Volume VI, 2006

U.S. Department of Energy • Office of Science

JOURNAL OF UNDERGRADUATE RESEARCH

Mentoring Relationships in the Field of Science

This year's cover for Volume VI of the *Journal of Undergraduate Research* recognizes the importance of mentoring relationships in the fields of science to current students who are future scientists. Beyond the learning of science content, the mentor relationships that students experience are critical because they introduce those students to collaboration in research and to a network of scientists.

The "tree" of mentoring shows that mentors pass on the science legacy to their students, who in turn become mentors for other students. One successful mentor may have an impact on several students, who each may impact even more students, just like the branches on a tree.

The images on the cover reflect past and current activities at the Lawrence Berkeley National Laboratory in Berkeley, California. The Lab is one in a network of laboratories supported by the U.S. Department of Energy (DOE). Students who conducted research at DOE National Laboratories during 2005 were invited to include their research abstracts, and for a select few, their completed research papers in this *Journal*. This *Journal* is direct evidence of students collaborating with their mentors.

Lawrence Berkeley National Laboratory (LBNL), the oldest Department of Energy National Lab, is celebrating its 75th anniversary. LBNL was founded on August 26, 1931 by Ernest O. Lawrence, the inventor of the cyclotron, an accelerator of subatomic particles, and a 1939 Nobel Laureate in physics for that achievement. The Radiation Laboratory he developed at Berkeley during the 1930s ushered in the era of "big science," in which experiments are no longer done by an individual researcher and a few assistants on the table-top of an academic lab, but by large, multidisciplinary teams of scientists and engineers in entire buildings full of sophisticated equipment and huge scientific machines.

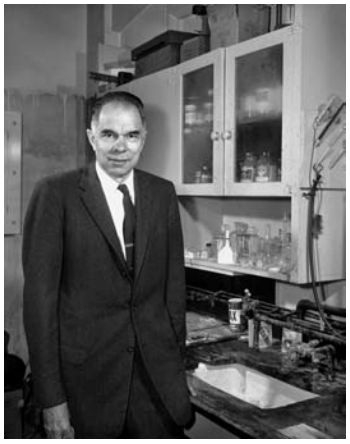

Glenn Seaborg

At the base of the tree of images is Marie Curie (1861-1934), followed by Ernest O. Lawrence (1901-1958), Glenn Seaborg (1912-1999), Al Ghiorso (1915-), Darleane Hoffman (1926-), and then followed by shots of recent educational groups. The claim to fame for these members of our "tree" is their contribution to the discovery of new elements from the 1940s to the 1970s. Lawrence was honored with Element 103, Lawrencium, in 1961; and Seaborg with Element 106, Seaborgium, in 1997. Curie created the phrase "radioactivity," and won two Nobel Prizes (1908 and 1911), the latter for the discovery of Radium and Polonium. Seaborg earned a Nobel Prize in 1951, codiscovered Plutonium, boldly predicted a new version of the Periodic Table, was an advocate for arms control and science education, and served as the Chairman of the Atomic Energy Commission (parent organization to the Department of Energy today). Ghiorso codiscovered 11 elements, a world record likely not to be matched. Darleane Hoffman took Glenn Seaborg's place on the UC Berkeley faculty and led the effort to confirm the discovery of element 106, paving the way for naming it Seaborgium.

The current Director of Education at the Lab, Rollie Otto, was mentored by Glenn Seaborg, and shared this reflection:

> "A mentor has a commitment to his or her life's work that is contagious. Certainly this was true of Glenn Seaborg. As I look back on my own career, I was guided by Glenn Seaborg's commitment and commitment to address critical problems and issues in nuclear science, energy independence and education.
>
> I learned from Glenn by example that mentors have a commitment to the successes of their students, as well as to raise students' expectations for what they can accomplish. Glenn Seaborg was a model mentor, who not only assigned his students to frontier projects, new element discoveries, but was a reliable supporter for these students' throughout their careers, creating a great legacy."

All photographs courtesy of Lawrence Berkeley National Laboratory. Darleane Hoffman photo taken by Roy Kaltschmidt.

A NOTE FROM THE EDITOR: SCIENTIFIC PROGRESS

Progress in scientific thought has helped to create societies with widespread security and comfort. The means by which science progresses have resulted in its reputation for being unbiased in its search for understanding. Contrary to what many school books purport, progress in science takes various forms, and is akin to organized chaos. When new innovative ideas arise, their defense can be especially absorbing. Numerous scientists have spent entire careers pursuing evidence that couldn't be found. Even more dramatic are the shifts from one paradigm to another. Paradigm shifts in science are often provoked by the discovery of phenomena antithetical to ideas that were so fundamental to current beliefs as to be unassailable. Newton extended the highest praise to Kepler because he was so audacious as to propose elliptical planetary orbits rather than the circular orbits so customarily accepted by others. Proponents of new paradigms have seldom found their ideas eagerly received. They are often roundly dismissed by those passionately adhering to prevalent theories. By gathering strong empirical evidence and enduring tests of their thinking, they sometimes succeed in radically shifting the course of scientific inquiry. Such progress embodies the expansion of knowledge that we call science.

Thomas Kuhn wrote in his 1962 monograph, *The Structure of Scientific Revolutions*, that so called normal science "is predicated on the assumption that the scientific community knows what the world is like. Scientists usually take great pains to defend this assumption and will make a strenuous and devoted attempt to force nature into the conceptual boxes supplied by professional education." Paradigm shifts occur when an anomaly "subverts the existing tradition of scientific practice."[1] In *Ideas and Opinions*, Albert Einstein wrote "our notions of physical reality can never be final. We must always be ready to change the notions … in order to do justice to perceived facts in the most logically perfect way."[2] Scientists must embrace curiosity and feed the desire to question for these are the fuel that fires the engine of discovery.

"Science and society are as interwoven as are observers and the observed."

Theories themselves can be viewed in different ways by different groups of scientists. Some see theories as a way to classify and systematize observations while others see them as attempts to describe the true nature of reality, even beyond the observable. These differing views can lead to diverse definitions of scientific progress. Those who adhere to theories as a way to systematize observations see scientific progress as an increase in the body of knowledge accessible to scientific thought. Adherents of this point of view often do not value theories as the genuine product of the scientific endeavor. Those who view theories as an attempt to describe the underlying truths of the universe see scientific progress as a never-ending movement towards a more valid description of the universe. A more inclusive description of scientific progress should avoid both of these extremes and incorporate aspects of each view.

Science, at its most basic level, is a human activity, and an integral part of human society. It is a way that we think about and rationally attempt to expose the underlying truth that confronts us. Progress in modern science is inextricably linked to societal affairs. Science and society are as interwoven as are observers and the observed. Throughout history, the intellectual freedom so prized by scientists has come with a price. For society, science is the bearer of security and well-being. Society typically grants science the freedom to explore and grow in almost any direction that discoveries warrant. As science has become more powerful and far-reaching, it has become the responsibility of all in society to understand the greater issues of science. Society guides the direction in which science is moving. Modern science relies on funds from government, industry, and private agencies in order to conduct research. It is through this funding that society is most able to exert its influence over scientific progress. Recent events, such as debates surrounding stem cell research and cloning, illustrate society's ability to exert such pressure.

In such an environment, science may need to address another of its long-standing paradigms – that within the bounds of ethical conduct, any question that is answerable should be open to scientific investigation. Given the extent to which science can affect the planet, it is no longer wise to ignore the concerns of society outside of the scientific establishment. The next generation of scientists will have to answer the question of whether or not we should pursue certain scientific developments simply because we can. Such discussions will require scientists to engage in dialogue with many different factions within society. This will present new and unique challenges to the scientists of the future.

Peter Faletra, Ph.D.
Director, Office of Workforce Development for Teachers & Scientists
Office of Science

Kevin M. Hartmann
Albert Einstein Distinguished Educator Fellow
Office of Science

References:

1. Kuhn, T. (1996). *The Structure of Scientific Revolutions*. Chicago: University of Chicago Press.
2. Einstein, A. (1954). *Ideas and Opinions*. New York: Crown Publishers.

SCIENTIFIC "GRANDCHILDREN"

Many things have been said about the value of mentoring, and in some sense not much can be added. A mentor is someone who is interested in the first steps of developing a student into a professional. There are many lessons that must be taught. For example, "Don't listen to orthodox explanations." Well, maybe listening is okay, but believing all you hear isn't okay. "Find the courage to stick to your conclusions." "Don't get discouraged when mistakes are made." "Understand what you are doing, and if things don't work you must evaluate what you did and make sure it's correct." The list goes on and on, and in some sense, a mentor must get the student through these obstacles.

In fact they are not obstacles, but really become a mind set for a scientist. Even though I could probably find more things to enumerate, I must emphasize that the most important thing to leave with a student is the sense of adventure in science, to try something no one has ever tried, and ultimately if your experiment or calculation goes well, to realize that you know more about something than anyone else in the world.

There was a very amazing surprise that happened a couple of summers ago. Noel Blackburn in our Office of Educational Programs indicated that he had a candidate in the Faculty and Student Team (FaST) program that might be a match for me, and was I interested. After looking at the credentials of Abebe Kebede of North Carolina A&T, he seemed to have experience in my area and I had a good project for him and his students. What's interesting is that in looking at his credentials he had reasonable publications, and better yet he got his Ph.D. with Jack Crow at Temple University. Jack Crow was a remarkable scientist with the vision to create the National High Magnetic Field Laboratory in Tallahassee Florida. Tragically, Jack died in September of 2004 from pancreatic cancer. In the memorial service information it says "The National High Magnetic Field Laboratory is truly the house that Jack built." It couldn't be put better.

So in the summer of 2004, Abebe Kebede, his students, and I agonized over Jack, as well as measuring the conductivity of percolating gold clusters. Interestingly, I had hired Jack when he left graduate school; we worked together for many years before he went to Temple. So, in some sense, Abebe, Jack's student, is really my scientific "grandson," which of course makes me a great-grandfather to Chris Jessamy and Tanina Bradley, the students who accompanied Abebe from North Carolina. Having a part in this as a mentor has been a great source of satisfaction for me as I see the excitement of science passed on to new generations.

"...the most important thing to leave with a student is the sense of adventure in science..."

There is another interesting aspect to this story, and that is the value of the FaST program where minority students can take part in some of the things that go on at a great laboratory. They can see ideas flying around, some good and some bad, and they get the

feeling of how science is done and whether this is what they want as a career. It's important to them, and it's important to America. In looking through the Web, I noticed that Chris and Tanina expanded some of the work they did here and presented it in the University of North Carolina Student Research Program. I gather that Tanina is finishing up at the University of North Carolina at Charlotte and Chris is about to graduate from North Carolina A&T. I like to think that somehow we all came together through Jack.

Myron Strongin
Bookhaven National Laboratory

"They can see ideas flying around, some good and some bad, and they get the feeling of how science is done and whether this is what they want as a career."

TABLE OF CONTENTS

Selected Student Papers:

Selected Student Papers Continued:

DOE Office of Science Programs

AMES LABORATORY
Ames, Iowa

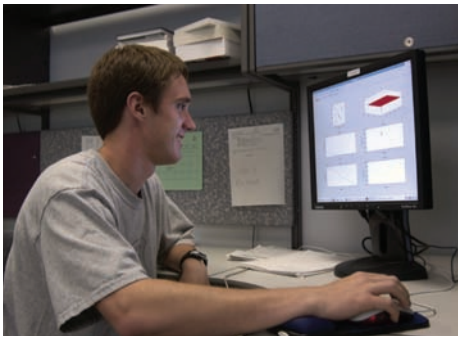

Scientists at the Department of Energy Office of Science's Ames Laboratory seek solutions to energy-related problems through the exploration of chemical, engineering, materials and mathematical sciences, and physics.

Established in the 1940s with the successful development of the most efficient process to produce high-purity uranium metal for atomic energy, Ames Lab now pursues much broader priorities than the materials research that has given the Lab international credibility.

Responding to issues of national concern, Lab scientists are actively involved in innovative research, science education programs, the development of applied technologies and the quick transfer of such technologies to industry. Uniquely integrated within a university environment, the Lab stimulates creative thought and encourages scientific discovery, providing solutions to complex problems and educating tomorrow's scientific talent.

Ames Laboratory is located in Ames, Iowa, on the campus of Iowa State University. Iowa State's 2,000-acre, park-like campus is home to more than 25,000 students. Ames is approximately 30 minutes north of Des Moines, Iowa's capital city.

ARGONNE NATIONAL LABORATORY
Argonne, Illinois

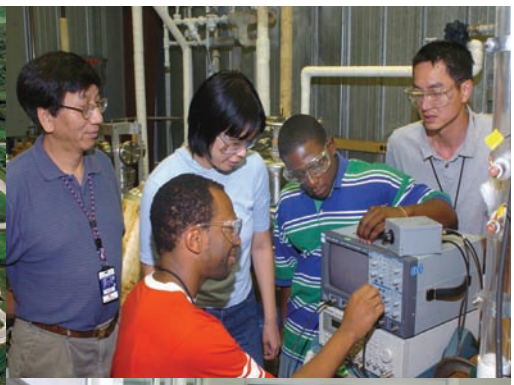

Argonne National Laboratory descends from the University of Chicago's Metallurgical Laboratory, part of the World War Two Manhattan Project. The laboratory has about 2,900 employees, including about 1,000 scientists and engineers. Argonne occupies 1,500 wooded acres in DuPage County, Illinois, about 25 miles southwest of Chicago's Loop. Argonne research falls into broad categories:

- Basic science seeks solutions to a wide variety of scientific challenges. This includes experimental and theoretical work in biology, chemistry, high energy and nuclear physics, materials science, and mathematics and computer science.
- Scientific facilities help advance America's scientific leadership and prepare the nation for the future. These facilities are used by scientists thousands of scientists and students from the U.S. and abroad. The laboratory is also home to the Advanced Photon Source, the Center for Nanoscale Materials, the Intense Pulsed Neutron Source, and the Argonne Tandem Linear Accelerator System.
- Energy resources programs help insure a reliable supply of efficient and clean energy for the future. Argonne scientists and engineers are developing advanced batteries and fuel cells, as well as advanced electric power generation and storage systems.
- Environmental management includes work on managing and solving the nation's environmental problems and promoting environmental stewardship.
- National Security has increased in significance in recent years for the nation and for Argonne research. Argonne capabilities developed over the years for other purposes are helping to counter the threats of terrorism.

Argonne's Division of Educational Programs provides workforce development for faculty and students from universities to regional K-12 schools.

BROOKHAVEN NATIONAL LABORATORY
Upton, New York

Established in 1947, Brookhaven National Laboratory is a Department of Energy, Office of Science multidisciplinary laboratory managed by Brookhaven Science Associates, a company founded by Battelle and Stony Brook University. Home to six Nobel Prizes, Brookhaven conducts research in the physical, biomedical, and environmental sciences, as well as in energy technologies and national security.

Located on a 5,300-acre site on eastern Long Island, New York, Brookhaven builds and operates major scientific facilities available to university, industry and government researchers. Among those facilities are the world's newest accelerator for nuclear physics research, the Relativistic Heavy Ion Collider (RHIC), and the National Synchrotron Light Source (pictured here) where approximately 2,500 researchers use beams of light, from x-rays to ultraviolet and infrared, to study materials as diverse as computer chips and proteins. In the near future, the Center for Functional Nanomaterials will be built at Brookhaven, one of five Department of Energy centers where researchers will study materials on the scale of a billionth of a meter, or only a few atoms.

A wide variety of both basic and applied research is conducted at Brookhaven. For instance, scientists are investigating the building blocks of matter using RHIC, the roots of drug addiction and brain metabolism using positron emission tomography, the effects of space radiation on astronauts using the newly built NASA Space Radiation Laboratory, and the effects of increased carbon dioxide in ecosystems. Brookhaven researchers also develop new technologies as varied as detectors for national security and oil burners with improved efficiency.

FERMI NATIONAL ACCELERATOR LABORATORY
Batavia, Illinois

Fermi National Accelerator Laboratory (Fermilab) is one of the world's foremost laboratories dedicated to high-energy physics research. It is operated for the Department of Energy Office of Science by a consortium of 90 research-oriented universities. More than 3,000 scientists from around the world use Fermilab for their experiments.

Fermilab is located on a 6,800-acre site about 35 miles west of Chicago, Illinois. The laboratory is home to the Tevatron Collider, the world's highest-energy particle accelerator. Two large detectors analyze the Tevatron's proton-antiproton collisions to unveil the fundamental forces and particles of the universe. Scientists at Fermilab discovered the bottom quark and the top quark, and first observed the tau neutrino.

Fermilab operates the world's most powerful proton beam for creating neutrinos. The Center for Particle Astrophysics at Fermilab includes groups studying cosmic rays, supernovae, dark energy and other phenomena.

IDAHO NATIONAL LABORATORY
Idaho Falls, Idaho

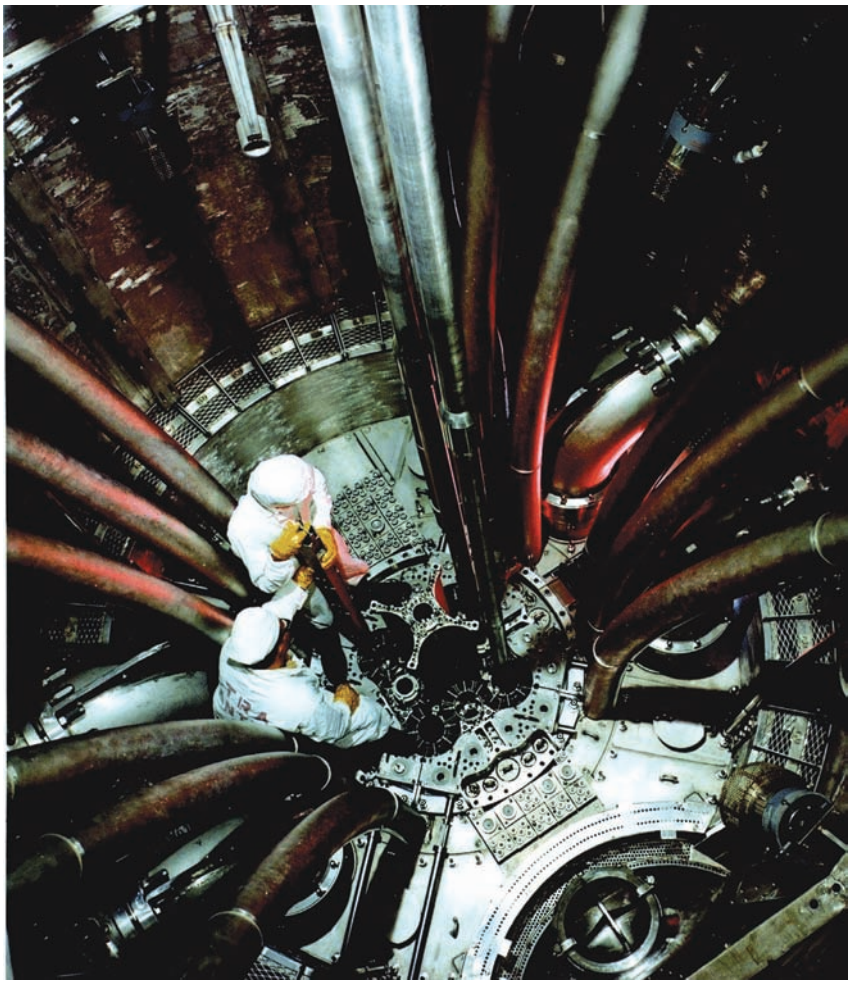

In operation since 1949, The Idaho National Laboratory (INL) is a science-based, applied engineering National Laboratory dedicated to supporting the U.S. Department of Energy's missions in nuclear and energy research, science, and national defense.

INL stands out as a unique national and international resource. Notably, the Lab has been formally designated as the nation's command center for advanced civilian nuclear technology research and development, and is home to the unparalleled Critical Infrastructure Test Range, with assets as diverse as an isolable electric grid and wireless test bed. Leveraging these and numerous other distinguishing features, the Lab and its more than 3,300 scientists, engineers and support personnel build on the potential and promise of the theoretical for the benefit of the real world.

Located in southeast Idaho, INL covers 890 square miles of the Snake River Plain between Idaho Falls and Arco, Idaho. Offices and laboratories are also in the city of Idaho Falls (population 50,000), located about two hours from Grand Teton and Yellowstone national parks and other areas offering prime recreational opportunities.

LAWRENCE BERKELEY NATIONAL LABORATORY
Berkeley, California

Lawrence Berkeley National Laboratory's research and development includes new energy technologies and environmental solutions with a focus on energy efficiency, electric reliability, carbon management and global climate change, and fusion. Frontier research experiences exist in nanoscience, genomics and cancer research, advanced computing, and observing matter and energy at the most fundamental level in the universe.

Ernest Orlando Lawrence founded the Berkeley Lab in 1931. Lawrence is most commonly known for his invention of the cyclotron, which led to a Golden Age of particle physics—the foundation of modern nuclear science—and revolutionary discoveries about the nature of the universe. Berkeley Lab's Advanced Light Source is its premier national user facility centrally located on the lab site overlooking the San Francisco Bay.

LAWRENCE LIVERMORE NATIONAL LABORATORY
Livermore, California

Lawrence Livermore National Laboratory (LLNL) is a premier applied science laboratory that is part of the National Nuclear Security Administration (NNSA) within the Department of Energy. With more than 8,000 employees, LLNL is located on a one-square-mile site in Livermore, California. A larger (10 square miles) remote explosives testing site (Site 300) is situated 18 miles to the east.

LLNL is managed by the University of California (UC) for the National Nuclear Security Administration. Being part of the University helps foster intellectual innovation and scientific excellence. This University connection allows LLNL to recruit and retain a diverse world-class workforce and partner with the UC's extensive research and academic community. These factors are essential to sustaining the laboratory's scientific and technical excellence.

Lawrence Livermore National Laboratory is a national security laboratory with responsibility for ensuring that the nation's nuclear weapons remain safe, secure, and reliable. LLNL also applies its special expertise and multidisciplinary capabilities to prevent the spread and use of nuclear and other weapons of mass destruction and strengthen homeland security.

The Lab has pioneered the application of many technologies, from high-performance computers to advanced lasers, to meet national security needs. Today, the special capabilities developed for our stockpile stewardship and nonproliferation activities enable us to also meet enduring national needs in conventional defense, energy, environment, biosciences, and basic science. Research programs in these areas enhance the competencies needed for the Laboratory's national security mission.

LOS ALAMOS NATIONAL LABORATORY
Los Alamos, New Mexico

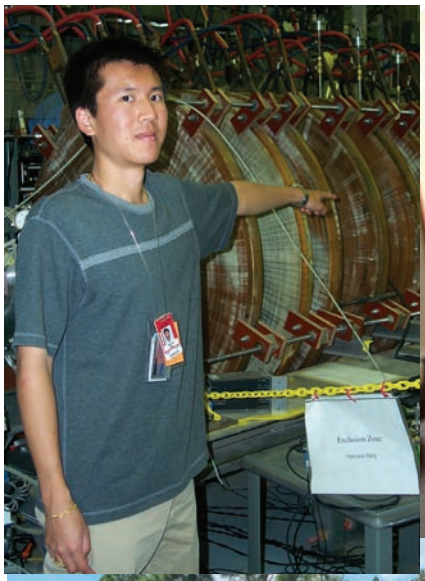

The Los Alamos National Laboratory (LANL), located in the Jemez Mountains of northern New Mexico, offers the opportunity for students to work at a multi-disciplinary, world-class research facility while enjoying a truly unique environment. Long known for its artistic community, northern New Mexico also offers a variety of exciting outdoor recreational opportunities, including rock climbing and hiking in the adjacent mountains and canyons, proximity to the Rocky Mountains, and exceptional skiing opportunities at many nearby locations.

We offer a diverse research experience for undergraduate and graduate students as a means of assuring the continued vibrancy of the science, engineering, and technology at the laboratory. Serve your internship with us and you will have the opportunity to work in a team environment with some of the world's top scientists and engineers on critical issues involving our national security, environment, infrastructure, and security. We offer internship opportunities in areas that include: Biology, Chemistry, Computer Science, Physics, Mathematics, Materials Science, Environmental Science, and Engineering: Chemical, Civil, Computer, Electrical, Mechanical, Nuclear, and Software.

If you are a problem solver and independent thinker, a team player, a good communicator, like a hands-on approach, and are self-motivated, we offer you the challenge of an internship at Los Alamos National Laboratory.

NATIONAL RENEWABLE ENERGY LABORATORY
Golden, Colorado

The National Renewable Energy Laboratory (NREL) is the Department of Energy's primary National Laboratory for renewable energy and energy efficiency research and development. From harvesting energy from the sun and wind, to advancing automotive systems, to developing biodegradable plastics form corn stalks, NREL develops renewable energy and energy efficiency technologies and practices, advances related science and engineering, and transfers knowledge and innovations to address the nation's energy and environmental goals. NREL is home to three nationals centers of excellence: the National Center for Photovoltaics, the National Bioenergy Center and the National Wind Technology Center.

NREL research has been recognized with 39 R&D 100 Awards, ranking first among National Laboratories per researcher, as well as numerous honors from *R&D*, *Discover*, and *Popular Science* magazines and leading scientific organizations.

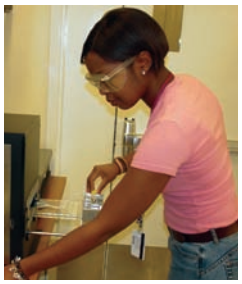

Innovative, challenging and dynamic—that's our culture. If you are interested in a research internship with an institution that believes creativity and individual uniqueness are at the core of our success, then explore your options at: www.nrel.gov. We value intern talent that adds to the rich pool of research findings produced by NREL each year. Intern accomplishments include:

- More than 24 students have been selected by the Office of Science to present major NREL research at the AAAS.
- More than 50 past student interns have been hired on to join the NREL family.
- Teacher researchers have produced over 50 renewable energy lessons for the classroom.
- NREL's Office of Education partners with over 75 universities throughout the nation.

NREL's main 327-acre site is in Golden, Colorado, just west of Denver. The Laboratory also operates the National Wind Technology Center on 307 acres about 20 miles north of Golden, adjacent to the Department of Energy's Rocky Flats Environmental Test Site. We are an equal opportunity employer committed to diversity.

OAK RIDGE NATIONAL LABORATORY
Oak Ridge, Tennessee

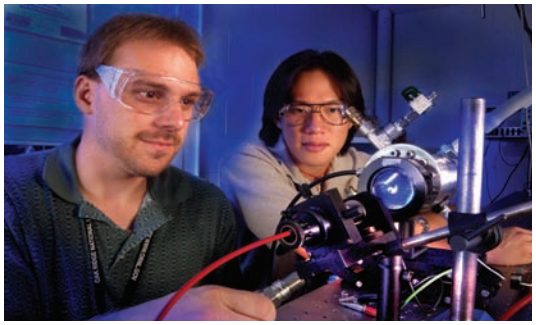

Oak Ridge National Laboratory is the Department of Energy's largest science and energy laboratory. Managed since April 2000 by a partnership of the University of Tennessee (UT) and Battelle, ORNL was established in 1943 as a part of the secret Manhattan Project to pioneer a method for producing and separating plutonium. More than 60 years later, ORNL's mission is to conduct basic and applied research that provides innovative solutions to complex problems.

ORNL, with funding that exceeds $1 billion, has a staff of more than 4,000 and approximately 3,000 guest researchers who spend two weeks or longer each year in Oak Ridge. The Laboratory's six major scientific competencies, in support of DOE's Office of Science, include neutron science, energy, high performance computing, complex biological systems, advanced materials and national security.

ORNL is in the final stages of a $300 million project to provide a modern campus for the next generation of great science. A unique combination of federal, state and private funds is building 13 new facilities. Included in these new facilities will be the Functional Genomics Center, the Center for Nanophase Materials Science, the Advanced Microscopy Laboratory, and the joint institutes for Computational Science, Biological Science and Neutron Science. ORNL is the site of the Office of Science's National Leadership Computing Facility for unclassified high-performance computing. On budget and on schedule for completion in 2006, the $1.4 billion Spallation Neutron Source will make Oak Ridge the world's foremost center for neutron science research.

UT-Battelle has provided more than $6 million in support of math and science education, economic development and other projects in the greater Oak Ridge region.

PACIFIC NORTHWEST NATIONAL LABORATORY
Richland, Washington

Pacific Northwest National Laboratory (PNNL) is a multi-purpose National Laboratory dedicated to delivering innovative science-based solutions to some of the nation's most pressing problems. PNNL conducts fundamental and applied research to address important issues including securing our homeland, reducing our dependence on foreign oil, transforming the energy system, making information access easier, and protecting our natural resources.

PNNL's facilities form a world-class campus, including many laboratories recognized as best-in-class for many research areas. With an international reputation for studies in chemistry, biology, computer sciences, and a wide range of other fields, award-winning PNNL researchers rapidly translate theory into concrete solutions. Many of the Laboratory's technologies have been developed into common consumer and industrial products including the compact disc (CD).

The Laboratory consistently attracts some of the world's leading scientific talents shaping the future of science through a variety of on-site educational programs. As mentors and research partners, the Laboratory's staff trains young scientists and engineers to become tomorrow's inventors. Student research opportunities at PNNL include appointments in atmospheric science and global change, computational sciences, experimental chemistry, marine sciences, molecular biology, environmental studies, remediation, environmental microbiology, wildlife and fisheries biology, materials research, process science and engineering, economics and political science.

Located in southeastern Washington near the base of the Blue Mountains and the confluence of the Columbia, Snake and Yakima rivers, PNNL staff enjoy year around recreation, locally-produced fine wines, and the community's commitment to the arts.

PRINCETON PLASMA PHYSICS LABORATORY
Princeton, New Jersey

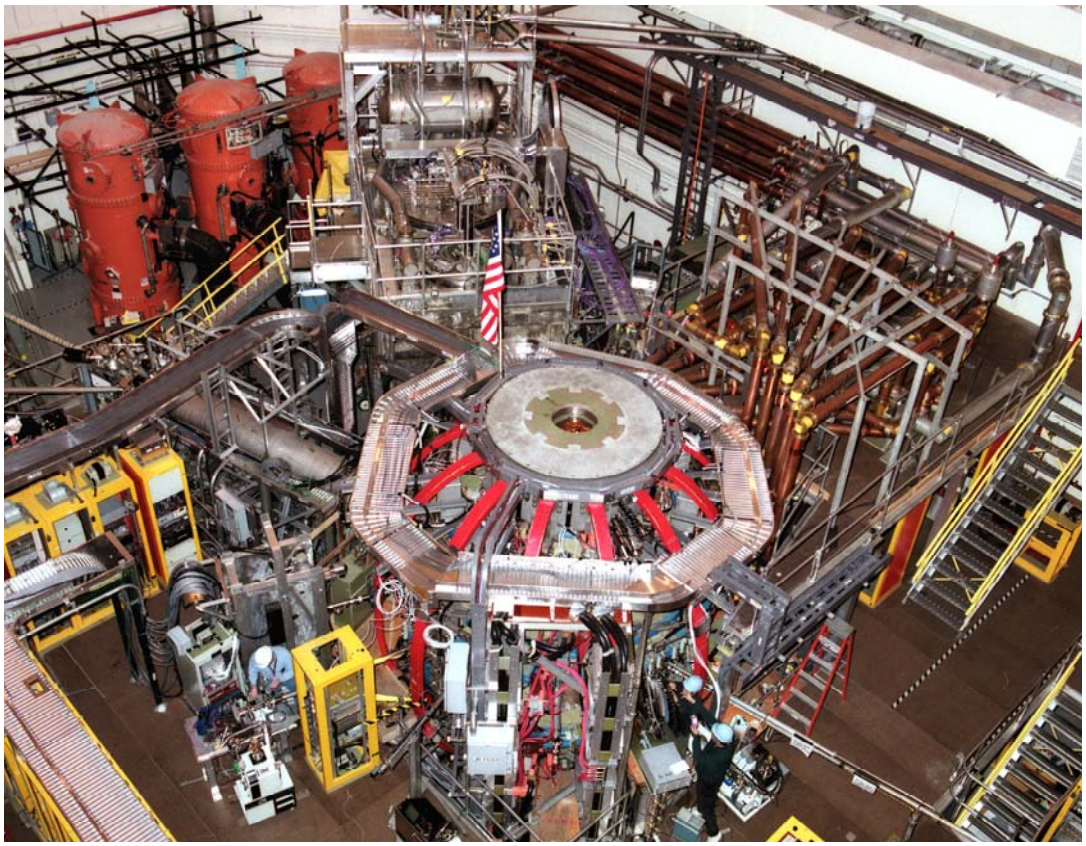

The world's reliance on fossil fuels is imperiling our environment. Fusion, the energy source of the sun and the stars, offers an inexhaustible alternative. A fusion-powered electric generator would not produce hydrocarbon emissions, greenhouse gases, or long-lived radioactive waste; nor would it emit chemicals that cause acid rain. Consequently, the U.S. Department of Energy (DOE) Office of Science has made the development of commercial fusion power one of its highest priorities.

DOE's Princeton Plasma Physics Laboratory (PPPL) is one of the world's leading facilities for fusion R&D.

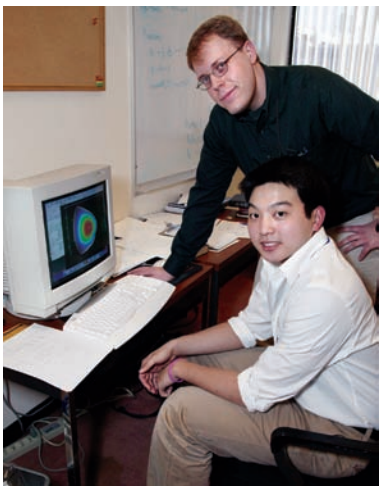

Currently the PPPL is operating the National Spherical Torus Experiment (pictured above) and is building the National Compact Stellarator Experiment, both use magnetic fields to confine hot ionized gas (plasma) that serves as the fusion fuel. PPPL's theoretical physicists are developing computational physics models that can predict how various plasma configurations will perform, saving time and money.

PPPL experimental physicists collaborate with their colleagues worldwide in a free, mutually beneficial, exchange of information. Princeton researchers and engineers are using knowledge and skills gained in fusion research to solve other problems, including the development of plasma-based propulsion systems for space vehicles, studies of plasma phenomena that occur in the sun's corona and the earth's magnetosphere, and research on plasma sterilization of plastic food and beverage containers. PPPL is located about three miles from Princeton University's main campus in Princeton, NJ.

STANFORD LINEAR ACCELERATOR CENTER
Menlo Park, California

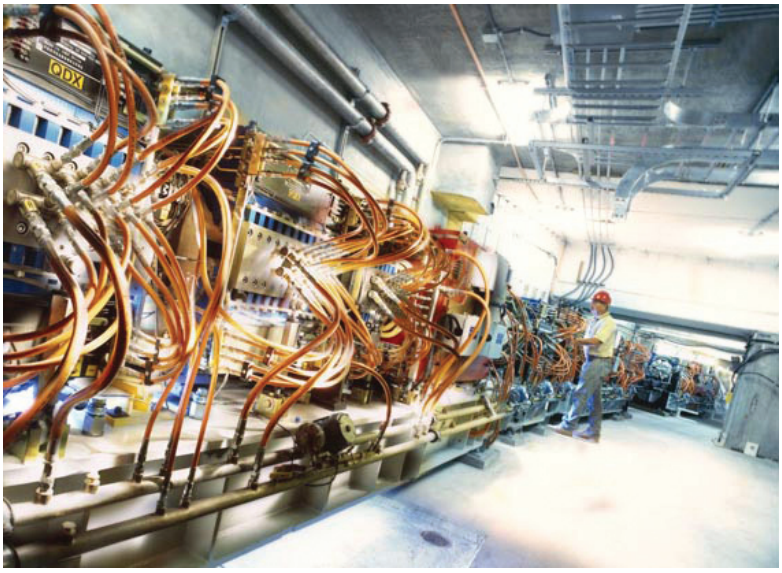

The Stanford Linear Accelerator Center (SLAC) is one of the world's leading laboratories for research in high-energy physics (HEP), particle astrophysics and cosmology, and synchrotron radiation research.

SLAC's HEP program seeks answers to fundamental questions about the ultimate structure of matter and the forces between these fundamental particles. The BABAR experiment investigates matter/anti-matter asymmetry and is the current focus of the HEP program. In addition, a vigorous R&D program is focused on realizing the next generation electron collider—the International Linear Collider, as part of a world-wide effort.

The Kavli Institute at SLAC for Particle Astrophysics and Cosmology bridges theoretical and experimental physics communities, and brings their combined strengths to bear on some of the most challenging and fascinating problems in particle astrophysics and cosmology to help us understand the birth and evolution of the universe.

The Stanford Synchrotron Radiation Laboratory (SSRL) at SLAC, provides high intensity x-ray beams for molecular and atomic scale studies in physics, biology, chemistry, medicine, and environmental science. The Linac Coherent Light Source (LCLS), a facility to provide even more intense x-ray capability is now under construction. Pioneering experiments at LCLS will advance our understanding of everything from the hidden physics inside planets, to how proteins function as the engines of life, to building nanotechnology devices for the backbone of future industry and technology.

THOMAS JEFFERSON NATIONAL ACCELERATOR FACILITY
Newport News, Virginia

The Thomas Jefferson National Acceleration Facility, or Jefferson Lab, is a nuclear physics research laboratory located in Newport News, Virginia. Nuclear physics research scientists who use Jefferson Lab are on a journey of discovery into the nucleus of the atom. Their goal is to develop a roadmap of matter that helps unlock the secrets of how the universe is put together. Nuclear physics funding from the Department of Energy provides Jefferson Lab with leading-edge instrumentation, world-class facilities and training and support for the people involved in these pursuits. Forefront nuclear physics research conducted at Jefferson Lab provides solid foundations for other fields. The accumulation of new results and the intellectual training of new generations of scientists foster important advances in medicine, chemistry and other sciences.

Scientists at Jefferson Lab use the Continuous Electron Beam Accelerator Facility — the first large-scale application of superconducting radiofrequency technology — to conduct physics experiments. Using accelerated electron beams, experimenters probe the sub-nuclear realm. Using this same technology, Jefferson Lab has built the world's brightest high average power Free Electron Laser that offers unique capabilities for defense, industry, basic research and medicine.

Yiwen Chu is a senior at Massachusetts Institute of Technology majoring in physics and mathematics. In the summer of 2005, she worked on the BaBar project at the Stanford Linear Accelerator Center as a SULI intern. In addition to the analysis of semileptonic B meson decays, which was presented at the 2006 AAAS conference, she worked on testing hardware for the detector drift chamber. She is currently working in an atomic physics group at MIT on cooling and trapping rubidium atoms in hollow core optical fibers. She will finish her B.S. degrees next year and then hopes to enter into a PhD program in physics.

Bryce Littlejohn is entering his first year of graduate school at the University of Wisconsin-Madison and is interested in studying particle physics. He received his B.S. in 2006 from Principia College, where he worked on the construction of a pulsed positronium beam for use in low-energy positron physics research. Fir his internship at SLAC in 2005, Bryce worked on semileptonic decay data analysis and hardware testing on BaBar.

Jochen Dingfelder is a postdoc at the Stanford Linear Accelerator Center (SLAC). He received his Ph.D. from the University of Heidelberg in 2003 for a study of anomalous production of top quarks in electron-proton collisions with the H1 experiment at DESY in Germany. He has performed a number of analyses searching for new particles and interactions beyond the Standard Model of particle physics. He came to SLAC as a Feodor Lynen fellow of the Alexander von Humboldt Foundation to study decays of B mesons with the BaBar experiment. His research activities have focused on semileptonic B-meson decays, in particular the study of exclusive charmless semileptonic decays such as B->\pi l nu or B->\rho l nu. Since 2005 he is co-convener of the semileptonic analysis working group in BaBar and coordinates the research activities of this group.

ANALYSIS OF $B \rightarrow \omega l\nu$ DECAYS WITH BaBar

YIWEN CHU, BRYCE LITTLEJOHN, AND JOCHEN DINGFELDER

ABSTRACT

As part of the BaBar project at SLAC to study the properties of *B* mesons, we have carried out a study of the exclusive charmless semileptonic decay mode $B \rightarrow \omega l\nu$, which can be used to determine the magnitude of the Cabbibo-Kobayashi-Maskawa matrix element V_{ub}. Using simulated event samples, this study focuses on determining criteria on variables for selection of $B \rightarrow \omega l\nu$ signal and suppression of background from other types of *BB* events and continuum processes. In addition, we determine optimal cuts on variables to ensure a good neutrino reconstruction. With these selection cuts, we were able to achieve a signal-to-background ratio of 0.68 and a signal efficiency of the order of 1%. Applying these cuts to a sample of 83 million *BB* events recorded by BaBar in e^+e^- collisions at the $\Upsilon(4S)$ resonance, we obtain a yield of 115 ± 19 $B \rightarrow \omega l\nu$ decays.

INTRODUCTION

The BaBar experiment at SLAC studies the properties of *B* mesons in $B\bar{B}$ events produced in e^+e^- collisions on the $\Upsilon(4S)$ resonance. We study the particular exclusive decay $B \rightarrow \omega l\nu$, which is called a charmless semileptonic decay due to the presence of a charged lepton, a neutrino, and a charmless hadron, the ω meson, in the final state. The study of charmless semileptonic decays allows for the determination of the Cabbibo-Kobayashi-Maskawa (CKM) matrix element $|V_{ub}|$, which determines the probability of a $b \rightarrow u$ quark transition in a weak interaction and is one of the smallest and least known elements. In the Standard Model, the CKM matrix is unitary, and this condition can be graphically represented as the Unitarity Triangle in the complex $(\rho - \eta)$ plane [1]. $|V_{ub}|$ indicates the length of one side of this triangle. A precise measurement of $|V_{ub}|$ would significantly improve the constraints on the Unitarity Triangle and provide a stringent test of the Standard Model mechanism for Charge-Parity (CP) violation.

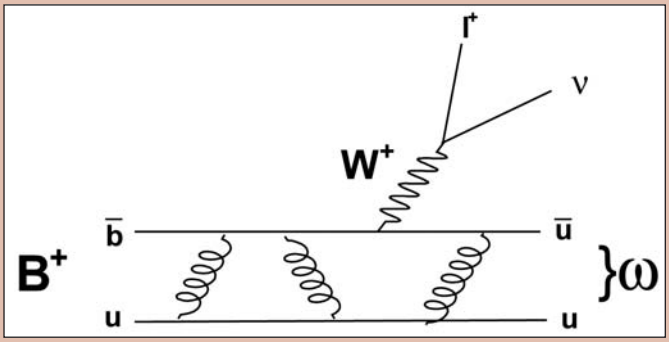

Figure 1. Feynman diagram of a B → $\omega l\nu$ decay.

The BaBar collaboration has already measured several other charmless semileptonic decays, such as $B \rightarrow \pi l\nu$ and $B \rightarrow \rho l\nu$ [2]. However, the $B \rightarrow \omega l\nu$ mode is experimentally more difficult and has not yet been studied in detail with sufficient signal statistics by BaBar. Recent studies at Belle have been able to identify these

events and measure a branching fraction of (1.3 ± 0.4 ± 0.3 ± 0.3) × 10^{-4} [3].

In this study, we focus on improving the selection of $B \rightarrow \omega l\nu$ decays by reducing the background from other processes and ensuring a reliable reconstruction of the neutrino kinematics. In the complex process of analyzing data, discrimination between signal and background is particularly important and challenging for a rare process such as $B \rightarrow \omega l\nu$. By looking at tracks made in different parts of the BaBar detector, we can reconstruct and identify the particles produced in the e^+e^- collision, thereby selecting signal decays. However, background events can be misidentified as signal, or a real signal decay may be wrongly reconstructed. The latter case may occur by, for example, assigning a particle from the other B decay to the signal B decay. Significant backgrounds include $B \rightarrow X_c l\nu$ decays, where X_c stands for a meson that contains a c quark, and $e^+e^- \rightarrow q\bar{q}$ processes ("continuum events"). Fortunately, the features of the signal events we are interested in differ in many ways from those of the background, which allows us to enhance the signal by applying selection cuts on variables that exhibit these differences. Another challenge of the analysis process involves the reliable reconstruction of the semileptonic decay kinematics. In particular, we study the quality of the neutrino reconstruction. Since these particles are not directly detectable, their kinematics must be inferred indirectly from the missing momentum and energy of the entire event, causing much room for error. We study several variables that can be used to ensure a good quality of the neutrino reconstruction.

After performing the above studies using Monte Carlo simulated samples, we can determine the number of signal events in a sample of 83 million $B\bar{B}$ events recorded with the BaBar detector.

MATERIALS AND METHODS

To identify a $B \rightarrow \omega l\nu$ decay, we look for the presence of a lepton with center-of-mass momentum greater than 1.3 GeV/c, a substantial missing momentum as indication of a neutrino in the event, and a reconstructed hadron consistent with an ω meson. The ω is reconstructed in its dominant decay mode $\omega \rightarrow \pi^+\pi^-\pi^0$, where the π^+ and π^- are identified as charged tracks in the drift chamber not consistent with a lepton or kaon and the π^0 as two photons in the electromagnetic calorimeter produced in the decay $\pi^0 \rightarrow \gamma\gamma$.

The data and Monte Carlo samples used in our analysis have been applied with preliminary selection criteria ("preselection"). In order to reduce continuum background events that are not produced on the Υ (4S) resonance, the preselection uses loose cuts on the number of charged tracks ($N_{track} > 3$), $R2 < 0.6$, $|\cos\theta_{BY}| < 1.5$ (see section 3.2 for definitions of $R2$ and $|\cos\theta_{BY}|$). In addition, we apply a loose cut on the invariant mass of the three pions forming the omega candidate of $0.70 < m_{\pi^+\pi^-\pi^0} < 0.86$ GeV and a cut on the ω decay amplitude of the three pions produced, given by

$$\lambda = \frac{|\vec{p}_{\pi^+} \times \vec{p}_{\pi^-}|^2}{\frac{3}{4}(\frac{1}{9}m_{3\pi}^2 - m_{\pi^+}^2)^2} > 0.25\ \mathrm{GeV}^{-2}. \qquad (1)$$

These criteria significantly reduce the requirements on CPU time and disk space and yield a data sample of manageable size for this analysis.

Neutrino Reconstruction

In addition to the energetic charged lepton, the presence of a neutrino in the decay products of the B meson is a characteristic feature of semileptonic modes, so we first try to isolate events with a well reconstructed neutrino. Since neutrinos cannot be detected, we must infer their mass and kinematics from all reconstructed particles. The four-momentum of the neutrino is taken to be the missing four-momentum of the event, given by

$$(\vec{p}_\nu, E_\nu) = (\vec{p}_{miss}, E_{miss}) = (\vec{p}_{beams}, E_{beams}) - (\sum_i \vec{p}_i, \sum_i E_i), \quad (2)$$

where $\vec{p}_{beams}$, E_{beams} are the sums of the known momenta and energies of the colliding e^+ and e^-, and $\vec{p}_i$, E_i are the momentum and energy of the i^{th} reconstructed particle [4]. We also reject events with $|\vec{p}_{miss}| < 0.7$ GeV. The missing-mass squared of the neutrino is then calculated as

$$m_{miss}^2 = E_{miss}^2 - |\vec{p}_{miss}^2|. \qquad (3)$$

In the simulated events, these reconstructed quantities can be compared to the true values for each event, which tells us how well the neutrino has been reconstructed. In particular, we are interested in the following resolutions:

1. $|\vec{p}_{miss}| - |\vec{p}_{\nu,true}|$: The difference in the magnitudes of the lab-frame momenta.
2. $q^2_{reco.} - q^2_{true}$: Here q^2 is the four-momentum transfer of the decay, given by

$$q^2 = (p_{lepton} + p_\nu)^2 = (p_B - p_{hadron})^2. \qquad (4)$$

It is equivalent to the invariant mass squared of the virtual W boson involved in the production of the lepton and neutrino.

We try to quantify the quality of the neutrino reconstruction by fitting the $|p_{miss}| - |p_{\nu,true}|$ distribution with a Gaussian function for the peak and a Landau function for the tail. The $q^2_{reco.} - q^2_{true}$ distribution was fitted with two Gaussian functions, one for the peak and the other to describe the tails. Although the fits are not perfect, they approximately quantify the quality of the reconstructed neutrino. We then study the width (σ_{peak}) and mean (μ_{peak}) of the peak Gaussian functions, along with the ratio N_{tail} / N_{all}, where N_{all} is the number of events in both the Gaussian and Landau functions, and N_{tail} is the number of events in the tail with selection criteria (as explained below) outside 2σ of the Gaussian peak without selection criteria.

As can be seen in Fig. 2, there are significant resolution tails due to poorly reconstructed events. These tails are mostly caused by events where particles are lost outside the detector acceptance region or by the production of an additional neutrino from, for example, the decay of the other B meson. By discarding events that do not satisfy selection criteria on the following variables that are directly affected by the neutrino reconstruction, we can reduce the resolution tails.

1. $Q_{tot} = \sum_i Q_{track,i}$: If a charged particle was lost, the total charge of the event will generally no longer be zero. To reduce the effect of losses due to detector acceptance, we use the typical cut of $Q_{tot} \leq 1$.

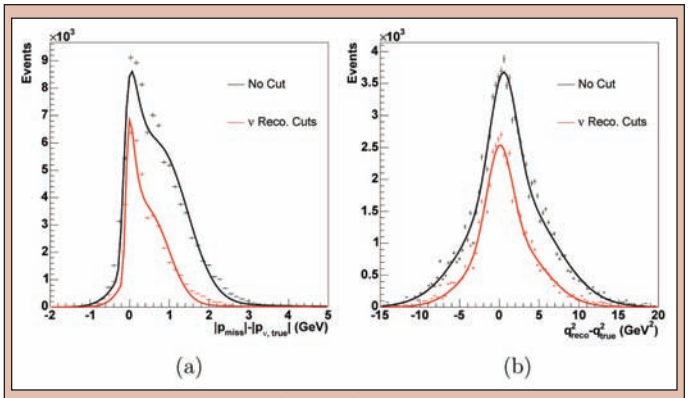

Figure 2. Resolutions (a) $|\vec{p}_{miss}| - |\vec{p}_{\nu;true}|$ and (b) $q^2_{reco.} - q^2_{true}$. Crosses are simulated signal events with statistical error and lines are fits. Black: No cuts applied. Red: Resolutions after chosen cut of $\frac{m^2_{miss}}{E_{miss}} < 2.6$ GeV, $\theta_{miss} > 0.5$ rad, and $Q_{tot} \leq 1$.

2. m^2_{miss}/E_{miss}: m^2_{miss} should be $m^2_{\nu} \approx 0$. Since the m^2_{miss} resolution broadens linearly with E_{miss}, a cut on this variable is more effective than a cut on m^2_{miss}.
3. θ_{miss}: This variable indicates the angle between the missing momentum and the e^- beam. When this angle is close to 0° or 180°, it is likely that the missing momentum was caused by a particle other than a neutrino traveling in the direction of the beamline, where it cannot be detected.

We vary the cuts from $m^2_{miss}/E_{miss} < 1.0$ GeV to $m^2_{miss}/E_{miss} < 3.8$ GeV and from $\theta_{miss} > 0$ rad to $\theta_{miss} > 0.6$ rad and then plot the signal efficiency $\epsilon_{sig} = N^{sig}_{cut}/N^{sig}_{uncut}$ and the characteristic parameters of the resolutions as functions of cut values in order to find the best combination of cuts (see Fig 3). While we see only a moderate improvement when tightening the cut on the missing mass, a tighter cut on θ_{miss} significantly improves the resolution. We choose the cuts $m^2_{miss}/E_{miss} < 2.6$ GeV, $\theta_{miss} > 0.5$ rad, and $Q_{tot} \leq 1$. This optimum combination of cuts, along with other cuts of similar efficiency, are presented in Table 1 for comparison.

Background Suppression and Signal Selection

The background for $B \rightarrow \omega l\nu$ decays can be categorized into several sources. Continuum background consisting of $e^+e^- \rightarrow q\bar{q}$ processes are the largest contribution, while another significant source is semileptonic $B \rightarrow X_c l\nu$ events with a charm meson in the final state. The continuum background has a more jet-like topology than $B\bar{B}$ events, which are isotropic in the center-of-mass frame. The continuum background is therefore significantly suppressed by preselection. However, preselection is not as effective on $B \rightarrow X_c l\nu$ decays, which are also much more abundant than the signal. In addition there is background from other $B \rightarrow X_u l\nu$ modes where X_u is $\pi^{\pm}$, π^0, $\rho^{\pm}$, ρ^0, etc. Even after applying the neutrino reconstruction cuts, the background completely overwhelms the signal (Fig. 4). Selection criteria on top of the neutrino re-construction cuts must be applied to reduce these various backgrounds with respect to the $B \rightarrow \omega l\nu$ signal.

We first studied the agreement between Monte Carlo and BaBar data for the two main background sources by comparing them using $B \rightarrow X_c l\nu$ and continuum enhanced samples. There was

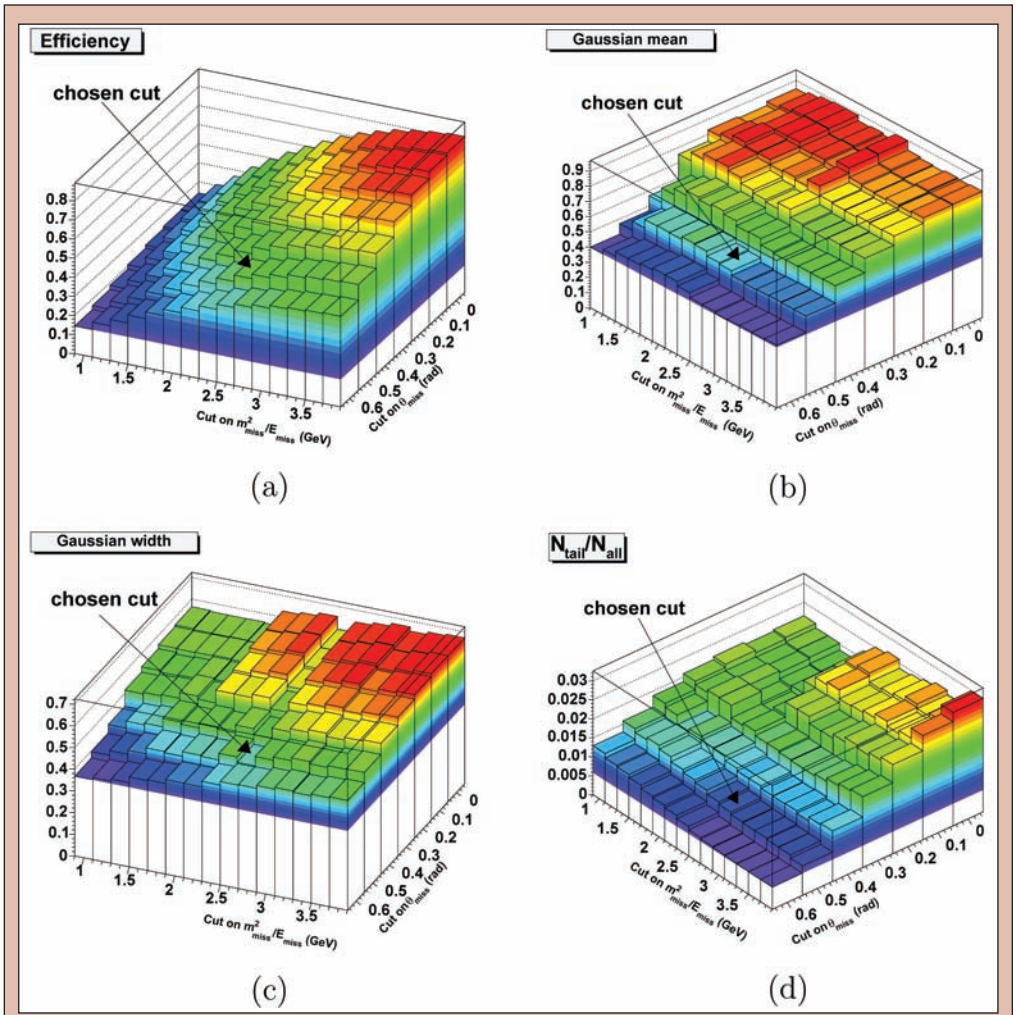

Figure 3. Characteristic quantities of ν momentum resolution for all combinations of cuts on m^2_{miss} / E_{miss} and θ_{miss}. (a) Signal efficiency with preselection, (b) Peak Gaussian mean μ_{peak}, (c) Peak Gaussian width σ_{peak}, and (d) the ratio $\frac{N_{tail}}{N_{all}}$. Similar plots were used with the q^2 resolution to determine the optimal cut.

Sets of Cuts				Signal Efficiency	$\lvert\vec{p}_{miss}\rvert$ — $\lvert\vec{p}_{v,true}\rvert$ (GeV)			$q^2_{reco.}$ — q^2_{true} (GeV)		
	Q_{tot}	θ_{miss} (rad)	$\frac{m^2_{miss}}{E_{miss}}$ (GeV)		σ_{peak}	μ_{peak}	$\frac{N_{tail}}{N_{all}}$	σ_{peak}	μ_{peak}	$\frac{N_{tail}}{N_{all}}$
No Cut:	-	-	-	1	0.66	0.848	0.03	1.659	0.474	0.41
Chosen Cuts:	≤ 1	> 0.5	< 2.6	0.552	0.481	0.554	0.010	1.556	0.0192	0.172
Cuts w/Similar Eff.:	≤ 1	> 0	< 1.8	0.574	0.556	0.889	0.0187	1.834	0.489	0.27
Cuts w/Similar Eff.:	≤ 1	> 0.3	< 2	0.559	0.597	0.783	0.0178	1.911	0.27	0.241

Table 1. Four combinations of m^2_{miss} / E_{miss}, θ_{miss}, and Q_{tot} cuts with their effect on ν resolutions and signal efficiencies. The chosen set of cuts is compared to the uncut signal Monte Carlo sample along with two other sets of cuts with similar signal efficiencies.

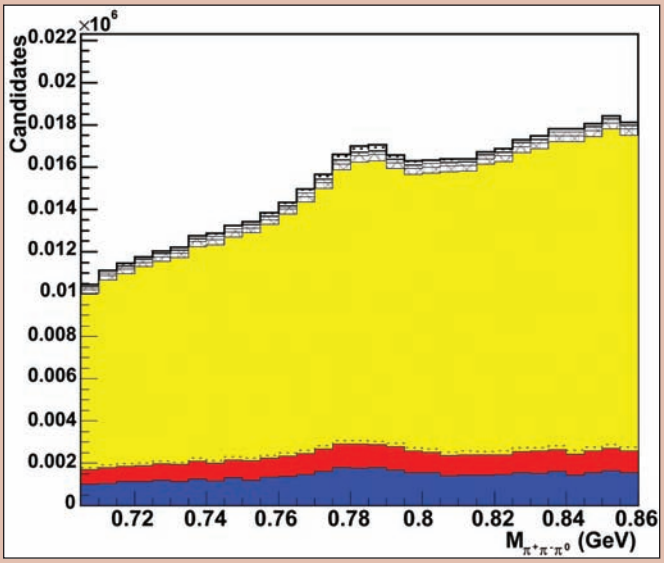

Figure 4. Invariant mass $m_{\pi^+\pi^-\pi^0}$ after only preselection and neutrino reconstruction cuts. Red and blue histograms are $e^+e^- \rightarrow q\bar{q}$ events with a real and fake lepton, respectively. Yellow histograms are $B\bar{B}$ background, dominated by $B \rightarrow X_c l\nu$ decays (above dotted line). Hatched histograms are other $B \rightarrow X_u l\nu$ decays. Simulated signal is shown as white histogram with the contribution from combinatoric signal (see last sentence before Sec. 3.3 for definition) marked as dotted line.

a relatively uniform normalization discrepancy in the continuum background, which may be caused by unsimulated continuum processes in the Monte Carlo. We simply scaled the continuum background by a factor of 1.1 in order to match the data. The shapes of the distributions for several kinematic variables in the $B \rightarrow X_c l\nu$ enhanced sample were also slightly different between data and Monte Carlo (at the 10% level). Within the scope of this study, we could not further investigate these deviations.

We define several variables that characterize each reconstructed event and will be used for selection cuts. The first three variables below describe the topology of the event.

- $|\cos\theta_{thrust}|$, where θ_{thrust} is the angle between the thrust axis [5] of the so-called Y system, consisting of the ω and lepton, and the thrust axis of the rest of the event. Here the thrust axis is the direction that maximizes the total longitudinal components of the particle momenta. This variable peaks around 1 for jet-like events like $e^+e^- \rightarrow q\bar{q}$.
- $L2 = \sum_i |\vec{p}^*_i| \cos^2\theta^*_i$ where $|\vec{p}^*_i|$ is the momentum of the i^{th} particle in the center-of-mass frame, and θ^*_i is the angle of the momentum with the thrust axis of the Y system. This quantity is large for jet-like events and small for isotropic ones such as semileptonic B decays.
- $R2$: the ratio of the 2^{nd} to 0^{th} Fox-Wolfram moments [6]. It is close to 0 for isotropic events and close to 1 for jet-like events.
- The cosine of the angle between the Y system and the B meson, given by

$$\cos\theta_{BY} = (2E^*_B E^*_Y - M^2_B - M^2_Y)/(2|\vec{p}^*_B||\vec{p}^*_Y|), \qquad (5)$$

  where the B momentum and energy are calculated from the known beam four-momenta and the Y momentum and energy are determined through the reconstruction of the lepton and ω. For correctly constructed $B \rightarrow \omega l\nu$ decays, $\cos\theta_{BY}$ should be between -1 and 1 so that θ_{BY} corresponds to a physical angle. The backgrounds, on the other hand, should have a broader distribution.
- $\Delta E = E^*_B - \sqrt{s}/2$, where E^*_B is the energy of the reconstructed B meson and $\sqrt{s}$ is the mass of the $\Upsilon(4S)$.
- $m_{ES} = \sqrt{s/4 - (\vec{p}^*_B)^2}$, the beam energy substituted mass of the reconstructed B meson.

We use the preselected Monte Carlo samples to determine which variables show a discrimination between signal and background and are therefore useful for selection cuts. We first optimized cuts on topology and kinematics variables. The topology variables showed significant differences between the signal and continuum backgrounds, while kinematic variables such as lepton and hadron momentum were very effective in suppressing other semileptonic decays (see Fig. 5). For example, $B \rightarrow X_c l\nu$ background tends to have lower lepton and hadron momenta than the $B \rightarrow \omega l\nu$ signal due to the heavier quark produced. Distributions for some of these variables can be found in Fig. 6. A list of selection cuts along with signal efficiencies and approximate amount of background reduction is given in Table 2. Fig. 6 also compares simulation with data selected from a sample of 83 million $B\bar{B}$ events. Simulated samples have been scaled to the data statistics. We see reasonable agreement between data and simulation and a clear excess of signal events above the dominant background. There are also contributions from other $B \rightarrow X_u l\nu$ decays, as well as a contribution from signal decays where the reconstructed ω includes a background pion or photon ("combinatoric signal").

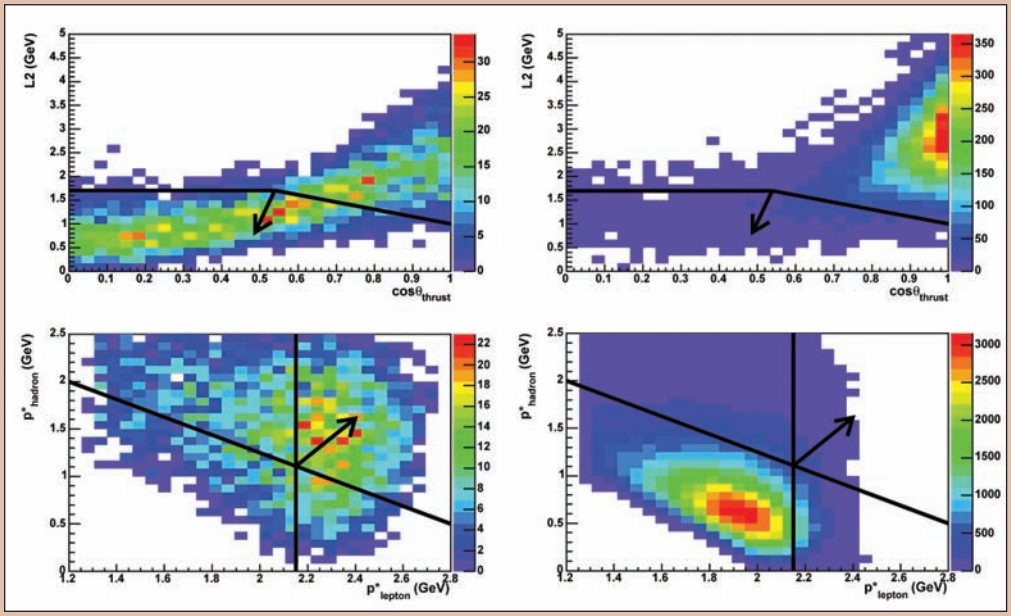

Figure 5. Top: Distributions of L2 vs. $\cos\theta_{thrust}$ for simulated signal (left) and continuum background (right). Bottom: Distributions of lepton vs. hadron momentum for simulated signal (left) and $B \rightarrow X_c l\nu$ background (right). Black arrow points to region selected.

	signal	$B \rightarrow X_c l\nu$	$B \rightarrow X_u l\nu$	$e^+e^- \rightarrow q\bar{q}$
	Efficiencies of preselection(%)			
preselection	35	1.8	6.1	0.4
	Efficiencies of individual cuts on top of preselection (%)			
$\lvert p_\nu \rvert > 0.7$ GeV	96	99	99	85
neutrino reconstruction	50	29	42	33
$R2 < 0.4$	92	99	97	64
$\lvert \cos\theta_{BY} \rvert < 1$	92	66	71	73
$p^*_{hadron} + 0.94p^*_{lepton} > 3.125$ GeV; $p^*_{lepton} > 2.15$ GeV	43	1.4	11	31
$L2 + 1.5 \cos\theta_{thrust} < 2.5$; $L2 < 1.7$ GeV	63	47	49	7.8

Table 2. Cut efficiencies for simulated signal and background samples.

Signal Extraction

After all other cuts have been optimized, we extract the $B \rightarrow \omega l\nu$ signal from the ΔE, m_{ES}, and $m_{\pi+\pi-\pi0}$ distributions. For signal decays, we expect ΔE to be close to 0; m_{ES} and $m_{\pi+\pi-\pi0}$ should correspond to the B mass and the ω mass, respectively. We require that $-0.3 < \Delta E < 0.5$ GeV, $m_{ES} > 5.23$ GeV, and $0.75 < m_{\pi+\pi-\pi0} < 0.81$ GeV. These three cuts had the most significant effects on our signal-to-background ratio. Fig. 6 and 7 show the distributions of these variables with their corresponding cuts.

RESULTS AND DISCUSSION

After all cuts we were able to see a distinct mass peak around the omega mass of 782 MeV in the $m_{\pi+\pi-\pi0}$ distribution (Fig. 7). This shows that we have effectively reduced the background and can extract the desired $B \rightarrow \omega l\nu$ signal. The final Monte Carlo signal efficiency is of the order of 1%, while the various backgrounds have been reduced by roughly 10^{-4} to 10^{-6}. A comparison between the effects of signal extraction on the Monte Carlo signal and background is given in Table 3. The final number of signal events

	Before Sig. Extr.	After Sig. Extr.
Signal Events	482	133
Background Events	2386	195
Signal-to-background ratio	0.20	0.68
Signal Efficiency (approximate)	0.04	0.01
Background Efficiency (approximate)	10^{-5}	10^{-6}

Table 3. Effects of signal extraction along with final numbers of events and efficiencies.

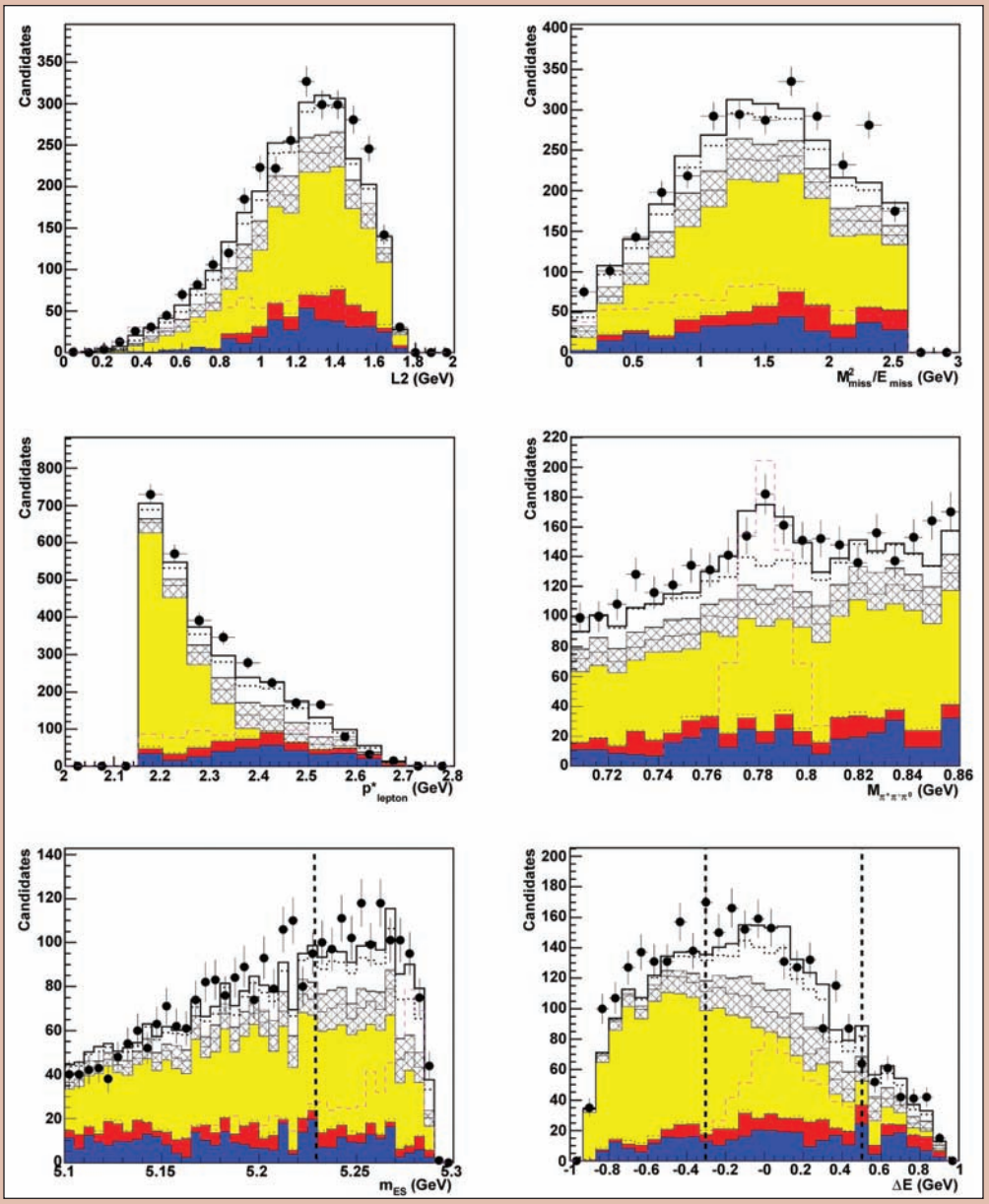

Figure 6. Distributions before signal extraction for six variables used in the selection cuts. ΔE and m_{ES} are shown with corresponding cuts indicated by vertical lines. Monte Carlo simulation (histograms) is compared to BaBar data (points). Magenta dashed histograms with arbitrary normalization indicate the signal shapes. See Fig. 4 caption for details.

predicted by the Monte Carlo simulation is 133, and the total number of expected background events is 195, giving a signal-to-background ratio of 0.68. This ratio is more than sufficient for isolating the signal processes above background uncertainties.

We determine the number of signal events in the data by subtracting out the Monte Carlo simulated background distributions. We find 115 ± 19 $B \to \omega l \nu$ decays in the data, where the error includes the statistical uncertainties of the data and Monte Carlo samples.

We hope to use the work presented here to calculate the $B \to \omega l \nu$ branching fraction, which can be obtained using the exact signal efficiency along with the number of signal events in the data. Another feature that calls for further investigation is the discrepancies between the data and $B \to X_c l \nu$ and continuum backgrounds observed in the dedicated background-enhanced samples. Eventually, the analysis of this decay mode can be used to extract the CKM matrix element $|V_{ub}|$ and thus constrain the Unitarity Triangle.

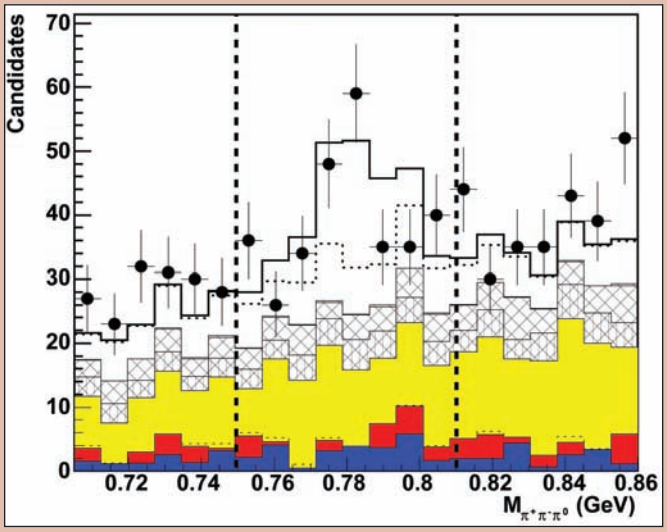

Figure 7. Invariant mass $m_{\pi+\pi-\pi0}$ after all selection cuts but the one on the mass itself. The final mass cut is indicated as vertical lines. The raggedness of the continuum background distribution is due to the low statistics of the Monte Carlo sample. See Fig. 4 caption for details.

ACKNOWLEDGEMENTS

We would like to thank the Department of Energy, Office of Science and SLAC for this opportunity to participate in the SULI program. We would especially like to express our gratitude to our mentor, Jochen Dingfelder, who always took time out of his extremely busy schedule to help us with our programming and explain the physics behind what we were doing. We would also like to thank Vera Lüth, Mike Kelsey, Kai Yi, and the rest of our colleagues in Group C for providing valuable help and advice.

REFERENCES

[1] L. Wolfenstein. *Phys. Rev. Lett.* 51, 1945 (1983).

[2] BaBar Collaboration. B. Aubert, et al. *Phys. Rev.* D72, 051102 (2005).

[3] Belle Collaboration. C. Schwanda, et al. *Phys. Rev. Lett.* 93, 131803 (2004).

[4] A.J. Weinstein. "Study of Exclusive Charmless Semileptonic Decays of the B Meson", PhD thesis, Stanford Linear Accelerator Center (2004).

[5] E. Farhi. *Phys. Rev. Lett.* 39, 1587 (1977).

[6] G.C. Fox and S. Wolfram. *Nucl. Phys.* B149, 413 (1979).

Kristen Maier graduated magna cum laude from the University of Illinois at Chicago (UIC) with a Bachelor's degree in elementary education in 2005. She is currently a full-time elementary teacher at Barry Elementary School in Chicago, Illinois. After graduating from UIC, she completed an internship in ecology and environmental studies at Fermi National Accelerator Laboratory in Batavia, Illinois. She plans to continue teaching and begin working on a master's degree.

Rod Walton is the coordinator for the DOE National Environmental Research Park (NERP) at Fermi National Accelerator Laboratory in Batavia, Illinois. While there he has worked on a wide variety of research projects, including plant-insect interactions, applications of game theory in animal behavior, and restoration ecology. He received his PhD in ecology and evolutionary biology from Indiana University.

Peter Kasper is a staff physicist at Fermi National Accelerator Laboratory, in Batavia, Illinois. He joined Fermilab in 1986 after postdoctoral appointments at Rutherford laboratory in England and at Saclay laboratory in France. His research has varied between neutrino and charm particle physics, and he is currently working on neutrino oscillations. He earned his Ph.D. in Physics from the University of Melbourne in 1981.

ANALYSIS OF THE HABITAT OF HENSLOW'S SPARROWS AND GRASSHOPPER SPARROWS COMPARED TO RANDOM GRASSLAND AREAS

Kristen Maier, Rod Walton, and Peter Kasper

ABSTRACT

Henslow's Sparrows are endangered prairie birds, and Grasshopper Sparrows are considered rare prairie birds. Both of these birds were abundant in Illinois, but their populations have been declining due to loss of the grasslands. This begins an ongoing study of the birds' habitat so Fermilab can develop a land management plan for the Henslow's and Grasshoppers. The Henslow's were found at ten sites and Grasshoppers at eight sites. Once the birds were located, the vegetation at their sites was studied. Measurements of the maximum plant height, average plant height, and duff height were taken and estimates of the percent of grass, forbs, duff, and bare ground were recorded for each square meter studied. The same measurements were taken at ten random grassland sites on Fermilab property. Several *t*-tests were performed on the data, and it was found that both Henslow's Sparrows and Grasshopper Sparrows preferred areas with a larger percentage of grass than random areas. Henslow's also preferred areas with less bare ground than random areas, while Grasshoppers preferred areas with more bare ground than random areas. In addition, Grasshopper Sparrows preferred a lower percentage of forbs than was found in random areas and a shorter average plant height than the random locations. Two-sample variance tests suggested significantly less variance for both Henslow's Sparrows and Grasshopper Sparrows for maximum plant height in comparison to the random sites. For both birds, the test suggested a significant difference in the variance of the percentage of bare ground compared to random sites, but only the Grasshopper Sparrow showed significance in the variation in the percentage of forbs

INTRODUCTION

Henslow's Sparrows and Grasshopper Sparrows are grassland birds found in Midwestern prairies during the summer months. Henslow's Sparrows have recently been considered the highest priority for conservation efforts in eastern and Midwestern North America [1]. Grasshopper Sparrows are considered rare and uncommon in the habitat where they have been known to reside [2]. Both of these birds' populations are declining because of diminishing grasslands [1,2].

Henslow's Sparrows were first sighted at Fermilab in the summer of 2000, and they have been increasing in population since then [3]. Grasshopper Sparrows have been seen on the site since the bird population first started being monitored and counted in 1987, but their populations have been decreasing in recent years [4,5]. The suspected cause of this population decline at Fermilab is the lack of a suitable habitat [1,2]. The birds' habitats were studied so that Fermilab could manage the grounds to optimize the preferred habitats for these declining bird species.

Henslow's Sparrows have a characteristic hiccup sound, and Grasshopper Sparrows make a high-pitched buzz sound. Both birds are small, 12 to 23 centimeters, and both have a flat head. Henslow's have an olive-colored head. They have a dark moustachial line and dark streaking all over their bodies. Grasshoppers are a buff color all over. They have virtually no markings or streaking on their pale breast, but their wings and backs have some dark streaking [6,7].

Both species have been found in prairies and European grasslands on Fermilab grounds [8]. Grasslands are dominated

by introduced European grasses, and prairies include native North American prairie plants. In this study, Henslow's Sparrows were seen in two different European grassland areas and one reconstructed prairie area. Grasshopper Sparrows were seen in two European grassland areas, and one reconstructed prairie area. The random sites were chosen to include either grassland or prairie sites, and did not exclude sites where the birds were sighted.

MATERIALS AND METHODS

Overview

Research was done in various prairie and grassland regions around Fermilab. Initial bird identification was by song, and visual identification confirmed the aural identification. A GPS (Global Positioning System) was used to record the position for each bird sighting. This enabled later measurement of the sites. The habitats were surveyed based on these characteristics: maximum plant height, average height of vegetation, amount of duff (dead plant material), and percent of the ground that was covered with grasses, forbs, duff, or left bare. A point-quarter study (see below) of the vegetation was conducted at each of the recorded bird sites. For comparison, a point-quarter study was also done in randomly selected prairie and grassland regions regardless of bird sightings.

To select random points, a 100-meter square grid was superimposed in a north-south, east-west direction on top of an aerial map of Fermilab. The prairie and grassland areas were then separated out from the agricultural lands, bodies of water, roads, and buildings [8]. The grid intersections in prairie or grassland were numbered; there were 963 such intersections. Ten random numbers between 1 and 963 (inclusive) were generated, and the area corresponding to each number was located on the aerial map [9].

The same measurements were taken at random grassland and prairie areas at Fermilab to serve as control areas. The characteristics of the vegetation in the bird areas were compared to control areas, and the data were analyzed for a statistical difference between the habitats where the birds live and the general prairie land.

Point-Quarter Methodology

Around the initial bird sighting point, an imaginary 10-meter line was drawn in four directions: north, south, east, and west, breaking the bird's territory into four quadrants. Each quadrant was subdivided into 100 one-square-meter quadrats. A list of random numbers, 1 through 100, was generated to select the one-square-meter quadrat for each 10-meter by 10-meter point-quarter quadrant [9]. A randomly selected 1 square meter quadrat of the vegetation around the bird's location could be surveyed in each of the four quadrants: northeast, northwest, southeast, and southwest.

Vegetation data were taken in four quadrats for every bird site and randomly selected site. Henslow's Sparrows were sighted at ten different locations (40 quadrats), Grasshopper Sparrows were sighted at eight different locations (32 quadrats), and there were ten random locations (40 quadrats).

Vegetation Survey

The maximum plant height was measured using a meter stick. The average plant height was measured by having one person hold the meter stick in the center of the quadrat while the other person stepped about five meters away, thus providing a complete view of the quadrat. The average plant height was estimated visually against the meter stick. Actual duff height was measured from the ground to the top of the vegetation litter in two places — one from the east and one from the west side of the quadrat. The two measurements were averaged together.

The ground cover percentages were taken as a visual estimate. While the quadrat was on the ground, the researchers mentally pictured each type of ground cover as though it was grouped together. Estimations were always performed by the same individual.

Statistical Analysis

Once the data was collected, the means were graphed with the standard error using Microsoft Excel. Then, *t*-tests were performed using SPSS (Statistical Package for the Social Sciences). The *t*-test was chosen because it is the standard way to statistically compare the means of a limited statistical sample [10]. Microsoft Excel was used for two-sample variance tests to determine if a difference in the variance between the bird sites and the random sites exists regardless of the difference in mean. All hypothesis tests were evaluated at a significance level of $\alpha = 0.05$.

RESULTS

Figure 1 shows the mean vegetation heights with standard error bars for each of the three types of sites: Henslow's, Grasshoppers, and random. Figure 2 shows the percent of ground cover for each of the three site types. Several *t*-tests were performed on this data to determine statistical significance.

The *t*-test suggested that Henslow's Sparrows prefer a significantly larger percent of grass than was found in random areas ($t(76) = 2.57$, $p = 0.012$). The *t*-test also suggested that Henslow's prefer less bare ground than was found in the random sites ($t(40)$

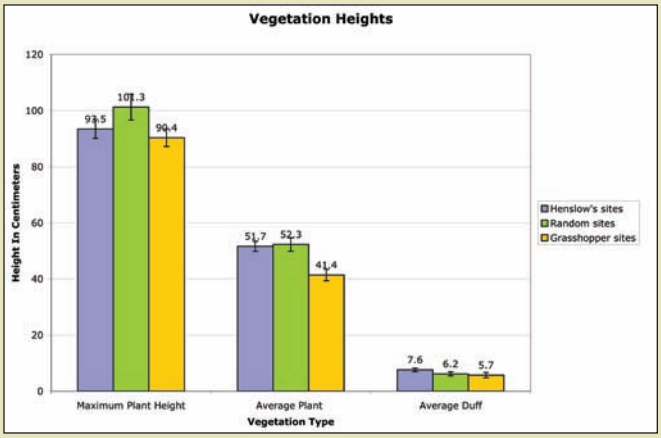

Figure 1. Vegetation heights for each site type with standard error of the means.

= 2.17, p = 0.036). The t-tests did not show significant differences for other variables for the Henslow's Sparrow.

Based on the t-tests, Grasshoppers appear to prefer a shorter average plant height than what was found in the random areas (t(70) = 3.45, p = .001). Further, it was found that Grasshoppers prefer a higher percent of grass than the amount of grass found at the random sites (t(70) = 3.51, p = 0.001). Additionally, the t-test suggested that Grasshopper Sparrows were sighted at places with a

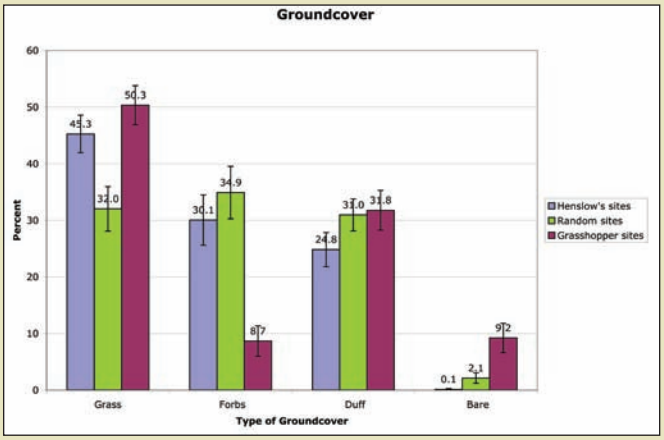

Figure 2. Percent of ground cover for each site type with standard error of the means.

significantly lower percentage of forbs than the random plots (t(61) = 4.91, p < 0.0005). They also suggested Grasshoppers preferred more bare ground than was found at the random sites (t(39) = 2.58, p = 0.014). There were no other statistically significant differences for the Grasshopper Sparrow sites.

Based on the two-sample variance tests, it was found that there was a significant difference in the variance for the percent of bare ground for Henslow's Sparrows compared to the variance of bare ground for the random sites (F(39, 39) = 53.4, p < 0.0001). It was also shown that there was significantly less variance for maximum plant height at Henslow's sites than at random sites (F(39, 39) = 1.93, p = 0.044).

For the Grasshopper Sparrow, the two-sample variance tests performed using Microsoft Excel showed that their sites have significantly less variance for the percent of bare ground compared to the random areas (F(31, 39) = 6.42, p < 0.0001). The test also suggested there was a significant variance difference for the percent of forbs compared to the random areas (F(39, 31) = 3.70, p = 0.0003). Further, it was seen that Grasshopper Sparrows have significantly less variance for the maximum plant height compared to random sites (F(39, 31) = 2.74, p = 0.0048).

DISCUSSION AND CONCLUSIONS

Based on the results of the statistical analyses, both Henslow's Sparrows and Grasshopper Sparrows appear to be particular about their habitats. They both prefer areas with more grass than random grasslands. The reason for this is unknown, but it is possible that a grassy area is more suited to their nest building. Both birds build their nests on the ground at the base of grass clumps [11].

Henslow's seem to prefer less bare ground than random sites, but Grasshoppers seem to prefer sites with more bare ground than random areas. Interestingly, Henslow's and Grasshoppers can live near enough to each other, an observer could hear both of their songs and sight them at the same time. Of course, this is not always the case.

Both sparrows eat insects they find on the ground. It is probable that Grasshoppers prefer more bare ground because they can find their food more easily. Even though Henslow's also eat insects from the ground, they do not appear to prefer bare ground [1]. Grasshopper Sparrows were also shown to prefer sites with a shorter average plant height and a shorter maximum plant height than random sites. The reason for this is unknown.

Henslow's Sparrow sites did not have a statistically significant difference from the random sites in maximum plant height; however, they did have a statistically significant difference in the variance for maximum plant height. This means Henslow's prefer a narrower variation in the plant height than random sites, even though the average height is statistically similar. The reason for the difference in the variance is unknown, and could be an idea for future research.

Grasshoppers seemed to prefer a lesser amount of forbs in their areas than the amount of forbs found in random grasslands. The reason for this is unknown; however, their preferred type of ground cover probably makes nest building and food acquisition more ideal.

Both sparrows are particular as to where they live, and in order to increase their populations, land managers must effectively control the grounds to be suitable for them. It would be advisable to continue studying these birds' habitats so that the land can be suited to their preferences, since they are both rare birds.

The continuation of this study will provide more information about the preferred habitat for the sparrows. Since this is the beginning of an ongoing study, further research and more data collection will increase the accuracy of the characterization of the habitat preference. In the future, the site should be thoroughly investigated for additional Henslow's and Grasshopper sites. For example, there were Henslow's Sparrows heard at three sites that were not characterized because they were found near the end of the study, and time did not permit their inclusion in the study.

Another interesting study would be to observe the behavior of these birds in order to determine their territories. It would be useful to find out how much area they take up for their territories in order to see if they need lots of space, or if a smaller section of the preferred ground would be enough to accommodate several birds.

A third suggested study would be to survey the vegetation heights for each bird in comparison to random areas. There has not been much research on the study of the vegetation heights, and this study found some significance between vegetation heights for Henslow's Sparrow sites, Grasshopper Sparrow sites, and random areas.

ACKNOWLEDGEMENTS

This research was conducted at Fermi National Accelerator Laboratory in Batavia, Illinois. We would like to thank the Department of Energy, Office of Science for giving us the opportunity to participate in the PST program. Maier also thanks Spencer Pasero and Anna Zuccarini for their patience and help in all areas of the internship. Thanks go to Charles Federowicz for creating the large aerial map and grid. We would also like to thank Waylon Meadors and Thomas Jordan for their technical support, and LaMargo Gill for her editing skills. Finally, Maier would like to thank Maria Varelas for encouraging her to participate in this incredible program.

REFERENCES

[1] J. R. Herkert, P. D. Vickery, and D. E. Kroodsma (2002). Henslow's Sparrow (*Ammodramus henslowii*). In *The Birds of North America*, No. 672 (A. Poole and F. Gills, eds.). The Birds of North America, Inc., Philadelphia, PA.

[2] P. D. Vickery (1996). Grasshopper Sparrow (*Ammodramus savannarum*). In *The Birds of North America*, No. 239 (A. Poole and F. Gill, eds.). The Academy of Natural Sciences, Philadelphia, PA, and The American Ornithologists' Union, Washington, D.C.

[3] P. Kasper. *Henslow's Sparrow*. Retrieved June 13, 2005. Available: http://www.fnal.gov/ecology/wildlife/specs/Henslows_Sparrow.html

[4] P. Kasper. *Grasshopper Sparrow*. Retrieved June 13, 2005. Available: http://www.fnal.gov/ecology/wildlife/specs/Grasshopper_Sparrow.html

[5] About Fermilab –The Fermilab Campus (August 8, 2005). Available: http://www.fnal.gov/pub/about/campus/ecology/wildlife/birds.html

[6] M. Waite (2002). *Percevia: The Ultimate Guide To Birds of North America*. Retrieved June 7, 2005. Available: http://www.percevia.com

[7] R. T. Peterson. *Peterson Field Guides Eastern Birds* (4th ed.). New York: Houghton Mifflin, 1980, pp. 282, 286-7.

[8] Fermilab ELM Map (July 5, 2005), Available: http://www.fnal.gov/ecology/map

[9] *Random.org True Random Number Service* (1998, October). Retrieved July 5, 2005. Available: http://www.random.org

[10] T. D. Swinscow (1997). *Stastistics at Square One*. Retrieved June 13, 2005. Available: http://bmj.bmjjournals.com/collections/statsbk/7.shtm

[11] M. Austen, R. Pratt, M. Cadman, D. Cuddy, & R. Knapton (1997). *National Recovery Plan for Henslow's Sparrow*. Retrieved June 21, 2005. Available: http://www.speciesatrisk.gc.ca/publications/plans/Sparrow_e.cfm#Citation%20for%20Recovery%20Plan

Lawrence Chyall is currently enrolled at the University of California Berkeley where he is completing his baccalaureate studies in the Microbial Biology Department. He became interested in the biological sciences while working as a San Francisco maitre d'hotel and sommelier. His curiosity about the processes that govern life and his desire to help reduce human suffering inspired him to leave his career and enroll at San Francisco City College. After completing the prerequisite courses for the study of upper division undergraduate biology, Chyall undertook a summer internship at the Lawrence Berkeley National Laboratory. He has returned to LBNL for a second summer where he continues under the mentorship of Amy Kronenberg and Stacey Gauny. His scientific interests include radiation biology and carcinogenesis. He looks forward to graduate study in the life sciences and fulfilling his dream of serving others through science.

Stacey Gauny is a Principal Research Associate at Lawrence Berkeley National Laboratory (LBNL). She received her B.S. in psychobiology from the University of California, Santa Cruz and a M.S. in physiology from the University of California, Davis. Her first professional research position was in the preclinical pharmacology department at the biotechnology company Cetus. For the past fourteen years she has been in Dr. Amy Kronenberg's lab at LBNL.

Amy Kronenberg received her undergraduate degree in biology from Brown University where she did undergraduate research on Compton scatter radiography of bone. She then joined the Medical Physics group at Brookhaven National Laboratory starting with a DOE summer fellowship and continuing for several years thereafter working collaboratively with physicists and engineers to apply nuclear physics techniques to biological problems. She received her Sc.D. in Cancer Biology at the Harvard School of Public Health. Dr. Kronenberg joined the Lawrence Berkeley National Laboratory after completing her doctorate, where she has lead a vigorous research program for more than fifteen years. Her major research interests are the factors that regulate genomic stability, mechanisms of mutagenesis in human and rodent cells and tissues, and the connections between programmed cell death and DNA repair.

CHARACTERIZATION OF A TK6-BCL-X_L GLY-159-ALA HUMAN LYMPHOBLAST CLONE

LAWRENCE CHYALL, STACEY GAUNY, AND AMY KRONENBERG

ABSTRACT

TK6 cells are a well-characterized human B-lymphoblast cell line derived from WIL-2 cells. A derivative of the TK6 cell line that was stably transfected to express a mutated form of the anti-apoptotic protein Bcl-x_L (TK6-Bcl-x_L gly-159-ala clone #38) is compared with the parent cell line. Four parameters were evaluated for each cell line: growth under normal conditions, plating efficiency, and frequency of spontaneous mutation to 6-thioguanine resistance (hypoxanthine phosphoribosyl transferase locus) or trifluorothymidine resistance (thymidine kinase locus). We conclude that the mutated Bcl-x_L protein did not affect growth under normal conditions, plating efficiency or spontaneous mutation frequencies at the thymidine kinase (*TK*) locus. Results at the hypoxanthine phosphoribosyl transferase (*HPRT*) locus were inconclusive. A mutant fraction for TK6-Bcl-x_L gly-159-ala clone #38 cells exposed to 150cGy of 160kVp x-rays was also calculated. Exposure to x-irradiation increased the mutant fraction of TK6-Bcl-x_L gly-159-ala clone #38 cells.

INTRODUCTION

Shortly after Wilhelm Roentgen discovered the existence of ionizing radiation in the form of x-rays in 1895, the adverse effects of the "New Rays" became apparent. Radiation pioneers frequently suffered from epilations, erythemas, and painful desquamation as a result of occupational exposure to x-rays. The premature death of Clarence Dally (Thomas Edison's assistant in the manufacture of x-ray equipment) from lymphoma and the subsequent cancer deaths of other early radiation investigators led scientists to hypothesize that x-rays might be carcinogenic. It is now well known that exposure to ionizing radiation may lead to chromosomal damage, mutagenesis, and cancer. It has been thought that programmed cell death (apoptosis) is a means of limiting the number of mutations that can be accumulated by an organism and that dysregulation of apoptosis may be implicated in the multi-step process of carcinogenesis.

The intracellular protein Bcl-x_L helps limit apoptosis by titrating the concentration of the pro-apoptotic protein Bax through the formation of a heterodimer [1]. Cells overexpressing the protein Bcl-x_L better survive assaults on the genome that would otherwise lead to cell death. Cherbonnel-Lasserre *et al.* [2] found that human lymphoblastoid TK6 cells stably transfected with *pSFFV-neo-bcl-x_L* and overexpressing the Bcl-x_L protein survived x-irradiation in greater numbers with a significantly higher mutant fraction at an autosomal locus than TK6 cells transfected with the control vector, *pSFFV-neo*. It is, however, not currently understood if Bcl-x_L facilitates mutagenesis independently of its function in blocking apoptosis. Our group plans to investigate this question using a TK6-Bcl-x_L gly-159-ala clone that expresses a mutated form of Bcl-x_L protein (Bcl-x_L gly-159-ala) that cannot dimerize with Bax to inhibit the pro-apoptotic activity of Bax. The Bcl-x_L gly-159-ala protein is not expected to inhibit radiation-induced apoptosis, however it

may still lead to increased levels of radiation-induced mutations if the pro-mutagenic effect requires a portion of the protein that does not include amino acid 159.

TK6 is a well characterized human cell line derived from WIL-2 cells with a known mutation that disables one copy of the thymidine kinase (*TK*) gene located on chromosome 17 [3, 4]. The other (active) copy of the *TK* gene is a useful genetic locus to study mutations at a model heterozygous autosomal locus. Cells that survive growth in medium containing trifluorothymidine (TFT) have been shown by others to be deficient in thymidine kinase [4]. Additionally, TK6 is a male cell line that is hemizygous for the hypoxanthine phosphoribosyl transferase gene (*HPRT*) on the X chromosome, providing another useful locus to study mutations. It has been shown by others that cells deficient in the HPRT protein survive growth in medium containing 6-thioguanine (6-TG) [4].

This paper reports on the growth properties and spontaneous mutant frequencies at the *TK* and *HPRT* loci of TK6-Bcl-x_L gly-159-ala clone #38 cells and compares them to similar data acquired for the parent TK6 cell line. In addition, the *TK* mutant fraction of TK6-Bcl-x_L gly-159-ala clone #38 cells exposed to 150 cGy of 160 kVp x-rays is compared to the *TK* mutant fraction of non-irradiated cells from the same cell line.

MATERIALS AND METHODS

Cells and cell culture conditions

The TK6-Bcl-x_L gly-159-ala clone #38 cell line was established in the Kronenberg laboratory from the parent TK6 cell line by stably transfecting TK6 cells with *pSFFV-neo-bcl-x_L-gly-159-ala* (kindly provided by S. Korsmeyer of the Dana Farber Cancer Institute and G. Nunez of the University of Michigan). Each cell line was grown in 100ml suspension cultures using T-175 culture flasks and RPMI 1640 medium + L-glutamine supplemented with 10% heat-inactivated horse serum and 50units/ml penicillin + 50µg/ml streptomycin (all from Gibco Laboratories, Grand Island, NY). Cultures were maintained at 37˚C in a humidified 5% CO_2 atmosphere. Cells were counted Monday through Friday using a Coulter Counter and diluted as necessary to a density of either 2 X 10^4 cells/ml (Fridays) or 4 X 10^5 cells/ml (Monday through Thursday) to keep them in exponential growth.

Growth curve

Growth curves were set up for TK6 and TK6-Bcl-x_L gly-159-ala #38 cells. Measurements of the cell density of 100ml cultures, each set up with an initial density of 1.0 X 10^4 cells/ml, were made over a six-day period. To avoid nutrient starvation or hypoxia, cells were diluted as necessary to 4.0 X 10^5 cells/ml. The growth of the two cells lines was compared by graphing cell density as a function of time on a semi-log plot.

To assess the effect on growth rate when TK6 cells are maintained at higher densities, a parallel TK6 culture was established at a density of 3.1 X 10^5 cells/ml after 3 days of standard growth under the conditions described above. This culture was not diluted further during the 6-day observation period. Cell density was measured on day 6 and growth was compared with the TK6 cells maintained in exponential growth throughout the experiment.

Plating efficiency

Plating efficiency (PE) is defined as the probability that a single cell will form a colony. The plating efficiency of each cell line was determined using a method of limiting dilution in 96-well plates [5]. Cells were diluted to a final density of 5 cells/ml and 200µl of cell suspension was seeded in each well using an 8-channel pipettor. This corresponds to delivering an average of one cell per well. Plates were incubated at 37˚C in a humidified 5% CO_2 atmosphere for 11 days. Following incubation, plates were visually inspected for the presence of macroscopic colonies. Wells without any apparent colony growth were counted as negative. Wells with evidence of growth may contain one or more individual colonies that are difficult to discriminate and were counted as positive for growth. Plating efficiency was calculated using the formula:

$$PE = -\ln \frac{\chi_0}{\eta_0}$$

χ_0 = number of negative wells
η_0 = number of total wells

Cleansing the population for pre-existing TK and HPRT mutants

The spontaneous mutant fraction (MF) at either the *TK* or *HPRT* locus was determined according to previously described methods [4, 5]. Cells without functional TK or HPRT proteins ($TK^{-/-}$ or $HPRT^-$ cells) were removed from the population by treating the culture for two days with normal growth medium supplemented with CHAT (10µM deoxycytidine, 200µM hypoxanthine, 0.2µM aminopterin, and 17.5µM thymidine, all from Sigma Chemical, St. Louis, MO). Following two days of treatment, the cells were spun out of the CHAT medium at 1000rpm for 5 minutes and re-suspended in standard medium supplemented with THC (17.5µM thymidine, 200µM hypoxanthine, and 10µM deoxycytidine). Cells were maintained in exponential growth for two additional days.

Selection for spontaneous HPRT-deficient mutants

Two days after re-suspension in medium supplemented with THC, cell cultures were diluted to 2 X 10^5 cells/ml and treated with 0.5µg/ml 6-thioguanine (6-TG, Sigma Chemical, St. Louis, MO). Cells were seeded in 96-well plates in 200µl of cell suspension per well, corresponding to 40,000 cells/well. Plates were incubated for 11 days under the conditions described above and inspected for the presence of macroscopic colonies.

Selection for spontaneous TK-deficient mutants

Cell cultures were diluted to 2 X 10^5 cells/ml following two days of growth in medium supplemented with THC. The cell cultures were treated with 2.0µg/ml triflurothymidine (TFT, Sigma

Chemical, St. Louis, MO) and seeded in 96-well plates at a density of 40,000 cells/well. To determine the plating efficiency, an aliquot of each culture was seeded in 96-well plates at low density in the absence of TFT. Following 11 days incubation under the above described conditions, plates were examined for the presence of macroscopic early-arising mutant colonies. Cells were re-fed with TFT by adding 20µl of growth medium supplemented with triflurothymidine (22.0µg/ml) to each well. Plates were returned to the incubator for an additional 7 days. On day 18 the plates were re-examined for the presence of late-arising *TK*-mutant colonies.

Selection for radiation-induced TK-deficient mutants in TK6-Bcl-x_L gly-159-ala clone #38 cells

Cell cultures were diluted to a density of 4 X 10^5 cells/ml one day after re-suspension in THC-supplemented medium. On the following day, samples were exposed to 150 cGy of x-rays using a 160 kVp Pantak Mk II x-ray generator. Unirradiated control cultures were maintained in parallel. Following irradiation, cultures were split to a density of 5 X 10^5 cells/ml and returned to the incubator for three days to allow expression of the *TK* mutant phenotype. Cells were split daily to prevent overgrowth. Cells were treated with TFT, plated, and scored for early-arising and late-arising mutant colonies as described above.

Calculation of mutant fraction

The mutant fraction (MF) at a given locus is defined as the ratio of mutants detected at a given time. The MF was calculated using previously described methods [5]. Microtiter plates were inspected for the presence of macroscopic colonies and the number of wells without apparent colonies was recorded. MF was calculated using the following formula:

$$MF = \frac{-\ln(\chi_s/\eta_s)}{-\ln(\chi_0/\eta_0)} \bullet \frac{(total\ cells/well\ of\ non-selective\ PE\ plates)}{(total\ cells/well\ of\ selective\ mutation\ plates)}$$

χ_0 = number of empty wells in non-selective conditions
η_0 = total number of wells in non-selective conditions
χ_s = number of empty wells in non-selective conditions
η_s = total number of wells in non-selective conditions

RESULTS

Growth curve

Figure 1 shows growth curves for the TK6 and TK6-Bcl-x_L gly-159-ala clone #38 cell lines. Each cell line grew exponentially with a doubling time of approximately 15 hours when maintained at a density of between 1 X 10^4 cells/ml and 1.2 X 10^6 cells/ml. The growth curve of TK6 cells grown without dilution is displayed on Figure 2. After six days, the total number of cells of this culture was 2.34 X 10^6 cells/ml compared with 1.19 X 10^7 cells/ml for the culture maintained under standard conditions, indicating that the culture maintained at a higher density grew at a slower rate.

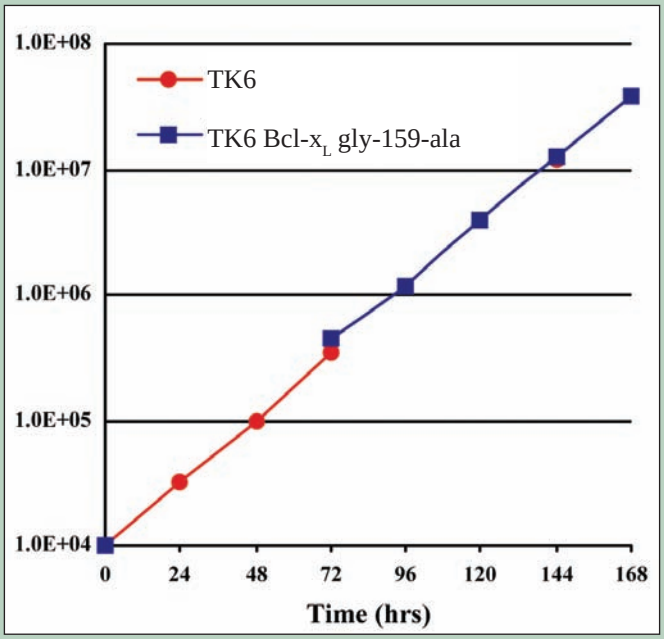

Figure 1. Growth rate comparison of TK6 cells and TK6 Bcl-x_L gly-159-ala clone #38 cells.

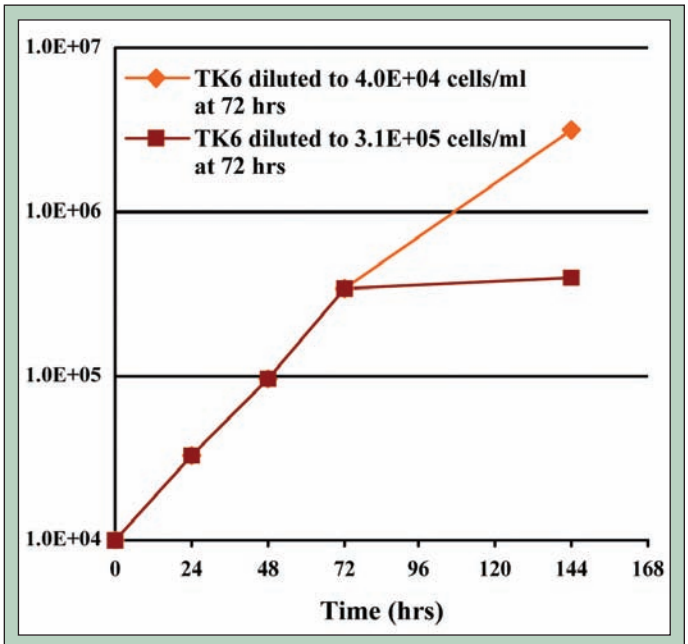

Figure 2. Growth rate comparison of TK6 cells maintained at normal density and high density.

Plating efficiency

Plating efficiency (PE) data for each cell line is given in Table 1. TK6 cells were found to have a mean PE of 62.8% (±10.2%). TK6-Bcl-x_L gly-159-ala #38 cells displayed a mean PE of 72.5% (±3.7%). A two tailed t-test (t= 1.84, p=0.116) showed no difference between the means.

TK6			TK6-pSFFV- Bcl-x_L gly-159-ala clone #38		
Sample	no. of plates	PE %	Sample	no. of plates	PE %
A	2	47.8	A	2	74.7
B	2	67.3	B	2	68.3
C	2	70.3	C	2	74.7
D	4	65.8			
mean PE = 62.8% ± 10.2%			mean PE = 72.5% ± 3.7%		
t= 1.84, p= 0.116, two tailed t-test					

Table 1. Plating efficiencies of TK6 cells and TK6 Bcl-x_L gly-159-ala clone #38 cells.

Spontaneous HPRT-deficient mutants

No mutant colonies were observed among the cells plated in the presence of the selective agent 6-TG. A significant amount of debris was observed in all of the wells prohibiting the scoring the wells as either positive or negative. The experiment did not produce useful results.

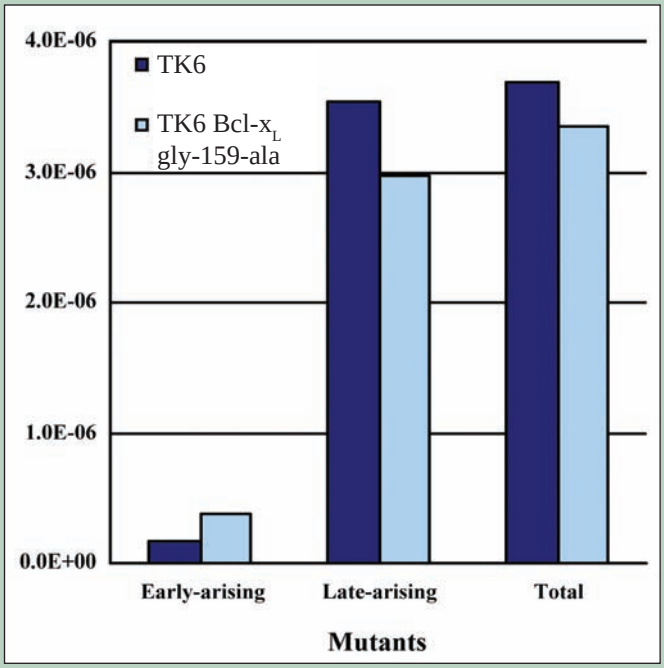

Figure 3. Comparison of spontaneous mutant fractions at the *TK* locus in TK6 cells and TK6 Bcl-x_L gly-159-ala clone #38 cells.

Spontaneous TK-deficient mutants

Figure 3 displays the TK mutant fraction in untreated TK6 and TK6-Bcl-x_L gly-159-ala #38 cells. The mutant fraction for early-arising TK-deficient mutants was 1.78 X 10^{-7} for TK6 cells and 3.71 X 10^{-7} for TK6-Bcl-x_L gly-159-ala #38 cells. TK6 cells had a late-arising mutant fraction of 3.54 X 10^{-6} compared with 2.97 X 10^{-6} for TK6-Bcl-x_L gly-159-ala #38 cells. The total mutant fraction (combined early-arising and late-arising) for TK6 cells was 3.69 X 10^{-6} and the total mutant fraction for TK6-Bcl-x_L gly-159-ala #38 cells was 3.34 X 10^{-6}. TK6-Bcl-x_L gly-159-ala #38 cells had a similar

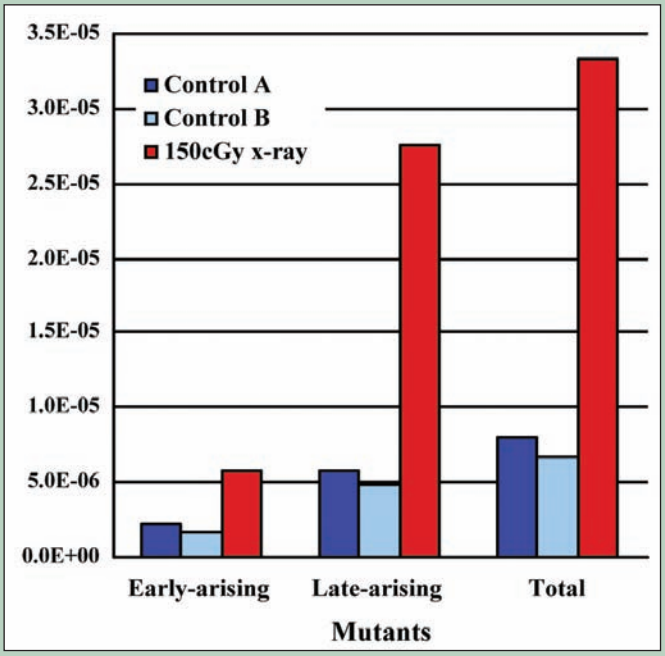

Figure 4. Radiation induces mutations at the *TK* locus in TK6 Bcl-x_L gly-159-ala cells.

MF to TK6 cells, with a similar proportion of early-arising and late-arising mutant colonies. No statistical analysis can be done since these data represent the results of a single experiment.

Radiation-induced TK-deficient mutants

Figure 4 summarizes the radiation-induced mutant fraction at the *TK* locus for TK6-Bcl-x_L gly-159-ala #38 cells. The early-arising MF for TK6-Bcl-x_L gly-159-ala #38 cells exposed to 150cGy of 160 kVp x-rays was 5.85 X 10^{-6}. Two unirradiated control cultures had early arising MF's of 2.15 X 10^{-6} and 1.75 X 10^{-6} respectively. The late-arising TK MF was 2.75 X 10^{-5} for irradiated cells, while the values for the two control cultures were 5.86 X 10^{-6} and 4.88 X 10^{-6}. Total MF (combined early-arising and late-arising) for irradiated cells was 3.34 X 10^{-5}. One control culture had a total MF of 8.01 X 10^{-6} while the second control culture had a total MF of 6.63 X 10^{-6}. Late-arising mutant colonies compromised the bulk of the observed mutants and x-irradiation increased the mutant fraction approximately five-fold above the control levels.

DISCUSSION AND CONCLUSIONS

TK6-Bcl-x_L gly-159-ala clone #38 cells behaved similarly to the parent TK6 cell line when cultured under normal conditions. Growth curves indicated that the two cell lines grew exponentially when diluted to optimal concentrations. It is noteworthy that growth of the parallel culture of TK6 cells slowed when the cell density exceeded 1 X 10^6 cells/ml. This may have been the result of hypoxia, nutrient depletion, an accumulation of waste products, or a combination of these events. It is reasonable to anticipate that TK6-Bcl-x_L gly-159-ala clone #38 cells would also grow non-exponentially when maintained in an over-dense environment, given the similarity of growth patterns of the TK6-Bcl-x_L gly-159-ala clone #38 cells to

the parent TK6 cell line. No statistically significant difference was found in the plating efficiencies of the two cell lines. A single cell from either cell line is, therefore, equally likely to form a colony.

The inconclusive findings for the selection for HPRT-deficient mutants may be attributable to two possible causes. One possibility is that the presence of an unusually high amount of debris (arising from dead cells) in wells obscured any mutant colonies that formed. A second possibility is failure of the selective agent 6-TG. An insufficient concentration of active 6-TG would have enabled $HPRT^+$ cells to survive 6-TG treatment, potentially resulting in the observed debris. Based on the clear results obtained from the plates treated with TFT, we do not believe that the high background on the 6-TG containing plates is due to failure of the aminopterin "pre-cleaning" procedure. Aminopterin blocks the *de novo* synthesis of thymidine by competitively binding with dihydrofolate reductase, thus inhibiting the reduction of dihydrofolate to tetrahydrofolate (a molecule required for the methylation of deoxyuridate to thymidine and many other one carbon transfer reactions). Cells treated with aminopterin cannot synthesize DNA by the *de novo* pathway. Only cells producing functional salvage pathway proteins (i.e. cells with at least one functional copy of the *TK* and *HPRT* genes) will be able to synthesize DNA and live in the presence of aminopterin. Thus, if the aminopterin had failed then we would expect to have seen a high background in both the 6-TG containing plates and the TFT containing plates.

Spontaneous mutant fractions for TK-deficient mutants were similar in both cell lines. In addition to similar total mutant fractions, both cell lines displayed a similar pattern of distribution between early-arising and late-arising colonies (the majority of mutant colonies were of the late-arising type for both cell lines). The frequency of spontaneous mutations at the *TK* locus of the TK6 cells does not appear to have been changed by transfecting the parent cell line with the *pSFFV-Bcl-x_L gly-159-ala* plasmid. TK6-Bcl-x_L gly-159-ala clone #38 cells were mutated by x-rays, displaying an elevated mutant fraction at the *TK* locus when exposed to 150cGy of x-rays. This data is consistent with earlier results noted by the Kronenberg group.

In summary, the growth under normal conditions and plating efficiency of the TK6-pSFFV-Bcl-x_L gly-159-ala clone #38 mirrors the parent TK6 cell line. Both cell lines undergo spontaneous mutation at the *TK* locus with a similar frequency. No conclusions could be reached about the spontaneous mutant fraction at the *HPRT* locus. Exposure of the TK6-pSFFV-Bcl-x_L gly-159-ala clone #38 cells to x-rays led to an increase in the TK mutant fraction as compared to the unirradiated controls.

ACKNOWLEDGEMENTS

This work was supported by the Director, Office of Science, Office of Science and Workforce Development, of the U.S. Department of Energy under contract No. DE-AC02-05CH11231. The patient and kind mentorship of Amy Kronenberg, Stacey Gauny, and all of the scientists and staff at the Kronenberg lab (Xing Kwoh, Caren Oto and Hiroko Sudo) is gratefully acknowledged. Additionally, heartfelt thanks is offered to the Lawrence Berkeley Laboratory Center for Science and Engineering Education program staff and to Philip Jardim of San Francisco City College.

REFERENCES

[1] T. W. Sedlak, Z. N. Oltvai, E. Yang, K. Wang, L. H. Boise, C. B. Thompson, and S. Korsmeyer, "Multiple Bcl-2 family members demonstrate selective dimerizations with Bax," *Proceedings of the National Academy of Sciences USA*, vol. 92, pp. 7834-7838, 1995.

[2] C. Cherbonnel-Lasserre, S. Gauny, and A. Kronenberg, "Suppression of apoptosis by Bcl-2 or Bcl-x_L promotes susceptibility to mutagenesis," *Oncogene*, vol. 13, pp. 1489-1497, 1996.

[3] J. A. Levy, M. Virolainen, and V. Defendi, "Human Lymphoblastoid Lines from Lymph Node and Spleen," *Cancer*, vol. 22, pp. 517-524, 1968.

[4] H. L. Liber and W. G. Thilly, "Mutation Assay at the Thymidine Kinase Locus in Diploid Human Lymphoblasts," *Mutation Research*, vol. 94, pp. 467-485, 1982.

[5] E. E. Furth, W. G. Thilly, B. W. Penman, H. Liber, and W. M. Rand, "Quantitative Assay for Mutation in Diploid Human Lymphoblasts Using Microtiter Plates," *Analytical Biochemistry*, vol. 110, pp. 1-8, 1981.

Shaun P. Garland is currently a senior at the University of California, Davis majoring in biochemical engineering. In 2005, he graduated from Shasta College, a community college in Redding, California and received an internship through the CCI program at Pacific Northwest National Laboratory where this research was done. The research in this article was presented at the AAAS convention in February 2006 at America's Center in St. Louis, Missouri. Shaun has received another internship through the Science Underground Laboratory Internships (SULI) program, again at Pacific Northwest under Michael Alexander. After receiving his degree from UC Davis, he hopes to attend graduate school in a program involving medical science.

Michael Alexander is involved with instrument development in the fields of chemical ionization and mass spectrometry at the Pacific Northwest National Lab. Specifically, he is using proton transfer reaction mass spectrometry (PTR-MS) to obtain direct measurements of volatile organic compounds in air to study air pollution. Dr. Alexander served as part of an air quality campaign in Mexico City and he also collaborated with Boeing to determine how jet engine oil is broken down in high temperatures. He received his B.S. in chemistry from the University of California, Berkeley in 1979 and his Ph.D. in chemical physics from the University of Colorado in 1987. Dr. Alexander is the recipient of several awards, including DOE Mentor of the Year Award (2002), a Fitzner-Eberhardt Award nominee (2002), and a PTR-MS Collaborator, University of Innsbruck, Austria.

CHARACTERIZING THE PERFORMANCE OF A PROTON-TRANSFER-REACTION MASS SPECTROMETER WITH A RAPID CYCLING TENAX PRECONCENTRATOR

Shaun P. Garland, Michael L. Alexander

ABSTRACT

Volatile organic compounds (VOCs) are species of interest for atmospheric modeling, worker chemical exposure and medical studies. Sometimes the required detection limits for these compounds is below the capability of existing real-time instrumentation. Preconcentrators have been implemented as an inexpensive way to amplify chemical signals and improve detection limits. Proton-transfer-reaction mass spectrometry (PTR-MS) has been used as a tool for studying low concentrations of VOCs, but it lacks the capability to differentiate chemical signal contributions from isobaric compounds. In this work, behavior of a newly designed Tenax TA preconcentrator when coupled with a PTR-MS is characterized. This novel preconcentrator design allows rapid temperature cycling, maintaining near real-time response. The preconcentrator was exposed to a sample gas of toluene in varying concentrations and loading times between and then thermally desorbed for analysis by PTR-MS. The effects of preconcentrating multiple analytes simultaneously were also investigated as well as the chromatographic effects of the preconcentrator. A linear behavior was observed when the integrated ion count rates (ICPS) from thermal desorption peaks were regressed against both varying loading times at a constant toluene concentration and varying concentrations with constant loading times. From these trends, it is possible to determine the concentration of a VOC by knowing its ICPS from thermal desorption peaks from a known preconcentration time. Peak height ion count rates representing ultimate detectability were amplified by factors up to 257 times the original signal, extending the range of the PTR-MS from 50pptv to nearly 250 parts per quadrillion. This corresponds to an ultimate sensitivity of 200 parts per quadrillion with 20 minute time resolution. Quantitative preconcentrator behavior was demonstrated using ICPS from these ion peaks and were amplified as much as 148 times their original signal. Results from multi-analyte desorption indicate that chromatographic separation is possible with a Tenax preconcentrator and further details are discussed. The dramatic increased in sensitivity with near real-time response, combined with chromatographic resolving capability opens up new areas of research requiring the detection of ultra-trace organic species using PTR-MS.

INTRODUCTION

Volatile organic compound (VOC) emissions to the atmosphere have been a topic of interest for some time now in relation to ozone formation and aerosol pollutants. The identity and fate of eventual products and destinations of organic reactions in the atmosphere is currently not well understood [1]. Industrial solvents and pollutants are commonly VOCs and their detection is important to ensure worker exposure safety limits [2]. Sometimes these exposure guidelines are below the lower detectible concentration of common detection equipment [3]. In order to overcome this problem without purchasing more expensive equipment that would be potentially difficult to implement, preconcentrators have been used. Preconcentrators are exposed to streams of gas containing compounds of interest for certain lengths of time at a known flow rate and then trapped compounds can either be thermally desorbed or extracted by solvents [4]. Solid absorbent preconcentrators have been employed in a variety of situations to increase the sensitivity

of common detection instruments such as for atmospheric study and health-related issues [2-6]. Another benefit that has been found is that if multiple analytes are adsorbed, various temperature programs can be used for chromatographic separation upon thermal desorption [6,7]. Tenax TA is an adsorbent polymer often used in preconcentrators to trap VOCs and its contents are thermally desorbed. Some of the benefits of Tenax TA compared to other sorbent materials are its stability at high temperatures, low water uptake in humid conditions, performs well with adsorbing VOCs in low concentrations, and its ability to be conditioned to give very low background interference in detection instruments [2].

Proton-transfer-reaction mass spectrometry (PTR-MS) has become an integral tool for studying VOCs by being capable of detecting them in low concentrations near 50 parts per trillion by volume (pptv). PTR-MS, which was developed by [8], has much literature [1,8,9] describing its methodologies and theory, so only a brief description is given here. Functionality of the PTR-MS consists of introducing a sample at 2mBar into the presence of H3O+ primary ions in a drift tube where the VOC is protonated if it has a proton affinity larger than that of water (165.2 kcal/mol) [8]. Once it leaves the drift tube, a linear quadrapole separates a selected mass which then collides with a secondary electron multiplier, giving a detectible signal. The utility of this type of mass spectrometry comes from relatively soft ionization and its selectiveness in what it can detect; largely only organic compounds have a greater proton affinity than water which eliminates interference from the carrier gas and most other common inorganic species found in the atmosphere. While the PTR-MS has great sensitivity, there are research areas where the required detection limits for VOC concentrations are below its detection limit. An example is very trace gas emissions from crop plants [10]. Proton transfers are also much less potent energetically than electron impact methods which results in very little fragmentation of an ionized molecule. While lack of fragmentation is useful when looking at an isolated source, it does not allow for the capability to distinguish between isobaric compounds which can be normally be done by the resulting fragmentation patterns. Because some molecules, like biogenic VOCs, share the same molecular weight, [1] points out the need for chromatographic separation prior to analysis in PTR-MS to differentiate signal contributions.

The goal of this work is to couple the preconcentrator and PTR-MS together and characterize its performance. Combining the rapid evolution of VOCs with the real-time detection capability of the PTR-MS has the potential to lower PTR-MS detection limits and help to distinguish signals between different compounds of the same molecular weight. The preconcentrator employed in this work used Tenax deposited on a nickel foam core as described [7] by a previous work. This novel setup allows for rapid, uniform heating of the Tenax allowing minimum time spread in evolution of a given VOC when heated, resulting in high preconcentration factors with near real-time response. Toluene gas solutions in nitrogen at concentrations between 50 and 1000pptv with various loading times are used to test the preconcentrative capability of a Tenax TA preconcentrator. Chromatographic trends and separation by thermal desorption are also demonstrated and discussed.

MATERIALS AND METHODS

Toluene samples were prepared by filling gas tanks with vapor generated by heating diffusion vials in a Dynacalibrator (Vici) using dry nitrogen as a carrier gas. The sample tanks were pressurized by a cylinder of ultra high pure nitrogen to approximately 100psi to provide enough sample for one run and to further dilute the toluene to a usable stock solution. Teflon permeation tubes provided another source of toluene.

The preconcentrator was fabricated according to a previous work [7] from a 12.7mm x 4.8mm x 12.7mm nickel foam core (Porvair Advanced Materials, Inc., 700 Shepherd Street, Hendersonville, NC 28792, 800-843-6105) filled with 25mg of the 60/80 mesh Tenax TA polymer (Supelco) fitted into 0.150in Inconel 600 tubing (Figure 1). The tubing containing the preconcentrator pellet was wrapped with

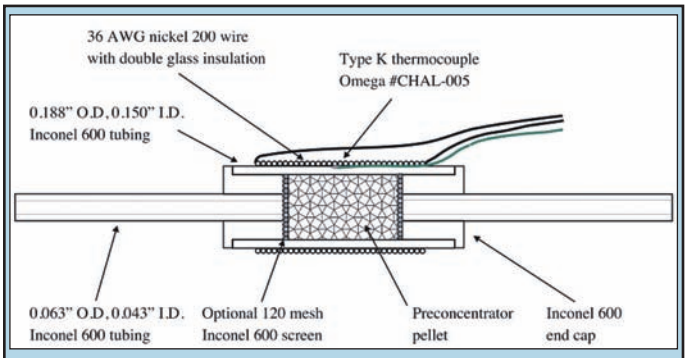

Figure 1. Tenax TA preconcentrator schematic.

a type K thermocouple (#CHAL-005, Omega, Stamford, CT, 800-848-4286) on the inner-most layer and approximately 61cm of 36 AWG nickel 200 double glass insulated wire (Pelican Wire Company, Inc., Naples, FL, 941-597-8555) was wrapped around the outside to act as a resistive heater. The assembly was then coated with an insulating zircon-based cement and Teflon tubing was connected to the Inconel tubing. Custom LabVIEW™ software written in a previous work [7] was used to control the resistive heater.

The proton-transfer-reaction mass spectrometer (PTR-MS) was calibrated for toluene by using a gas cylinder with a standardized toluene concentration connected to a gas dilution system shown in Figure 2. The standard toluene gas was diluted with dry nitrogen gas. All gas flows were controlled with mass flow controllers and the dilution flow was varied from 800 to 200sccm in 100sccm decrements to yield different toluene concentrations. The PTR-MS settings were U_{drift} = 540V, P_{drift} = ~2.0mBar, and multiplier voltage was 3400V. Dwell time for toluene (m/z 93) was 1 second and hydronium (m/z 21) was 500 milliseconds. The resulting data was linearly regressed to an equation, as shown in Figure 3, and was used to determine toluene concentrations for the remainder of the experiment.

Flow from the sample gas tanks was regulated by a mass flow controller which could be diluted further by nitrogen flow from another mass flow controller. From the resulting diluted flow, 30sccm of it was diverted and regulated to a gas switching apparatus by a mass flow controller. The output of the switching apparatus was

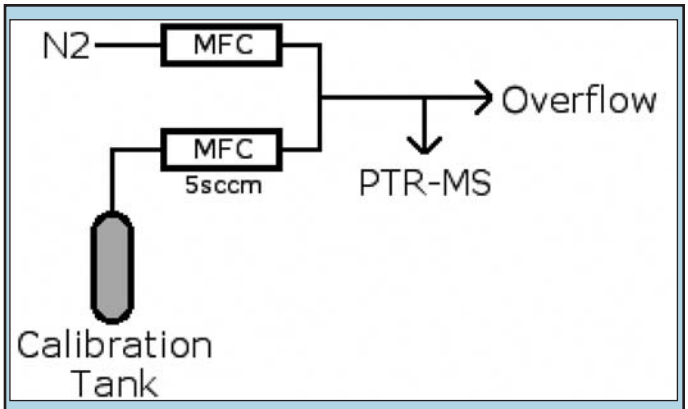

Figure 2. This is the experimental setup used to calibrate the PTR-MS for toluene. Static flow rates are indicated. MFC = mass flow controller

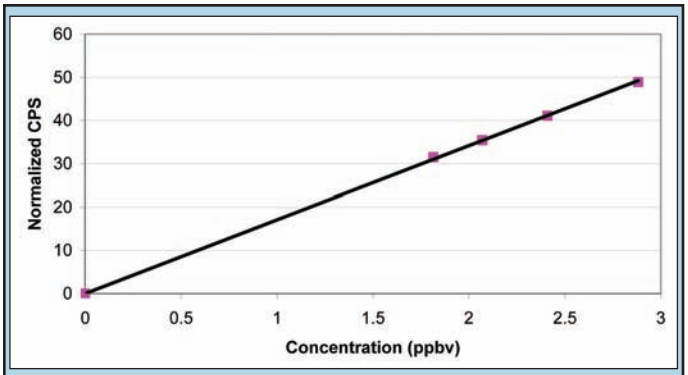

Figure 3. Calibration curve for toluene. The regression is forced through the origin.

connected to the preconcentrator, which in turn was connected to the PTR-MS. Operation of the switching apparatus was controlled by the same LabVIEW™ software [7]. The length of the tube from the preconcentrator to the PTR-MS was minimized to 3cm to retain sharp count rate peak shape during gas analysis with the PTR-MS. The setup is outlined in Figure 4. The intake flow of the PTR-MS was adjusted to 30sccm.

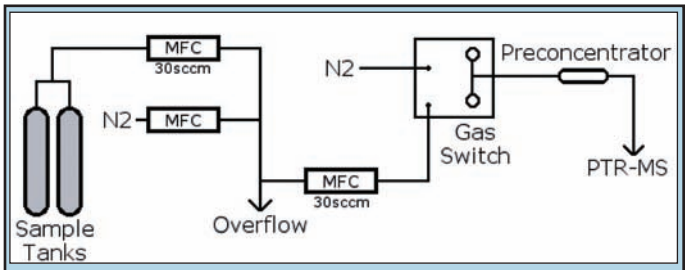

Figure 4. This is the experimental setup used to load the preconcentrator. Static flows rates are indicated. (MFC = mass flow controller)

Prior to starting a perconcentration loading time test for a particular toluene concentration, the sample vapor concentration was measured by the PTR-MS in the absence of the preconcentrator for 100 cycles. The preconcentrator was then reconnected in series to the PTR-MS and was thermally cycled with a dry nitrogen flow of 30sccm. During a thermal cycle, the preconcentrator was thermally ramped from 25°C to 200°C linearly in 20 seconds by running electrical current through the 36 AWG heater wire. The peak temperature was held for 10 seconds before the preconcentrator was allowed to conventionally cool by aid of a cooling fan. Once the preconcentrator reached a temperature of 30°C, the thermal cycle restarted. A complete thermal cycle finished in about 150s. Thermal cycles continued until observed toluene ion count peaks were at consistent, minimal heights, then sample loading commenced on the next thermal cycle.

Toluene vapor concentrations of 56, 199, 534, and 975 parts per trillion by volume were then flowed in turn through the preconcentrator at 30sccm for loading times of 60, 150, 300, 600, and 1200 seconds. After each loading time, the thermal cycle previously described was performed with the exception that only dry nitrogen gas was flowed through the preconcentrator during the cool down process by the gas switching apparatus. Toluene ion count rates were observed by the PTR-MS during the thermal cycle with a dwell time of 1 second. This procedure was performed 5 times for loading times of 60, 150, and 300 seconds and 3 times for the loading times of 600 and 1200 seconds.

The toluene vapor source was then changed with a standard gas calibration tank that contains various gases outlined in Table 1.

Species	Protonated m/z	Concentration, ppbv	Temperature at Peak Height for 120s Ramp, °C
Methanol	33	641	58.0
Acetonitrile	42	515	73.8
Acetone	59	390	70.9
Isoprene	69	405	80.1
Methyl Vinyl Ketone Methacrolein	71	727	92.7
Methyl Ethyl Ketone	73	272	95.9
Benzene	79	362	108.5
Toluene	93	299	133.7
p-Xylene	107	232	158.9
1,2,4-Trimethylbenzene	121	215	171.5
α-Pinene	137	179	89.6

Table 1. Contents and concentrations of VOC mixture tank. Temperature and peak data is provided from a 120s ramp time.

The flow from the tank was regulated to 5sccm and the nitrogen dilution flow to 1500sccm by mass flow controllers resulting in a dilution factor of 3.3%. The same cleaning procedure used prior to running the tests for varied loading times was carried out. The same loading and thermal cycle sequence previously performed was used with the exceptions that the loading time remained constant at 300 seconds and the thermal ramping time was varied to 20, 40, 60, 90, and 120 seconds. During the thermal ramping process all organic species' count rates were monitored simultaneously by the PTR-MS with a dwell time of 100 milliseconds.

RESULTS

Data points acquired during the calibration phase for each dilution were recorded and averaged (arithmetic mean) over the 50 cycles. Toluene count rates were normalized to 1,000,000 H_3O^+ count rates averaged (arithmetic mean) over the same cycles. The resulting normalized ion counts per second were plotted and linearly regressed against toluene concentration, resulting in the equation displayed in Figure 2. The concentrations of toluene for the samples used in this work were determined from this regressed formula.

Count rate peak areas obtained from thermal ramping of the preconcentrator were obtained by numerically integrating over 6 points using the trapezoid method. The selected points for the peak started 2 data points before the highest recorded count rate for that particular run. The average time integrated for each peak was approximately 8.2 seconds. All peaks belonging to the same toluene concentration and loading time were averaged (arithmetic mean). This process was used for determining the areas of all peaks in this work. Peak areas were divided by the interval of time over which they were measured to calculate integrated ion counts per second.

Table 2 compares the preconcentration factors of toluene for peak height and normalized integrated ion count rate methods

	60s Loading		150s Loading		300s Loading		600s Loading		1200s Loading	
	NICPS	Height	NICPS	Height	NICPS	Height	NICPS	Height	NICPS	Height
56pptv	11	16	17	27	30	51	58	102	113	189
199pptv	8	14	16	27	25	46	54	101	92	157
534pptv	10	16	21	34	38	63	69	118	132	242
975pptv	10	17	21	35	39	65	78	151	148	257

Table 2. Comparison of preconcentration factors of ICPS and ion peak height calculation methods for the loading times and concentrations used. NICPS = Normalized Integrated Counts Per Second

calculated by dividing either the normalized integrated counts per second or normalized peak heights by the original normalized ion count rate. Mean peak heights from the same concentration and preconcentration time are used in this calculation.

Figure 5 is a compressed time plot of the peaks recorded from a 20s thermal ramp with a 150s loading time at 56pptv. The deviation of peak heights in the figure is due to small variations in peak width. The true measure of reproducibility is integrated peak area as discussed later. Temperature is included in the graph for reference.

Figure 6 is a composite that demonstrates typical variation of ion count peaks with different loading times for the same concentration (56pptv). Time between the peaks is compressed.

The integrated ion count rates from each loading time belonging to the same toluene concentration were plotted against the respective loading time. This plot was then linearly regressed to demonstrate the relationship between integrated ion count rates and loading times. A graph of all concentrations is shown in Figure 7. In a similar manner, Figure 8 shows the linear correlation between toluene concentration and integrated ion count rates for each loading time.

Table 1 is a list of the contents and concentrations of the gas mixture used to test the chromatographic ability of the

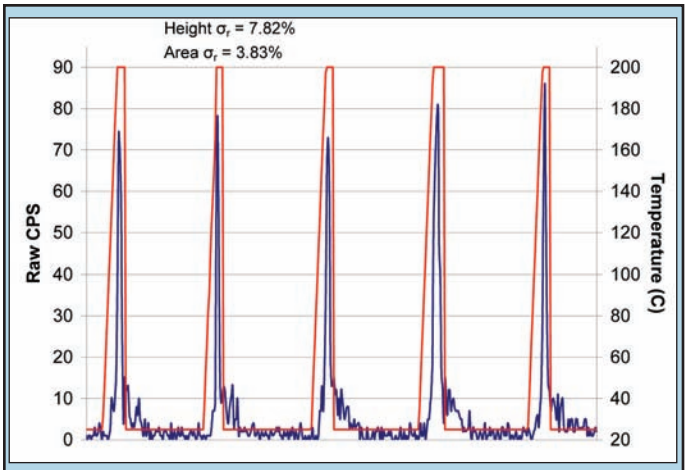

Figure 5. Demonstration of repeatability. Toluene peaks resulting from 20s thermal desorption from 150s of loading time at 56pptv are in blue. Target temperature for the thermal ramps is shown in red. Time between the peaks is condensed for greater peak detail. Relative standard deviations are shown for peak areas and heights.

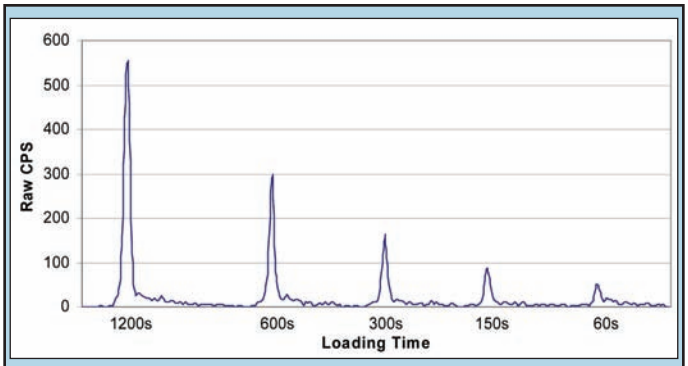

Figure 6. Composite of typical desorption peaks from indicated loading times at 56pptv. Thermal ramp time is 20s. Time between the shown peaks was compressed for better peak clarity.

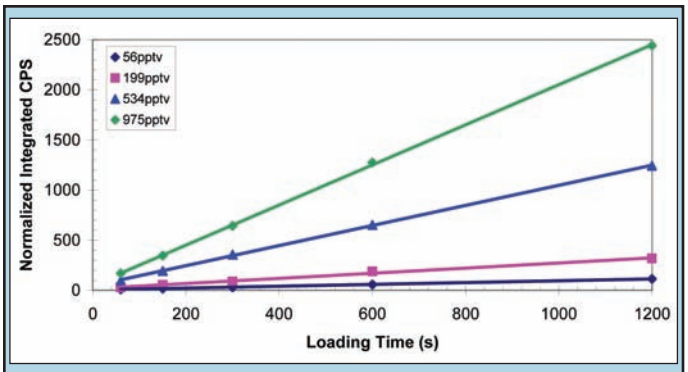

Figure 7. Linear regression of normalized, integrated CPS (counts per second) of toluene against preconcentrator loading times for the toluene concentrations used.

preconcentrator. The temperature at which each compound had its maximum ion count rate from the 120s ramp is provided to show the order of desorption for the various compounds.

Figures 9 and 10 show the behavior and comparison of the organic species described in Table 2 when different thermal ramp times are performed. The count rate for each data point was

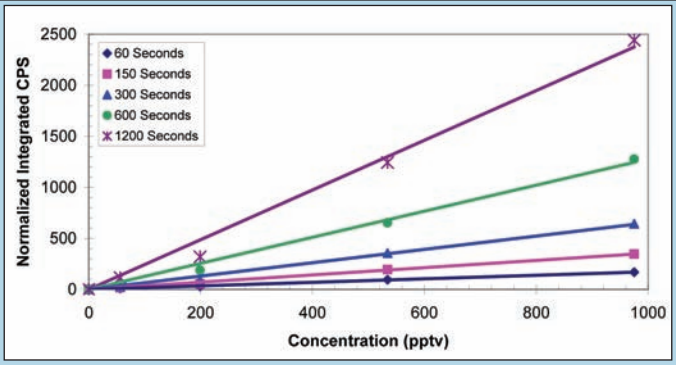

Figure 8. Linear regression of normalized, integrated CPS (counts per second) of toluene against the concentrations used for each preconcentrator loading time. The regressions are forced through the origin.

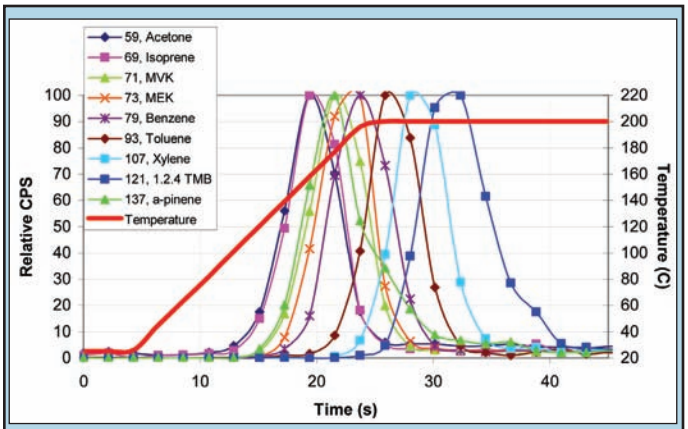

Figure 9. Time and temperature of peak separations for listed organic species over a 20s thermal ramp. Peaks are normalized to their maximum height. MVK = methyl vinyl ketone, MEK = methyl ethyl ketone, 1.2.4 TMB = 1,2,4-trimethylbenzene.

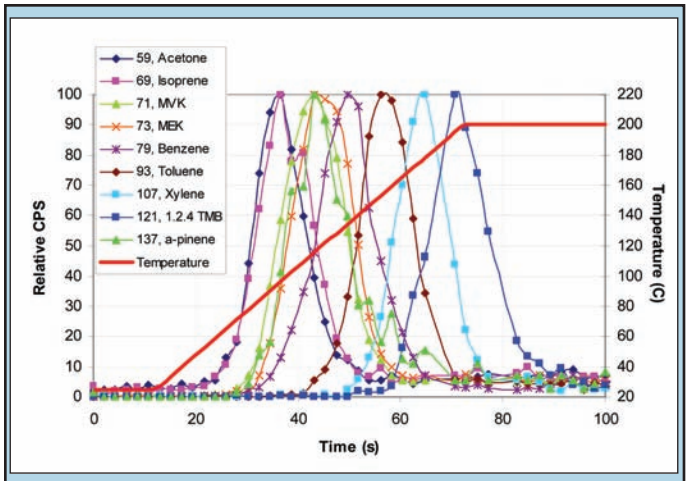

Figure 10. Time and temperature of peak separations for listed organic species of a 60s thermal ramp. Peaks are normalized to their maximum height. MVK = methyl vinyl ketone, MEK = methyl ethyl ketone, 1.2.4 TMB = 1,2,4-trimethylbenzene

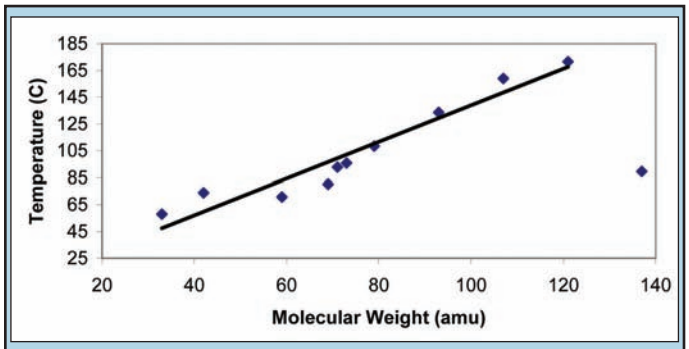

Figure 11. Temperature at maximum count rate height against molecular weight. A line is regressed to show a trend. Mass 137 (α-pinene) exhibits atypical behavior and was excluded in the calculation of the trend line.

normalized to the maximum value recorded for that specie for that run. The temperature line is included for reference.

Data taken from the 120s ramp was taken to plot molecular weight against the temperature at which each VOC had its maximum count rate and is shown in Figure 11. A linear regression was done to show the observed relationship between molecular weight and temperature at peak height.

DISCUSSION AND CONCLUSIONS

Current PTR-MS instruments are able to detect some VOCs with a lower limit of approximately 50pptv. This detection limit can be improved when a preconcentrator is used to collect a sample VOC over a brief collection time and then desorb the analyte to the PTR-MS in a short time. Our results showed that a preconcentrator can successfully increase the lower sensitivity of a PTR-MS by 2 orders of magnitude with a 1200s loading time. With the smallest concentration at the shortest loading time tested (56pptv at 60s), we increased the signal from 0.996 normalized counts per second to 10 normalized integrated counts per second, an amplification by a factor of 11.

Calibration of the PTR-MS was done with a standardized mixture gas tank and diluted with nitrogen by mass flow controllers. Proton transfer efficiencies for toluene were not accounted for in this calibration because another work showed that such considerations ultimately integrate themselves into the calibration curve when standardized gases are used [9].

The data presented in Figure 5 demonstrates the repeatability of the desorption peaks for a set loading time and toluene concentration. The peaks slightly vary in heights due to the time resolution of the PTR-MS. Due to this limitation, we chose to take data from the peaks by numerically integrating their area using a trapezoidal method rather than ratios of peak height and width. Further justification for integrating can be found in the standard deviations for the particular series in Figure 5; the standard deviations for the peak area and peak heights were 3.83% and 7.82%, respectively. The consistent temperature of thermal desorption is also observed in the figure. Peak tails were observed after each thermal desorption which can clearly be seen in Figures 5 and 6. This phenomenon is noted in another work [7].

Integrating over the peaks also reduces the calculated preconcentration factors by averaging over the entire range of concentrations emitted during heating. Table 2 compares the preconcentration factors for normalized peak height and normalized integrated ion count rate methods. Recent developments [12]

improving the time resolution of PTR-MS can eliminate the need for peak integration allowing full utilization of preconcentrator capability. With a preconcentration time of 1200s, the detection limits are improved from about 50pptv to nearly 250 parts per quadrillion.

Behavior of the preconcentrator is found to be very linear with respect to varying loading times at constant concentrations or toluene concentrations at constant loading times as shown in Figures 7 and 8. This dual linear behavior demonstrates the potential utility of the preconcentrator-PTR-MS combination in real-world applications. Figure 8, which indicates that for any of the loading times shown, it is possible to determine the concentration of a sample by its integrated ion count rate. However, because both figures show a linear trend, it is possible to determine the concentration of a sample by its integrated count rate with any 2 loading times by plotting the slopes of the regressions in Figure 7 against their concentrations and use that regression to determine the concentration by the slope between the 2 arbitrary loading times. This linearity is presumed to hold true for the low toluene concentrations and loading times here as the total accumulation of toluene in the Tenax is far below its saturation point.

The resulting peaks as seen in Figure 9 demonstrate two important analytical capabilities of the preconcentrator. The mean time from the beginning of the thermal ramp to the time of toluene's maximum peak height was 22s for any thermal desorption peak with a 20s ramp time. In the presence of various other organic species, the time from the beginning of the thermal ramp to toluene's peak height in Figure 9 was 21.6s. The difference of 0.4s can be attributed to the time resolution of the sampling rate of the PTR-MS, which was about 2s per cycle. The close relationship of these times indicate that the temperature of desorption of an analyte is unaffected by the presence of other molecules in the Tenax preconcentrator. The chromatographic property of the preconcentrator can be seen in both Figures 9 and 10. The difference in these plots show that the slower the temperature is increased, the greater the resolving power between the peaks. This observation supports the findings of another work [7]. However our results show that as the thermal ramp time is increased, the peaks become consistently shorter and wider at the base. Temperatures determined to correspond with maximum peak height for a particular species should be only taken as an approximation as there is a short time delay for the gas to travel from the preconcentrator to the drift tube of the PTR-MS. Longer ramp times yield more accurate temperatures at maximum thermal desorption as it makes the delay less significant. An attempt was made to reduce the length of the tubing between the preconcentrator and the PTR-MS in the experimental setup as much as possible to minimize this time delay and peak widening.

It is of interest to note the order in which each of the organic species desorbed from the preconcentrator. The plot shown in Figure 11 shows a linear trend of increasing maximum desorption temperature with molecular weight. These results differ from another work [6] which show order of thermal desorption is greatly influenced by boiling points rather than molecular weight. However α-pinene (m/z 137) distinctly deviates from this linear relationship found in the figure. It is because of this deviance that the utility exists to allow separation of certain chemical compounds of the same molecular weight. The light weight organic species methanol and acetonitrile broke though the preconcentrator easily and did not show distinct peaks upon thermal desorption. This is consistent with the behavior of Tenax TA described elsewhere [4]. Further investigations will be necessary to study the mechanism of thermal desorption in Tenax TA to determine the order of elution among a set of VOC analytes.

The results of this work show that a Tenax TA preconcentrator can be used to extend the lower detection limits of a PTR-MS while giving it the advantage to chromatographic separation of analytes. Another benefit of this type of preconcentrator is its ability to reduce water vapor in a sample. Other works [9,11] have shown that humidity effects can water clusters to form in the drift tube which hinder proton transmission rates to aromatic hydrocarbons like toluene. Although this experiment was performed in dry nitrogen gas, a Tenax preconcentrator could help alleviate some of this problem where sampling conditions contain humidity since it is fairly hydrophobic [2] and would not adsorb water with the VOCs of interest contained within the sample stream. Samples could then could be purged with a dry gas like nitrogen when desorption into the PTR-MS occurs to avoid sensitivity issues.

Further investigations into the characterization of other types of preconcentrators with PTR-MS would be beneficial to help determine which preconcentrator technology would be best suited for a particular task. Studies should not only include their capacitive capabilities for certain compounds but also chromatographic behaviors. Like gas chromatograph columns, different preconcentrators may resolve some types of organic species' peaks better than others. The improvements in sensitivity and chromatographic ability to resolve peaks demonstrated in this work can potentially open up a greater number of applications for detecting time-resolved ultra-trace gas emissions by PTR-MS.

ACKNOWLEDGEMENTS

This research was conducted at the W. R. Wiley Environmental Molecular Science Laboratory at Pacific Northwest National Laboratory. I acknowledge support from the U.S. Department of Energy's Office of Science and thank them for this opportunity to participate in their CCI program. A great many thanks goes to my mentor, Michael Alexander, for his encouragement, time, assistance, and consideration. I also thank Matt Newburn for his help in the laboratory, Norman Anheier for fabricating the preconcentrator, its setup, documentation, and programming LabVIEW™ software, and Jay Grate for information and documentation about the preconcentrator. Credit for Figure 1 goes to Norman Anheier. Pacific Northwest National Laboratory is operated by the Battelle Memorial Institute for the U.S. Department of Energy.

REFERENCES

[1] Joost de Gouw, Carsten Warneke, Thomas Karl, Gunter Eerdekens, Carina van der Veen, Ray Fall, "Sensitivity and specificity of atmospheric trace gas detection by proton-transfer-reaction mass spectrometry," *International Journal of Mass Spectrometry*, vol. 223-224, pp. 365-382, 2003.

[2] Martine Harper, "Sorbent trapping of volatile organic compounds from air," *Journal of Chromatography* A, vol. 885, pp. 129-151, 2000.

[3] C.E. Davis, C.K. Ho, R.C. Hughes, M.L. Thomas, "Enhanced detection of m-xylene using a preconcentrator with a chemiresistor sensor," *Sensors and Actuators* B, vol. 104, pp. 207-216, 2005.

[4] Nader Vahdat, Peter M. Swearengen, James S. Johnson, Steve Priante, Keith Mathews, Amalia Neidhardt, "Adsorption capacity and thermal desorption efficiency of selected adsorbents," *American Industrial Hygiene Association Journal*, vol. 56, no. 1, pp. 32-38, 1995.

[5] Junji Ito, Takamichi Nakamoto, Hiroshi Uematsu, "Discrimination of halitosis substance using QCM sensor array and a preconcentrator," *Sensors and Actuators* B, vol. 99, pp. 431-436, 2004.

[6] T. Nakamoto, Y. Isaka, T. Ishige, T. Moriizumi, "Odor-sensing system using preconcentrator with variable temperature," *Sensors and Actuators* B, vol. 69, pp. 58-62, 2000.

[7] Jay W. Grate, Norman C. Anheier, David L. Baldwin, "Progressive thermal desorption of vapor mixtures from a preconcentrator with a porous metal foam internal architecture and variable thermal ramp rates," *Analytical Chemistry*, vol. 77, no. 6, pp. 1867-1875, 2005.

[8] W. Lindinger, A. Hansel, A. Jordan, "On-line monitoring of volatile organic compounds at pptv levels by means of proton-transfer-reaction mass spectrometry (PTR-MS): medical applications, food control, and environmental research," *International Journal of Mass Spectrometry and Ion Processes*, vol. 173, pp. 191-241, 1998.

[9] M. Steinbacher, J. Dommen, C. Ammann, C. Spirig, A. Neftel, A.S.H. Prevot, "Performance characteristics of a proton-transfer-reaction mass spectrometer (PTR-MS) derived from laboratory and field measurements," *International Journal of Mass Spectrometry*, vol. 239, pp. 117-128, 2004.

[10] J. Kesselmeier, M. Staudt, "Biogenic volatile organic compounds (VOC): an overview on emission, physiology and ecology," *Journal of Atmospheric Chemistry*, vol. 33, pp. 23-88, 1999.

[11] C. Warneke, C. Van der Veen, S. Luxembourg, J.A. de Gouw, A. Kok, "Measurements of benzene and toluene in ambient air using proton-transfer-reaction mass spectrometry: calibration, humidity, and field comparison," *International Journal of MassSpectrometry,* vol. 207, pp. 167-182, 2001.

[12] P. Prazeller, M. Alexander, B.T. Jobson, E. Boscaini, P. Palmer, "Proton Transfer Reaction Ion Trap Mass Spectrometer (PTRITMS)," *Rapid Communications in Mass Spectrometry*, vol. 7, pp. 1593-1599, 2003.

Jennifer Chentzu Pai received a B.S. in chemical engineering from Cornell University in May 2006. At Cornell, she studied the characteristics of synthetic polymers formed from the dimer dihydroxyacetone for use in drug delivery. During the summer of 2005, Jennifer participated in the DOE Summer Undergraduate Laboratory Internship program at Brookhaven National Lab. Her research involved exploring the effects of acetone using a conditioned place preference (CPP) paradigm, was funded by the Department of Energy and Office of Science and supervised by Dr. Stephen Dewey. This CPP research was presented at the AAAS Annual Conference in 2006. She is currently preparing to pursue a PhD in chemical engineering at the University of Texas at Austin, where she hopes to focus on new methods of drug uptake.

Stephen Dewey's research interests include neurotransmitter interactions in healthy and diseased states, functional regulation of neurotransmitter systems, behavioral pharmacology, animal models of addiction, and in vivo neurochemical monitoring techniques. He received his B.S. from Fairleigh Dickinson University in 1981 and his Ph.D. from the University of Iowa in 1985. Dr. Dewey has been tenured scientist at the Brookhaven Lab since 1995 and a senior chemist since 1998.

CONDITIONED PLACE PREFERENCE TO ACETONE INHALATION AND THE EFFECTS ON LOCOMOTOR BEHAVIOR AND ^{18}FDG UPTAKE

Jennifer C. Pai, Stephen L. Dewey, Wynne Schiffer, and Dianne Lee

ABSTRACT

Acetone is a component in many inhalants that have been widely abused. While other solvents have addictive potential, such as toluene, it is unclear whether acetone alone contains addictive properties. The locomotor, relative glucose metabolism and abusive effects of acetone inhalation were studied in animals using the conditioned place preference (CPP) paradigm and [^{18}F]2-fluorodeoxy-D-glucose (^{18}FDG) imaging. The CPP apparatus contains two distinct conditioning chambers and a middle adaptation chamber, each lined with photocells to monitor locomotor activity. Adolescent Sprague-Dawley rats (n=16; 90-110 g) were paired with acetone in least preferred conditioning chamber, determined on the pretest day. The animals were exposed to a 10,000 ppm dose for an hour, alternating days with air. A CPP test was conducted after the 3rd, 6th and 12th pairing. In these same animals, the relative glucose metabolism effects were determined using positron emission tomography (PET) imaging with ^{18}FDG. Following the 3rd pairing, there was a significant aversion to the acetone paired chamber (190.9 ± 13.7 sec and 241.7 ± 16.9 sec, acetone and air, respectively). After the 6th pairing, there was no significant preference observed with equal time spent in each chamber (222 ± 21 sec and 207 ± 20 sec, acetone and air-paired, respectively). A similar trend was observed after the 12th pairing (213 ± 21 sec and 221 ± 22 sec, acetone and air-paired, respectively). Locomotor analysis indicated a significant decrease ($p<0.05$) from air pairings to acetone pairings on the first and sixth pairings. The observed locomotor activity was characteristic of central nervous system (CNS) depressants, without showing clear abusive effects in this CPP model. In these studies, acetone vapors were not as reinforcing as other solvents, shown by overall lack of preference for the acetone paired side of the chamber. PET imaging indicated a regionally specific distribution of ^{18}FDG uptake following acetone exposure. Further studies using different concentrations are required to better understand the locomotor and behavioral effects of acetone. This study confirms that the combination of microPET and the CPP paradigm can be used to elucidate the effects of abused solvents vs. non-abused solvents in inhalants.

INTRODUCTION

Inhalant abuse has become an increasing problem in the United States and around the world, a major problem especially among children and adolescents [1,2] even though it does not carry the same publicity as illegal drug use. Inhalants, due to the inexpensiveness and unrestricted availability, frequently become the first substance abused by children. While most teenagers cease to abuse inhalants, many progress to drugs with larger consequences, including marijuana, cocaine and opiates, or even using them alongside inhalants [3,4]. As a result, it becomes important to determine which inhalants carry the greatest risk of abuse.

Commonly abused products, such as paints, varnishes, paint thinners and adhesives, consist of many solvent components. In

the literature, toluene is known to be a major component that causes abusive effects in inhalants in a dose dependent manner [5]. Solvents such as acetone have not been as extensively covered in literature. Acetone, commonly found in some paint thinners and nail polish, has high water solubility. This causes the acetone to diffuse rapidly into the blood while entering the brain at a much slower rate than solvents such as toluene. As a result it creates central nervous system (CNS) effects that are not as strong but have a much longer presence in the system [6]. It seems unlikely that solvent abusers would select acetone because of its slow onset and prolonged duration of action however, preliminary studies indicate a preference which is why we plan to study it further.

Conditioned Place Preference (CPP) is an indirect model of drug seeking behavior. Focusing on environments previously associated with a drug, it is used to measure the motivational effects of inhalants rather than the actual act of administering [7]. We will use the CPP paradigm to test the hypothesis that acetone is reinforcing to laboratory animals. We will also test the secondary hypothesis that acetone, like other CNS depressants, alters locomotor activity [6, 8]. Our unique conditioning chamber is equipped with automated photocells capable of measuring locomotor activity simultaneously as conditioning occurs and will allow us to assess acetone's role in CNS depression shown in other abused solvents [9]. Determine whether acetone produces locomotor sensitization (increase response to drug) or tolerance (decrease response to drug), two measures of altered CNS functions studied with drugs of abuse [10,11].

In addition to measuring locomotor behavior and place preference, the neurochemical effects of acetone will be studied using microPET (positron emission tomography). PET studies can be used to measure the acute neurochemical responses to an abused drug or track the addictive drug's path in the brain [12,13]. Neuroimaging studies with 2-deoxy-2-[^{18}F]fluoro-D-glucose (^{18}FDG), an analog of glucose, allow measurement of relative glucose metabolism, more importantly local cerebral metabolism [14]. PET allows us to study drug effects and how they contribute to reward and reinforcement. Pet can also be used to investigate the impact drug abuse has on the system [13]. Information from this study will affect the attention given to inhalants, prevention efforts currently in process as well as pharmacologic treatment strategies.

MATERIALS AND METHODS

Subjects

Adolescent Sprague-Dawley rats (n=16; Taconic Farms, Germantown, NY) measuring 90-110 grams at the beginning of the study were used. The rats were housed randomly in pairs and kept on a 7am/7pm light cycle and given free access to food and water. All testing and conditioning of the animals were preformed daily at 9am. All experiments were conducted in accordance with the Institutional Animal Care and Use Committee.

Conditioned Place Preference Apparatus

The conditioned place preference apparatus (ENV-013 MED Associates Inc.) consists of two conditioning chambers (21×21×27.5 cm) separated by a middle chamber with access to each chambers facilitated by two guillotine doors. One conditioning chambers contains black walls with a white smooth floor, the other contains white walls with a steel mesh floor. The middle adaptation chamber has gray walls and a smooth floor. Conditioning chambers contain clear plexiglass ceilings that becomes airtight when shut. Infrared photocells line the walls of each chamber to monitor locomotor activity and time spent in each chamber. The photocells, positioned at the level of the animal's head, are connected to MED-PC for Windows and Delphi TM4 and programmed to measure beam breaks when the animal enters the chamber (head and the front torso).

In order to maintain the equilibrium concentration of acetone vapor in the conditioning chambers. Each of the conditioning chambers contains an opening at the far top end that delivers the inhalant vapors and along the bottom to allow stabilization of atmospheric pressure. Before the initial exposure to the vapors, concentration equilibration required for 20 minutes.

Acetone Administration

Acetone (99%) was purchased from Sigma-Aldrich (Milwaukee, WI). Mixtures of acetone vapors and air were metered using two mass flow controllers (Dyna-Blender by Matheson Tri-Gas, Mongomerville, PA) with a total flow of gas mixture set at 2 L/min. During conditioning, the acetone was kept at 0°C and bubbled to retard evaporation (1.75 L/min of pure air and 0.25 L/min of acetone) for a concentration of 10,000 ppm (calibration on a gas chromatograph). During conditioning, rats were exposed to the acetone vapors or air at 24 hours intervals for an hour duration.

CPP Procedure

Preconditioning phase: The animals were transported between the Brookhaven Laboratory Animal Facility and the Chemistry department and handled to adjust them to the transportation procedure and conditioning environment for three days.

Pretest day: Each rat was placed into the middle chamber for 5 minutes of adaptation. The animals were allowed to freely explore the three chambers for 15 min. The time spent in each chamber was recorded.

Conditioning phase: For the first group of animals (n=8), a CPP test was conducted following the 6th and 12th pairing. For the second group of animals (n=8), a CPP test was conducted after 3 pairings. The pairings (one acetone and air dose) were administered on consecutive days, including weekends, alternating the doses of acetone and air. The rats were assigned acetone in the side they had least preferred on the pretest day. During conditioning, noise was brought to the minimum and presence of humans were restricted.

Test day: 24 hours after last acetone administration, the animals were tested for a place preference. Animals were placed into the middle adaptation chamber for 1.5 minutes (since animals have now habituated to the chamber) and then allowed to freely explore the three chambers for 15 minutes. The time was recorded as well as the number of chamber crossings that occurred during the test.

MicroPET Imaging

Before animals were imaged, an additional pairing was administered. The animals received an intraperitoneal (IP) injection of ^{18}FDG (~ 1.0 mCi; $t_{1/2}$ 110 min) for a 45-minute uptake in their home cage and scanned for 10 or 20 minutes. MicroPET images were taken using an R4 tomograph (Concorde Microsystems, Knoxville, TN). Following the scan, a plasma glucose value was measured (standard glucose testing strips) from the lateral tail vein. MicroPET images were analyzed by spatial pre-processing (realignment, coregistration and normalization) with SPM2 (Statisical Parametric Mapping 2) and dose corrected. A ROI (region of interest) template was applied and analyzed using the PMOD (Pixel-wise Modeling tool 2.65) software package.

Statistical Analysis

A student's T test (1-tailed, 2-variance) was used to determine significance ($p < 0.05$). Determination of locomotor activity was defined as the break of two consecutive beams. Locomotor analysis was analyzed using area under the curve with SigmaPlot (9.0).

RESULTS

Conditioned Place Preference

At the pretest, the first group of animals (n=8) spent 215.4 ± 32.11 sec and 197.6 ± 28.7 sec (mean ± standard deviation) in the white and black chambers, respectively. Following 6 pairings of acetone and air exposure, the animals did not exhibit a significant preference for either the acetone paired side (221.7 ± 20.6 sec) or the air paired side (206.9 ± 20.0 sec). After the 12th pairing (Figure 1), these same animals as a group did not show a significant preference

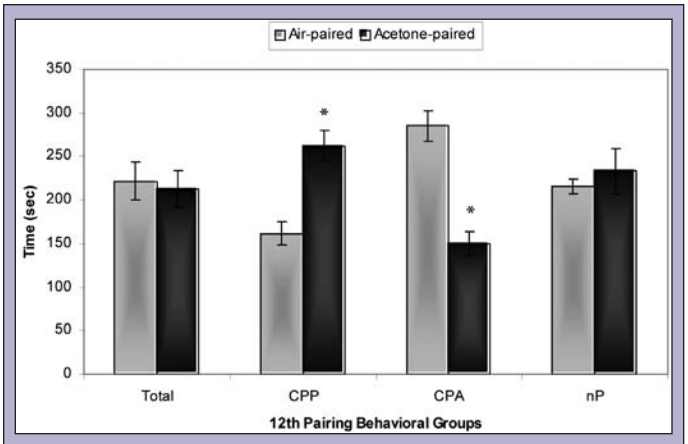

Figure 1. CPP results after the 12th pairing with the preference of the animals as a group. The three distinct groups were separated out into CPP (n=3), CPA (n=3) and nP (n=2).

toward either conditioning chamber (212.7 ± 21.1 sec and 221.4 ± 21.6 sec, acetone paired and air paired chamber, respectively). Three animals out of this group expressed a positive place preference ($p < 0.006$) with 262.0 ± 17.5 sec in the acetone-paired chamber and 161.3 ± 13.3 sec in the air-paired chamber. Three animals expressed a significant ($p < 0.002$) conditioned place aversion (CPA) with 149.6.4 ± 13.6 sec in the acetone paired side and 285.2 ± 17.3 sec in the air paired side. Two animals expressed no preference (nP) for either chamber (233.5 ± 25.8 sec and 216 ± 8.3 sec; acetone and air paired chamber, respectively).

A separate group of animals (n=8) at the pretest had no preference for either side of the conditioning chamber spending 217.1 ± 19.1 sec and 176.3 ± 32.9 sec in the white and black chamber, respectively. Following the 3rd pairing, there was a significant ($p < 0.02$) aversion for the acetone paired side of the chamber with the animals spending 190.9 ± 13.7 seconds in the acetone paired side vs. 241.7 ± 16.9 seconds in the air paired side. Figure 1 illustrates the preference for the behavioral groups after the 12th pairing.

Locomotor Activity

Figure 2 illustrates the average locomotor activity comparison per minute between acetone and air showed a significant ($p<0.01$)

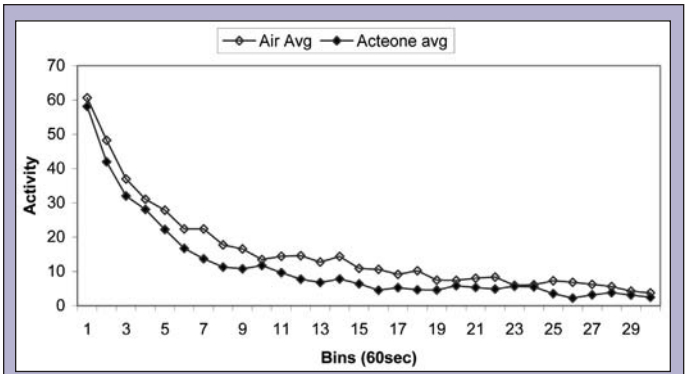

Figure 2. Locomotor activity during each initial 30 minutes of air and acetone conditioning days, average of all the pairings days combined.

decrease during the first 30 minutes of conditioning from the air exposed days to the acetone exposed day in the same pairing. Standard deviations of the curves fell in the range of 0-2, therefore not displayed on the figure. During the initial first 5 minutes of the locomotor activity the respective slopes for the air and acetone were –6.7009 and –7.8685 (set at an intercept of 60) with a marked difference of 18% between the two exposures.

During the hour conditioning period, there was a gradual decrease in the locomotor activity throughout the initial six pairings with the exception of the 3rd pairing, revealing significantly lower acetone locomotor activity than on the air exposure day, shown in Figure 3. From the first pairing to the sixth pairing, there was a decrease in the ratio of acetone exposed locomotor activity to air exposed locomotor activity. For the first six pairings the average ratio was 69.2%. During the final six pairings there was a fluctuation in the locomotor activity with no pattern displayed. The animals no longer displayed a significant difference between the acetone and air activity, though acetone is still lower than the air. For the final six pairings the average ratio of the acetone to air exposures of each pairing was 83.6%.

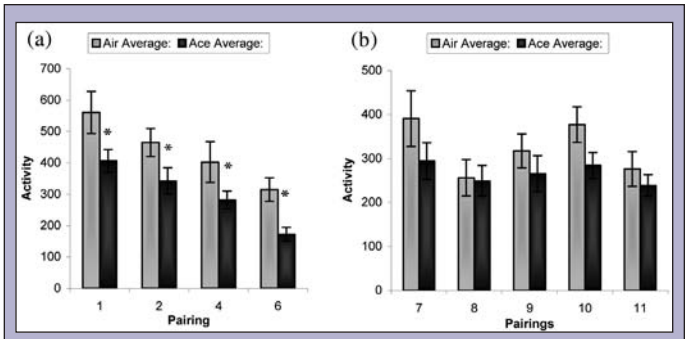

Figure 3. 1, 2, 4, and 6th pairing in the initial six pairings: (a) the first five pairings (b) final six pairings of exposure. Values were determined using an area under the curve for the first 20 minutes during each conditioning period.

FDG Neuroimaging

The baseline images (Figure 4) for which all acetone exposed animals were compared to were taken from other animals that were

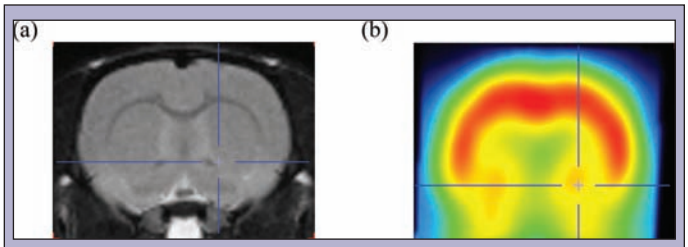

Figure 4. Baseline Images: (a) MRI map of the coronal plane of a rat brain (b) image of the FDG uptake in the frontal cortex and striatum.

of the same group, age, and weight when they arrived. Images of the animals after the 12th baseline (Figure 5), displaying the ^{18}FDG uptake for each of the behavioral groups are on the top row, along the bottom row the images are overlapped onto an MRI scan to distinguish regions of the brain, specifically the striatum and cortex.

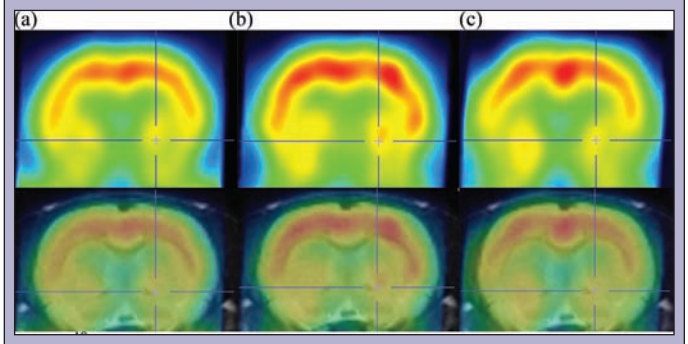

Figure 5. ^{18}FDG uptake following chronic exposure of acetone on the relative brain metabolism for the (a) conditioned place preference (CPP); (b) conditioned place aversion (CPA); and (c) no preference (nP) behavioral groups.

Analysis of the relative glucose metabolism for regional changes to whole brain (Figure 6) showed there were differences in the regional distribution between the three different behavioral groups. Observed

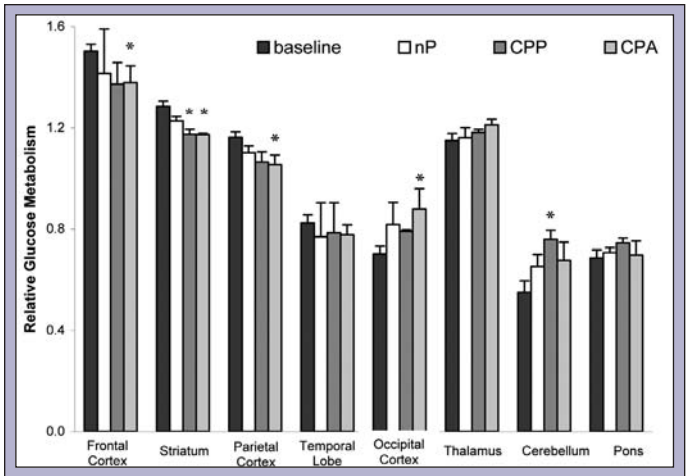

Figure 6. Relative glucose metabolism with regionally specific ^{18}FDG uptake. *Significant differences ($p < 0.05$).

that FDG uptake was regionally specific with decreases in the frontal cortex, striatum, parietal cortex and temporal coretex while there were increases in the occipital cortex, thalamus, cerebellum and pons. The CPA group displayed a significant ($p < 0.05$) difference from the baseline in the Frontal Cortex, the Striatum, the Parietal Cortex and the Occipital Cortex, CPP group: the striatum and cerebellum were the regions that displayed a significant difference. Results analyzed through percent injected dose/cc (Figure 7) indicated only CPA behavioral group had a significant difference from the baseline.

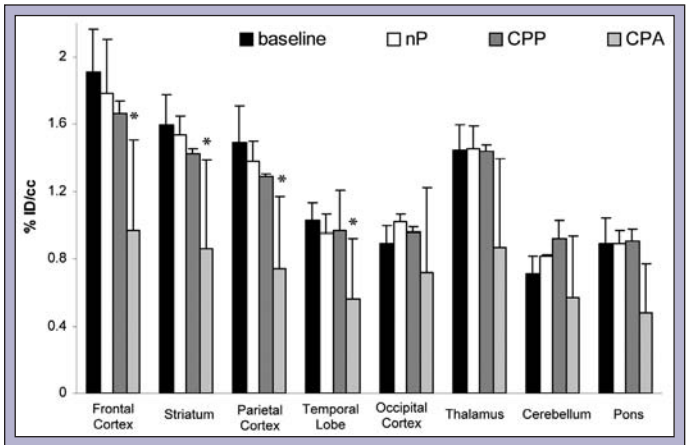

Figure 7. Percent injected dose/cc of brain tissue. *Significant decreases ($p < 0.05$) in the frontal cortex, striatum, parietal cortex and temporal lobe in the CPA behavioral group.

DISCUSSION

The lasting behavioral effect of abused drugs is an extremely important question relating to drug addiction research. The animal model for abuse liability of solvents has been very successful for toluene. Nevertheless, the abuse potential of other solvents common to household products remains to be established. We therefore extend out previous method for determining the abuse liability of toluene [5,15] to acetone, a common ingredient in products such as fingernail polish remover. Based on our previous data and data

from biochemical studies [6,16] reinforcing doses of acetone should be roughly five times higher than reinforcing doses of toluene. Our studies indicate the optimal reinforcing dose of toluene as 2,000 ppm, so therefore we chose a dose of 10,000 ppm acetone, since acetone is much less potent that toluene for producing intoxicating effects in mice (Bruckner and Peterson). We also obtained parallel measures of locomotor activity and regional changes in brain energy demand. Our overall goal was to obtain a better understanding of the effects that acetone has on locomotor behavior, place preference and metabolic consequences for reinforcing or aversive exposures to acetone.

Our results provides evidence that a dose-dependent CPP could not be obtained with an exposure of 10,000 ppm and a pairing duration of 60 minutes. The "dose" of inhaled solvent incorporates both the concentration during exposure and the duration for which animals are exposed to that concentration. Here, the dose was based on preliminary data which showed that six pairings of 30 minutes, followed by three pairings of 60 minutes, yielded a significant CPP to acetone. Based on this and biochemical data, there are several reasons why this particular 'dose' did not produce a place preference for acetone. First, the reinforcing concentrations of acetone have not been established and it is possible that 10,000 ppm is in excess; second, the metabolic response in acetone-preferring animals differs significantly from the acetone — averse animals; and third, our compiled data would suggest that the 'dose' of acetone may need the incorporation of a third variable: exposure titration. Animals may need to be exposed to smaller doses of acetone prior to being exposed to a concentration that is as reinforcing as toluene.

While there was no preference following the 6^{th} and the 12^{th} pairing, it is significantly important that the animals showed an aversion to the vapor. With the addition of the preliminary data showing a significant preference. Hypothesis on the addictive effects of acetone based on the duration that animals were exposed to the volatile vapors can be formed. The sensitivity of the dose would explain distinct behavioral groups exhibited after the 12^{th} pairing. The hour duration chosen was established by the pharmakinetics of the solvent. Acetone is more water soluble than toluene allowing it to absorb into the blood stream more rapidly but less inclined to diffuse into the brain. Known as an unmetabolized vapor, enzymes are unable to break it down [17,18]. As a result, higher levels of acetone have been found in the blood than in the brain [6,19], creating less potent CNS effects with a gradual but longer duration. It seems that initially the hour doses are too overpowering for the animals and cause the aversive affects. Instead the animals need smaller doses to adjust to the solvent before increasing the doses (or titrating up) to create the preference found with preliminary data.

Analysis of locomotor activity indicates that the solvent carries the characteristics of a CNS depressant producing concentration-dependant narcoses in animals [6]. The significant decrease in average activity on acetone exposure days and air exposure days seems to provide evidence of this characterization [8]. Individual pairings were examined to study if acetone effects became more evident with increasing pairings. These measures demonstrated a marked decrease in the ratio between the acetone and air for the initial 6 pairings, indicating that acetone is producing a behavioral effect on the animals during acute exposure. This supports previous studies that indicated a decrease in locomotor activity following acetone exposure [6,8] and provides evidence that the concentration used in this study was sufficiently high. The return of the acetone locomotor activity to 83% of the acetone and remaining approximately at the level seems to suggest that larger doses of acetone are needed in order for the similar trend of effect to continue. It can be hypothesized that a titration increase could carry the decreasing trend found after the initial six pairings through the final 6 pairings. Our results indicate that reinforcing effects of acetone can not clearly be established, as toluene that has been shown to have large reinforcing properties through the use of the CPP paradigm [5,15]. Unlike studies done on dose-dependent effects with other drugs of abuse [20,21], acetone is unique in that there are numerous various variables that can be manipulated (number of pairings, pairing duration, pairing concentration and pairing titration). Further studies need to be conducted to verify the affect of these variables on preference.

The PET studies provide evidence that acetone contains a differential regional uptake distribution in various regions of the CNS that possibly denote the signs and symptoms that are related to its abuse. The application of ^{18}FDG is key in determining the brain regions that are most sensitive to the effects of the given drug. By analyzing the data, regional to whole brain measures of relative glucose metabolism can be used to identify distinct changes to chronic exposure of acetone. Of these regions, striatum and orbitofrontal cortices have been associated with addiction and reward related behaviors of drugs of abuse [22]. Overall it can be determined that there was a regionally specific distribution in the brain following the acetone exposure. The animals will be imaged two months after the initial scan to determine if there was a return to the baseline or if there were permanent effects of these animals.

Further studies are needed to determine the reinforcing 'dose' of acetone. These data clearly distinguish toluene and acetone in terms of pharmacodynamic effects, consistent with their differing pharmacokinetic profiles. Further, these studies substantiate the hypothesis that not all inhalants produce their intoxicating effects by non-specific mechanisms. Our results with acetone are very different than equipotent doses of toluene, suggesting that each inhalant possesses a unique behavioral and metabolic profile, which may effect its dependence liability. Clearly the reinforcing properties of acetone, and of inhalants as a whole, are far more complex than previously thought.

ACKNOWLEDGEMENTS

Thankful to mentors, Dr. Stephen Dewey, Dr. Wynne Schiffer and Dianne Lee, for support and insight into my research. Would like to thank, Joseph Carrion, David Alexoff, Doug Marsteller and Nicole Barbarich-Marsteller for assisting in the technical aspects of the research. Thank the Chemistry Department, Animal Facility Center and MicroPET at Brookhaven National Lab for the use of their facilities. This work was supported by the U.S. Department of Energy and the Office of Science's Summer Undergraduate Laboratory Intern (SULI) Program.

REFERENCES

[1] C. E. Anderson and G. A. Loomis, "Recognition and prevention of inhalant abuse," *Am Fam Physician*, vol. 68, pp. 869-74, 2003.

[2] N. I. o. D. Abuse, "NIDA *InfoFacts*, Inhalants, 2004," 2005, pp. <http://www.nida.nih.gov/ResearchReports/Inhalants/Inhalants2.html#scope>.

[3] S. H. Dinwiddie, "Abuse of inhalants: a review," *Addiction*, vol. 89, pp. 925-39, 1994.

[4] C. G. Schutz, H. D. Chilcoat, and J. C. Anthony, "The association between sniffing inhalants and injecting drugs," *Compr Psychiatry*, vol. 35, pp. 99-105, 1994.

[5] M. R. Gerasimov, L. Collier, A. Ferrieri, D. Alexoff, D. Lee, A. N. Gifford, and R. L. Balster, "Toluene inhalation produces a conditioned place preference in rats," *Eur J Pharmacol*, vol. 477, pp. 45-52, 2003.

[6] J. V. Bruckner and R. G. Peterson, "Evaluation of toluene and acetone inhalant abuse. II. Model development and toxicology," *Toxicol Appl Pharmacol*, vol. 61, pp. 302-12, 1981.

[7] T. M. Tzschentke, "Measuring reward with the conditioned place preference paradigm: a comprehensive review of drug effects, recent progress and new issues," *Progress in Neurobiology*, vol. 56, pp. 613-72, 1998.

[8] S. O. Burmistrov, O. N. Mashek, and Stepanova, II, "[The effect of the inhalation of ethanol and acetone on the indices of the antioxidant protection system and on lipid peroxidation in the brain tissue and blood serum of rats]," *Eksp Klin Farmakol*, vol. 55, pp. 56-8, 1992.

[9] E. B. Evans and R. L. Balster, "CNS depressant effects of volatile organic solvents," *Neurosci Biobehav Rev*, vol. 15, pp. 233-41, 1991.

[10] K. A. Trujillo, K. S. Kubota, and K. P. Warmoth, "Continuous administration of opioids produces locomotor sensitization," *Pharmacol Biochem Behav*, vol. 79, pp. 661-9, 2004.

[11] J. Timar, Z. Gyarmati, and Z. Furst, "The development of tolerance to locomotor effects of morphine and the effect of various opioid receptor antagonists in rats chronically treated with morphine," *Brain Res Bull*, vol. 64, pp. 417-24, 2005.

[12] J. S. Fowler, N. D. Volkow, G. J. Wang, Y. S. Ding, and S. L. Dewey, "PET and drug research and development," *J Nucl Med*, vol. 40, pp. 1154-63, 1999.

[13] W. K. Schiffer, D. E. Lee, J. D. Brodie, and S. L. Dewey, "Imaging addiction with PET: is insight in sight?" *Drug Discov Today*, vol. 10, pp. 547-62, 2005.

[14] M. Reivich, D. Kuhl, A. Wolf, J. Greenberg, M. Phelps, T. Ido, V. Casella, J. Fowler, E. Hoffman, A. Alavi, P. Som, and L. Sokoloff, "The [18F]fluorodeoxyglucose method for the measurement of local cerebral glucose utilization in man," *Circ Res*, vol. 44, pp. 127-37, 1979.

[15] M. Funada, M. Sato, Y. Makino, and K. Wada, "Evaluation of rewarding effect of toluene by the conditioned place preference procedure in mice," *Brain Res Brain Res Protoc*, vol. 10, pp. 47-54, 2002.

[16] E. Frantik, L. Vodickova, M. Hornychova, and M. Nosek, "Pattern of inhalation exposure: blood levels and acute subnarcotic effects of toluene and acetone in rats," *Cent Eur J Public Health*, vol. 4, pp. 226-32, 1996.

[17] L. Ernstgard, E. Gullstrand, G. Johanson, and A. Lof, "Toxicokinetic interactions between orally ingested chlorzoxazone and inhaled acetone or toluene in male volunteers," *Toxicol Sci*, vol. 48, pp. 189-96, 1999.

[18] J. B. Morris, D. N. Hassett, and K. T. Blanchard, "A physiologically based pharmacokinetic model for nasal uptake and metabolism of nonreactive vapors," *Toxicol Appl Pharmacol*, vol. 123, pp. 120-9, 1993.

[19] H. W. Haggard, L. A. Greenberg, and J. M. Turner, "The physiological principles governing the action of acetone together with determination of toxicity," *J Ind Hyg Toxicol*, vol. 26, pp. 133-151, 1984.

[20] G. A. Barr, W. Paredes, and W. H. Bridger, "Place conditioning with morphine and phencyclidine: dose dependent effects," *Life Sci*, vol. 36, pp. 363-8, 1985.

[21] T. C. Durazzo, D. V. Gauvin, K. L. Goulden, R. J. Briscoe, and F. A. Holloway, "Cocaine-induced conditioned place approach in rats: the role of dose and route of administration," *Pharmacol Biochem Behav*, vol. 49, pp. 1001-5, 1994.

[22] N. D. Volkow and J. S. Fowler, "Addiction, a disease of compulsion and drive: involvement of the orbitofrontal cortex," *Cereb Cortex*, vol. 10, pp. 318-25, 2000.

Kristen Ann Record has been a physics teacher at Bunnell High School in Stratford, Connecticut since August 2000. She graduated Phi Betta Kappa with a B.S. in physics from Fairfield University in 1999, received her Ed.M. in teaching and learning from Harvard Graduate School of Education in 2000, and her C.A.S. in Science Instruction and Study from Southern Connecticut State University in 2006. She has conducted scientific research in near-contact transport in semiconductor devices and education research in causal model instruction and factors influencing conceptual understandings in physical science. During the summer of 2005 she participated in the Laboratory Science Teacher Professional Development Program (LSTPD) at the National Renewable Energy Laboratory (NREL). Mentored by Dr. John Turner, her project investigated the conductivity of synthesized heteropoly acid membranes for use in PEM fuel cells. She presented this work at the 2005 Fuel Cell Summit and the 2006 National Science Teacher's Association's National Conference on Science Education. Since her LSTPD Fellowship, she has worked with the Connecticut Clean Energy Fund to raise awareness of renewable energy resources at both the state and local level.

Brenna Haley graduated from the University of Northern Colorado in 2006 with a degree in chemistry and a minor in secondary education. She participated in the Pre-Service Teacher (PST) program and the National Renewable Energy Laboratory during the summer of 2005 conducting research on fuel cell membranes. While at UNC she was active in numerous honor societies including Golden Key, Phi Lambda Theta, and Sigma Alpha Lambda. She was recognized on the Dean's List of Academic Distinction throughout her four years in college. In addition to academic pursuits she was a member of the UNC Sugar Bears Dance Team and is currently a professional cheerleader/dancer for a Colorado sports team. She is currently making decisions regarding which graduate degree she would like to pursue.

John A. Turner is a Principal Scientist at the National Renewable Energy Laboratory. He received his B.S. from Idaho State University, his PhD from Colorado State University, and completed a postdoctoral appointment at the California Institute of Technology before joining the Laboratory (then the Solar Energy Research Institute) in 1979. His research is primarily concerned with enabling technologies for the implementation of hydrogen systems into the energy infrastructure. This includes direct conversion (photoelectrolysis) systems for hydrogen production from sunlight and water, advanced materials for high temperature fuel cell membranes, and corrosion studies of fuel cell metal bipolar plates.

CONDUCTIVITY MEASUREMENTS OF SYNTHESIZED HETEROPOLY ACID MEMBRANES FOR PROTON EXCHANGE MEMBRANE FUEL CELLS

KRISTEN ANN RECORD, BRENNA TAMIKO HALEY, AND JOHN TURNER

ABSTRACT

Fuel cell technology is receiving attention due to its potential to be a pollution free method of electricity production when using renewably produced hydrogen as fuel. In a Proton Exchange Membrane (PEM) fuel cell H_2 and O_2 react at separate electrodes, producing electricity, thermal energy, and water. A key component of the PEM fuel cell is the membrane that separates the electrodes. DuPont's Nafion® is the most commonly used membrane in PEM fuel cells; however, fuel cell dehydration at temperatures near 100°C, resulting in poor conductivity, is a major hindrance to fuel cell performance. Recent studies incorporating heteropoly acids (HPAs) into membranes have shown an increase in conductivity and thus improvement in performance. HPAs are inorganic materials with known high proton conductivities. The primary objective of this work is to measure the conductivity of Nafion, X-Ionomer membranes, and National Renewable Energy Laboratory (NREL) Developed Membranes that are doped with different HPAs at different concentrations. Four-point conductivity measurements using a third generation BekkTech® conductivity test cell are used to determine membrane conductivity. The effect of multiple temperature and humidification levels is also examined. While the classic commercial membrane, Nafion, has a conductivity of approximately 0.10 S/cm, measurements for membranes in this study range from 0.0030 – 0.58 S/cm, depending on membrane type, structure of the HPA, and the relative humidity. In general, the X-ionomer with $H_6P_2W_{21}O_{71}$ HPA gave the highest conductivity and the Nafion with the 12-phosphotungstic (PW_{12}) HPA gave the lowest. The NREL composite membranes had conductivities on the order of 0.0013 – 0.025 S/cm.

INTRODUCTION

As an energy conversion device, Proton Exchange Membrane Fuel Cells (PEMFCs) can potentially produce greater operating efficiency and no harmful emissions compared to conventional fossil fuel power sources. While PEMFCs have been shown to be an option for replacing petroleum based generators and engines, it will be necessary to overcome some economic and engineering problems in order for them to become commercially viable [1,2]. PEMFCs utilize a Poly (perfluorosulfonic acid) (PFSA) as the proton conducting electrolyte, most commonly DuPont's Nafion®. Literature has shown Nafion can produce high power densities at temperatures below 100°C. Nafion performs optimally at 80°C and at a high relative humidity, with a proton conductivity of 0.075 S/cm [3]. Full hydration is necessary for maximum proton conductivity, making Nafion not viable under high-temperature (>100°C) or low relative humidity conditions [4].

Membrane hydration presents a challenge to the PEMFC community, as operating temperatures of 120 and 200°C are optimal for automobile and stationary applications, respectively. In addition, reducing the need for external humidification would significantly reduce the complexity and cost of fuel cell systems [1]. PEMFC performance is governed by the conductivity of their PFSA membranes, which depends on the hydration state of the membrane. If the hydration is too low, the conductivity of the cell drops due to the decay of the electrolyte membrane, resulting in poor fuel cell performance. High levels of hydration, and the resulting excess water in the fuel cell, lead to cathode flooding, which also decreases a fuel cell's performance. Thus, the humidification of gases in the PEMFC is a crucial part of maintaining membrane conductivity and material stability [5,6].

Recent research on the improvement of PEM conductivity has focused on the use of hybrid membranes containing inorganic super acids [7,8]. Of these, heteropoly acids (HPAs) are a diverse group of materials known to have high proton conductivities at ambient temperatures. This, coupled with their ability to hold water at high temperatures, makes HPAs appealing candidates for high-temperature and/or low humidity PEMFC operation [9,10]. Vernon et al [11] have done work with heteropoly acids ($H_8SiW_{11}O_{39}$ and 11-SiWA) attached covalently to a polymer backbone in a PEM. Results suggest that, when fully hydrated, the hybrid membranes can achieve proton diffusion coefficients as high as those found in Nafion 117. The ex situ conductivity tests of these membranes showed that conductivity increases more rapidly with temperature, as compared to Nafion 117, suggesting that these hybrid membranes may be developed for higher operating temperature applications [11]. Additionally, results from Reed et al show that heteropoly silicotungstic acid (HSiW) and heteropoly arsenotungstic acid (HAs_2W) doped Nafion 112 have a higher conductivity at elevated temperatures when compared to pure Nafion 112 [12]. Data from Ramani et al suggests that, like pure Nafion, the conductivity of hybrid membranes is also strongly humidity dependent [13]. Thus, there is a need to develop a better understanding of the factors related to the humidification needs of various HPA doped membranes.

This work investigates the effect of relative humidity on HPA doped membranes in an effort to meet the DOE specifications for high-temperature, low humidity PEMFC membranes (120°C, 25-50% relative humidity). Multiple types of synthesized HPA doped Nafion, X-Ionomer, and NREL Developed Membranes (NDMs) at various levels of relative humidity are examined. Information about the fabrication of X-Ionomer is proprietary.

MATERIALS AND METHODS

The Nafion and X-Ionomer hybrid membranes were prepared at Colorado School of Mines. The membranes were each doped with 3 different HPAs: 12-phosphotungstic (PW_{12}), Keggin boron (α-$BW_{12}H$), and $H_6P_2W_{21}O_{71}$ at concentrations of either 1% or 5% by weight. Commercial samples of PW_{12} (Fisher Scientific A248-500) were employed; the other 2 HPAs were synthesized by chemists at Colorado School of Mines. Preparation of the Keggin boron and H6P2W21O71 followed the procedures of Rocchiccioli-Deltcheff et al [14] and Brauer [15] respectively. The HPAs were physically blended with one of the ionomers. Each solution was then casted on a 280 X 175 mm glass plate and placed in an 80°C oven. A multiple clearance applicator was used to attain a membrane with a consistent thickness. The film remained in the oven for 20 minutes. Each membrane cooled to ambient temperature and was then placed back into the oven at 120°C for five minutes to execute the annealing process. After removal from the glass plate, each membrane of a specific HPA and ionomer combination were cut into squares of approximately 50 X 50 mm and placed into a small (~25 mL) vial.

In order to determine the hydration state of the membranes, we utilized isopiestic equilibration of the samples with water vapor above salt solutions, as described by Zawodzinski et al [16]. To completely dry the samples, the open vials were sealed in jars containing phosphorous pentoxide for several days. Weight measurements were taken periodically until a steady state was observed. The sample vials were placed in sealed saturated salt solution jars containing either NaBr, NaCl, MgCl, or KCl. These humidifying jars were then put in an 80°C hot water bath. Again, a constant sample weight was used to indicate equilibrium. Humidity values were determined using values established by Greenspan [17].

The NREL Developed Membranes (NDMs) were prepared by covalently bonding HPAs at a high weight percent (>100 weight percent HPA/polymer) to a host polymer, glycidyl methacrylate-type copolymer (PEMAGMA or PMG for short). While high HPA loadings in previous studies tended to result in mechanically fragile films, the current formulation used a dimethacrylate monomer molecular cross-linker, EGDMA, to improve the integrity of the membranes [18]. The fabrication process first included reacting saturated Keggin 12-HSiW or custom-synthesized Lacunary $H_8SiW_{11}O_{39}$ (11-HSiW) with a methacrylate-based binding silane. Next, a sol-gel approach was employed to produce nano-scaled SiO_2 with functional silanes to immobilize the HPA in a 3D network. EGDMA, a thermal curing agent, and the polymer host of PMG were introduced. PEM-type films were then made by casting the solution in PFA Petri dishes. The resulting films were next processed in an 80°C oven. After a one-hour drying period, the films were heated to approximately 145°C for 10 minutes under a 2-ton pressure to initiate the cross-linking reaction.

The ex situ membrane conductivity measurements of all membranes were determined via a third generation four-point BekkTech® conductivity test cell. Membrane samples were cut into strips of approximately 24 mm in length and 3.6 mm in width and were held in the four-point probe apparatus with temperature and humidity controlled hydrogen gas. A back-pressure regulator (Globe Tech, Compu Cell GT) was used at the outlet of the anode and cathode. The temperature of the gas was controlled by a Scribner Associates, Inc. Series 890 and associated software, while the temperature of the conductivity cell was controlled by a separate bench-top controller (Omega CSC32). Gamry Instruments Potentiostat and Framework software was used to apply the external voltage to the cell. The conductivity of the hybrid membranes was calculated using the equation, $\sigma = L / (R \times W \times T)$, where L is the distance in the direction of ion flow between voltage probes, W is the measured width of the sample, T is the measured thickness of the sample, and R is the calculated resistance. The resistance

of the sample was calculated via the current and voltage drop measurements, based upon the distance between the 2 measurement electrodes. Sample thickness was obtained by using a Mitutoyo digital micrometer at 5 different locations along the length of the membrane. An average was then taken as representative of the membrane's thickness.

All conductivity tests were performed at a cell temperature of 80°C and with a hydrogen backpressure that varied from 14-20 psi. The humidification of the conductivity cell was determined using the Clausius-Clapeyron equation. The hydrogen gas in the experimental setup leaves the humidifiers at 100% relative humidity at a preset temperature and enters the cell, which was held at constant 80°C. By knowing the initial relative humidity and final temperature of the hydrogen gas, it is then possible to calculate the ΔT necessary to achieve the desired humidity level in the conductivity cell. The Nafion and X-Ionomer hybrid membranes were each tested at the same relative humidity to which they were equilibrated in the afore mentioned humidification jars. The NDMs were each tested at 25%, 50%, and 100% relative humidity.

RESULTS

Table 1 shows conductivity values for Nafion and X-Ionomer control samples; both were tested in 79%, 74%, 51%, and 26% relative humidity environments. The conductivity values for the Nafion Control ranged from 0.0050 S/cm at 26% RH to 0.44 S/cm at 79% RH. The values for the X-Ionomer Control ranged from 0.023 S/cm at 26% RH to 0.27 S/cm at 79% RH.

	Nafion Control Average Conductivity	X-Ionomer Control Average Conductivity
79% Relative Humidity	0.44 S/cm	0.270 S/cm
76% Relative Humidity	0.28 S/cm	0.255 S/cm
51% Relative Humidity	0.22 S/cm	0.330 S/cm *
26% Relative Humidity	0.0050 S/cm	0.023 S/cm
* Represents anomalous data ranging from 0.190 S/cm to 0.530 S/cm		

Table 1. Conductivity Results for Nafion and X-Ionomer Control Samples

Figures 1-4 show topical current-voltage results, and corresponding conductivity calculations, for Nafion hybrid membrane samples. Figure 1 shows results for membranes doped with α-$BW_{12}H$ (1% by weight). Samples were tested at relative humidities of 79%, 51%, and 26% and demonstrated conductivities of 0.21, 0.15, and 0.21 S/cm respectively. Nafion membranes doped with $H_6P_2W_{21}O_{71}$ (5% by weight) tested at relative humidities of 79%, 74% and 51%, demonstrated conductivities of 0.58, 0.10, and 0.15 S/cm respectively (Figure 2). Nafion doped with PW_{12} at 1% by weight, tested at relative humidities of 79%, 74% and 51%, demonstrated conductivities of 0.0061, 0.0081, and 0.53 S/cm respectively (Figure 3). Membrane samples containing PW_{12} at 5% by weight, tested at two relative humidities — 51% and 26%, demonstrated conductivities of 0.27 and 0.0030 S/cm respectively.

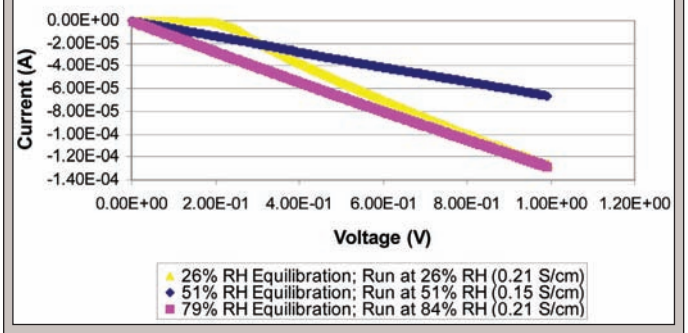

Figure 1. RH Comparison of Nafion with Alpha - $BW_{12}H$ (1% by weight) (4 mV/sec Scan Rate)

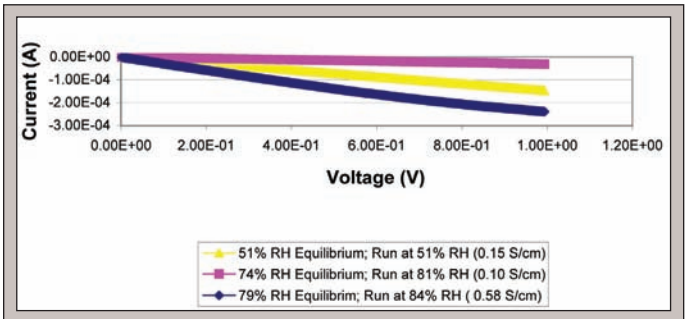

Figure 2. RH Comparison of Nafion with $H_6P_2W_{21}O_{71}$ (5% by weight) (5 mV/sec Scan Rate)

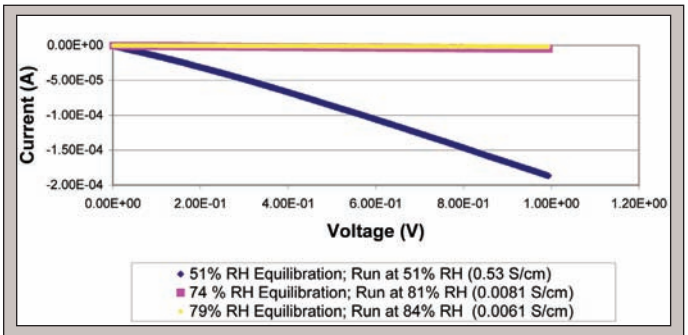

Figure 3. RH Comparison of Nafion with PW_{12} (1% by weight) (5 mV/sec Scan Rate)

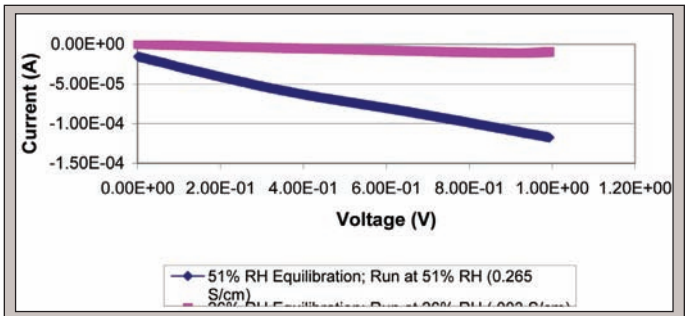

Figure 4. RH Comparison of Nafion with PW_{12} (5% by weight) (5 mV/sec Scan Rate)

Figures 5 and 6 show the current-voltage results, and corresponding conductivity calculations, for X-Ionomer hybrid membrane samples. Figure 5 shows results for membranes doped with α-$BW_{12}H$ at 5% by weight, tested at relative humidities of 79%, 74%, and 51%. They demonstrated conductivities of 0.42, 0.19, and 0.18 S/cm respectively. The results for X-Ionomer membranes doped with $H_6P_2W_{21}O_{71}$ (1% by weight), tested at four relative humidities — 79%, 74%, 51%, and 26%, show conductivities of 0.44, 0.16, 0.16, and 0.38 S/cm respectively (Figure 6).

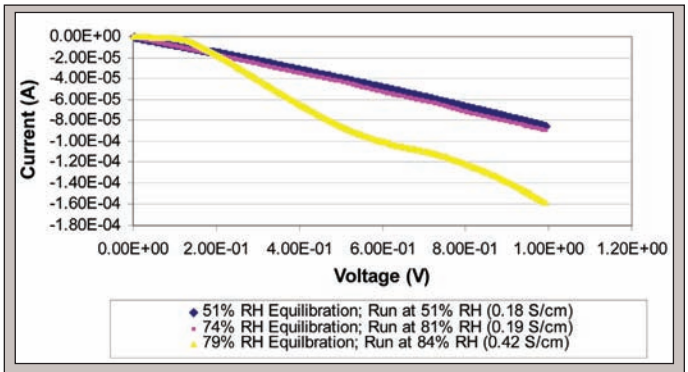

Figure 5. RH Comparison of X-Ionomer with Alpha - $BW_{12}H$ (5% by weight) (5 mV/sec Scan Rate)

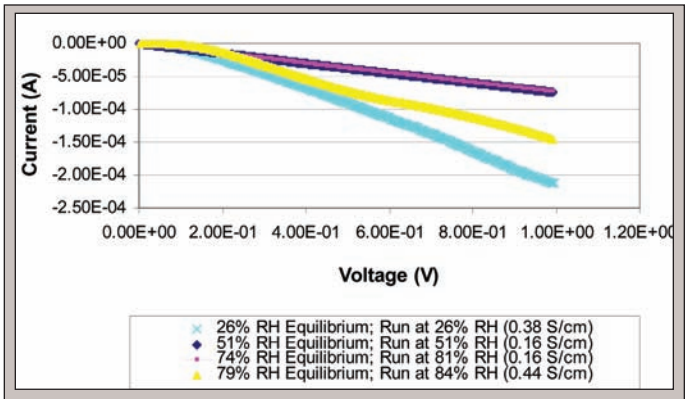

Figure 6. RH Comparison of X-Ionomer with $H_6P_2W_{21}O_{71}$ (1% weight) (5 mV/sec Scan Rate)

Conductivity results for the NDMs are shown in Table 2. Four membrane types were tested, two of which had two different casting dates. Data were collected for each membrane type and each casting date at a constant cell temperature of 80°C at 100%, 50%, and 25% relative humidity. The conductivity data from membrane 20050401B varied between the two casting dates with measurements at 25% RH of 0.0026 S/cm and 0.0000061 S/cm and measurements at 100% RH of 0.0065 and 0.0069 S/cm. Variation was also found between the two castings of membrane 20050404A. Here the data ranged from 0.0050 and 0.00013 S/cm at 25% RH to 0.0059 and 0.013 S/cm at 100% RH. The conductivities of membrane 20050426A ranged from 0.00093 S/cm at 25% RH to 0.0012 S/cm at 100% RH, while those of membrane 20050714B1#1 ranged from 0.0011 S/cm at 25% RH to 0.025 S/cm at 100% RH.

	Conductivity at 100% RH	Conductivity at 50% RH	Conductivity at 25% RH
Cast Date 4/12/05			
20050401B	0.0065 S/cm	0.0045 S/cm	0.0026 S/cm
20050404A	0.0059 S/cm	0.0025 S/cm	0.0050 S/cm
Cast Date 5/11/05			
20050401B	0.0069 S/cm	0.0043 S/cm	0.0000061 S/cm
20050404A	0.0130 S/cm	0.009 S/cm	0.000128 S/cm
20050426A	0.0012 S/cm	0.00027 S/cm	0.00093 S/cm
Cast Date 7/20/05			
20050714B1#1	0.025 S/cm	0.025 S/cm	0.0011 S/cm

Table 2. Conductivity Results for NREL Developed Membranes.

DISCUSSION AND CONCLUSIONS

Conductivity results suggest that the doping of our Nafion and X-Ionomer hybrid membranes with the HPAs of this study increased the conductivity of the membranes. The conductivity values for the Nafion control ranged from 0.0050 S/cm at 26% RH to 0.44 S/cm at 79% RH. Comparatively, at 26% RH the Nafion membranes doped with α-$BW_{12}H$ (1% by weight) and PW_{12} (5% by weight) showed conductivities of 0.21 and 0.0030 S/cm respectively. For the α-$BW_{12}H$, this represents an increase over two orders of magnitude compared to the control. Though the PW_{12} sample showed a conductivity slightly lower than that of the control, this same sample at 51% RH showed a conductivity of 0.27 S/cm, which is twice the conductivity reported in the literature for Nafion 117. The results shown for Nafion doped with α-$BW_{12}H$ (1% by weight) in Figure 1 demonstrate a relatively constant conductivity (near 0.20 S/cm) as the RH is decreased from 79% to 26%. It is notable that at 26% RH this sample showed an increase in conductivity of almost two orders of magnitude compared to the control. Thus, it would be useful to study the effect doping this HPA at a higher weight percent (i.e. 5% by weight) into our Nafion membranes. Figure 2 for Nafion doped with $H_6P_2W_{21}O_{71}$ (5% by weight) shows conductivity at 79% RH of nearly six times that of Nafion 117. Even at a lower RH (51%), this membrane had a conductivity that was comparable the Nafion Control. The anomalous results shown in Figure 3 for Nafion doped with PW_{12} (1% by weight) do not allow for a comparison of the effects of a higher weight percent for this HPA. As shown in the figure, the conductivity of the 1% by weight PW_{12} varies from 0.0061 to 0.53 S/cm as the relative humidity is decreased from 79% to 51%. This is the opposite trend that would be expected and indicates possible systematic error or manufacturing defects during membrane preparation. Thus, further studies should be completed to better understand the relationship between conductivity and higher doping levels for PW_{12}.

The values for the X-Ionomer Control ranged from 0.023 S/cm at 26% RH to 0.27 S/cm at 79% RH. The data collected at 51% RH represent anomalous measurements for the membrane. Three scans were run at this RH — scan A yielded a conductivity of 0.19 S/cm, scan B yielded a conductivity of 0.53 S/cm, and scan C yielded a conductivity of 0.27 S/cm. This data trend suggests the possibility that excess water may have entered the conductivity cell

between scans A and B, resulting in an abnormally high conductivity measurement. The drop seen in the conductivity measurement of scan C indicates that the excess water could have begun to evaporate between the later two scans. Thus, this control membrane should be retested at 51% relative humidity to insure the accuracy of control comparisons.

Figure 5 shows that at 79% RH, doping the X-Ionomer with α-$BW_{12}H$ (5% by weight) increased the conductivity by over 60%, while results at 74% and 51% are on the order of the conductivity of the control. All results presented indicate increased conductivity compared to Nafion 117. Similar results are shown in Figure 6 for the X-Ionomer doped with $H_6P_2W_{21}O_{71}$ (1% by weight). Here, again, at 79% RH, this membrane shows an increase in conductivity of over 60% compared to the control. Though the conductivity drops by a factor of three at 74% and 51% RH, the results at 26% RH (0.38 S/cm) are an order of magnitude higher than that of the control (0.023 S/cm). Thus, it would be useful to study $H_6P_2W_{21}O_{71}$ further, particularly the effect of doping this HPA at a higher weight percent (i.e. 5% by weight). In conclusion, results from this study show promising results for the doping of Nafion and X-Ionomer membranes with HPAs, in particular, α-$BW_{12}H$ and $H_6P_2W_{21}O_{71.}$ The results shown for Nafion doped with PW_{12} suggest that this HPW should also be tested in the X-Ionomer membrane. Overall, in order to advance the technology of low-relative humidity fuel cell membranes, further research is recommended related to the dopant levels of these HPAs.

Though the conductivity results for the NDMs are all significantly lower than that of Nafion 117 (0.0012 – 0.013 at 100% RH), these data represent the first time mechanically flexible PEM films based on PMG with high HPA loading (>100% HPA/ polymer) were fabricated. While more work is needed in modifying the formulation and improving the procedural details in solution preparation and film making, this represents a promising beginning for future work related to covalently bonding HPAs to their host polymer.

ACKNOWLEDGEMENTS

We would like to thank the U.S. Department of Energy, Office of Science for the opportunity to participate in the LSTPD and PST programs and NREL's Hydrogen and Electricity, Systems and Infrastructure Group for hosting us. Special thanks goes to Dr. John Turner for his expertise and patience while mentoring us, and to Jen Leisch and Todd Deutsh for their continuous support. We also thank the Fuel Cell Group at Colorado School of Mines, particularly Dr. Andrew Herring and Niccolo Aieta. Additionally, we thank Dr. John Pern, Dr. Fan-Quin (Jane) Meng, Mei-Chen Kuo, and Jim Horan for membrane and HPA fabrication. Kristen Record would like to thank the Connecticut Clean Energy Fund, Joseph Briganti, Peter Banks, Robert Tramaglio, and the Stratford Board of Education, Stratford, CT. for supporting this fellowship experience.

REFERENCES

[1] W. Vielstich, A. Lamm, H. Gasteiger (Eds.), *Handbook of Fuel Cells – Fundamentals, Technology, Applications*, Wiley, 2003.

[2] S. Yoshioka, A. Yoshimura, H. Fukumoto, O. Hiroi, and H. Yoshiyasu, "Development of a PEM fuel cell under low humidified conditions," *Fuel Cells Bulletin*, 2005, pp. 11-15.

[3] M.A. Sweikart, "Heteropoly Acids for Use as Proton conductors in High Temperature Proton Conducting Membrane Fuel Cells," M.S. Thesis. Golden, CO: Colorado School of Mines, 2004.

[4] I. Honma, H. Nakajima, S. Nomura, "High temperature proton conducting hybrid polymer electrolyte membranes," *Solid State Ionics*, vol. 154-155, 2004, pp. 707-712.

[5] M. Cappadonia, J.W. Erning, S.M.S. Niaki and U. Stimming, "Conductance of Nafion 117 membranes as a function of temperature and water content," *Solid State Ionics*, vol. 77, 1995, pp. 65-69.

[6] T.A. Zawodzinski, T.E. Springer, F. Uribe and S. Gottesfeld, "Characterization of polymer electrolytes for fuel cell applications," *Solid State Ionics*, vol. 60, 1993, pp. 199-211.

[7] I. Honma, H. Nakajima, O. Nishikawa, T. Sugimoto, S. Nomura, "Family of High-Temperature Polymer-Electrolyte Membranes Synthesized from Amphiphilic Nanostructured Macromolecules," *Journal of the Electrochemical Society*, vol. 150, 2003, pp. A616.

[8] H. Nakajima, S. Nomura, T. Sugimoto, S. Nishikawa, I. Honma, "High Temperature Proton Conducting Organic/Inorganic Nanohybrids for Polymer Electrolyte Membrane," *Journal of the Electrochemical Society*, vol. 149, 2002, pp. A953.

[9] R.C.T. Slade, M.J. Omana, "Protonic Conductivity of 12-Tungstophosphoric Acid (TPA, $H_3PW_{12}O_{40}$) at Elevated Temperatures," *Solid State Ionics*, vol. 58, 1992, pp. 195.

[10] S. Malhotra, R. Datta, "Membrane-Supported Nonvolatile Acidic Electrolytes Allow Higher Temperature Operation of Proton-Exchange Membrane Fuel Cells," *Journal of the Electrochemical Society*, vol. 144, 1997, pp. L23-L26.

[11] D.R. Vernon, F. Meng, S.F. Dec, D.L. Williamson, J.A. Turner, A.M. Herring, "Synthesis, characterization, and conductivity measurements of hybrid membranes containing a mono-Lacunary heteropolyacid for PEM fuel cell applications," *Journal of Power Sources*, vol. 139, 2005, pp. 141-151.

[12] R. Reed, J.A. Turner, "Conductivity Analysis of Membranes for High-Temperature PEMFC Applications," *U.S. Department of Energy Journal of Undergraduate Research*, vol. V, 2005.

[13] V. Ramani, H.R. Kunz, J.M. Fenton, "Investigation of Nafion/HPA composite membranes for high temperature/low relative humidity PEMFC operation," *Journal of Membrane Science*, vol. 232, 2004, pp. 31-44.

[14] C. Rocchiccioli-Deltcheff, M. Fournier, R. Franck, R. Thouvenot, "Vibrational Investigations of Polyoxometalates. 2. Evidence for Anion-Anion Interactions in Molybdenum (VI) and Tungsten (VI) Compounds Related to the Keggin Structure," *Inorganic Chemistry*, vol. 22, 1983, pp. 207-216.

[15] G. Brauer, *Handbook of Preparative Inorganic Chemistry*, vol. 2, 2nd Edition, Academic Press, New York, 1963-1965.

[16] T.A. Zawodzinski, M. Neeman, L.O. Sillerud, and S. Gottesfeld, "Determination of Water Diffusion Coefficients in Perfluorosulfonate Ionomeric Membranes," *Journal of Physical Chemistry*, vol. 95, 1991, pp. 6040-6044.

[17] L. Greenspan, "Humidity fixed points of binary saturated aqueous solutions," *Journal of Research*, National Bureau of Standards, vol. 81A, 1977, pp. 89-96.

[18] F.J. Pern, J.A. Turner, A.M. Herring, "Hybrid Proton-Carrier Polymer Composites for High Temperature FCPEM Applications," in *Nanostructured Materials in Alternative Energy Devices*, edited by Erik M. Kelder, Edson Roberto Leite, Jean-Marie Tarascon, and Yet-Ming Chiang (Mater. Res. Soc. Symp. Proc. 822, Warrendale, PA, 2004), S8.6.

Matt Pharr is a junior at Rice University where he is pursuing a double major in mechanical engineering and materials science. He participated in the Science Undergraduate Laboratory Internships (SULI) program in the summer of 2005 at ORNL where he tested properties of silicon carbide for potential use in nuclear fusion and fission reactors. This coming summer he will be doing an internship at the University of Tennessee where he will be examining scintillation materials for use in SPECT/CT/PET scanners. He plans to attend graduate school to earn a PhD in either mechanical engineering or materials science.

Yutai Katoh is a Staff Scientist at Oak Ridge National Laboratory's Materials Science and Technology Division. He received his PhD in materials science from the University of Tokyo and he was Associate Professor of Advanced Energy Materials at Kyoto University for seven years. He specializes in advanced ceramics and composites for energy system applications and is in charge of several DOE fusion and advanced nuclear materials programs. His current research includes development and characterization of ceramic composites for severe environment applications; neutron and high energy particle irradiation effects in metals, alloys and ceramics; and helium effect on irradiation-induced phenomena in metals and ceramics.

Hongbin Bei is currently a Postdoctoral Research Associate at Department of Materials Science and Engineering at the University of Tennessee. He received his PhD in materials science and engineering from the University of Tennessee at Knoxville in 2003, working on directional solidification of intermetallics for high temperature application. His current research includes synthesis of intermetallic composites with well-controlled microstructures and investigation of their small-scale mechanical behavior.

DEPENDENCE OF FRACTURE TOUGHNESS ON CRYSTALLOGRAPHIC ORIENTATION IN SINGLE-CRYSTALLINE CUBIC (β) SILICON CARBIDE

MATT PHARR, YUTAI KATOH, AND HONGBEN BEI

ABSTRACT

Along with other desirable properties, the ability of silicon carbide (SiC) to retain high strength after elevated temperature exposures to neutron irradiation renders it potentially applicable in fusion and advanced fission reactors. However, properties of the material such as room temperature fracture toughness must be thoroughly characterized prior to such practical applications. The objective of this work is to investigate the dependence of fracture toughness on crystallographic orientation for single-crystalline β-SiC. X-ray diffraction was first performed on the samples to determine the orientation of the crystal. Nanoindentation was used to determine a hardness of 39.1 and 35.2 GPa and elastic modulus of 474 and 446 GPa for the single-crystalline and polycrystalline samples, respectively. Additionally, crack lengths and indentation diagonals were measured via a Vickers micro-hardness indenter under a load of 100 gf for different crystallographic orientations with indentation diagonals aligned along fundamental cleavage planes. Upon examination of propagation direction of cracks, the cracks usually did not initiate and propagate from the corners of the indentation where the stresses are concentrated but instead from the indentation sides. Such cracks clearly moved along the {1 1 0} family of planes (previously determined to be preferred cleavage plane), demonstrating that the fracture toughness of SiC is comparatively so much lower along this set of planes that the lower energy required to cleave along this plane overpowers the stress-concentration at indentation corners. Additionally, fracture toughness in the <1 1 0> direction was 1.84 MPa·m$^{1/2}$, lower than the 3.46 MPa·m$^{1/2}$ measured for polycrystalline SiC (which can serve as an average of a spectrum of orientations), further demonstrating that single-crystalline β-SiC has a strong fracture toughness anisotropy.

INTRODUCTION

For the last three decades, silicon carbide (SiC) has been considered a promising candidate for use in nuclear fusion and fission reactors [1-5]. Desirable properties of SiC for such applications include high strength and chemical stabilities [1], low density, low neutron activation [2], and safety at high temperatures [3]. However, before this material is implemented into such nuclear reactors, much care must be taken in extensively examining its properties.

One such property in need of examination is that of room temperature fracture toughness, as SiC demonstrates a relatively low one, with a maximum for polycrystalline SiC of ~4 MPa·m$^{1/2}$ [6-7]. Although basic fracture properties have previously been measured, fracture toughness as a function of spatial orientation has not yet been investigated. Such investigation is important in fully characterizing the fracture properties of SiC, as stresses applied along a certain cleavage plane (in a single-crystalline material) may yield a different value for fracture toughness than would be observed along a different cleavage plane. This phenomenon is related to the number of bonds broken per unit area along different cleavage planes. Since more energy is required to break more bonds, higher fracture toughness is expected along cleavage planes with a higher bond density. Thus, in this study we investigate the crystallographic orientation dependence of fracture toughness in single-crystalline β-(cubic or 3C) SiC.

MATERIALS AND METHODS

Specimen description, preparation, and initial examination

Two different forms of SiC were examined. The first was a 200-micron-thick sample of single-crystalline β-SiC (Hoya Advanced Semiconductor Technologies Co, Ltd.). These crystals were grown as described by H. Nagasawa et al. [8], using an "Undulant-Si" substrate and a process that eliminates most planar defects. Laue back-scattered x-ray diffraction revealed the orientation of the flat edge of the sample, allowing for alignment relative to certain cleavage planes. The other sample was a 2.54-mm-thick film of polycrystalline chemical-vapor-deposited (CVD) SiC. This sample was included to provide direct comparison to the properties associated with fracture toughness in the single-crystalline sample.

Both of these were grinded down to their desired thicknesses. To finalize the preparation of the samples, they were polished using a diamond powder slurry. This polishing process increases the optical reflectivity of the surface so that the crack length can be more accurately measured [10]. Additionally, polishing may eliminate problems associated with initial surface stresses, as a compressive initial surface stress would decrease crack length while a tensile surface stress would do just the opposite [10]. The samples were then mounted to a cylindrical piece of aluminum using CrystalBond™.

Vickers indentation

A micro-indenter with a Vickers tip was used as it has many pertinent advantages as described by Ponton and Rawlings [9]. Primarily, it can be used on a very small sample, proving highly important as the single-crystalline sample was only 200 microns thick. Further advantages include quickness of experimentation and cost effectiveness [9]. However, the most important advantage is that associated with the shape of the indenter. For the single-crystalline sample, it was crucial to implement an indenter that could potentially activate key cleavage planes. In a cubic structure, the shape of the Vickers indenter (a diamond shape with corners situated 90° apart) is highly conducive to cleavage along certain fundamental planes. Additionally, to more easily attempt this activation along key cleavage planes, a rotating stage was implemented. This stage contained 360 degree marks on the circumference so that the sample could be easily rotated by a specified angle.

The samples were first tested with a 2001 Micromet™ (Buehler, Ltd.) Vickers micro-hardness tester. Indentations were performed on each sample at a load of 100 gf for a dwell time of 15 s. Since the single-crystalline sample was relatively thin, a small load was used to help prevent crack breakthrough. However, a load lower than 100 gf was not employed, as crack measurement at such loads is highly difficult and a slight error in determination of crack length has a more significant impact on fracture toughness estimation at these lower loads.

The single-crystalline specimen was first observed under an optical microscope so that the indentation corners were aligned with the {1 0 0} plane. Then, a series of indentations was made at this orientation. Crack lengths and indentation diameters were measured with an optical microscope immediately after indentation to prevent the effect of time dependent slow-crack propagation. A model of the lengths measured is included in Figure 1. As suggested by Osborne, et al., these indentations were spaced both away from the edges of

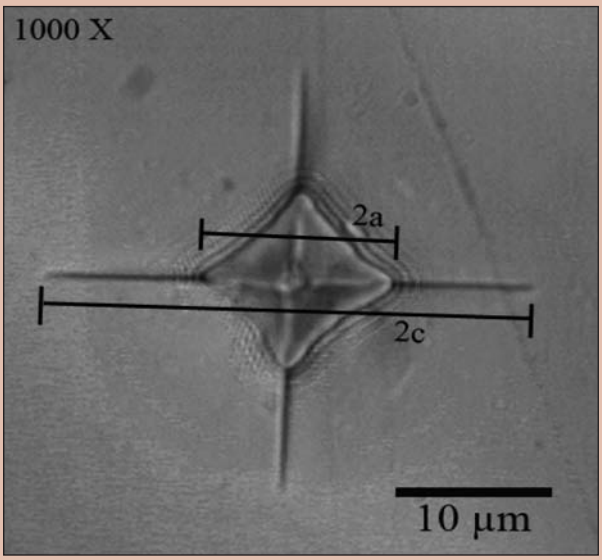

Figure 1. Indentation on single-crystalline β-SiC at load = 100 gf. 2a is indentation diameter, 2c is twice the crack length.

the sample and from one another to prevent possible influence from another indentation or edge [2]. The specimen was then rotated (clockwise) by 22.5° and another series of indentations was made to activate the {2 1 0} family of cleavage planes. Finally, the specimen was rotated (clockwise) by an additional 22.5° and a final series of indentations was made to activate the {1 1 0} cleavage plane. At least five indentations were made at each orientation depending on whether or not crack lengths could clearly be observed. There was no need to rotate the polycrystalline SiC sample. Thus, the procedure simply consisted of making about ten indentations and measuring crack and indentation diameter lengths.

Nanoindentation

Nanoindentation was performed on both samples to determine hardness and elastic modulus by means of a Nanoindenter XP (Nano-instruments, Oak Ridge, TN) equipped with a Berkovich tip. 50-micron-thick single-crystalline and polycrystalline samples were used as larger samples were not necessary since chance of crack breakthrough and effect of substrate can be avoided with such small indentation depths. These samples were mounted with Crystalbond™ on a piece of sapphire was to increase the stiffness. The Oliver and Pharr [14] method was used to calculate the hardness and modulus of the samples. The Berkovich indenter and machine stiffness were carefully calibrated by testing a standard sample of fused quartz. The continuous stiffness mode (CSM) was used in all tests with a maximum depth of 500 nm. Elastic modulus and hardness for each sample were then obtained by taking averages of numerous indentations over the range of a 100-200 nm indentation

depth. This depth was deep enough to avoid problems associated with surface roughness of the specimen and shallow enough that the substrate did not begin to significantly impact the properties of the specimen.

RESULTS AND DISCUSSION

Method used for measurement of fracture toughness

Fracture toughness can be estimated through one of many models present today. Ponton and Rawlings state that the best "all-around" models are those that display the ability to correlate K_C and K_{IC} and demonstrate the best correlating ability as regards five main material classes[10]. After extensive examination into which models appear to work the best, Ponton and Rawlings [10] conclude that the best "all-around" equations are those of the Evans and Charles [11] equation, the Evans and Davis equation [12], and the Shetty, Wright, Mincer, and Clauer equation [13]. However, specifically for SiC, Osborne et al. [2] state that the Evans and Davis equation is quite appropriate. Even though there is no real evidence that models based on half-penny cracks model half-penny cracks prove any better than models based on Palmqvist cracks, this may be because of its pertinence to radial-median (half-penny) cracks as opposed to Palmqvist cracks (as is modeled by Shetty, Wright, Mincer, and Clauer). Thus, for the purposes of this experiment, the Evans and Davis equation will be and is as follows:
where the indentation half-diameter and crack length are represented by 'a' and 'c', respectively, as shown in Figure 1; K_C is the fracture toughness (or critical stress intensity factor); H_V is the Vickers Hardness; and E is the elastic modulus. The relationship between the nano-hardness and the Vickers hardness is found by simple geometric conversion, which is H_V=.9272H_{nano}[9].

$$K_C = H_V \sqrt{a}\left(\frac{E}{H_V}\right)^{2/5} \times 10^F \quad (1a)$$

$$F = -1.59 - .34B - 2.02B^2 + 11.23B^3 - 24.97B^4 + 16.32B^5 \quad (1b)$$

$$B = \log_{10}\left(\frac{c}{a}\right) \quad (1c)$$

Fracture anisotropy in single-crystalline β-SiC

Predictions for fracture toughness were based on the notion that different cleavage planes have different bond densities. Since more energy is required to break more bonds, cleavage planes with higher bond densities should demonstrate higher fracture toughness. Based on the crystal structure of β-SiC (zincblende cubic structure), it was predicted that within the planes normal to the {1 0 0} surface, fracture toughness would be lowest along the {1 1 0} plane, highest along the {1 0 0} plane, and somewhere in-between for the {2 1 0} plane. However, only activation of the {1 1 0} plane was obtained with Vickers indentation testing, as shown in Figure 2. This figure demonstrates that although indentation corners were aligned with different cleavage planes, actual crack propagation did not occur along those desired planes. Thus, the fracture of the single-crystalline sample exhibits very strong crystallographic orientation dependence, as cracks tend to propagate along the preferred cleavage plane, the {1 1 0}, even with higher stress concentration along other planes. Unfortunately, quantifying this dependence proves impossible with the method used as the Evans and Davis equation is based on a wedge-shaped indentation with cracks propagating from indentation corners (as they do not except along the preferred cleavage plane). However, it is important to note that Table 1 demonstrates similar crack length at each orientation despite the cracks not propagating as the Evans and Davis method suggests. Thus, the assumed mechanism may not be exactly responsible for the observed crack extension.

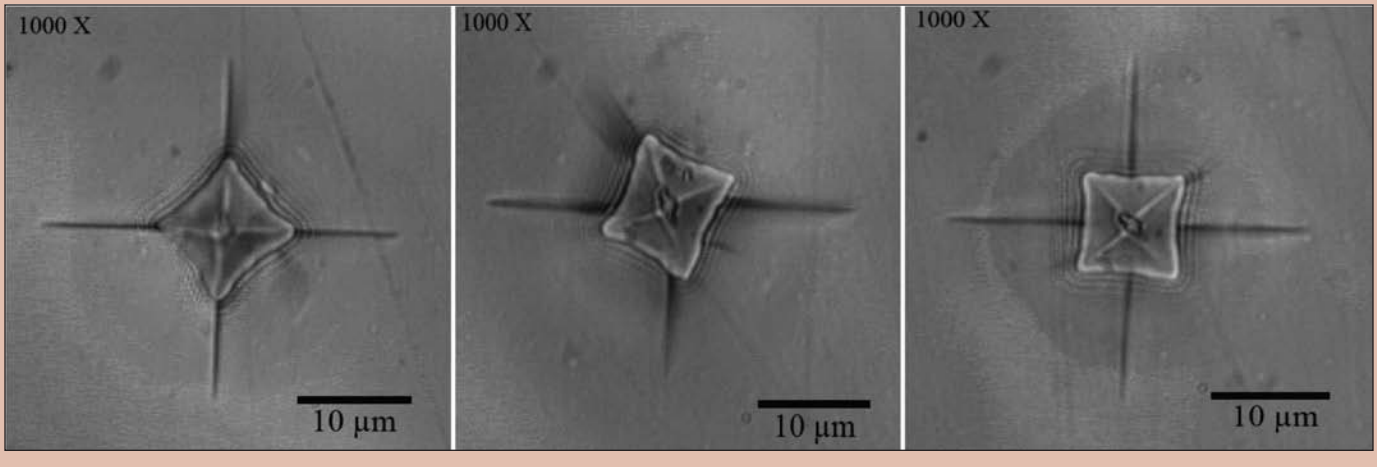

Figure 2. Micrographs showing single-crystalline β-SiC crack propagation directions with indentation diagonals along the: (a). {1 1 0} plane, (b). {2 1 0} plane, and (c). {1 0 0} plane. In all cases, cracks propagate along the {1 1 0} plane.
*Note: Pictures were taken from 50-micron-thick sample; similar behavior was observed in 200 micron sample.

Crystal Type	Degree of Rotation from {1 1 0} plane	Average Crack Length (μm)	Std. Dev.	Average Indentation Diameter (μm)	Std. Dev.	Average Fracture Toughness ($MPa \cdot m^{1/2}$)	Std. Dev.
Single	0	11.60	.569	6.42	.231	1.84	.200
Single	22.5	11.59	.398	6.61	.116	1.95*	.122
Single	45	11.88	.510	6.85	.009	2.02*	.131
Poly	N/A	8.81	.608	8.5	.266	3.46	.156

* - indicates that the following cracks do not propagate along the assumed plane and thus do not follow the method used.

Table 1: Results of micro-indentation with load = 100 gf. Fracture Toughness values were obtained by Eq. (1).

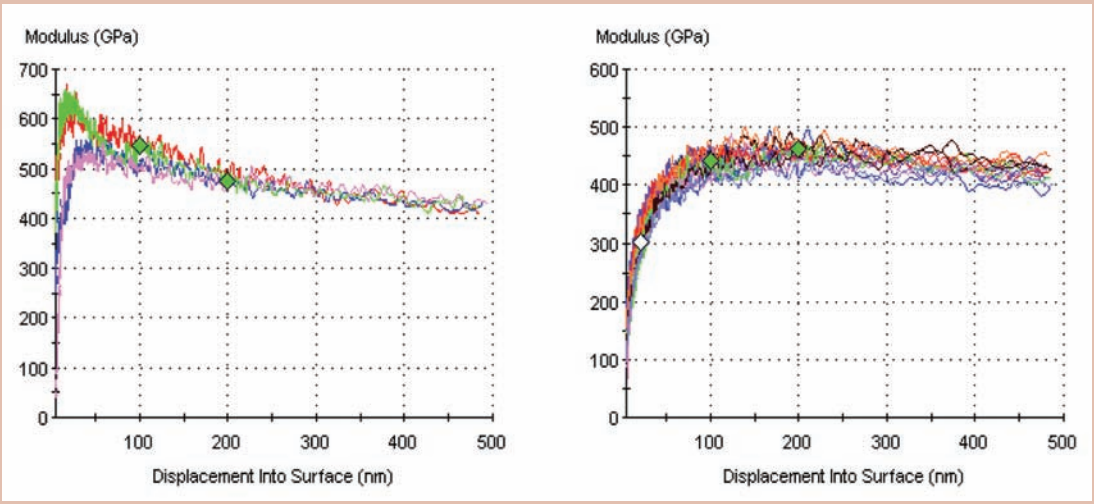

(a) Single-Crystalline Sample (b) Polycrystalline sample

Figure 3. Determination of elastic modulus in the (a) single-crystalline and (b) polycrystalline samples. Averages were taken over the 100 nm to 200 nm depth range.

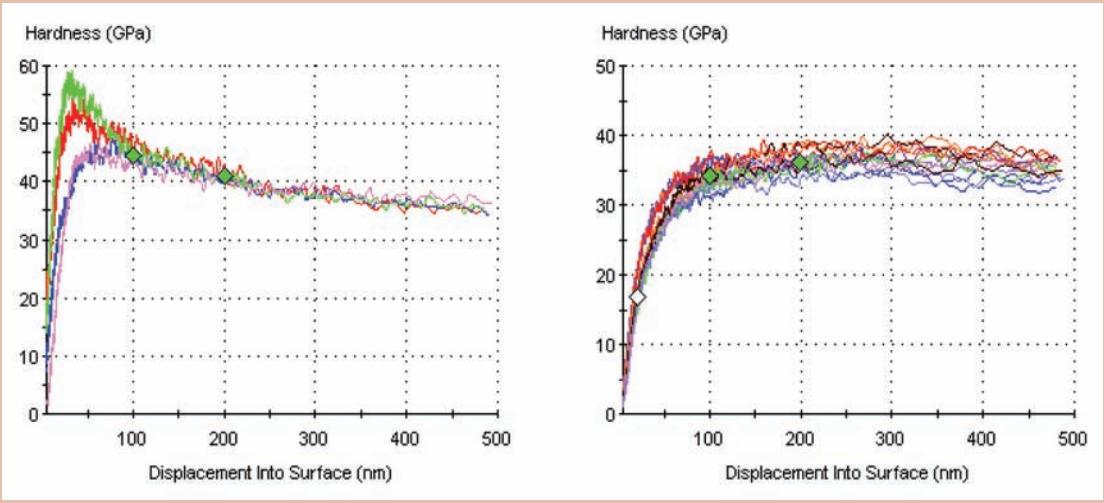

(a) Single-Crystalline Sample (b) Polycrystalline Sample

Figure 4. Determination of nano-hardness in the (a) single-crystalline and (b) polycrystalline samples. Averages were taken over the 100 nm to 200 nm indentation depth range.

Comparison between single-crystalline and polycrystalline samples

Despite the model not being appropriate for each of the orientations within the single-crystalline sample, since cracks did propagate from indentation corners in the <1 1 0> direction, it can be used for comparison between the single-crystalline and polycrystalline samples. For the single-crystalline sample, nanoindentation gave an elastic modulus of ~474 GPa and a hardness of ~39.1 GPa (Figures 3a,4a).

For the polycrystalline sample, nano-indentation gave an elastic modulus of ~446GPa and a hardness of ~35.2 GPa (Figures 3b,4b), indicating a crystallographic orientation dependence of elastic modulus. The results of plugging these and the corresponding crack/indentation diameter lengths into equation (1) are given in Table 1. The important numbers are that of fracture toughness, ~1.84 MPa·$m^{1/2}$ for the single-crystalline sample as opposed to ~3.46 MPa·$m^{1/2}$ for the polycrystalline sample (Table 1). Furthermore, comparison of the cracks in the <1 1 0> direction in the single-crystalline sample and the cracks in the polycrystalline samples (Figures 2, 5) demonstrates that the cracks are straighter in the single-crystalline sample. This deflection found in the polycrystalline sample may show that the cracks are deflecting as to move along cleavage planes with lower bond densities, further demonstrating the orientation dependence of fracture toughness. Unfortunately, it is hard to tell if this deflection is occurring at each grain boundary as it is difficult to determine exactly where the cracks are actually deflecting. However, even if these cracks are not deflecting at each grain boundary, the polycrystalline sample should serve somewhat as an average of all crystallographic orientations possible on a {1 0 0} surface. Thus, the lower fracture toughness found along the preferred cleavage plane in the single-crystalline is sample consistent with the supposition that fracture toughness should be lower along planes with lower bond densities.

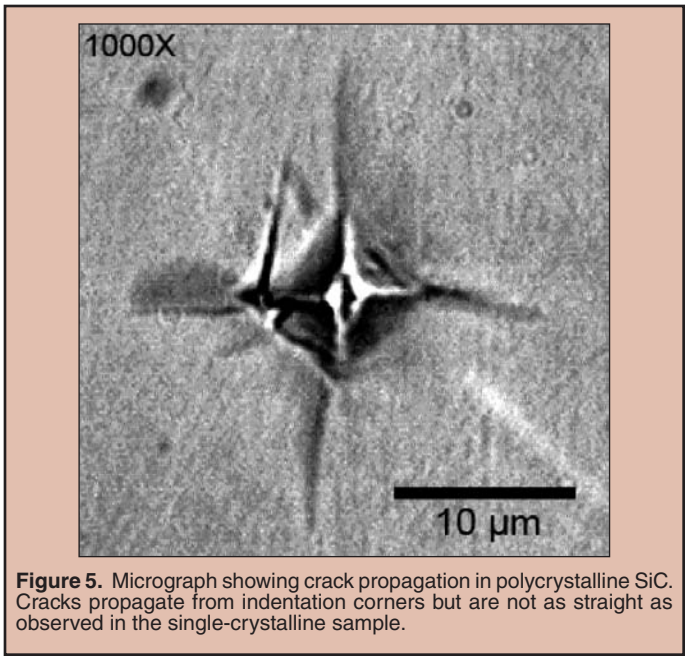

Figure 5. Micrograph showing crack propagation in polycrystalline SiC. Cracks propagate from indentation corners but are not as straight as observed in the single-crystalline sample.

CONCLUSIONS

Fracture morphology demonstrated that cracks did not initiate from indentation corners. Thus, the cleavage planes were not activated as desired, making direct comparison of fracture toughness data obtained at each angle of rotation invalid according to the assumed model. However, this morphology did demonstrate that strong dependence on crystallographic orientation does exist as the cracks clearly initiated and propagated along a preferred cleavage plane despite higher stress concentration along other planes. Additionally, the fracture toughness of the single-crystalline sample along the preferred cleavage plane was much lower than the polycrystalline sample, further demonstrating that fracture toughness does strongly depend on the crystallographic orientation.

ACKNOWLEDGMENTS

This project was performed at Oak Ridge National Laboratory in Oak Ridge, Tennessee. I would like to thank the United States Department of Energy Office of Science for providing funding for the Summer Undergraduate Laboratory Internship (SULI) program that allowed my participation in this rewarding internship. I would additionally like to thank my mentor, Yutai Katoh for his scientific expertise, guidance, and willingness to answer my numerous questions. Special thanks is extended to Hongbin Bei for his help with the micro-indentation and x-ray diffraction equipment and this paper and to Andrei Rar for his help with the nano-indentation equipment.

REFERENCES

[1] A. R. Raffray, R. Jones, G. Aiello, M. Billone, L. Giancarli, H. Golfier, A. Hasegawa, Y. Katoh, A. Kohyama, S. Nishio, B. Riccardi, and M.S. Tillack "Design and material issues for high performance SiC_f/SiC-based fusion power cores," *Fusion and Engineering* Design, 55 [1] 55-95 (2001).

[2] M. Osborne, J. Hay, L. L. Snead, and D. Steiner, "Mechanical- and physical-property changes of neutron-irradiated chemical-vapor-deposited silicon carbide," *Journal of the American Ceramic Society*, 82 [9] 2490-2496 (1999).

[3] R. H. Jones, L. Giancarli, A. Hasegawa,Y. Katoh, A. Kohyama, B. Riccardi, L. L. Snead, and W. J. Weber"Promises and Challenges of SiCf/SiC composites for fusion energy applications," *Journal of Nuclear Materials*, 307, 1057-1072 (2002).

[4] T. Noda, A. Kohyama, and Y. Katoh, "Recent progress of SiC-fibers and SiC/SiC-composites for fusion applications," *Physica Scripta*, 91, 24-29 (2001).

[5] R. H. Jones, D. Steiner, H. L. Heinisch, G. A. Newsome, and H. M. Kerch, "Radiation Resistant Ceramic Matrix Composites," *Journal of Nuclear Materials*, 245, 87-107 (1997).

[6] H. Kodama and T. Miyoshi, "Study of Fracture Behavior of Very Fine-Grained Silicon Carbide Ceramics," *Journal of the American Ceramic Society*, 73 [10] 3081 (1990).

[7] K. Niihara, "Mechanical Properties of Chemically Vapor Deposited Nonoxide Ceramics," *American Ceramic Society Bulletin*, 63 [9] 1160-1164 (1984).

[8] H. Nagasawa, K. Yagi, and T. Kawahara "3C-SiC hetero-epitaxial growth on undulant Si(0 0 1) substrate," *Journal of Crystal Growth*, 237, 1244-1249.

[9] C. B. Ponton and R. D. Rawlings, "Vickers indentation fracture toughness test-part 1-Review of literature and formulation of standardized indentation toughness equations," *Materials Science and Technology*, 5, 865-872 (1989).

[10] C. B. Ponton and R. D. Rawlings, "Vickers indentation fracture toughness test-part 2-application and critical evaluation of standardised indentation toughness equations," *Materials Science and Technology*, 5, 961-976 (1989).

[11] A. G. Evans and E. A. Charles, "Fracture Toughness Determinations by Indentations," *Journal of the American Ceramic Society*, 59 [7-8] 371-372 (1976).

[12] A. G. Evans, "Fracture Toughness: The Role of Indentation Techniques," pp. 112-135 in *Fracture Mechanics Applied to Brittle Materials*. Edited by S. W. Freiman, American Society for Testing and Materials, Philadelphia, PA, 1979.

[13] D. K. Shetty, I. G. Wright, P. N. Mincer, and A. H. Clauer, "Indentation Fracture of WC-Co Cermets," *Journal of Materials Science*, 20, [5] 1873-1882 (1985).

[14] W.C. Oliver and G. M. Pharr, "An Improved Technique for Determining Hardness and Elastic Modulus Using Load and Displacement Sensing Indentation Experiments," *Journal of Materials Research*, 20, 1564–1583 (1992).

Jonathan Huang was born in New Brunswick, NJ and grew up in Princeton. He attended Dartmouth College, double-majoring in math and physics. During his undergraduate career, he held two SULI internships at the Princeton Plasma Physics Laboratory in the winter and summer of 2005. He hopes to enter a PhD program in mathematics and become a professor. His interests include chess and ultimate frisbee.

Jon Menard, Princeton Plasma Physics Laboratory (PPPL), received the Presidential Early Career Award for Scientists and Engineers. He is an experimental plasma physicist who works primarily on the National Spherical Torus Experiment (NSTX) at PPPL. Dr. Menard's research interests include the linear and non-linear magnetohydrodynamic (MHD) stability properties of spherical torus (ST) plasmas, advanced operating scenarios in the ST, plasma startup, and high-harmonic fast wave physics, and performing studies to optimize the stability of fusion plasmas and providing the heart of the physics basis for a new, spherical plasma fusion reactor. After receiving a bachelor's degree in nuclear engineering from the University of Wisconsin-Madison in 1992, Dr. Menard went on to receive a master's and a Ph.D. in plasma physics from Princeton University, Department of Astrophysical Sciences, in 1994 and 1998, respectively. He conducted post-doctoral research at PPPL before joining the research staff in 1999. Among his honors, Menard was awarded the Presidential Early Career Award in Science and Engineering in 2004, the "Best Student Paper" award from the American Nuclear Society Fusion Energy Division in 1998, the Princeton University Honorific Fellowship in 1996, and the U.S. Department of Energy Magnetic Fusion Science Fellowship in 1993. The PPPL is funded by the DOE and managed by Princeton University.

DEVELOPMENT OF AN AUTO-CONVERGENT FREE-BOUNDARY AXISYMMETRIC EQUILIBRIUM SOLVER

JONATHAN HUANG, JON MENARD

ABSTRACT

The calculation of the magnetic flux given an assumed value for the current profile in axisymmetric toroidal plasmas is essential in studying the effects of various magnetohydrodynamic (MHD) instabilities upon controlled fusion. To this end, an iterative, modular algorithm coupled with a fast, direct elliptic solver for the Grad-Shafranov equation has been used to reconstruct the desired free-boundary equilibrium solution. This free-boundary Grad-Shafranov (FBGS) equilibrium algorithm is modified with the application of the von Hagenow method for determining the flux on the computational boundary, greatly reducing the time cost from $O(N^3)$ to $O(N^2 \ln N)$ machine operations as compared to current Green's function methods. The inherent variance in implementing the von Hagenow method gives a mean error bound of 0.1 percent with respect to the normal Green's method. The improvements will allow the grid resolution to be increased efficiently and automatically to reduce the maximum Grad-Shafranov error to values needed for accurate stability calculations on a more effective time scale.

INTRODUCTION

The National Spherical Torus Experiment (NSTX) is a medium-sized, low aspect ratio spherical torus (ST) device—a cost-effective, innovative, and compact magnetic confinement concept designed to explore high-beta stability and plasma confinement as a "proof of principle" for controlled fusion. Parameters for the machine are a major radius of R = 0.85 m, minor radius a = 0.67 m, and an aspect ratio R/a = 1.26, with a typical toroidal field B_T < 0.6 T and plasma current of 0.3–1.5 MA.

The shape of the plasma and location of the plasma boundary greatly affect its stability and, therefore, its attractiveness for controlled fusion. Since the electromagnetic fields influence the movement of the plasma which itself induces electromagnetic fields, determining this shape may quickly lead to nonlinear equations. One simple way of studying magnetically confined plasmas with an emphasis on the shaping magnetic field topology is magnetohydrodynamics (MHD), the principle whereby the plasma is treated as a single, electrically-conducting fluid. Certain MHD modes cause alterations in the plasma topology that form magnetic islands, which may lead to large disruptions in a magnetic confinement device. For instance, in NSTX plasmas the 1/1 internal kink mode has been observed to induce energetic ion loss by a factor of 3–5 and cause flattening in the toroidal rotation profile within the plasma core [1].

To understand these and others MHD modes and their resulting impact, it is essential to be able to both accurately predict and reconstruct free-boundary MHD equilibria based on experimental measurements. Moreover, these equilibria are important in reproducing plasma configurations, implementing plasma shape control, and studying the plasma-wall interactions. Equilibria represent the simplest solution to a dynamical system, and thus are a natural starting point. Furthermore, reconstructing sequences of equilibria may be used to model the time evolution of the plasma as a quasi-static approximation.

MHD equilibrium is predicated upon the force balance equation, $\nabla p = \mathbf{J} \times \mathbf{B}$, where p is the pressure, $\mathbf{J}$ the current density,

and **B** the magnetic field. This is the static solution to the ideal MHD equations; it determines the plasma shape and the external fields required for confinement. Noting that from Ampére's Law, $\nabla \times \mathbf{B} = \mu_0 \mathbf{J}$, and from Maxwell's equations, $\nabla \cdot B = 0$, the force balance equation may be simplified in a toroidally symmetric system to the so-called Grad-Shafranov equation. In cylindrical coordinates, this is a non-linear, two-dimensional elliptic partial differential equation whose solution is obtained by a freeboundary Grad-Shafranov (FBGS) algorithm.

In this paper, we present the development of a predictive free-boundary auto-convergent axisymmetric equilibrium solver named ISOLVER. ISOLVER takes normalized pressure and current profiles and boundary shape as input, matches a specified plasma current and β, and computes coil currents as its output. At its core, it contains a modular, iterative algorithm coupled with a fast, direct elliptic solver to the Grad-Shafranov equation. To improve the calculation of the boundary condition for the elliptic equation, the von Hagenow method is implemented. This greatly reduces the time cost of the algorithm, making the time-limiting factor the solution to the differential equation. The grid resolution may be efficiently increased to reduce the maximum Grad-Shafranov error to necessary values for accurate stability calculations. Furthermore, a convergent solution may be calculated once and stored for a given computational grid, and accessed for a particular current profile on a much faster time scale.

In the following section, we shall describe in detail the main FBGS algorithm, including an analysis of the time cost. In Section 3, we shall explain the von Hagenow method, including the nuances of dealing with the inherent logarithmic singularity, and fully describe the significant reduction in time cost. In Section 4 we present a full error analysis of the code, and in Section 5 we shall give concluding remarks and discuss future work.

Main Algorithm

A good example of a FBGS algorithm is the EFIT code which has been used as a freeboundary equilibrium reconstruction technique for many magnetic confinement devices, including DIII-D, JET, and JT-60U. Here we shall describe the main components of codes like EFIT; more rigorous derivations may be found in [2].

The FBGS algorithm solves the Grad-Shafranov equation, which is derived from the force balance equation. Using cylindrical (R, ϕ, Z) coordinates, Maxwell's equations imply that the magnetic field may be expressed as the curl of a vector potential $\mathbf{A} = (A_R, A\phi, A_Z)$. Exploiting of axisymmetric geometry results in the following form for the magnetic field

$$\mathbf{B} = \nabla\phi \times \nabla\Psi(R,Z) + g(R,Z)\nabla\phi \qquad (1)$$

where we define the poloidal flux function $\Psi(R,Z) = -RA_\phi$ and the toroidal field function $g(R,Z) = R(\partial A_R/\partial Z - \partial A_Z/\partial R)$. From Ampére's Law we recognize that the current may be expressed as

$$\mu_0 \mathbf{J} = \Delta^* \Psi \nabla\phi + \nabla g \times \nabla\phi \qquad (2)$$

where we have defined the toroidal elliptic operator as $\Delta^*\Psi \equiv R^2\nabla \cdot (1/R^2)\nabla\Psi$.

Using the axisymmetric forms for the magnetic field from Equation (1) and the current from Equation (2) in the force balance equation, and taking the projection onto the vectors **J** and $\nabla\phi$, we see that p and g are functions of the poloidal flux Ψ. Taking the projection onto the vector $\nabla\Psi$, we obtain the Grad-Shafranov equation $\Delta^*\Psi + \mu_0 R 2p'(\Psi) + gg'(\Psi) = 0$. Equivalently, we may define the toroidal current density $J\phi$ as constructed from the two flux functions $p(\Psi)$ and $gg'(\Psi)$ which are the plasma pressure gradient and the poloidal current functions, respectively, and thus represent the Grad-Shafranov equation as $\Delta^*\Psi = \mu_0 R J_\phi(R,\Psi)$. Hence, an assumed form for the toroidal current profile is dictated by the 3 plasma pressure gradient and the poloidal current functions. In EFIT, these are usually given by a set of basis functions of the normalized flux Ψ_n which are second order polynomials for $p(\Psi)$ and second or third order polynomials for $gg(\Psi)$ [3]. In ISOLVER, $p(\Psi)$ and $\langle \boldsymbol{J} \cdot \boldsymbol{B} \rangle(\Psi)/\langle B \cdot \nabla\phi \rangle$ are the specified profiles and the sound-speed Mach number $M_S(\Psi)$ is also specified to include the effects of plasma rotation on the equilibrium.

The Grad-Shafronov equation given in cylindrical coordinates,

$$R\frac{\partial}{\partial R}\frac{1}{R}\frac{\partial\Psi}{\partial R} + \frac{\partial^2\Psi}{\partial Z^2} = \mu_0 R J_\phi R J\phi(R,\Psi) \qquad (3)$$

is a separable elliptic partial differential equation. This may be handled by using Fast Fourier Transform techniques or applying the generalized Buneman Algorithm. A consistent solution to the elliptic equation is found by iterating on the Ψ dependence in the source function $\mathbf{J}_\phi(R,\Psi)$ with a Picard iteration technique, $\Delta^*\Psi^{n+1} = \mu_0 R J\phi(R,\Psi^n)$. The iteration is kept convergent by altering $J\phi$ through the free functions $p(\Psi)$ and $g(\Psi)$ to meet the specified constants.

In order to solve Equation (3), the flux along the computational boundary must be provided as a boundary condition for the elliptic solver. To determine the boundary flux given the plasma toroidal current density and the current Ic measured in conductors located outside the plasma boundary at positions (R^i_c, Z^i_c), we employ the Green's function for the differential operator $\Delta^*\Psi$,

$$G(R,R') = \frac{\mu_0}{2\pi}\frac{\sqrt{RR'}}{k}[(2-k^2)K(k^2) - E(k^2)] \qquad (4)$$

$$\text{where the argument } k2 = \frac{4RR'}{(R+R')^2 + (Z-Z')^2}$$

and $K(k^2)$ and $E(k^2)$ are the complete elliptic integrals of the first and second kind, respectively. The Green's function by definition satisfies $\Delta^*G(\mathbf{R},\mathbf{R}') = \delta(\mathbf{R}-\mathbf{R}') = R\delta(\mathbf{R}-\mathbf{R}')\delta(Z-Z')$ and the flux function satisfies

$$\Delta^*\psi(R) = \mu_0 R J\phi(R) = \mu_0 R J\phi(R,Z) \text{ in plasma}$$
$$= \mu_0 \Sigma\, RIi\delta(R-R^c_i)\delta(Z-Z^c_i) \text{ in vacuum}$$

where Nc is the total number of coils, and (R^c_i, Z^c_i) is the position of and I_i the current in the ith coil.

In order to use these relations to solve for the boundary flux, first consider the following vector identity applied to Ψ and G,

$$\nabla \cdot \left(\Psi\frac{1}{R^2}\nabla G - G\frac{1}{R^2}\nabla\Psi\right) = \Psi\frac{\Delta^*G}{R^2} - G\frac{\Delta^*\Psi}{R^2} \qquad (5)$$

Letting the observation point (R', Z') lie on the computational boundary, integrate Equation (5) over all space. Using the Divergence Theorem, the left hand side reduces to surface integrals which vanish

at infinity. After integration, the first term on the right hand side becomes the boundary flux. Integration over the second term on the right hand side may be broken into integrating over the plasma and the vacuum. Hence, we have for the flux boundary

$$\begin{aligned}\Psi_b(R',Z') &= \int_{\text{plasma}} G(\mathbf{R};\mathbf{R}')\frac{\Delta^*\Psi(\mathbf{R})}{R^2} + \int_{\text{vacuum}} G(\mathbf{R};\mathbf{R}')\frac{\Delta^*\Psi(\mathbf{R})}{R^2} \\ &= \mu_0 \int_{\text{plasma}} G(\mathbf{R},\mathbf{R}')J_\phi(\mathbf{R})\,dR\,dZ + \mu_0 \sum_{i=1}^{N_c} G(R_i^c, Z_i^c; R', Z')I_i \qquad (6)\end{aligned}$$

In summary, a FBGS algorithm takes an initial guess for the toroidal current profile J_{ϕ} and executes an iterative technique to compute a convergent flux solution. Once given a boundary condition flux, the algorithm solves Equation (3) using a fast direct method for elliptic equations. Inverted, the elliptic equation has the following finite difference form

$$\begin{aligned}&\frac{R_i}{\Delta R^2}\left[\frac{1}{R_{i+1/2}}\left(\Psi_{i+1,j}^{n+1} - \Psi_{i,j}^{n+1}\right) - \frac{1}{R_{i-1/2}}\left(\Psi_{i,j}^{n+1} - \Psi_{i-1,j}^{n=1}\right)\right] \\ &\quad + \frac{1}{\Delta Z^2}\left[\Psi_{i,j+1}^{n+1} - 2\Psi_{i,j+1}^{n+1} + \Psi_{i,j+1}^{n+1}\right] = \mu_0 R_i J_{\phi i,j}^n \qquad (7)\end{aligned}$$

A Fast Fourier Transform technique would require N transforms for $J_{\phi ij}$, where N is the number of grid points in the Z direction (index j), each requiring $O(N\ln N)$ operations. After solving the $5M$ tri-diagonal equations where M is the number of grid points in the R direction (index i), another N transforms are required to bring the solution back into $\Psi_{i,j}$. In total, the number of operations required to solve the elliptic equation is $O(N^2 \ln N)$.

To arrive at a boundary solution, the integral in Equation (6) must be evaluated. The two dimensional integral becomes a double sum over R and Z, which can be expensive to evaluate. Assuming there are N grid points in each direction, to evaluate this sum requires $O(4N^3)$ operations, and determining the flux on the computational boundary can become the limiting factor in the FBGS algorithm. The algorithm iterates the boundary flux computation through the current profile given by a consistent flux solution until the boundary flux and other profiles converge

Von Hagenow Method

The von Hagenow Method[4] is a technique used to greatly reduce the time cost in calculating the boundary flux Ψ_b. Namely, it implements a new method of evaluating the costly integral in Equation (6).

First, consider a psuedo-flux function $U(R,Z)$ that satisfies the same elliptic equation as Ψ but is canonically 0 on the boundary. Then, applying the same vector identity as in Equation (5) now to U and G, we have that

$$G\frac{\Delta^* U}{R^2} = U\frac{\Delta^* G}{R^2} - \nabla\cdot\left(U\frac{\nabla G}{R^2}\right) + \nabla\cdot\left(G\frac{\nabla U}{R^2}\right) \qquad (8)$$

where we choose the observation (R',Z') to be a small distance outside the computational boundary, and we take the limit as $\epsilon \to 0$.

Integrating the expression in Equation (8) over the computational domain, and using the relations for $\Delta^* U$, the term on the left hand side becomes the sought-after integral in Equation (8). Noting the behavior of U on the boundary, the integral of the first term on the right hand side vanishes, and so does the second term after application of the divergence theorem. Thus, we arrive at the following expression for the desired integral

$$\mu_0 \int_{\text{plasma}} G(\mathbf{R},\mathbf{R}')J_\phi(\mathbf{R})\,d\mathbf{R} = \int_{\text{boundary}} \frac{G(\mathbf{R},\mathbf{R}')}{R}\frac{\partial U}{\partial n}\,d\ell \qquad (9)$$

This line integral around the boundary is much cheaper to evaluate than the whole integral over the computational domain. First, the inherent symmetries in the Green's function for the toroidal elliptic operator reduce the number of total evaluations needed. Noting closely the form in Equation (4), we see that $G(\mathbf{R},\mathbf{R}')$ is symmetric in its arguments and is only dependent on the three variables R, R', and $(Z - Z')^2$. These symmetries reduce the number of calculations of the Greens function from $16N^2$ to close to $3N^2$ machine operations. The solution to the psuedo-flux U may be found using similar fast direct methods as for the original flux, which takes $O(N^2 \ln N)$ as previously discussed. The derivative may be easily and accurately approximated by analytically differentiating a three-point bicubic spline interpolation. Thus, the time limiting factor has been reduced to solving the elliptic equation.

The problem that arises using this method to compute the boundary flux is the behavior of the Green's function $G(\mathbf{R},\mathbf{R}')$ at the point $(R,Z) = (R',Z')$. The boundary integral that we seek to evaluate given by Equation (9) has a logarithmic singularity which can be removed analytically. The Green's function term behaves like

$$g(\mathbf{R},\mathbf{R}') \equiv \frac{G(\mathbf{R},\mathbf{R}')}{R} \simeq -\frac{1}{4\pi}\ln\left(\frac{\ell - \ell_0}{2R_0}\right)^2 \qquad (10)$$

with a singularity at the boundary $\ell = \ell_0$, where we have parameterized $\mathbf{R} = \mathbf{R}(\ell)$ and $\mathbf{R}' = \mathbf{R}(\ell_0)$

The removal of the logarithmic singularity may be dealt with in several ways, the most accurate and straightforward of which is to express the derivative as $\partial U/\partial n$ = constant + $\partial U'/\partial n$ where the variable term $\partial U'/\partial n$ vanishes at the singularity. Thus, we may analytically evaluate the singular behavior of the Green's function term $g(\mathbf{R},\mathbf{R}')$ around the boundary and numerically integrate the remaining terms which are no longer exhibit singularities.

Specifically, to evaluate the integral at the boundary point given by ℓ_0, we first express the derivative as

$$\frac{\partial U(\ell)}{\partial n} = \frac{\partial U(\ell_0)}{\partial n} + \left(\frac{\partial U(\ell)}{\partial n} - \frac{\partial U(\ell_0)}{\partial n}\right) \qquad (11)$$

And the total Green's function term is broken into its singular component $gs(\boldsymbol{\ell})$ given by Equation (10) and non-singular component $gns(\boldsymbol{\ell})$ which is determined by simply subtracting out the singular component from the total. Thus the line integral may treated by three separate integrands,

$$\int g(\ell)\left(\frac{\partial U(\ell)}{\partial n} - \frac{\partial U(\ell_0)}{\partial n}\right)d\ell + \frac{\partial U(\ell_0)}{\partial n}\int g_s(\ell)d\ell + \frac{\partial U(\ell_0)}{\partial n}\int g_{ns}(\ell)d\ell \qquad (12)$$

The first integral no longer has a singularity due to the behavior of the variable derivative term, and the third integral is easily evaluated. The second integral may be determined analytically.

RESULTS

In the implementation used for the following results, we have used for computational convenience a simpler approximation to the integration through the logarithmic singularity. Instead of the method described in Section 3, we simply treat the singularity locally at the two points closest to the singularity, replacing the entire Green's function term by the singular approximation and ignoring the non-singular part. Though less accurate, this calculation remains viable since the local contribution missing from the non-singular term at the singularity is almost negligible around the whole boundary. The mean relative contribution is 0.00035, decreasing the computed boundary flux result from its actual value.

Figure (1) shows the entire computed boundary solution plotted linearly for the von Hagenow method (plotted in black) and the slower summing Green's function method (plotted in red). Figure (2) shows a closer comparison at each side of the computational boundary. The maximum error against the Green's method calculated boundary values was observed to be 0.00019 for the bottom, 0.00196 for the right, 0.00022 for the top, and 0.00016 for the left, with respective mean relative errors of 0.02326, 0.02326, 0.00301, and 0.00598. Figure (3) shows the ratio of the regular computed value over the von Hagenow computed value. Figure (4) shows the inherent computational variance in the von Hagenow and Green computed boundary, and the ratio of disagreement. The inherent mean relative error is 0.00174.

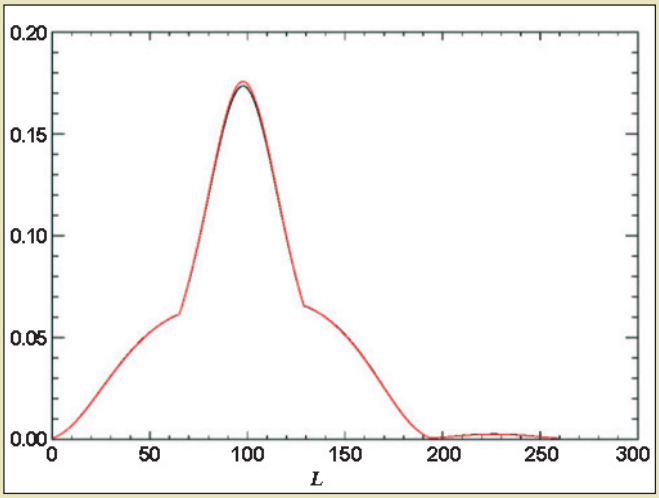

Figure 1. Linear plot of the entire boundary solution with and without von Hagenow implementation

Figure (5) contains contour plots of the equilibrium flux computed using the von Hagenow and the Green's method to compute the boundary flux.

A more exact application of the von Hagenow method should differ from the normal Green's method by a limiting inherent relative error of 0.1 percent. However, it is clear from Figure (2) that the error in the bottom and right side of the boundary are off by an order of magnitude, which is larger than expected from ignoring the local contribution of the non-singular Green's term to the boundary flux. These systematic errors affect the entire equilibrium solution. Furthermore, the behavior of the error and ratios at the corners of the boundary are not consistent with the fact that the approximation of the pseudo-flux derivative $\partial U/\partial n$ is canonically set to vanish at the corner values. This points at possible minor errors in the specific application of the von Hagenow method and treatment of the Green's function term at the singularity.

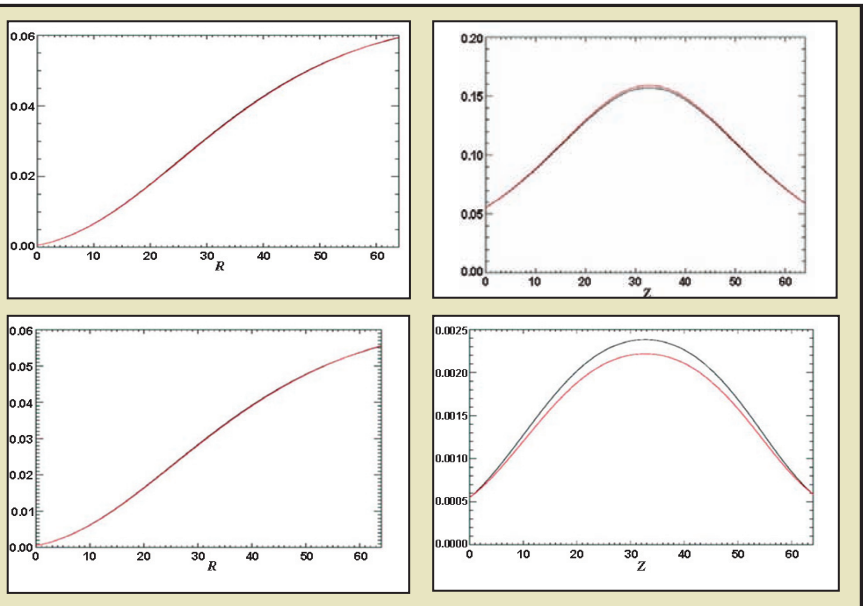

Figure 2. Plots of the boundary flux.

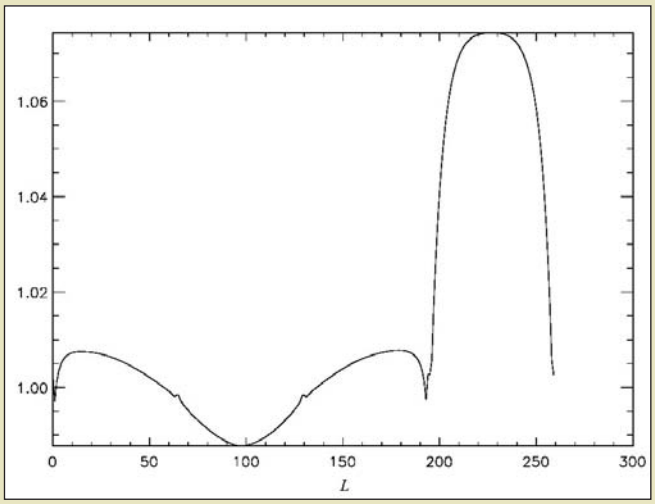

Figure 3. Ratio of von Hagenow computed value versus normal value.

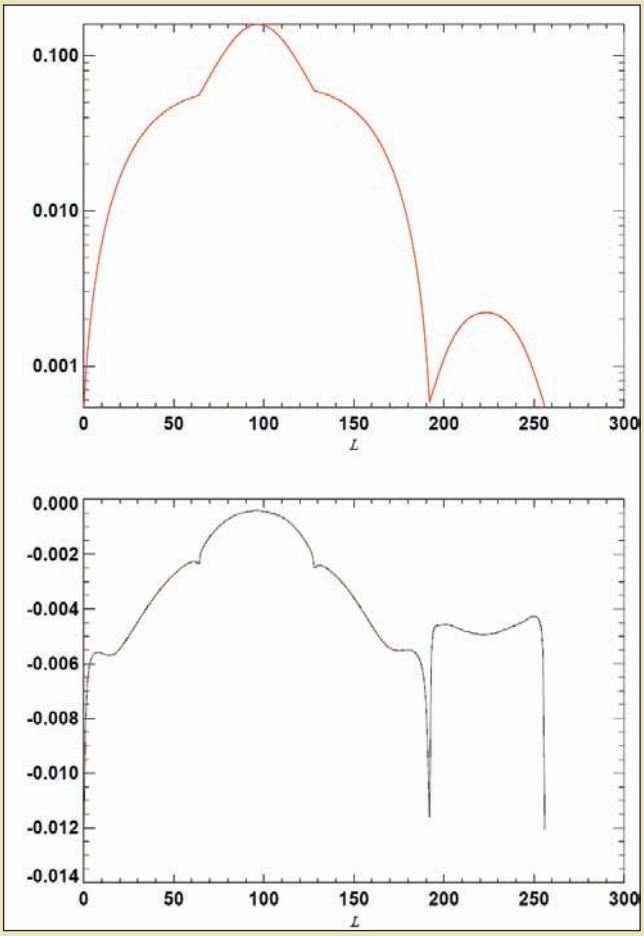

Figure 4. Inherent variance in von Hagenow method and ratio.

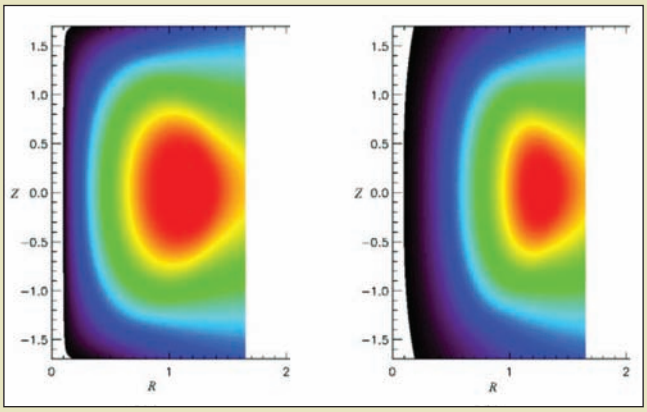

5(a) Contour plot of Ψ using von Hagenow method

5(b) Contour plot of Ψ using normal Green's method

Figure 5. Contour plots of the equilibrium flux.

DISCUSSION AND CONCLUSIONS

A sufficiently accurate application of the von Hagenow method in a modified implementation of the FBGS algorithm has been accomplished. The costly computation of the boundary flux has been greatly reduced so that the limiting factor in the total equilibrium algorithm becomes the solution of the differential equation, which may be handled using fast direct elliptic methods. The total time cost reduces from $O(N4)$ to $O(N^2 \ln N)$.

Future studies should investigate the behavior of the Green's function term at the corner boundary values, and reduce the disagreement in the von Hagenow method to below 0.1 percent. Furthermore, the method should be implemented to create a more modular FBGS algorithm, computing the necessary values once for a given grid resolution, which may be changed efficiently to reduce the maximum Grad-Shafranov error. The improved FBGS algorithm may be implemented within ISOLVER, which computes free-boundary equilibria.

ACKNOWLEDGEMENTS

The author would like to thank Dr. J. Menard for his guidance throughout this project and many helpful discussions and Mr. J. Morgan for his support. The work was completed within the Science Undergraduate Laboratory Internship program in the Office of Science of the U. S. Department of Energy under DE-AC02-76CH0307.

REFERENCES

[1] J. E. Menard, R. E. Bell, E. D. Fredrickson, et al., "Internal kink mode dynamics in high-beta nstx plasmas," *Nucl. Fus.,* vol. 45, pp. 539–556, 2005.

[2] L. L. Lao, H. St. John, R. D. Stambaugh, et al., "Reconstruction of current profile parameters and plasma shapes in tokamaks," *Nucl. Fus.,* vol. 25, no. 11, p. 1611, 1985.

[3] S. A. Sabbagh, S. M. Kaye, J. Menard, et al., "Equilibrium properties of spherical torus plasmas in nstx," *Nucl. Fus.,* vol. 41, no. 11, p. 1601, 2001.

[4] S. C. Jardin, N. Pomphrey, and J. Delucia, "Dynamic modeling of transport and positional control of tokamaks," *Journal of Comp. Phys.,* vol. 66, no. 2, pp. 481–507, 1986.

Scott Pinegar received a B.A. in physics from the University of Colorado at Boulder in 2001 and has been an astrophysics and earth science Teacher at Pomona High School since 2001. He is a second year Laboratory Science Teacher Professional Development (LSTPD) teacher at the National Renewable Energy Laboratory (NREL). He is in the beginning stages of a masters program in Applied Mathematics at the University of Colorado at Denver.

Derek Nalley is a student at Purdue University who plans on becoming a physics teacher. During the summer of 2005, he worked on research at National Renewable Energy Laboratory as part of the Pre-Service Teacher Program.

Keith Emery is currently a Group Manager in Cell and Module Performance and acting Group Manager of the Electro-Optical Characterization Groups at the National Renewable Energy Laboratory, responsible for photovoltaic cell and module calibrations and efficiency verification. He leads a team that is ISDO 17025 accredited for primary reference cell, secondary reference cell, and secondary module calibrations. Over the past 26 years, his group has supplied the PV community with a formal calibration traceability path and developed internationally accepted PV performance measurement procedure. Mr. Emery graduated from Michigan State University with a B.S. degree in Physics and a Masters in Electrical modeling chemical lasers. He also worked at Colorado State University on transparent conducting oxides on Si and chemical vapor deposited oxides and nitrides using lasers and electron beams.

LINEARITY TESTING OF PHOTOVOLTAIC CELLS

Scott Pinegar, Derek Nalley, and Keith Emery

ABSTRACT

Photovoltaic devices are rated in terms of their power output or efficiency with respect to a specific spectrum, total irradiance, and temperature. In order to rate photovoltaic devices, a reference detector whose response is linear with total irradiance is needed. This procedure documents a procedure to determine if a detector is linear over the irradiance range of interest. Testing the short circuit current versus the total irradiance is done by illuminating a reference cell candidate with two lamps that are fitted with programmable filter wheels. The purpose is to reject nonlinear samples as determined by national and international standards from being used as primary reference cells. A calibrated linear reference cell tested by the two lamp method yields a linear result.

INTRODUCTION

Photovoltaic devices are rated by their power output over a specific total irradiance, spectrum, and temperature. Rating these systems requires a reference detector that must have a linear response over the ranges of interest according to the ASTM and IEC standards [8]. Measurements of linearity are usually done in two ways; measuring the short circuit current versus total irradiance as the total irradiance is varied, or measuring the quantum efficiency versus bias light [1,2,3,4,5,6,7].

Short Circuit Current vs. Total Irradiance

The short circuit current (I_{sc}) is measured over a shunt resistor connected to a sample that is illuminated over a varied total irradiance (E_{tot}) [1,2,3,4]. Measuring I_{sc} versus E_{tot} assumes that the spatial non-uniformity does not change as the total irradiance is varied. This method also assumes that the spectrum does not change with total irradiance because if the spectrum changes with total irradiance then the spectral error changes with total irradiance causing an error in the measured total irradiance. The last assumption is the temperature and ambient light stays constant throughout the test [1,2,3,4].

Quantum Efficiency vs. Bias Light

Quantum efficiency or spectral irradiance $E_s(\lambda)$ is measured versus the bias light [5,6,7]. The quantum efficiency versus bias light test requires a low noise quantum efficiency system that operates at low light levels and at the one sun value of 1000W/m^2. The National Institute of Standards and Technology (NIST) in Boulder Colorado cannot perform this measurement in the range of irradiances useful to photovoltaics (PV) [9]. This method requires that the temperature of the sample stays constant which is critical because the quantum efficiency changes rapidly with cell temperature near the band gap. Finally the quantum efficiency method requires that

the noise in the quantum efficiency measurement be independent of the bias light [5,6,7].

The Two Lamp Method

The two lamp method circumvents some of these assumptions as well as factor them out completely. This method does not require a linear detector, takes a shorter time period to perform and does not require attended operation. In the absence of ambient lab light the following is true:

$$I_{sc,AB} = I_{sc,A} + I_{sc,B} \quad (1)$$

where $I_{sc,AB}$ is the short circuit current produced when lamp A and lamp B are both incident on the reference cell. $I_{sc,A}$ and $I_{sc,B}$ are the short circuit currents produced when only lamp A or lamp B is incident on the reference cell. In order to factor out the ambient light ohms law says the following:

$$V_{lab} = (I_{sc,lab})R \quad (2)$$

where V_{lab} is the voltage produced and $I_{sc,lab}$ is the short circuit current across a 0.10 ohm shunt resistor (R) produced by the ambient light in the lab. When a single lamp, lamp A, is incident on the sample the resulting voltage follows:

$$V_A = (I_{sc,A} + I_{sc,lab})R \quad (3)$$

where V_A is the voltage produced and $I_{sc,A}$ is the short circuit current produced by the light on the reference cell from lamp A alone. A similar situation follows for lamp B:

$$V_B = (I_{sc,B} + I_{sc,lab})R \quad (4)$$

again where V_B is the voltage produced and $I_{sc,B}$ is the short circuit current produced by the light on the sample from lamp B alone. Measuring the voltage from the reference cell when both lamp A and B are incident yields:

$$V_{AB} = (I_{sc,AB} + I_{sc,lab})R \quad (5)$$

where

$$V_{AB} = V_A + V_B \quad (6)$$

and

$$I_{sc,AB} = I_{sc,A} + I_{sc,B} \quad (7)$$

substituting equations (1) – (4) into equation (6) yields:

$$V_{AB}/R = V_A/R + V_B/R - V_{lab}/R. \quad (8)$$

A plot of V_{AB} versus $(V_A + V_B - V_{lab})$ should give a straight line which according to the ASTM and IEC standards must have a percent standard deviation of the slope of 0.02%. The percent standard deviation (s) in percent is:

$$s = \text{standard deviation/slope x } 100. \quad (9)$$

Some advantages to this method are that the test is insensitive to spatial non-uniformity, insensitive to spectral variation and does not require a linear detector. Also the ambient light from the lab can be factored out completely. According to ASTM standards E1143 and E1125 a primary reference cell is required to be linear. The primary goal of this test is to reject nonlinear samples from being used as primary reference cells.

MATERIALS AND METHODS

Four assumptions made with the two lamp method test are that the lamp outputs, the filter transmittance, the ambient lab light, and test cell temperature all stay constant throughout the test. The equations we use allow us to factor out the ambient lab light (V_{lab}) completely which eliminates one source of error. The test bed for the experiment consists of two Spectra-Physics lamps model number 66860 and 66861 powered by IEEE-488 programmable low noise Sorensen DCS60-18E power supplies [13,14]. The 400 watt lamps operate at a maximum 19 volts and 8 amps (see Figure 1). The spectral irradiance of the lamps illuminating a single area both at 8 amps is shown in Figure 2. The spectral irradiance shown in Figure 2

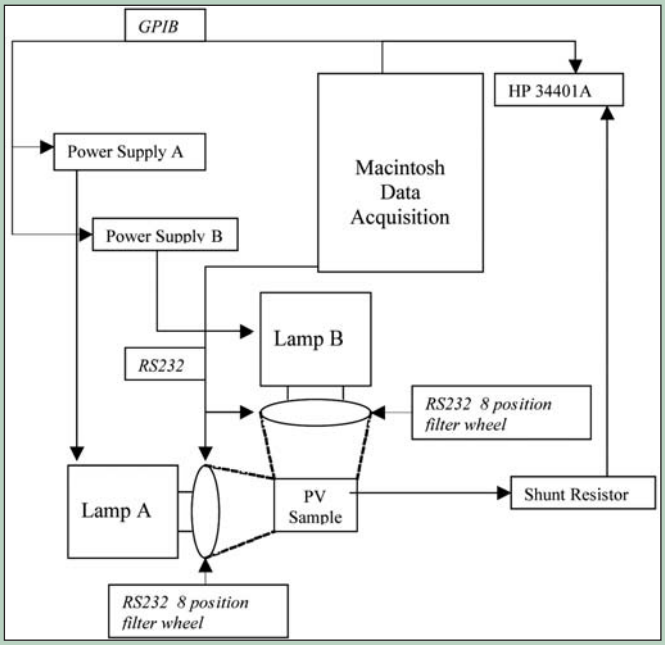

Figure 1. Block diagram of Linearity Test Bed.

is approximately 2 suns or 2000 W/m^2/nm. The spectral irradiance is taken over a wavelength range of approximately 300 nm to 1200 nm. The lamps intensity is controlled with metallic neutral density filters mounted in eight position RS232 programmable filter wheels [12]. The transmission curve for each filter as a function of wavelength can

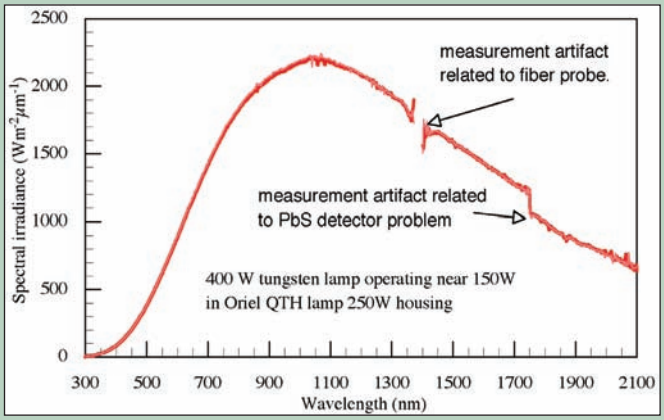

Figure 2. Unattenuated Spectral Irradiance versus Wavelength of Lamp A measured twice.

be seen in Figure 9 as well as a table of the percent transmission for each filter in Table 1. The transmission ranges from 100% where no filter is added to opaque which has 0% transmittance. To minimize

Wheel	Filter Transmittance		Wheel	Filter Transmittance
A1	Opaque		B1	Opaque
A2	Blank		B2	Blank
A3	79%		B3	79%
A4	63%		B4	63%
A5	50%		B5	50%
A6	40%		B6	40%
A7	33%		B7	33%
A8	25%		B8	25%

Table 1. Filter Transmittance for lamp A and B.

uncertainties, the maximum and minimum level of the lights should be within a factor of 5. Different ranges of total irradiances are achieved by varying the lamp voltage. The sample is placed in the test plane where it will be illuminated by light from each lamp after the light has passed through the filter wheels. This allows the sample to be illuminated by the two light sources as if it were from one light source. The ability to apply different voltages to the lamps allows a wide range of light levels to be tested which results in a wide range of E_{tot} on the sample. This gives us an I_{sc} across the current sense resistor which is chosen in such a way to allow only 20 mV across the sample as specified in the standards [8]. The I_{sc} versus E_{tot} curve will determine the linearity or nonlinearity of the sample. The voltages and filter rotations are chosen by us which allows a view of certain regions of the sample response. The Labview program that runs our test bed collects the data and displays a graphical representation on the screen while saving the data to a designated file.

RESULTS

The 930216-1 primary reference cell calibrated by Physikalisch-Technische Bundersanstalt (PTB) in Braunschweig Germany and determined to be linear is used to test the validity of the two lamp method [10,11]. Figure 3 shows linear calibration data from PTB done two different times. Once PTB calibrated the 930216-1 reference cell to be linear in 1998 as published in PEP'93 [10] and again in 2004 given in the calibration certificate [11]. Figure 3 also shows the National Renewable Energy Lab (NREL) results from the two lamp method. The data has been normalized such that a

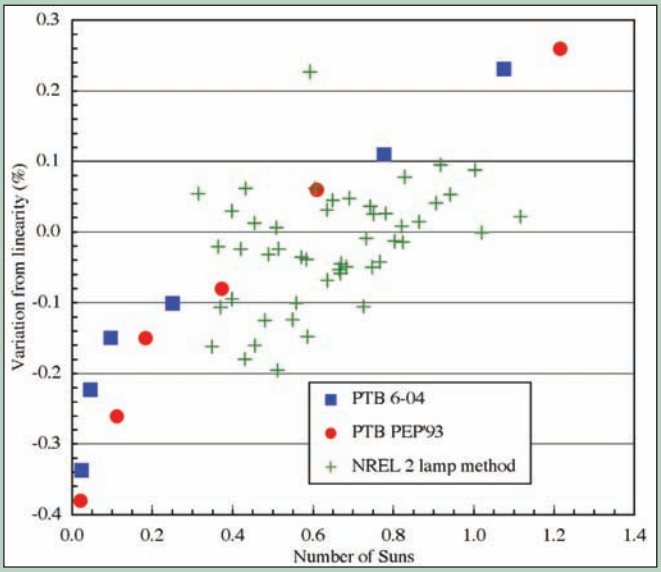

Figure 3. Reference Cell 930216 PTB and NREL Normalized Data.

horizontal line shows linearity. This method of determining linearity differs from the standards which state the standard deviation from the slope where this method looks at the variation from linearity which may be a more accurate method of looking at linearity. The PTB data varies from linear by almost 0.7% ranging from -0.4% to 0.3%. The NREL data also falls within this range of variation. Over the irradiance of interest (0.6 – 1.1 suns) the range for both PTB and NREL is a much better range, approximately -0.15 to 0.1%. This is a difference of approximately 0.25% variation from linearity. The PTB and NREL data both result in a s of less than 2% classifying the reference cell to be linear as specified in the standards [8]. This gives evidence of the validity of the two lamp method as a legitimate test for linearity.

Doing a numerical study using functions that are known to be nonlinear overall helps in further determining the validity of the two lamp method. For convenience and clarity, E_{tot} on the x-axis for Figures 5-8 has been transformed to the number of suns. The exponential function in the form of $y = Ae^{Bx}$ gives the results as seen in Figure 4, where A is 100, B is 0.00015, x represents Etot and y represents I_{sc}. With these values given in the equation and specifying the range of 0 – 1 suns for E_{tot} a *s* value of 0.02% results. Using the two lamp method with the same E_{tot} range gives a *s* value of 0.00001%, much less than the actual *s* value (see Figures 5-6). This fact is due to the chosen function and the range over which the A + B method is collected. Over a small enough range the A + B method will give a linear result of any curve but widening the range between A and B when added together the *s* value will be greater.

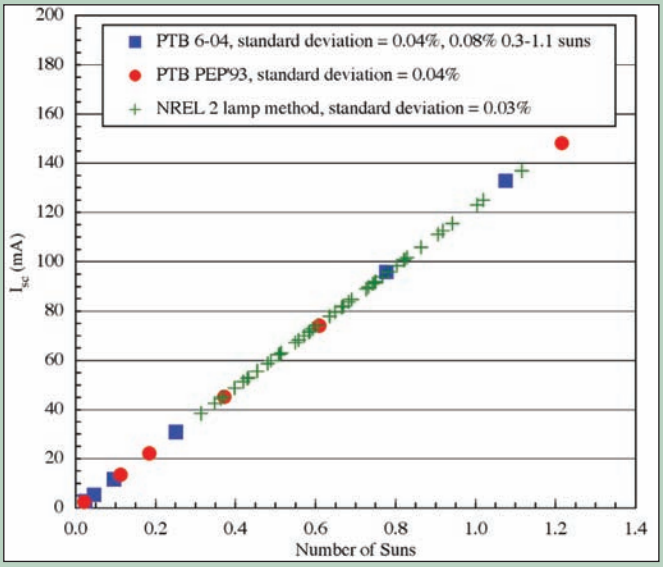

Figure 4. PTB and NREL Data. PTB standard deviation = 0.04%, NREL standard deviation = 0.03%.

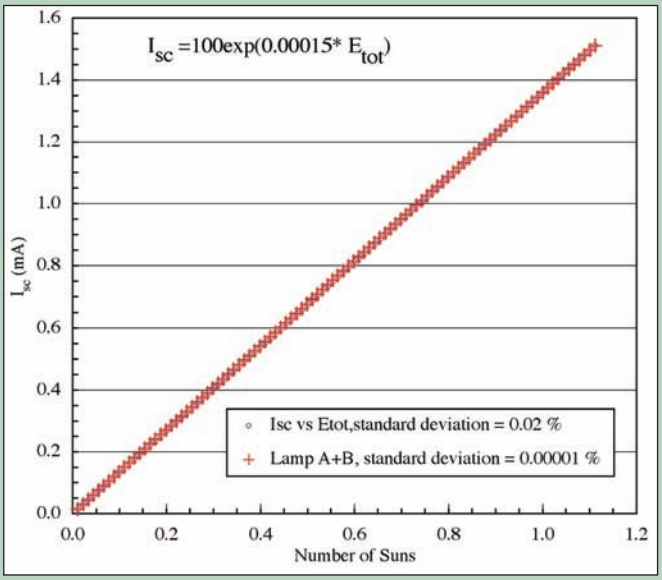

Figure 6. Exponential numerical analysis Isc vs E_{tot} standard deviation = 0.02%. Lamp A + B standard deviation = 0.00001%. E_{tot} is transformed to number of suns.

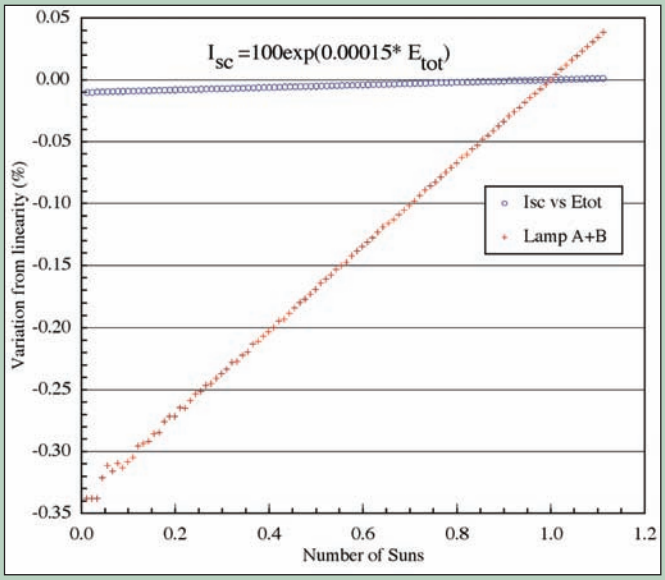

Figure 5. Exponential normalized numerical analysis. E_{tot} is transformed to number of suns.

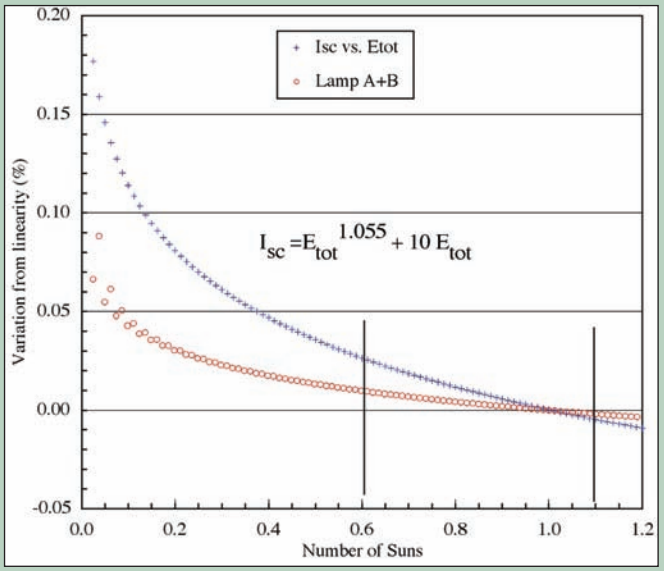

Figure 7. Quadratic normalized numerical analysis. E_{tot} is transformed to number of suns.

Similarly doing the same study using the quadratic function in the form of y = xA + Bx, where A is 1.0055, B is 10, and y represents I_{sc} and x represents E_{tot} further investigates the validity of the two lamp method. Using this function and graphing I_{sc} versus E_{tot} gives the graphs seen in Figures 7-8. Similar to the exponential function, the graph of the quadratic function results in a *s* value of 0.02% while the two lamp method results in a *s* value of 0.0006%. The two lamp method gives a value less than the actual *s* value again due to the chosen range for A + B.

DISCUSSION AND CONCLUSIONS

The standards require that primary reference cells be linear over the total irradiance of interest [8]. Linearity is determined to be 2% standard deviation from the linear slope according to calibration standards [8]. The purpose of this test is to pass or fail primary reference cells as linear or nonlinear using the two lamp method. The 930216-1 sample calibrated by PTB is linear [10,11] and the two lamp method also yields a linear response. This gives validity to the ability of the two lamp method to classify a reference cell as linear or nonlinear. What is found is that the two lamp method does not give the actual *s* value of the response for the reference cell. A factor of at least 2 must be applied to the *s* value given by the two lamp method in order to classify the cell as linear or nonlinear. Applying this factor in the Labview code is easily done so that the program will either pass or fail the cell immediately. A better approach may be

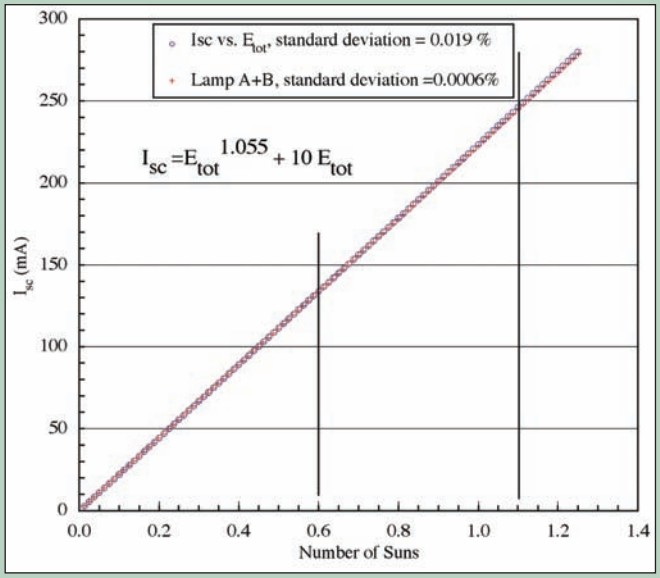

Figure 8. Exponential numerical analysis. I_{sc} vs E_{tot} standard deviation = 0.019%. Lamp A + B standard deviation = 0.006%. E_{tot} is transformed to number of suns.

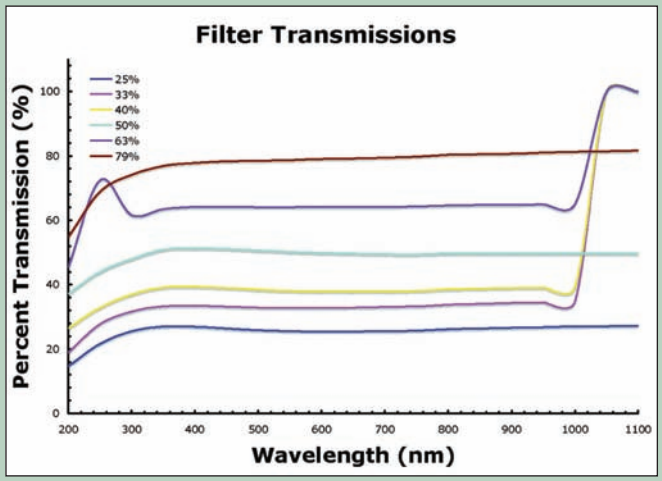

Figure 9. Percent transmission of filters in filter wheel. The opaque filter has a 0% transmission while the empty filter has 100% transmission (not shown on graph).

to set a window like the variation in nonlinearity over the intensity range of interest must be less than 2%.

The overall response of a cell cannot be known before testing and by assuming nonlinearity overall, this test can be used at least as an initial check. The two lamp method places rather strict standards on a cell to be considered linear over the irradiance region of interest and correlates well with other linearity methods done around the world. This method gives a quick and easy way to classify linearity of the reference cell but this test will not however give the degree of nonlinearity if the cell is classified nonlinear.

ACKNOWLEDGEMENTS

The research was conducted at the NREL. We would like to thank the Department of Energy, Office of Science for the opportunity afforded to us in the PST and LSTPD programs. We would like to give special thanks to our mentor Keith Emery who guided us through this project. We would also like to thank the Franhofer Institute for Solar Energy Systems in Freidburg Germany for suggesting the concept. Thank you finally to the National Center for Photovoltaics and the NREL Office of Education Programs for their support.

REFERENCES

[1] R. J. Chaffin and J.J. Wiczer, “Nonlinear response of GaAs Concentrator Cells to Solar Insulation,” *IEEE PVSC*, vol. 15, no. 81, pp. 243–244, 1981.

[2] Joseph Burdick and Troy Glatfelter, “Spectral Response and I-V Measurements of Tandem Amorphous-Silicon Alloy Solar Cells,” *Solar Cells*, vol. 18, pp. 301–314, 1986.

[3] R. W. Sanderson, J. D. Birkeland, S. C. Martin and C. E. Backus, “Performance of Silicon Solar Cells in the Concentration Range of 150 - 1500 Suns,” *IEEE PVSC*, vol. 7, pp. 1309–1313, 1984.

[4] V. Augelli, L. Vasanelli, M. Leo, R. A. Leo, and G. Soliani, “Nonlinear Behavior of the Short Circuit Current of a Solar Cell with Minority Carrier Lifetime Dependent on the Light Intensity,” *Journal of Applied Physics*, vol. 53, no. 3, pp. 1558–1562, 1982.

[5] J. Metzdorf, H. Kaase, “Nonlinearity and Spectral Mismatch Problems of Solar Cells,” *European Symposium Photovoltaic Generators in Space*, vol. 4, no. 0, pp. 273–277, 1984.

[6] J. Metzdorf, “Calibration of Solar Cells 1: The Differential Spectral Responsivity Method,” *Applied Optics*, vol. 26, pp. 1701–1708, 1987.

[7] H. Mullegans, H. Bossong, E. D. Dunlop, “Temperature and Bias Light Dependence of Spectral Response Measurement,” *PV in Europe from PV Technology to Energy Solutions*, pp. 7–10, 2002.

[8] American Society for Testing and Materials “Standard Test Method for Determining the Linearity of a Photovoltaic Device Parameter with Respect to a Test Parameter,” *ASTM Standard E1143*, 1999

[9] National Institute for Standards and Technology (2004, July) Calibration Services [online] http://ts.nist.gov/ts/htdocs/230/233/calibrations

[10] C.R. Osterwald, S. Anevsky, A.K. Barua, K. Bucher, P. Chauduri, J. Dubard, K. Emery, D. King, B. Hanses, J. Metzdorf, F. Nagamine, R. Shimokawa, Y.X. Wang, T. Wittchen, W. Zaaiman, A. Zastrow, and J. Zhang, “The Results of the PEP’93 Intercomparison of Reference Cell Calibrations and Newer Technology Performance Measurements: Final Report” pp. A3-3 – A3-4, 1998.

[11] Physikalisch-Technische Bundesanstalt “Calibration Certificate” PTB 930216-1, 2004.

[12] DFM Engineering, Inc. “DFM Engineering, Inc. filter Wheel System Description and Control Interface Manual Model FW-82” Longmont, CO, pp. 1-5.

[13] Spectra-Physics Lasers and Photonics “QTH/IR Lamp Housing Models 66860, 66861 Through 66884 Users Manual” Stratford, CT, pp. 1–17.

[14] Sorensen DC Products (2004, July) Power Supplies [online] http://www.elgar.com/products/Sorensen/index.htm

[15] Keith Emery, “ Measurement and Characterization of Solar Cells and Modules,” *Handbook of Photovoltaic Science and Engineering*, 1 ed., Ed. Antonio Luque and Steven Hegedus, West Sussex, England: John Wiley and Sons Ltd., 2003, pp. 701–752.

Jun Zhang participated in the Science Undergraduate Laboratory Internships (SULI) program at Brookhaven National Laboratory as a rising sophomore from Cornell University during the summer of 2005. His project involved characterizing the electric and magnetic properties of a doped nickelate compound that is closely related to the high temperature superconductors. During the summer of 2006, he worked in the SRF group at Cornell's Laboratory for Elementary-Particle Physics, where he helped set up, program and run a bead-pull apparatus that measures the electric axis of RF cavities. His work was used to optimize the beam quality inside the cavity. Jun plans on pursuing a PhD in Physics after he graduates from Cornell University.

Markus Hücker is an Associate Physicist in the Condensed Matter Physics & Materials Science Department at Brookhaven National Laboratory. He received a diploma (1994) and a Ph.D. (2000) in Physics, both from the University of Cologne, Germany. Prior to doing research at Brookhaven, he did postdoctoral research at the University of Paris, France. He earned the Karl Liebrecht Award, Faculty of Natural Sciences, from the University of Cologne, Germany, in 2000.

MAGNETIZATION, CHARGE TRANSPORT, AND STRIPE PHASES IN $Nd_{5/3}Sr_{1/3}NiO_{4+\delta}$ SINGLE CRYSTAL

JUN Z. ZHANG, MARKUS HÜCKER

ABSTRACT

Stripe phases, in which doped charges are localized along domain walls between antiferromagnetic insulating regions, provide a framework for the electronic structure of doped antiferromagnets such as the superconducting layered copper-oxides. Layered nickel-oxides, such as $Nd_{2-\chi}Sr_{\chi}NiO_4$, though non-superconducting, exhibit stripe phases in which charges are more localized, resulting in higher charge density modulation amplitudes than their cuprate analogs, thus are more amenable for experimental investigations. We study the magnetic and electric-transport properties of a $Nd_{5/3}Sr_{1/3}NiO_{4+\delta}$ single crystal by means of magnetic susceptibility, isothermal magnetization, and electric resistivity measurements. We observe a transition of the magnetic susceptibility with applied field parallel to the c-axis at $T \approx 15$ K, which is due to the long-range ordering of Nd^{3+} magnetic moments. A transition of the in-plane resistivity (ρ_{ab}) is observed at $T \approx 230$ K, which indicates the charge stripe ordering that has also been observed in $La_{2-\chi}Sr_{\chi}NiO_4$ at about the same temperature. The out-of-plane resistivity (ρ_c) exhibits a milder transition at $T \approx 200$ K. After the stripe phase transition takes place, the electronic transport exhibits variable range hopping behavior. The resistivity anisotropy (ρ_c/ρ_{ab}) shows a sharp drop at the ρ_{ab} transition temperature with decreasing temperature, which indicates the strong localization of charge carriers in the ab-plane as charge stripes become statically ordered and the system becomes less two-dimensional electronically. Our results are in support of the stripe phase picture of the electronic structure in layered metal-oxides.

INTRODUCTION

Since the discovery of high-temperature superconductivity in layered cuprates, the mechanism of charge transport in strongly correlated electronic systems has remained one of the most challenging problems in condensed matter physics. There is strong evidence that selforganized local inhomogeneities are responsible for the electrical properties of these systems. Stripe phases, in which charge carriers are confined to a single dimension between antiferromagnetic insulating regions, were theoretically predicted and experimentally observed in doped antiferromagnets by means of neutron scattering studies [1]. Extensive investigations of these materials in recent years have revealed that stripe correlations occur as a consequence of a complex interplay among spin, charge, and lattice degrees of freedom.

Isostructural nickelates, which remain insulating when doped with holes, are easier to study experimentally because they exhibit relatively static stripe order with higher charge density modulation compared with their cuprate analogs in which stripes are fluctuating. In recent years stripe correlations in $La_{2-\chi}Sr_{\chi}NiO_4$ have been studied extensively with many different experimental techniques such as neutron scattering, x-ray diffraction, thermal conductivity, NMR, specific heat, etc [2]. Nd substitution for La causes the lattice to change from the tetragonal structure to the orthorhombic structure, resulting in an anisotropic distortion of the NiO_2-planes. It has been

shown that stripes in $Nd_{2-\chi}Sr_{\chi}NiO_4$ align themselves in preferred direction, parallel to the [100] direction [3].

The goal of our research is to study the magnetic and electric-transport properties of $Nd_{5/3}Sr_{1/3}NiO_{4+\delta}$ by means of magnetization and electric resistivity measurements. Studies have shown that $La_{2-\chi}Sr_{\chi}NiO_4$ exhibits the most pronounced charge-ordering for a Sr doping of χ = 1/3 below 235 K [4]. Therefore we expect that $Nd_{2-\chi}Sr_{\chi}NiO_4$ with a Sr doping of χ = 1/3 would also exhibit the most distinct transitions in our experiments. Figure 1 shows the lattice structure of $Nd_{2-\chi}Sr_{\chi}NiO_4$ in its three structural phases, the high-temperature tetragonal (HTT) phase, the low-temperature orthorhombic (LTO) phase, and the low temperature tetragonal (LTT) phase [5].

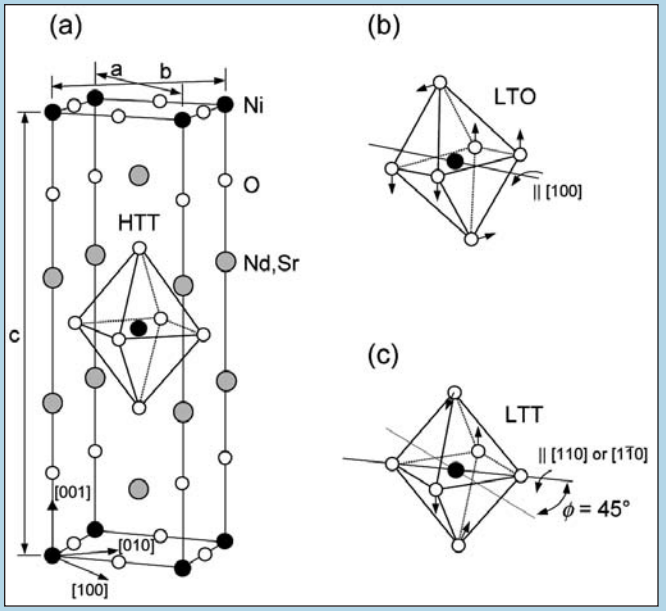

Figure 1. Lattice structure of $Nd_{2-\chi}Sr_{\chi}NiO_4$ and its three structural phases.

MATERIALS AND METHODS

Our single crystal sample of $Nd_{5/3}Sr_{1/3}NiO_{4+\delta}$ was grown by the Traveling-Solvent Floating-Zone (TSFZ) technique. Two pieces from the same grown crystal were used in our experiment. They were mounted with QuickCure acrylic on mounting blocks. We used the x-ray back-reflection Laue method to determine the crystallographic axes of both pieces and to orient them on a goniometer. Because our crystal has twinned domains in the ab-planes, we refer to the two in-plane axes as the ab1 and ab2 axes throughout this paper. The oriented crystals were then cut along the desired axes with a diamond blade sectioning machine. One sample with a flat surface parallel to the ab-plane (Figure 2(a)) was prepared for magnetization measurements so that we could easily orient its crystallographic axes with respect to the applied magnetic field. For the magnetization measurements, a bulky sample is preferred, to reduce the effects due to an anisotropic sample geometry. Two samples for resistivity measurements were shaped into thin bars (approx. 3.9 × 0.75 × 0.50 mm^3 and 2.0 × 0.70 × 0.50 mm^3) with each of their longest dimensions parallel to the ab1-axis and the c-axis, respectively.

Magnetic susceptibility and isothermal magnetization measurements were carried out using a superconducting quantum interference device (SQUID) magnetometer in a temperature range from 2 to 300 K with magnetic fields up to 7 T. For every measurement we took, the sample was first heated to high temperature and then zero-field-cooled to 2 K. The magnetic susceptibility was measured with magnetic field parallel to the ab1, ab2, and c directions with increasing as well as decreasing temperature. The mass of our as-prepared magnetization sample was determined to be m = 0.384 g using an electric balance. The molar susceptibility was calculated using the formula

$$\chi = \frac{\mu M}{Hm},$$

where μ is the measured magnetic moment, M is the molar mass of $Nd_{5/3}Sr_{1/3}NiO_{4+\delta}$ which is 2 about 392 g/mol, and H is the applied magnetic field strength. The isothermal magnetization was measured with field parallel to the c direction at 2 K, 5 K, 7.5 K, 10 K, etc. up to 30 K and with field parallel to the ab2 direction at 2 K.

The in-plane and out-of-plane resistivities (ρ_{ab} and ρ_c) were measured using the standard 4-terminal method. We used 0.002" pure platinum wires as contact leads, which were applied to polished sample surfaces with silver epoxies, followed by a heat treatment at 100°C in air for about an hour and then at 350°C in pure Ar gas for about two hours. This procedure was found to result in a very low contact resistance of the order of 1-10 Ω per lead. The Ar atmosphere was chosen to prevent oxygen annealing of the sample. The contacted sample for ρ_{ab} is shown in the photograph in Figure 2(b). The samples were then mounted on the probe with their leads soldered on the corresponding connectors. The probe was inserted in the magnet cryostat and connected to the resistance bridge which has an upper limit of 2 MΩ. The resistivity was calculated using the formula

$$\rho = \frac{RA}{L},$$

where R is the measured resistance, A is the cross-sectional area of the sample and L is the distance between the two voltage leads.

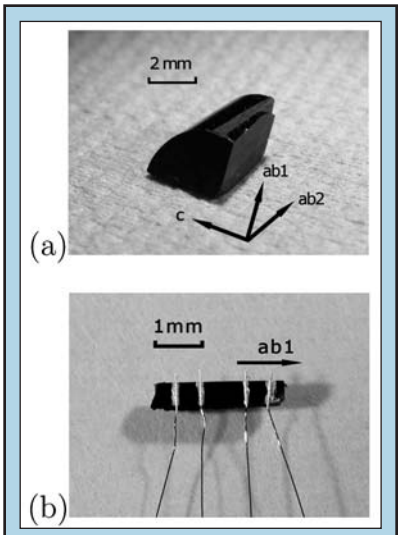

Figure 2. (a) The sample for susceptibility and isothermal magnetization measurements. (b) The ρ_{ab} sample with lead wires attached.

RESULTS AND DISCUSSION

Magnetic Susceptibility

Figure 3 shows the magnetic susceptibility $\chi(T)$ of $Nd_{5/3}Sr_{1/3}NiO_{4+\delta}$ for H = 1 T applied parallel to the three principal axes. The corresponding data will be referred to as χ_{ab1}, χ_{ab2}, and χ_c. For all the magnetic susceptibility measurements taken, measuring up and down with respect to temperature show no discrepancy within experimental error; therefore we only present the susceptibility data taken with increasing temperature. As indicated in Figure 3, χ_c shows an antiferromagnetic transition known as the Néel transition at $T_N \approx 15$ K, which is due to the long-range ordering of the Nd^{3+} moments. No apparent anisotropy in the NiO_2-planes is observed as we can see from the similar behaviors of χ_{ab1} and χ_{ab2}. However, the discrepancy between $\chi_{ab1,2}$ and χ_c suggests the presence of a crystal field perturbation.

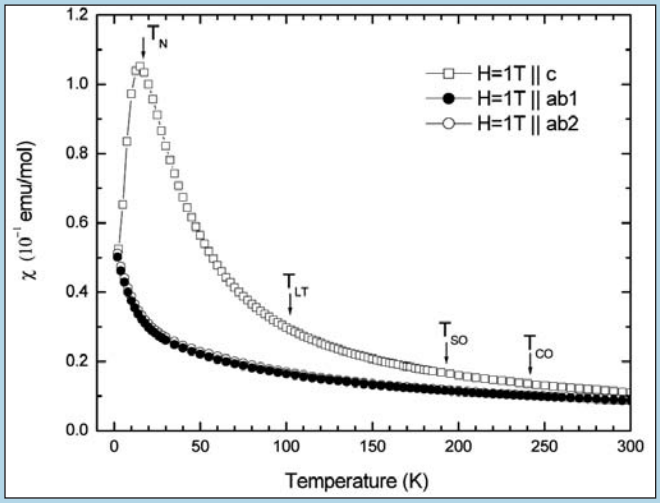

Figure 3. Temperature dependence of χ_{ab1}, χ_{ab2}, and χ_c. The expected transition temperatures are indicated.

Other than the Néel transition, we do not observe any other anomalies, for example, the transitions associated with the charge stripe and spin stripe orderings that have been observed in the susceptibility measurements on $La_{5/3}Sr_{1/3}NiO_4$ at about 240 K and 190 K, respectively [2]. The overall susceptibility can be attributed to the composition of different microscopic magnetic sources:

$$\chi_{NSNO} = \chi_{core} + \chi_{pauli} + \chi_{Ni} + \chi_{Nd},$$

where χ_{core} is the diamagnetic contribution of the closed electron shells, χ_{pauli} is the paramagnetic contribution of the conduction electrons, χ_{Ni} is the contribution due to Ni spins, and χ_{Nd} is the contribution due to the Nd moments. Both χ_{core} and χ_{pauli} are of the order of 10^{-4} emu/mol with opposite signs. χ_{Ni} is of the order of 10^{-3} emu/mol [4,6]. Therefore we think that the anomalies in the susceptibility due to charge stripe and spin stripe ordering are completely masked by the large contribution of the paramagnetic Nd^{3+} ions, which is of the order of 10^{-1} emu/mol (see Figure 3). The structural phase transition from the LTO phase to the LTT phase at T_{LT} = 100 K is also not apparent in the susceptibility data, which is unusual because in La_2NiO_4 [7] and $Nd_{1.8}Sr_{0.2}NiO_{3.72}$ [6] the transition leads to weak ferromagnetism.

The temperature dependence of the inverse susceptibility is plotted in Figure 4. The linear relationships at high temperature are indicated with lines fitted over $1/\chi_{ab2}$, and $1/\chi_c$. We see that the susceptibility clearly behaves according to the Curie-Weiss law [8]

$$\chi = \frac{C}{T - \theta},$$

where C is the Curie constant, in the high temperature regime (T > 100 K) for magnetic field applied parallel (χ_{ab1} and χ_{ab2}) as well as perpendicular (χ_c) to the NiO_2-planes. From the curve for $1/\chi_c$, the Weiss constant θ is approximated to be –10 K. The Curie-Weiss law predicts an antiferromagnetic transition near $T = |\theta| \approx 10$ K, which is indeed observed at TN ≈ 15 K. However, for field parallel to the ab-plane $1/\chi$ has a Weiss constant of about -100 K in which case the Curie-Weiss law is obviously a too simple model because it does not take into account the effects of the crystal electric field.

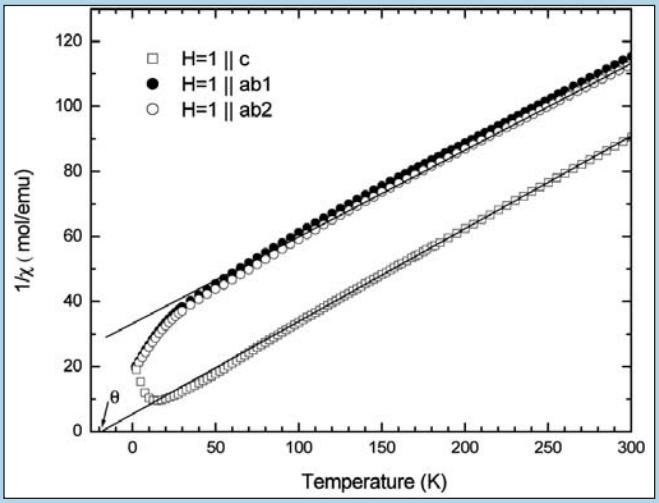

Figure 4. Temperature dependence of $1/\chi_{ab1}$, $1/\chi_{ab2}$, and $1/\chi_c$. Lines are fitted over $1/\chi_{ab2}$, and $1/\chi_c$ at high temperature.

Figure 5 shows the susceptibility for magnetic fields of various magnitudes applied parallel to the c-axis. We note that field strength has no noticeable effect on the susceptibility in the paramagnetic regime ($T > T_N$). However, a higher magnetic field tends to drive the Néel transition to lower temperature. Moreover, the susceptibility in higher magnetic field tends to decrease at a less rapid pace in the antiferromagnetic regime ($T > T_N$), indicating the suppression of the antiferromagnetic order by a uniform magnetic field. We have also measured the low field susceptibility (H = 20, 50, 100, 200 gauss) but again no additional anomalies are detected.

Isothermal Magnetization

Figure 6 shows the magnetization data $M(H)$ taken at T = 2 K, 5 K, 10 K, 15 K, 20 K, and 30 K with field parallel to the c-axis and at T = 2 K with field parallel to the ab2-axis. The measurements

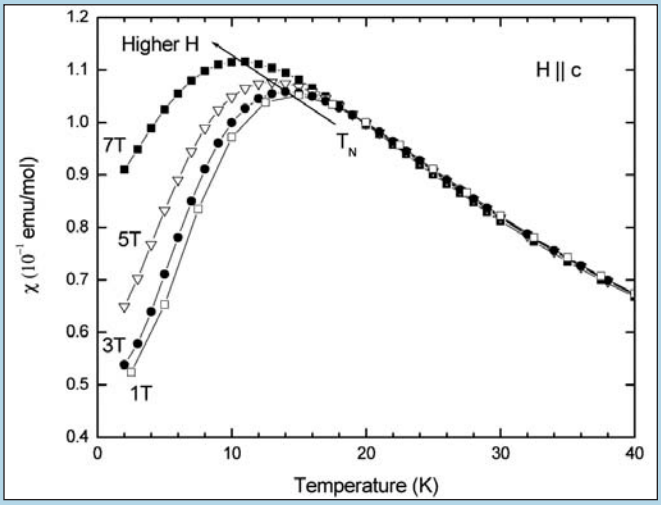

Figure 5. Temperature dependence of χ_c in different magnetic fields.

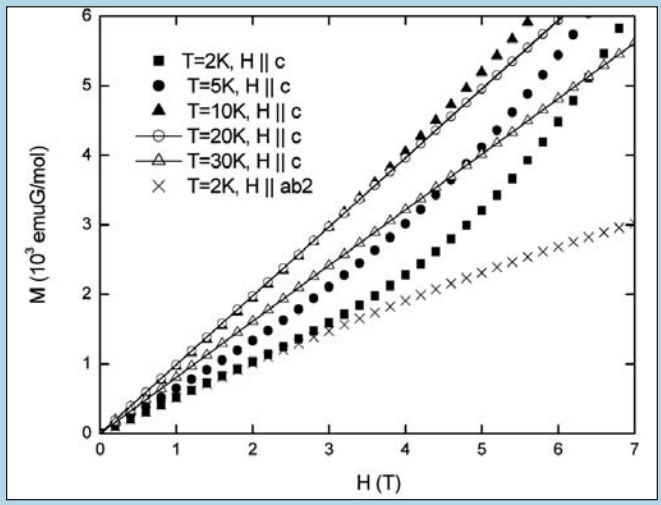

Figure 6. Field dependence of the magnetization at various temperatures with fields parallel to c-axis and ab2-axis.

were performed by increasing the field from H = 0 up to 7 T and then back to H = 0 at constant temperatures. The magnetization measurements at temperatures higher than T_N all exhibit linear field dependence, which is in agreement with the paramagnetic behavior at $T > T_N$ shown in Figure 3. Below T_N the field dependence of the magnetization is curving up, which indicates the onset of a magnetic transition. Unfortunately, we are limited by the 7 T capacity of our magnetometer, which prevents us from determining the critical field and the type of the magnetic transition.

Resistivity

Plotted in Figure 7 are the temperature dependence of the in-plane and out-of-plane resistivities (ρ_{ab} and ρ_c) with the vertical axis in the logarithmic scale and their temperature derivatives in the inset. Both ρ_{ab} and ρ_c clearly show insulating temperature dependence ($d\rho/dT < 0$) in the temperature range we studied. One feature in Figure 7 is that ρ_{ab} increases abruptly at about 230 K, indicative of a phase transition. The temperature derivative of $\log_{10} \rho$ in the

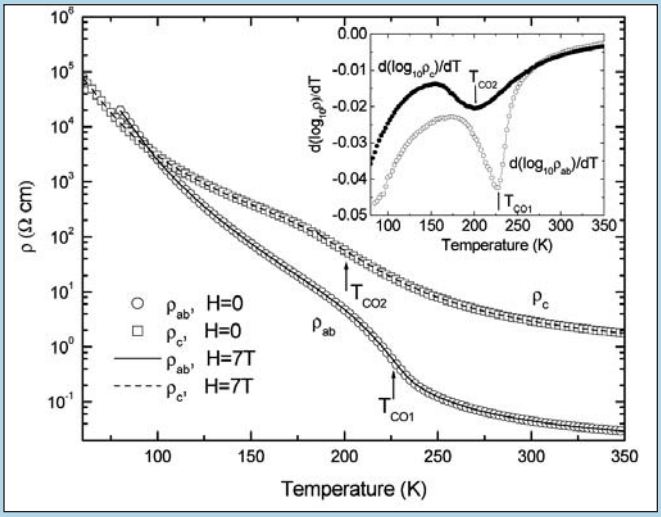

Figure 7. Temperature dependence of the in-plane and out-of-plane resistivities. The inset shows the temperature derivative of the resistivities.

inset of Figure 7 shows a sharp dip at $T_{CO1} \approx 228$ K, identifying the phase transition temperature. A similar transition in the in-plane resistivity of $La_{2-\chi}Sr_\chi NiO_4$ with $\chi = 1/3$ has also been observed and thought to be attributed to the segregation of doped holes to form the preferred charge-ordered state [4]. Neutron scattering and other experiments performed on $La_{2-\chi}Sr_\chi NiO_4$ showed conclusive results that the transition is due to the charge stripe ordering in the NiO_2-planes [9,10,11].

It is interesting to note that at $T_{CO2} \approx 200$ K ρ_c also exhibits a similar transition with a much milder feature. It is very likely that both transitions we see in ρ_{ab} and ρ_c are due to the charge stripe ordering. The fact that the charge stripe ordering takes place at two different temperatures may be attributed to the difference in the oxygen contents of our two samples. To verify this, we applied two more contact leads at the bottom of our ρ_c sample to measure the in-plane resistance across the bar-shaped sample and the out-of-plane resistance along the sample with the 2-terminal method using an electrometer, which has a build-in current source. To our surprise, the out-of-plane resistance shows a transition at 200 K, same as what we have observed before; however, the transition for the in-plane resistance is shifted down to 130 K (not shown in the figures). We suspect that the oxygen content of the sample has changed again; and it seems to affect only the in-plane resistivity. Further experiments are needed to determine the reason for the difference in the transition temperatures of ρ_{ab} and ρ_c. No anomalies due to the spin stripe transition and the LTO to LTT structural phase transition are observed in the resistivity.

We have also plotted ρ_{ab} and ρ_c on a logarithmic scale against $T^{-1/3}$ in Figure 8. The linear relationships below T_{CO1} and T_{CO2} suggest that the system's nonmetallic behavior is described within the variable range hopping (VRH) model as

$$\rho(T) \propto \exp\left[\left(\frac{T_0}{T}\right)^{\alpha}\right],$$

where T_0 is a measure of the localization of charges and the exponent α depends on the dimensionality of the VRH process. In our case

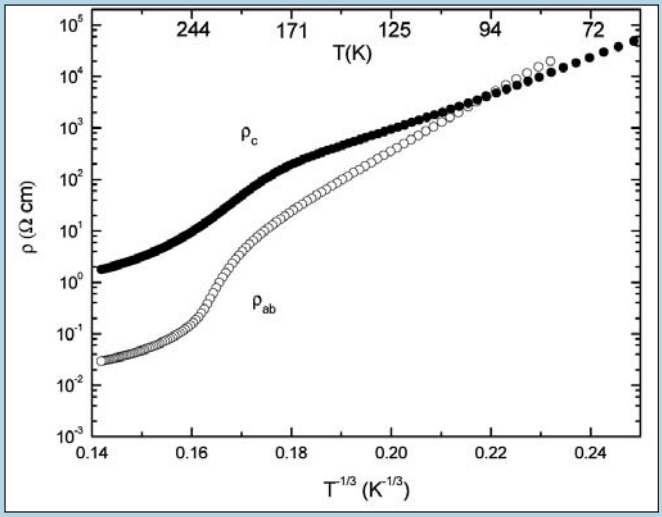

Figure 8. The in-plane and out-of-plane resistivities plotted against $T^{-1/3}$

ρ_{ab} and ρ_c are well described assuming α = 1/3 which corresponds to a two-dimensional hopping [12].

The resistivity anisotropy (ρ_c/ρ_{ab}) is calculated and shown in Figure 9. A strong temperature dependence of ρ_c/ρ_{ab} is noted. An abrupt decrease of ρ_c/ρ_{ab} is observed near the charge stripe ordering transition in ρ_{ab} at $T_{CO1} \approx 230$ K. When one compares Figure 9 to Figure 7, it becomes clear that the sudden drop in the resistivity anisotropy corresponds to the onset of the insulating behavior in ρ_{ab}. In other words, the rapid increase in ρ_{ab} causes the decrease of ρ_c/ρ_{ab} with decreasing temperature. The strong localization of charge carriers as charge stripes become statically ordered causes ρ_{ab} to rise more rapidly than ρ_c. As the more favorable in-plane charge transport mechanism breaks down, the system becomes a quasi-isotropic insulator. This can be seen in Figure 7 in which the two resistivities are of the same order of magnitude below 100 K. A similar phenomenon has also been observed in the cuprates [13].

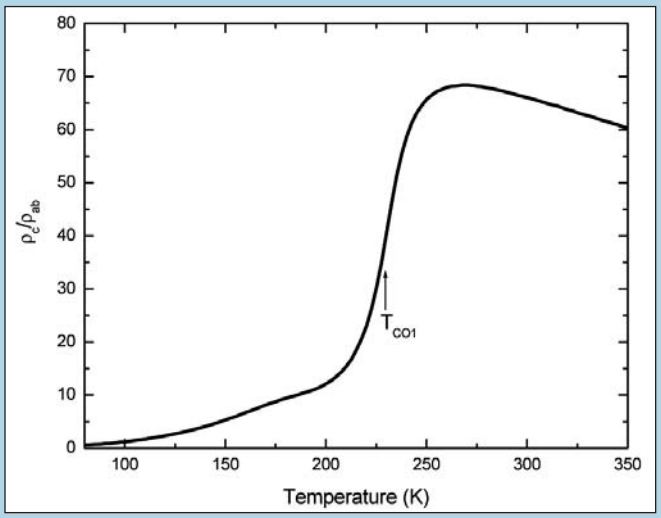

Figure 9. Temperature dependence of the resistivity anisotropy ratio ρ_c/ρ_{ab}.

CONCLUSION

Our research constitutes an important part of the characterization of $Nd_{2-\chi}Sr_\chi NiO_4$, a member of the nickelate family that has aroused considerable interest in the study of high temperature superconductivity. In this paper we have presented the measurements of the magnetization and of the resistivity of a $Nd_{5/3}Sr_{1/3}NiO_{4+\delta}$ single crystal. We observe an antiferromagnetic transition of magnetic susceptibility with applied field perpendicular to the NiO_2-planes at TN ≈ 15 K, which is due to the ordering of Nd^{3+} magnetic moments.

Charge stripe ordering is observed at $T_{CO1} \approx 230$ K in ρ_{ab} and $T_{CO2} \approx 200$ K in ρ_c. The discrepancy between T_{CO1} and T_{CO2} needs to be analyzed in future experiments. More suitable experimental techniques such as neutron scattering are needed to detect the spin stripe ordering and structural transitions in $Nd_{5/3}Sr_{1/3}NiO_{4+\delta}$. The resistivity anisotropy (ρ_c/ρ_{ab}) shows a sharp decrease at the ρ_{ab} transition temperature with decreasing temperature, which indicates the strong localization of charge carriers in the NiO_2-planes as charge stripe order takes place. Our results are in support of the stripe phase picture of the electronic structures in layered metal-oxides.

ACKNOWLEDGEMENTS

This research was conducted at the Brookhaven National Laboratory in Upton, NY. I would like to thank the U.S. Department of Energy, Office of Science for giving me the opportunity to participate in the SULI program. My sincere gratitude is given to my mentor Markus Hucker for his patient guidance and support. I would also like to thank Myron Strongin and John Tranquada for helpful discussions and assistance as well as Genda Gu for growing such a beautiful $Nd_{5/3}Sr_{1/3}NiO_{4+\delta}$ single crystal.

REFERENCES

[1] V. J. Emery, S. A. Kivelson, and J. M. Tranquada, "Stripe phases in high-temperature superconductors", *Proceedings of the National Academy of Sciences*, vol. 96, 8814 (1999).

[2] R. Klingeler, B. Büchner, S-W. Cheong, and M. Hücker, "Weak ferromagnetic spin and charge stripe order in $La_{5/3}Sr_{1/3}NiO_4$", *Physical Review B*, accepted for publication.

[3] M. Hücker, M. v. Zimmermann, S. Kiele, J. Geck, S. Bakehe, Revcolevschi, J. Hill, Büchner, and J. Tranquada, unpublished.

[4] S-W. Cheong, H. Y. Hwang, C. H. Chen, B. Batlogg, L. W. Rupp, Jr., and S. A. Carter, "Charge-ordered states in $(La,Sr)_2NiO_4$ for hole concentrations n_h = 1/3 and 1/2 ", *Physical Review B*, vol. 49, no. 10, 7088 (1994).

[5] M. Hücker, K. Chung, M. Chand, T. Vogt, J. M. Tranquada, and D. J. Buttrey, "Oxygen and strontium codoping of La_2NiO_4: Room-temperature phase diagrams", *Physical Review B*, vol. 70, no. 6, 064105 (2004).

[6] M. Medarde, J. Rodríguez-Carvajal, B. Martínez, X. Batlle, X. Obradors, "Magnetic ordering and spin reorientations in $Nd_{1.8}Sr_{0.2}NiO_{3.72}$", *Physical Review B*, vol. 49, no. 13, 9138 (1994).

[7] O. Friedt, "Preparation, characterization, and structure of $La_{2-\chi}Sr_\chi NiO_{4+\delta}$", diploma thesis 1998, University of Cologne, Germany.

[8] N. W. Ashcroft, N. D. Mermin, *Solid State Physics*, Philadelphia: Holt, Rinehart and Winston, 1976.

[9] S.-H. Lee and S-W. Cheong, "Melting of quasi-two-dimensional charge stripes in $La_{5/3}Sr_{1/3}NiO_4$ ", *Physical Review Letter*, 79, 2514 (1997)

[10] R. Kajimoto, K. Ishizaka, H. Yoshizawa, and Y. Tokura, "Spontaneous rearrangement of the checkerboard charge order to stripe order in $La_{1.5}Sr_{0.5}NiO_4$", *Physical Review B*, vol. 67, no. 1, 014511 (2003).

[11] A. Vigliante, M. von Zimmermann, J. R. Schneider, T. Frello, N. H. Andersen, J. Madsen, D. J. Buttrey, D. Gribbs, and J. M. Tranquada, "Detection of charge scattering associated with stripe order in $La_{1.775}Sr_{0.225}NiO_4$ by hard-x-ray diffraction", *Physical Review B*, vol 56, no. 13, 8248 (1997).

[12] M. Hücker, V. Kataev, J. Pommer, J. Harraβ, A. Hosni, C. Pflitsch, R. Gross, and B. Büchner, "Mobility of holes and suppression of antiferromagnetic order in $La_{2-\chi}Sr_\chi CuO_4$", *Physical Review B*, vol 59, no. 2, 50102 (1999).

[13] S. Komiya, Y. Ando, X. F. Sun, and A. N. Lavrov, "c-axis transport and resistivity anisotropy of lightly to moderately doped $La_{2-\chi}Sr_\chi CuO_4$ single crystals: Implications on the charge transport mechanism", *Physical Review B*, vol. 65, no. 21, 214535 (2002).

Christopher Rosenthal graduated in 2005 with a B.S. in computer engineering from the Illinois Institute of Technology. While completing his undergraduate degree, he began coursework for his M.S. in mathematics education. Christopher is currently finishing his graduate degree while teaching mathematics at Andrew High School in Tinley Park, Illinois. During the summer of 2005, he worked in the Physics Division of Argonne National Laboratory as part of the Pre-Service Teacher (PST) Program sponsored by the Department of Energy and the Office of Science. His research focused on developing a mathematical model and meaningful visualizations for the particle beam in a proposed particle accelerator.

Bela Erdelyi holds a joint appointment between the Department of Physics at Northern Illinois University and the Physics Division of Argonne National Laboratory. He received his PhD in physics from Michigan State University in 2001, followed by a three-year postdoctoral research scientist appointment at Fermi National Accelerator Laboratory. His current research interests are in the general field of beam physics, more specifically nonlinear beam dynamics, accelerator modeling, simulations and design, and applications of symplectic geometry to Hamiltonian dynamics.

MODELING AND VISUALIZING THE PARTICLE BEAM IN THE RARE ISOTOPE ACCELERATOR

Christopher Rosenthal, Bela Erdelyi

ABSTRACT

Argonne National Laboratory is actively pursuing research and design for a Rare Isotope Accelerator (RIA) facility that will aid basic research in nuclear physics by creating beams of unstable isotopes. Such a facility has been labeled as a high priority by the joint Department of Energy and National Science Foundation Nuclear Science Advisory Committee because it will allow more study on the nature of nucleonic matter, the origin of the elements, the Standard Model, and nuclear medicine. An important part of this research is computer simulations that model the behavior of the particle beam, specifically in the Fragment Separator. The Fragment Separator selects isotopes based on their trajectory in electromagnetic fields and then uses absorbers to separate particles with a certain mass and charge from the rest of the beam. This project focused on the development of a multivariate, correlated Gaussian distribution to model the distribution of particles in the beam as well as visualizations and analysis to view how this distribution changed when passing through an absorber. The distribution was developed in the COSY INFINITY programming language. The user inputs a covariance matrix and a vector of means for the six phase space variables, and the program outputs a vector of correlated, Gaussian random variables. A variety of random test cases were conducted in two, three and six variables. In each case, the expectation values, variances and covariances were calculated and they converged to the input values. The output of the absorber code is a large data set that stores all of the variables for each particle in the distribution. It is impossible to analyze such a large data set by hand, so visualizations and summary statistics had to be developed. The first visualization is a three-dimensional graph that shows the number of each isotope present after each slice of the absorber. A second graph plots any of the six phase space variables against any of the others to see the change in the beam's distribution. Also, the expectation values, variances and covariances of the phase space variables were calculated after the absorber. The distribution that models the particle beam gives the variability that physicists need to simulate many different situations in the Fragment Separator. The statistics and visualizations will allow quick analysis of the particle beam. Both of these developments will contribute to the overall viability of the RIA proposal.

INTRODUCTION

Argonne National Laboratory (ANL) is actively pursuing research and design for a Rare Isotope Accelerator (RIA) facility that will aid basic research in nuclear physics. The joint Department of Energy (DOE) and National Science Foundation (NSF) Nuclear Science Advisory Committee stated in their long range plan that "The Rare Isotope Accelerator (RIA) is our highest priority for major new construction" [8]. RIA will allow further study on the nature of nucleonic matter, the origin of the elements, the Standard Model, and nuclear medicine. It will make this research possible by creating beams of unstable, short-lived isotopes for scientific analysis.

There is a lot of planning that goes into the design for such a facility. An important part of this design is the creation of a

computer model of the beam line. In the Fragment Separator, isotopes with a specific mass over charge ratio are selected based on their trajectories in electromagnetic fields. Those with the same mass over charge ratio are further separated by an absorber that allows for the selection of a specific isotope by decoupling mass and charge. This project focuses on modeling and visualizing the particle beam in the Fragment Separator.

The development of such a model requires a multivariate, correlated Gaussian distribution to model the particle beam before it passes through the absorber. Each particle in the distribution is given six variables (phase space variables) that track its position, momentum, and energy. This distribution will allow physicists to vary the dependence and mean of the six phase-space variables as they run simulations. This type of flexibility will make it possible to test the fragment separator in a variety of conditions as research is done to design RIA.

As the beam passes through the absorber, the particle distribution changes and new particles are developed. Currently, very large output files of numbers are created as the result of the absorber simulation. An extension was written to represent the data meaningfully in a graphic form and calculate statistics on the large data set. This will allow physicists and non-physicists alike to make quick and accurate analysis of the particle beam distribution generated by the fragment separator model.

These two important pieces, creating a multivariate, correlated Gaussian distribution and generating graphics to show how the distribution that models the particle beam changes, will be integrated into the existing model in the COSY INFINITY language. "COSY INFINITY is an arbitrary order beam dynamics simulation and analysis code. It allows the study of accelerator lattices, spectrographs, beamlines, electron microscopes, and many other devices" [7]. It is especially useful in the Fragment Separator simulations because its implementation of differential algebra allows it to quickly compute high-order derivatives.

MATERIALS AND METHODS

The development of the Gaussian distribution that models the particle beam required research in both mathematics and computer science. A random vector $X = [X_1,..., X_N]$ follows a multivariate, Gaussian distribution [6],[12],[13] if there is a vector $\mu = [\mu_1,...,\mu_N]$ and a symmetric, positive definite covariance matrix S (N x N matrix) such that X has density

$$p(X_1,...,X_N) = \frac{1}{\sqrt{(2\pi)^N |S|}} e^{-\frac{1}{2}(X-\mu)^T S^{-1}(X-\mu)}.$$

The covariance matrix of x_i is S, which is equal to

$$S \equiv \begin{pmatrix} < X_1^2 > & < X_1 X_2 > & \dots \\ \dots & < X_2^2 > & \dots \\ \dots & \dots & \dots \end{pmatrix},$$

where $< X_1^2 >, < X_2^2 >, \dots, < X_n^2 >$ are the variances of the Gaussian variants and $< X_1 X_2 >, < X_i X_j >, \dots, < X_n X_n >$ are the covariances.

In order to create such a distribution, an uncorrelated X was created, with means, $\mu = 0$ and a covariance matrix D, such that

$$D \equiv \begin{pmatrix} < X_1^2 > & 0 & \dots \\ 0 & < X_2^2 > & \dots \\ \dots & \dots & \dots \end{pmatrix}.$$

In this case, D was diagonal with all of the covariances equal to zero. Then the density function was rewritten as

$$p(X_1,...,X_N) = \frac{1}{\sqrt{(2\pi)^N |D|}} e^{-\frac{1}{2}X^T D^{-1} X}.$$

Next, a linear transformation A was applied to X, such that $Y = AX$ and $\det(A) \neq 0$. This meant that $X = A^{-1}Y$ and $X^T = (A^{-1}Y)^T = Y^T (A^{-1})^T$. Looking back at the exponential part of the density function, $X^T D^{-1} X$, this was rewritten as $Y^T (A^{-1})^T D^{-1} A^{-1} Y$. Therefore the density function for a multivariate Gaussian distribution in Y was written as

$$p(Y_1,...,Y_N) = \frac{1}{\sqrt{(2\pi)^n |S|}} e^{-\frac{1}{2}Y^T S^{-1} Y},$$

where S, the covariance matrix was given by

$$S = \left\{ (A^{-1})\mathrm{T}\, D^{-1}\, A^{-1} \right\}^{-1} = ADA^T$$

Since A was chosen to be orthogonal,

$$A^{-1} = A^T,$$
$$|A| = \pm 1,$$
$$|S| = |ADA^T| = |D|.$$

This allowed the density function to be rewritten as

$$p(Y_1,...,Y_N) = \frac{1}{\sqrt{(2\pi)^n |D|}} e^{-\frac{1}{2}Y^T S^{-1} Y}.$$

Then Y could generate a correlated Gaussian distribution centered at zero. In order to allow for any mean as an input, Z was defined as a function of μ and S where

$$Z = Y + \mu.$$

Based on this theory, the COSY function developed took a covariance matrix, S, as an input to describe the dependence between the Gaussian random variables that were generated. The other inputs were the number of variables (n), and a vector (μ) containing the desired means for the variables. It output the vector Z as a set of correlated Gaussian random variables. Generally, it is expected for this calculation to be done in a six-dimensional phase space, but the algorithm was generalized for any number of variables.

In order to develop such a function, first the covariance matrix S was diagonalized and the diagonalization matrix T was stored. Then, n independent Gaussian random variables were generated, using the Eigen values of S as the variances. Finally, T was multiplied by W, where W was the vector formed by the independent Gaussian random variables, and the resulting vector was output as a set of correlated Gaussian random variables [9].

COSY has a built-in function that writes a matrix as $B^{-1}DB$, where D is a diagonal matrix with the Eigen values on the diagonal. This Jordan decomposition of sorts was rewritten for better

integration with the model and to decompose the matrix into the form BDB^{-1}. However, this decomposition does not guarantee that the transformation matrix B is orthogonal. Without this guarantee, BDB^{-1} does not have to equal the decomposition for S, ADA^T. Therefore, a new decomposition, the Schur decomposition which writes a matrix as ADA^T (with A being orthogonal) was needed. To transform from the Jordan BDB^{-1} form available in COSY to the Schur ADA^T form needed, the following calculation was performed:

$$S = ADA^T = BDB^{-1}.$$

Because A was orthogonal, $A^T = A^{-1}$. Therefore, $ADA^{-1} = BDB^{-1}$. Then it was shown that $(B^{-1}A)D = D(B^{-1}A)$, and thus $B^{-1}A$ commuted with D. D was an arbitrary diagonal matrix, and only diagonal matrices commute with such matrices. Therefore, $B^{-1}A$ was set equal to some diagonal matrix d. This meant that

$$B^{-1}A = d,$$
$$A = Bd.$$

Because A was orthogonal,

$$AA^T = I,$$
$$(Bd)(Bd)^T = I,$$
$$Bdd^T B^T = I,$$
$$BddB^T = I,$$
$$Bd^2 B^T = I,$$
$$d^2 = (B^T B)^{-1},$$
$$d = \sqrt{(B^T B)^{-1}}.$$

Therefore, the transformation was concisely written as

$$A = B\sqrt{(B^T B)^{-1}}.$$

Now that the covariance matrix was diagonalized in the proper form, the next step was creating the independent Gaussian random variables. This was done with the Box-Muller transform [11]. Given r and φ independently, uniformly distributed random variables in (0,1), then

$$z_0 = \cos(2\pi\varphi)\cdot\sqrt{-2\ln(r)},$$

where z_0 is the Gaussian random variable. A procedure was written in COSY to generate a Gaussian random variable based on this transformation and taking a desired variance and mean. In this case the variance was the Eigen value from the covariance matrix.

Finally, the diagonalization matrix, T, obtained after changing the Jordan decomposition to the Schur decomposition was multiplied by the vector of independent, Gaussian random variables and this created a vector of correlated, Gaussian random variables. This procedure was then called many times, and the results were analyzed to determine their validity.

In order to generate valid covariance matrices to input as test cases, another math theorem was used. If a matrix A is an *m x n* real matrix with $m > n$, then A can be written using a singular value decomposition of the form $A = UDV^T$. In this case, U is an *m x n* matrix and V is an *n x n* square matrix, both of which have orthogonal columns such that $U^TU = V^TV = I$, and D is a *n x n* diagonal matrix [10]. This decomposition was used to generate orthogonal matrices (U,V) which could then be used with a diagonal matrix containing the test Eigen values to generate a symmetric, diagonalizable test covariance matrix S.

As part of the testing, a statistics procedure was written to recalculate the expectation values, variances, and covariances produced and display them alongside the expected input values. Optimizations were added to this computationally intensive code so that the memory for the calculation arrays was dynamically allocated. Another enhancement took advantage of the symmetric nature of the covariance matrix, only calculating the upper half of the covariance matrix and thereby cutting the runtime of the statistics calculation nearly in half.

After completing work on the particle distribution to model the beam before the absorber, the project focused on visualizing and analyzing the output files produced by the absorber simulation code. An isotope file is created after each slice of the absorber that shows how many of each type of isotope are present in the beam. A particle file is created for each isotope present in the beam after the last slice and it contains the six phase space variables for each particle of that type.

Procedures were written in COSY to read in this data, calculate statistics on the data set, and visualize the important elements. The expectation values, variances and covariances were calculated for each of the phase space variables. These values summarized large amounts of data and were output to a single file. One visualization was developed in three-dimensions to show the amount of each type of isotope present after each slice of the absorber. Another visualization plots any of the phase space variables against any other phase space variable. The statistics and visualizations were tested with a variety of cases to ensure that they would be accurate representations of the data set.

RESULTS

The multivariate, correlated Gaussian distribution was developed with the following two-variable test case [9]. The covariance matrix S, was given as $\begin{pmatrix} 3 & 2 \\ 2 & 4 \end{pmatrix}$.

The Eigen values of S are $\frac{(7 \pm \sqrt{17})}{2}$,

which is approximately equal to 5.562 or 1.438. The corresponding Eigen vectors are

$$s_1 = \begin{pmatrix} 0.615 \\ 0.788 \end{pmatrix} \qquad \text{and } s_2 = \begin{pmatrix} 0.788 \\ -0.615 \end{pmatrix}..$$

In order to generate pairs (z_1, z_2) of Gaussian random numbers with the given covariance matrix, draw (y_1, y_2) Gaussian, uncorrelated, with variances 5.562 and 1.438. Then compute (z_1, z_2) as

$$\begin{pmatrix} z_1 \\ z_2 \end{pmatrix} = \begin{pmatrix} 0.615 & 0.788 \\ 0.788 & -0.615 \end{pmatrix} \cdot \begin{pmatrix} y_1 \\ y_2 \end{pmatrix}.$$

This test case was used until it was shown that the Eigen values and Eigen vectors could be calculated correctly in order to create correlated, Gaussian random numbers. The uncorrelated random variables were created with the Box-Muller transform from a uniform random number generator. However, when tested with 25,000 iterations centered at 100, the uniform random number generator was not perfectly uniform (Figure 1). This non-uniformity introduces a small amount of error.

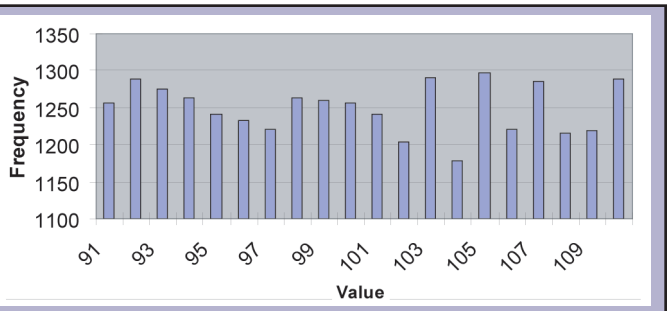

Figure 1. Uniform Random Distribution (25,000)

The next test was to see if the distribution of one variable was indeed Gaussian. A single, Gaussian, random variable was created using the Box-Muller transform 25,000 times and the distribution is shown in Figure 2. The bell curve is instantly recognizable.

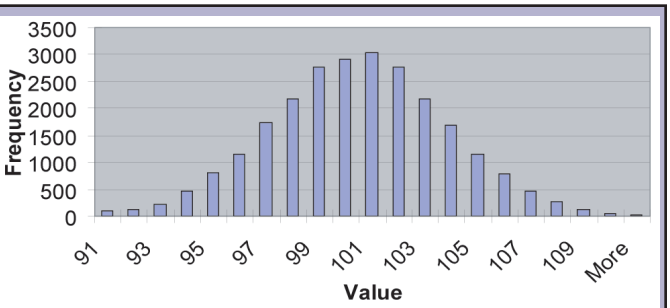

Figure 2. Gaussian Random Distribution (25,000)

A procedure was written to generate somewhat random test cases in two, three and six variables. In the two variable case, rotation matrices were used as orthogonal matrices to create symmetric, diagonalizable covariance matrices to use as inputs. These rotation matrices were of the form

$$\begin{pmatrix} \cos(\theta) & \sin(\theta) \\ -\sin(\theta) & \cos(\theta) \end{pmatrix}.$$

The three variable tests were also created from orthogonal matrices. These were generated in Mathematica® and were of the form

$$\begin{pmatrix} a & c & b \\ b & a & c \\ c & b & a \end{pmatrix}.$$

The six-variable tests took advantage of the singular-value decomposition to create 6 x 6 orthogonal matrices that could be used to generate valid covariance matrices. All of these cases created the covariance matrix from an orthogonal matrix A by multiplying $A^{-1} * D * A$, where D was a diagonal matrix with the Eigen values on the diagonal.

While many tests were run in two, three, and six variables during development, an example of a typical six variable test is as follows. The covariance matrix generated is given in Figure 3. The rounded input Eigen values in the D matrix were 12.469, 4.0517, 13.839,

10.598	.18021	-1.3869	.39434	2.6909	1.2784
.18021	11.444	.77670	4.1156	-1.9797	-2.6044
-1.3869	.77670	9.3385	2.3855	1.8617	2.0057
.39434	4.1156	2.3855	11.462	1.4981	-2.1241
2.6909	-1.9797	1.8617	1.4981	9.0835	-.84000
1.2784	-2.6044	2.0058	-2.1241	-.84000	13.125

Figure 3. Input Covariance Matrix

10.531, 18.005, and 6.1554. After the matrix was decomposed, the Eigen values were output and they were exactly the same out to 15 significant digits. The input covariance matrix was also recalculated and it was exactly the same out to 14 significant digits. The Jordan transformation matrix is given in Figure 4 and the Schur transformation matrix is given in Figure 5.

.41612	-.07196	.12966	-1.1971	.57873	1.1005
-.36983	.70910	.45016	-1.1276	-.23231	-.07353
.46467	.12289	.47397	.81362	-.43161	1.2441
.06911	.70659	-.69796	.06343	-.09364	1.0310
-.61197	.02728	.18875	.90775	.43519	1.2549
-.30797	-.65899	-.18193	-.82532	-.47606	1.1901

Figure 4. Jordan Transformation Matrix

.41612	-.05961	.12966	-.54214	.57873	.42144
-.36983	.58737	.45016	-.51068	-.23231	-.02816
.46467	.10179	.47397	.36846	-.43161	.47644
.06911	.58530	-.69796	.02872	-.09364	.39484
-.61197	.02260	.18875	.41109	.43519	.48057
-.30797	-.54587	-.18193	-.37376	-.47606	.45577

Figure 5. Schur Transformation Matrix

The test created 25,000 sets of six correlated, Gaussian random variables. All of the expectation values were set to zero and the output expectation values are given in Table 1. The variances and covariances were also calculated and the results are shown in Table 2. These variances and covariances should converge to the values given in the input covariance matrix.

Other tests were conducted to examine the correlation of two variables. Figure 6 shows two variables with a correlation coefficient of zero. Figure 7 shows a perfect correlation, where the coefficient is

	Input Expectation Value	Experimental Expectation Value (25,000 iterations)
E(X)	0.00000000000000	-.1164935988960410E-001
E(A)	0.00000000000000	-.2874439761976170E-001
E(Y)	0.00000000000000	.5855313062040197E-002
E(B)	0.00000000000000	-.1004700561425346E-001
E(L)	0.00000000000000	.4222684426054750E-002
E(D)	0.00000000000000	-.1427094209738337E-001

Table 1. Expectation Values.

	X	A	Y	B	L	D
X	10.671	.20779	-1.4274	.34818	2.6728	1.3420
A		11.307	.69172	4.0452	-2.0736	-2.6828
Y			9.2482	2.3314	1.8719	1.9073
B				11.326	1.4360	-2.1624
L					9.2897	-.80201
D						13.138

Table 2. Variances and Covariances.

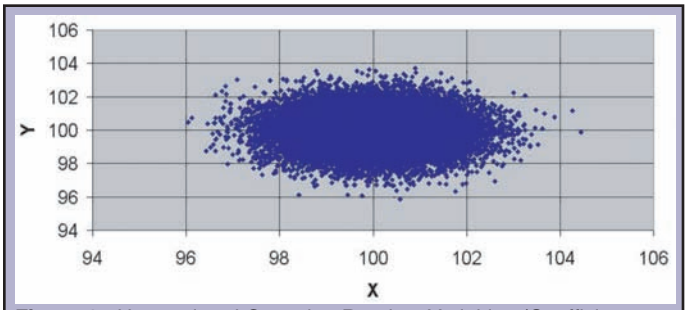

Figure 6. Uncorrelated Gaussian Random Variables (Coefficient = 0, {25,000}.

one. Figures 8 and 9 show correlations of $\frac{2}{3}$ and $-\frac{3}{4}$. With 25,000 pairs of correlated, Gaussian variables in each figure, the shape of the correlation can be seen.

The visualizations were checked to ensure that they were accurate and usable in many situations. The 3D isotope visualization was developed with a small data set of three slices. The test data set can be seen in Table 3. Figure 10 shows the number of each type of isotope present before slice one. Figures 11 and 12 show the number of each type present before slices two and three. Figure 13 shows the final results after slice three. Each isotope was represented in the proper location with a scaled bar to show its height. The scales on the axes adjusted appropriately and new isotopes did show up in the correct locations on subsequent slices.

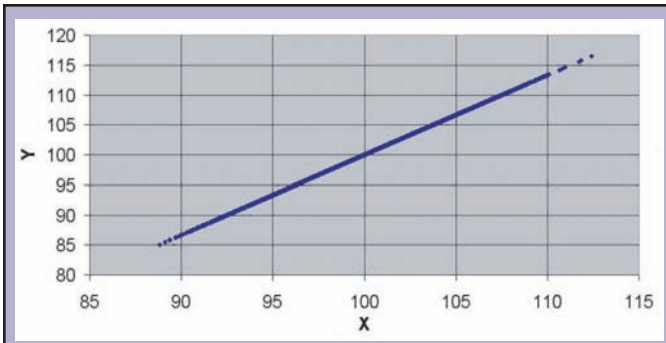

Figure 7. Correlated Gaussian Random Variables (Coefficient = 1) {25,000}.

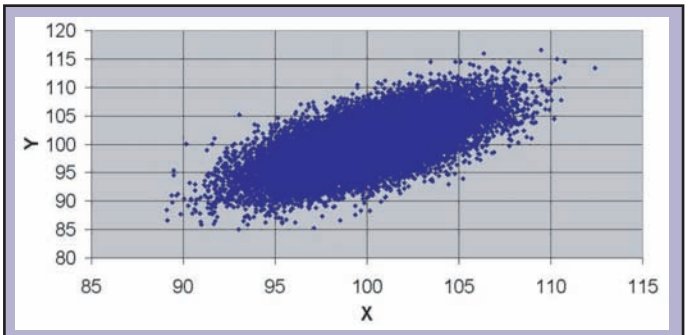

Figure 8. Correlated Gaussian Random Variables (Coefficient = 2/3) {25,000}.

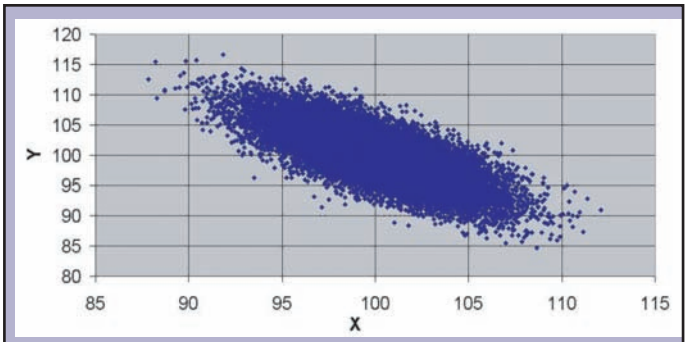

Figure 9. Correlated Gaussian Random Variables (Coefficient = -3/4) {25,000}.

A larger data set with ten slices was also run and the final graph can be seen in Figure 14. The isotopes with the top five yields have been colored and the rest are dark blue. A filter was created to allow physicists to focus on a particular subset of data, and an example of this can be seen in Figure 15 where only isotopes with a mass greater than 110 are considered.

	BEFORE SLICE 1			BEFORE SLICE 2			BEFORE SLICE 3			AFTER SLICE 3		
	Mass	Charge	Count	Mass	Charge	Count	Mass	Charge	Count	Mass	Charge	Count
1	132	50	1500	132	50	1200	132	50	1400	132	50	1700
2	100	38	1200	100	38	1100	100	38	1300	100	38	1000
3	180	10	1000	180	10	1050	180	10	800	180	10	900
4	58	80	800	58	80	900	58	80	400	58	80	750
5	150	20	500	150	20	300	150	20	350	150	20	550
6				120	8	250	120	8	300	120	8	400
7							45	93	150	45	93	100

Table 3. Test Data Set for Isotopes Graph (three slices).

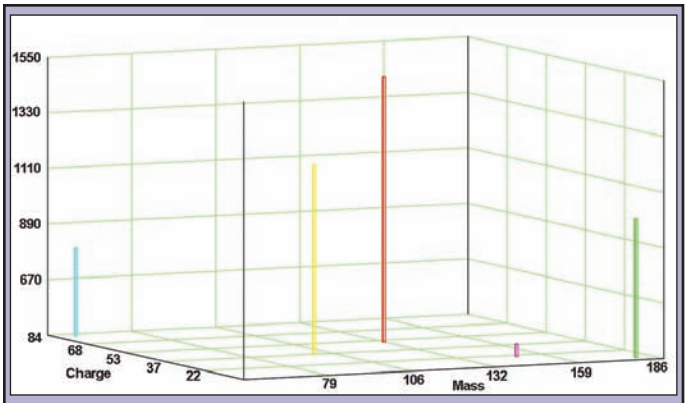

Figure 10. Isotope Graph Before Slice One (Test Data Set)

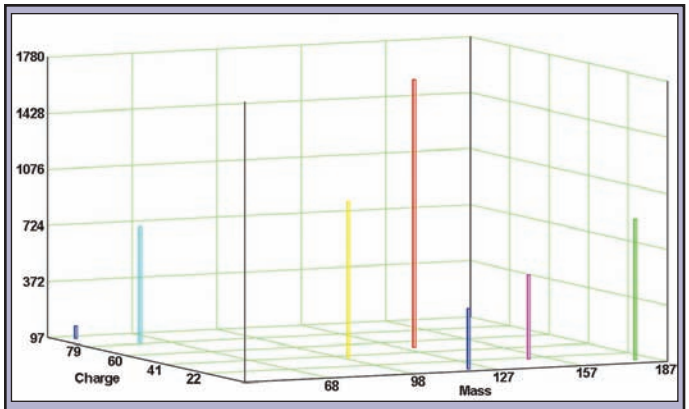

Figure 13. Isotope Graph After Slice Three (Test Data Set)

The 2D plots of any one phase space variable against any other phase space variable were tested by using this filtering capability to reduce the data to a very small set. Adding in one particle at a time, it could be seen that the scale was correct and the plot was a good representation of the data set. Figure 16 shows X versus Y, which is the horizontal position of the particle versus the vertical position. This is like looking right at the particle beam. The data set is the same as the ten slice run from Figures 14. The colors of each dot correspond to the colors given to each isotope in Figure 14. Figure 17 shows X versus A, the horizontal position versus the horizontal momentum.

The final test was to make sure that the expectation values, variances and covariances that summarized all of the particle data in the particle files were accurate. This was done in a similar fashion, where the data set was first filtered to one particle. Then, as each particle was added, the new statistics were calculated by hand and confirmed.

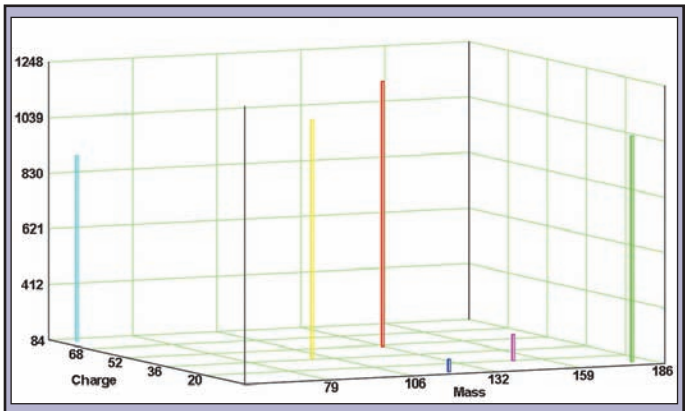

Figure 11. Isotope Graph Before Slice Two (Test Data Set)

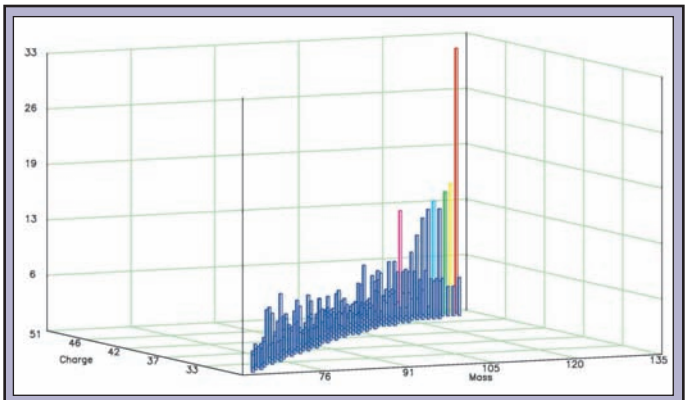

Figure 14. Isotope Graph After Slice Ten (Large Data Set)

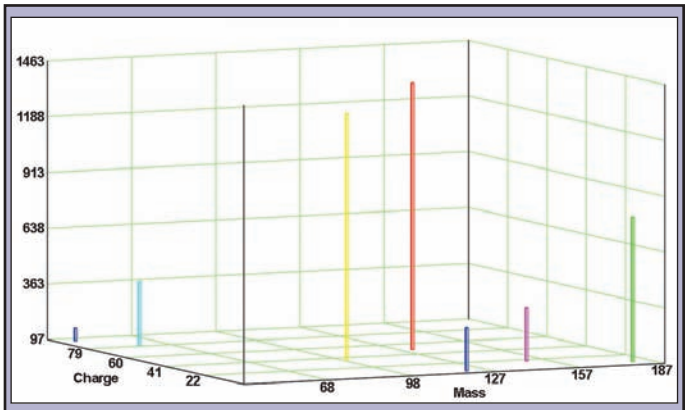

Figure 12. Isotope Graph Before Slice Three (Test Data Set)

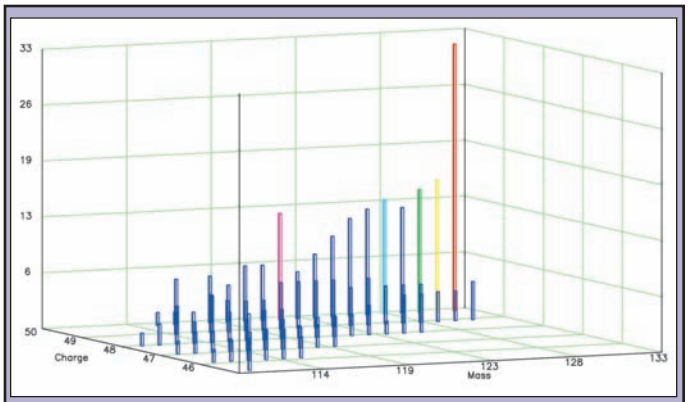

Figure 15. Filtered Data Subset (mass > 110)

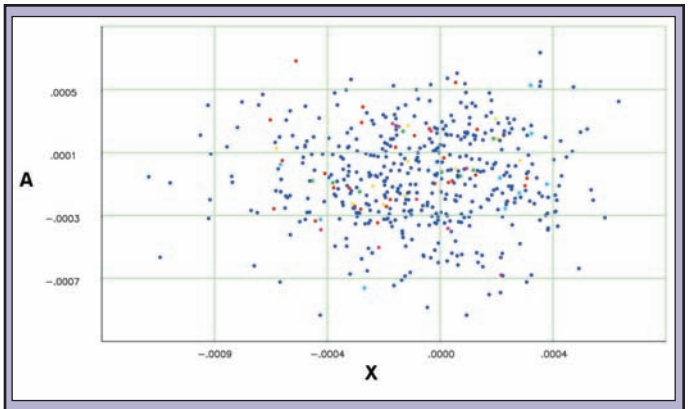

Figure 16. Particle Plot of X vs. Y (horizontal vs. vertical position)

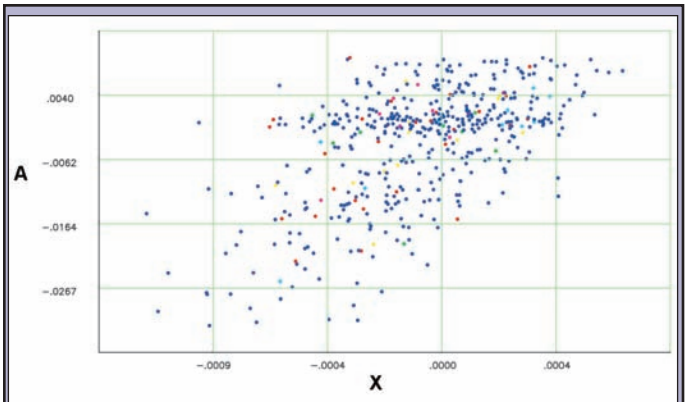

Figure 17. Particle Plot of X vs. A (horizontal position vs. horizontal momentum)

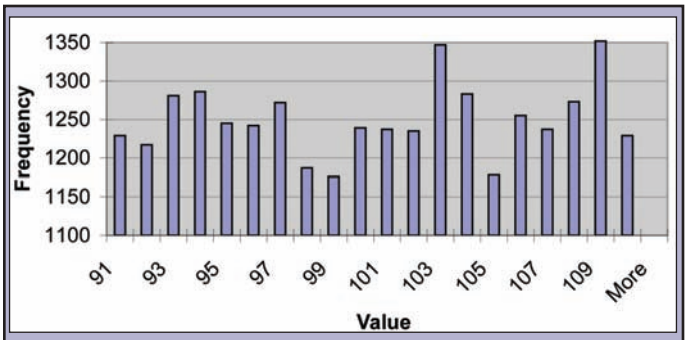

Figure 18. COSY's Uniform Random Number Generator (RERAN) {25,000}

DISCUSSION AND CONCLUSION

The major question was what was causing the small amounts of error in the Gaussian distribution. It is estimated that most of the error in the calculations is due to the non-uniformity of the random number generator (Figure 1). Another generator that is included in COSY (RERAN) was tested, but was actually a bit worse (Figure 18). However, the amount of error was small and the distribution will still be quite useful for running a variety of simulations in RIA's Fragment Separator. Also, the visualizations and statistics will make it possible for physicists to analyze the results of different types of absorbers. Both of these will contribute to the research necessary to design a Rare Isotope Accelerator.

ACKNOWLEDGMENTS

The author would like to acknowledge the Office of Science and the Department of Energy for providing such a great research opportunity. Argonne National Laboratory and the Physics Division were both excellent hosts. Lou Harnisch, Nancy Nega, Frank Vivio, Natalie Kremer, Lisa Reed and the rest of the education staff were outstanding. Dr. Bela Erdelyi was a brilliant mentor who taught, challenged, and made this project possible. Finally, I would like to thank my wife Amanda, whose support and encouragement was indispensable.

REFERENCES

[1] M. Berz, J. Hoefkens, and K. Makino, "COSY INFINITY Version 8.1 Programming Manual," MSUHEP-20703, Department of Physics and Astronomy, Michigan State University (2002).

[2] M. Berz and K. Makino, "COSY INFINITY Version 8.1 User's Guide and Reference Manual," MSUHEP-20704, Department of Physics and Astronomy, Michigan State University (2002).

[3] O. Knill. Multivariable Calculus in Probability [Online]. Available: http://abel.math.harvard.edu/archive/21a_spring_03/handouts/statistics.pdf (June 2005).

[4] T. Barlow, "Task 23: COSY Absorber Addition," Argonne National Laboratory, Argonne, IL (June 2005).

[5] T. Barlow, "Task 25: COSY Absorber Addition," Argonne National Laboratory, Argonne, IL (June 2005).

[6] E. Kreyszig, *Advanced Engineering Mathematics*, 8th ed. Hoboken: John Wiley & Sons, Inc. (1999).

[7] The COSY INFINTY web page [Online]. Available: http://www.bt.pa.msu.edu/index_files/cosy.htm

[8] The DOE/NSF Nuclear Science Advisory Committee, "Opportunities in Nuclear Science A Long-Range Plan for the Next Decade" (April 2002).

[9] F. J. Vesely. Introduction to Computational Physics Course Material [Online]. Available: http://homepage.univie.ac.at/Franz.Vesely/cp0102/dx/dx.html (October 2001).

[10] E. Weisstein, "Singular Value Decomposition", MathWorld-A Wolfram Web Resource [Online]. Available: http://mathworld.wolfram.com/SingularValueDecomposition.html

[11] Wikipedia, "Box-Muller Transform," [Online]. Available: http://en.wikipedia.org/wiki/Box-Muller_transform

[12] R. Walpole, R. Myers, S. Myers and K. Ye, *Probability & Statistics for Engineers & Scientists*, 7th ed. Upper Saddle River: Prentice-Hall Inc. (2002).

[13] Wikipedia, "Multivariate Normal Distribution," [Online]. Available: http://en.wikipedia.org/wiki/Multivariate_normal_distribution

Rebecca M. Ward graduated from McDaniel College in May 2006 with a B.A. in chemistry and physics. She participated in the Science Undergraduate Laboratory Internships (SULI) program during the summer of 2005, completing an internship in the Chemical Engineering Division of Argonne National Laboratory, where she contributed to the development of novel electrode materials for lithium ion batteries. She presented this work in February 2006 at the AAAS conference. She has also conducted dosimetry research at the National Institute of Standards and Technology and worked on laser cooling and trapping of rubidium atoms at Wellesley College as a NSF-REU student. In addition to her academic pursuits, she was a member of the McDaniel College Women's soccer team. She will be teaching physics at Pope John Paul II High School in Hendersonville, TN in the fall of 2006.

John T. Vaughey is a chemist at Argonne National Laboratory in the Electrochemical Technology Program within the Chemical Engineering Division. In 1987, he received his undergraduate degree in chemistry from Worcester Polytechnic Institute and in 1992 received his PhD in Inorganic Chemistry from Northwestern University. After completing postdoctoral studies at the University of Houston and Iowa State University/Ames Laboratory he started at Argonne National Laboratory in 1997. His efforts have concentrated on materials development and characterization of electroactive ceramics and metals. He has been active in the area of portable power developing novel electrode materials that have applications in hybrid electric vehicles, implantable medical devices, and consumer electronics.

OLIVINE COMPOSITE CATHODE MATERIALS FOR IMPROVED LITHIUM ION BATTERY PERFORMANCE

REBECCA M. WARD, JOHN T. VAUGHEY

ABSTRACT

Composite cathode materials in lithium ion batteries have become the subject of a great amount of research recently as cost and safety issues related to $LiCoO_2$ and other layered structures have been discovered. Alternatives to these layered materials include materials with the spinel and olivine structures, but these present different problems, e.g. spinels have low capacities and cycle poorly at elevated temperatures, and olivines exhibit extremely low intrinsic conductivity. Previous work has shown that composite structures containing spinel and layered materials have shown improved electrochemical properties. These types of composite structures have been studied in order to evaluate their performance and safety characteristics necessary for use in lithium ion batteries in portable electronic devices, particularly hybrid-electric vehicles. In this study, we extended that work to layered-olivine and spinel-olivine composites. These materials were synthesized from precursor salts using three methods: direct reaction, ball-milling, and a core-shell synthesis method. X-ray diffraction spectra and electrochemical cycling data show that the core-shell method was the most successful in forming the desired products. The electrochemical performance of the cells containing the composite cathodes varied dramatically, but the low overpotential and reasonable capacities of the spinel-olivine composites make them a promising class for the next generation of lithium ion battery cathodes.

INTRODUCTION

Lithium ion battery materials have recently become the subject of intense research interest. The use of these batteries in numerous portable devices, including mobile phones, laptop computers and medical devices has increased the demand for performance improvement. This demand is augmented by the potential use of lithium ion batteries for electric and hybrid electric vehicles where replacing the currently used nickel metal hydride batteries would provide the same performance but using only 20% of the space. For these large number of cell applications, the performance of lithium ion batteries is limited by abuse tolerance issues and the desire for higher energy storage capacities.

Attempts at improving the capacity of these batteries have historically focused on synthesizing and developing more lithium rich cathode materials. The presently used commercial cathode is a material with a layered structure, $LiCoO_2$, and is shown in Figure 1. Layered structures are useful for applications requiring high energy because they have a relatively high ratio of transition metal to lithium and they typically display good lithium diffusion properties. The energy of a cell is related to its ability to cycle large amounts of lithium over a long period, as opposed to the power of a cell, which is related to the rate at which lithium can be extracted. Most applications of the lithium ion batteries require high-energy batteries (e.g. laptops, mobile phones); however, the use of lithium ion batteries in

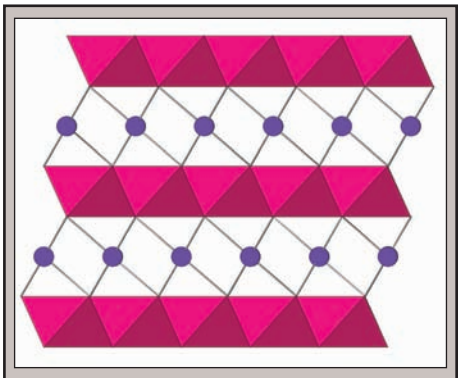

Figure 1. The structure of $LiCoO_2$. The blue spheres are Li cations, the red polyhedra represent cobalt centered octahedra.

hybrid-electric vehicles would require a battery that can also deliver excellent power.

There are several issues related to the continued the use of $LiCoO_2$, specifically its relatively low cycling capacity of 140 mAh/g [1], and, more importantly, the rising price of cobalt. Structural analogues containing nickel, manganese, and several combinations thereof have been studied as possible alternatives to $LiCoO_2$, but each of these materials presents different problems. $LiNiO_2$ has serious safety issues, namely at top of charge it can violently release oxygen. $LiMnO_2$, due in part to the Jahn-Teller nature of the Mn(III) cation, is unstable to delithiation, rapidly converting on cycling to a material with the three-dimensional spinel structure [1].

Spinels provide much faster cycling (higher power) than layered structures because of the three-dimensional structure, which usher lithium ions into and out of the cell more efficiently while maintaining electronic conduction via the three dimensional lattice. The use of the spinel $LiMn_2O_4$ (or $Li_{1+x}Mn_{2-x}O_4$) as a cathode material offers a higher power alternative to layered structures. Figure 2 displays the structure of a spinel. Although it is a cheaper and more powerful alternative to $LiCoO_2$, spinels have a lower capacity (100-120 mAh/g) and show poor cycling characteristics at elevated temperatures due to dissolution problems [2]. Another low-cost alternative to $LiCoO_2$ is the olivine $LiFePO_4$, the structure is shown in Figure 3. It can be made using simple low cost starting materials and provides a higher energy alternative ($LiFePO_4$ typically delivers 160 mAh/g; a ~15% improvement) to the layered materials. Because of its three dimensional structure, the volume change that occurs upon intercalation and deintercalation of lithium ions in olivine is smaller than in layered structures, resulting in increased electrode stability upon subsequent cycling. Additionally, there are less abuse tolerance concerns related to the energetic release of oxygen gas, as the $[PO_4]_{3-}$ group will not release oxygen under operating conditions. Unfortunately, incorporating the phosphate anion also makes olivine a very poor electrical conductor in comparison to other electrode materials [3]. In order to promote its utility as a cathode material, the conductivity of olivine must be increased. This has been addressed mainly by surface coating nano-sized materials with a conductive carbon or slightly reducing the surface to create a coating of highly conductive FeP_x or Fe_3O_4 [3, 4].

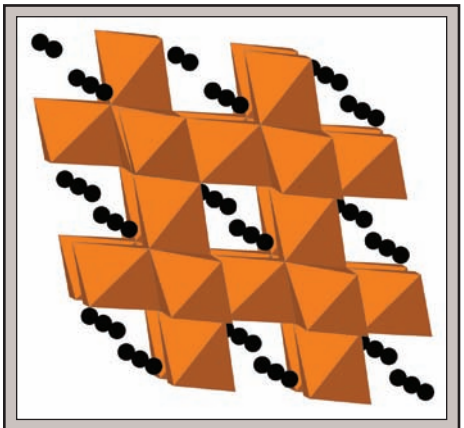

Figure 2. The structure of the spinel $LiMn_2O_4$. Black spheres represent lithium cations, the orange polyhedra are Mn-centered octahedra.

The purpose of this study was to improve the limited capacity of lithium ion batteries by developing layered-olivine and spinel-olivine composites that could serve as safe, cheap and effective cathode materials. The composite structures should produce a stabilizing effect on the cathode, allowing more lithium to be intercalated and deintercalated without encountering the thermodynamically driven structural collapse that occurs when too much lithium is extracted, while the spinel (or layered) component would increase the average conductivity of the sample. Three different approaches were taken in an attempt to synthesize these composites materials: direct reaction, ball milling and the core-shell approach. Materials were analyzed by X-Ray Diffraction and tested in half cells (vs. Li) for electrochemical performance.

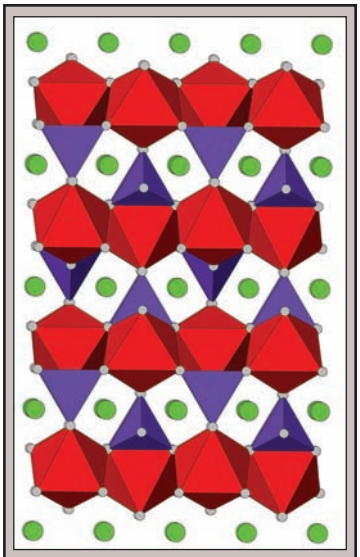

Figure 3. The structure of olivine, $LiNiPO_4$. The greens spheres are lithium cations, the blue polyhedra are phosphorus centered tetrahedral, the red polyhedra are nickel centered octahedra.

MATERIALS AND METHODS

The first method employed to synthesize layered-olivine composites was the direct reaction of precursor materials with the general stoichiometry $x\ LiNiPO_4 \bullet y\ Li(Ni_{0.5}Mn_{1.5})O_4$ and $x\ LiNiPO_4 \bullet y\ Li(Ni_{0.5}Mn_{0.5})O2$ (x = 0.9, 0.5; y = 0.1, 0.5). Physical mixtures of Li_2CO_3, $Ni(OH)_2$, $MnCO_3$, $NH_4H_2PO_4$, $(CH_3CO_2)_2Mn \bullet 4H_2O$ were prepared and ground by hand, and then fired to either 400 °C or 800 °C. The resultant powders were analyzed using X-Ray diffraction. Laminates containing the composite materials were made using 80% active material, 10% PvDF binder (Kureha), 5% acetylene black (Chevron C-55), and 5% carbon fiber (Osaka Gas) on aluminum foil. Cells were constructed in an argon-filled glovebox using a lithium metal anode, LP-40 electrolyte ($50\%_{wt}$ EC (ethylene carbonate)/ $50\%_{wt}$ DEC (diethyl carbonate), 1 M $LiPF_6$, Merck KG), and a Celgard polyethylene / polypropylene separator using methods described previously by the Argonne group [1].

The second technique utilized to prepare the same four composite stoichiometries outlined above was high energy ball milling. The same precursors were ground together and heated to 400 °C for 12 hrs in air. The materials were then broken down vigorously in the ballmill for approximately two hours. After processing, the materials were laminated and cells were constructed as described above.

The third procedure for producing composite materials was a core-shell synthetic method, which was used to synthesize both layered-olivine and spinel-olivine materials. The composites being made are listed in Table 1. Precursor salts, $(CH_3CO_2)_2Co \bullet 4H_4O$, $(CH_3CO_2)_2Mn \bullet 4H_2O$, $(CH_3CO_2)_2Ni \bullet 4H_2O$, $CH_3CO_2Li \bullet 2H_20$, were dissolved in ethanol and stirred constantly using a magnetic stirring bar. The individual stoichiometries were set to yield the compounds $LiCoO_2$, $Li_4Mn_5O_{12}$, and $LiNi_{0.5}Mn_{1.5}O_4$. $LiNiPO_4$

Composite	XRD Analysis	Cycling Cap. (mAh/g)	Theoretical Cap. (mAh/g)
10% $LiNiO_2$ / 90% $LiNiPO_4$	$(LiNi)O_2$, LiNiPO4	40	30
10% $LiMn_2O_4$ / 90% $LiNiPO_4$	$LiMn_2O_4$, $LiNiPO_4$	30	30
50% $LiNiO_2$ / 50% $LiNiPO_4$	$(LiNi)O_2$, $LiNiPO_4$	125-150	150
50% $LiMn_2O_4$ / 50% $LiNiPO_4$	$LiMn_2O_4$, $LiNiPO_4$	160	150
80%$LiCoO_2$ / 20%$LiNiPO_4$	$LiCoO_2$, $LiNiPO_4$	20-40	120
80% $Li_4Mn_5O_{12}$ / 20% $LiNiPO_4$	$Li_4Mn_5O_{12}$, $LiNiPO_4$	120-140	130
80% $LiNi_{0.5}Mn_{1.5}O_4$ / 20% $LiNiPO_4$	$LiNi_{0.5}Mn_{1.5}O_4$, $LiNiPO_4$	120-130	120
50% $LiCoO_2$ / 50% $LiNiPO_4$	$LiCoO_2$, $LiNiPO_4$	90	75
50% $Li_4Mn_5O_{12}$ / 50% $LiNiPO_4$	$Li_4Mn_5O_{12}$, $LiNiPO_4$	90	85
50% $LiNi_{0.5}Mn_{1.5}O_4$ / 50% $LiNiPO_4$	$LiNi_{0.5}Mn1.5O_4$, $LiNiPO_4$	80	80

Table 1. Results of the core-shell method for synthesis of layered-olivine and spinel-olivine composite materials (assuming LiNiPO4 is inactive in the testing window).

was made separately by heating a stoichiometric mixture of Li_2CO_3, $(CH_3CO_2)_2Ni \cdot 4H_2O$, and $NH_4H_2PO_4$ at 800 ºC for two days with one intermittent grinding. After analysis by powder XRD, the resulting material was then ground to a fine powder and sifted to remove any particles larger than 63 microns. This powder was added to the ethanol solution, stirred, and heated until dryness. The resultant powder was ground by hand and heated to 400 °C in air. Laminates and cells were constructed as described above.

Cells were tested on a Maccor battery cycling station, discharging and charging in a specified voltage window under constant current. A typical cycling window was 4.8 – 2.0 V (vs Li) using a 0.1 mA current. The amount of lithium passed between the electrodes as well as voltage profiles was monitored by the Maccor cycling software during charge and discharge of the electrochemical cell.

RESULTS AND DISCUSSION

Direct reaction synthesis and high energy ball milling — Several attempts were made to synthesize composite material with the general stoichiometry x $LiNiPO_4 \cdot$ y $Li(Ni_{0.5}Mn_{1.5})O_4$ and x $LiNiPO_4 \cdot$ y $Li(Ni_{0.5}Mn_{0.5})O_2$ (x = 0.9, 0.5; y = 0.1, 0.5). Lithium can only be extracted from $LiNiPO_4$ above 5.2 V (vs Li) but it was chosen for this study primarily because it is one of the few lithium olivine materials that can be synthesized in air. Analysis of powder X-Ray diffraction results for the composite direct reaction or balled milled samples revealed that all were a complex mixture of phases, rather than actual composites of an olivine ($LiNiPO_4$) and a layered or spinel structure. Figure 4 shows a typical XRD spectrum for these mixed phase materials, specifically the $LiNiPO_4$/ $LiNi_{0.5}Mn_{0.5}O_2$ (50/50%) for the 400 and 800 °C samples. All of the materials synthesized by this method were found to be physical mixtures of

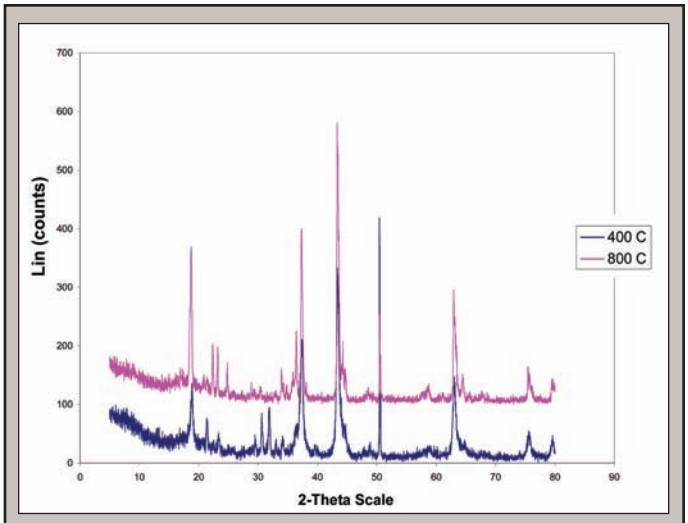

Figure 4. X-ray diffraction spectra of $LiNi_{0.5}Mn_{10.5}O_2$/ $LiNiPO_4$.

$(Li,Ni)O_2$, $Ni_3(PO_4)_2$, Li_3PO_4, $Li(Ni,Mn)O_2$, MnP_2O_7, and Li_2CO_3. Electrochemical and powder XRD analysis of the materials subjected to high energy ball-milling showed no significant differences between those samples and the ones produced by direct reaction.

The limiting factor in the formation of the layered-olivine composites in the direct reaction method appeared to be the formation of $LiNiPO_4$. The complex reaction mixture placed in the oven had three cations and two anions, from which the layered-olivine composite was expected to form. It appears that binary phosphates are too stable with respect to ternary phosphates at the stoichiometries loaded, resulting in Li_3PO_4 and $Ni_3(PO_4)_2$ to be formed preferentially over the desired $LiNiPO_4$ in the presence of Mn and excess oxide. This physical mixture of components is responsible for the poor electrochemical performance of the cells. The disordered structure of the cathode and the uneven dispersal of compounds with different electrical and ionic conductivities caused poor cycling demonstrated by the cells.

Core-shell synthesis method — Table 1 presents information on the materials synthesized using the core-shell type method. The 50/50 $LiNiO_2$ and $LiMn_2O_4$ composites materials performed much better than the 10/90 composites, as expected, and is shown in Figure 5. Though the cycling efficiency of these cells was lower than for the 10/90 composites, the capacities were significantly

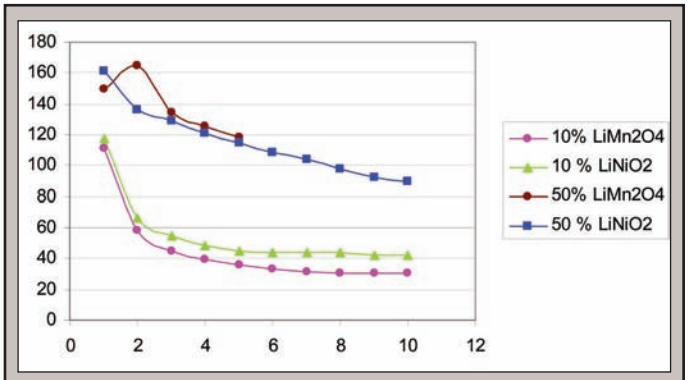

Figure 5. Discharge capacities for various core-shell composites. Balance of composition is $LiNiPO_4$.

higher. Both sets of materials cycled near their theoretical values, assuming the $LiNiPO_4$ component was electrochemically inactive in the voltage window used. The $LiNiO_2$/$LiNiPO_4$ cell had the highest capacity, ranging from 125-150 mAh/g, while the $LiMn_2O_4$/ $LiNiPO_4$ performed the best, with an initial capacity of 160 mAh/g and a fade rate of only 3-4 % per cycle. The time profile for this sample is shown in Figure 6, during charge reveals two plateaus, one around 3 V corresponding to the extraction of the first Li-ion

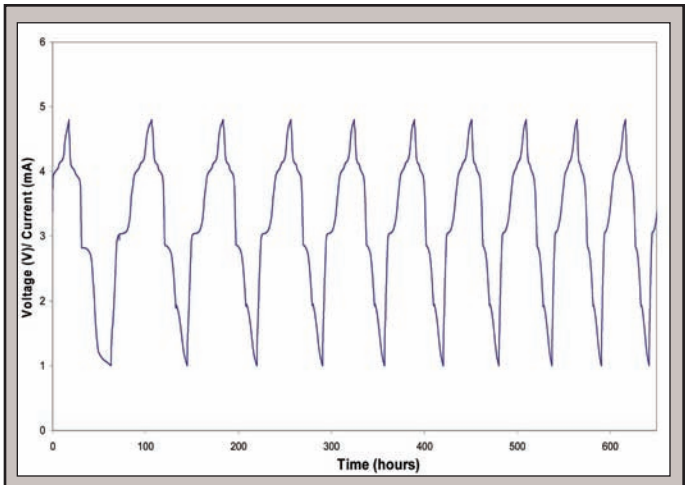

Figure 6. The time profile for $LiMn_2O_4$/ $LiNiPO_4$ (50/50).

from the fully charged material $Li_2Mn_2O_4$, resulting in a $LiMn_2O_4$ cathode material, and the second around 4.2 V corresponding to the extraction of a second Li-ion, forming Mn_2O_4 [5]. The plateaus for intercalation and deintercalation occur at nearly the same voltages, representing a small overpotential, which suggests the electrical conductivity was not seriously hindered by the underlying insulating phosphate. For many of these materials the initial first cycle capacity exceeded theoretical capacity. This is usually associated with one time side reactions between the electrode and electrolyte, current collector passivation, and reactions between amorphous phases in the electrode and lithium.

The improved electrochemical performance of the samples prepared using the core-shell synthesis method as compared to those produced by the direct reaction method suggests more structured products. The x-ray diffraction patterns for the layered-olivine and spinel-olivine composites are featured in Figure 7 and 8, respectively. Figure 9 shows the hypothetical composite structure of the layered-olivine composite. Figures 10 and 11 show the first three cycles of some representative spinel-olivine composites. The lattice constants for all of the spinels formed in this study are shown alongside the literature lattice constants in Table 2. Lattice constants were determined by full pattern fitting and analysis using the Rietveld method. The lattice constants of the spinel coating help give a better idea of the exact Li/Mn distribution over the various possible lattice sites when compared to literature precedent.

In general the $LiCoO_2$/$LiNiPO_4$ composites, ideally layered-olivine composites, showed poor electrochemistry. Both the 80/20 and 50/50 composites showed poor capacity retention. Over 50 cycles, the capacity of the 80/20 sample dropped from 55 to

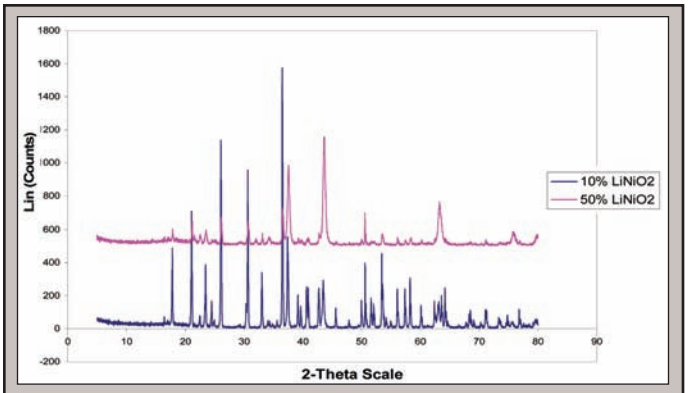

Figure 7. X-ray diffraction spectra for $LiNiO_2$/ LiNiPO4 composites. The two series have been offset for representation purposes.

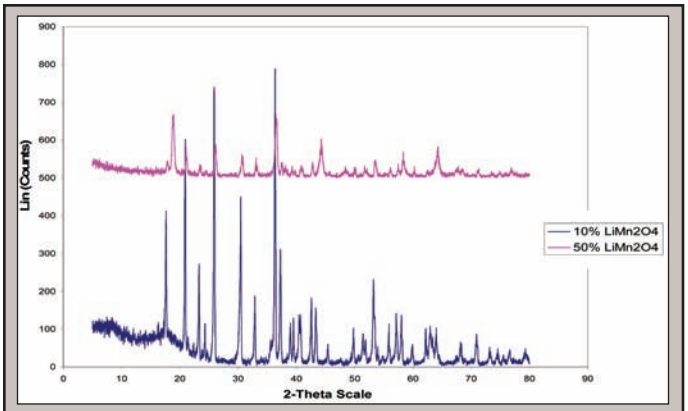

Figure 8. X-ray diffraction spectra for $LiMn_2O_4$/ $LiNiPO_4$ composites. The two series have been offset for representation purposes.

20 mAh/g, while the 50/50 sample showed an initial capacity of 95 mAh/g, but faded quickly. The powder x-ray diffraction analysis for this material indicated that the synthesized material contained the expected product, $LiCoO_2$ coated with $LiNiPO_4$, however some ambiguity exists in determining the exact form of the $LiCoO_2$ formed [6].

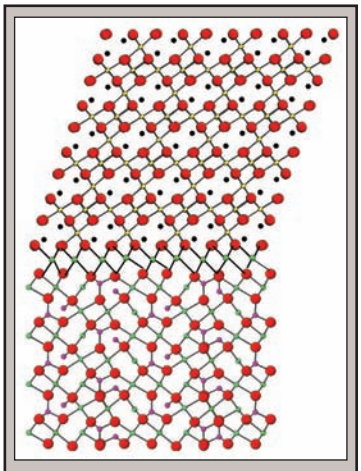

Figure 9. The ideal structure of the spinel-olivine composite.

The poor performance of these cells could reflect the poor crystallinity of the coating material. The synthesis of $LiCoO_2$, which involved the firing of the precursor materials to 400 °C, is well below the temperature at which $LiCoO_2$ is usually synthesized (700 °C), and can result in a poorly ordered sample. At these temperatures several other structures with inferior electrochemical properties have been reported with the same ratio of lithium to cobalt, notably $Li_2[Co_2]O_4$ or $(Li,Co)_2[Co]_2O_4$ spinels [6]. At the concentration levels used in this study, it would be difficult to distinguish a spinel structure from the desired layered structure by powder XRD as many of the main

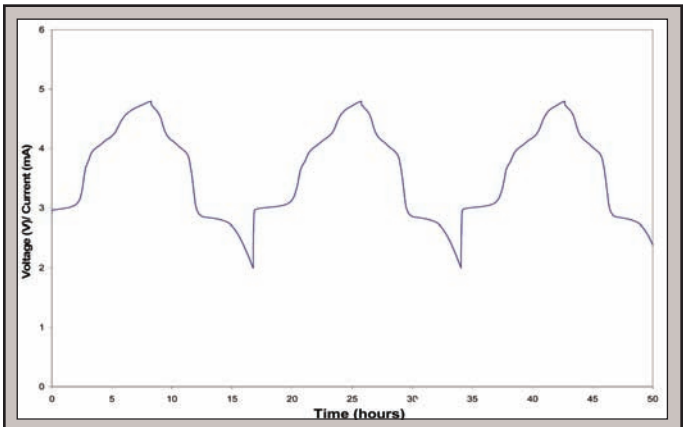

Figure 10. The time profile for $LiNi_{0.5}Mn_{1.5}O_4$/ $LiNiPO_4$ (80/20).

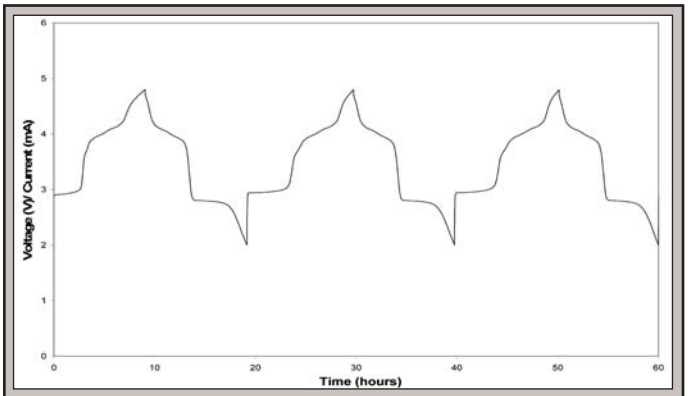

Figure 11. The time profile for $Li_4Mn_5O_{12}$/ $LiNiPO_4$ (50/50).

diagnostic peaks overlap. The low-temperature synthetic method used may have yielded a disordered or non-uniform coating material, resulting in poor electrical and ionic conductivity. It is very possible that the optimization of this composite material could produce a good cathode material for Li-ion batteries, possibly by annealing the material at a higher temperature.

The $LiNi_{0.5}Mn_{1.5}O_4$ / $LiNiPO_4$ composite produced using the core-shell synthesis method performed much better than the $LiCoO_2$ composite. The x-ray analysis for this data indicated that the product was the intended $LiNi_{0.5}Mn_{1.5}O_4$ spinel coating on $LiNiPO_4$. The time profile for the battery made with this composite material featured the two plateaus for the deinsertion of lithium at 3 V and 4 V, much like the $LiMn_2O_4$ composite, but with added capacity above 4.5 V (vs Li) indicative of the mixed Ni-Mn spinel and inclusion of some electrochemically active Ni(II) [7]. Figure 10 shows the time profile for the 80/20 composite. Furthermore, this material showed the same low overpotential as the spinel composite. The 50/50 composite showed a low but stable capacity, and the 80/20 composite had about the same capacity as a commercial $LiCoO_2$ cathode, but in a larger voltage window.

The final composite material synthesized and tested in this study was the $Li_4Mn_5O_{12}$/ $LiNiPO_4$ composite [8]. This composite is another spinel-olivine composite, and had a time profile very similar to that of $LiMn_2O_4$, as shown in Figure 11. This lithium rich Mn (IV) spinel is supposed to have all of its capacity at 3V, instead of a two plateaus at 3V and 4V as seen for $LiMn_2O_4$. Although by XRD analysis it has a lattice constant closer to that reported for

Composite	Experimental Lattice Constant (Å)	Literature Lattice Constants (Å)
50% $LiMn_2O_4$ / 50% $LiNiPO_4$	8.189(2)	8.244
80% $LiNi_{0.5}Mn_{1.5}O_4$ / 20% $LiNiPO_4$	8.148(1)	8.173
50% $LiNi_{0.5}Mn_{1.5}O_4$ / 50% $LiNiPO_4$	8.174(2)	8.173
80% $Li_4Mn_5O_{12}$ / 20% $LiNiPO_4$	8.139(2)	8.135
50% $Li_4Mn_5O_{12}$ / 50% $LiNiPO_4$	8.155(2)	8.135

Table 2. Table of spinel coating lattice constants.

$Li_4Mn_5O_{12}$, its electrochemistry is much more similar to $LiMn_2O_4$. The exact reason for these discrepancies is not known at this time. The batteries produced using this $Li_4Mn_5O_{12}$/ $LiNiPO_4$ composite as a cathode material behaved much like the batteries with the $LiNi_{0.5}Mn_{1.5}O_4$ / $LiNiPO_4$ composite cathode. The 50/50 composite showed a capacity just above that of the $LiNi_{0.5}Mn_{1.5}O_4$ 50/50, as did the 80/20 composite. Both the 50/50 and 80/20 composites had low overpotentials.

CONCLUSIONS

Of the two primary composite synthesis methods presented in this paper, direct reaction and core-shell, the core-shell synthesis method was far more successful. The direct reaction method proved inadequete for compounds with such a complex mixture of constituent anion and cations, especially when the synthesis required the anion to form a specific ternary compound within a collection of so many choices. The core-shell method was particularly effective for the synthesis of spinel-olivine materials. The synthesis of layered-olivine structures proved more problematic, though it was still successful the majority of the time.

The layered-olivine composites in general showed high overpotentials, suggesting the conductivity of the underlying olivine may have been an issue and the coating may have not been complete. The disordered nature of the layered compounds synthesized makes the intercalation / deintercalation of lithium ions much more difficult. This overpotential issue is a major problem that must be addressed before such composite materials can be seriously considered for use in commercial lithium ion batteries.

Unlike the layered-olivine composites, the spinel-olivine composites show low overpotentials, which suggests the excellent conductivity of the spinel structure compensates for the insulating nature of the phosphate group, producing a sufficiently conductive material. The spinel-olivine composite materials also show capacities ranging from 100-160 mAh/g, which will be a viable operating capacity if the fade rate can be reduced. A major problem these cells present is cycling efficiency, which is higher for the spinel composites than for the layered composites. Despite this shortcoming, the low overpotentials, capacity, safety benefits and ease of production of

spinel-olivine composite materials could make them an ideal class of materials from which to build the cathodes of next generation of lithium ion batteries.

ACKNOWLEDGMENTS

This research was conducted at Argonne National Laboratory. RW thanks the U.S. Department of Energy, Office of Science for funding and the organization of the SULI program. Financial support from the Office of Basic Energy Sciences and the Office of FreedomCar and Vehicle Technologies of the U.S. Department of Energy under Contract No. W31-109-Eng-38 is gratefully acknowledged.

REFERENCES

[1] M. Thackeray, C. Johnson, J. Vaughey, N. Li and S. Hackney, "Advances in Manganese-Oxide 'Composite' Electrodes for Lithium-Ion Batteries," in *Journal of Materials Chemistry*, Vol. 15, 2005, pp. 2257-2267.

[2] J.-M. Tarascon and M. Armand, "Issues and Challenges Facing Rechargeable Lithium Batteries," in *Nature*, Vol. 414, November 2001, pp. 359-367.

[3] P. Subramanya Herle, B. Ellis, N. Coombs and L.F. Nazar, "Nano-Network Electronic Conduction in Iron and Nickel Olivine Phosphates," in *Nature Materials*, Vol. 3, March 2004, pp. 147-152.

[4] M. Doeff, Y. Hu, F. McLarnon, R. Kostecki, "Effect of Carbon Surface Structure on the Electrochemical Performance of $LiFePO_4$" in *Electrochemical and Solid State Letters*, Vol. 6, October 2003, pp. A207-209.

[5] J. Greedan, C. Wiebe, A. Willis and J. Stewart, "Neutron-Scattering Studies of the Geometrically Frustrated Spinel," in *Physical Review B*, Vol. 65, May 2001, pg. 184424.

[6] R. Gummow, D. Liles, M. Thackeray, "Spinel versus Layered Structures for Lithium Cobalt Oxide Synthesized at 400°C" *Materials Research Bulletin*, Vol. 28, March 1993, pp 235-246.

[7] K. Takahashi, M. Saitoh, M. Sano, M. Fujita and K. Kifune, "Electrochemical and structural properties of a 4.7 V-class $LiNi_{0.5}Mn_{1.5}O_4$ positive electrode material prepared with a self-reaction method," in *Journal of Electrochemical Society*, Vol. 151, Jan 2004, pp. A173-A177.

[8] Y. Zhang, B. Want, H. Yan, A. Ahniyaz and M. Yoshimura, "Low Temperature Synthesis of Nanocrystalline $Li_4Mn_5O_{12}$ by a Hydrothermal Method," in *Materials Research Bulletin*, Vol. 37, July 2002, pp. 1411-1417.

Jennifer Wang received her B.S. in chemistry from Rice University in 2006. At NREL she participated in the Science Underground Laboratory Internships (SULI) program, working on the nanoscale manipulation of zinc oxide structures to improve their functionality in hybrid ZnO/organic nanocomposite photovoltaic devices. She presented this work with a poster at the 2006 AAAS Meeting in St. Louis. At Rice she performed additional undergraduate research on magnetic and semiconductor nanomaterials and the analysis of biodiesel by gas chromatography. Her interests outside the lab are in sustainable design and environmental advocacy, with the aim of integrating research and fieldwork with application and outreach. She is currently working in this field and will pursue a graduate degree in a related discipline.

David S. Ginley is currently a Group Manager in Process Development and Advanced Concepts at the National Renewable Energy Laboratory, leading activities in the applications of nanotechnology, organic electronics, transition metal oxides (ferroelectric materials, rechargeable Li batteries, and transparent conductors) and ink jet printing. He leads a team in the development of nanoparticle-based precursors to electronic materials, particularly as they apply to photovoltaic and optoelectronic technologies. Recent activities include a program on combinatorial approaches to electronic materials and a program on polymer-based photovoltaic cells and OLEDs. For more than 25 years, he has been active in developing a basic understanding of the relationships between structure and the optoelectronic properties in a variety of materials. Dr. Ginley graduated from the Colorado School of Mines with a B.S. in mineral engineering chemistry. He subsequently received a PhD from MIT in inorganic chemistry, where he worked in inorganic photochemistry and in the emerging area of photoelectrochemistry.

Sean Shaheen is a senior scientist at the National Renewable Energy Laboratory (NREL) in Golden, CO. He received his B.S. in physics from Carnegie Mellon in 1991 and his PhD in physics from the University of Arizona in 1999. His current research is focused on organic and nanostructured photovoltaic devices using novel polymers, dendrimers, and solution-grown organic/inorganic composite nanostructures. His research interests include studies of the complex interplay between molecular structure and bulk material properties and device behavior, with the goal of producing low cost solar cells from "smart" materials. He currently advises several graduate students and postdocs at NREL.

ORDERED NUCLEATION SITES FOR THE GROWTH OF ZINC OXIDE NANOFIBERS

JENNIFER WANG, DAVID S. GINLEY, AND SEAN SHAHEEN

ABSTRACT

Organic photovoltaics (OPVs) offer a promising route to low cost photovoltaic (PV) technology that can be inexpensively manufactured on a large scale for use in power generation and commercial products. Solar power conversion efficiencies of laboratory scale OPV devices have recently reached ~5%; however, projected efficiencies of at least 10% will be required for commercialization. An analogous approach that has arisen recently that can potentially increase efficiencies employs metal oxide semiconductors as the electron acceptor, creating a hybrid organic-inorganic device. This approach offers the advantage that the conduction band of the oxide can be tuned in a systematic way through doping, thus potentially achieving higher photovoltages in the device. Additionally, nanostructures of these materials can be easily grown from precursor solutions, providing a technique to precisely control the nanoscale geometry. This work focuses on using ZnO, which is known to have high electron mobility (>100 cm^2/Vs), as the electron acceptor. Nanofibers of ZnO can be grown from precursors such as zinc acetate or zinc nitrate to form arrays of nanofibers into which a conjugated polymer can be intercalated to form a composite PV device. The morphology of the nanofiber array is critical to the performance of the device, but current methods of nanofiber growth from a flat, polycrystalline nucleation layer allow for little morphological control. To overcome this limitation, we have created ordered arrays of ZnO nucleation sites with controllable size and spacing. Toluene solutions of diblock copolymer micelles with $ZnCl_2$ incorporated into the micellar cores were spin-coated onto glass substrates and etched with an O_2 plasma to yield hexagonally ordered arrays of ZnO nanoparticles that functioned as nucleation sites. Changing the concentration of $ZnCl_2$ and the molecular weight and ratio of the diblock copolymer resulted in systematic variation in the size and spacing of the nucleation sites. Thermal anneal treatment provided further modification of the nucleation layer, from which ZnO nanofibers were successfully grown from solution, although at present it is not known if the geometry of the as-grown ZnO nanofibers precisely reflects that of the underlying nucleation layer. This work provides a simple and useful method for potentially controlling the nucleation of ZnO nanofibers to be used in hybrid ZnO/organic nanocomposite PV devices.

INTRODUCTION

Photovoltaic (PV) technology is regarded as an essential component in the future of global energy production. By harvesting energy directly from sunlight, PV systems are a renewable resource that can address growing global energy demands and reduce the consumption of fossil fuels with its detrimental effects on the environment. A PV device, or solar cell, converts absorbed photons directly into electrical charges, which then drive an external circuit. Current PV technologies utilize crystalline silicon and thin film inorganic materials, but the costs of these technologies limit their competitiveness in energy production. As such, the development of PV technologies with very high efficiencies or very low costs is a potentially lucrative endeavor.

Low-cost, moderate efficiency (15-20%) PV technologies require inexpensive materials for the active components and packaging, low-temperature atmospheric processing, and high fabrication throughput. All of these attributes can theoretically be realized in organic-based photovoltaics (OPVs). The use of organic materials provides great versatility in the alteration of key properties such as molecular weight, electronic properties, and surface and structural properties [1]. The ease and economy of production combined with a theoretical efficiency that matches that of conventional semiconductor PVs give OPVs a competitive edge in the overarching search for a PV technology that is both economically and technically viable for large-scale power production. Additionally, the flexibility of the materials allows for the incorporation of PV devices into myriad commercial products such as fabrics, plastics, and roofing.

Recent OPV devices fabricated in the research laboratory have exhibited solar power conversion efficiencies of ~5% [2]. Such devices are based on composite blends of a π-conjugated semiconducting polymer, such as poly(3-hexylthiophene) (P3HT), and a soluble fullerene derivative, such as [6,6]-phenyl C_{61}-butyric acid methyl ester (PCBM). The method of photoconversion in these composite blends is based on the ability of the polymer to absorb light and create excitons, which are dissociated through an ultra-fast photoinduced charge transfer between the polymer, the electron donor, and the fullerene, the electron acceptor.

An alternative to the polymer blend devices involves the use of metal oxide semiconductors such as SnO_2, TiO_2, or ZnO, all of which exhibit ultra-fast photoinduced charge transfer with conjugated polymers [3,4]. A major advantage to this approach is that the conduction band of the oxide can be tuned in a systematic way through doping, potentially resulting in increased photovoltages in the device. Additionally, nanostructures of these materials can be easily grown from precursor solutions, allowing for precise control over the nanoscale morphology. This work focuses on the use of ZnO, which is known to have high electron mobility (>100 cm^2/Vs), as the electron acceptor.

A solution-based growth method employs precursors such as zinc acetate or zinc nitrate to form arrays of vertically aligned ZnO nanofibers into which a conjugated polymer can be intercalated to form a composite PV device [5]. The use of ZnO nanofiber arrays offers several advantages: a) increased donor-acceptor interfacial area leads to increased charge transfer, b) the electron transport pathways toward the negative electrode possesses very high electron mobility, c) the fixed morphology assures that the donor-acceptor interface does not change, potentially leading to better device lifetimes, d) material costs are reduced in device fabrication due to the lower cost of metal oxides compared to fullerenes, and e) the direction of current flow is inverted with respect to traditional blend devices, allowing for the use of more stable high work function counter electrodes [5]. Figure 1 is a schematic representation of the ZnO nanofiber/polymer PV device.

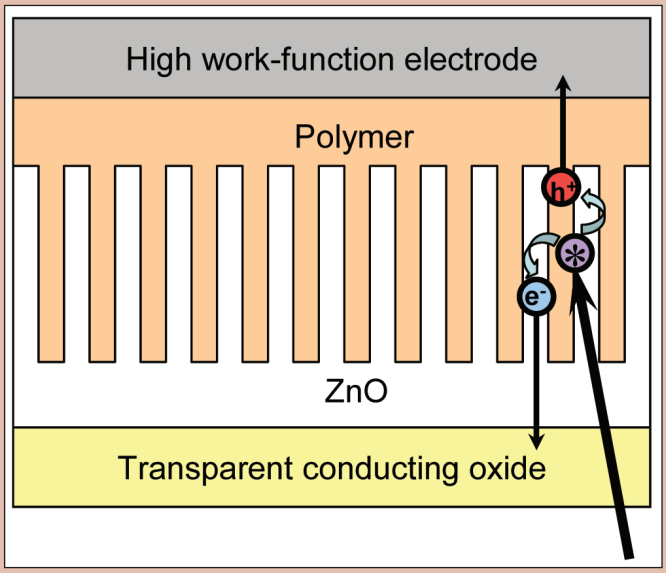

Figure 1. Schematic of a ZnO nanofiber/polymer PV device. The large black arrow represents an incident photon that creates an exciton (purple) in the polymer (eg. P3HT). The exciton diffuses into an electron (blue), which is transported through the ZnO fibers to the transparent conducting oxide (eg. ITO) electrode, and a hole (red), which is transported through the polymer to the high work function counter-electrode (eg. Ag).

The morphology of the nanofiber array is critical to the performance of the device, as defects and disorder in the nanostructure and large nanofiber spacing lead to charge recombination. Increased efficiency may be achieved by reducing the nanofiber spacing to within the P3HT exciton diffusion length, which is presumed to be less than 10 nm. None of this necessary morphological control is provided by the current method of ZnO nanofiber growth from a continuous, polycrystalline nucleation layer.

To overcome this limitation, we have created ordered arrays of ZnO nucleation sites with controllable size and spacing. The method used was based on previously published work in which the nanoparticle arrays were self-assembled from monolayer films of diblock copolymer micelles [6]. The diblock copolymer used in this study, poly(styrene-*block*-poly4-vinylpyridine) (PS-P4VP), consists of a hydrophobic PS solvate block and a hydrophilic P4VP functional block. Because toluene is a selective solvent for the PS block, spherical micelles with a PS corona and a P4VP core form in dilute toluene solution [7]. $ZnCl_2$ is then added to the solution, whereupon it dissolves in the P4VP block [6]. We spin-coated the solution onto a glass substrate and exposed the resulting film to O_2 plasma, which served to both remove the PS-P4VP and oxidize the zinc salt to ZnO. The size and spacing of the ZnO nanoparticles were controlled through modification of the amount of $ZnCl_2$ and the

molecular weight and ratio of the copolymer blocks. Thermal anneal treatment of the nucleation layer allowed for successful growth of ZnO nanofibers using a chemical solution growth technique [8].

MATERIALS AND METHODS

Chemicals

All chemicals were used as received: $ZnCl_2$ (Aldrich), Toluene (Aldrich), Zinc acetate dihydrate (Aldrich), Zinc nitrate hexahydrate (Aldrich), NaOH (J. T. Baker), and PS-P4VP (Polymer Source). Three different PS-P4VP polymers were used: M_n^{PS} [kg mol^{-1}]/M_n^{PVP} [kg mol^{-1}]/polydispersity index = 47.6/20.9/1.14, 31.9/13.2/1.08, and 32.9/8.0/1.06, which will be referred to in this paper as PS-P4VP-1, PS-P4VP-2, and PS-P4VP-3, respectively.

Formation and Characterization of Ordered Nucleation Sites

0.5 wt% toluene solutions of PS-P4VP were stirred at 70 °C for 2 h. $ZnCl_2$ was added to the micelle solutions and stirred at

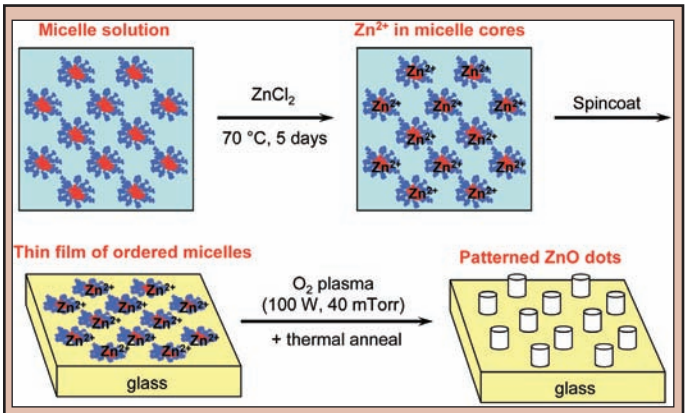

Figure 2. Schematic of the formation of ordered ZnO nucleation sites from diblock copolymer micelles.

70°C for 3-5 days to maximize loading of $ZnCl_2$ into the P4VP core. Glass microscope slides (Fisher) were cut into 1 inch squares and cleaned by ultrasonic agitation in isopropanol for 10 minutes, followed by oxygen plasma cleaning (150 W, 500 mTorr) for 5 min. The $ZnCl_2$/PS-P4VP solution was spin-coated onto the glass at 2000 rpm for 1 min with an initial ramp speed of 2000 rpm/s. The films were then exposed to oxygen plasma (100 W, 40 mTorr) for 10 min, resulting in an array of ZnO nanoparticles. The films were subsequently annealed in air on a hot plate. A schematic of this entire process is given in Figure 2. The nucleation layers were characterized by atomic force microscopy (AFM) in tapping mode on a nanoSurf DFM and by scanning electron microscopy (SEM) on a FEI Quanta 400 FEG ESEM and a JEOL 6320 FE-SEM.

Hydrothermal Growth and Characterization of Nanofibers

The films of ZnO nanoparticles were rinsed with deionized water and ethanol and submerged in a stirring solution of 1 mM zinc nitrate hexahydrate and 80-90 mM NaOH at 70°C for 20 min [3,8].

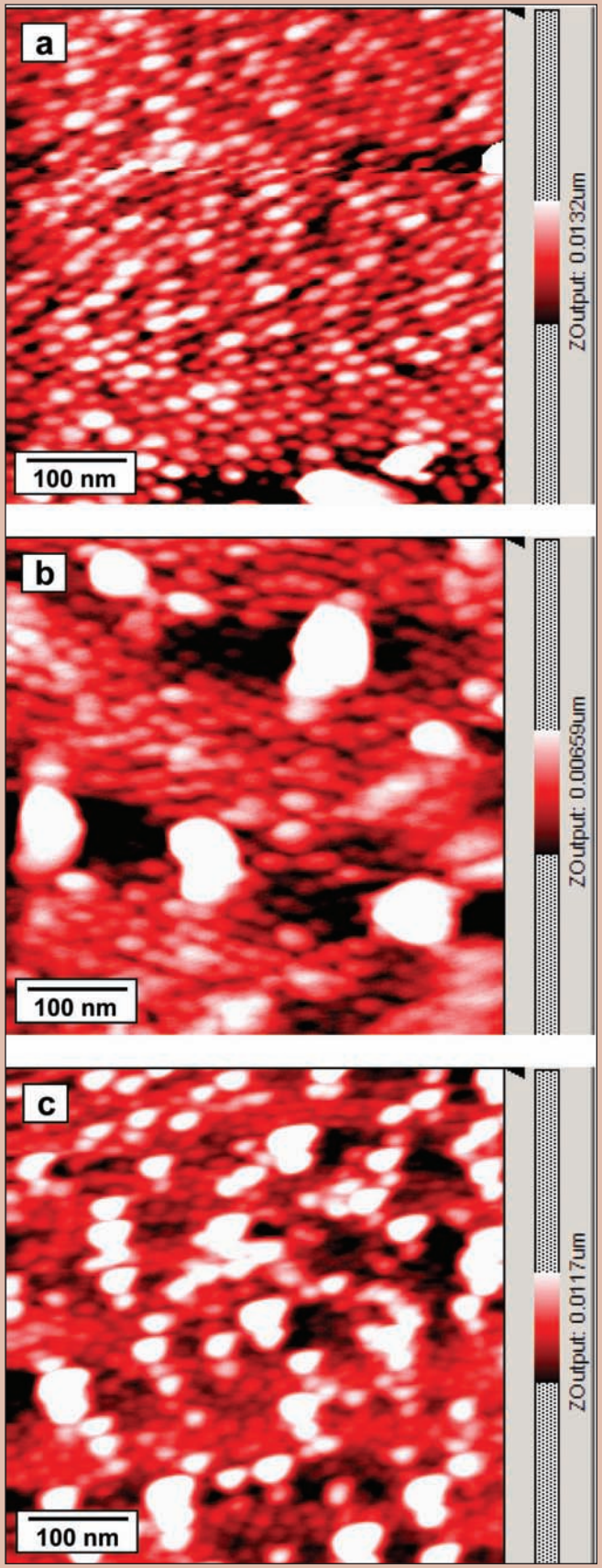

Figure 3. AFM images of films spin-coated from identical toluene solutions of PS-P4VP-1 with different ZnCl2:4-vinylpyridine molar ratios: a) 1:1.1, b) 1:2.1, and c) 1:2.7.

The samples were rinsed again and dried in air at room temperature. The nanofiber arrays were characterized by SEM.

RESULTS

Nucleation Layer

Zinc Ion Concentration: Different amounts of $ZnCl_2$ were added to identical solutions of PS-P4VP-1 in toluene. The molar ratios of $ZnCl_2$:4-vinylpyridine were: a) 1:1.1, b) 1:2.1, and c) 1:2.7. After spin-coating the solutions onto glass and treating with O_2 plasma, the films were annealed for 2 h at 300°C to reduce noise and streaking effects in AFM imaging, the results of which are presented in Figure 3. Qualitatively, reduction of zinc ion concentration resulted in a decrease in the size of the nanoparticles, but it also resulted in the formation of several large nanoparticles randomly scattered across the substrate.

M_{PS}:M_{P4VP} (x 10^3)	47.6:20.9 (PS-P4VP-1)	32.9:8.0 (PS-P4VP-2)	32.9:8.0 (PS-P4VP-2)
% P4VP	31	29	20
Diameter	37 nm	13 nm	15-20 nm
Edge-to-edge spacing	22 nm	9 nm	Variable
Height	4.0-5.5 nm	2.7-3.5 nm	1.5-4.2 nm
% Coverage	67	61	Unknown

Table 1. Effect of PS-P4VP molecular weight and ratio on nucleation layer morphology. Numbers are based on visual estimation.

PS-P4VP molecular weight and ratio: The three different PS-P4VP polymers were used to make 0.5 wt % toluene solutions, followed by addition of $ZnCl_2$ at a constant molar ratio to 4-vinylpyridine of 1:2. After spin-coating the solutions onto glass and treating with O_2 plasma, the films were annealed for 30 min at 300°C. AFM images of the resulting nucleation layers are shown in Figure 4. Morphological changes are tabulated numerically in Table 1. Keeping a constant molecular weight ratio of approximately 30% P4VP and reducing the molecular weights of both copolymer blocks resulted in a significant decrease in the size, edge-to-edge spacing, height, and % coverage of the nanoparticle array, which maintained its hexagonal ordering. The hexagonal ordering was lost upon changing the molecular weight ratio to 20% P4VP while keeping a nearly constant M_{PS}.

M_{PS}:M_{P4VP} (x 10^3)	47.6:20.9 (PS-P4VP-1)	32.9:8.0 (PS-P4VP-2)	32.9:8.0 (PS-P4VP-2)
% P4VP	31	29	20
Diameter	37 nm	13 nm	15-20 nm
Edge-to-edge spacing	22 nm	9 nm	Variable
Height	4.0-5.5 nm	2.7-3.5 nm	1.5-4.2 nm
% Coverage	67	61	Unknown

Table 2. Effect of thermal anneal on nucleation layer morphology. Image analysis was performed using Igor Pro by fitting to a model assuming a perfect hexagonal lattice.

Thermal anneal: Figure 5 shows SEM images of two nucleation layers spin-coated from the same PS-P4VP-1 toluene solution with 1:1.3 $ZnCl_2$:4-vinylpyridine and treated with O_2 plasma. One of the films received no anneal treatment and the other was

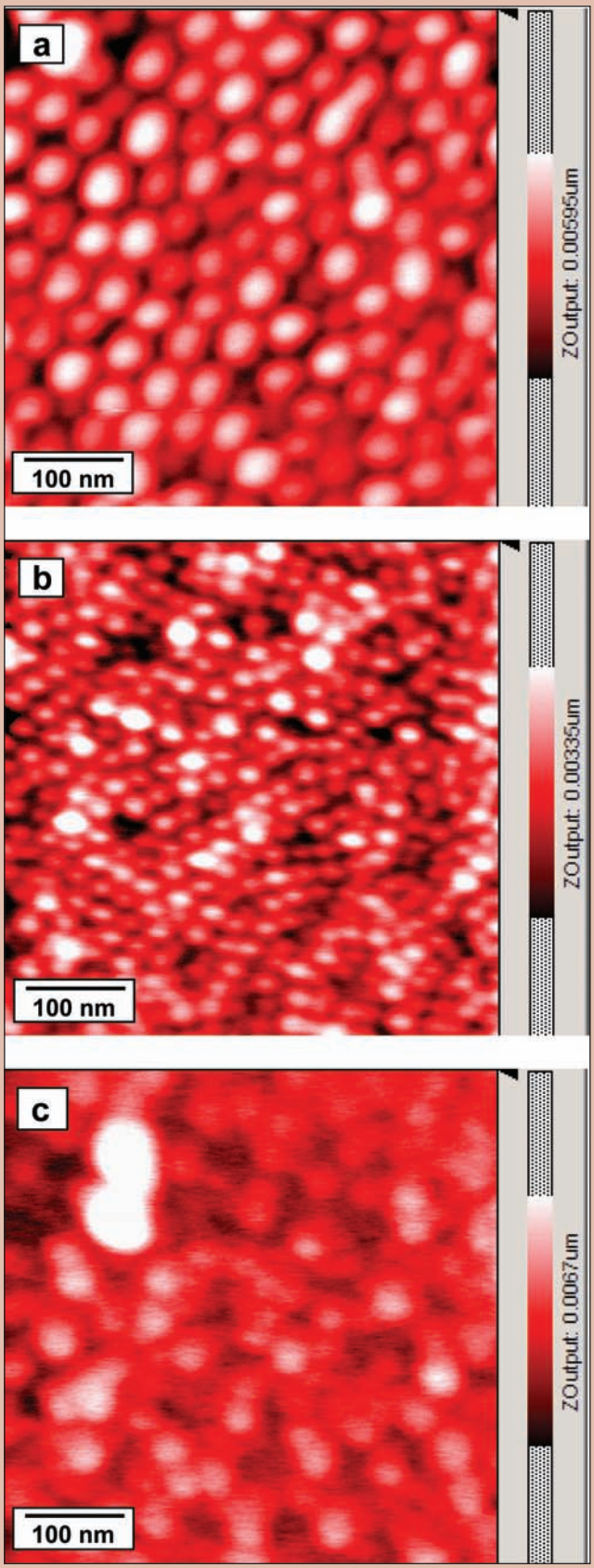

Figure 4. AFM images of films spin-coated from toluene solutions of a) PS-P4VP-1, b) PS-P4VP-2, and c) PS-P4VP-3. The ZnCl2:4-vinylpyridine molar ratio was kept constant at 1:2.

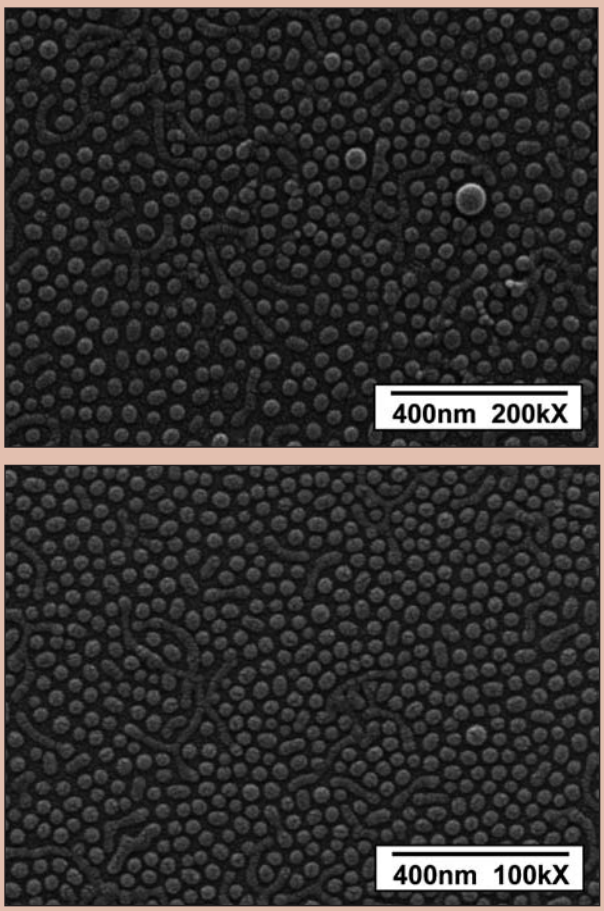

Figure 5. SEM images of films spin-coated from the same PS-P4VP-1 toluene solution with 1:1.3 ZnCl2:4-vinylpyridine and were subject to a) no anneal, and b) 10 min anneal at 300 °C.

annealed for 10 min at 300°C. Morphological changes are tabulated numerically in Table 2. Anneal treatment did not change the size of the nanoparticles, but it did result in better monodispersity, larger % coverage, and decreased edge-to-edge spacing.

Nanofibers

ZnO nanofibers were grown from solution on nucleation layers spin-coated from the same solution (PS-P4VP-1, $ZnCl_2$:4-vinylpyridine = 1:1.3) and had received different anneal treatments. SEM images of the results are presented in Figure 6. No anneal treatment caused the nucleation sites to be etched away during growth, and the resulting nanofibers appeared randomly on the substrate in isolation or arranged in small clusters (Figure 6a). Annealing at 300°C for 10, 30, and 60 min, and at 400°C for 20 min all resulted in the formation of "egg" structures, dense regions of vertically aligned nanofibers strewn about the substrate (Figure 6b). Each "egg" consisted of an outer circle full of nanofibers and an inner "yolk" of nanofibers that seemed to form an additional layer (Figure 6c). Only with a 2 h anneal at 300°C did a dense film of nanofibers form across the substrate (Figure 6d). With a 2 h anneal at 500°C, the isolated nanoparticles on the nucleation layer aggregated (Figure 6e), and the resulting nanofibers were randomly arranged on the substrate in small clusters similar to the result of no anneal, but the fiber diameter increased (Figure 6f).

DISCUSSION AND CONCLUSIONS

Morphological Control of ZnO Nucleation Sites

We have examined three approaches to changing the size and spacing of ZnO nucleation sites formed from diblock copolymer micelles incorporated with a zinc salt. One route was to change the concentration of the zinc salt while keeping the size of the diblock copolymer micelles constant. With less precursor available to infiltrate into the micellar cores, the total precursor amount should be distributed evenly among the micelles. After spin-coating and O_2 plasma treatment, the film should exhibit smaller ZnO nanoparticles, while the center-to-center spacing should have remained constant (edge-to-edge spacing should have increased). Close examination of the Z-scales in Figure 3 reveals that decreased $ZnCl_2$ concentration does result in shorter nanoparticles. Due to the AFM tip resolution, however, this result is strictly qualitative, and it is unclear whether there was any change in the nanoparticle diameter. Decreasing the $ZnCl_2$ concentration caused the film to exhibit larger, aggregated nanoparticles scattered randomly across the surface. This suggests that the ratio of the zinc salt to the P4VP cores can be optimized so that the zinc-loaded micelles can achieve optimal monodispersity. Our experience showed that larger amounts of $ZnCl_2$ ($ZnCl_2$:4-vinylpyridine = 1:1.1 -1:1.3) led to greater monodispersity in the resulting nanoparticle array.

Another route to morphological control over the nucleation sites was to change the molecular weight and ratio of the diblock copolymer as purchased. As seen in Figure 4a and 4b, decreasing the molecular weight of each block while keeping their ratio constant to be a highly effective way of decreasing the size and spacing of the nanoparticles. Table 1 shows that by switching from PS-P4VP-1 to PS-P4VP-2, the estimated diameter decreased from 37 nm to 13 nm, and the estimated spacing decreased from 22 nm to 9 nm. The estimated height and % coverage also decreased. Further decreasing only M_{P4VP} seemed to hinder the formation of ordered micelles, and the resulting nanoparticles had variable size, spacing, and ordering (Figure 4c). Changing the PS-P4VP ratio, therefore, may be a more challenging approach that will require further investigation.

Lastly, thermal anneal treatment of the nucleation layer provided morphological control in that the nanoparticles became more monodisperse in size and exhibited closer spacing. Since the amount of ZnO remains constant during anneal, this result suggests that the nanoparticles became flatter and possibly more crystalline during the anneal process. Future work will examine changes in the crystallinity of the nanoparticles using X-ray diffraction.

Nucleation and Growth of ZnO Nanofibers

Thermal anneal of the ZnO nucleation layer was a critical factor affecting the morphology of the nanofibers that were subsequently grown. Figure 6 shows that a uniform film of vertically oriented ZnO nanofibers grew only from the nucleation layer that was annealed for 2 h at 300°C (Figure 6d). At the same temperature, shorter anneal

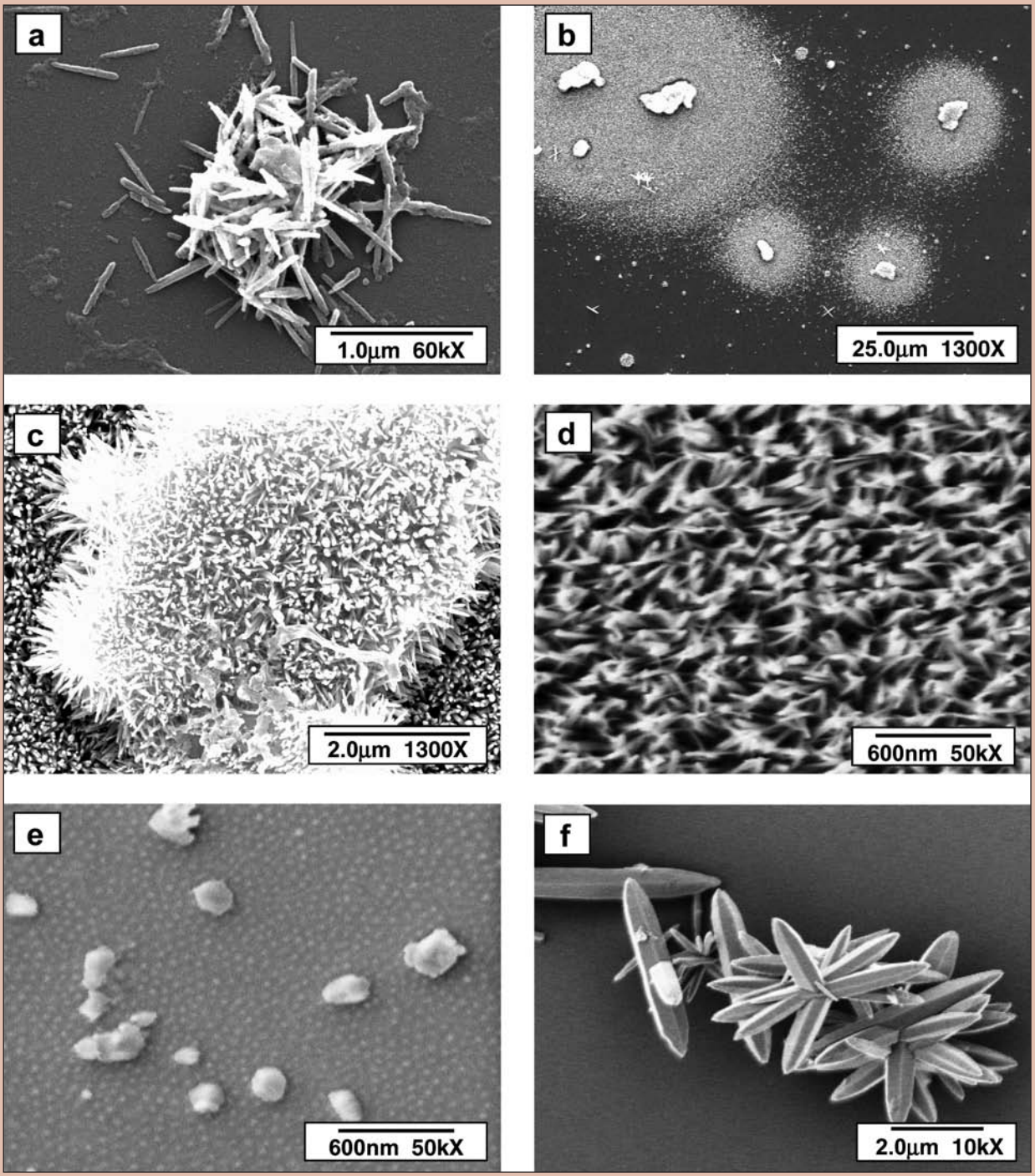

Figure 6. SEM images of ZnO nanofibers grown from nucleation layers that were annealed for: a) no anneal, b) and c) 10 min at 300 °C, d) 2 h at 300 °C, and f) 2h at 500 °C. The nucleation layer from which f) was grown is shown in e).

times ranging from 10 min to 1 hr resulted in the "egg" structure seen in Figures 6b and 6c. No anneal and anneal for 2 h at 500°C yielded isolated clusters of nanofibers, as seen in Figures 6a and 6f, respectively. These results suggest that adhesion of the nucleation sites is a possible factor contributing to successful nanofiber growth. Annealing for a long period of time (2 h) at a moderate temperature (300°C) may have provided the ideal rate and amount of interaction between the nanoparticles and the substrate, allowing for proper adhesion to nucleate the growth of nanofibers.

The vertical alignment of the nanofibers must also be addressed, as poorly aligned nanofibers can lead to incomplete intercalation of the polymer [5]. Figure 6d shows an array of nanofibers whose vertical orientation is fair at best, which presents another reason to further examine the anneal treatment. Previous work has shown

that improved ZnO nanofiber alignment can be achieved through adjustment of the anneal time and temperature of the nucleation layer [5]. As mentioned in the previous subsection, thermal anneal may have an effect on the crystallinity and lattice orientation of the nucleation sites. Such properties affect the surface free energy of the nucleation layer, which in turn determines the epitaxial growth of ZnO nanofibers [8].

Another route to improving the crystallinity and orientation of the nucleation sites is to use a different zinc precursor in the diblock copolymer micelles. Zinc acetate is one potential candidate, as it is unique in its tendency to form textured ZnO surfaces upon decomposition, with the (0001) planes parallel to the substrate [9]. Lastly, the use of structure-directing agents in the growth solution may also provide control over the morphology of the nanofibers grown.

This report has presented a simple method for controlling the morphology of ZnO nucleation sites for the growth of ZnO nanofibers. The use of diblock copolymers with adjustable molecular weights provides valuable flexibility in the size and spacing of ZnO nanoparticle arrays formed from micelle solutions. These arrays functioned adequately as nucleation sites for the growth of a uniform film of ZnO nanofibers. Further investigations into the effect of thermal anneal and chemical precursors on the nucleation sites and resulting nanofiber morphology may result in the development of well-aligned ZnO nanofibers of optimal diameter and spacing for use in composite PV devices.

ACKNOWLEDGEMENTS

This research was conducted at the National Renewable Energy Laboratory. I gratefully acknowledge my mentors, Drs. Sean Shaheen and David Ginley, and my unofficial graduate student mentor, Dana Olson, for their invaluable advice and encouragement throughout the summer. Special thanks to Drs. Don Selmarten, Bobby To, and Manuel Romero for the SEM images, and to Nikos Kopidakis for training on the AFM. Finally, I thank the U.S. Department of Energy, the Office of Science, and the NREL Office of Education for facilitating my participation in the SULI program, which proved to be an excellent research and learning experience.

REFERENCES

[1] S. E. Shaheen, D. S. Ginley, and G. E. Jabbour, Guest editors, “Organic-based photovoltaics: Toward low-cost power generation,” *MRS Bulletin*, vol. 30, pp. 10-15, Jan. 2005.

[2] C. Brabec et al., “Advances in the Performance of Organic Bulk Heterojunction Solar Cells: Towards First Products,” presented at the SPIE Conference for Organic Photovoltaics VI, San Diego, CA, USA, Aug. 2005.

[3] T.J. Savenije, J.M. Warman, and A. Goosens. “Visible light sensitisation of titanium dioxide using a phenylene vinylene polymer, *Chem. Phys. Lett.*, vol. 287, pp. 148-153, Apr. 1998

[4] P.A. van Hal et al., “Photoinduced Electron Transfer and Photovoltaic Response of a MDMO-PPV:TiO2 Bulk Heterojunction”, *Adv. Mater.*, vol. 15, pp. 118-121, 2003.

[5] D. C. Olson, J. Piris, R. T. Collins, S. E. Shaheen, and D. S. Ginley, “Hybrid photovoltaic devices of polymer and ZnO nanofiber composites,” *Thin Solid Films*, vol. 496, pp. 26-29, 2006.

[6] S. I. Yoo, B. H. Sohn, W. C. Zin, S. J. An, and G. C. Yi, “Self-assembled arrays of zinc oxide nanoparticles from monolayer films of diblock copolymer micelles,” *Chem. Comm.*, pp. 2850-2851, Nov. 2004.

[7] S. Förster and M. Antonietti, Amphiphilic block copolymers in structure-controlled nanomaterial hybrids, *Adv. Mater.*, vol. 10, pp. 195-217, 1998.

[8] R. B. Peterson, C. L. Fields, and B. A. Gregg, “Epitaxial Chemical Deposition of ZnO Nanocolumns from NaOH,” *Langmuir*, vol. 20, pp. 5114-5118, May 2004.

[9] L. E. Greene, M. Law, Dawud H. Tan, M. Montano, J. Goldberger, G. Somorjai, and P. Yang, “General Route to Vertical ZnO Nanowire Arrays Using Textured ZnO Seeds,” *Nano Lett.*, vol. 5, pp. 1231-1236, Jun. 2005.

Ashley Vollmar completed this research as a senior at the University of Tennessee and Pellissippi State Technical Community College in Knoxville, TN. She graduated with a Bachelor of Science degree in Ecology and Evolutionary Biology from the University of Tennessee in May 2006. Her previous publications include research on salamanders along the Appalachian Trail, published in the Tennessee Junior Academy of Sciences Handbook. She is continuing research on global climate change and its impacts on temperate deciduous ecosystems through a post-graduate internship with Oak Ridge National Laboratory, Oak Ridge, TN, and will present a poster at the 2006 Annual Meeting of the Ecological Society of America. She plans to attend graduate school in the near future in ecosystem studies; particular interests are climate change effects on forest floor vertebrate communities.

Carla Gunderson is a research staff scientist at Oak Ridge National Laboratory (ORNL), in the Environmental Sciences Division. At ORNL, her research has centered on plant and ecosystem responses to atmospheric and climatic changes. Her research career began at the University of Tennessee (UT), Knoxville, where she assisted in an algal research lab and completed an independent study of the flora of Corsica. She earned her B.A. degree in 1977, in both Botany and French. She completed graduate studies in plant physiology, plant-insect interactions, and insect foreign compound metabolism, obtaining an MS in environmental toxicology from UT. In 1983 she joined ORNL to work in air-pollution effects research. Much of Carla's ORNL research has focused on photosynthesis and respiration, and the influence of elevated CO_2, atmospheric warming, and drought on forest structure and function. She is principal investigator of the project on temperature response and adjustment in trees, and collaborates with ORNL modelers to predict impacts of climatic change on forests of the future. She still enjoys an occasional eco-toxicology project, or translating French research articles for her colleagues.

PHYSIOLOGICAL ADJUSTMENTS OF LEAF RESPIRATION TO ATMOSPHERIC WARMING IN *BETULA ALLEGHANIENSIS* AND *QUERCUS RUBRA*

ASHLEY VOLLMAR, CARLA GUNDERSON

ABSTRACT

Global air temperatures are predicted to rise 1° to 4.5° Celsius by the year 2100. This climatic change is expected to have a great effect on the succession and migration of temperate deciduous forest species. Most physiologically based models of forest response to climatic change focus on the ecosystems as a whole instead of on individual tree species, assuming that the effects of warming on respiration are generally the same for each species, and that processes can not adjust to a changing climate. Experimental data suggest that physiological adjustments are possible, but there is a lack of data in deciduous species. In order to correctly model the effects of climate change on temperate species, species-specific respiration acclimation (adjustment) to rising temperatures is being determined in this experiment. Two temperate deciduous tree species *Betula alleghaniensis* (BA) and *Quercus rubra* (QR) were grown over a span of four years in open-top chambers and subjected to two different temperature treatments; ambient and ambient plus 4° Celsius (E4). Between 0530 hours and 1100 hours, respiration was measured over a range of leaf temperatures on several comparable, fully expanded leaves in each treatment. Circular punches were taken from the leaves and dried at 60°C to determine leaf mass per area (LMA). Respiration rates at a common temperature decreased by 15-18% in both species, and the entire resperation versus temperature curve shifted by at least 4°C, indicating a large degree of physiological acclimation. Foliar mass per area decreased with increasing growth temperature for both species. It can be concluded that there is a relationship between leaf respiration and foliar mass as it relates to respiratory acclimation, and that these two species had similar patterns of adjustment to warming.

INTRODUCTION

Global air temperatures are expected to rise 1° to 4°C by the year 2100 as a result of increasing concentrations of greenhouse gases [4]. Such a change in air temperatures can have a tremendous effect on the succession and migration of temperate deciduous forest species. Most models of forest response to climatic change focus on the ecosystems as a whole instead of each individual tree species, assuming that the effects of warming on respiration are generally the same for each species, and that physiological responses can not adjust to a changing climate [2]. Although it is predicted that forest species will not be able to adjust to the increasing temperatures [5], experimental data suggests that physiological adjustments can and do occur. Plant respiratory adaptations have been documented and reported, particularly in evergreen species, but little information is available for temperate deciduous species [2]. In order to correctly model the effects of warming on respiration, growth, and survival in temperate species, their ability to acclimate must be assessed and included in model predictions [6].

The objective of this study was to investigate the potential respiratory acclimation of two temperate deciduous trees with different geographic and climatic distributions. A broadly distributed temperate species, *Quercus rubra* (northern red oak, mean annual temperatures from 5°-16°C over its natural range) was grown

with *Betula alleghaniensis* (yellow birch), which typically grows in somewhat cooler climates (mean annual temperatures from 5°-7°C) [1,8]. Respiratory responses to increased growth temperatures and differences in foliar mass per area for each species were determined. It is hypothesized that leaf respiration will decrease with an increase in growth temperatures, thus moderating the impacts of warming on respiratory CO_2 losses. Likewise, it is hypothesized that foliar mass per area will decrease with an increase in growth temperatures, as respiration is often correlated with mass and nitrogen (N) content [7,9].

MATERIALS AND METHODS

Plant Material and Growth Conditions

Bare root seedlings were planted directly in the ground in open-top chambers (OTCs) at the Global Change Field Research Site on the Oak Ridge National Environment Research Park in the spring of 2002. Seedlings were maintained in naturally varying rainfall, day length, and sunlight. Additional watering was provided in the summer of 2002 to ensure seedling establishment. The trees were grown in three blocks and subjected to two temperature treatments: ambient and ambient + 4°C (E4). Each block contained one ambient treatment and one E4 treatment chamber. Chamber temperatures were maintained by a combination of evaporative coolers through spring, summer, and fall months and electrical resistance heaters throughout all months.

Plants of *Quercus rubra* and *Betula alleghaniensis* were purchased as one year old bare root seedlings from commercial nurseries. The seedlings were grown with two other temperate species, *Liquidambar styraciflua* and *Populus grandidentata,* within the chamber. The trees were positioned so that all trees would potentially receive the same amount of rain and sunlight. *Q. rubra* and *B. alleghaniensis* grew in the southeast and southwest quadrant respectively.

Gas Exchange and Leaf Properties

Two comparable, fully expanded leaves were chosen from two trees of each species in each chamber and marked with flagging tape for easy recognition in the dark. Between 0530 hours and 1100 hours, respiration was measured using a LI-6400 portable photosynthesis system (LiCOR INC. Lincoln, NE) on marked leaves in a darkened 2cm by 3cm cuvette over a range of leaf temperatures. Starting block temperature was, on average, 6°C below ambient outside air temperature. Block temperatures were increased by 2.5°C to cover a span of 14°C from the starting block temperature. Five measurements were taken at each block temperature using an auto program with a minimum wait time of 0.6 minutes, a maximum wait time of 4 minutes, and a maximum coefficient of variance of 0.3%. CO_2 concentration for the measurements was set at 450 ppm based on nighttime CO_2 concentrations at the site, and flow rate at 400 µmol s^{-1}.

Average respiration and leaf temperature were calculated for each block temperature and used to determine the temperature responses of each leaf. Exponential respiration curves were linearized by taking $\log_{10}$ of the respiration rate in order to calculate slope and intercept values for each leaf and generate an average equation for each treatment.

After respiration measurements were completed, leaf chlorophyll content was estimated using a Minolta SPAD 502, taking the average of four readings per leaf. Arbitrary SPAD units are strongly correlated with area based chlorophyll content (chlorophyll mg cm^{-2} = 0.885 x SPAD – 3.5614 for these species, data not shown) and are used to estimate leaf N in agricultural applications. Several 6.38 mm diameter punches were taken from each measured leaf. The punches were dried at 60°C for 2-4 days. Once dry, the punches were weighed using a digital top loading balance to determine leaf mass per area (LMA). The remainder of the leaf was freeze-dried for later biochemical analyses.

RESULTS

Respiration rates increased exponentially with temperature in each treatment (Fig. 1), but respiration rates in the E4 treatment were shifted to the right by 4°C relative to the ambient treatment. Respiration rates in *Q. rubra,* measured at a common temperature (25°C), decreased by as much as 0.1 µmol $m^{-2}s^{-1}$ from the ambient treatment to the E4 treatment as represented in Figure 2. The mean

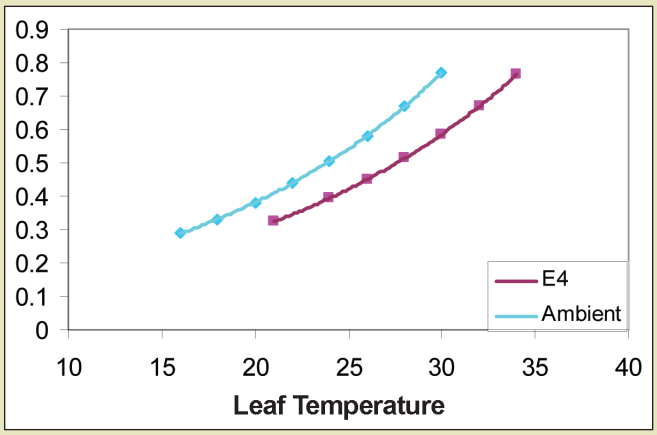

Figure 1. Response of foliar respiration as a function of leaf temperature in *Quercus rubra*. Fitted curves are based on average rates and leaf temperature as described. Error bars are obscured by symbols.

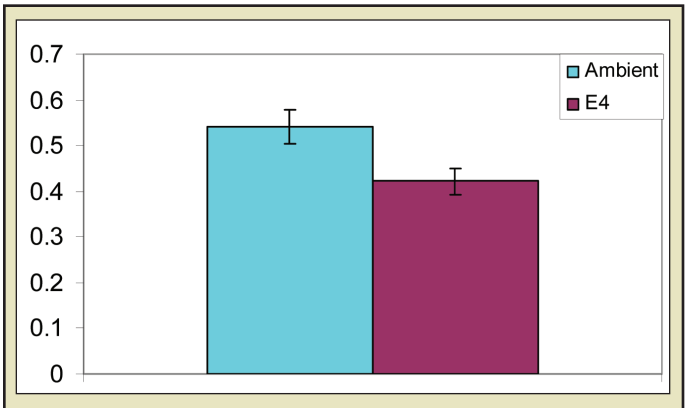

Figure 2. Average foliar respiration measured at 24°C in *Quercus rubra*. Error bars represent SE

respiration rate for the ambient treatment at 25°C was 0.51 µmol $m^{-2}s^{-1}$ ± 0.037. The mean respiration rate for the E4 treatment was 0.42 µmol $m^{-2}s^{-1}$ ± 0.028. Figure 3 shows a decrease of 0.326 mg cm^{-2} in foliar LMA between treatments. The LMA for the ambient

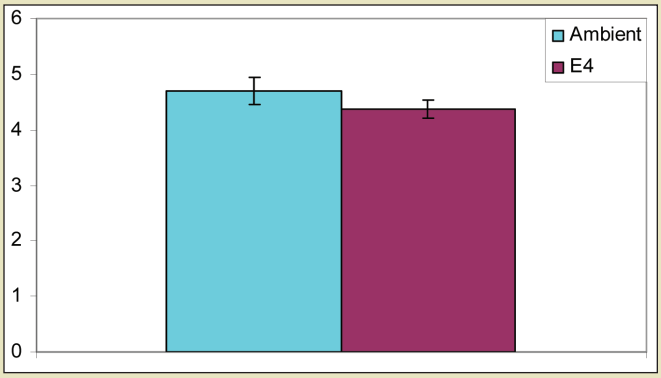

Figure 3. Average foliar mass per area measured in mg cm^{-2} in *Quercus rubra*. Error bars as in Fig 2

treatment was found to be 4.70 mg cm^{-2} ± 0.255, and the LMA for the E4 treatment was 4.37 mg cm^{-2} ± 0.173. Mean leaf chlorophyll content of *Q. rubra* leaves was 33.27 ± 2.32 for the ambient treatment and 33.08 ± 2.06 for the E4 treatment, in SPAD units. However, there was no significant difference (P=0.7) in the average leaf chlorophyll content between treatments.

Respiration rates increased exponentially with temperature in each treatment (Fig. 4), but respiration rates in the E4 treatment

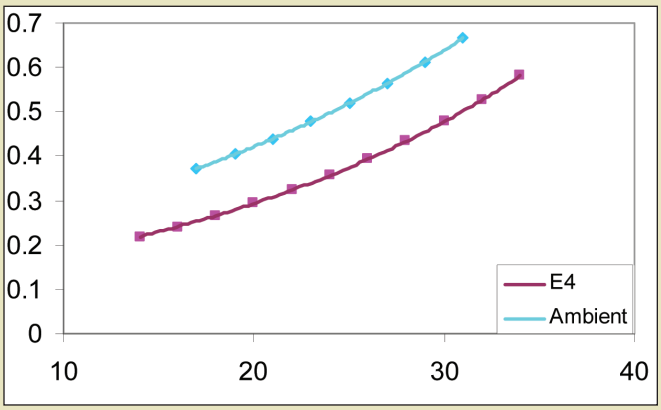

Figure 4. Response of foliar respiration as a function of leaf temperature in *Betula alleghaniensis*. Fitted curves are based on average rates and leaf temperature as described. Error bars are obscured by symbols.

were shifted to the right by 6°C relative to the ambient treatment. Similar to *Q. rubra*, respiration rates in *B. alleghaniensis* measured at 22°C decreased by as much as 0.1 µmol $m^{-2}s^{-1}$ from the ambient treatment to the E4 treatment, as represented in Figure 5. The mean respiration rate for the ambient treatment was 0.46 µmol $m^{-2}s^{-1}$ ± 0.026. The mean respiration rate for the E4 treatment was lower; 0.39 µmol $m^{-2}s^{-1}$ ± 0.054. Foliar LMA decreased by 0.618 mg cm^{-2} in the E4 treatment (Fig. 6). The LMA for the ambient treatment was 5.49 mg cm^{-2} ± 0.230, and the LMA for the E4 treatment was

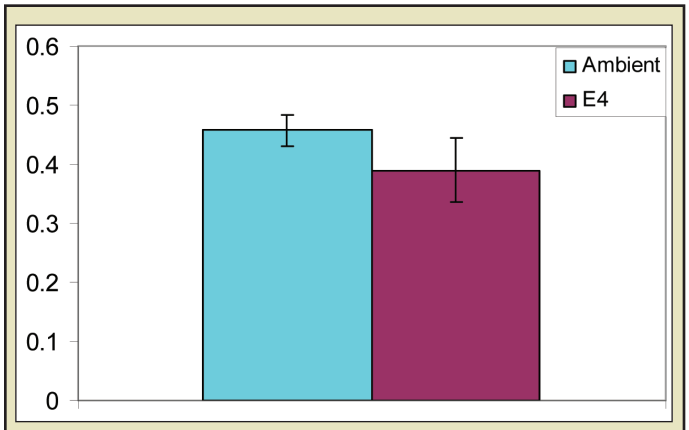

Figure 5. Average foliar respiration measured at 22°C in *Betula alleghaniensis*. Error bars represent SE.

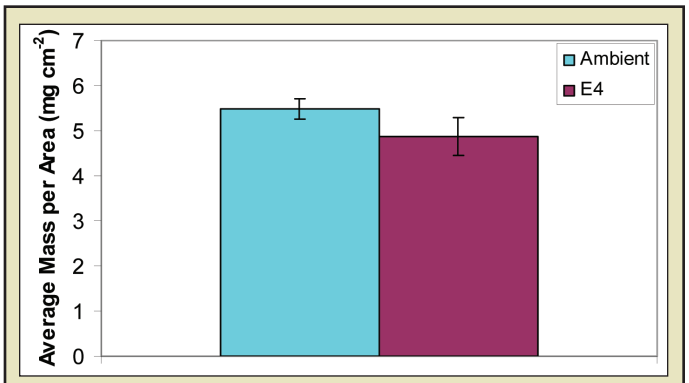

Figure 6. Average foliar mass per area measured in mg cm^{-2} in *Betula alleghaniensis*. Error Bars as in Fig 5.

4.87 mg cm^{-2} ± 0.420. Leaf chlorophyll for *B. alleghaniensis* was 31.6 ± 2.439 for the ambient treatment and 33.6 ± 5.019 for the E4 treatment. However, there was no significant difference (P=0.48) in the average leaf chlorophyll content between treatments.

DISCUSSION AND CONCLUSIONS

In *Q. rubra,* respiration at 24° was 17.6% lower in E4 leaves than in ambient leaves (P=0.026) on an area basis, in µmol $m^{-2}s^{-1}$, suggesting that models based on ambient leaf responses would overestimate respiratory losses. LMA in E4 leaves was only 6.9% lower than in ambient, but not significantly different (ns, P=0.32). Chlorophyll content was 0.6% higher in E4 than in ambient, but also not significantly different (ns, P=0.95). Thus, changes in LMA and N, if N correlates with chlorophyll content, do not account for the decrease in respiration in *Q. rubra.*

Similarly, in *B. alleghaniensis*, respiration at 22°C was 15.2% lower in E4 leaves than in ambient leaves (P<0.01) on an area basis, µmol $m^{-2}s^{-1}$. LMA in E4 leaves was 11.2% lower than ambient, but not significantly different (ns, P=0.22). Chlorophyll content was 6.22% lower in ambient than in the E4, but also not significantly different (ns, P=0.48). Thus changes in LMA and N, again if N correlates with chlorophyll content, do not account for the decrease in respiration in *B. alleghaniensis.* The mechanisms behind

respiratory acclimation in both species remain to be determined and may be related to substrate (carbohydrate) availability.

Q. rubra and *B. alleghaniensis* both showed complete acclimation of leaf respiration to increased growth temperatures. This is shown by the decrease in respiration rates, measured at a common temperature, with warmer growing temperatures, and by the right shift of the respiration curves of both species. A shift of 4°C when growing temperatures are 4° different represents a complete homeostatic adjustment. Both species maintained a constant respiration rate that is lower than would be predicted from a respiration curve developed in ambient-grown seedlings. There was no significant correlation between respiration and chlorophyll content, so if leaf nitrogen content is correlated with chlorophyll content, then nitrogen content will not explain the differences in respiration rates and thus can not be used to model acclimation to warming. Leaf N and carbohydrates will be measured later to directly test correlations with respiration. Current forest models predict accelerated carbon losses and negative carbon balance associated with increased respiration as temperatures rise. These data suggest no such acceleration in carbon losses as plants acclimate to warming. The complete acclimation observed here implies a need for models to incorporate physiologically based research in order to correctly portray ecosystem function in a changing environment and to interpret which changes could ultimately influence species survival [3,7].

ACKNOWLEDGEMENTS

The author would like to thank Carla Gunderson for her guidance and knowledge and Christina Campion for assistance in data collection. The author would also like to thank the Oak Ridge Institute for Science and Education (ORISE), U.S. Department of Energy, Department of Energy's Community College Institute of Science and Technology (CCI), and Oak Ridge National Laboratory for this opportunity. Funding for this project was provided by the U.S. Department of Energy (DOE) Office of Science (Biological and Environmental Research) as part of the Program for Ecosystem Research. Oak Ridge National Laboratory is managed by UT-Battelle, LLC, for DOE under contract DE-AC05-00OR22725. The experimental site is located on the Oak Ridge Environmental Research Park.

REFERENCES

[1] Burns, Russell M., and Barbara H. Honkala, tech. coords. 1990. Silvics of North America: 1. Conifers; 2. Hardwoods. *Agriculture Handbook* 654. U.S. Department of Agriculture, Forest Service, Washington, DC. vol.2, 877 p.

[2] Gunderson, C.A., R.J. Norby, and S.D. Wullschleger. 2000. Acclimation of photosynthesis and respiration to simulated climatic warming in northern and southern populations of *Acer saccharum*: laboratory and field evidence. *Tree Physiol.* 20: 87-96.

[3] Hansen, P, S.Wullschleger, R. Norby, T.Tschaplinski and C. Gunderson. (2005) Importance of changing CO_2, temperature, precipitation, and ozone on carbon and water cycles of an upland-oak forest: incorporating experimental results into model simulations. *Global Change Biology*: In Press.

[4] Houghton JT, Ding Y, Griggs DJ, Noguer M, van der Linden PJ, Xiaosu D. (2001) *Climate Change 2001*: The Scientific Basis: Contribution of Working Group I to the Third Assessment Report of the Intergovernmental Panel on Climate Change (IPCC). (eds, Maskell K, Johnson CA), Cambridge University Press, Cambridge, England.

[5] Kirschbaum, M.U.F. and A.Fischlin. 1996. In: *Climate Change 1995*: Impacts, Adaptations and Mitigation of Climate Change: Scientific-Technical Analyses. Contribution of Working Group II to the Second Assessment Report of the Intergovernmental Panel on Climate Change (R.T. Watson, M.C. Zinyowera, R.H. Moss, eds) pp.95-129. Cambridge University Press, Cambridge

[6] Körner, Ch. 1995. Towards a better experimental basis for upscaling plant responses to elevated CO_2 and climate warming. *Plant Cell & Environment* 18: 1101-1110.

[7] Mitchell, K.A., P.V. Bolstad and J.M. Vose. 1999. Interspecific and environmentally induced variation in foliar dark respiration among eighteen southeastern deciduous tree species. *Tree Physiol*. 19: 861-870.

[8] Prasad, A. M. and L. R. Iverson. 1999-ongoing. A Climate Change Atlas for 80 Forest Tree Species of the Eastern United States [database]. http://www.fs.fed.us/ne/delaware/atlas/index.html, Northeastern Research Station, USDA Forest Service, Delaware, Ohio.

[9] Whitehead, D., K.L. Griffin, M.H. Turnbull, D.T. Tissues, V.C. Engel, K.J. Brown, W.S.F. Schuster, and A.S. Walcroft. (2004). Response of total night-time respiration to differences in total daily photosynthesis for leaves in a *Quercus rubra* L. canopy: implications for modelling canopy CO_2 exchange. *Global Change Biol*. 10: 925-938.

Jeff Head received his B.S. in chemistry from Colorado State University in the spring of 2006. As an undergraduate Jeff worked with Dr. Bruce Parkinson in a combinatorial analysis of metal oxides capable of driving the water-splitting reaction for hydrogen production. Before and after senior year at CSU Jeff completed two Science Undergraduate Laboratory Internships (SULI) at the National Renewable Energy Laboratory (NREL). While at NREL the focus of his studies were to carry out the photoelectrochemical characterization of various nitride compounds. Specifically, the goal of the research was to determine the water-splitting capabilities of the compounds with light as the only energy input. Advising him on the project was Dr. John Turner (NREL). He is currently pursuing graduate studies in analytical chemistry at the University of Arizona for his PhD.

John A. Turner is a Principal Scientist at the National Renewable Energy Laboratory. He received his B.S. from Idaho State University, his PhD from Colorado State University, and completed a postdoctoral appointment at the California Institute of Technology before joining the Laboratory (then the Solar Energy Research Institute) in 1979. His research is primarily concerned with enabling technologies for the implementation of hydrogen systems into the energy infrastructure. This includes direct conversion (photoelectrolysis) systems for hydrogen production from sunlight and water, advanced materials for high temperature fuel cell membranes, and corrosion studies of fuel cell metal bipolar plates.

SILICON NITRIDE FOR DIRECT WATER-SPLITTING AND CORROSION MITIGATION

Jeff Head, John A. Turner

ABSTRACT

Todays fossil fuels are becoming harder to obtain, creating pollution problems, and posing hazards to people's health. One alternative to fossil fuels is hydrogen, capable of serving as a clean and efficient energy carrier. Certain semiconductors are able to harness the energy of photons and direct it into water electrolysis in a process known as photoelectrochemical water splitting. Triple junction devices integrate three semiconductors of different band gaps resulting in a monolithic material that absorbs over a broader spectrum. Amorphous silicon (a-Si) is one such material that, when stacked in tandem, possesses water-splitting capabilities. Even though a-Si is capable of splitting water, it is an unstable material in solution and therefore requires a coating to protect the surface from corrosion. A stable, transparent material that has the potential for corrosion protection is silicon nitride. In this study, silicon nitride thin films were grown using DC magnetron sputtering with varying amounts of argon and nitrogen added to the system. X-ray diffraction indicated amorphous silicon nitride films. Current as a function of potential was determined from cyclic voltammetry measurements. Mott-Schottky analysis showed n-type behavior with absorption and transmission measurements indicated variation in flatband potentials. Variation in band gap values ranging from 1.90 to 4.0 eV. Corrosion measurements reveal that the silicon nitride samples exhibit both p-type and n-type behavior. Photocurrent over a range of potentials was greater in samples that were submerged in acidic electrolyte. Silicon nitride shows good stability in acidic, neutral, and basic solutions, indicative of a good material for corrosion mitigation.

INTRODUCTION

Energy resources have and always will be a cause for concern in order to meet the energy needs and requirements that society deals with in everyday life. To date, most of the world's energy is obtained from fossil fuels, nuclear power, and renewable processes from the power of the sun and wind. However, pollution from fossil fuels used to power today's society create many environmental and health problems. Global warming is also linked to the exponentially increasing anthroprogenic carbon dioxide concentrations in the atmosphere that has been taking place over the past 200 years [1]. Hydrogen fuel can be obtained from biomass conversion or using any renewably generated electricity for water electrolysis. Renewably produced hydrogen is a clean and efficient way of storing energy harnessed through typically intermittent renewable technologies such as wind, and solar power.

One of the most efficient ways of producing hydrogen is using sunlight to directly split water into hydrogen and oxygen on semiconductor surfaces [2]. At least 1.23 V are required for splitting water into hydrogen and oxygen. A cathodic overpotential of 100 mV and an anodic overpotential of 200 mV means an efficient photoelectrolysis system should have a band gap of at least 1.53 eV, where band gaps above 2.0 eV absorb less of the solar spectrum [3]. Two other requirements for water splitting are stability of the semiconductor in solution and "straddling" of the redox potentials of the hydrogen and oxygen evolution reactions by the energy bands

[3]. Specifically, the energy bands must encompass the potentials at which the following half reactions occur:

$$2H^+ + 2e^- \rightarrow H_2 \quad (1)$$

$$2H_2O \rightarrow O_2 + 4e^- + 4H^+ \quad (2)$$

Semiconductors are classified as either n-type or p-type. Semiconductors in which the majority charge carriers are electrons are n-type whereas those in which the majority charge carriers are holes are p-type [4]. Oxygen is produced on the surface of n-type materials and hydrogen on the surface of p-type materials. Preliminary characterization of semiconductors can be carried out with open circuit potential measurements, photocurrent measurements, and Mott-Schottky analysis [5]. In considering the location of the band edges one must factor in the Fermi level of the material, which for n-type materials lies just below the conduction band, and for p-type materials lies slightly above the valence band. The flatband potential, or the energy of the Fermi level when the bands are flat, can be estimated from Mott-Schottky plots [4], based on the equation

$$\frac{1}{C^2} = \frac{1.41x10^{32}}{\varepsilon N_D}\left[E - \left(V_{fb}\right)\frac{kT}{e}\right] \quad (3)$$

where C is the capacity of the space charge layer, ε is the static dielectric of the semiconductor, e is the electronic charge, N_D is the doping density, and E is the electrode potential [4]. Plotting the inverse square of capacitance versus voltage will give a linear plot with x-intercept equal to the flatband potential and a slope inversely proportional to the doping density.

Currently there exist solid-state multijunction devices that can generate the potential energy required for hydrogen and oxygen production from water while accessing a large fraction of the solar spectrum. For example, triple junction amorphous silicon (a-Si), devices can produce potentials greater than 1.8 V, sufficient for water-splitting and can be manufactured for maximum efficiency. However, a-Si exhibits a lack of stability when in solution, and therefore requires a protective coating. Previous studies have shown that the use of amorphous silicon carbide as a protective coating offers protection but attenuates too much light, thereby preventing maximum efficiency of hydrogen production by a-Si [6]. A possible solution is the use of silicon nitride which can offer the transparent qualities that silicon carbide lacks.

Previous work has shown that silicon nitride is a stable material, has transparent and nontransparent qualities, and its composition can be varied to be an absorber for the direct water splitting reaction itself [7]. With the ability to vary the composition of silicon nitride, and therefore the band gap of this material, it is the goal of this research to offer a transparent protective coating for a-Si, and thereby realize the USDOE 2005 goal of 7.5% solar to hydrogen efficiency and 1000 hours of stability. With the ability to vary the band gap of this compound, silicon nitride will also be considered for driving the water-splitting reaction as a single-gap device.

MATERIALS AND METHODS

Silicon nitride samples were deposited by means of DC magnetron sputtering at room temperature using a power of 200W at 4.5 mTorr. Nitrogen was used as a sputtering gas and varying amounts of argon, between 0 and 10.0 sccm were added. Glass with a thin indium-tin-oxide (ITO), film was used as a substrate (Colorado Concept Coatings). Once grown, x-ray diffraction and raman measurements were taken of the material for structural analysis. Photocurrent spectroscopy was carried out using a set-up containing a light source (tungsten lamp, LPS-220 PTI), which gives light in the visible spectrum; a lock-in amplifier (Stanford research systems SR830 DSP), which measures frequency with which the chopped light passes through to the sample; a potentiostat (Potentiostat/Galvanostat Model 263A), which applies an appropriate potential and measures the current being passed; a monochromater (PTI), that varies the energy of light hitting the sample; and a chopper (Chopper SR540), which regulates the frequency of light allowed to illuminate the sample. Using ocean optics equipment, reflectance and transmission measurements were taken, and initial conductivity measurements were carried out using four-point conductivity (Probe and Hall Probe).

Samples were cut into smaller fractions with a diamond scribe and made into electrodes using front face contact. A top portion of the sample was scraped off and contacted to a copper wire using silver paint (Ted Pella 16034 Colloidal Silver Liquid). The entire assembly was sealed with epoxy leaving only the front surface of the silicon nitride exposed (Loctite 9462 Hysol epoxy adhesive). Surface areas of the electrodes were determined with a photocopy technique which resulted from the ratio of the photocopy area mass to that of a standard 1 cm^2 cutout. Semiconductor characterization was carried out with electrodes submerged in a pH 6 buffer (Metrepak 06914KY), to see whether the open circuit potential became more negative under illumination, or more positive, indicating an n-type semiconductor or a p-type semiconductor.

Using a potentiostat and frequency response analyzer (Solartron 1286 electrochemical interface/SI 1260 Impedance/Gain-Phase Analyzer), various electrochemical measurements were taken using the SiN as the working electrode, a platinum counter electrode, and a silver/silver chloride reference electrode in a 50 mL beaker. Cyclic voltammetry, (I-V), scans were taken in the dark and light (100mW/cm^2), to see if the material passed anodic or cathodic photocurrent. Mott-Schottky analysis was carried out to determine flat band potentials as well as doping densities. Intensely illuminated open circuit potential measurements were taken using a DC power supply with a tungsten bulb at 10A for determining flatband positions.

Potentiodynamic scans were carried out in 3M H_2SO_4 (J.T. Baker), pH 7 buffer (Hydrion Buffer Kenvelopes 280-7.00), and 1M KOH (J. T. Baker) under dark and light conditions, for stability assessment, photocurrent response, as well as photovoltage behavior. Electrodes were platinized for further photocurrent analysis using chloroplatinic acid at a coverage of 10mC/cm^2.

Cyclic voltammetry and potentiodynamic measurement analyses were carried out using CorrWare2 software, and Mott-Schottky analysis was carried out using Zplot software from the vendor Scribner Associates International.

RESULTS

Photoresponse spectra of the samples were taken and divided by the tungsten lamp spectrum giving a normalized photocurrent response for transmittance and absorbance as seen in Figure 1 and 2, respectively. Samples containing less nitrogen were less transparent and showed more absorbance in the range of 500 to 600 nm, 2.48 to 2.07 eV. Samples containing more nitrogen, more transparent samples, showed less absorbance. Using ocean optics, reflectance and transmission measurements were taken on samples

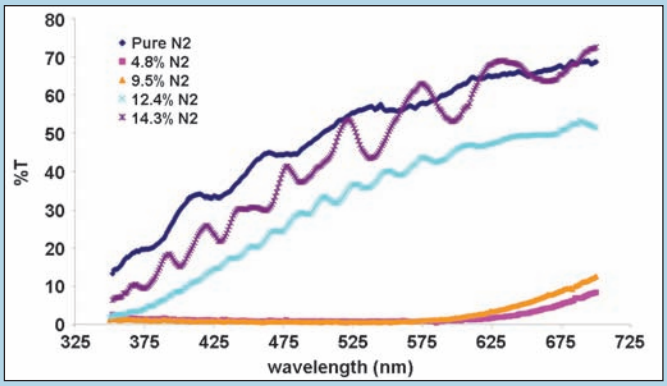

Figure 1. Raw transmission data of each sample from 350 to 700 nm using sample as a filter in front of thermopile.

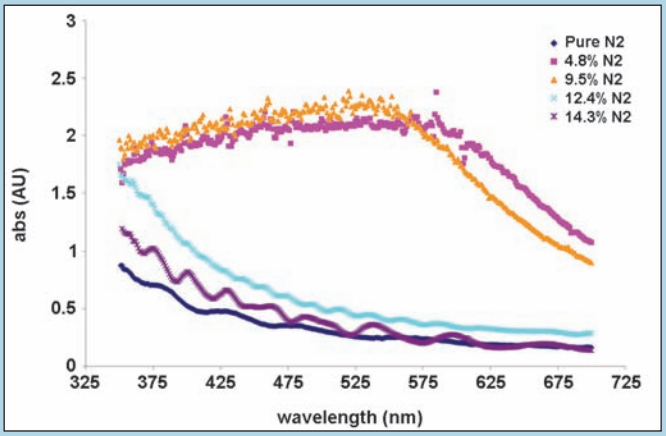

Figure 2. Initial absorbance measurements of each sample from 350 to 700nm at 1nm steps using the sample as a filter in front of a thermopile normalized to a tungsten lamp spectrum extrapolated from Figure 1.

sputtered with pure N_2 and 4.8% N_2, as seen in Figure 3 and 4, respectively. This relates to initial absorbance and transmittance measurements giving a bandgap equal to 1.90 eV for the 4.8% N_2 material. X-ray diffraction measurements of the samples showed no peak shifts as compared to ITO as seen in Figure 5. This result indicated amorphous compounds which was further supported by raman analysis.

Preliminary photovoltage shift measurements revealed small changes in electrode potential when illuminated. The largest change in potential occurred for the sample sputtered with 4.8% N_2 giving a potential difference of -131 mV when illuminated as seen in Table 1.

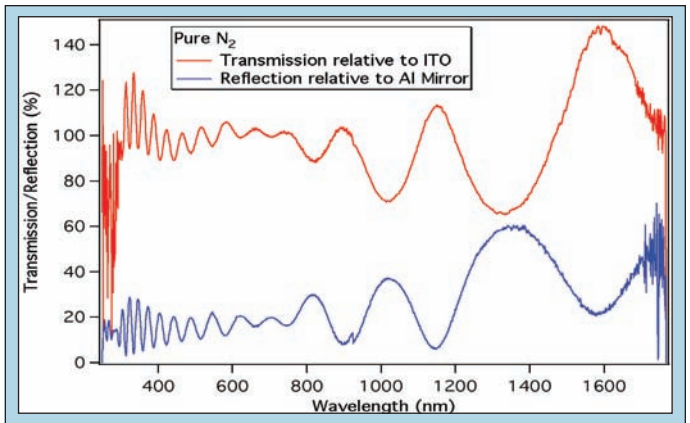

Figure 3. Wavelength as a function of percent transmission and reflection of silicon nitride containing pure nitrogen, measured with ocean optic instruments.

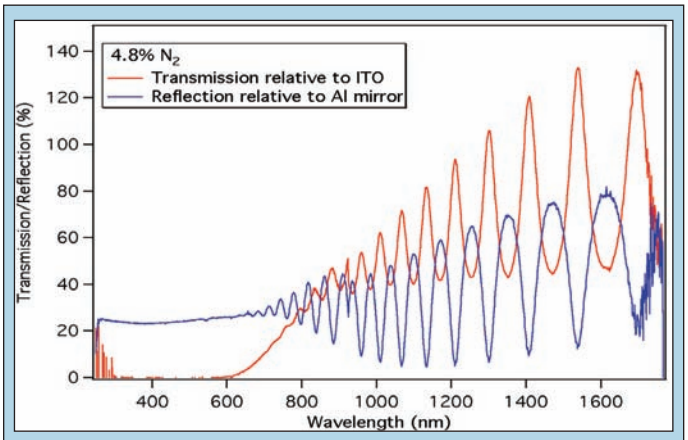

Figure 4. Percent transmission and reflection of silicon nitride sample containing 4.8% N_2 using ocean optic instruments.

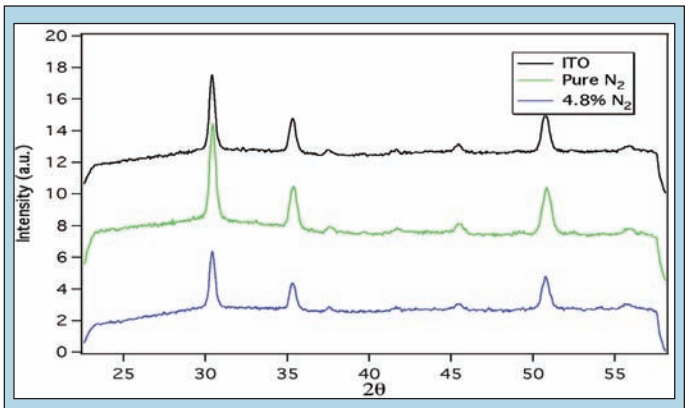

Figure 5. X-ray diffraction measurements of ITO as a control, a pure nitrogen sample, and sample containing 4.8% N_2.

Sample	Pure N_2	Pure N_2	Pure N_2	52.4%N_2	23.8%N_2	14.3%N_2	9.52%N_2	4.8%N_2
Dark	-0.008	-0.059	-0.011	-0.093	-0.02	-0.018	-0.012	-0.23
Light	-0.031	-0.083	-0.021	-0.128	-0.036	-0.064	-0.035	-0.361
ΔV	-0.023V	-0.024V	-0.01V	-0.035V	-0.016V	-0.046V	-0.023V	-0.131V

Table 1. Open circuit potential measurement changes in pH 6 buffer under dark and light conditions.

Out of the 10 samples deposited by magnetron sputtering, those that were more transparent showed the least photopotential, whereas the less transparent samples showed more change in potential under illumination. All of the samples revealed a more negative potential reading in the light. Four-point conductivity resulted in values greater than 10^7 Ω/square.

A sample was submerged in a 50 mL beaker with pH 6 buffer and multiple scans of current versus potential were obtained. Measurements showed a minimal shift in anodic and cathodic current when illuminated for the 10 different batches, including 4.8% N_2 measurements, as seen in Figure 6. However, when submerged in 3M H_2SO_4 the same 4.8% N_2 sample responded to chopped light, with illumination marked by an increase in cathodic current as seen in Figure 7.

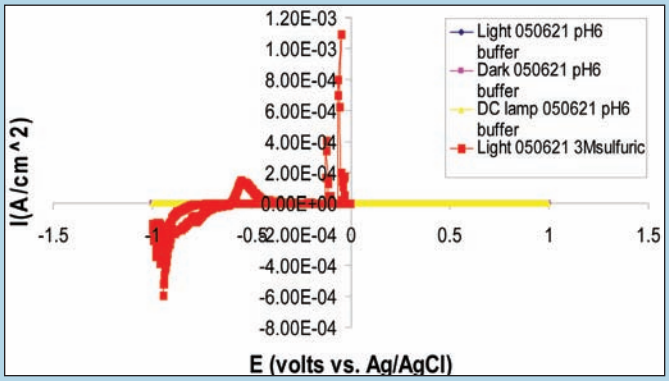

Figure 6. I-V cyclic voltammetry scan of sample containing 4.8% N_2 in dark and light conditions with a fiber optic lamp at 0.100 W/cm2 in pH 6 buffer and 3M H_2SO_4.

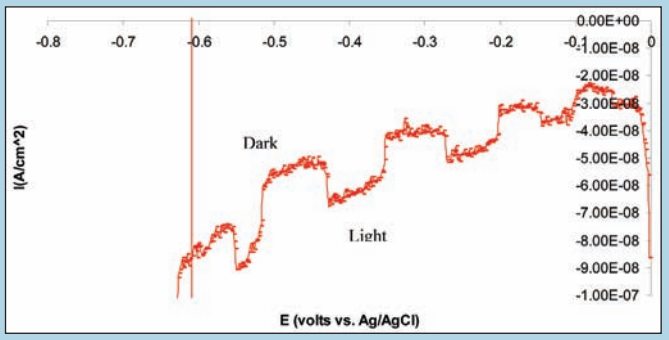

Figure 7. I-V scan of sample 4.8% N_2 in 3M H_2SO_4 obtained from hand chop method resulting in a stepwise plot with dark measurements at a lower current and light measurements at the higher cathodic current. Zoomed in from Figure 6.

Varying the frequency between 1000 and 20,000 Hz in the dark and light, while in pH 6 buffer, Mott-Schottky analysis was performed on each sample as seen in Figure 8. All plots obtained from analysis revealed doping densities on the order of 10^{15} to 10^{17}/cm^3, with varied aphysical x-intercepts, and all positive slopes. Analysis on the 4.8% N_2 sample revealed flatband potentials near -1.46 V while in pH 6 buffer at 1000 Hz in the light.

Potentiodynamic scans were carried out in acidic, neutral, and basic solutions in the light and dark. As seen in Figure 10, both anodic and cathodic current increased for the sample sputtered with 4.8% N_2 when illuminated. Also, there is a drop in the photovoltage when illuminated, and as seen from the plot, low noise activity. Table 2 depicts the intercept values for the current, which are on the order of 10^{-7} A/cm^2.

	Current (Amps/cm^2)		
Sample	3M H_2SO_4	pH 7	1M KOH
ITO	10^{-7}	10^{-8}	10^{-7}
Pure N_2	10^{-8}	10^{-7}	10^{-7}
4.8% N_2	10^{-7}	10^{-8}	10^{-7}

Table 2. Current measurements for ITO, pure N_2, and 4.8% N_2, in acidic, neutral, and basic solution when potential is at zero.

DISCUSSION AND CONCLUSIONS

The absorbance of the sample increases, Figures 1 and 2 show nitrogen content in the sample decreases, as expected from the transparent and nontransparent characteristics of the samples. In Figure 2, the raw absorbance data of the pure nitrogen samples shows minimal absorbance, which would indicate high band gap values for these transparent samples. In contrast, the materials containing 4.8% N_2 and 14.3% N_2 show strong absorbance, with a drop off in absorbance near ~600 nm, as expected because their red-orange color. These measurements reveal a band gap of ~2.0 eV. Further measurements with ocean optics, as seen in Figure 3, show strong correlation in that for the 4.8% N_2 material the transmission increases at 600 nm giving a band gap equal to 1.90 eV, near the estimated band gap given by photoresponse, and therefore are sufficient for water-splitting. Also, for a sample sputtered with pure nitrogen, in Figure 4, transmission levels remain high across the spectrum, giving a band gap around 4.0 eV, too large of a value to absorb terrestrial radiation.

Figure 5 shows there is good overlap of the x-ray diffraction peaks when looking at the ITO, pure N_2, and 4.8% N_2. This lack of shift in peaks would suggest that this material is non crystalline and has amorphous qualities. Results from raman analysis show no peak behavior, also suggesting non crystalline material.

From Table 1, multimeter conductivity measurements show small changes in potential under illumination. The four-point conductivity measurements of greater than 10^7 Ω/square further support silicon nitride films being a resistive material. Comparing changes in potential it can be seen that the less transparent, 4.8% N_2 sputtered sample, has the greatest change, -131 mV. Therefore, of these samples, this material has the greatest ability to absorb photons to excite electrons. The common trend of a more negative potential resulting under illumination suggests that silicon nitride behaves as an n-type semiconductor. For n-type semiconductors, the bands bend up at the semiconductor/electrolyte interface. Illuminating the semiconductor and holding the circuit open results in a flattening of the bands which is measured as a negative shift in the Fermi level, or measured potential [4].

I-V plots also give an indication of whether the semiconductor exhibits p-type or n-type behavior, as seen in Figure 6. In comparing

light and dark measurements, minimal photocurrent is generated in pH 6 buffer. However, when the sample is placed in 3M H_2SO_4, a photocurrent is observed (Figure 7). For p-type semiconductors, photocurrent is negative because of the orientation of the electric field surface, which is seen in Figure 7, inferring p-type behavior of the 4.8% N_2 sputtered material.

Mott-Schottky analysis is also a good indicator of the type of semiconductor. With Mott-Schottky plots having polarization as a function of the inverse of capacitance squared, it is suggested that for p-type materials that, when there is an increase in negative potential there is an increase in the depletion layer width. This in turn causes the capacitance of the material to decrease, thereby causing $1/C^2$ to increase, resulting in a negative slope for the M-S plot as seen in Figure 8. This suggests the silicon nitride as an n-type material, as expected from measurements determined by open circuit potential.

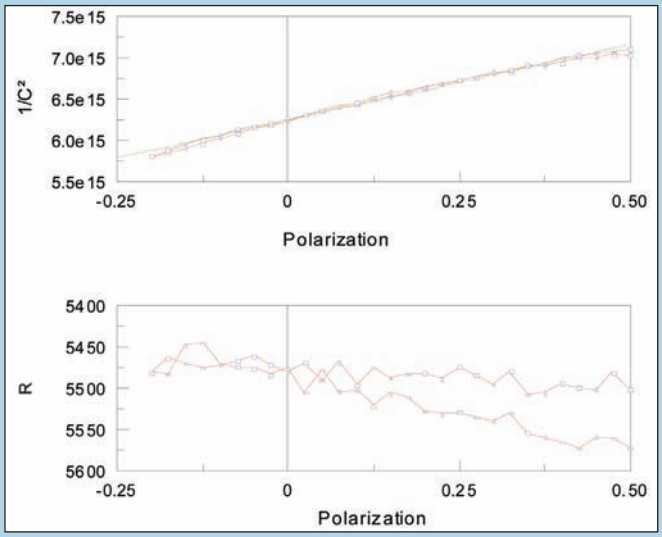

Figure 8. Mott-Schottky plot of polarization as a function of the inverse of capacitance squared above and polarization as a function of resistance below with regression performed on above plot.

Mott-Schottky analysis can also indicate where the flatband potential lies as well as the doping density. Performing linear regression on the M-S plot for 4.8% N_2 yields an x-intercept value of -1.46 V. Since the slope of this material indicates n-type behavior, this would suggest the location of the Fermi level, giving an accurate location of the conduction band. From the obtained band gap of 1.90 eV, the valence band is then estimated to be 0.44 V. Because this measurement was carried out in pH 6 buffer, the reduction potential of H_2O lies at -0.56 V and the oxidation potential lies at 0.67 V. Therefore, even though the band gap of this material is sufficient for splitting water and the conduction band lies more negative of the reduction potential, the valence bands does not lie more positive than the oxidation potential, which suggests that silicon nitride is not capable of splitting water in pH 6 buffer, due to this non band edge "straddling" as seen in Figure 9. Doping densities of all 10 batches of materials were on the order of 10^{15} to $10^{17}/cm^3$, typical values for a semiconductor.

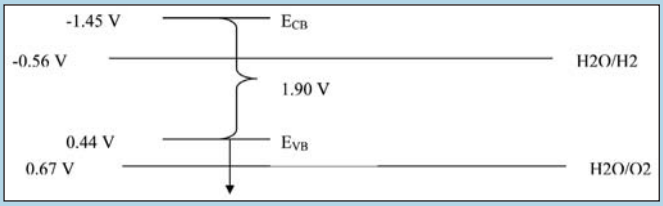

Figure 9. Representation of the band edge locations with respect to the redox potentials when submerged in pH 6 buffer. Arrow indicates where energy of valence band should be located.

Potentiodynamic scans, which look at logarithm of current as a function of potential, can be used for stability . Figure 10 shows that when the dark scan and light scan are compared, there is a drop in the photovoltage in the light indicating an n-type material,

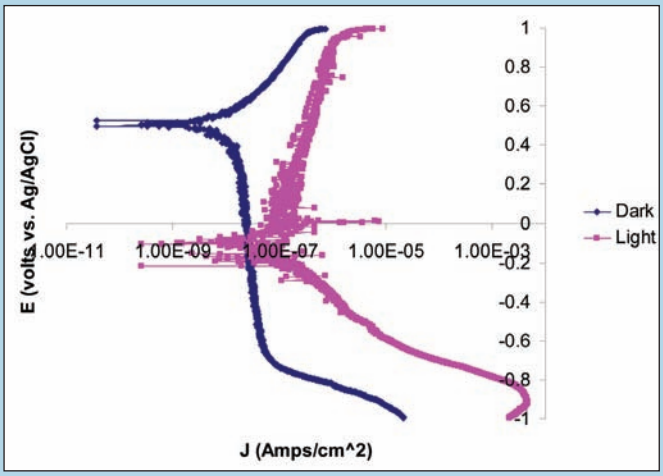

Figure 10. Potentiodynamic scan in 3M H_2SO_4 of sample containing 4.8% N_2 in the dark and light. Light scans show a drop in photovoltage when illuminated, as well as an increase in the anodic and cathodic current from shifts in current both above and below the horizontal peak where the shift from cathodic to anodic current takes place. Stability exhibited in both the dark and light plot.

as expected from open circuit potential measurements. However, when in the light there is an increase in anodic as well as cathodic current, indicating both n-type and p-type behavior when in 3M H_2SO_4. This would suggest that the 4.8% N_2 material has intrinsic, or compensated, characteristics.

Table 2 shows that when compared with ITO as a control, samples sputtered with both pure N_2 and 4.8%N_2, silicon nitride seems to pass a similar current when there is zero potential in the system. This further supports the suggestion that silicon nitride is a resistive material due to it crossing at a low current. Factoring in the low noise level shown in Figure 10, and the low current measurements from Table 2 of both pure N_2 and 4.8% N_2, silicon nitride appears to be a stable material, characteristic of a protective coating.

In conclusion, the goals of this research were realized in that silicon nitride was studied for its water-splitting and corrosion-protection capabilities. The results of this study suggest that silicon nitride is a resistive material that has intrinsic semiconductor characteristics. Corrosion measurements revealed low current and low noise plots suggesting not only a resistive material, but also a

stable material. With the ability to manufacture transparent silicon nitride, these results will allow for further corrosion and protective coating measurements to be made, such that this material has the potential to solve the problems of using silicon carbide as a protective coating. Future work at NREL will look at possible dopants for the material to enhance the n-type or p-type behavior, as well as growth on other substrates. The stable characteristic of this material needs further quantitative analysis.

ACKNOWLEDGEMENTS

This research was conducted at the NREL. I would like to thank the U.S. Department of Energy, Office of Science for the opportunity to participate in the SULI program to further my knowledge of science and renewable energies. I would like to thank Dr. John Turner for his patience, humor, and knowledge of this research. I would also like to thank Todd Deutsch and Jen Leisch for their expertise in this area of research and for taking the time to instruct me on the concepts used in this study. I would also like to thank Maikel van Hest for growing my samples, and my other coworkers in the Electric & Hydrogen Technologies & Systems Center at NREL.

REFERENCES

[1] IPCC Third Assessment Report. 2003.

[2] Turner, John A. "Photoelectrochemical Water Splitting". 2004 DOE Hydrogen, Fuel Cells & Infrastructure Thechnologies Program Review. 2004.

[3] Kocha, Shyam S., Turner John A. "Study of the Schottky barrier and determination of the energetic positions of band edges at the n- and p-type gallium indium phosphide electrode /electrolyte interface". *Journal of Electroanalytical Chemistry*. Vol. 367, 1994 pp. 27-30.

[4] Bott, Adrian W. "Electrochemistry of Semiconductors". *Current Separations*. Vol. 17, 1998. pp. 87-91.

[5] Turner, John A. Energetics of the Semiconductor-Electrolyte Interface". *Journal of Chemical Education*. Vol. 60, 1983 pp.327-329.

[6] Varner, K. "Evaluation of Amorphous Silicon as a Direct Water Splitting System". 2002 National Renewable Energy Laboratory Internal Report.

[7] Y. Hirohata. "Properties of silicon nitride films prepared by magnetron sputtering". *Thin Solid Films*. Vol. 253, 1994. pp. 425-429.

Stephanie Freeman graduated with an honors B.S. in chemical engineering from the University of Arizona in December of 2005. During the summer before her final semester she participated in the Science Undergraduate Laboratory Internships (SULI) program at Idaho National Laboratory in Idaho Falls, Idaho. Her SULI project involved investigating the use of nucleotide primers designed for the ammonia monooxygenase gene in detection of ammonia oxidizing bacteria in environmental samples. She is an incoming graduate student at Massachusetts Institute of Technology (MIT) in the MS of chemical engineering practice program and is currently completing an independent research project on perchlorate reducing bacteria at Wageningen University in The Netherlands. She will graduate in August 2007 and hopes for a PhD position afterward.

David W. Reed is a scientist in the Biological Sciences Department at the Idaho National Laboratory in Idaho Falls, Idaho. He received a B.S. in microbiology) and M.S. in zoology from Brigham Young University and a subsequent PhD in microbiology, molecular biology and biochemistry from the University of Idaho. He has more than twelve years of experience using molecular methods to probe environments for microbial activity and diversity, characterizing microbial enzymatic and metabolic systems, and conducting comparative proteomic and genome analysis in microbial systems. He is experienced working with anaerobes, hyperthermophiles, sulfate reducers, and industrially relevant bacteria. He is an affiliate faculty member in biological sciences at Idaho State University and in environmental science at the University of Idaho. He is published in peer-reviewed journals and has given numerous presentations.

Yoshiko Fujita is a researcher in the Biological Sciences Department at the Idaho National Laboratory (INL) in Idaho Falls, Idaho. She received a B.A. in chemistry from Williams College, and M.S. and PhD degrees in civil and environmental engineering from Stanford University. Her primary research focus has been the characterization of microbial activity in subsurface environments using cultivation-based and molecular techniques, and examining the associated effects on contaminant fate and transport. She also has expertise in the identification of metabolic products and intermediates, and is interested in changes in organic water quality that occur during aquifer recharge with reclaimed water. Recently she has been interested in the interactions between microorganisms and minerals, and on the coupling between hydrologic transport and microbially induced mineralization in porous media.

TESTING THE SPECIFICITY OF PRIMERS TO ENVIRONMENTAL AMMONIA MONOOXYGENASE (*AMO*A) GENES IN GROUNDWATER TREATED WITH UREA TO PROMOTE CALCITE PRECIPITATION

Stephanie Freeman, David W. Reed, and Yoshiko Fujita

ABSTRACT

Bacterial ammonia monooxygenase (*amo*A) genes in DNA isolated from microorganisms in groundwater were characterized by amplification of *amo*A DNA using polymerase chain reaction (PCR), Restriction Fragment Length Polymorphism (RFLP) analysis, and sequencing. The *amo*A gene is characteristic of ammonia oxidizing bacteria (AOB). The DNA extracts were acquired from an experiment where dilute molasses and urea were sequentially introduced into a well in the Eastern Snake River Plain Aquifer (ESRPA) in Idaho to examine whether such amendments could stimulate enhanced ureolytic activity. The hydrolysis of urea into ammonium and carbonate serves as the basis for a potential remediation technique for trace metals and radionuclide contaminants that can co-precipitate in calcite. The ammonium ion resulting from ureolysis can promote the growth of AOB. The goal of this work was to investigate the effectiveness of primers designed for quantitative PCR of environmental *amo*A genes and to evaluate the effect of the molasses and urea amendments upon the population diversity of groundwater AOB. PCR primers designed to target a portion of the *amo*A gene were used to amplify *amo*A gene sequences in the groundwater DNA extracts. Following PCR, amplified gene products were cloned and the clones were characterized by RFLP, a DNA restriction technique that can distinguish different DNA sequences, to gauge the initial diversity. Clones exhibiting unique RFLP patterns were subjected to DNA sequencing. Initial sequencing results suggest that the primers were successful at specific detection of *amo*A sequences and the RFLP analyses indicated that the diversity of detected *amo*A sequences in the ESRPA decreased with the additions of molasses and urea.

INTRODUCTION

One of the crucial steps in the nitrogen cycle is the oxidation of ammonia to nitrite. The ammonia monooxygenase (*amo*A) gene has been identified as an integral gene in the conversion of ammonia to hydroxylamine, the first step in overall ammonia oxidation [1]. The *amo*A gene codes for the catalytic subunit of the ammonia monooxygenase enzyme. The *amo*A gene is present in all nitrosifying bacteria that take part in this critical step of the global nitrogen cycle [2]. This gene was previously thought to be unique to bacteria, but recent research has identified ammonium oxidizing

archaeal species that have a similar archaeal *amo*A gene and that may play an important role in marine nitrogen cycling [3].

Along with collaborators, Idaho National Laboratory (INL) is currently investigating a remediation technique for radioactive strontium-90 (^{90}Sr) contamination of aquifers based on the incorporation of strontium into calcite (calcium carbonate, $CaCO_3$). In calcite-saturated aquifers such as the Eastern Snake River Plain Aquifer (ESRPA) in Idaho, co-precipitated strontium in calcite is expected to remain stable for hundreds of years. The specific remediation method under investigation is greatly dependent upon the acceleration of calcite precipitation by native groundwater microorganisms' hydrolysis of urea:

$$H_2NCONH_2 + 2H_2O \rightarrow 2NH_4^+ + CO_3^{2-}$$
(Urea + Water → Ammonium + Carbonate)

The carbonate ion reacts with metals to form carbonate minerals, while the ammonium can serve to displace metal cations (such as Ca^{2+} and Sr^{2+}) from ion exchange sites on aquifer solids, making them available for reaction with the carbonate. However, the ammonium could also serve as an electron donor for ammonia oxidizing bacteria (AOB) present in the aquifer.

At INL, a quantitative Polymerase Chain Reaction (qPCR) technique is being developed to evaluate the effect of urea additions on native AOB populations present in groundwater. This qPCR method utilizes primers designed to specifically target the *amo*A gene in environmental microbial communities. Methods based on the presence of the *amo*A gene for detection and quantification of AOB species have been previously developed based on conventional Polymerase Chain Reaction (PCR) [4], competitive PCR (c-PCR) [5] and real-time PCR [6]. In this work, we used real-time PCR primers originally developed by others [4,6] with slight modifications in an effort to capture more environmental *amo*A genes and exclude sequences for the similar *pmo*A gene, a subunit of the membrane bound methane monooxygenase gene (pMMO). Parts of the *pmo*A gene have high sequence similarity to *amo*A and non-specific priming is common [6].

The specific objective of the work reported here was to test the effectiveness of these primers in targeting *amo*A genes in environmental samples and to characterize the diversity of genes that could be detected. The primers were applied to genomic DNA extracts collected previously as part of a field experiment in the ESRPA where dilute molasses and urea were added to the aquifer in order to stimulate ureolytic activity. After amplification of genomic DNA with these primers, initial diversity was observed through the use of Restriction Fragment Length Polymorphism (RFLP) analysis. Sequencing was then performed in order to compare these environmental *amo*A gene sequences with *amo*A sequences reported by others for clones and known AOB species.

MATERIALS AND METHODS

Sample Origin: Genomic DNA extracts from microorganisms in groundwater samples taken during the course of a 2002 field experiment using an ESRPA well located at University Place, Idaho Falls, ID, were used as PCR templates during this study. During the first phase of the field experiment, Pre-Treatment, groundwater samples were taken prior to the addition of experimental amendments to establish the background conditions. Dilute molasses (0.00075%) was delivered into the well during the second phase (two weeks in duration), known as Post-Molasses, and urea (and no molasses) was added in the third and final phase (also a two week period), known as Post-Urea. Groundwater samples were collected periodically throughout the experiment and DNA was extracted from cells collected on filters (20 L filtered per extract) [7] using conventional methods. A more detailed description of the field experiment and the DNA extractions is provided in Tyler (2004) [7].

Primer Name	Direction	Sequence	Ref.
A189	Forward	5' - GGHGACTGGGAYTTCTGG - 3'	[8]
A189 DR	Forward	5' - GGNGACTGGGAYTTCTGG - 3'	[9]
*amo*A-2R'	Reverse	5' - CCTCKGSAAAGCCTTCTTC - 3'	[4]
*amo*A-2R' DR	Reverse	5' - CCCCTSBGSRAAVCCTTYTTC - 3'	[9]

Table 1. *amo*A primers. Primers A189 and *amo*A-2R' are shown along with the primers used in this study, A189 DR and *amo*A-2R' DR. Primers were designed from alignments of sequences of *amo*A genes from *Nitrosomonas* and *Nitrosospira genera*. Changes made to the standard *amo*A primers are indicated with bold and underlined typeface. Sequences, given from 5' to 3' end, include degeneracies represented by B, H, K, N, R, S, Y, and V. B represents CGT (implying a C, G, or T at that position). Similarly, H represents ATC, K represents GT, N represents ACGT, R represents AG, S represents CG, Y represents CT, and V represents ACG.

***amo*A Gene Specific Primers**: Primers A189 DR and amoA-2R' DR were used for the PCR amplification (Table 1). The primers were based on primers A189 and amoA-2R' developed in previous studies [4,8]. Primer A189 DR targets both bacterial *amo*A and *pmo*A genes while the amoA-2R' DR primer is designed to target the *amo*A gene only, excluding the *amo*A gene present in *Nitrosococcus* species [9].

PCR Amplification: The optimized PCR reaction mixture consisted of Taq2000 Polymerase (1U, Stratagene, La Jolla, California, USA), 1X Taq2000 buffer, dNTPs (0.2 mM; Roche Applied Science, Indianapolis, Indiana, USA), BSA (0.2 μg/mL; Roche Applied Science), A189 DR forward primer (900 nM), amoA-2R' DR reverse primer (300 nM), and DNA template (2 μL). Genomic DNA from *Nitrosomonas europaea* was used as template for a positive control reaction. Multiple negative reactions used either no added genomic DNA (water) or genomic DNA extracts from *Escherichia coli* and *Methylococcus capsulatus*. The reactions were performed on a GeneAmp PCR System 9700 thermocycler (Applied Biosystems, Foster City, California, USA) using the following thermal program: 94°C (4 mins), then 38 cycles of 94°C (45 secs), 57°C (60 secs), and 72°C (60 secs), with a final hold of 72°C (5 minutes). PCR products were verified for correct size (670bp) and purity by electrophoresis on an ethidium bromide stained 1.3% agarose gel.

Cloning: Prior to cloning, PCR products derived from multiple samples taken from each of the three phases of the field experiment were pooled (five products for Pre-Treatment, three products from Post-Molasses, and two products for Post-Urea) and then purified by affinity column and gel purification (Qiagen PCR Purificaiton

and Q1Aquick Gel Extraction Kits; Qiagen, Valencia, California, USA). Cloning reactions were performed using the TOPO® TA Cloning system (Invitrogen, Carlsbad, California, USA) following the manufacturer's directions. Cloning reactions were performed on the pooled PCR products from the three different phases, as well as a positive control (*N. europaea*) and a negative control (only the reaction with no DNA template), resulting in the generation of 5 separate clone libraries. PCR products were ligated and added to 50 µL of One Shot® TOP10 *Escherichia coli* competent cells (Invitrogen, Carlsbad, California, USA) for transformation. The transformed cells were plated on LB agar plates containing S-Gal, ITPG, and kanamycin (50 µg/mL; Sigma-Aldrich Corp., St. Louis, Missouri, USA), and grown overnight at 37°C. For each treatment phase clone library, 50 colonies were transferred to new LB agar kanamycin plates, grown overnight, and stored for further analysis.

Restriction Fragment Length Polymorphism (RFLP): Clones from each library were analyzed using RFLP. Individual colonies from each library were re-suspended in 10 µL of sterile water and lysed for 10 mins at 99°C. The lysed cells' DNA was used as template for PCR as described previously, after which the PCR product (20 µL) was used for the restriction analysis. The restriction reaction also contained enzymes HinP1 and MsPI (0.4 U each; New England Biolabs, Ipswich, Massachusetts, USA) in 1X NEBuffer 2, and Triton X-100 (1%; Promega, Madison, Wisconsin, USA). The restriction mixture was incubated at 37°C for 4.5 hours. RFLP products were analyzed by electrophoresis on a 3% MetaPhor® agarose (Cambrex, East Rutherford, New Jersey, USA) gel and stained with ethidium bromide.

Plasmid Purification and Sequencing: After RFLP analysis, plasmid purification was performed on the clones selected for sequencing. Plasmids were extracted from the *E. coli* cells using the QIAprep Spin Miniprep Kit (Qiagen, Valencia, California, USA) according to manufacturer's instructions. Each purified plasmid (50-100 ng) was subjected to cycle sequencing (10 µL reaction) with 2 µL 2.5X sequencing buffer and 1 µL BigDye, both part of the BigDye® Terminator Cycle Sequencing Kit (Applied Biosystems, Foster City, California, USA), and 1 µL primer (T7, M13F, and M13R; Operon Technologies, Huntsville, Alabama, USA). The sequencing reaction products were purified using a MultiScreen$_{384}$-SEQ filter plate (Millipore, Billerica, Massachusetts, USA). The reactions were subsequently washed with 0.3 mM EDTA, pH 7.8 and re-suspended in 0.3 mM EDTA, pH 7.8. Sequencing was performed in an ABI Prism Model 3700 sequencer (Applied Biosystems, Foster City, California, USA).

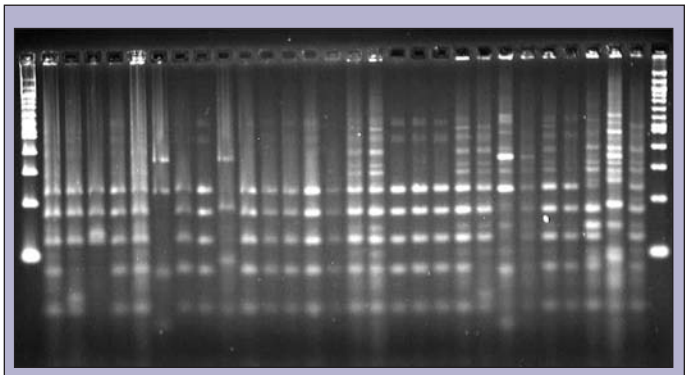

Figure 1. Example of an RFLP gel from Pre-treatment groundwater sample. The outer lanes contain 100 bp DNA ladder (New England Biolabs, Ipswich, Massachusetts, USA) while the inner 28 lanes contain clones from the Pre-treatment groundwater sample. Samples were digested with HinP1 and MsP1 restriction enzymes and were electrophoresed on a 3% agarose gel and stained with ethidium bromide.

RESULTS

The diversity of the *amo*A sequences detected in the UP-1 groundwater samples was characterized using RFLP. The RFLP gels (see for example Figure 1) were analyzed visually to identify unique banding patterns. Initially, PCR products with a common RFLP banding pattern within each library were assigned to the same RFLP group (A through BB; Table 3). Then, patterns were compared between the libraries to see if similar RFLP patterns were found in more than one clone library. In this way, some patterns were found in multiple libraries and resulted in more than one RFLP group label. RFLP analysis of the Pre-Treatment clones showed 12 unique banding patterns from the 50 clones of that library whereas RFLP analysis of the second library, Post-Molasses, and the third library, Post-Urea, showed 8 and 7 unique banding patterns respectively. Two unique banding patterns, namely RFLP Groups A/J_1-J_2/Q and C/L/R, were found in all three samples. This may indicate that the bacterial species represented in these patterns were present throughout the course of the UP-1 experiment. There was also one common pattern found in the Pre-Treatment and Post-Molasses libraries, RFLP Groups G/P, and one pattern present in only the Pre-Treatment and Post-Urea libraries, RFLP Groups E/V. All other banding patterns from each library appeared to be unique.

Primer Name	Direction	Sequence
T7	Forward	5' - TAATACGACTCACTATAGGG - 3'
M13F (-20)	Forward	5' – GTAAAACGACGGCCAG - 3'
M13R	Reverse	5' – CAGGAAACAGCTATGAC - 3'

Table 2. Primers used in sequencing reaction. The oligonucleotide sequences complementing these primers are all found on the TOPO TA vector used during cloning. A majority of the clones chosen for sequencing after RFLP were sequenced with at least two of the primers listed above.

Sequencing was performed on unique RFLP clones and the clones derived from the PCR control reactions. The positive control reaction used a *N. europaea* genomic DNA template while the negative control reaction used no added DNA template in the initial PCR reaction. All of the clones were sequenced using at least two of the three sequencing primers (Table 2) and the majority of clone sequences were visually analyzed to confirm the accuracy of the automatically generated sequence produced by the sequencing software. The sequences were manually fitted if necessary and both the primer sites and vector nucleotides were removed. Since multiple sequences were obtained for each clone, a consensus sequence was generated for each clone. Consensus sequences were compared to the NCBI (National Center of Biotechnology Information) database

RFLP Group	Common RFLP Patterns	Number of clones assigned to each RFLP Group		
		Pre-Treatment	Post-Molasses	Post-Urea
A	J_1-J_2, Q	32	35	41
B		2	0	0
C	L, R	1	7	4
D		2	0	0
E	V	2	0	1
F_1-F_2		3	0	0
G	P	1	1	0
H		1	0	0
I		1	0	0
K	O	0	2	0
M		0	1	0
N		0	1	0
S		0	0	1
T		0	0	1
U		0	0	1
W		1	0	0
X		1	0	0
Y		1	0	0
Z		0	1	0
AA		0	1	0
BB		0	0	1
Number of Unique RFLP Patterns		12	8	7

Table 3. Comparison of RFLP groups found after cloning UP-1 groundwater samples. The three UP-1 clone libraries, Pre-Treatment, Post-Molasses, and Post-Urea all had varying numbers of unique RFLP banding patterns, decreasing in number from Pre-Treatment to Post-Urea. The Common RFLP Patterns column indicates the RFLP patterns that are common between different clone libraries. RFLP groups were first assigned for each library and then compared between the different libraries, resulting in multiple labels in some instances.

using BLAST (Basic Local Alignment Search Tool) [10] to observe how the sequences obtained were related to known *amo*A gene sequences.

As expected, BLAST analysis of the gene sequences obtained for the positive controls (clones Pos1 and Pos2) indicated a very close relationship to *N. europaea* (complete genome, NCBI ascension number |BX321863.1|). Although only a very faint band of DNA was visualized in the ethidium bromide gel from the negative control sample, the DNA was cloned (clones Neg1 and Neg2), and the sequences closely matched a portion of the *N. europaea* genome, indicating that contamination of the negative control from the positive control might have occurred during PCR amplification. For the clones derived from environmental samples, data was not obtained for 5 groups (RFLP pattern A, L, S, T, and X clones) because of inefficient sequencing reactions that produced unreadable outputs. The remaining 25 clones were submitted to BLAST for analysis. A majority of the sequenced clones, 14 in total (representing RFLP groups B, C, F1, F2, G, I, J1, J2, N, P, Q, R, Z, and BB), matched most closely to the *amo*A gene from two unidentified bacteria (isolate E-207M, NCBI ascension number |AJ317947| and clone W10 682 7 |DQ008439|). With respect to known isolated bacteria, the output from the BLAST search indicated that the sequence from the clones matched most closely to the *amo*A gene of *Nitrosomonas sp*. AL212 (NCBI ascension number |AF327918|).

Three additional clones were very similar to those obtained for the positive control. The BLAST analysis of these clones E, H, and V indicated that the highest similarity was to the *amo*A gene region of *N. europaea*,. The remaining 8 clone sequences (D, K, M, O, U, W, Y, and AA) were similar in size to the expected *amo*A PCR products yet the sequencing suggested improper priming during the sequencing reaction.

DISCUSSION AND CONCLUSIONS

Analysis of the RFLP screening results showed differences between the banding patterns of the clones obtained from the three UP-1 experimental treatment phases. The RFLP diversity of the *amo*A gene fragments apparently decreased over the course of the experiment with the first experimental period, Pre-Treatment, having the greatest number of unique banding patterns. It is possible that some species might have been more responsive than others in this changing environment and dominated the AOB community during the different phases of the experiment. Only two banding patterns were common in all three clone libraries, while only two other patterns were found in multiple clone libraries. The other banding patterns were unique to the sample library in which each was found. As a majority of the banding patterns were changing with each sample, with only a few being maintained throughout the various samples, the RFLP analysis seems to indicate that the molasses and urea amendments have a large impact on the subsurface microbiological community.

Sequence data for three of the four RFLP groups with the most common RFLP pattern (J_1, J_2, and Q; unfortunately the sequencing reaction for the clone representing group A did not provide a usable sequence) matched closely with the sequence of the *amo*A gene of known AOB species. Additionally, clones that represented eleven other RFLP banding patterns indicated a close match with this same, known AOB species. Because a majority of the clone sequences were found to closely match known AOB species, it appears that our primers successfully detected bacterial *amo*A genes in the environment. The fact that at least 14 clones shared a similar BLAST output suggests that one particular species or closely related AOB may dominate the nitrosifying subsurface microbial community of the ESRPA. However, potential biases in DNA extraction, PCR, and cloning mandate caution in extrapolating results from clone libraries to the extant microbial communities [11].

The correlation of the gene sequences of RFLP groups E, H, and V to that of *N. europaea* and the finding of this same sequence in the negative control suggested that contamination might have occurred during PCR. Another possibility is that the subsurface community in the ESRP aquifer did in fact naturally contain *N. europaea* or closely related organisms.

In summary, preliminary sequencing results indicate that the primers used in this study were selective for the *amo*A gene region of various AOB. This finding supports the use of these primers to gauge the effect of urea addition on both the quantity and composition of the AOB community of the subsurface. However, further work is needed to elucidate the relationships between the gene sequences obtained here and the *amo*A gene sequences of known AOB species.

ACKNOWLEDGEMENTS

This work was conducted at the Idaho National Laboratory in Idaho Falls, Idaho, USA. I would especially like to thank the Department of Energy and the SULI program for allowing me the opportunity to complete this work and gain valuable research experience. Special thanks go to Dr. David Reed for his instruction and assistance during every step of my project. Also, I would like to acknowledge Dr. Yoshiko Fujita, my mentor, who offered valuable advice throughout the project and Lynn Petzke for her technical assistance and Tina Tyler for DNA samples.

REFERENCES

[1] T. C. Hollocher, M. E. Tate, and D. J. D. Nicholas, "Oxidation of ammonia by *Nitrosomonas europea*: definitive 18O-tracer evidence that hydroxylamine formation involves a monooxygenase," in *The Journal of Biological Chemistry*, Vol. 256, No. 21, pp. 10834-10836, Nov. 1981.

[2] C. D. Sinigalliano, D. N. Kuhn, and R. D. Jones, "Amplification of the amoA Gene from Diverse Species of Ammonium-Oxidizing Bacteria and from an Indigenous Bacterial Population from Seawater," in *Applied Environmental Microbiology*, Vol. 61, No. 7, pp. 2702-2706, July 1995.

[3] C. A. Francis, K. J. Roberts, J. M. Bemen, A. E. Santoro, and B. B. Oakley, "Ubiquity and Diversity of Ammonia-oxidizing Archaea in Water Columns and Sediments of the Ocean," in *PNAS*, Vol. 102, No. 41, pp. 14683-14688.

[4] J. H. Rotthauwe, K. P. Witzel, W. Liesack, "The Ammonia Monooxygenase Structural Gene amoA as a Functional Marker: Molecular Fine-Scale Analysis of Natural Ammonia-Oxidizing Populations," in *Applied Environmental Microbiology*, Vol. 63, No. 12, pp. 4704-4712, Dec. 1997.

[5] G. Harms, A. C. Layton, H. M. Dionisi, I. R Gregory, V. M. Garrett, S. A. Hawkins, K. G. Robinson, and G. S. Sayler, "Real-Time PCR Quantification of Nitrifying Bacteria in a Municipal Wastewater Treatment Plant," in *Environmental Science and Technology*, Vol. 31, No. 2, pp. 343-351, 2003.

[6] A. J. Holmes, A. Costello, M. E. Lidstrom, and J. C. Murrell, "Evidence that particulate methane monooxygenase and ammonia monooxygenase may be evolutionarily related," in *FEMS Microbiology Letters*, Vol. 132, No. 3, pp. 203-208, October 1995.

[7] T. L. Tyler, "Detection and Characterization of Urease Genes in Groundwater Bacterial Communities," Ph.D. thesis, Department of Biology, Idaho State University, Pocatello, Idaho, 2004.

[8] Y. Okano, Y. R. Hristova, C. M. Leutenegger, L. E. Jackson, R. F. Denison, B. Gebreyesus, D. Lebauer, and K. M. Scow, "Application of Real-Time PCR To Study Effects of Ammonium on Population Size of Ammonia-Oxidizing Bacteria in Soil," in *Applied Environmental Microbiology*, Vol. 70, No 2, pp. 1008-1016, Feb. 2004.

[9] D. W. Reed, S. Freeman, L. M. Petzke, and Y. Fujita, "Quantification of Ammonia Oxidizing Bacteria in Groundwater Treated With Urea to Promote Calcite Precipitation," poster presented at the *2005 International Symposia for Subsurface Microbiology and Environmental Biogeochemistry*, August 14th-19th, 2005, Jackson Hole, Wyoming, USA.

[10] "BLAST Database (Basic Local Alignment Search Tool)", Online document, Version BLAST 2.2.11 released, National Center for Biotechnology Information, National Library of Medicine, and National Institutes of Health. http://www.ncbi.nlm.nih.gov/BLAST/

[11] F. von Wintzingerode, U. B. Gobel, and E. Stackebrandt, "Determination of microbal diversity in environmental samples: Pitfalls of PCR-based rRNA analysis", in *FEMS Microbiology Reviews*, Vol. 21, pp. 213-229, November 1997.

ABSTRACTS

TABLE OF CONTENTS

Biology

A Pseudo-Broad Beam Approach to Low-LET Radiation Biology Studies Using an Electron Microbeam. *BENJAMIN ARTHURS (Washington State University, Pullman, WA 99163) MARIANNE SOWA (Pacific Northwest National Laboratory, Richland, WA 99352).* Microbeam technology has been widely successful in studies of low-dose radiation biology. Using an electron microbeam to mimic low-linear energy transfer (LET) radiation it is possible to study the biological effects of γ-rays and x-rays, which contribute to background radiation exposure and carcinogenesis. By taking advantage of the scattering properties of electrons in air, one can use the microbeam in a pseudo-broad beam mode. This procedure lends itself well to low-dose explorations of genomic instability and bystander effects in mammalian cells. We have used 50 keV electrons and a 5 mm air gap to show the effectiveness of the electron microbeam in a pseudo-broad beam configuration. Using GafChromic® film we have developed a method of dosimetry allowing for accurate low-dose irradiations. Also, we have designed aluminum plates acting as shielding for measuring non-targeted bystander effects resulting from low-LET radiation exposure. The effectiveness of pseudo-broad beam irradiations in producing biological damage was determined by formation of DNA double strand breaks measured using a γ-H2AX foci assay. After irradiating mammalian RKO cells, we have observed an increased number of these foci above the background levels seen in unirradiated controls. These results support the use of the electron microbeam in pseudo-broad beam mode to study low dose low-LET radiation effects and their implications to cancer formation in mammalian cells.

Mammary Epithelial Cell Survival Following Exposure to Ionizing Radiation and the Radiomimetic Bleomycin. *EMILY ASHJIAN (University of Washington, Seattle, WA 98105) LEE OPRESKO (Pacific Northwest National Laboratory, Richland, WA 99352).* Bleomycin is an effective radiomimetic drug which, when administered to cells, induces DNA double strand breaks (DSBs) similar to those caused by ionizing radiation. These DSBs can be measured using the γ-H2AX assay, as each γ-H2AX focus represents a DSB. In order to use bleomycin in place of ionizing radiation in studies where the delivery of ionizing radiation by x-ray or charged particle microbeam is not feasible, a survival curve for bleomycin is needed. Using the MCF 10A and 184 A1 lines of human mammary epithelial cells, survival curves for doses of radiation, ranging from 0.5 Gy to 9 Gy, and bleomycin, ranging from 0.1 µg/ml to 2.5 µg/ml were created for each cell line. When the survival curves of MCF 10A and 184 A1 cells were compared, the MCF 10A cells tended to be more resistant to all doses of radiation and bleomycin than the 184 A1 cells. Both cell lines demonstrated only slight differences between the trends of the bleomycin survival curve and the radiation survival curve. Use of the γ-H2AX assay confirmed the occurrence of DNA DSBs in the survival curve experiments, as the number of γ-H2AX foci per cell increased with increasing doses of bleomycin and radiation. This corresponds to the decreasing surviving fraction of both MCF 10A and 184 A1 cells as the doses of bleomycin and radiation were increased. Results from this study will be used to administer doses of bleomycin to MCF 10A and 184 A1 three dimensional cell structures in accordance with a much larger project researching mechanism(s) of three dimensional intercellular signaling in mammary epithelial cells in response to low dose, low-LET radiation.

Discovering Peptide Ligands for Intersectin - SH3 A1 using Phage Display and comparison with src SH3. *TEISHA BARNES (Grambling State University, Grambling, LA 71245) BRIAN KAY (Argonne National Laboratory, Argonne, IL 60439).* Phage display is a tool that has many applications. It can be used for the study of molecular interactions and especially in the generation of monoclonal antibodies. (1) The main goal of phage display is to determine the properties of the target protein through its interaction with the peptides displayed on the surface of M13 phage. Some typical targets for isolation of phage displayed peptide ligands include antibodies, certain receptors and other full size proteins. Our group chose to use phage-display as a tool to isolate the peptide ligands to our target protein: ITSN SH3 A1 (Intersectin Src Homology 3). This protein has not been very much studied making this research fairly new. In order to begin the process, the protein first had to be purified. Several attempts to purify SH3 A1 did not yield a soluble protein, thereby creating a problem. After the purification process is completed Affinity Selection Experiments are performed to prepare for an ELISA. After all of this is done we performed an ELISA (Enzyme Linked Immuno-Sorbent Assay). In this procedure the target protein is immobilized in a 96 well plate where it is incubated with the peptides displayed on the phage (in this case the binders resulting from selections against libraries ANL 6 & 7). The phage is detected by anti-M13 antibody with its HRP conjugate. The ELISA shows if the phage is bound to its target protein, another protein, or the plastic of the wells. A signal is determined with ABTS + H_2O_2 which produce a colorimetric change upon reacting with HRP. Screening the libraries yields information about protein-peptide interactions. The major task in phage display is to determine the properties of the protein and to give the identity of the clones that were selected from the process. One identifying process used in the lab is PCR (Polymerase Chain Reaction). The PCR amplifies the DNA of the phage displaying the selected peptides. Once the amplification of the DNA has occurred, sequencing is then done to see how the peptides compare to each other, if they are similar and if so how many residues are similar. Then the common trend of the peptides is studied as to figure out the interacting partners of the target protein.

Sequence-Based Identification of Extremophilic Filamentous Fungi. *LAMEKA BERRY (Jackson State University, Jackson, MS 39217) TAMAS TOROK (Lawrence Berkeley National Laboratory, Berkeley, CA 94720).* Fungi have been found to survive and grow at environmental extremes of low pH, high temperatures, and high radiation. These extremophilic fungi have become of great interest to scientists because of their ability to survive such great extremes. To understand fungi and their ecological role, they first have to be identified taxonomically. Currently, research is being conducted at Berkeley Lab to identify fungi based on biomarker gene sequencing. Fungal isolates from the exploded Unit-4 and the 10-km “exclusion zone” surrounding the failed nuclear power plant in Chernobyl, Ukraine, are being characterized using this method. The strains were grown up and genomic DNA was extracted from these pure cultures. Polymerase chain reaction (PCR) was used to amplify the D1/D2 domains of the 28S rRNA- coding gene, and agarose gel electrophoresis was applied to analyze the amplicons. DNA sequencing was done at the University of California at Berkeley DNA Sequencing Facility. Raw sequences were edited online using FinchTV Version 1.3.1. The edited sequences were blasted against the National Center for Biotechnology Information (NCBI) database for preliminary identification. Of the 48 fungal strains, the identification of 75% of the strains is pending due to a lack of available DNA sequence data for filamentous fungi in the database. For the remaining 25%, about one-third matched with their classical identification. Our final results show the limitation of available public databases for fungal identification. Many of the strains that were included in this study do not have submitted sequences in databases. In the future, as more species of fungi are entered into online databases, the efficiency of fungal identification will improve. In addition, a wider selection of fungal species may prove in the future that the biomarker D1/D2 domains alone are not sufficient for identification. If additional biomarker genes were used, the identification of these fungi would become less of a problem.

Sequence-Based Identification of Extremophilic Filamentous Fungi. *SHAMEKA BERRY (Jackson State University, Jackson, MS 39217) TAMAS TOROK (Lawrence Berkeley National Laboratory, Berkeley, CA 94720).* Fungi have been found to survive and grow at environmental extremes of low pH, high temperatures, and high radiation. These extremophilic fungi have become of great interest to scientists because of their ability to survive such great extremes. To understand fungi and their ecological role, they first have to be identified taxonomically. Currently, research is being conducted at Berkeley Lab to identify fungi based on biomarker gene sequencing. Fungal isolates from the exploded Unit-4 and the 10-km “exclusion zone” surrounding the failed nuclear power plant in Chernobyl, Ukraine, are being characterized using this method. The strains were grown up and genomic DNA was extracted from these pure cultures. Polymerase chain reaction (PCR) was used to amplify the D1/D2 domains of the 28S rRNA- coding gene, and agarose gel electrophoresis was applied to analyze the amplicons. DNA sequencing was done at the University of California at Berkeley DNA Sequencing Facility. Raw sequences were edited online using FinchTV Version 1.3.1. The edited sequences were blasted against the National Center for Biotechnology Information (NCBI) database for preliminary identification. Of the 48 fungal strains, the identification of 75% of the strains is pending due to a lack of available DNA sequence data for filamentous fungi in the database. For the remaining 25%, about one-third matched with their classical identification. Our final results show the limitation of available public databases for fungal identification. Many of the strains that were included in this study do not have submitted sequences in databases. In the future, as more species of fungi are entered into online databases, the efficiency of fungal identification will improve. In addition, a wider selection of fungal species may prove in the future that

the biomarker D1/D2 domains alone are not sufficient for identification. If additional biomarker genes were used, the identification of these fungi would become less of a problem.

Protein to Gene Annotation of Human Proteomics Data using Public Bioinformatics Tools and Databases. *JESSICA BIAN (Yale University, New Haven, CT 06520) KATRINA WATERS (Pacific Northwest National Laboratory, Richland, WA 99352).* Mass spectroscopy-based proteomics explores cell response pathways through the epithelial growth factor receptor, which is constitutively active in malignant breast cancer cells. To correlate protein abundance with gene expression data, the specific gene that produces each protein must be identified and annotated. Incompatibility and redundancy among bioinformatics databases makes this a complex task. A workflow incorporating several bioinformatics tools and databases was developed to annotate proteins initially identified by International Protein Index (IPI) numbers with their corresponding gene symbols. On a dataset of 7694 IPI identified proteins, 7334 (95%) were successfully annotated with gene symbols using this workflow. Invalid IPI numbers (201) accounted for the majority (56%) of unsuccessful cases. Other factors that prevented successful annotation were hypothetical or predicted proteins of unknown function and IPI identified peptide fragments without assigned gene identifiers. Manual annotation methods, like the ones employed in this project, are currently the most common means by which scientists interpret experimental data. However, this is a time-consuming and inefficient process that has become too costly to continue practicing, especially with the advent of high-throughput technologies, which generate datasets of thousands of genes and proteins. Future research demands call for the development of a computer program with the ability to annotate proteins with gene identifiers using a workflow that mimics the accuracy of manual annotation methods.

Domain Analysis of the DNA Repair Proteins TFB5, XPD, and CSB. *JESSICA BLANTON (Amherst College, Amherst, MA 01002) JILL FUSS (Lawrence Berkeley National Laboratory, Berkeley, CA 94720).* Damage to an organism's DNA can cause severe defects in gene function, and to counter such damage, all organisms have developed mechanisms of DNA repair. The nucleotide excision repair pathway (NER) is responsible for the removal of helix-distorting lesions in the DNA, both for global genome repair (GG-NER) that maintains the genome and transcription coupled repair (TCR-NER) that preferentially removes damage that blocks transcription. In humans, mutations in either the GG-NER or the TC-NER pathway lead to three severe but rare autosomal recessive disorders: Xeroderma pigmentosum (XP), Cockayne's syndrome (CS) and Trichothiodystrophy (TTD). Three proteins implicated in these diseases are investigated in this study: the recently identified protein TFB5, associated with TTD; the DNA helicase XPD, associated with XP, CS and TTD; and CSB, from the SWI/SNF family of DNA-dependent ATPases, which is associated with CS. Standard molecular and biochemical techniques were used to express in *E. coli* and purify these proteins for biochemical analysis. TFB5, at 8kDa, has proven to be relatively simple to clone and express. Expression of the larger XPD (86 kDa) has been moderately successful, with three of four truncations proving to have straightforward amplification and cloning, and two of those three yielding soluble protein expression in *E. coli* cells. The truncations of the 170kDa CSB protein thus far appear to express as soluble protein, but further testing must be done to verify presence of the full-length segments. Continued progress and large-scale expression of these proteins will hopefully provide material for structural and functional studies, in turn enlightening further the mechanisms of NER and human DNA repair associated disorders.

Reconstructing Genetic Regulatory Networks Using Pearson Correlation, Mutual Information and Bayesian Network Inference Algorithms. *MERIDITH BLEVINS (Case Western Reserve University, Cleveland, OH 44106) RONALD C. TAYLOR (Pacific Northwest National Laboratory, Richland, WA 99352).* Network inference algorithms exist to understand network structure by searching for correlations across huge datasets. By applying inference algorithms to high-throughput data of RNA and protein expression levels, it is possible to establish transcriptional regulatory network structure. Such a structure or 'wiring diagram' can serve as a foundation for dynamic modeling to understand the behavior of the network over time and under different environmental conditions. This understanding will someday allow scientists to control microorganisms and lead to directed intelligent genetic engineering-an important directive to the Department of Energy's Genome to Life effort. This work will establish a baseline for future development of inference algorithms in the field of Bayesian networks and graphical models in general. Genetic regulatory network data was simulated based on a Boolean gene state model. Three techniques that use correlation in gene states were applied and compared-Pearson correlation, mutual information, and Bayesian Markov Chain Monte Carlo (MCMC) structure learning. The output of each algorithm was examined based on three common metrics-Recall, Precision and F-Measure. Results were collected for varying parameters with the goal of determining the best score cut-off to use for each method in identifying the regulatory edges. A fourth technique modified the dataset for Bayesian MCMC network inference by introducing some simulated lab experiments where genes were silenced or over-expressed. It is our conclusion that Bayesian MCMC network inference is superior to Pearson correlation and mutual information methods. The algorithm's performance improved further with the simulated blocking of genes. The future directive is to further investigate MCMC and other Bayesian network structure learning algorithms and their parameters using additional simulated topologies.

Live Cell FT-IR Spectroscopy of Macrophage Response to Endotoxin. *ERIN BLOMQUIST (University of Arizona, Tucson, AZ 85721) THOMAS WEBER (Pacific Northwest National Laboratory, Richland, WA 99352).* Fourier transform infrared spectroscopy coupled with attenuated total reflectance (FT-IR/ATR) has sufficient sensitivity to identify and measure chemical alterations of a cellular system following exposure to environmental agents. In this study, FT-IR/ATR measurements of the ensuing apoptotic response to lipopolysaccharide (LPS) were investigated using murine macrophage cells (RAW 264.7) maintained on a zinc selenide (ZnSe) ATR crystal. To decrease the time required for cell attachment to the ZnSe crystal, the adhesion molecule fibronectin was used as a coating on the ZnSe crystal. This shortened the attachment time to 1 day, whereas it had previously been as long as 6 days. The conundrum surrounding fibronectin use was the fear the fibronectin would cause the cells to sit higher than 1 μm which might place them above the sensing zone of the evanescent field and hence would provide no spectroscopic signal. Results using fibronectin mirrored the results obtained from the earlier studies not employing fibronectin, thus indicating that the fibronectin coating is thin and does not cause the cells to sit more than 1 μm above the ZnSe crystal. FT-IR/ATR spectroscopy was then used to examine the spectroscopic signatures of the murine macrophages before LPS treatment and 2, 4, 6, 8, and 24 hours following LPS treatment. LPS treatment induces the activation of the macrophages to produce iNOS and COX-2, which through inflammatory pathways leads to apoptosis of the macrophage. In particular, spectral changes were apparent at 1,575 cm^{-1}, 2,925 cm^{-1}, and 1034 cm^{-1}, indicative of alterations in cellular components Amide II proteins, lipids, and sugars, respectively. Visualization of the cell death response of the murine cells to LPS treatment also was supported through immunofluorescence microscopy imaging. Our results indicate that FT-IR/ATR spectroscopy can be used to investigate live cell responses to environmental toxins.

Biopanning of the Single Chain Fragment Variable T7 Phage Display Library for Immunoprecipitation of Target Proteins. *PAVEL BOGOMIAKOV (Johns Hopkins, Baltimore, MD 21218) JOHN DUNN (Brookhaven National Laboratory, Upton, NY 11973).* Antibody-antigen binding interactions can be exploited to selectively bind to specific proteins or other molecules of interest. One potentially rapid and efficient method for screening for reactive antibodies is antibody phage display, which relies on affinity selection of antibodies displayed on the surface of bacteriophage. We are developing a chicken Single chain Fragment variable (ScFv) T7 phage display system as a powerful method for immunoprecipitation of target proteins. ScFv antibodies are attractive for phage display because of their small fragment size, easy expression, and high clonal diversity. DNA sequencing verified that a previously constructed chicken ScFv T7 phage library exhibits considerable antibody diversity. To further develop protocols for using this phage display system, we are screening this library for antibodies specific for the *E. coli* cAMP receptor protein (CRP), which we crosslinked to a solid support for affinity biopanning. Four rounds of selection for CRP-specific antibodies have been completed and confirmed by immunoblotting of plaque lifts. Once specific phage clones are isolated, the single chained antibodies they encode will be expressed and used in chromatin immunoprecipitation (ChIP) experiments to examine CRP-DNA interactions that mediate gene expression changes. Long term implications of this research include the rapid production of antibodies to target molecules for disease research, pathogen detection, and protein structure studies.

Isolation and Characterization of a Novel Enzyme from a Thermoacidophilic Organism. *MORGAN BRUNO (University of Idaho, Moscow, ID 83844) VICKI THOMPSON (Idaho National Laboratory, Idaho Falls, ID 83415).* Extremophilic organisms live and

thrive at extremes of temperature, pH, salt and pressure. The enzymes produced by these organisms share their extreme nature and operate under conditions that normal enzymes can not. These enzymes are valuable industrially where conditions are often very extreme. In this study, an enzyme from a thermoacidophilic organism was produced, purified and characterized. The organism was grown in liquid media pH 3.5 and 60°C. After growing up to 1L, the cultures were harvested. Centrifugation at eight thousand rpm yielded supernatant that was adjusted to pH 3.0 and vacuum filtered with a 0.22µL filter. Cation exchange HPLC was performed on the supernatant to purify the enzyme. The column solution was desalted, concentrated 3X, and assayed for protein content and activity. Based upon the results of the fraction activity assay, select fractions were run in an SDS-PAGE gel and Silver stained for visualization. The fractions showing the isolated enzyme were pooled together. The enzyme was concentrated 10X via ultrafiltration. Activity assays were performed on the purified enzyme over a temperature range of 20–90°C with 10-degree increments to determine the optimum temperature of the enzyme. Activity assays were also performed on the purified solution over a pH range of 2.0–8.0 with 1.0-pH unit increments to determine the optimum pH of the enzyme. These activity assays showed that this novel enzyme follows the expected activity trends for a thermoacidophilic enzyme.

Probing the Proteomic Overlap Between Angiogenesis and Neurogenesis. *MARGARET BUELL (Brown University, Providence, RI 02912) DIANE J. RODI (Argonne National Laboratory, Argonne, IL 60439)*. During the past few years it has become increasingly apparent that many of the molecules first characterized in developing neurons that guide their growth and migration (here called neurogenesis) are also involved in angiogenesis, the process of blood vessel formation from pre-existing capillary networks. A growing number of studies are now beginning to explore the parallels between nervous and vascular system development; however, the majority of these studies approach the topic one protein at a time. Using in vitro models of both angiogenesis and neurogenesis our group is instead conducting an exploration of about 50 proteins implicated in both processes (only 6 could be presented here). Immunofluorescence was used to test for the presence and subcellular localizations of these proteins in human microvascular endothelial cells (HMVECs) and SH-SY5Y neuroblastoma cells cultured on Matrigel™, in which they undergo tubulogenesis and neurogenesis. The majority of the proteins investigated in this study were found during both HMVEC tubulogenesis at 7-hours post-plating and SH-SY5Y neurogenesis 6 days post-plating, but certain patterns in the data indicate that more temporal investigations of these and other proteins are needed to fully determine the nature of their participation in angiogenesis and neurogenesis. Ultimately, this study and others like it promise to advance our knowledge regarding normal and pathological angiogenesis, including tumor angiogenesis, and nerve regeneration following damage to the peripheral and central nervous systems.

Expression, Purification and X-ray Crystallographic Analysis of Hypothetical Protein PG0823 from *Porphyromonas gingivalis*, APC 80877. *JOHN BUELT (Xavier University, Cincinnati, OH 45207) ANDRZEJ JOACHIMIAK (Argonne National Laboratory, Argonne, IL 60439)*. Hypothetical protein PG0823 is a protein derived from source organism Porphyromonas gingivalis, a bacterium which produces enzymes that contribute to the destruction of gum tissue and bone that supports the teeth. Hypothetical protein PG0823 has been labeled as hypothetical due to the fact that its function in the source organism is unknown. Hypothetical protein PG0823 was cloned and expressed in *Escherichia coli*. The protein was then purified and crystallized using the hanging-drop method of vapor diffusion. The crystal structure has been determined at a resolution of 2.2 Å using a synchrotron-radiation source, courtesy of the Advanced Photon Source at Argonne National Laboratory. The protein structure exposes a helix-turn-helix motif which is commonly associated with DNA-binding proteins. Based upon the helix-turn-helix motif and similarity to protein amino acid sequences that serve as transcriptional regulators, it can be hypothesized that hypothetical protein PG0823 may serve as a transcriptional regulator in *P. gingivalis*. The discovered structure and hypothesized function may be used in further research in order to develop a drug intended to inhibit the transcription of *P. gingivalis*.

Use of the Program DISTANCE to Assess Population Size of the Eastern Hognose Snake (*Heterodon platirhinos*) at the Brookhaven National Laboratory. *CHRIS CAMACHO (Wesleyan University, Middletown, CT 06459) JEREMY FEINBERG (Brookhaven National Laboratory, Upton, NY 11973)*. The eastern hognose snake (Heterodon platirhinos) is a species of particular interest on Long Island and throughout the northeast, where habitat loss and declines in reported sighting have become a cause for concern. The program DISTANCE, a Windows based software package that aids in the design and analysis of wildlife population surveys, was used in an attempt to determine the population size of *H. platirhinos* at Brookhaven National Laboratory (BNL). Line transects were generated with the DISTANCE software and walked from early May to early July. Only one hognose snake was found in approximately 114 hours of walking transects, whereas six hognose snakes were found in 29 hours when conducting random pedestrian surveys in preferred *H. platirhinos* habitat. Thus, it is likely that DISTANCE is inefficient for generating a population estimate of hognose snakes at BNL and may not be appropriate for surveying other cryptic animals overall.

Purification and Crystallization of Conserved Hypothetical Protein APC 82795 Using X-Ray Diffraction Protein Crystallography. *DIAN CANADAY (University of Illinois at Urbana-Champaign, Urbana-Champaign, IL 61801) ANDRZEJ JOACHIMIAK (Argonne National Laboratory, Argonne, IL 60439)*. Protein crystallization is used to determine the structure, and in turn, the function, of certain proteins in specific targets. We use many systems of purification and optimization to grow these crystals and once the diffraction is above a minimum level of three angstroms, crystallographers study the crystals and determine the structure. The machines implemented in this process included AKTA Express, Hydra, Mosquito, Cartesian, and RoboDesign. I worked under Andrzej Joachimiak and Lour-Evelyn Lezondra on the protein APC 82795. This protein resulted in many crystals but none diffracted more than three angstroms. The structure of this protein, consequently, has not been solved. With more variable processes, including different temperature and screens, this protein may be solved in the near future.

Design and Development of a PDA Interface for Cloning and Purification Database Systems. *RICO CARRELL (Governors State University, University Park IL 60466) SOON-OK PARK (Argonne National Laboratory, Argonne, IL 60439)*. The objective of the research being conducted in the Midwest Center for Structural Genomics (MCSG) and Bioscience division is to develop, and optimize new, rapid integrated methods for highly cost-effective determination of protein structures through x-ray crystallography. Our near term goal is to improve a user application, which the biologist use, for the advancement of research data storage and mobility. In working towards are goal of advancing mobility. We are faced with the task of modifying the cloning application so that it will be feasibly useable on all PDA's. We want to provide some of the desktop functionality of the application on PDA's. While developing the application there were precautions we took. We developed the application to be user friendly and made sure we had data validation, to reduce errors on data entry that is stored in the database. There are several advantages to this application: Increases the quality and efficiency on the data collection and analysis; minimizes data entry errors; data is collected electronically from various sources; scans the data directly into the database by using a PDA scanner; increases accessibility and mobility.

Characterization of a TK6-Bcl-x_L gly-159-ala Human Lymphoblast Clone. *LAWRENCE CHYALL (San Francisco City College, San Francisco, CA 94720) AMY KRONENBERG (Lawrence Berkeley National Laboratory, Berkeley, CA 94720)*. TK6 cells are a well-characterized human B-lympoblast cell line derived from WIL-2 cells. A derivative of the TK6 cell line that was stably transfected to express a mutated form of the anti-apoptotic protein Bcl-x_L (TK6-Bcl-x_L gly-159-ala clone #38) is compared with the parent cell line. Four parameters were evaluated for each cell line: growth under normal conditions, plating efficiency, and frequency of spontaneous mutation to 6-thioguanine resistance (hypoxanthine phosphoribosyltransferase locus) or trifluorothymidine resistance (thymidine kinase locus). We conclude that the mutated Bcl-x_L protein did not affect growth under normal conditions, plating efficiency or spontaneous mutation frequencies at the thymidine kinase (TK) locus. Results at the hypoxanthine phosphoribosyltransferase (*HPRT*) locus were inconclusive. A mutant fraction for TK6-Bcl-x_L gly-159-ala clone #38 cells exposed to 150cGy of 160kVp x-rays was also calculated. Exposure to x-irradiation increases the mutant fraction of for TK6-Bcl-x_L gly-159-ala clone #38 cells.

Breeding Population Status and Nest Site Characteristics of Hawks. *KELLY CLAYTON (Washington State University, Pullman, WA 99163) JANELLE DOWNS (Pacific Northwest National Laboratory, Richland, WA 99352)*. Field surveys of potential nesting sites for 3 Buteo hawks and common raven were conducted on the U.S. Department of Energy (DOE) 560-mi2 Hanford Site in spring and summer 2005 to document nesting pairs on central Hanford and describe nest site characteristics. Nest sites were mapped and characteristics of nest sites (i.e., species identification, active/inactive),

type of nesting structure, tree species, nest height, and aspect of nest (8 cardinal directions) were recorded. Surveys documented 4 Ferruginous hawk, 10 Swainson's hawk, 14 Red-tailed hawk, and 45 common raven nests that were active in central Hanford. Current survey data were also compared to survey information compiled for 1990 through 2005 to examine trends in the number of nesting birds. Nesting pairs of common ravens on the Hanford Site appear to have significantly increased over the past decade, although survey information for this species has not been consistently collected. Ferruginous hawks (a state threatened species), Swainson's hawks (a state monitor species) and red-tailed hawks appear to have experienced a slight overall decrease in the numbers of nesting pairs between the years 1990 and 2005. Ravens and red-tailed hawks, which nest primarily on electric transmission towers, preferred nesting sites at higher elevation, and Ferruginous hawks nest at lower elevations on the towers. Swainson's hawk nests were found only in trees at lower elevations.

Biopanning of the Single Chain Fragment Variable T7 Phage Display Library for Immunoprecipitation of Target Proteins. *DIANA CONNOLLY (Hofstra University, Hempstead, NY 11549) JOHN DUNN (Brookhaven National Laboratory, Upton, NY 11973).* Antibody-antigen binding interactions can be exploited to selectively bind to specific proteins or other molecules of interest. One potentially rapid and efficient method for screening for reactive antibodies is antibody phage display, which relies on affinity selection of antibodies displayed on the surface of bacteriophage. We are developing a chicken Single chain Fragment variable (ScFv) T7 phage display system as a powerful method for immunoprecipitation of target proteins. ScFv antibodies are attractive for phage display because of their small fragment size, easy expression, and high clonal diversity. DNA sequencing verified that a previously constructed chicken ScFv T7 phage library exhibits considerable antibody diversity. To further develop protocols for using this phage display system, we are screening this library for antibodies specific for the *E. coli* cAMP receptor protein (CRP), which we crosslinked to a solid support for affinity biopanning. Four rounds of selection for CRP-specific antibodies have been completed and confirmed by immunoblotting of plaque lifts. Once specific phage clones are isolated, the single chained antibodies they encode will be expressed and used in chromatin immunoprecipitation (ChIP) experiments to examine CRP-DNA interactions that mediate gene expression changes. Long term implications of this research include the rapid production of antibodies to target molecules for disease research, pathogen detection, and protein structure studies.

Reverse Transcription (RT) PCR Analysis of Transcript Levels in Mutants Attenuated in Hydrogen Photoproduction. *ZUZANNA CZERNIK (Scripps College, Claremont, CA 91711) MATT WECKER (National Renewable Energy Laboratory, Golden, CO 89401).* The green alga, *Chlamydomonas reinhardtii* is capable of sustained H_2 photoproduction under anaerobic conditions. Algae could be an excellent renewable, cheap and clean source of hydrogen, if the levels of production could be increased. One hope for increasing hydrogen levels is the creation of algae mutants which are more efficient producers of the gas. In order to do this the genetic pathway has to be properly understood. NREL has many mutants ready for study to. However, the current method for studying these mutants is long. In order to streamline the process a new protocol using RT-PCR was developed. RT-PCR allows for the presence of RNA to be detected, and the amount present to be quantified. Various parameters involved in the procedure were tested, adjusted and changed to create a working protocol. Once the protocol was working a dark adaptation experiment was repeated for mutant strain 103-9 and wild-type 425. RNA was isolated, and PCR on control genes and genes involved in the hydrogen pathway was performed. The results confirm the previous results obtained: mRNA for HydEF, which assembles a working hydrogenase enzyme, is not present in the mutant. Since the new method also allows quantification a new discovery was made. The relative abundance of HydA, which codes for the hydrogenase enzyme, is higher in the mutant than in the wild-type. Since the mutant is unable to produce hydrogen, perhaps it reacts by up-regulating hydrogenase production under conditions that would normally force it to create hydrogen. These results will need to be verified still. The protocol can now be used to study other mutants as well.

Anaerobic Co-Cultures of Purple Non-Sulfur Photosynthetic Bacterium *Rhodopseudomonas palustris* and Metal-Reducing Bacterium *Shewanella oneidensis*. *WILLIAM DABBS (University of Tennessee, Knoxville, TN 37996) ABHIJEET P. BOROLE (Oak Ridge National Laboratory, Oak Ridge, TN 37831).* *Rhodopseudomonas palustris* is a metabolically versatile organism whose genome was recently sequenced. *R. palustris* is capable of fixing nitrogen, sequestering carbon dioxide (greenhouse gas reduction) and producing hydrogen gas (alternate energy solution). It is also capable of growing under different metabolic states, namely photoheterotrophic, photoautotrophic, chemoheterotrophic and chemoautotrophic. Under these different metabolic states, the organism produces different proteins to carry out various functions. These proteins act as markers for identifying the metabolic state of the bacterium using Proteomics. Therefore, by knowing the metabolic status of *R. palustris*, in theory, one could infer the status of an entire community. Due to *R. palustris*' versatility and familiarity, it has been selected by a group at ORNL to be used as a sentinel organism in a study of microbial communities. The goal of this specific study is to examine the possibility of designing a minimal medium to grow an anaerobic co-culture of *R. palustris* and *Shewanella oneidensis. S. oneidensis* is of interest to DOE due to its metal reducing ability which could aid in the cleanup of heavy metals. One major concern, while designing this medium, is ensuring each organism has an optimal carbon source for growth. On its own, *R. palustris* has had positive results by using both succinate and acetate as a carbon source. In studies with lactate as a carbon source and fumarate as an electron acceptor, *S. oneidensis* has grown well reducing fumarate to succinate and partially oxidizing lactate to acetate. Therefore, there is a possibility that *R. palustris* can utilize the succinate or acetate produced by *S. oneidensis* for its own benefit. This may mean that *S. oneidensis* could supply the carbon source for *R. palustris* for this experiment without one being provided in the medium. *R. palustris* and *S. oneidensis* have been grown in separate anaerobic cultures in a variety of different media. The results thus far, for *R. palustris*, have been concordant with the predicted results, and it has grown optimally in the medium with succinate. Testing the growth of *R. palustris* and *S. oneidensis* will be the final step in creating the anaerobic medium which will support the co-culture of *R. palustris* and *S. oneidensis*.

Water Absorption Levels of Willows (*Salix alba var. tristis*), Walnuts (*Juglans nigra*) and Oaks (*Quercus alba*), in a Closed System. *ELIZABETH DAVIS (Kennedy King College, Chicago, IL 60621) ARLICIA CORLEY (Argonne National Laboratory, Argonne, IL 60439).* Phytoremediation is the cost effective use of green plants to sequester or detoxify pollutants from groundwater or damaged land. Because of the enormous cost associated with the removal of water and soil pollutants in the environment, the use of green plants is useful as it can decrease cost. A controlled study is warranted to determine how they perform. Phreatophytic and non-phreatophytic plants were then used in controlled tree well cartridges. These tree well cartridges were designed by Argonne National Laboratory (ANL) and Applied Natural Science (ANS) who owns patented technologies (Tree Mediation® and Tree Well® systems). Trees pre-installed in these controlled cartridges are 3-Willows (*Salix alba var. tristis*), 3-Oaks (*Quercus alba*), 3-Walnuts (*Juglans nigra*) and 3-cartridges with no-trees are used as controls. Trees and no-tree cartridges were installed in order to evaluate root density, water absorption levels, and soil carbon balances. Water absorption was monitored during the mornings and afternoon with a Solinst Water Level Indicator, which was inserted into a piezometer tube that was installed in the cartridges and the result are measured in centimeters. Five to 15 gallons of water was added after the initial reading to the cartridges periodically as their measurement dropped below 240 cm. The height and diameter was taken on all of the trees to follow up on the data from last summer. The weather was monitored and correlated with the fluctuation of water intake of the cartridges containing the Willows (*Salix alba var. tristis*), Oaks (*Quercus alba*), Walnuts (*Juglans nigra*) and cartridges with No-Trees installed. Major components of Phytoremediation studies at Argonne National Laboratory, currently being conducted, is to determine which species of trees are better suited to remediate contaminated, semi-arid and marginal soil depending on the depth and severity of the pollutant or conditions; as well as, determining various avenues unto which various soil depths can be exploited in order to increase carbon sequestration.

Development of Corrugated Patterning of CVD Diamond Foils. *VASHTI DAVIS (Grinnell College, Grinnell, IA 50112) ROBERT SHAW (Oak Ridge National Laboratory, Oak Ridge, TN 37831).* Stripper foils are used in the technology of linear accelerators to change a negative ion beam to an ion beam that is positively charged. Most commonly, carbon stripper foils are employed. However the Spallation Neutron Source (SNS) at Oak Ridge National Laboratory requires a foil that can withstand a 1GeV beam at 10's of mA, which is beyond the capability of carbon foils. Research investigating the use of diamond stripper foils found that the material could meet the 1GeV requirement. In order to use diamond foils in the SNS the diamond stripper foil is suspended into the beam by only a one edge handle and must be 12mm x 20 mm.

Unfortunately, the stress created by the film growth process causes the diamond foil to curl. Research was conducted to find a method to keep the foil lying flat. A silicon etching process was used to create corrugations in the diamond foils, making the film lie flat. Variations of several patterns in the corrugations were investigated to determine the best design for keeping the foil lying flat and also maintaining the integrity of the diamond film. Patterns resembling a horseshoe shape with various radii of curvature and frequency of corrugations were investigated. When comparing patterns, preliminary results indicated that 100 corrugations per inch produce the best results. Furthermore, the pattern that maintained the desired results on a regular basis was designed with a radius of curvature of 80 mils and only a 40% corrugation coverage of the film. Ideally the corrugations will cover only a small amount of the diamond foil so the results that have been initially observed are well accepted. As part of investigation into the use of diamond stripper foils, research will continue to explore the possibilities of nanocrystalline technology to further the lifetime of stripper foils used at linear accelerators.

Environmental Chemical Exposure and Genetic Polymorphisms of the CYP1B1 Gene in Breast Cancer Susceptibility. *JOHN DEACON (Contra Costa College, San Pablo, CA 94806) REGINE GOTH-GOLDSTEIN (Lawrence Berkeley National Laboratory, Berkeley, CA 94720).* Polycyclic Aromatic Hydrocarbons (PAHs) are common lipophilic organic chemicals metabolized in the body through the Cytochrome P-450 1B1 (CYP1B1) enzyme pathway, where CYP1B1 metabolizes PAHs into electrophilic intermediates that can form adducts with DNA. CYP1B1 is strongly expressed in mammary tissue where PAH-DNA adducts can cause mutation and cancer. Single Nucleotide Polymorphisms (SNPs) are versions of genes differing by one base-pair and can differ from each other in function. Difference in catalytic function between SNPs of CYP1B1 may extend the electrophilic presence, thus effecting cancer susceptibility. An ongoing epidemiologic study in Brazil compares CYP1B1 genotype, CYP1B1 expression levels, and PAH-DNA adduct levels in normal breast tissue of breast cancer patients and controls, and estimates participant PAH exposure by questionnaire. The genotyping of participants for two CYP1B1 SNPs has produced a partial data set and is herein discussed. DNA was isolated from mammary tissues of participants and genotyped for two SNPs by Polymerase Chain Reaction and Restriction F igest SNPs for visualization by electrophoresis. 42 genotyped samples show 38 samples with SNP M1 (90.5%) and 11 samples with SNP M2 (26.2%). The M1 and M2 genotypic and allelic frequencies are consistent with other studies of European populations. These data represent only 1/3 of the study's total participants. Once all data is collected, a case v. control comparison may show correlation between these parameters and breast cancer incidence.

Determining the 3-Dimensional Structure of Proteins From *Mycobacterium tuberculosis*. *DINICIO DELGADO (Fresno State, Fresno, CA 93722) EVAN BURSEY (Lawrence Berkeley National Laboratory, Berkeley, CA 94720).* Determining the 3-Dimensional Structure of proteins from *Mycobacterium tuberculosis* Dr. Hung leads the X-ray Crystallography Center for the *Mycobacterium tuberculosis* Structural Genomics Consortium. The role of the center is to conduct experiments to determine the 3-dimensional structure of various proteins from the bacterium *Mycobacterium tuberculosis*. To identify the 3-dimensional structure of the *Mycobacterium tuberculosis* protein we use a technique called x-ray crystallography. This technique requires a source of x-rays and crystallized protein. The Advance Light Source, here at Lawrence Berkeley National Laboratory, supplies the x-rays. Dr. Hung's collaborators at Lawrence Livermore National Laboratory provide the crystallized proteins. The crystallized protein is irradiated with x-rays. The x-rays bounce off of the electrons in the protein. The experiment consists of collecting the x-rays that scatter off of the crystallized proteins. If we can describe the x-rays going into the protein crystal, and if we can describe the x-rays going out of the crystal, then we can mathematically determine what has to be inside the crystal. In other words, we can determine the position of all the atoms in the crystal. This research is important so that scientists can develop antibiotics for tuberculosis disease. I spent time working on our protein expression system, and also participating in x-ray diffraction data collection when we have time at the Advanced Light Source (approximately twice a month). I gained experience with Polymerase Chain Reaction techniques, protein expression techniques (*in vivo* and *in vitro*), and basic protein analysis methods such as dot blots and western blots. I learned to use the automated liquid-handling robot. I participated in the wet lab to learn to make buffer reagents, use the PCR thermo cycle, performed gel electrophoresis, and took inventory when needed. I became a crucial asset in a team environment, along side Dr. Hung, Dr. Bursey, Dr. Yu and Dr. Radhakannan who provided me with a memorable experience in research.

Teaching Students About Evolution and Genetics: Analyzing DNA Polymorphisms to Test Competing Hypotheses. *AMY DEMARCO (Columbia University, New York, NY 10027-6902) SCOTT BRONSON (Brookhaven National Laboratory, Upton, NY 11973).* People often get caught up in comparing one another based on broad, macro, and external criteria such as skin color or ethnicity. However, this can be extremely misleading, and it overlooks the fact that genetically, we are all very similar. The present experiment was performed to teach thirty high school students to think of themselves on a micro, genomic level. Two regions of the genome were analyzed. First, each student isolated and amplified by PCR a 440 nucleotide sequence from the control region of the mitochondrial DNA of their cheek cells. This region of the mitochondrial DNA is also known as the hypervariable region, because it accumulates point mutations at a very high rate. The students sequenced this region and then compared their sequences to each other and to the sequences of other people of various backgrounds all around the world. Assuming that mutations occur at a constant rate, the number of mutations is proportional to the length of time that two groups have diverged. Thus, by comparing different sequences, it is possible to analyze relative relatedness. It was stressed to the students that so-called race is actually not genetically visible, and that members of the same background may have relatively more sequence differences than members of different backgrounds, which adds further evidence to the Out of Africa, or Displacement Hypothesis. Second, each student amplified a region of chromosome 16 in order to determine the presence or absence of an Alu jumping gene. Alu insertions represent ten percent of the human genome, and since these transposable DNA sequences are inherited in a Mendelian fashion, they can be used to track lineages. The ancestral state of chromosome 16 does not include an Alu insertion. This fact tells us that two people with an Alu insertion at the chromosome 16 locus have inherited this additional DNA from a common ancestor. Together, these two experiments not only provide students with basic knowledge concerning evolution and genetics, as well as laboratory skills such as PCR, DNA isolation, and gel electrophoresis, but they also allow students to realize how genetically similar people are even despite large phenotypic differences.

Effect of Hexavalent Chromium Uptake in *Chironomus dilutus* Mg. (Diptera: Chironomidae) Larvae. *JESSICA DEROUSSE (University of New Hampshire, Durham, NH 03824) AMORET BUNN (Pacific Northwest National Laboratory, Richland, WA 99352)*. Hexavalent chromium (Cr^{+6}) has been listed as a priority pollutant throughout the United States, including the eastern Washington State area of the Colombia River basin. As a result of disposal of cooling water containing Cr^{+6} from the nuclear reactors, low levels of Cr^{+6} have been entering the sediment water interface of the river. In response to the contamination, *Chironomus dilutus (C. dilutus)* larvae were used in a seven day toxicity study to test for phenotypic and genotypic consequences occurring from Cr^{+6} contamination found in the form of $K_2Cr_2O_7$. Using 4 treatments, 8 chambers containing 420 larvae each were exposed to 0 µg /L $K_2Cr_2O_7$ (treatment 1), 5 µg /L $K_2Cr_2O_7$ (treatment 2), 50 µg /L $K_2Cr_2O_7$ (treatment 3), and 500 µg /L $K_2Cr_2O_7$ (treatment 4). Each day pH levels monitored as well as marinating a temperature range of 13–15°C. The larvae were counted, and ashed for dry weight. Substrate samples > 2.0 g were, weighed, and ashed. RNA extraction preformed using standard protocol for microarray analysis. Ashed larvae, substrate, and water samples have not yet been analyzed for Cr^{+6}. Expected outcome should show uptake of higher levels of Cr^{+6} affecting *C. dilutus* negatively both phenotypically and genotypically. Upregulated proteins expressed on microarray slides will show how the organism is responding to the different levels of toxicity. This work directly relates to the environmental cleanup and remediation being done on site as well as the rivers ecosystem and stability.

The Potential of Highly Stable Proteins to Act as Protein Scaffolds on M13 phage. *CLARE DESMOND (University of Notre Dame, Notre Dame, IN 46556) JOHN KEHOE (Argonne National Laboratory, Argonne, IL 60439).* Antibodies are very capable of obtaining affinity reagents but are limited in their scope of use due to factors such as flexibility, size, folding efficiency and stability. Protein scaffolds are emerging as a useful alternative to antibodies. A potential scaffold protein must be exceptionally stable and therefore resistant to mutation. A highly stable protein, Top 7, was tested for its potential as a protein scaffold. The protein was ligated into a SAM vector and transformed into SS320 *E. coli* cells. The cells were plated in top agar that contained 0.04% X-gal and 1mM IPTG in a series of dilutions. No positive plaques showed on the plates containing the ligation

of the SAM vector and Top 7 insert. The negative result was most likely due to Top 7 rendering the phage non-viable. Other methods of protein display on the M13 phage pIII will be attempted in the future to determine if this method affects the viability of the phage. Another protein, PknD, was also tested for its potential as a protein scaffold. Both a periplasmic PknD and cytoplasmic PknD were expressed. After expressing both types at 25°C and 37°C, they were subjected to trypsin for specific amounts of time (5 min, 10 min, 20 min, 40 min, and 2 hours) and at different concentration ratios of protein to enzyme (10:1, 100:1, and 1,000:1). The results of the digest displayed that only the PknD expressed at 25°C was properly folded as evidenced by the presence of a strong band in a polyacrylamide gel. PknD expressed at 37°C was presumably cut into small fragments, as evidenced by no discernible bands on the protein gel. Since phage are not efficiently viable at 25°C , the folding capacity of PknD will be tested at 30°C with the same trypsin experiment.

Comparison of Automated and Manual Methods for DNA Hybridization. *ASHTON EASTERDAY (Santa Clara University, Santa Clara, CA 95053) RICHARD OZANICH (Pacific Northwest National Laboratory, Richland, WA 99352).* There is a great interest in the use of DNA hybridization for the detection of harmful biological pathogens. Optimizing this process is important for sensitive and rapid detection in a variety of samples. A fluidics system utilizing oligonucleotide-coupled microbeads was used to perform automated hybridizations and was compared with standard bench-top hybridization procedures at 15 and 30 minutes. Automated hybridization had greater hybridization efficiency relative to manual bench-top methods. Hybridization efficiencies of four oligonucleotides (invA, lacZ, stx1, uidA1), each complementary to a gene in *Salmonella typhimurium* or *Escherichia coli* O157:H7, were compared. Automated hybridization was 26–37% and 117–121% greater relative to manual hybridizations for stx1 and uidA1, respectively. Hybridization efficiency for invA was 2–11% greater for the manual method. LacZ had poor hybridization efficiencies for both manual and automated approaches. The total hybridization procedure time was considerably reduced when performed by the automated system. This apparatus provides a new tool for rapid and sensitive pathogen detection.

Shrub Cover and Arthropod Diversity in a Landscape Altered by Fire. *JEREMY ENDSLEY (Sacramento City College, Sacramento, CA 95822) ROBIN DURHAM (Pacific Northwest National Laboratory, Richland, WA 99352).* Little is known about the relationships that exist between post-wildfire big sagebrush (*Artemisia tridentata*) plant communities and arthropod diversity and richness on eastern Washington's ecologically sheltered Hanford Site. Following a fire on the Hanford site in 2000, a study was conducted in the summer of 2005 which compared the diversity and richness of arthropods to shrub cover on both burned and unburned sites. This investigation was used to test the hypothesis that a positive relationship would exist between shrub cover and arthropod diversity and richness. No comparisons of understory vegetation were made. Three 200-m x 100-m biological resource management (BRMaP) plots, one unburned and two burned, were studied. Arthropods were sampled using pitfall traps in May 2005 after four trap nights. The arthropod collection was keyed to family, and to species where possible, to determine richness and diversity. Shrub cover was measured in July 2005 along each of the pitfall trap lines. Surveys found greater arthropod family richness on sites with greater shrub cover. Plant bugs (*Lygaeidae*) and most of the spiders were found on the unburned plot while grasshoppers and ants were more abundant on the burned plots. These differences may be the result of diverse niches made available by fire and exploitation of those niches by arthropods of differing life strategies. Suggestions for future research include a systematic and seasonal survey of arthropod abundance and diversity immediately following a fire event and in intervals thereafter to track changes.

Purification of the Phospholipase A2 Domain from the B19 Parvovirus. *MATTHEW ENGEL (State University of New York - Stony Brook, Stony Brook, NY 11790) MARC ALLAIRE (Brookhaven National Laboratory, Upton, NY 11973).* The human parvovirus B19 is a 5.6 kb single-stranded DNA containing virus. Its structure and genetics are similar to other parvoviruses, including the adeno-associated virus (AAV), a promising vector for gene therapy. The genetic material of B19 is contained in the capsid which governs infectivity, receptor binding, immune response, host cell range and tissue tropism. The capsid of B19 is composed of two structural proteins named VP1 and VP2. VP1 contains the 554 amino acids (aa) of VP2 but stretches for an additional 227aa at the N-terminus. This unique overhanging portion of VP1 (VP1up) exhibits phospholipase A2 (PLA2) activity and is essential for infectivity. To further understand the PLA2 interfacial enzymology and its role in the viral life cycle, a high resolution three-dimensional structure is necessary. In collaboration with Z. Zádori and P. Tijssen (INRS-Institut Armand-Frappier, Laval, QC Canada), the PLA2 domain of B19 was expressed in *E.Coli* as a fusion protein flanked by thioredoxin and a histidine tag. The 399 aa fusion protein was digested to remove these fragments and the region of interest was purified with high performance liquid chromatography (HPLC). This method relies on intrinsic biochemical and physical properties of the protein fragments for separation. The purification method consisted of anion exchange chromatography followed by gel filtration. The size of VP1up was verified by mass spectroscopy during HPLC to correlate each fraction with its corresponding fragment. Results have yielded samples pure enough for crystallization studies of the B19 PLA2 domain. We expect the high resolution atomic structure of VP1up will contribute to the further understanding of B19 PLA2 enzymology and its role in infectivity.

Microbeam Radiation Therapy. *JASMINE ESCALERA (Pace University, New York, NY 10038) AVRAHAM DILMANIAN (Brookhaven National Laboratory, Upton, NY 11973).* Conventional radiation therapy has proven to have clinical limitations due to the overall risk of radiation-induced tissue damage. One of the new forms of radiation therapy used to treat a wide variety of cancers is Microbeam Radiation Therapy (MRT) which was first initiated at the National Synchrotron Light Source (NSLS), Brookhaven National Laboratory. MRT uses a parallel array of microscopically thin planar slices of synchrotron-generated X-rays (microplanar beams, or microbeams). The unique feature of MRT is that the radiation exposure comprises thin, single-fraction, unidirectional microbeams. These microbeams have been shown in animal models to spare normal tissues, including the normal central nervous system, while damaging malignant tissue at therapeutic doses. This 'sparing' effect has been attributed to the rapid and selective regeneration of the normal-tissue capillary blood vessels damaged in the direct paths of the microbeams. Dr. Avraham Dilmanian has originated the novel use of microbeams in a special geometry called "interlaced bidirectional microbeams." This procedure produces a solid beam at the target from two interlacing arrays of microbeams. The method was used to irradiate targets in two animal models a) the normal rat brain, and b) a subcutaneous carcinoma tumor implanted in mice. The interlaced microbeams consist of two arrays, one array is shifted vertically with respect to the other by half the beam spacing, causing the two beams to interlace at the target, producing a solid beam there. In a study conducted while interning at Brookhaven, Balb/C mice were subcutaneously inoculated with the EMT-6 mammary carcinoma tumors behind their neck. They were then exposed in an upright position to a) bidirectional interlaced microbeams, or b) bidirectional broad beams. The neck site was chosen to use salivary glands as the normal tissue model. Results are still pending on this study. But earlier similar studies have concluded that a) "thick" microbeams (0.68 mm) spaced twice the beam thickness on-center retain their sparing effect on the normal brain, and b) interlaced microbeams combine the sparing effect of microbeams in the normal tissue around the tumor with the tumoricidal effect of broad beams. It is expected for the same conclusions to be seen in this new study.

Optimal Lengths For Genome Sequence Tags. *LOGAN EVERETT (Binghamton University, Binghamton, NY 13902) SEAN MCCORKLE (Brookhaven National Laboratory, Upton, NY 11973).* A Genome Sequence Tag (GST) is a short (less than 50 base pairs) sequence of nucleotides which is extracted from a DNA fragment of interest and used to identify the same position in a known gene sequence. GSTs are experimentally useful because fragmentation processes often provide no indication of where in the genome each fragment came from. GSTs provide a method for determining the original location of the fragment with minimal sequencing. Shorter GSTs can lead to higher throughput experiments because more GSTs can be concatenated and sequenced as a group. However, GSTs below a certain length become useless because they are less likely to be unique. This work studied the theoretical effectiveness of GSTs over a range of lengths in order to identify the optimal lengths for various experiments. The method of studying GSTs was in silico analysis of known genomes, specifically: simulating the fragmentation and tag sequencing processes and comparing all potential GSTs of a fixed length to calculate how many are unique. The comparison is computationally intensive due to the large amount of GSTs to be considered (tens of millions for mammalian genomes). Several methods of optimizing the comparison were used, including a hash table, a 4-ary tree, and a sorted array. This work produced several computationally feasible methods for predicting the effectiveness of GSTs in experiments using specific splicing enzymes on mammalian DNA. Predicting GST effectiveness for sonicated DNA (randomly fragmented) has proved to be more complex; however,

statistical approximations have shown to be equally effective and far less time consuming than an exhaustive analysis. These results have been used by other lab teams to design in vitro experiments using GSTs. In conclusion, in silico analysis is a powerful tool for designing a GST-based in vitro method because it can predict the effectiveness of any restriction enzyme. Sonication-based methods can also be predicted in silico although a statistical, rather than exhaustive analysis, is recommended.

Characterization of the Cobalamin and Fep Operons in *Methylobium petrolphilum* PM1. *JANE EWING (Merced College, Merced, CA 95340) ANU CHAKICHERLA (Lawrence Livermore National Laboratory, Livermore, CA 94550).* The bacterium *Methylobium petroleophilum* PM1 is economically important due to its ability to degrade methyl tert-butyl ether (MTBE), a fuel additive. Because PM1 is a representative of all MTBE degraders, it is important to understand the transport pathways critical for the organism to survive in its particular environment. In this study, the cobalamin pathway and select iron transport genes will be characterized to help further understand all metabolic pathways in PM1. PM1 contains a total of four cobalamin operons. A single operon is located on the chromosome. Located on the megaplasmid are two tandem repeats of cob operons and a very close representative of the cob operon located on the chromosome. The fep operon, an iron transport mechanism, lies within the multiple copies of the cob operon. The cob operon and the fep operon appear to be unrelated except for a shared need for the TonB-dependent energy transduction complex to assist the operons in moving large molecules across the outer membrane of the cell. A genomic study of the cob and the fep operons with that of phylogenetically related organisms helped to confirm the identity of the cob and fep operons and to represent the pathways. More study of the pathways should be done to find the relationship that positions the two seemingly unrelated cob and fep genes together in what appears to be one operon.

Selective Breeding of *Drosophila melanogaster* to Achieve Gene Excision. *BRESHELLE FARB (California State University Fresno, Fresno, CA 93710) BILL FISHER (Lawrence Berkeley National Laboratory, Berkeley, CA 94720).* Modeling is an important part of Cancer research. It allows researchers to better understand the function of cancer genes by using animal systems which can be altered via powerful genetic tools. Using *D. melanogaster* as our model we strove to discover the function of two genes. Both genes have been found to be over expressed in human breast cancer cells. We selected *Drosophila* cognates for each gene. In an effort to understand the function of the genes Trap 220 and Ppla-96A special mutations were planned. The goal of these mutations was to make the genes non-functional. By using a transposable element near each gene we hoped to create a small deficiency which will knock out gene function. The transposable elements are known as P-elements. P-elements need the enzyme transposase to mobilize. A four-generation cross scheme was developed to introduce transposase into flies carrying the P-elements. We scored and collected the progeny that were positive for the phenotypic marker telling us a P-element jump had occurred. Out of 100 parental crosses 18 excisions were found for P-element EY01286. Whereas, 58 excisions were found for P-element EY012810. The F1 generational crosses also had low success rates. Low success rates coupled with faltering supplies of the TM3/TM6 virgins prevented the completion of the final cross. It was not previously known, however, it has now been confirmed that P-element EY01286 does not jump as well as other p-elements. Since P-element EY01286 has a lower success rate this cross scheme will need to be repeated with a substantial increase in the number of parental crosses to obtain the desired amount of progeny with the intended genotype. An increase initial parental crosses coupled with better care of weak TM3/TM6 strains is likely to produce a more desirable result.

Ligand-Independent Preformation of EGFR Homodimers Visualized Utilizing Flow Cytometric Fluorescence Resonance Energy Transfer (FRET) Techniques. *DEMETRA FARLEY (Prairie View A&M University, Prairie View, TX 77448) GAYLA ORR (Pacific Northwest National Laboratory, Richland, WA 99352).* The growth factor-induced epidermal growth factor receptor (EGFR) signal transduction pathway, which promotes proliferation and differentiation in cells of varying lineage, requires for its commencement the homodimerization of EGF receptor monomers. While dimeric association of EGF receptors is primarily invoked through ligand binding, recent studies elucidate that pre-formed EGFR homodimers innately exist at the cell surface independent of activation by ligand. Here, corroboration of this finding was achieved by illustrating, via flow cytometric fluorescence resonance energy transfer (FCET-FRET), the presence of EGFR homodimers on the surface of 184A1 cells prior to epidermal growth factor (EGF) insertion. Analysis of the molecular interactions occurring between EGF receptors before introduction of growth factor involved the fusion of EGFRs to the fluorescent labels Alexa Fluor 488 (A488) and Alexa Fluor 546 (A546) using antibodies to the ectodomains of EGFR proteins. Based on FRET theory, it was anticipated that marked energy transfer, or indirect stimulation of the acceptor molecule via donor excitation and quenching, would occur between A488 and A546 only if the fluorescently-tagged EGF receptors were less than ten nanometers apart, a distance relatively suggestive of direct intermolecular activity. Upon excitation of dually stained EGFR fusion proteins, both a slight decline in A488 emission and a considerable enhancement in A546 fluorescence were visualized, substantiating the presence of FRET in the system prior to the addition of epidermal growth factor. Perceivably, a significant proportion of pre-formed EGFR homodimers must inherently exist at the surface of cells independent of activation by ligand. While the incidence of ligand-independent EGFR homodimerization has adequately been validated, the function of pre-formed EGF receptor dimers in the overall mechanism of EGFR activity remains uncertain.

Imaging Compositional Changes in Mouse Bone at High Resolution. *THEODORE FELDMAN (State University of New York — Stony Brook, Stony Brook, NY 11776) LISA MILLER (Brookhaven National Laboratory, Upton, NY 11973).* Understanding the changes in material properties of bone during formation is critical for diagnosing and treating bone disease. Mechanical properties can be studied using assays such as nanoindentation (NI), whereas synchrotron-based infrared microspectroscopy (SIRMS) provides information on the chemical makeup of bone. In order to correlate the mechanical and chemical properties, these two techniques must be performed on the same sample. Typically, NI is performed on an embedded and polished thick specimen, whereas SIRMS data are collected by measuring the transmission of infrared light through thin, microtomed sections. We have developed a new method for collecting SIRMS data in a reflection geometry, such that NI and SIRMS can be performed on the same sample. This study validates the accuracy and quality of reflection SIRMS, while investigating spatially-resolved chemical changes in developing bone with respect to the sagittal axis. The tibia of two male BALB/cByJ mice, 10 to 21 days of age, were dehydrated and embedded in poly-methyl-methacrylate (PMMA). A 3μm-thick sagittal section was cut from the surface of each embedded bone. IR microspectroscopic imaging was performed on both the thin section and the surface of the sample block in transmission and reflection geometry, respectively. Transmission data were converted to absorbance using Beer's Law. Reflection data were converted to absorbance through a Kramers-Kronig (KK) transformation. The KK transformation will also be validated theoretically. The data from the two imaging methods were compared using common visible landmarks. Peak area ratios were performed on data from both the thin section and sample block to provide quantitative measures of mineral and matrix content and stoichiometry (i.e. phosphate-to-protein ratio; carbonate-to-phosphate ratio). Data analysis indicates that there are disparities between transmission and reflection data, particularly within the global phosphate-to-protein ratio. Chemical indices of collagen cross-linking and the carbonate-to-phosphate ratio appear consistent in trend and value across both time points and data collection modes. Future studies will be necessary to determine the source(s) of these differences.

New Insights into the Cellular Actions of the Plant Defense Hormone, Methyl Jasmonate. *ABIGAIL FERRIERI (College of the Holy Cross, Worcester, MA 01610) RICHARD FERRIERI (Brookhaven National Laboratory, Upton, NY 11973).* Studies have shown that exposing a plant to insect herbivory or to exogenous methyl jasmonate (MeJA), a known defense hormone linked to insect herbivory, will cause increased sucrose loading in phloem sieve tube elements with subsequent long-distance transport to sink tissues. Little is known, however, about the early actions of MeJA at the cellular level which can impact leaf sugar synthesis, its active loading, or long-distance transport. Recent in vitro cellular studies suggest that MeJA increases lipid membrane polarization enhancing the proton electromotive force which drives synthesis of adenosine triphosphate (ATP), the primary energy currency for cellular function. If true, changes in sugar synthesis and active loading could be a consequence of this action. The objectives of this project were, first, to establish a direct association between MeJA and lipid membrane polarization at whole-organism levels; and second, to test for correlations between chemical structure and membrane polarization for future radioligand design for *in vivo* imaging of membrane function. We hypothesized that exogenous

jasmonate treatment in cut leaf studies will counter the inhibitory effects of treatment using an uncoupling agent such as carbonyl cyanide 3-chlorophenylhydrazone (CCCP). Such agents prevent oxidative phosphorylation of adenosine diphosphate (ADP) back to ATP with consequences to sugar synthesis and its transporters. Sucrose loading was quantified by administering $^{11}CO_2$ to cut leaves, and measuring vascular loading of [^{11}C]sucrose in leaf tissue using phosphor plate imaging. Tobacco leaves, treated with 40 uM CCCP through the cut petiole for 15 minutes displayed 0.2 ± 0.2% (n=3) loading in comparison with 7.0 ± 3.1% (n=4) loading in control cut leaves. Similar inhibitory effects were observed using another uncoupling agent, 2, 4-dinitrophenol (DNP). We also noted that cut and intact control leaves exhibited the same loading. Furthermore, cut leaves pre-treated with 1 mM MeJA prior to CCCP treatment displayed 3.4 ± 1.6% (n=3) loading. Our results provide additional evidence supporting the hypothesis that MeJA increases membrane polarization. Subsequent studies compared dose responses for [^{11}C]sucrose loading between DNP and 4-fluoro-2-nitrophenol (FNP) with an intent to assess efficacy for using [^{18}F]FNP in subsequent imaging studies. Although less acidic, FNP was found to be a more potent uncoupling agent than DNP.

Detection of Hydrogen Peroxide (H_2O_2) in a Sol-Gel Embedded Amplex Red/ Horse Radish Peroxidase (HRP) Solution Using a Miniature Fluorescence Spectrometer. *MARK FISHER (Yale University, New Haven, CT 06520) GUY GRIFFIN (Oak Ridge National Laboratory, Oak Ridge, TN 37831).* Under appropriate conditions, the non-fluorescent compound amplex red is selectively oxidized by H_2O_2, the posited precursor of other reactive oxygen species believed to be involved in cellular inflammation and damage, in the presence of HRP catalyst to form the fluorescent dye resorufin. Entrapment of the dye /enzyme (Amplex Red/ HRP) molecules in a matrix enables their better-controlled localization and increased robustness in non-ideal conditions. Based on a fluorescence intensity measurement and data from a calibrated concentration curve, concentrations of H_2O_2 in an unknown solution can be determined. A sol stock was prepared by stirring a mixture of tetramethylorthosilicate (TMOS), water, and 0.1M HCl for three hours. The dye solution was prepared by mixing 50 mM phosphate buffer with HRP (10 U/mL) and 10 mM amplex red, after which 0.125 mL was vortexed with 0.125 mL of the sol stock. The mixture was then pipetted into a test tube, allowed to solidify on the side of a cuvette, or coated on a polished 800 nm fiber. After being rinsed or dipped in water for one minute, the gel was dried for 24 or 48 hours in darkness at ambient temperature. Concentrations of H_2O_2 ranging from 0.5 uM to 10 uM were introduced to the sol-gel tubes in 0.25 mL aliquots and were allowed to diffuse for an hour in darkness at room temperature. The intensity of fluorescence for each tube was then measured. A similar process was repeated using 1 mL of various concentrations of H_2O_2 for ten minutes on the cuvette slides. A few droplets of 0.5 uM H_2O_2 were added to the tips of the fibers, and the fluorescence intensity was again measured. The results so far suggest that sol-gel encapsulation of the dye does not inhibit the linear relationship between H_2O_2 concentration and the fluorescence intensity of resorufin in the tubes or cuvettes. The intensities are overall lower than those measured in liquid solution, but this is most likely caused by the kinetics of H_2O_2 diffusion through the sol-gel and the decrease in volume of Amplex Red inherent in the sol-gel encapsulation process. In the cases of the fibers, detection of resorufin has been achieved, but no linear relationship has yet been established. Resorufin detection has also proved to be extremely sensitive to drying time of the sol-gel. The long-term goal of the project is to coat a pulled nano-scale fiber with the sol-gel dye matrix and use it as a reagentless optic sensor for intracellular detection of hydrogen peroxide.

Sampling Strategies of *Populus tremuloides* in Rocky Mountain National Park for Assessment of Somatic Mutations and Diversity Within Clonal Populations. *TODD FLEMING (Ball State University, Muncie, IN 49307) LEE GUNTER (Oak Ridge National Laboratory, Oak Ridge, TN 37831).* Quaking aspen (*Populus tremuloides* Michx.), has the widest distribution of any tree species in North America, and may also have one of the longest lifespans due to its clonal propagation. Large aspen stands in the west primarily consist of clones made up of individual ramets connected by extensive root systems. Estimates of the age of some clones extend upwards of 10,000 years. There is no current way of measuring the age of these clones due the fact that individual ramets live only 100–150 years. Accumulated somatic mutation rates may be used to age aspen clones if a method can be developed for determining the basal genotype and thus allowing for the assessment of total mutations generated over time. Comparing Single Nucleotide Polymorphisms (SNPs) from several meristems sampled across the crown of a single ramet to isolate the most frequent meristematic genotype should allow the identification of the basal genotype, and combining genotypes for an entire stand would allow the average number of mutations within a given ramet cohort to be calculated. Investigators will travel to Rocky Mountain National Park in early August to sample leaf tissue from aspen stands. Park officials have also requested a diversity study be done on sampled aspen. Suitable stands will be selected and sampling points and distances measured prior to arrival using geographical information system software Arcmap. Meristems of ramets will be sampled individually, but the possible pooling of these samples for DNA extraction prior to SNP analysis could save thousands of hours of lab work. The process of pooling leaf sample tissue prior to extraction is being tested using individual genotypes of the hybrid cottonwood family 52124 (TD '52-225' by 'D124') developed by the University of Minnesota – Duluth (UMD) Natural Resources Research Institute (NRRI). In addition, the use of commercial cat litter in place of silica gel as an affordable, convenient desiccant for preserving tissue samples in the field is being tested.

Experimental Studies on Near Frictionless Carbon Coatings for Industrial Applications. *LEO GERDOV (Benedictine University, Lisle, IL 60532) ALI ERDEMIR (Argonne National Laboratory, Argonne, IL 60439).* Near frictionless carbon coatings (NFC) are structurally amorphous but exhibit some of the lowest friction and wear coefficients when tested in inert environments. The main characteristics of these coatings are that due to their very impressive friction and wear properties, they can significantly increase energy efficiency and durability of many moving parts. If the coatings live up to the expectations and are indeed appropriate for certain applications, the next step will be to offer this technology for industrial exploitation. In our laboratory, we use a Plasma Enhanced Chemical Vapor deposition system to deposit these nearly frictionless carbon coatings. This system is very small and hence not appropriate for large scale production. For most industrial applications, we have been looking for new deposition systems and/or companies that can scale-up the production of these coatings. At the moment, we are working with an industrial company that is capable of producing our NFC coatings in their big deposition systems. These systems use a Pulse DC power source to grow the NFC coatings on the surfaces of metallic samples. After deposition, this company is sending the coated samples back to us and we are then testing these samples to determine if the coatings produced in their systems have the same friction and wear properties as our original NFC coatings. We are also performing structural and chemical studies on these coatings using microscopes and a micro Raman spectroscopy. So far, we have conducted a series of friction tests on these samples using a Pin-on-Disk tribometer under different environmental conditions. After the tests, we determined wear rate and studied the fine details of sliding surfaces using a MicroXAM non-contact optical profilometer. We have also studied the chemical structure of the coatings using micro Raman spectroscopy. The results obtained so far suggest that this company has come very close to duplicating our coating. After the completion of our examination of the sample coated by the outside company, we will be able to suggest further adjustments to them so that the next batch of samples will hopefully be identical to our NFC coating. The implications of this achievement are mostly aimed at the industrial market.

Using Furfural Derivatives for Quantification of Detergent Concentration During Dialysis. *JOSEPH GONCALVES (State University of New York – Stony Brook, Stony Brook, NY 11743) DAX FU (Brookhaven National Laboratory, Upton, NY 11973).* Monitoring detergent concentration during dialysis is a difficult task, primarily due to hydrophobic effects causing monomeric units to aggregate at or above the critical micellular concentration, an intrinsic property unique to specific detergents. A convenient procedure for quantifying the concentration of glycosidic detergents exploits the saccharide head group of detergents in this class. The concerted reaction of these molecules with phenol in the presence of concentrated sulfuric acid results in a furfural derivative, an aromatic compound capable of absorbing light with a wavelength of 490nm. Varying concentrations of n-dodecyl Beta-D maltoside were added to 20mM Hepes pH7.5, 100mM NaCl, 20% Glycerol and dialyzed against one another. A series of 50 ul fractions were collected from both external and internal dialyzing solutions for each trial daily over the course of 14 days. Upon collection of the final sample, a calibration curve was constructed using differing detergent concentrations in otherwise identical solutions. When analyzed as a function of dialysis time, detergent concentrations closely correlate to theoretical exponential decay, which allow for the calculation of a rate constant indicating that dialysis is virtually completed after four days.

PyMOL Made EZ – A Tool for Simplifying Molecular Viewing in PyMOL. *LAURA GRELL (Rochester Institute of Technology, Rochester, NY 14623) LEN SLATEST (Brookhaven National Laboratory, Upton, NY 11973).* PyMOL is a molecular modeling program that can be used in a wide range of studies within the scientific community. Its ability to produce informative, detailed, stereoscopic images makes it a very powerful tool both in the laboratory and in the classroom. However, the PyMOL user interface is difficult to use and its "development has been focused on capabilities, not on ease-of-use for new users." (PyMOL Users Manual) To resolve this, we set out to develop a new interface for PyMOL that can be installed as a plugin and helps to eliminate the need for command line interactions, making it a much more user-friendly interface. Using tools from Python's Tkinter and PMW toolkits, we created a tabbed interface called PyMOL Made EZ. The interface contains a series of buttons and entry fields that allow users to select given attributes of a molecule and make changes to it with the click of a button as opposed to issuing highly syntactical commands. Other features of the interface include a Chime/PyMOL command converter, nine preset molecular views, four molecular movies, and molecular sequence and hetero atom information all at the click of a button. The ongoing and continued development of PyMOL Made EZ could help to further the use of PyMOL which we believe to be one of the most powerful molecular viewing programs currently available.

Mapping Protease Substrates using Phage Display. *JUSTIN HENRY (Grambling State University, Grambling, LA 71245) MICHAEL D. SCHOLLE (Argonne National Laboratory, Argonne, IL 60439)*. Proteases comprise approximately 2 percent of the human and bacterial genome, thus making it important to map substrate specificity for known proteases. Proteases hydrolyze the peptide, or scissile bonds of proteins; a cleavage event commonly observed in cancer, inflammation, and infectious diseases. The substrate library (ANL16) produced by the Kay Lab contains a 7-mer randomized peptide sequence fused to the N-terminus of gene III of M13 bacteriophage. In this study, ANL 16 was utilized to map substrates for human, SARS, and *E. coli* proteases. Substrate selections yielded eight positive substrates that were cleaved by the SARS protease 3CL Pro with an efficiency of ~70 percent. A dihydrophobic amino acid motif was common from the 3CL Pro substrates whereas substrates from StcE, in comparison to a known substrate of the protease, were glutamine rich. To further characterize the ANL 16 library, phage were biotinylated in vitro to map the substrates cleaved by native host cell proteases. These results showed that the majority of the substrates contained arginine and lysine rich dibasic motifs, similar to substrates cleaved by the outer membrane protease OmpT of *E. coli*.

Comparison of the Bioavailability of 1, 2 Diethylbenzene and 1, 3 Diethylbenzene in F344 Control Rats. *SUSAN HIATT (Eastern Washington University, Cheney, WA 99004) KARLA THRALL (Pacific Northwest National Laboratory, Richland, WA 99352).* The compound Diethylbenzene (DEB) is a colorless liquid that is mixture of isomers and is used as a solvent. Humans are exposed to DEB through household chemicals, such as paint thinners. Through these chemicals, DEB can come in contact with drinking water and enter the human body. The purpose of the study was to look at two isomers of DEB; 1, 2-DEB and 1, 3-DEB and compare the amount absorbed in an in vitro system using F344 rat tissue as a model for the human body. Tissues used in this study included liver, brain, fat and blood from F344 control rats. The vial equilibrium method and a gas chromatography system were used to determine partition coefficients for each sample. For the compound 1, 2 DEB the tissue to blood ratios for fat were 2.56, for liver 1.45, and for brain 1.09. The tissue to blood ratios showed that 1, 2 DEB preferred to stay in fat tissue and equally distribute between liver/blood, and brain/blood. For the compound 1, 3 DEB the tissue to blood ratios for fat were, 0.59, for liver 0.13, and for brain 0.19. Tissue to blood ratios showed that 1, 3 DEB preferred to stay in blood rather than distribute into the tissues. These are significant results due studies showing that 1, 2 DEB is neurotoxic to experimental animals, while 1, 3 DEB is not. This research suggests that one reason for this occurrence is the difference in the amount of compound reaching the tissue. To understand the structural impact, further research will be needed to evaluate metabolic and kinetic differences.

Coatings as a Variable in Acoustic Telemetry. *ELIZABETH HOBBS (Truman State University, Kirksville, MO 63501) RICHARD S. BROWN (Pacific Northwest National Laboratory, Richland, WA 99352)*. Scientists commonly use acoustic transmitters to conduct research on salmon. Acoustic transmitters for juvenile salmon are used for short term studies since their battery life is limited and transmitters may not stay in the salmon. Transmitters can be expelled through the suture wound, by pressure necrosis or by transintestinal expulsion. Pressure necrosis occurs when an irregular part of the transmitter rubs against the body wall, causing stress on the tissue and eventual ejection of the tag. Transintestinal encapsulation involves the encapsulation of the tag by the intestine and then evisceration through the anus. Chisholm and Hubert (1985), noted that transintestinal expulsion occurred within a 42–175 day timeframe for expulsion for rainbow trout (17.5–22.5cm in length). This research will study the effect of different coatings in relation to expulsion of transmitters. The long term study of rainbow trout, (*Oncorhynchus mykiss*), a model species for salmon, will monitor the expulsion rates of transmitters coated in beeswax, KISS-COTE, and also expulsion rates of a control group (tags as they are currently used in salmon research). KISS-COTE is a thin, clear coating created to provide a slick surface that is hard for barnacles and other organisms to attach. This may make encapsulation difficult and possibly prolong the amount of time a transmitter can remain free floating in the body cavity. Beeswax may prevent irritation from irregular objects on the transmitter. With less irritation, the encapsulation and possible necrosis process might slow down. Helm and Tyus (1992) found that transmitters coated in beeswax had a 3% expulsion rate, significantly less than the other coatings used in their study (paraffin wax and silicone). The long term study of the effect of transmitter coatings on expulsion rates will provide data on alternate coatings and the possible implementation of the coatings for commercial/scientific use. Also, a more precise prediction of transmitter retention in the fish will create a more accurate timeframe of when scientists can expect the tag to be expelled. This will help scientists decide whether they are tracking a fish, or just an expelled tag. This information may create a clearer picture of fish migration.

Improvements in the Isolation and Purification of Nucleic Acids and Proteins Using a Renewable Microcolumn Fluidics System. *JERRAH HOLTH (Harvey Mudd College, Claremont, CA 91711) RICHARD OZANICH (Pacific Northwest National Laboratory, Richland, WA 99352).* Detection of biological substances in the environment is an important part in the defense against bioterrorism and keeping water and air supplies safe. The rapid and sensitive capture and purification of cells, nucleic acids, and proteins is necessary for these efforts. Detection systems must be transportable and automatic for work in the field and be able to process samples that are dirty and/or have targets present in low concentrations. The Biodetection Enabling Analyte Delivery System (BEADS) uses microbeads to capture and purify the desired cells, nucleic acid, or protein. A variety of bead types can be used including polymer, glass, sepharose and magnetic. The following experiments were conducted: 1) Benchtop comparison of different antibodies for capturing Botulinum neurotoxin recombinant fragment, 2) Comparison of benchtop vs. BEADS for measuring six different proteins in a single sample using a multiplex bead suspension array, and 3) Purification of nucleic acid using BEADS. Flow cytometry was used to analyze the efficiency of four primary antibodies and two fluorescent labeled, secondary antibodies to bind Botulinum neurotoxin fragment in a sandwich immunoassay. The fluidics system was also compared to the traditional benchtop method, using flow cytometry, for a six-plex protein assay to examine the time needed for the procedure and the amount of capture achieved. The final part of this investigation used Real Time Polymerase Chain Reaction and an intercalating fluorescent dye to investigate and attempt to eliminate contamination, increase capture and elution efficiency, and determine the best method for automated DNA purification. The combination of AR-4 primary antibody and Alexa 488 fluorescence bound Raz-1 secondary antibody is the most effective at binding Botulinum neurotoxin. For the 6-plex protein assay, the benchtop was shown to have a greater capture than BEADS. However, for all concentrations of protein, BEADS took less time than the benchtop with the 50 µL sample taking less than one fourth the time of the manual method. The preliminary DNA investigation showed that small pore silica beads are better for elution but the larger pores capture a greater amount of nucleic acid. These three experiments produced preliminary data that will allow further enhancement of the BEADS method.

A Comparison of Different Protein Staining Techniques in 2-Dimensional Electrophoresis Gels: Coomassie Blue-Green, Coomassie Blue-Red, Silver and Sypro Ruby Fluorescent-Stained Shewanella Oneidensis Proteins. *NICOLE JENKINS (Hampton University, Hampton, VA 23668) CAROL GIOMETTI (Argonne National Laboratory, Argonne, IL 60439).* The goal of this study was to compare staining techniques used to visualize spots on 2DE gels in order to determine the most qualitative and time efficient staining of proteins. Mini-gels were stained with the following dyes: Coomassie Blue Red, Serva colloidal Coomassie Blue Green, Invitrogen Simply Blue Coomassie Blue Green, Silver Stain and SYPRO Ruby Fluorescent stain, and compared. A destaining time course study was performed

to determine the sensitivity of CB-Green using either a green or red scanner filter. A product brand comparison was done, comparing Invitrogen CB-Green to Serva CB-Green. A concentration sample loading comparison was done to determine the most appropriate amount of sample to load for substantial staining results using CB-Red. Lastly, a total comparison of all of the staining techniques was done, which evaluated all stains for optimal results. The 6 hour destain with CB-Red, and the use of a red filter are best for spot detection. Loading 60µg, in comparison to 40µg of protein, provides a better sensitivity of spot detection for CB-Red staining. The Serva brand of CB-Green has a more pronounced staining of spots than the Invitrogen Simply Blue CB-Green. The silver stain, although having the lowest protein concentration, is most sensitive when staining, producing the greatest number of spots. However, because silver staining involves the lowest protein concentrations, specific spots are more difficult to identify using mass spectrometry. Also, silver staining takes a greater amount of time and produces the most expensive waste disposal.

Visualization of Inner Ear Hair Cell Machines by Electron Tomography. *DANIELLE JORGENS (California State University Fresno, Fresno, CA 93740) MANFRED AUER (Lawrence Berkeley National Laboratory, Berkeley, CA 94720).* The inner ear hair cells are responsible for the transduction of mechanical force into an electrical signal which is the starting point of hearing. Protruding from the apical surface of the hair cell is a hair bundle made up of multiple stereocilia and one kinocilium. The stereocilia are composed of actin filaments, unconventional myosins, ERM proteins and other actin or myosin binding proteins. The actin filaments are cross-linked by either espin or fimbrin, both of which are documented actin-bundling proteins. Fimbrin has been found to cross-link actin in vitro by either a slanted or straight pattern. The outer most actin filaments of the actin bundle are also suspected to be connected to the plasma membrane via linker proteins. To examine these two lines of thought we dissected the saccular maculae out of the bullfrog and subjected it to progressive lowering of temperature dehydration. This method of dehydration resulted in excellent preservation of the stereocilia and actin bundle. Using electron tomography, we three-dimensionally visualized, with a resolution of ~4-6 nm, the actin-actin structure and actin-membrane structure. We found surprisingly that the actin filaments were cross-linked in both slanted and straight patterns; however we were unable to conclusively identify the cross-linking protein. When we examined the connection between the actin bundle and the adjacent membrane, there were many regions whose size and shape were consistent with myosin. This first glimpse at the actin bundle of stereocilia in vivo is also evidence that stereocilia do not undergo shrinkage due to the resin embedding procedure. When actin filament models were docked to the tomogram we found that the regularly spaced actin filaments were 12 nm apart, supporting in vitro studies of actin filaments. For further study of these protein interactions and for certain identification of such targeted proteins, double tilt-series tomography combined with labeling techniques should be employed.

Screening *Bacillus* spp. for Crystalline Endotoxin Production. *HAIG KASSABIAN (Diablo Valley College, Pleasant Hill, CA 94523) TAMAS TOROK (Lawrence Berkeley National Laboratory, Berkeley, CA 94720)*. Members of the bacterial genus *Bacillus* are microorganisms that, when deprived of nutrients, have the capability to develop endospores and concurrently produce δ-endotoxins. The crystalline δ-endotoxins are toxic to insects but not to humans because insects have an enzyme, which breaks down the crystalline structure and releases the toxic protein. The high insect specificity of the toxins makes the producing bacilli good candidates for their use as natural bio-insecticides. In this study, extremophilic *Bacillus* spp. were screened for the production of crystalline δ-endotoxins. The strains were grown in 96-well plates containing TB medium for one day and stressed in C2 medium for six days. We used high-throughput screening to detect crystalline toxins. Crystal-positive strains were grown in larger volume for further screening of the novel compounds. So far, 30.5% of the 583 strains screened showed positive crystalline toxin production. The two most prevalent toxin producing species were *B. subtilis* and *B. megaterium*. The area where the highest numbers of positive crystal producing bacilli were collected was Solovetskie Island, Russia with 30.3% of the 178 strains screened. Continuing work will concentrate on screening more toxin producing strains, sequencing the novel proteins, and detecting their new insect specificities that will benefit crop protection.

High Throughput Analysis of Stress Response in *Shewanella oneidensis* MR-1. *NATALIE KATZ (Laney College, Oakland, CA 94607) TERRY C. HAZEN (Lawrence Berkeley National Laboratory, Berkeley, CA 94720)*. *Shewanella oneidensis* MR-1 has shown extraordinary metabolic diversity through its use of a variety electron acceptors. It can grow both aerobically and anaerobically, and can use nitrate, fumarate, sulfur compounds, and oxidized metals as electron acceptors. It has the ability to grow in almost any environment, and its entire genome has been sequenced and most of the genes annotated, which makes *S. oneidensis* an excellent candidate for environmental remediation of sites contaminated with toxic metals and radionuclides. The Natural and Accelerated Bioremediation Research (NABIR) Field Research Center (FRC) in Oak Ridge, Tennessee, like most other U.S. Department of Energy uranium contaminated sites, has very high concentrations of nitrate and various salts from the metal processing wastes that contained nitric acid. To rapidly screen the response of *S. oneidensis* to stressors of interest, e.g. nitrate, nitrite, and osmotic stress – the Biolog Omnilog Phenotype Microarray system was utilized. The Omnilog uses digital imagery sensing technology to track the changes in turbidity of cultures growing in individual wells of a 96-well microarray plate over a given time period. The Omnilog was calibrated with two other methods in order to determine the final cell yield of *S. oneidensis* by correlating the digital readings produced by Omnilog with OD600 readings and direct cell counts. After the calibration, *S. oneidensis* was subjected to varying concentrations of each stressor of interest, coupled with either sodium or potassium as the carrier salt. Inhibition of growth was determined by calculating the maximum cell yield achieved by the control and stressed cultures to see which concentration of stressor decreased the final yield by at least fifty percent. In general, final cell yields decreased with increasing concentrations of stressor. A fifty percent inhibition of the final cell yield for nitrate stress was seen at 250 and 6,000 ppm nitrate for $NaNO_3$ and KNO_3, respectively. Fifty percent inhibition of the final cell yield for nitrite stress was seen at 125 ppm nitrite for both $NaNO_2$ and KNO_2. Fifty percent inhibition of the final cell yield for salt stress was seen at 100 and 250 mM salt for NaCl and KCl, respectively.

Nondestructive Decontamination of Radiological Dispersal Devices from Porous Materials. *NADIA KIVENAS (Richard J. Daley College, Chicago, IL 60629) MICHAEL KAMINSKI (Argonne National Laboratory, Argonne, IL 60439)*. Technologies are needed for non-destructive removal of radioactivity from porous surfaces such as concrete and marble. We are developing a process based on superabsorbing hydrogels. The optimized process would involve three conceptual steps: (1) penetrate the pore structure with a water-based wash solution to promote the removal of radionuclides from their sorption sites and into the pore water; (2) pull water from the pore structure with a superabsorbing hydrogel, and (3) remove the radioactivity-loaded gel by wet vacuum. We report aqueous solution absorbency as a function of potential wash solution compositions by gravimetric analysis of the swelling capacity of gel formulations ("tea bag test"). We discovered that the addition of anionic non-crosslinked polymers to the formulations decreased the retention capacity. We found that polymer absorbency is dependent on the salt concentration in the following wash solutions: NH_4Cl, $CaCl_2$, and $NH_4H_2PO_4$. Reducing the molarity of the wash solution increases the absorption capacity of the polymer formulation. This trend is apparently in contrary to the theory of osmotic pressure.

Trichloroethylene Co-metabolism by *Methylosinus trichosporium* OB3b at Maintenance Level Activity. *ALICIA KRUPP (Brigham Young University, Provo, UT 84602) FREDERICK COLWELL (Idaho National Laboratory, Idaho Falls, ID 83415)*. Methanotrophs are aerobic microorganisms that metabolize methane. Some methanotrophs have the ability to aerobically co-metabolize trichloroethylene (TCE), a contaminant in the Snake River Plain Aquifer (SRPA) through the action of the enzyme soluble methane monooxygenase (sMMO). The methanotroph, *Methylosinus trichosporium* OB3b, was grown in a biomass recycle reactor (BRR), simulating groundwater conditions, to determine rates of methane oxidation and TCE co-metabolism. sMMO activity was measured in the presence and absence of TCE, using the coumarin oxidation assay, which monitors the oxidation of coumarin (in place of methane) to a fluorescent product, 7-hydroxycoumarin. Quantitative real-time PCR and acridine orange direct counts (AODC) were used to determine cell numbers of *M. trichosporium* in the BRR. Data suggests that starved cells exposed to TCE have lower rates of sMMO activity. From this data and from current literature, we infer that cells under stressed conditions may be less affected by TCE compared to cells under ideal growth conditions. The rates of methane oxidation and TCE co-metabolism measured in *M. trichosporium* will assist the development of models that describe natural attenuation of TCE in the SRPA.

Number of Active, Active-Sites in the SARS CoV Main Proteinase Homo-dimer. *JOYCE LAI (University of California Berkeley, Berkeley, CA 94720) WALTER MANGEL (Brookhaven National Laboratory, Upton, NY 11973).* During the first SARS epidemic, 10% of patients died. The infection was contained by quarantine. There still is no vaccine available; therefore, anti-viral agents are needed urgently. The SARS CoV main proteinase is an attractive target for antiviral agents as it is an enzyme required for viral replication. We have shown that the monomeric form of the enzyme is inactive; the active form of the enzyme is the homo-dimer. Are the two active sites in the homo-dimer functional or is only one of them active? To answer this question, the specific activity of dimers made from a mixture of potentially active monomers and inactivated monomers will be measured. If the specific activity of the active homo-dimer is twice that of the hetero-dimer, then both active sites in the homo-dimer are indeed functional. On the other hand, if the specific activity of the active homo-dimer is equal to that of the hetero-dimer, then only one of the active sites in the homo-dimer is functional. As a control, small angle x-ray scattering will be used to confirm that hetero-dimers form under the conditions used to measure enzyme activity. In order to do these experiments, a series of preliminary experiments were performed. Conditions were found under which a preparation of SARS CoV main proteinase dimers was completely inactivated by treatment with dithiodipyridine (dTdP). About 66% of the inhibition could be reversed by TCEP, a strong reducing agent. The mono-dimer equilibration rate was shown to be extremely fast. Finally, equations were derived to quantitate the distribution of monomers and dimers at equilibrium. Eventually the results of these experiments will be used to design antiviral agents.

Multimodality Nanopartcle for Targeted in Vivo Imaging with Xe NMR and Fluorescence. *LESLEY LARA (Contra Costa College, San Pablo, CA 94806) FANQING FRANK CHEN (Lawrence Berkeley National Laboratory, Berkeley, CA 94720).* One of the major challenges for antibody-based therapeutics is the lack of sensitive and convenient methods for *in vivo* imaging that track the distribution, metabolism, movement of the drug delivery system, and provide an effective means to monitor the treatment efficacy of the drugs. The lack of sensitivity also made early detection of cancerous tumors unrealistic. Currently, radiolabels are the most sensitive labeling technology; however, radioactivity labels are undesirable for large-scale use due to the harmful effects of ionizing radiation to both the technicians and the patients. Current generation MRI contrasting reagents work in a very high concentration range of several millimolars, and there is a high false positive rate. To solve this problem, we have constructed a novel class of imaging reagent that uses near-infrared CdSe nanocrystals. The nanocrystals are clustered with Gd-based MRI contrasting reagents for regular MRI imaging, or with a novel zero- to low-field MRI agent. This dual modality nanoparticle composite would be detectable with both deep tissue near infrared in vivo imaging and MRI/zero-field MRI. To target this to breast cancer, the nanoparticle also uses single-chain antibody against ErbB2, which is a protein in the EGFR family over expressed in 15% to >50% of breast cancers, depending on the stage of the disease. The nanoparticle is highly fluorescent with a high quantum yield and the clustering of the Gd chelating compound or zero-field MRI agent is demonstrated to be at least 500 per nanoparticle. This new class of nanoparticle based imaging solution can be applied to diagnostic and monitory imaging of other cancers, or even other diseases.

Microbeam Radiation Therapy. *ANN LAYVEY (Lehman College CUNY Bronx, NY 10453) AVRAHAM DILMANIAN (Brookhaven National Laboratory, Upton, NY 11973).* Microbeam Radiation Therapy (MRT) is a new experimental form of radiation treatment for cancers. We studied irradiation of normal and tumor-bearing rats with arrays of parallel thin, planes of synchrotron-generated x-rays at the National Synchrotron Light Source (NSLS). The rats were monitored after the irradiations, and their brain was dissected upon euthanasia for histology. Previous studies suggest that MRT seems to be less damaging to healthy tissue than conventional radiation therapy. The aim of this study was to compare the efficacy of MRT to the conventional radiation therapy. First, we anesthetized the rats using a ketamine-xylazine solution and inoculated them in their brain with 9LGS tumor cells. The cells are injected into the striatum at the level of bregma 4 mm left of the midline, and 4mm deep into the brain. After fourteen days, the rats were irradiated at the NSLS; two groups of rats were irradiated at 60 Gy incident dose using two different array sizes. After the Light Source irradiation, the rats are weighed on a weekly basis. We also checked them daily for their general health, and euthanized them at the first sign of sickness due to the tumor growth. Euthanasia was carried out using either tissue perfusion with paraformaldehyde, or by subjecting the rats to a mixture carbon dioxide and oxygen. Few of the tumor bearing rats also had subcutaneous tumor and have to be euthanized. The brains of the euthanized rats were then preserved in formaldehyde for twenty-four hours and then placed into sucrose solution until they are needed for histology analysis. Behavior studies were conducted using an Open field test and RotoRod on the normal rats, irradiated with similar beams in their brain earlier, to determine the possible central nervous system effect produced by radiations. The study is inconclusive because some animals are still being followed up.

Expression of Parkin. *NICHOLAS LEIBY (Massachusetts Institute of Technology, Cambridge, MA 02139) KENNETH DOWNING (Lawrence Berkeley National Laboratory, Berkeley, CA 94720).* Parkinson's Disease is the second most common neurodegenerative disorder, affecting 1-2% of the population over 60 years of age. The pathogenesis of the disease is still unknown, but it's believed that a complex interaction of genetic and environmental influences are involved. Mutations in the park2 gene, encoding the parkin protein, account for up to 50% of familial recessive cases of the disease. Previous studies have shown that parkin binds strongly with microtubules, but the specifics of the bond between are unknown. A better understanding of this interaction may help to determine the pathogenesis of Parkinson's Disease. We tried 2 different methods to isolate parkin protein: *E. coli* and cell-free expression. *E. coli*: We transformed an IPTG inducible, GST-tagged pGEX-6P1 vector containing park2 into BL21 *E. coli*, grew a 2L culture of cells, then induced expression by adding IPTG to a concentration of 1 mM. We spun down the cells, resuspended them in 20mL of PBS, and lysed by sonication. We then centrifuged the lysate at 120 G for 45 minutes and mixed the supernatant with GST bind resin. The beads were washed with PBS and then the bound substrates were eluted with 60mM reduced glutathione in PBS. The elution was concentrated using a centrifugal concentrator. Cell-free: We used the Invitrogen Expressway Plus cell-free kit. Park2 was inserted into a pEXP1-DEST vector, and the reaction was run using different plasmid concentrations. A pEXP-lacZ vector was used as a positive control and a reaction without DNA was used to determine background. The reaction product from the cell-free system and the concentrated elution from the *E. coli* expression were denatured in SDS at 90 degrees C for 15 minutes and run out on gels. Some gels were stained with coomassie blue, and others were used to run western blots using anti-parkin antibody. Our results were inconclusive in both cases. There was too much background protein in the cell-free system coomassie stain to be certain there was parkin, and the *E. coli* expression bead wash was not stringent enough to remove all the background protein. The western blots were also inconclusive. The anti-parkin antibody was polyclonal and not selective enough for our purposes- multiple bands were visible in both cases. More work will have to be done to isolate parkin. The Westerns will have to be redone using Xpress and GST antibodies, and the GST column will have to be run with a stronger wash.

Thermodynamics of the Activation of the Adenovirus Proteinase by an 11-Amino Acid Peptide. *RICHARD LIU (Stanford University, Stanford, CA 94305) WALTER MANGEL (Brookhaven National Laboratory, Upton, NY 11973).* The adenovirus proteinase (AVP) is unusual in that it requires cofactors for maximal enzyme activity. One cofactor is pVIc, the 11-amino acid peptide from the C-terminus of the precursor to adenovirus protein VI; the other cofactor is the viral DNA. The thermodynamics of the binding of AVP to pVIc was investigated by isothermal titration calorimetry (ITC). Before those experiments could be done, both the solubility of AVP and the binding constant for pVIc had to be increased. Lower pH increased the solubility of AVP to at least 50 mM; a mutant of pVIc had an increased binding constant. In one ITC experiment the measured change in enthalpy (ΔH) was -6000 cal/mol, the calculated change in entropy (ΔS) was 6.38 cal/deg/mol, and the calculated change in free energy (ΔG) was -7,902.2 cal/mol. This implies the binding reaction was driven by the formation of hydrogen bonds and ion pairs. The ITC titration curve was complex, indicating several types of reactions were releasing heat. Understanding the thermodynamics of the binding of pVIc to AVP should offer profound insights into the activation mechanism of the proteinase by the cofactor. Ultimately, this information will be used to develop drugs that will act as antiviral agents for treating medical ailments caused by adenoviruses.

The Use of Spectroscopic Analysis Tools To Evaluate Changes in the Composition of Pretreated Biomass. *KILEY MACK (University of Colorado, Boulder, CO 80309) STEVE KELLEY (National Renewable Energy Laboratory, Golden, CO 89401).* The biomass that is used for production of ethanol must generally be pretreated before it is converted. These pretreatments change the chemical and structural

properties of biomass and make it more easily converted to ethanol. The changes can be evaluated using spectroscopic techniques like Near Infrared (NIR) spectroscopy and Fourier Transform Infrared (FT-IR) spectroscopy. These methods offer comprehensive information on changes in the chemical composition of pretreated biomass. They are also faster and less expensive than traditional wet chemical methods used to analyze biomass. The purpose of this study was to use these spectroscopic tools to understand changes in the composition and structure of spruce wood chips that had been subjected to different pretreatment processes. A secondary goal was to compare the rapid analysis methods in terms of their reproducibility and chemical insight. Multivariate statistical tools were used to relate changes in the composition of the samples to the pretreatment conditions (temperature, time, acid concentration, etc.) and to compare the rapid analysis methods. The chemical analysis indicated a strong correlation between the concentration of the acid used in the pretreatment and the loss of acetate from the hemicellulose. Both of the spectroscopic tools, in combination with multivariate analysis (MVA) techniques, were valuable for differentiating between the samples; however, the FT-IR was more useful for discerning the chemical changes that took place during the pretreatment process.

Radiation Effects on Connexin 50 Expression in Human Lens Epithelial Cells. *LYDIA MCCLURE (Carleton College, Northfield, MN 55057) ELEANOR BLAKELY AND KATHY BJORNSTAD (Lawrence Berkeley National Laboratory, Berkeley, CA 94720).* Astronauts encounter risks of chronic exposure to ionizing radiation, which is potentially damaging to sensitive cells of the body such as the lens of the eye, causing a heightened risk for cancer and cataracts. An estimated medical risk for astronauts in space is uncertain without an understanding of the effects of ionizing radiation. The lens of the eye includes two distinct cell types. Nucleated epithelial cells differentiate as they approach the equator of the lens, losing their nucleus and other organelles while becoming fully differentiated fiber cells. An internal circulation of fluid and ions flows away from the center of the lens at the equator, through connexons, and then inward at the poles, creating a current that washes the cells in essential solutes and metabolites. Connexons are molecular aggregates of intercellular channels between cells composed of a pair of hexameric assemblies of integral membrane proteins belonging to the connexin (Cx) family. Three connexins are expressed in the mammalian lens: Cx43 (α1) is predominant in epithelial cells, Cx46 (α3) and Cx50 (α8) are more prevalent in fiber cells. To examine the specific role of Cx50 during normal cell growth and differentiation after radiation exposure, human lens epithelial (HLE) cell cultures were irradiated with 4 and 0.5 Gy 600 MeV/amu Fe ions at Brookhaven National Laboratory and processed for immunofluorescence, RNA and protein. The cells were fixed for immunofluorescence at varying times, post-irradiation, using 4% paraformaldehyde. Cx50 was identified using secondary antibodies conjugated to red Cy3. A Zeiss Axiovert 200M immunofluorescent optical microscope was used to digitally capture fluorescent images. Additionally, protein lysates were separated using SDS-PAGE and analyzed with a Western blot. The irradiated HLE cells demonstrated increased expression of Cx50 protein within 5-7 hours after exposure as evidenced by immunofluorescence and Western analysis. However, this effect is not significant after a similar 0.5 Gy exposure time course. Since Cx50 is more prevalent in lens fiber cells, the radiation-induced increase in Cx50 in HLE cells may be linked to an aberrant induction of differentiation. Increased expression of Cx50 may play a role in the effects of radiation exposure experienced by astronauts in space.

Skin & Hair Development: Examining the Role of Tg737, Kif3a, & the Primary Cilium. *MICHAEL MILLER (Albion College, Albion, MI 49224) EDWARD J. MICHAUD (Oak Ridge National Laboratory, Oak Ridge, TN 37831).* The primary cilium is an organelle that is found singly on the surface of most vertebrate cell types. The primary cilium functions as a cellular antenna, receiving both mechanical and chemical signals from neighboring cells. This organelle plays a critical role in the development and function of many mammalian organ systems, as exemplified by mutations in Tg737 and Kif3a, two genes needed to build the primary cilium. Previous work has also shown that mutations in the Tg737 and Kif3a genes alter the Sonic hedgehog (Shh) and Wnt signaling pathways, which are vital to the development of many organ systems, including the skin and hair follicles. Additionally, uncontrolled activation of the Shh and Wnt pathways causes a variety of cancers, including basal cell carcinoma (BCC) of the skin, which is the most common form of human cancer. Here mice with a hypomorphic mutation in Tg737 or a conditional mutation in Kif3a were utilized to examine the roles of these two genes in skin and hair follicle development. Specifically, quantitative real-time PCR (QRT-PCR) was used to examine the expression profiles of Shh and Wnt pathway genes in the skin of the mutant mice. By using a statistical analysis program and comparing each mutant mouse to its wild-type littermate control, relative gene expression levels were determined. The results demonstrate that both mutations altered Shh signaling; however, they affected the pathway at two different levels. In the Tg737 mutant, the Ptch1, Gli1, and Gli3 genes were down-regulated, but the Shh and Gli2 genes were unaffected. In the Kif3a mutant, the Shh, Gli1, and Gli3 genes were down-regulated, but the Ptch1 and Gli2 genes were unaltered. In the Wnt pathway, four different genes were studied. Catnb, an activator of the pathway, was not significantly affected in the Tg737 mutant but was down-regulated in the Kif3a mutant. Lef1, a repressor of the pathway, was down-regulated in both mutants. However, Ccnd1 and Myc, two genes activated by the Wnt pathway, were normal in both mutants. Taken together, these results demonstrate that the Shh and Wnt pathways are altered in the skin of Tg737 and Kif3a mutant mice. As the next step, in situ hybridization, immunohistochemistry, and immunofluorescence microscopy will be performed to complement the present results. Ultimately, the goal of this study is to determine the function of primary cilia in skin and hair follicle development, as well as the mechanisms involved in BCC.

The Effect of PAHs and PCBs on Eelgrass (*Zostera marina L.*) Growth. *RACHEL MOFFITT (Yakima Valley Community College, Yakima, WA 98903) RON THOM (Pacific Northwest National Laboratory, Richland, WA 99352)*. Despite the importance of eelgrass (*Zostera marina L.*) in improving water quality and as an ecosystem, little is known about how eelgrass meadows respond to indirect human impacts such as climate change and increases in nutrients, pollutants, and water temperature. The effects of light availability on the plants, including how epiphytes can reduce the amount of light available to eelgrass, is well understood. Long term monitoring of eelgrass may help us understand how indirect impacts such as pollution affect the meadows and to observe the natural dynamics of the meadow. In order to observe how the meadows can change from one year to the next, an eelgrass meadow (Site A) in Sequim Bay near the Pacific Northwest National Laboratory (PNNL) Marine Sciences Laboratory (MSL) was monitored for growth. To determine the impact of organic chemical pollutants on eelgrass, another site within the meadow was used as a control (Site B) and growth was measured for it, two experimental tanks (containing organic pollutants of PAHs (polynuclear aromatic hydrocarbon) and PCBs (polychlorinated biphenyls) and eelgrass transplanted from Site B), and also a control tank. Samples were marked and harvested at two-week intervals at low tide from June to August 2005. Growth was determined by dry weight samples of new leaf material and compared between sites. Site A was also compared to previous data from the site collected since 1991 [1]. Epiphytic mass and light attenuation were also measured for their impact on the sampling locations. Site A had a higher growth rate than Site B, but Tank 3 had the highest average growth rates, while Tank 2 had the lowest. Site B appeared to be affected by epiphyte levels, which were higher by weight than for any other sampling location. The growth in the eelgrass tanks were primarily affected by light, due to the use of different light sources, some with lower intensity than others. In general, the organic pollutants do not appear to have affected the growth in either experimental tank.

BDE-47 Metabolism and Effects on Fecundity in Japanese Medaka (*Oryzias latipes*) and Fathead Minnows (*Pimephales promelas*). *ELISABETH MUIRHEAD (University of Puget Sound, Tacoma, WA 98416) IRVIN SCHULTZ (Pacific Northwest National Laboratory, Richland, WA 99352).* Brominated diphenyl ethers (BDEs) are commonly used flame retardants in textiles, electronics, plastics and paints. Environmental concerns associated with release of BDEs has increased due to structural similarities with polychlorinated biphenyls and reported toxic effects, which include disruption of the endocrine/thyroid system. In this study, the kinetics of BDE in Japanese Medaka (*Oryzias latipes*), an organism that is being used increasingly as an alternative animal model for testing the chronic toxicity of chemicals, were examined, along with the effect of repeated oral exposure to BDE on reproductive performance in Fathead minnows (*Pimephales promelas*). Medaka and fathead minnows were orally exposed to BDE-47 by bioencapsulation in brine shrimp, *Artemia sp.* For the Medaka studies, a single oral exposure was administered followed by termination at specific timepoints. Pair-breeding fathead minnows were given daily BDE-47 exposures that were continued for 25 days, during which daily fecundity was measured as an indicator of reproductive performance. In Medaka studies, measurable levels of BDE-47 were detected in the carcass within 0.25 hr with peak levels occurring at 8 hrs. The body levels of BDE-47 slowly declined and were still 25% of

peak levels at 624 hrs after dosing. The BDE 47 concentration-time profile was fitted to a one-compartment clearance-volume toxicokinetic model; the model-predicted values for elimination half-life was determined to be 281 hrs. In the fathead minnow reproductive study, egg laying in the BDE-treated breeding pairs stopped after 10–11 days. Cumulatively, the results of these two studies suggest that it will be increasingly important to predict the kinetic behavior of BDEs, as well as the effects of BDE accumulation in wildlife, to begin to consider regulatory constraints on production and use that avoids toxic overexposure.

Nanoplasmonic Molecular Ruler for DNA-Protein Interaction. *BIPASHA MUKHERJEE (University of California Berkeley, Berkeley, CA 94720) FANQING CHEN (Lawrence Berkeley National Laboratory, Berkeley, CA 94720).* One of the major challenges of quantitative biochemistry and molecular biology is to monitor enzymatic activity within a femtoliter volume in real time. We have constructed a novel nanoscale plasmonic probe-based molecular ruler, which can perform label-free, real-time, and sensitive monitoring of DNA length during nuclease enzymatic reactions. The bionanoplasmonic molecular ruler was fabricated by tethering specificly-designed double-stranded DNA to single Au nanoparticles. Nuclease enzymatic activity was tracked via the evolution of the plasmon signal of a single Au-DNA nanoconjugate, which reflects DNA size changes introduced through site-specific DNA digestion by endonuclease. The scattering spectra of individual Au-DNA nanoconjugates are measured continuously in real time during nuclease incubation. The scattering spectra of Au-DNA nanoconjugates show a blue-shift of the plasmon resonance wavelength, as well as decrease in intensity and a time-resolved dependence on the reaction dynamics. With a series of enzymes that generate DNA incisions at different sites, the shifts of the plasmon resonance wavelength are observed to correlate closely with the positioning of the nuclease-targeted sites on the DNA, demonstrating DNA axial resolution in nanometer precision (5 nm of wavelength shift per nm of DNA length change, or 1.4 nm wavelength shift per base pair difference). DNA length differences of as little as 2 nm (6 base pairs) after nuclease digestion are differentiated by the corresponding plasmon resonance shifts of the Au-DNA nanoconjugate. Based on the mapping relationship between the DNA length and the plasmon resonance wavelength of the nanoconjugate, we further develop the nanoparticles into a new DNase footprinting platform. This DNase footprint mapping is demonstrated through the binding of DNA repair enzyme XPG to DNA bubbles. This work promises a novel molecular ruler that can monitor nuclease enzymatic reactions with single-particle sensitivity in real-time. It suggests the possibility of developing ultra-high density nanoarrays for parallel enzyme activity measurement in functional proteomic studies or biofunctional nanoprobe for intracellular enzymatic studies.

Preparation, Purification, and Crystallization of ORFan Proteins from Pathogenic Bacteria. *ELIZABETH OSTRANDER (University of Missouri, Columbia MO 65211) STEPHEN R. HOLBROOK (Lawrence Berkeley National Laboratory, Berkeley, CA 94720)*. Open Reading Frame orphan proteins (ORFans), proteins unique to a single organism or close family members, are potential targets for new drug therapies such as inhibitors designed to interfere with the roles of enzymes essential to the life cycle of infectious bacteria. Lacking sequence homology with other proteins, ORFans of unknown function can be crystallized and subjected to X-ray diffraction to determine their structure and thereby infer their function. We targeted two ORFans: MPN675 a member of the PFAM protein family denoted as “Domain of Unknown Function 16” found only in Mycoplasma pnuemoniae; and BA2578, a Nucleotide Diphosphate linked to X (Nudix) hydrolase of unknown function found only in Bacillus anthracis and close relatives. A selenomethionine derivative of MPN675 was successfully purified through a two-step process of metal affinity chromatography and ion exchange chromatography. Initial crystals of the purified derivative were obtained and diffracted to a resolution of 4.2Å. Data from this crystal as well as native and samarium derivative crystals are being analyzed in order to obtain phases and thereby solve the protein structure. Growth experiments using different *E. coli* background strains determined the induction conditions most suitable to obtaining expression of BA2578. The strain BL21-AI induced at 37°C with arabinose and isopropyl ß-D-1-thiogalactopyranoside (IPTG) gave the least amount of background expression. BA2578 was localized and enriched in the insoluble fraction. Solubilization and purification experiments are in progress.

PyMOL Made EZ - A Tool for Simplifying Molecular Viewing in PyMOL. *CHRISTOPHER PARKIN (Rochester Institute of Technology, Rochester, NY 14623) LEN SLATEST (Brookhaven National Laboratory, Upton, NY 11973).* PyMOL is a molecular modeling program that can be used in a wide range of studies within the scientific community. Its ability to produce informative, detailed, stereoscopic images makes it a very powerful tool both in the laboratory and in the classroom. However, the PyMOL user interface is difficult to use and its “development has been focused on capabilities, not on ease-of-use for new users.” (PyMOL Users Manual) To resolve this, we set out to develop a new interface for PyMOL that can be installed as a plugin and helps to eliminate the need for command line interactions, making it a much more user-friendly interface. Using tools from Python’s Tkinter and PMW toolkits, we created a tabbed interface called PyMOL Made EZ. The interface contains a series of buttons and entry fields that allow users to select given attributes of a molecule and make changes to it with the click of a button as opposed to issuing highly syntactical commands. Other features of the interface include a Chime/PyMOL command converter, nine preset molecular views, four molecular movies, and molecular sequence and hetero atom information all at the click of a button. The ongoing and continued development of PyMOL Made EZ could help to further the use of PyMOL which we believe to be one of the most powerful molecular viewing programs currently available.

Phytoremediation Potential of *Arabidopsis thaliana* for Soil Contaminated with Chromium and Arsenic Heavy Metal Stressors. *ALEXANDER PATANANAN (University of California Los Angeles, Westwood, CA 90095) K. PRASAD SARIPALLI (Pacific Northwest National Laboratory, Richland, WA 99352)*. With increases in heavy metal contamination due to industry and agriculture occurring worldwide, the use of plants to phytoremediate polluted environments have become a cost-effective and efficient alternative to mechanical equipment. Data acquired by two-dimensional gel electrophoresis and mass spectrometry from *Arabidopsis thaliana* exposed to chromium and arsenic heavy metal stressors was analyzed with PDQuestTM protein database computer software. The results provide strong arguments for site-specific activation and deactivation of proteins associated with environmental stresses. Substantial alterations in protein abundance occurred on the two-dimensional gel electrophoresis (2-DE) protein samples for arsenic at comparable standard spot positions (SSP) 120 and 6406. Proteomic data for SSP 2006 and 3006 were erratic in trend for chromium and were therefore inconclusive. In response to adding 100, 250, and 750 ppm excess heavy metal contaminants in the plant’s soil, two remediation processes can occur. Either glutamylcysteinylglycine (GSH) molecules neutralize the metals or phytochelatins are produced, which transport the toxins to a vacuole within the cell where they are stored in a nontoxic form until later use. A more intense analysis of different environmental stresses on plants are predicted to reveal a global species of protein responses, suggesting that microarrays and mass spectrometry assays may lead to genetic and protein engineering of plants for rapid phytoremediation purposes.

Design and Operation of a Continuous Flow Bioreactor to Determine the Effect of Growth Conditions on Monooxygenase Expression by Methanotrophic Bacteria. *CHUCK PEPE-RANNEY (Colorado School of Mines, Golden, CO 80401) DEBORAH NEWBY (Idaho National Laboratory, Idaho Falls, ID 83415).* Methane monooxygenase (MMO) shows promise for use in biocatalysis because of its broad substrate range. MMO is produced by methanotrophic bacteria and allows the bacteria to utilize methane as both a carbon and energy source. This research project involved designing and operating a continuous flow bioreactor to determine the effect of growth conditions on monooxygenase expression by methanotrophic bacteria. Understanding MMO expression under various growth conditions will allow for more efficient biocatalysis with MMO. A bioreactor consisting of a 1 L vessel, mixing impeller, sparger, media inlet and outlet, and gas outlet was assembled. The bioreactor was continuously sparged with 25% methane in air at approximately 350 mL/min. Within the reactor, Methylosinus trichosporium OB3b was grown to log phase under batch conditions in a total volume of 500 mL. Once the culture reached log phase, the bioreactor was converted to continuous flow and brought to steady state. Copper-free nitrate mineral salts medium was pumped into the reactor while reactor contents were pumped from the vessel at the same flowrate. Biomass was monitored via optical density measurements to verify steady state was achieved and sustained. The bioreactor maintained constant biomass when the influent and effluent flowrates were approximately 13 mL/hour. Samples were periodically collected and analyzed for enzymatic activity; however, not enough data has been collected to report any meaningful enzymatic activity results. Future research will involve changing growth conditions and monitoring the enzymatic response as well as monitoring MMO gene expression using molecular techniques. Research done with this bioreactor will

ultimately aid in the operation of a methanotrophic bioreactor for the production of value added chemicals.

Phytoremediation Potential of *Arabidopsis thaliana* for Soil Contaminated with Chromium and Arsenic Heavy Metal Stressors. *JACOB PHILLIPS (Roane State Community College, Harriman, TN 37748) K. PRASAD SARIPALLI (Pacific Northwest National Laboratory, Richland, WA 99352)*. With increases in heavy metal contamination due to industry and agriculture occurring worldwide, the use of plants to phytoremediate polluted environments have become a cost-effective and efficient alternative to mechanical equipment. Data acquired by two-dimensional gel electrophoresis and mass spectrometry from *Arabidopsis thaliana* exposed to chromium and arsenic heavy metal stressors was analyzed with PDQuestTM protein database computer software. The results provide strong arguments for site-specific activation and deactivation of proteins associated with environmental stresses. Substantial alterations in protein abundance occurred on the two-dimensional gel electrophoresis (2-DE) protein samples for arsenic at comparable standard spot positions (SSP) 120 and 6406. Proteomic data for SSP 2006 and 3006 were erratic in trend for chromium and were therefore inconclusive. In response to adding 100, 250, and 750 ppm excess heavy metal contaminants in the plant's soil, two remediation processes can occur. Either glutamylcysteinylglycine (GSH) molecules neutralize the metals or phytochelatins are produced, which transport the toxins to a vacuole within the cell where they are stored in a nontoxic form until later use. A more intense analysis of different environmental stresses on plants are predicted to reveal a global species of protein responses, suggesting that microarrays and mass spectrometry assays may lead to genetic and protein engineering of plants for rapid phytoremediation purposes.

Relative Comparison of mRNA Concentration of Target *E.coli* Membrane Proteins Through Real-Time PCR. *YURI POLUEKTOV (University of Illinois at Urbana-Champaign, Urbana-Champaign, IL 61801) PHILIP D. LAIBLE (Argonne National Laboratory, Argonne, IL 60439*). Real-time PCR is a very efficient way to measure the amount of starting DNA template in a PCR reaction relative to another PCR reaction. It is a very sensitive method that can detect up to a 2-fold difference in the concentration of DNA template between two PCR reactions. And it can work with as much as 10pmol of DNA to produce conclusive results. This method was used to determine the relative concentrations of mRNA, upon transcription into cDNA, of membrane proteins that could be detected using western blots versus ones that could not. Although this experiment would not be able to tell us why certain membrane proteins fail to be expressed in *Rhodobacter (R.) sphaeroides* cells while others do not, it would be able to tell us what part of the protein expression process the problem occurs in. For this purpose 10 *R. sphaeroides* cultures were processed, 5 that contained plasmids with target *E.coli* membrane proteins that were detectible with western blots and 5 that were not. In addition to the experimental cultures 2 more *R. sphaeroides* cultures expressing ß,α light harvesting complexes were processed to serve as controls. One of the cultures was grown just like the experimental cultures while the other one was grown aerobically. Using the fact that the ß,α light harvesting complexes have an absorption peak at 875 nm, it was determined that the culture grown aerobically did not express the light harvesting complexes and so it should probably have a very low concentration of ß,α mRNA. Strangely enough the Real-Time PCR did not register any difference in mRNA concentration between the aerobic and the unaerobic cultures, which suggests that there is some other mechanism along the lines of translation and protein degradation that inhibits the expression of the light harvesting complexes. The experimental cultures, however, did register a 2-fold difference in mRNA concentration between the non-expressing and the expressing membrane proteins. Although this indicates that transcription is involved in the failure of certain membrane proteins to express, it also tells us that there is a more extensive mechanism that prevents those proteins from being expressed. Perhaps the real problem lies within translation and protein degradation.

A Suicide Plasmid System for Targeted Gene Deletion in *Shewanella oneidensis* MR-1 utilizing a cre-lox Based Recombination Method. *ANGELA REEVELY (Tuskegee University, Tuskegee, AL 36088) SOUMITRA BARUA (Oak Ridge National Laboratory, Oak Ridge, TN 37831).* The versatile respiratory capabilities of the Gram-negative facultative anaerobic bacterium *Shewanella oneidensis* MR-1 cause it to be at the height of environmental interest for purposes of developing new bioremediation strategies for removing toxic chemicals and pollutants from groundwater. *S. oneidensis* is a metal-ion reducing bacteria that can convert nitrate to ammonium and soluble forms of Uranium and Chromium to a reduced and insoluble form. The Shewanella Federation, which includes the DOE's Oak Ridge National Laboratory, is presently conducting a comprehensive study of the sequenced genome *S. oneidensis*. The protocol for research included setting up a suicide plasmid system for targeted gene deletion in *S. oneidensis* MR-1 utilizing a cre-lox based recombination method. A pJK102 suicide plasmid was prepared involving PCR amplification and cloning of the N' and C'-terminal flanking regions of the targeted deleted gene in separate reactions. PCR purified restriction digests of both the N'and C'-terminal inserts were ligated in the respective restriction enzyme digested pJK100 in separated reactions. Screenings of KmR/TetR colonies of *Escherichia coli* containing pJK102 suicide plasmids with the correct size insert were tested and reviewed by PCR. This suicide plasmid was then moved from the DAP (diaminopimelic acid) auxotroph *E. coli* to *S. oneidensis* MR-1 through conjugation. The resultant MR-1 strain is KmR/TetS which contains the loxP-KmR-loxP cassette. Then another cre-recombinase enzyme producing plasmid, pCM157/TetR was moved into the MR-1 strain to resolve the loxP-KmR-loxP cassette through conjugation. Finally, the TetR plasmid pCM157 was cured from the *S. oneidensis* MR-1 by conducting a three to four day continuous culture in non-selective rich Luria-Bertani medium. The c-type cytochrome genes of MR-1 were targeted and obtained mutant strains of SO0479 and SO4484. These constructs will be used to explore the versatile metabolic capability of this organism. The goal of this research is to understand the function of these multiple c-type cytochrome genes of *S. oneidensis*. Future efforts will continue to correlate the function of these c-type cytochrome genes on bioremediation strategies for removing toxic chemicals and pollutants from groundwater.

Folate Receptor Binding nanoparticles Targeted Against Ovarian Cancer. *SONIA REVECO (Contra Costa College, San Pablo, CA 94806) FANQING CHEN (Lawrence Berkeley National Laboratory, Berkeley, CA 94720).* The Folate Receptor Protein (FR) is found in over 90% of ovarian carcinomas. Ovarian cancer is one of the deadliest types of cancer due to few symptoms until advanced stages. Since the FR has a high affinity for folic acid, nanoparticles can be conjugated with folic acid and targeted specifically to only ovarian cancer cells. The goal of this research was to attach aminated DNA conjugated to folic acid to a dendrimer, and then attach thiolated DNA conjugated to Doxorubicin (a cancer treatment pharmaceutical) to the same dendrimer. Then the dendrimer was to be tested on live cells. After each conjugation, agarose gels were run and then photographed under ultraviolet light. The gel from the conjugation of folic acid to aminated DNA showed a distinctly brighter band. Unfortunately, the gel with the dendrimer and DNA showed no DNA bands under ultraviolet light. The gel with Doxorubicin and thiolated DNA gave inconclusive results. Although the folic acid/DNA conjugation was successful, further testing using radioactive labeling is needed to determine the success of the dendrimer. This work is a portion of a larger project that would use the completed dendrimer to kill only ovarian cancer cells *in vitro* and finally *in vivo*.

Single-Cell Noise Spectrum Analysis for Gene Circuit Characterization. *DAR ROY (The Hebrew University of Jerusalem, Jerusalem, ISRAEL 91904) MICHAEL L. SIMPSON* (Oak Ridge National Laboratory, Oak Ridge, TN 37831). The capability to characterize natural and engineered gene circuits could be beneficial on both academic and industrial fronts by gaining more understanding of intra- and inter-cellular biological processes and structure-function relationships. To explore the frequency distribution of stochastic processes in gene circuits, Green Fluorescent Protein (GFP) expressing gene circuits were constructed on high copy number plasmids in *Escherichia Coli* bacterial cells. Experiments concentrated on two different types of circuits: (1) Non-regulated gene constructs differing in protein degradation rates, and (2) Autoregulated negative-feedback gene constructs where gene expression is repressed by the binding of a repressor protein at an operator site in the promoter. Laser confocal microscopy (Leica SP2) with a 488 nm Ar source was used to acquire 4-8 hour time-series fluorescence data (500-550 nm) from excited bacterium populations. Cell doubling time was controlled by varying growth temperatures. Single-cell fluorescent output was extracted from microscopy images by tracking individual cells using computer-imaging software to calculate mean pixel intensity. GFP noise was defined as this output's deviation from the population's mean fluorescence. A common reference point from calculated biased Autocorrelation Functions (ACFs) for this time-series noise data (time lag at which the ACF decayed by ½) was used as a measure of noise bandwidth (Fnbw) for gene circuits. An increase in Fnbw with decreasing cell doubling time was observed for all the gene constructs. In addition, an increased bandwidth of about two-fold was seen for the autoregulated

gene circuit as opposed to the unregulated circuit. This increase in bandwidth was predicted by a previous theoretical study for these gene circuits and is consistent with negative feedback theory. Additional spectral measurements and model interpretation may reveal significant information on enzyme kinetics, feedback mechanisms, and kinetic parameter fitting of these gene circuits. Ultimately the physical sciences approach to biological systems may be at the forefront of molecular-scale engineering and help enhance the biologist's tools for discovering underlying structure of gene circuits and networks.

Utilizing DNA Microarray Technology for the Analysis of Gene Expression Changes Between Normal and Tumor Human Kidney Cells. *NICOLE SADLER (University of California Davis, Davis, CA 95616) CHITRA F. MANOHAR (Lawrence Livermore National Laboratory, Livermore, CA 94550)*. DNA Microarray Technology is a remarkably powerful tool for the study of various physiological processes and cellular mechanisms. It is now possible to analyze the expression of over 25,000 genes using the information from the 2003 sequencing of the Human genome. The genetic blueprint, or genome, of a cell defines the patho-physiology of a cell and can provide insight into downstream health implications. With nearly 1.4 million new cancer cases and 500,000 cancer related deaths annually in the U.S. alone, a greater understanding of the differences in genetic processes between normal and cancerous cells is dire. Tumor formation is the first stage in the progression of cancer. In this study, to better understand the differences between normal and tumor kidney cells, gene transcript profiles were analyzed using DNA Microarray Technology. Each gene can be correlated to gene transcripts (mRNA) in a cell. Gene transcript profiles are unique for different cell types. The quantity of each transcript in normal and tumor cells was measured using the mRNA from seven pairs of microarray experiments. Biotin reporter tags were incorporated into the processed mRNA molecules, and the tagged molecules bind to precise DNA spots that are complementary on the GeneChip®. Gene transcripts derived from normal and tumor samples from the Hoag Hospital were analyzed using DNA Microarray Technology. Microarray experiments were performed at the LMAC using in-house validated protocols. Quality control experiments were conducted on all RNA samples, and the RNA was linearly amplified, labeled, and fragmented. The samples were then hybridized onto GeneChip® Human Genome U133 Plus 2.0 arrays overnight, washed the following morning and scanned with a laser scanner. The data is currently being analyzed to identify gene transcript markers aberrantly regulated in kidney tumor cells using LMAC statistic and bioinformatics procedures. Scatter plots from the raw data comparing control versus experimental samples indicated differences in gene expression in many genes between the control and experimental samples, and those comparing two control groups indicated few gene expression differences. It is not hard to visualize that newer tools of biological measurement like DNA Microarray Technology will enable personalized medicine in the future.

Comparisons of Solvent Effects on Horseradish Peroxidase Stability. *JONATHAN SALAZAR (New Jersey Institute of Tech, Newark, NJ 07102) A.J. FRANCIS (Brookhaven National Laboratory, Upton, NY 11973*). Enzymes can function as catalysts in non-aqueous solvents containing little or no water. This provides many advantages, such as increasing substrate solubility, shifting of thermodynamic equilibria and improving enzyme stability. Ionic liquids have been considered potentially environmentally friendly solvents because of their unique properties, and more importantly, have been shown to be effective co-catalysts. This research explores the different solvent effects (hydrophilic and hydrophobic properties) on enzyme stability, and compares the effects of ionic liquids with a conventional organic solvent. It also provides data that can lead to new opportunities of bio-catalysis in ionic liquids. Horseradish peroxidase (HP) was chosen in this study for its broad applications in industry and organic synthesis. HP was incubated in different solvent systems, containing different concentrations of acetone, 1-butyl-3-methyl imidazolium hexafluorophosphate ([BMIM]PF_6), or ethylpyridinium tetrafluoroborate ([EtPy]BF_4) Enzyme activities were monitored by spectrophotometric methods for 48 hours.

Proteomic Analysis of *Phanerochete chrysosporium's* Pelleted and Filamentous Fungal Morphologies. *AARON SCHNEBLY (Eastern Arizona College, Thatcher, AZ 85552) ELLEN PANISKO (Pacific Northwest National Laboratory, Richland, WA 99352)*. The white-rot fungi *Phanerochaete chrysosporium* is one of the only organisms able to completely degrade lignin, a main component of plant cell walls. This wood fungi has great potential to decompose biomass as an alternative source of energy, chemicals, and enzymes for industrial applications. Proteins produced by pelleted (yeast like) and filamentous morphologies were compared in an attempt to find differences in protein production. These different morphologies were induced by changing glucose concentrations in liquid media cultures. The cells were broken with liquid nitrogen and processed with several buffers. 2-Dimensional gel electrophoresis and mass spectrometry were used to analyze the proteins produced. The 2D gels showed completely different protein expressions for the two growth types. Variables to study in the future include incubation time, temperature, and different chemical levels within the media. Such changes could stimulate the production of other desirable enzymes and provide valuable insight into what genes are responsible for them.

A Comparative Study of *Shewanella oneidensis* Cytosol Proteins in Cells Grown in Aerobic and Anaerobic Environments. *CAMILLE SMITH (Hampton University, Hampton, VA 23668) CAROL GIOMETTI (Argonne National Laboratory, Argonne, IL 60439). Shewanella oneidensis* is a facultative microorganism with metal-ion reducing capabilities that function under anaerobic conditions. The microbe has the potential to remove toxic metals and pollutants from the environment and, thus, is considered a possible bioremediation agent. To further understand the capability of this microbe to live in different growth environments, an investigation was developed to analyze the protein changes in *S. oneidensis* grown with and without oxygen as an electron acceptor. Using the two-dimensional electrophoresis system (2DE), we evaluated the protein content after different growth conditions. We also compared sample preparations done under varying temperatures: refrigerated versus non-refrigerated. The different sample preparation methods had no effect on the appearance of proteins in the patterns of the seventeen centimeter silver nitrate gels; the patterns were indistinguishable. By comparing the images using a software program specifically designed for analysis of 2DE patterns, Progenesis, the proteins from cells grown with or without oxygen were examined for significant differences. We used mass spectrometry to identify the protein content of the cytosol samples. In classifying the proteins the metabolic shifts from oxygen to oxygen-free were recognized. By displaying the changes in intensities from the proteins their appearances decreased, increased, or disappeared and this showed a major separation between the aerobic and anaerobic growth patterns.

Multiple-Locus Variable-Number Tandem Repeat Analysis (MLVA) in *Bacillus anthracis*. *CHAD SMITH (Merced College, Merced, CA 95348) SHARON L. MESSENGER (Lawrence Livermore National Laboratory, Livermore, CA 94550)*. Anthrax, caused by the bacterium *Bacillus anthracis*, is a serious disease that if used in a biocrime or bioterrorism incident could cause widespread illness in any community. The anthrax letters of 2001 awoke the United States to the realization that a bioterrorism attack could occur in our country and demonstrated the need to rapidly identify the source of production and route of distribution for biothreat agents. Historically, *B. anthracis* strains have been difficult to differentiate due to the overall similarity within the genome. Multiple-Locus Variable-Number Tandem Repeat Analysis (MLVA), however, differentiates among most *B. anthracis* strains. Within *B. anthracis* strains there are unique Variable-Number Tandem Repeats (VNTRs) that are short sequences repeated numerous times within genomic regions. The varying number of these repeats enables differentiation among strains. In order to type these VNTRs within the DNA of each *B. anthracis* strain PCR is used to amplify eight loci (vrrA, vrrB1, vrrB2, vrrC1, vrrC2, CG3, pX01, pX02) containing these VNTRs. Agarose gel electrophoresis is used to qualitatively analyze the amplicons created by each locus. Fragment analysis by acrylamide gel electrophoresis is used to accurately size the VNTRs fragments at each of the eight loci based upon the fact that each *B. anthracis* strain will exhibit variation in the number of tandem repeats present at each locus. By analyzing the pattern of fragment sizes at the eight loci enables a genetic profile or "fingerprint" of each known *B. anthracis* strain to be made. This genetic typing system allows investigators to potentially trace the source of the *B. anthracis*. This technique provides a useful tool for forensic investigation and has been employed in the ongoing investigation of the anthrax letters sent out in 2001.

Stereoscopic Imaging of Scanning Electron Micrographs. TIMOTHY SMITH (Nassau Community College, Garden City, NY 11530) JOHN SPILETIC (Brookhaven National Laboratory, Upton, NY 11973). Scanning electron micrographs exhibit three-dimensional qualities due to the high depth of field inherent in the use of the scanning electron microscope (SEM). Using the program Stereo Photo Maker, we have attempted to render these micrographs viewable in three dimensions. For this to be accomplished, a routine procedure was developed that permitted movement from trial-and-error to a method that yields consistent results. As in conventional photography,

creation of a stereoscopic image using the SEM requires a left-eye and right-eye image. SEM stage controls permit sample movement in the X and Y axis, 360 degree rotation, and a tilt of 90 degrees toward and 15 degrees away from the signal detector. Images were captured using successive 2.5 degree increments, horizontal and vertical shifting, and sample rotation. Since rotation could not be measured directly, the SEM-generated scale bar was used to measure increments depending upon magnification. The resultant two-dimensional images were opened in a software application known as Stereo Photo Maker and combined to form a stereoscopic image based on two images of differing perspectives. In addition to the routine method of generating stereo pairs through sample tilting, other methods were also tested. It was determined that lateral shifting does not allow for the production of a visually satisfying stereo image. Rotation, however, produced three dimensional images of equal quality to that of tilted samples. We find that the greater variation of surface structure a sample has, a higher initial degree of tilt is required. However, the study of many more samples will be needed to verify this hypothesis.

The Effects of Transmitter Size to Fish Body Weight on Transmitter Expulsion and Mortality in Rainbow Trout. *SARAH STABLES (University of Virginia, Charlottesville, VA 22903) RICHARD S. BROWN (Pacific Northwest National Laboratory, Richland, WA 99352*). Acoustic telemetry is used in the Pacific Northwest for tracking salmon migrating up and down stream, including their passage through the many dams along the Columbia River. This type of telemetry on juvenile salmon is fairly new and little research has been conducted on transmitter expulsion and mortality rates in these studies. We chose to study these variables in rainbow trout (*Oncorhynchus mykiss*) because their body structure is similar to that of salmon and they are readily available for lab studies. We are attempting to gather information about fish mortality and tag expulsion rates for juvenile rainbow trout after the insertion of acoustic transmitters into the abdominal cavity. We salvaged 0.65 gram acoustic transmitters from prior studies and inserted them into four groups of fish. The fish were grouped into categories based on the ratio of body mass to transmitter mass. The groups were at transmitter mass percentages of 2, 6 9, and >10, along with a control group that consisted of all 4 sizes. Fish in the control group were not implanted with a transmitter. The study will be long term, possibly lasting up to a few years. The fish were implanted with transmitters on July 21, 2005. As of August 4, 2005, a total of nineteen fish have died in the study. Tag expulsion occurred in eight of these fish, although it is unclear whether the tags were expelled before or after death. Thirteen of the nineteen mortalities (68%) occurred in the group with the smallest fish (>10%). The other six deaths occurred in the 9% and 5% groups, while the fish in the control and 2% group experienced no mortality or tag expulsion. We expect that the majority of deaths occurred in the >10% group due to the smaller abdominal cavity in these fish. Since there is less room for the transmitter, more pressure is put on the incision wound and internal organs. This pressure often resulted in tag expulsion at the incision wound or death. Previous studies on tag expulsion in salmon and rainbow trout suggest using tags that take up no more than 2% of fish body weight. However, since little research has been conducted in this field, more testing on transmitter expulsion may prove otherwise. If scientists find that salmon can hold transmitters that take up more than 2% of their body mass, tracking studies may benefit greatly. Scientists could then use smaller fish in studies and also conduct longer studies due to the ability to increase battery size.

Live Cell FT-IR Spectroscopy of Macrophage Response to Endotoxin. *JUSTINA TAM (University of Arizona, Tucson, AZ 85721) TOM WEBER (Pacific Northwest National Laboratory, Richland, WA 99352)*. Fourier transform infrared spectroscopy coupled with attenuated total reflectance (FT-IR/ATR) has sufficient sensitivity to identify and measure chemical alterations of a cellular system following exposure to environmental agents. In this study, FT-IR/ATR measurements of the ensuing apoptotic response to lipopolysaccharide (LPS) were investigated using murine macrophage cells (RAW 264.7) maintained on a zinc selenide (ZnSe) ATR crystal. To decrease the time required for cell attachment to the ZnSe crystal, the adhesion molecule fibronectin was used as a coating on the ZnSe crystal. This shortened the attachment time to 1 day, whereas it had previously been as long as 6 days. The conundrum surrounding fibronectin use was the fear the fibronectin would cause the cells to sit higher than 1 μm which might place them above the sensing zone of the evanescent field and hence would provide no spectroscopic signal. Results using fibronectin mirrored the results obtained from the earlier studies not employing fibronectin, thus indicating that the fibronectin coating is thin and does not cause the cells to sit more than 1 μm above the ZnSe crystal. FT-IR/ATR spectroscopy was then used to examine the spectroscopic signatures of the murine macrophages before LPS treatment and 2, 4, 6, 8, and 24 hours following LPS treatment. LPS treatment induces the activation of the macrophages to produce iNOS and COX-2, which through inflammatory pathways leads to apoptosis of the macrophage. In particular, spectral changes were apparent at 1,575 cm^{-1}, 2,925 cm^{-1}, and 1,034 cm^{-1}, indicative of alterations in cellular components Amide II proteins, lipids, and sugars, respectively. Visualization of the cell death response of the murine cells to LPS treatment also was supported through immunofluorescence microscopy imaging. Our results indicate that FT-IR/ATR spectroscopy can be used to investigate live cell responses to environmental toxins.

Environment, Health, and Safety: Issues Related to Exposure to Beryllium of Electronics Workers and Occupational Noise Exposure. *KANDACE TAYLOR (Strayer University, Chesapeake, VA 23320) PATRICIA HUNT (Thomas Jefferson National Accelerator Facility, Newport News, VA 23606)*. Jefferson Lab is charged with providing employees with a safe and healthful workplace. Beryllium exposure and occupational noise exposure are two issues monitored by the Environment, Health and Safety Department (EH&S). Conducting a beryllium inventory, using Product Specification Sheets, is necessary when examining and implementing safety procedures for handling electronic articles. Electronic components Product Specification Sheets were evaluated for beryllium by contacting manufacturers by phone and email. There were "articles," beryllium components, at Jefferson Lab. Safety procedures for handling articles will be updated into the EH&S Manual. Data was categorized to focus and implement safety procedures related to beryllium at Jefferson Lab. The occupational noise monitoring includes personal monitoring of staff exposed to noise, and area measurements of noise areas. Two download noise meters were used: octave band dosimeter and personal decibel (dB) noise dosimeter. There were employees exposed to high noise levels, but most were not in excess of 85 decibels, dBA, Occupational Safety and Health Administration (OSHA) set limitations for noise exposure. Annual Monitoring of occupational noise exposure will continue in compliance to Jefferson Lab's (EH&S) Manual. Thomas Jefferson Accelerator Facility will continue to monitor these issues to ensure the health and safety of its employees.

Spore Disruption Analysis and Detection Limit Determination at Low Volume Amplifications Using eTags. *LAUREN TRACY (University of California Berkeley, Berkeley, CA 94720) SHANAVAZ NASARABADI (Lawrence Livermore National Laboratory, Livermore, CA 94550)*. In the post 9/11 world the threat of bioterrorism attacks in public venues has ignited a demand to develop a cost effective autonomous pathogen detection system capable of detecting the multitude of biological agents that can pose a threat to public safety. The major cost of such a pathogen detection system is the large volume of reagents it must expend. With the goal of reducing the reagent consumption, and therefore cost, of a pathogen detection system, we used the bacteria *Bacillus globigii* (Bg) as a surrogate for the pathogen *Bacillus anthracis* (anthrax) to determine the lowest amplifiable volume and concentration of amplified sonicated and unsonicated Bg spores that would still be detectable using capillary electrophoresis. We created a serial dilution of unsonicated Bg spores ranging in concentration from 10^8 to 10^1 cfu/mL. From each of these unsonicated spore dilutions we formed three aliquots that were sonicated to disrupt the spores. These sonicated aliquots were analyzed alongside the unsonicated spore samples for each dilution at reaction volumes of 25, 10, and 2 μL. All samples were amplified through a polymerase chain reaction (PCR) in the presence of small fluorescent molecules known as electrophoretic tags (eTags), which were analyzed with capillary electrophoresis to detect the presence of certain nucleic acid signatures. Using this process, Bg samples with concentrations as low as 10^1 cfu/mL and total reaction volumes of amplification as small as 2 μL were readily detectable. Interestingly, detection was more consistent for Bg samples with initial spore concentrations between 10^6 and 10^3 cfu/mL, with the higher and lower concentrations yielding less compelling results. The volume of the sample also affected the efficacy of detection, with detection for 2 μL samples compromised in relation to 25 and 10 μL samples. Detection of sonicated Bg spores appeared to be just as efficient as detection of unsonicated Bg spores. This work is a small portion of a larger project being researched at LLNL and Sandia National Laboratory to develop a low cost briefcase size autonomous detector for small-scale 24/7 detection of a variety of common biothreat agents.

Structural Analysis of Helical RNA. *CHARLES TREATMAN (Oberlin College, Oberlin, OH 44074) STEPHEN R. HOLBROOK (Argonne National Laboratory, Argonne, IL 60439)*. Gene regulatory networks are essential in understanding and manipulating cells. However, there

exists no tool for testing the validity of inference algorithms used to infer GRNs from experimental gene expression data. We have created three Java modules to create artificial networks, generate perturbation sets for those networks, and use perturbation data to infer the topology of the original artificial network, all three modules working on a single relational database.

Western Analysis of the Effects Cadmium has on Expression of CRY61 in Osteoblast and Osteoclast Cell Lines: New Insights into the Mechanism by Which Cadmium Might Lead to Osteoporosis. *MARYN VALDEZ (University of Maryland, College Park, MD 20742) MARYKA H. BHATTACHARYYA (Argonne National Laboratory, Argonne, IL 60439*). Cadmium (Cd) is a natural metal that has been shown to cause bone loss, sometimes drastically, which was the case in Japan, when it was leaked into the Jinzu River and caused an extreme case of osteoporosis/osteomalacia. The mechanism by which Cd causes bone loss has yet to be deciphered. The long-term goal of our research is to determine how Cd causes bone loss. Previous research using micro array analysis methods has found that the gene for Cry61 was greatly upregulated in bone from mice treated with Cd. Cry61 is a secreted Cysteine rich, matrix associated protein. Cry61 interaction with the integrin aVß3 isoform has been shown to lead to adhesion in different cell types. We hypothesize that Cd provokes expression of Cry61 in osteoblast (OB) or osteoclast (OC) cells, which bind to aVß3 integrin located on the surface of OC precursors. The binding activates the precursors, which then can increasingly differentiate into OC, which ultimately leads to bone resorbtion, and eventually to osteoporosis. Here I report specifically on the presence of Cry61 in pre-OB or OC cell lines treated with Cd. We used 7F2 cells lines and RAW cell lines for our OC and OB. We treated the RAW cells and 7F2 cells with Cd, and estrogen, or nothing. After 48 hours and 1hr, we collected the media and cells, than used immunoblotting to confirm the presence of the protein. In our immunoblots we saw very little difference in the bands for each condition in the 7f2 cells and RAW cells. Conversely, we did notice that the control band differed from the Cd band in the media of the RAW cells and 7F2 cells at 48 hours. In the 7F2 media at 48 hours, we observed an increase in band strength in the Cd verses control samples; however, the increase was not as great as that displayed in the RAW cells. Based on those observations, we tentatively concluded that Cry61 is not enhanced in 7F2 or RAW cells by Cd. On the other hand, we hesitantly conclude that Cd may be inducing Cry61 secretion in the media of 7F2 cells. Furthermore, Cd is inducing greater Cry61 secretion into the media at 48 hours for RAW cells. All of these conclusions are provisional; more trials need to be run. Additional time points would also be very enlightening. We would also like to evaluate Cry61 expression on the RNA level or see if, when we add an antagonist, the expression would cease. We need to do further research, but we feel we have made a good first step in elucidating the mechanism by which cadmium causes bone loss.

Selecting Peptide Ligands for Intersectin SH3 A2 using Phage Display and Comparison with Src SH3. *MARQUISHA WASHINGTON (Grambling State University, Grambling, LA 71245) BRIAN KAY (Argonne National Laboratory, Argonne, IL 60439)*. The Src homology 3 (SH3) domain is a unique protein interaction module. The domain is approximately 50-70 amino acids in length and directs protein-protein interactions through the recognition of proline rich sequences. Intersectin (ITSN) SH3 A2 is a human protein cloned into *E. coli* host cells. Our goal was to determine the properties of Intersectin (ITSN) SH3 A2, and determine the identity of the peptides that were selected to bind with it. These peptides were obtained using M13 phage display. After expressing and purifying the protein, affinity selection experiments were performed to select binders for ITSN SH3 A2. The protein was screened against libraries ANL 6 and ANL 7. After three rounds of selections, the phage were plated to obtain plaques. These single plaques were picked and used to perform an ELISA. The results of this experiment are still in progress. After initial testing of the protein, it is believed that the protein was not folded properly; however, experiments are in progress to reclone the gene, and retest for binders.

Use of SDS-PAGE to Determine Protein Variability of Soybean Cyst Nematode Populations in Tennessee. *JACULINE WILGAR (Salt Lake Community College, Salt Lake City, UT 84130) STEVE GOHEEN (Pacific Northwest National Laboratory, Richland, WA 99352)*. Soybean cyst nematode (SCN) is the most serious pest to soybean crops in the U.S. Previous published research on the variability in members of the Heteroderidae (cyst nematode family) has examined potential molecular differences to identify species and to attempt to describe population variability. The primary objective is to identify protein patterns of four significantly different Tennessee SCN populations and to determine common proteins that may be involved in the attachment to or degradation of the soybean root. The first step in identification of SCN proteins was to perform sodium dodecyl sulfate-polyacrylamide gel electrophoresis (SDS-PAGE) to determine whether there are gross differences in the proteins when separated according to size. Identification of proteins will help identify biochemical differences and help determine a common genetic link. Initially more similarities than differences have been found. Future work will focus on using additional techniques that may include capillary electrophoresis, and matrix-assisted laser desorption ionization (MALDI) coupled with mass spectrometry to differentiate between the nematode cyst proteins. However, it is possible that all SCN populations are nearly identical bio-chemically and that differences need to be found in the specific organelles of the adult nematodes. Other subtle differences could be found in DNA fragments, which will also be examined in future studies.

Investigation of Cell Signal Transduction Pathways that Account for Anti-Apoptotic Effects of Basic Fibroblast Growth Factor in Radiation-Induced Apoptosis Models II: Bis-Benzimide Staining in Human Umbilical Vein Endothelial Cells. *ALICIA WILLIAMS (Fort Valley State University, Fort Valley, GA 31076) LOUIS PENA (Brookhaven National Laboratory, Upton, NY 11973).* In cell biology, apoptosis is a process of deliberate suicide by an unwanted cell in a multicellular organism. Apoptosis can be initiated in a number of ways, including ionizing radiation. In cells, this process results in DNA damage and activation of signaling pathways that lead to cell death. Basic fibroblast growth factor (bFGF), known to cause cell proliferation, can inhibit apoptosis in irradiated cells. LY294002 hydrochloride is a Phosphatidylinositol 3 Kinase (PI3K) inhibitor. It blocks the action of PI3K thereby inhibiting the Protein Kinase B (AKT/PKB) pathway. This pathway functions to promote cell survival by inhibiting apoptosis. U73122 is a toxin that inhibits the hydrolysis of polyphosphoinositide (PPI) to inositol triphosphate (IP_3). It blocks the action of the Phospholipase C-γ (PLC-γ) hydrolase enzyme thereby inhibiting the Protein Kinase C (PKC) pathway. This pathway functions to promote cell differentiation. Endothelial cells can be used as a model system in which to study radiation-induced apoptosis. About two hours prior to irradiation, cells were serum starved from 10% fetal bovine serum (FBS) to 0.5% FBS. After irradiating the cells at 0.5 Gy/min with the Philips RT 100 X-ray machine, the samples were placed back in the incubator for varying lengths of time, harvested, stained with bis-benzimide (Hoechst 33258), and finally the cells were examined with fluorescent microscopy for changes in nuclear morphology (condensation and fragmentation) associated with apoptosis. In this project, several parameters were tested: time period after irradiation (4–24 hours), radiation doses (0–24 Gy), and harvesting methods (*in situ* fixation versus trypsinization). The best time interval to score apoptosis appeared to be about 18 hours after irradiation. For radiation doses, the range between 8 and 16 Gy were found to be adequate amounts of radiation for the samples because too much radiation can damage the cells and it would be difficult to determine whether a cell was apoptotic or not. Trypsinization was found to be the best harvesting method because the cells are easy to recover. The overall results indicate that there is still some work to be done on what inhibits apoptosis the most. Therefore, we are continuing working with other inhibitors to see which one blocks apoptosis without killing the cells.

Investigation of Signal-Transduction Pathways Accounting for Anti-Apoptotic Effect of bFGF in Radiation Induced Apoptosis I: Growth and Toxicity Assays in Murine Clonal Myoblast (MC3T3) and Human Umbilical Vein Endothelial (HUVEC) Cells. *JEREMIE WILLIAMS (Fort Valley State University, Fort Valley, GA 31030) LOUIS PENA (Brookhaven National Laboratory, Upton, NY 11973)*. Apoptosis is a programmed cell death in which cells use specialized cellular machinery to kill themselves. Basic Fibroblast Growth Factor (bFGF) is a growth factor that causes cell proliferation, but can also inhibit apoptosis from occurring in cells. There are specific signal transduction pathways that are activated by bFGF. These include the AKT/PKB pathway and the PKC pathway. The Phosphatidylinositol 3 Kinase (PI3K) acts upon the protein kinase AKT which functions to promote cell survival by inhibiting apoptosis. The Protein Kinase C (PKC) pathway controls cell differentiation. There are also fungal-derived toxins that can inhibit these pathways. LY294002 blocks the action of the PI3K and thus blocks the AKT/PKB pathway. U73122 inhibits the hydrolysis of PPI to IP3, by PLCg and thus blocks the PKC pathway. The goal of this project is to find the optimum assay conditions in which we can test the anti-apoptotic culture effects of bFGF and to determine which the most critical pathway is. The XTT assay is used to measure bFGF effects in a growth assay and in a toxicity assay to assess the potency of the inhibitors. We tested LY294002 and U73122 at a concentration range from 1-1,000 µM. The results revealed that over 5 µM the fungal

toxins kill the cells, but below 5 µM no toxicity was measured. We then irradiated the cells to see if they underwent apoptosis. The results revealed that they indeed did undergo this process and that the specific pathways that were targeted for this experiment were indeed correct.

X-Ray Microbeam Bystander Effects: Cell-Type Dependent? *CHRISTY WISNEWSKI (Las Positas Community College, Livermore, CA 94551) ELEANOR BLAKELY (Lawrence Berkeley National Laboratory, Berkeley, CA 94720).* When a tumor is irradiated, the normal tissue surrounding it exhibits a response to radiation called bystander effect. Bystander effect occurs when normal cells adjacent to irradiated cells exhibit radiation damage through DNA double-strand breaks. One way to identify the crosstalk within bystander effect is to tag protein markers within the ATM/TP53 signaling pathway (a pathway that is initiated through DNA damage). To do this, human mammary epithelial cells and fibroblasts were irradiated with 100 cGy using a Pantak 150 kVp X-ray machine and up to 50 cGy in a 100 µm wide stripe using a 12.5 keV X-ray microbeam at beamline 10.3.1 at the Advanced Light Source. The cells were fixed at varying times, post-irradiation, using -20°C/100% methanol. Two protein markers within the signaling pathway, TP53 and ATM, were identified using immunofluorescence with secondary antibodies that were tagged with green FITC fluorescent dye. Alexa-fluor 488 anti-rabbit was used for detecting TP53 and Alexa-fluor 488 anti-mouse was used for detecting ATM. A Zeiss Axiovert 200M immunofluorescent optical microscope was used to digitally capture fluorescent images. The 100 µm dose stripes were visible as low as 10 cGy in the epithelial cells tagged with anti-TP53 and in the fibroblasts tagged with anti-ATM. Additionally, there was no stripe that was visually detected in the epithelial cells tagged with anti-ATM or in the fibroblasts tagged with anti-TP53 at less than 400 cGy. While quantitation of the images is still in progress, there is the suggestion of a greater bystander effect in the ATM-positive fibroblasts, than there is in the TP53-positive epithelial cells.

Chemistry

A Comparison of the Reduction of Benzoquinone in Solvents of Two Different Polarities. *JUAN ALICEA (Dowling College, Oakdale, NY 11769) JOHN MILLER (Brookhaven National Laboratory, Upton, NY 11973).* Benzoquinone derivates are biologically active compounds that are important in photosynthesis as electron carriers. The first and second reduction potentials of benzoquinone are –0.4V and –1.24V, respectively. These potentials; however, have been determined electrochemically in polar solvents with high concentrations of electrolyte. Previously, it was reported from electrochemistry that solvent polarity has little effect on the reduction potential. We believe that our data questions that report. Low polarity calculations have been made, but there is little experimental data. We have titrated a fixed amount of benzoquinone with cobaltocene as a reducing agent in tetrahydrofuran (THF) and acetonitrile, separately. THF and acetonitrile have dielectric constants of 7.6 and 38, respectively. Cobaltocene was added to a solution of benzoquinone in increments of one tenth of one equivalent of cobaltocene to benzoquinone up to one equivalent. Thereafter, cobaltocene was added in increments of one fifth of one equivalent up to four equivalents. Continuous wave spectra were obtained after each addition from 200–800 nm. The experiments were carried out in an inert atmosphere. The data was analyzed using the data analysis program Igor with functions that we created. The fit for the THF spectra at 454 nm yielded an equilibrium constant of 1.316 and molar extinction coefficient of 5039. The free energy change at 298K was calculated to be –7.05V. The reduction in acetonitrile produced a much different result. The concentration of benzoquinone anion increased with each addition of cobaltocene up to 1.3 equivalents linearly. Thereafter, the concentration of benzoquinone anion decreased. We believe that cobaltocene reduces the benzoquinone anion to the dianion. Thus we conclude that, if the reduction potential change due to solvent polarity is distributed equally to cobaltocenium and benzoquinone, each has a change of –0.4V. In an attempt to characterize the equilibrium between the benzoquinone anion and dianion we will attempt the reaction in a solvent of intermediate polarity. We will also attempt to react less easily reduced quinones.

Investigation of Non-Platinum Based Electrocatalysts for Proton Exchange Membrane Fuel Cell Cathodes. *MICHAEL AMOLINS (Augustana College, Sioux Falls, SD 57197) XIAOPING WANG (Argonne National Laboratory, Argonne, IL 60439).* The energy crisis has forced the scientific community to investigate possible alternative, renewable energy sources for transportation applications. One such possibility is the proton exchange membrane fuel cell (PEM fuel cell). This fuel cell uses hydrogen gas as fuel and oxygen from the air to produce electricity, which can be used to power a vehicle. Emissions include only water, making it an environmentally friendly process. One of the major issues, however, is that the only PEM fuel cell cathode electrocatalysts currently capable of the most efficient reduction of oxygen to water are platinum-based, making them too expensive for commercial applications. In order to address this cost issue, research has been performed to investigate equally efficient and less expensive non-platinum-based electrocatalyst alternatives. Several transition metal-based bimetallic systems on carbon support have been synthesized using methods of co-precipitation deposition and co-impregnation. The activity for the oxygen reduction reaction (ORR) of a select number of these electrocatalysts has been tested using cyclic voltammetry and rotating disk electrode technique. Some show promise as PEM fuel cell cathodes. Specifically, one bimetallic system has shown ORR potentials as high as 0.85 V, nearly comparing to that of platinum at about 0.95 V. The effect of oxidized carbon support on ORR activity was also studied and showed an increase in electrocatalyst performance at a lower metal loading. These features have given promise to the possible use of bimetallic transition metal electrocatalysts in future PEMFC developments.

Characterizing Trypsin Behavior during Protein Digests in Mixed Organic Aqueous Solvent Systems Used for Automated High-Throughput Protein Mapping. *JASON ASKEW (Arizona State University, Tempe, WA 85281) DEANNA AUBERRY (Pacific Northwest National Laboratory, Richland, WA 99352).* Our current understanding of trypsin behavior during protein digests is limited because there is no direct way to measure the activity under normal digest conditions. Our work focuses on characterizing trypsin activity in various mixed organic aqueous solvents. In order to measure this we used chromogenic and fluorogenic substrates that would change colors as trypsin digests them. These changes in color could be accurately measured using various spectroscopic detection methods. Our results suggest that solvent systems containing acetonitrile produce higher activity rates then methanol systems, but methanol systems are more stable over long periods of time. There was also evidence that large protein substrates stabilize trypsin from the denaturing effects of the solvents. The degree of this stabilization was dependent on the concentration of protein. Future work will focus on measuring the rate of protein denaturation in solvents, and testing mixed acetonitrile and methanol solvent solutions.

Electrospray Mass Spectrometry of Selected Uranyl Amide Complexes. *SIGRID BARKLUND (The College of St. Catherine, St. Paul, MN 55105) ANITA GIANOTTO (Idaho National Laboratory, Idaho Falls, ID 83415).* Uranyl complexes are significant for several reasons: they are necessary for the actinide separations needed to produce fuel for nuclear energy, have untapped catalytic potential, and play a major role in solution phase chemistry influencing movement in the environment and living systems. Amides are important functional groups in both advanced extraction agents and complex biomolecules, so amide interactions with actinides are of interest. The presence of closely spaced d and f orbitals enables formation of multiple, interconverting species, making experimental studies complicated. Coupled with radioactivity and toxicity concerns, this has motivated utilization of computational chemistry (high-level density functional theory (DFT)) for the investigation of actinide-ligand coordination complexes. However, computational efforts have not been verified by experimental data. Here, trapped-ion mass spectrometry is used to evaluate the extent of coordination and ligand binding preference in uranyl ($[UO_2]^{2+}$) complexes. A Finnigan LCQ-Deca XP Plus electrospray ion trap mass spectrometer was used to identify the composition of sprayed $[UO_2(anion)(amide)n]^+$ complexes using collision-induced dissociation. Six amide ligands of increasing nucleophilicity were compared: formamide (F), N-methylformamide (NMF), N,N-dimethylformamide (DMF), acetamide (AA), N-methylacetamide (NMA), and N,N-dimethylacetamide (DMA). Tetraligated $[UO_2(NO_3)(F)_3]^+$ adducts underwent extensive substitution of weakly basic MeOH and water, indicating that F is weakly bound. NMF and AA also form $[UO_2(anion)(amide)_3]^+$ complexes, but because NMF and AA are stronger nucleophiles, there is little solvent substitution. DMF, a much stronger base, shows almost no solvent substitution in the anion complexes, and forms abundant doubly charged ions, suggesting that it is outcompeting the anions for uranyl coordination sites. These trends continue for NMA and DMA, even stronger nucleophiles. Although no calculations on the uranophilicity of the simple amide ligands exist, it was expected that they would echo the proton affinity values. In the gas phase with all solvent effects removed, the intrinsic order of amide uranophilicity mirrors proton affinity. These conclusions will be

compared with those generated using DFT calculations, which are currently underway.

Examination of the Hydrogenation of Aqueous 1,4-Pentadien-3-ol on Pd-black Using Cavitating Ultrasound Verses the Traditional Stirring Process. *KELLY BOYLES (Columbia Basin College, PasCO WA 99301) ROBERT S. DISSELKAMP (Pacific Northwest National Laboratory, Richland, WA 99352).* This study explores the effects of cavitating ultrasound and silent stirred processing on hydrogenation of the five carbon alcohol 1,4-pentadien-3-ol on the catalyst Pd-Black in water (H_2O) or deuterium oxide (D_2O) using H_2 or D_2 gas. In separate hydrogenation experiments, the methods of silent stirring or cavitating ultrasound at 20 kHz and 270W sonifier output power with 60psig H_2 or D_2 were applied to the substrate in a batch reactor at 298K. The scientific phenomena of hydrogen addition/elimination/isomerization were observed to take place during these hydrogenations. In all experiments the intermediate species of 1-penten-3-ol and 1-penten-3-one were observed to rise to a summed maximum of less than 53% then fall back to zero, at the same time the products 3-pentanol and 3-pentanone continued to rise in abundance throughout the experiment. The final ratio of the products formed is the subject of interest in these experiments. Hydrogenation of the 1,4-pentadien-3-ol species involves fairly complicated multiple reaction paths leading to two possible products. Hydrogen addition yields 3-pentanol and hydrogen elimination, through an enol intermediate, yields 3-pentanone. Cavitating ultrasound is believed to promote the pathway to the 3-pentanol product (e.g., enhanced hydrogenation) and these experiments appear to support that hypothesis. This investigation of fundamental aspects of hydrogenation of this 5 carbon species continues to be encouraging with the anticipated result of using these methods to selectively partially hydrogenate, while minimizing isomerization in non-hydrogenated olefins, 18 carbon species (i.e., seed oils) used in the commercial production of food products. By controlling the conditions that alter selectivity, it is hoped that unwanted trans-fats can be reduced, helping our diets to become healthier. This investigation is just beginning the work needed to reach the 18 carbon seed oil species. If these methods are going to yield the desired reduction of trans-fats in commercial food products, then further exploration will need to be performed on progressively longer carbon chain species until we reach the seed oil systems.

Proton Conducting Molecular Species Towards the Development of Polymer Electrolyte Membranes. *KATELYN BRYLL (Washington University in St. Louis, St. Louis, MO 63130) SUHAS NIYOGI (Argonne National Laboratory, Argonne, IL 60439).* A cost effective proton conducting membrane preparation work for a hydrogen fuel cell was done. Membranes were made by attaching two different types of dendrimeric molecules to polyepichlorhydrin and post sulfonation. Besides G1 and G2 that do not have any functional groups, Alt-G1 with ester groupswas used. The amount of the dendrimeric molecule Alt-G1 that was attached to the polymer was varied to optimize the composition. The sulfonic acid contents in these materials were determined and found to be a function of the ratio of [Cl:[Alt-G1] used. It was found that the ratio of 6.67:1 produces an insoluble membrane. Material of two other compositions with the ratios of 1:1 and 3:1 were insoluble in water and gave acid concentrations of 5 meq/g and 1.56 meq/g. The thermal stability of PECH-Alt-G1-SO_3H was found to be higher than that of PECH-G2-SO_3H. Two distinctly different routes were used to synthesize Alt-G2 and only one was met with partial success. New pathways to synthesize Alt-G2 are being worked out.

31P NMR Analysis of the Resistance of Tripoly- and Trimetaphosphate to Cation-Accelerated Hydrolysis under Groundwater-
Compatible Conditions. *BART BUTLER (Dartmouth College, Hanover, NH 03755) DAWN WELLMAN (Pacific Northwest National Laboratory, Richland, WA 99352).* Phosphate barriers have been proposed as durable and relatively inexpensive methods of subsurface uranium remediation. Metal orthophosphate compounds exhibit high stability and rapid precipitation kinetics which afford the potential for fouling the injection well for subsurface remediation. Therefore, identification of a time-released source of orthophosphate may facilitate subsurface remediation. Also, any components of the subsurface which catalyze this degradation must be identified. The degradation of sodium tripolyphosphate ($Na_5P_3O_{10}$) and sodium trimetaphosphate ($Na_3P_3O_9$) were systematically evaluated in under relevant environmental conditions to identify variables present within the subsurface which may catalyze the degradation condensed phosphates. Specific variables considered in this investigation consisted of common groundwater cations (Al^{3+}, Fe^{3+}, Ca^{2+}, Mg2+, and Na+ and Hanford groundwater) and heterogeneous surfaces (FeOOH(s) and Hanford site sediment). A 0.2 M sample of each candidate phosphate compound was subjected to subsurface-relevant pH, temperature, and one of the listed potential catalysts for a period of 3 to 4 weeks. The percent degradation of each condensed phosphate and formation of orthophosphate was monitored at predetermined intervals using ^{31}P nuclear magnetic resonance (NMR). Accelerated degradation of sodium tripolyphosphate was detected in the presence of FeOOH(s) and Hanford site sediment. FeOOH was also catalytic with respect to sodium trimetaphosphate degradation, but Hanford site sediment had no effect. All homogeneous potential catalysts (cations and groundwater) were also catalytically inert.

Relative Cerebral Glucose Metabolism and Behavioral Studies of Toluene Abuse using 18FDG in Toluene-Exposed Rats. *JOSEPH CARRION (City College of New York, New York, NY 10031) STEPHEN DEWEY & WYNNE SCHIFFER (Brookhaven National Laboratory, Upton, NY 11973).* The addictive dynamics of inhalants, along with the possible physiological and biochemical disruptions they may cause in the brain are not fully understood. Toluene, an abused solvent used as a base in many glues and household products, has been shown to produce a reinforcing response in a Conditioned Place Preference (CPP) paradigm. The expression of positive reinforcement behavior that is connected with a perceived reward may be reflected with changes in cerebral glucose metabolism, the brain's main metabolic source of energy. In this study we used a three chambered (black/gray/white) conditioning apparatus in an unbiased-design. Before any exposure, a pretest was conducted and the time spent in each chamber was measured by automated photocells; with animals spending equal time in each chamber (black: 258.7 ± 28; white: 269 ± 28 sec). A conditioned response to 2000 ppm of toluene vapors was obtained after 7 and 13 pairings from male Sprague-Dawley rats (n=8). On the 13th pairing test, n=3 animals showed a significant ($p = 0.001$) preference for the drug-paired side. Conditioned Place Aversion (CPA) was expressed by n=4 animals ($p > 0.06$). The locomotor activity measured were significantly lower ($p < 0.05$) for toluene-paired days as compared to the air-paired days. We have conducted an analysis of relative cerebral glucose metabolic rate using 2-deoxy-2-fluro-D-glucose (18FDG) and Micro Positron Emission Tomography (MicroPET). The results of these scans indicate significant increases in the striatum, thalamus, and parietal cortex for animals that expressed a preference, and decreases in these same areas for animals that showed an aversion. Further studies on toluene's lipid solubility may clarify the aforementioned changes, as well as give insight into whether these changes in the animal model are permanent or reversible.

Imaging Live Cells with Quantum Dots. *SARAH CARTER (University of Illinois at Urbana-Champaign, Urbana-Champaign, IL 61820) FANQING CHEN (Lawrence Berkeley National Laboratory, Berkeley, CA 94720).* Quantum dots are small semiconductor particles ranging in size from several nanometers to a few microns in diameter. The dots are spherical in structure with a special arrangement of electron shells that allows them to fluoresce. The luminescence emitted is non-bleaching, making them useful reagents for long-term in vivo studies. The surface of the nano-particles can be modified so that they can be linked to various other molecules, including water-soluble biomolecules. In order to develop a better reagent for detecting breast cancers, the quantum dot was linked to a DNA aptamer specific for breast cancer cells. The cells were then imaged using fluorescence microscopy.

Protein Adsorption and its Role in Smart Bandage Design. *NATHAN CASTRO (El Paso Community College, El Paso, TX 79915) STEVE GOHEEN (Pacific Northwest National Laboratory, Richland, WA 99352).* Protein adsorption can be characterized as the extemporaneous adhesion of protein to a surface. Although extensive research and investigations have been undertaken, a comprehensive biomechanistic understanding of protein adsorption remains quite ubiquitous. This is due to the diverse interactions resulting from the presence of amphoteric and amphiphilic moieties on both the protein and surface. The adsorption isotherm is a common first-step towards quantifying and understanding the adsorption of proteins. A comparative examination of two methods, the classical- and chromatographic, commonly used to study adsorption isotherms is presented. Both methods were used to study the solid/liquid interface of two different derivatives of cotton fiber and bovine serum albumin (BSA). Albumin is the most prominent globular protein in blood plasma and cotton fiber is the most utilized material for the treatment of wounds. Cotton is composed of nearly pure cellulose. The two derivatives under investigation are an untreated cotton sample and a carboxymethylcellulose (CMC) cotton sample. Protein adsorption of collected samples was studied utilizing a colorimetric protein assay coupled with spectrophotometric measurements of absorbance at 595

nm. Applicability of smart bandage design to acute wounds also merits investigation.

Probing the H/D Isotope Effect for Hydrogenation using H_2/D_2 in H_2O/D_2O of 3-Buten-2-ol on Pd-Black Catalyst. *SARAH CHAJKOWKI (Waynesburg College, Waynesburg, PA 15370) ROBERT DISSELKAMP (Pacific Northwest National Laboratory, Richland, WA 99352).* Partial hydrogenation is a process used for manufacturing seed oils, which are comprised of multiple cis-olefins. A large percentage of the residual (non-hydrogenated) cis-olefins during traditional heterogeneous catalytic processing are inevitably isomerized to their trans forms. This study was undertaken to examine the isotope effect of H_2 versus D_2 addition to aqueous 3-buten-2-ol on Pd-black by using the process of cavitating ultrasound compared to stirred/silent methods. Both selectivity and activity measurements were made. The effects of the cavitating ultrasound at 20 kHz and 280 W were investigated. The products formed were 2-butanone and 2-butanol. Comparing the ultrasound assisted to blank (stirred) experiments revealed an enhanced selectivity of the alcohol product formed.For the different combinations of gases and solvents employed, the final ratios of 2-butanol to 2-butanone were: H_2/H_2O 5.67 (cavitated) and 1.44 (stirred), H_2/D_2O 5.25 (cavitated) and 1.86 (stirred), and D_2/H_2O 10.11 (cavitated) and 2.125 (stirred).The hydrogenation employing D_2 did not show a decrease in the yield of 2-butanol product formed. It is anticipated that this information will yield insight into hydrogenation in general, and about cavitating ultrasound processing in particular. For example, it may be possible to quantify the enhancement in the hydrogenation rate caused by cavitating ultrasound.

Low Temperature Spectroscopy of ZnO Nanowires. *CANDACE CHAN (Rice University, Houston, TX 77005) SAMUEL MAO (Lawrence Berkeley National Laboratory, Berkeley, CA 94720).* ZnO is a direct, wide bandgap semiconductor with many interesting optical properties, such as room temperature excitonic recombination and UV photoluminescence and lasing capabilities. Recent advances in nanomaterial synthesis and characterization have suggested that ZnO nanowires may have potential use in nanoscale optoelectronics. Photoluminescence (PL) spectroscopy on ZnO nanowires synthesized by laser-assisted evaporation was conducted in order to study the optical properties of the nanowires at different temperatures. The nanowires were excited with a Nd:YAG laser (266 nm, 10 Hz, 6 ns) at constant pumping energy in a liquid helium cooled closed-cycle cryostat. PL spectra were taken at different temperatures from 12 K to room temperature. At low temperatures, well-defined emission peaks corresponding to donor-bound exciton and free-exciton recombination were observed at 3.342 eV and 3.306 eV. The first, second, and third order longitudinal optical phonon replicas were also observed at 3.231 eV, 3.161 eV, and 3.084 eV. With increased thermal energy, the peaks broadened and converged due to the decomposition of the bound-excitons into free-excitons. Room temperature PL was dominated by a broad free-exciton emission at 3.179 eV. The presence of the free-exciton emission at very low temperatures suggests that the nanowires synthesized were of high optical quality and have potential application for use in nanoscale optoelectronic devices.

Arsenic Removal Using Bottom Ash (ARUBA). *EBERECHUKWU CHUKWUEKE (Contra Costa College, San Pablo, CA 94806) ASHOK GADGIL (Lawrence Berkeley National Laboratory, Berkeley, CA 94720).* Arsenic is a naturally occurring heavy metal found in the earth's crust. Its presence in drinking water has become an issue of global concern due to numerous lethal occurrences particularly in countries in Bangladesh where the situation is called the largest mass poisoning in human history. The current guideline by World Health Organization (WHO) for arsenic is 10 µg/L. In Bangladesh, about 60 million people are exposed to levels higher than 50 µg/L (the Bangladeshi guideline) arsenic in drinking water and about 10% of the adults (about 13 million) will die of arsenic poisoning if nothing is done. Long term exposures of low concentrations may cause internal cancers including bladder, skin, lung and prostate cancer. Other effects of arsenic exposure include cardiovascular, pulmonary, immunological and neurological effects. Arsenic is mostly present as two species in ground water, arsenate (As^{5+}) and arsenite (As^{3+}). Previous studies have shown the removal efficiency of both species to be highly dependent on pH. The objective of this project is to develop a cheap and effective method to remove arsenic from drinking water as to make it affordable even to the poorest residents in Bangladesh. Our overall approach is based on coating small sized particles (1-10um) of bottom coal ash (a finely powdered and sterile waste material from coal-fired power plants) with ferric hydroxide and using them to immobilize and remove arsenic in water supplies. In this study, we examined the capacity of LBNL media to remove both As(V) and As(III) from water. We also examined the effect of pH on adsorption efficiency of As(V) and As(III). Finally, to make the LBNL approach more cost effective, we examined the effect of recycling excess $FeSO_4$ solution on the capacity of resulting media. Our results demonstrate that the removal of arsenite is more effective at high pH while the removal of arsenate is more effective at low pH. Based on Inductively Coupled plasma mass spectrometric (ICP-MS) analysis, 1g of the LBNL media can effectively remove 1mg of arsenate and about 0.2mg of arsenite. In the future, we will proceed to test the capacity of our media in real groundwater where inhibiting factors like phosphate are present and will design "ARUBA Up-flow Sand Filter" for domestic use.

Determination of Diisopropyl Methylphosphonate and Dimethyl Methylphosphonate and Their Degradation Products in Complex Biological Matrices. *RYAN CLARK (Washington State University, Richland, WA 99352) ERIC HOPPE, JIM CAMPBELL (Pacific Northwest National Laboratory, Richland, WA 99352).* The organophosphorous compounds, diisopropyl methylphosphonate (DIMP) and dimethyl methylphosphonate (DMMP), are of interest to national security and also play a role as environmental contaminants. Research on the degradation products and their toxicities in diverse matrices is needed. This study describes instrumental and sample preparation techniques used to identify and monitor these compounds and their degradation products in agar, saliva, serum, and aqueous media with the purpose of producing a degradation analysis model for analogous compounds of interest. Residue analysis using gas chromatography/mass spectrometry (GC/MS) and headspace sampling followed by GC/MS were the methods developed for analysis. DIMP and DMMP were successfully analyzed in agar, saliva, serum, and aqueous matrices. The methods were extended to analyze for DIMP and DMMP and their degradation products after fungal decontamination with Poria Cocos. This bioremediation technique could lay the groundwork for clean up of areas contaminated with these and similar compounds. The fungal-based technology will be potentially applicable to decontaminate personnel, equipment, structures, and wide-area sites without damage to items and/or individuals.

Photoelectrochemical Characterization of Gallium Indium Nitride Phosphide. *CALONDRA COLVIN (Baylor University, Waco, TX 76706) JOHN TURNER (National Renewable Energy Laboratory, Golden, CO 89401).* Hydrogen gas is evolved from the surface of Gallium Indium Nitride Phosphide (GaInNP) when placed in aqueous solution, along with a platinum counter electrode under an applied current. The success of hydrogen as an energy carrier is dependent on both how well the semiconductor material, in this case gallium indium nitride phosphide, can hold up to corrosion in aqueous solution, along with how efficiently it produces hydrogen. The focus of our research is quantizing both of these abilities for GaInNP by measuring the flat band potential, band gap and corrosion susceptibility. Band gap is calculated with data from photocurrent spectroscopy, and flat band potential using illuminated open circuit potentials, photocurrent onset measurements, and Mott-Schottky analysis values. Although the band gap of GaInNP lies above the necessary 1.8 eV, valence band values failed to realize potentials capable for water splitting. Ultimately, to split water the sample would need both a valence band more positive of the oxygen redox potential, and a conduction band more negative of the hydrogen redox potential. GaInNP fulfills the hydrogen part of this requirement but not the oxygen compliment. Durability tests showed a steady, minimal amount of corrosion occurring at the electrode surface over a period of 24-hours. Future work includes investigating the effects the quantization techniques using atomic force microscopy and profilometry. Corrosion results in fragmentation of the electrode surface, so by measuring the elemental composition using inductively coupled plasma atomic emission analysis, specific changes will be realized.

Functionalized Mesoporous Silica Modified Disposable Screen Printed Electrodes for Detection of Metal Ions. *LISA DEIBLER (Washington State University, Pullman, WA 99163) WASSANA YANTASEE (Pacific Northwest National Laboratory, Richland, WA 99352).* We have developed the self assembled monolayers on mesoporous silica (SAMMS) modified screen printed carbon electrode (SPCE) which has advantages of being mercury-free, reusable, and low cost, yet as sensitive as Hg based SPCEs. The self-assembled monolayer chemistry of SAMMS allows easy installation of a wide variety of functional interfaces on mesoporous MCM-41 silica, leading to excellent specificity and selectivity for many desired metal ions when the materials are used as modifiers in electrochemical sensors. The voltammetric detection procedure consisted of preconcentration by utilizing the affinity of the functional group to the target metal ions, cathodic electrolysis at -1 V, and stripping steps by scanning from -0.7

V to -0.49 V. After optimization of this procedure, a low detection limit of 0.91 ppb $Pb2^{+}$ was achieved and preliminary work on Cd detection in urine was completed. The SAMMS modification can be done during the manufacturing process which will increase the measurement precision and reproducibility from one sensor to another. The strong covalent bonding between the functional group and the mesoporous silica on SAMMS resulted in reusability of sensors for tens of measurements, making the establishment of the calibration curve easier (e.g., from 2.5 ppb to 100 ppb Pb^{2+} after 5 minutes of preconcentration) and the costs more competitive compared to single-use electrodes.

Preparation of Alkamides for Evaluation as Insecticides. *AMANDA DEVRIES (Buena Vista University, Storm Lake, IA 50588) GEORGE KRAUS (Ames Laboratory, Ames, IA 50011).* The idea of a biorefinery is modeled after the highly successful oil refinery wherein petroleum is converted into gasoline, oil and monomers such as ethylene and propylene. Unlike petroleum refineries, corn grain and soy biorefineries are in their first stages of development. For biorefineries to be successful on a long-term basis, they must produce: 1) high volume fuels such as ethanol or biodiesel; and, 2) a portfolio of high value products and chemicals. One such chemical is 1,3-propanediol, which can be polymerized for use in textiles and fabrics, such as in DuPont's Sorona. Another high value product would be an insecticide or herbicide based on alkyl amides derived from natural oils. Some alkamides have been shown to inhibit the hatching of larvae. Alkamides can be synthesized by using a Wittig reaction with the amide portion coming from the phosphonium ylide and the alkyl chain coming from the aldehyde. To synthesize the phosphonium salts needed for the production of the alkamides, a variety of organic synthesis techniques were used. Synthesizing the first phosphonium salt required initial reflux of chloroacetyl chloride with isobutylamine in ethyl ether. In a bimolecular nucleophilic substitution reaction (SN2) the resulting amide was then added to triphenylphosphine in toluene and boiled to produce the phosphonium salt. The preparation of the second phosphonium salt began with crotonic acid and a bromination reaction. The bromoacid then underwent halogen substitution with thionyl chloride under reflux conditions. The resulting acid chloride was added to a solution of isobutylamine in ethyl ether with stirring. An SN2 reaction was used by adding the amide to triphenylphosphine in toluene to produce the second phosphonium salt. To synthesize the seven-carbon aldehyde, 5-hydroxy-1-pentyne in methanol and potassium hydroxide reacted with iodine. The product of this reaction then underwent a coupling reaction with trimethylsilylacetylene, and the resulting alcohol was oxidized to create the aldehyde. Each product synthesized was confirmed using nuclear magnetic resonance (NMR). Future work will include carrying out the Wittig reaction to synthesize the desired alkamides. The alkamides will be evaluated as insecticides. The biological studies will be conducted by DuPont.

Chamber Experiments to Develop a New Air Pollution Measuring Method. *ELIZABETH DOMINGUEZ (Yakima Valley Community College, Yakima, WA 98902) YANBO PANG (Lawrence Berkeley National Laboratory, Berkeley, CA 94720).* Whether indoors or out, the air we breathe contains particulate and gaseous pollutants that can adversely affect human health. Semi-volatile organic compounds (SVOCs), which come from incomplete combustion of organic compounds, exist in both particulate and gas phases. Many of these SVOCs are toxic. Previous methods to measure air pollutants like annular denuders are not sufficient to understand the effects of semi-volatile organic compounds. They are typically made of glass and are large, fragile, and costly. Foam denuder technique could potentially be good for collecting a range of hazardous species, especially semi-volatile organic compounds. The objective is to develop a foam denuder technique that is lightweight, simple, cost effective, accurate, and easy to use to collect gaseous pollutants. But in order to accomplish this, we needed to understand how SO_2 gas diffuses in Polyurethane foam and how well the foam absorbs SO_2. Polyurethane foam was used as the primary foam material in the experiments. Two general approaches were taken in consideration, foam thickness and pore size. For the foam thickness, 1/8 in. thick foam sheets were stacked to reach 0.5–5 in. high. Each thin foam layer was analyzed separately. For the pore size, 20ppi, 50ppi, 80ppi, and 110ppi (pores per inch) were used. In addition, different face velocities 5, 20, 40, and 100 (cm/sec) and different SO_2 concentrations ~0.01, ~0.1, and ~1 (ppm) were tested. Data on SO_2 collection for different foam thickness were used to derive the empirical model. Our results demonstrated that when we decreased the pore size (increasing ppi) of foam and decreased the face velocity it can help to improve the collection efficiency for gaseous pollutants. Overall, there was good correlation when we compared the SO_2 concentration measured by foam denuder vs. the SO_2 concentration measured by annular denuders. In conclusion, it was demonstrated that foam denuders could achieve 100% collection efficiency for gaseous pollutants. Future experiments will be done to test foam denuders for SVOC collection efficiency.

A Systematic Search for New Bismuth and Lead Based Oxides Scintillators and Semiconductors. *ANGELA EDWARDS (North Carolina Agricultural and Technical State University, Greensboro, NC 27411) STEPHEN DERENZO (Lawrence Berkeley National Laboratory, Berkeley, CA 94720).* In recent times, the steady increase in the uses of radiation detectors has imposed a great need for higher efficiency and lower costs of detector production. Through such an achievement, applications ranging from medical imaging to weapons detection may be realized. Prompted by this demand, our research focuses on the discovery of new radiation detectors. In this manuscript we report the results of a systematic search for such detectors that have structures based on lead and bismuth. In this work we synthesized and characterized four compounds: Bi_2TeO_5, $PbTeO_3$, $Ca_2Bi_2O_5$, and Compound A. We were able to identify four semiconductors (Compound A and Compounds 1-3) by DC ionization under gamma irradiation.

Aqueous Alkaline Actinide Chemistry for Advance Nuclear Materials Processing. *MELISSA ENSOR (The University of the South-Sewanee, Sewanee, TN 37383) WOLFGANG RUNDE (Los Alamos National Laboratory, Los Alamos, NM 87545).* As an alternative to the acidic PUREX reprocessing of spent nuclear fuel, SNF, oxidative dissolution of UO_2 into alkaline aqueous solutions and subsequent separation of fission products is considered. The efficiency and kinetics of dissolution depends heavily on the solution and solid-state chemistry of actinides and fission products in carbonate media. Peroxide has been shown to be a primer oxidizing agent in carbonate solutions. However, the addition of peroxide increases the complexity of actinide solution chemistry, creating a dynamic system of multiple ligands. Uranium in carbonate solution forms the anionic complex $UO_2(CO_3)_{34}$- in solution with ternary uranyl(VI) phases of the general formula $M4UO_2(CO_3)_3 \bullet nH_2O$ as the solid equilibrium phase. We determined the solubility of these solids using M = NH_4, K, Na, and Cs in 0.1 M, 0.5 M, 1 M, and 2 M M_2CO_3 solutions. To establish an accurate interpretation of the experimental data the solids were characterized using X-ray diffraction, Raman spectroscopy, and diffuse reflectance spectroscopy. The uranyl(VI) concentration in the carbonate solutions was determined spectroscopically using the characteristic absorbance of the triscarbonate complex between 380 and 450 nm. The data from the pure carbonate system serves as a foundation to study the competing complexation behavior that occurs upon the addition of peroxide. Spectroscopic titrations of U(VI) carbonate in Na_2CO_3, $NaHCO_3$, and $(NH_4)_2CO_3$ were performed with varying peroxide molar ratios, and the solution speciation was characterized. We identified the predominant solution species, $UO_2(O_2)(CO_3)_{24}$-, and determined its formation constant. For comparison, we also performed spectroscopic titrations in the mixed hydroxide/peroxide system, where the data indicates a significantly different solution chemistry and complexation behavior. In this study, the structure and solubility of the relevant solid U(VI) carbonate phases will be discussed in terms of their dependence on the nature of the metal cation and the carbonate concentration. Also the results of solution speciation of U(VI) in mixed peroxide/carbonate (or hydroxide) solutions will be presented and, for the first time, thermodynamic data for ternary U(VI) carbonate solution complexes.

Aggregation of Granular Glass Forming Chemicals in Pretreated Radioactive Tank Waste Simulant. *CHRISTOPHER ESCOTT (Yakima Valley Community College, Yakima, WA 98908) RICHARD DANIEL (Pacific Northwest National Laboratory, Richland, WA 99352).* To vitrify the liquid fraction of radioactive tank waste, glass forming chemicals (GFC) composed primarily of ground silica glass and orthoboric acid must be added. When GFC are added to the high ionic strength, alkaline waste to make the melter feed material, the solution pH is lowered resulting in significant precipitation. While these precipitates are not a problem for the vitrification process during continuous operation, if given a chance to settle during an event such as prolonged maintenance, they may aggregate and become difficult to redisperse. The addition of polymers to the melter feed may provide steric stabilization to the solids, helping prevent strong aggregation. Here a physically adsorbed polymer layer repels close contact and interaction between adjacent particles. The degree of protection provided by the polymer depends on the amount adsorbed and its configuration at the particle-solution interface. While these are well characterized in low-ionic strength environments, few studies have examined conditions similar to the high ionic strength, alkaline environment of the Hanford tank waste. This study sought

to characterize the effectiveness of polymers as stabilizers against aggregation in the waste. Using a non-radioactive simulant solution that mimics the chemical and physical properties of actual tank waste, samples were observed under various pH levels with varying concentrations of the polymers Poly(acrylic acid) (PAA), Polyacrylamide (PAM), and Poly(diallyl dimethyl ammonium chloride) (Cat-Floc). In these samples, the occurrences of precipitates and the rheology of the melter feed were characterized. As the pH was lowered, the samples were found to develop increasing amounts of precipitates, thought to be aluminum hydroxide. Flow curve and shear strength tests were then performed. The addition of polymers resulted in an unwanted increase in the viscosity of the mixed slurry and offered no steric stabilization in the melter feed material. These findings show that simple addition of polymers will not stabilize the solids against aggregation. Future studies of radioactive tank waste treatment will be required to determine how the vitrification process can recover from periods of downtime.

Experiment Design and Setup for Laser-Induced Fluorescence Spectroscopy of Metal-Containing Free Radicals. *LAURA FREDRIKSEN (University at Albany, Albany, NY 11934) TREVOR SEARS (Brookhaven National Laboratory, Upton, NY 11973).* Small, metal-containing free radicals are models for the active site in heterogeneous catalysts, such as those used industrially for hydrodesulfurization of petroleum and in automobile exhaust gas treatment to remove oxides of nitrogen. Most catalysts employed in these processes today employ expensive, rare, or precious metals, and one of the goals of the research is to investigate the properties of potential cheaper replacements made from compounds of common, less expensive transition metals. A new experimental apparatus is being built to study the electronic structure of these metal-containing radicals in the gas phase. The new experiment will use laser ablation combined with a supersonic expansion of inert gas or inert gas seeded with a small percentage of reactive molecules to form beams of small metal clusters or cluster compounds. The beams will be studied spectroscopically using an optical parametric oscillator based laser system that provides narrow-band tunable light at wavelengths ranging from the infrared to the ultraviolet. The primary spectroscopic technique to be used is laser-induced fluorescence. We are particularly interested in the lowest energy excited states of the radicals, since their energies and properties can be used to infer likely chemical properties. As a first test for the machine, we will attempt to record the spectrum of vanadium nitride (VN), which has a strong visible spectrum that is well understood from previous studies. However, VN is also predicted to have several low-lying electronic states for which little experimental information is presently available. This experiment is within the first stages of being organized and built; considerable attention has been focused on building structures vital to the experiment, such as a table designed to support the vacuum system, laser shrouds, etc. This experiment should be expected to carry on for years, covering the spectra of a number of different metal-containing molecules.

Development of Sandwich Immunoassay for Use in the Detection of Biological Toxins by Flow Cytometry. *ALLYSON FRY (Vanderbilt University, Nashville, TN 37235) MARVIN WARNER (Pacific Northwest National Laboratory, Richland, WA 99352).* An autonomous pathogen detection system (APDS) was developed at Lawrence Livermore National Laboratory which analyzes aerosol samples using a Luminex flow cytometer in order to detect biological toxins that might be present during a bioterrorism attempt. We are currently developing reagents that could be used in a flow cytometer like the one found in the APDS that targets botulinum toxin. These reagents consist of fluorophore (e.g. phycoerythrin (PE) or Alexa 633) labeled antibody and internally labeled fluorescent microspheres. Our approach to carrying out the immunoassay employed biotinylated antibodies that were combined with antibody-coupled microspheres. These antibodies were specifically engineered to have a high affinity toward botulinum toxin. A second approach was to develop a model system that consisted of a biotinylated monoclonal antibody specific to Dinitrophenyl (DNP), monoclonal antibody specific to keyhole limpet hemocyanin (KLH) coupled to microspheres, and dinitrophenyl keyhole limpet hemocyanin. Both sets of assays were created using a washed capture sandwich immunoassay procedure and fluorescently labeled using streptavidin phycoerythrin (SA-PE). Median fluorescence was measured using a flow cytometer to quantitate assay efficiency. Future work will focus on optimizing these reagents and applying them to systems designed to employ quantum dot labels, fluorescent semiconducting nanocrystals.

Unsaturated Release and Migration of Uranium from 300-Area Contaminated Sediments. *CARMEN GARBERG (Columbia Basin College, PasCO WA 99301) DAWN M. WELLMAN (Pacific Northwest National Laboratory, Richland, WA 99352).* The Hanford Site in southeastern Washington State is among the most contaminated facility within the Department of Energy (DOE) complex due to operations related to nuclear energy and weapons production. Remediation at DOE facilities is a top priority due to the potential risks and hazards associated with groundwater. The objective of this investigation is to quantify the release of uranium from contaminated sediments under hydraulically unsaturated conditions. Experiments were conducted on two disturbed sediments from beneath the North Process Pond on the Hanford site, southeastern Washington State, at 20% saturation. These experiments were accomplished using centrifugation techniques to achieve steady-state, hydraulically unsaturated conditions. Results suggest that occasional spikes in uranium concentration may exceed EPA drinking water limits. However, the total amount of uranium released from either sediment does not exceed 5% of the total available amount. This indicates that under unsaturated conditions the migration of uranium from sediments beneath the North Process Pond may be controlled by the interplay of desorption and adsorption/desorption on uncontaminated sediments at the leading edge of the plume. Moreover the sediments may function as a partial barrier for the future migration of uranium within the vadose zone.

The Relationship of Soil and Water Chemistry to the Preservation of Salamander Habitats in the Long Island Pine Barrens. *CASSANDRA GILL (North Carolina Agricultural and Technical State University, Greensboro, NC 27411) TIM GREEN (Brookhaven National Laboratory, Upton, NY 11973).* Although salamanders are the dominant vertebrate population in the ponds of the eastern United States, little is known about their habits. As a result, the extent of their decline worldwide is unknown. Growing urban development is converting woodlands and wetlands, reducing aquatic and terrestrial salamander habitat. Consequentially, most salamanders are threatened by habitat loss and water pollution. Forty percent of North American salamander species are considered to be at risk and the Eastern Tiger Salamander has been listed as endangered since 1983. Long Island Pine Barrens is the northern limit of the tiger salamander in its known range and a stronghold for this species. The purpose of this study is to develop an understanding of the chemical and biological factors that affect salamander population and distribution, identify possible threats to viability, and contribute to the development of a management plan to protect this species. Field studies and analysis activities include soil and water measurements important to the ecological functioning of coastal ponds in the Long Island Pine Barrens—Peconic River Complex. Water and soil samples were collected and analyzed in four natural ponds and were analyzed using colorimetric and spectroscopic methods. Multiple soil samples prepared in accordance and water samples were further analyzed for metals using inductively coupled plasma –atomic emission spectrometer (ICP). Tiger salamanders appeared to thrive in areas with low concentrations of pollutants and moderate levels of natural factors such as dissolved oxygen. The presence of tannin—lignin and the amount of suspended solids had an affect on the salamander populations showing that salamanders prefer an oxygen-rich environment that contains a low amount of decaying matter. According to our research, steady water depths are desired by the species as well. This work was completed as a small portion of the implemented Wildlife Management Plan being conducted by the Environmental and Waste Management Services Division at Brookhaven National Laboratory. The soil and water chemistry of ponds with and without tiger salamanders was analyzed in order to further investigate the decline of the species as well as aid in the conservation of salamander habitats.

Synthesis and Characterization of Novel Nanoporous Metal Thiophosphates. *JULIA GLOVACK (SUNY Fredonia, Fredonia, NY 14063) DAWN WELLMAN (Pacific Northwest National Laboratory, Richland, WA 99352).* The first organically templated tin (II) thiophosphates have been synthesized using cetyltrimethylammonium chloride as the surfactant. The synthetic materials were characterized by x-ray diffraction, HR-TEM, and ICP-OES. Chemical analysis confirmed the material was composed of tin, phosphorus, sulfur, and oxygen, with sulfur being a minor constituent. The nanoporous tin (II) thiophosphate was found to be an effective adsorbent for Hg (14.03 mg-15.05 mg/g adsorbent).

Conductivity Measurements of Synthesized Heteropoly Acid Membranes for Proton Exchange Membrane Fuel Cells. *BRENNA HALEY (University of Northern Colorado, Greeley, CO 80639) JOHN TURNER (National Renewable Energy Laboratory, Golden, CO 89401).* Fuel cell technology is receiving attention due to its potential to be a pollution free method of electricity production when using renewably produced hydrogen as fuel. In a Proton Exchange Membrane (PEM) fuel cell H_2 and O_2 react at separate electrodes, producing electricity,

thermal energy, and water. A key component of the PEM fuel cell is the membrane that separates the electrodes. DuPont's Nafion® is the most commonly used membrane in PEM fuel cells; however, fuel cell dehydration at temperatures near 100°C, resulting in poor conductivity, is a major hindrance to fuel cell performance. Recent studies incorporating heteropoly acids (HPAs) into membranes have shown an increase in conductivity and thus improvement in performance. HPAs are inorganic materials with known high proton conductivities. The primary objective of this work is to measure the conductivity of Nafion, X-Ionomer membranes, and National Renewable Energy Laboratory (NREL) Developed Membranes that are doped with different HPAs at different concentrations. Four-point conductivity measurements using a third generation BekkTech® conductivity test cell are used to determine membrane conductivity. The effect of multiple temperature and humidification levels is also examined. While the classic commercial membrane, Nafion, has a conductivity of approximately 0.10 S/cm, measurements for membranes in this study range from 0.0030–0.58 S/cm, depending on membrane type, structure of the HPA, and the relative humidity. In general, the X-ionomer with $H_6P_2W_{21}O_{71}$ HPA gave the highest conductivity and the Nafion with the 12-phosphotungstic (PW_{12}) HPA gave the lowest. The NREL composite membranes had conductivities on the order of 0.0013 - 0.025 S/cm.

Physical Properties of Racemic Ionic Liquids Containing a 2,3-dihydroxyl-propyl Unit. *JASMINE HATCHER (Queensborough Community College, Bayside, NY 11364) JAMES WISHART (Brookhaven National Laboratory, Upton, NY 11973).* Ionic liquids have generated much interest due to their potential green chemistry applications. Green chemistry focuses on the design of chemical processes that reduce or eliminate the use and production of environmentally hazardous substances. Ionic liquids are environmentally friendlier solvent alternatives to traditional volatile (and hazardous) organic solvents because of their lack of vapor pressure. This means that they do not evaporate and therefore are considered safer. Ionic liquids are organic salts that have a melting point that is less than 100°C. They usually have a large cation and a relatively small anion. We report here on the synthesis and preliminary characterization of chiral ionic liquids. Chirality describes a molecule that is non-super imposable on its mirror image. This makes the molecule more asymmetrical and discourages solidification because it frustrates packing. In order to make the molecule chiral, we took a chiral auxiliary, 3-chloro-1,2-propanediol, and added it to a tertiary amine. Some of the tertiary amines used were DABCO (diazobicyclo [2,2,2] octane) and 1-methyl imidazole. We then converted the chiral halide salt into potential ionic liquids by anion exchange. Anion exchange was accomplished by reacting the halide salt with an acid or a metal salt that has the desired anion. Anions studied include phosphate, dicyanamide and bis (trifyl)imide. A large problem with ionic liquids is that they are very viscous. This makes it difficult to work with them at room temperature. Preliminary results suggest that adding a chiral center reduces viscosity. Future work will focus on conductivity and viscosity measurements of these new species.

Silicon Nitride for Direct Water-Splitting and Corrosion Mitigation. *JEFF HEAD (Colorado State University, Fort Collins, CO 80120) JOHN TURNER (National Renewable Energy Laboratory, Golden, CO 89401).* Today's fossil fuels are becoming harder to obtain, creating pollution problems, and posing hazards to people's health. One alternative to fossil fuels is hydrogen, capable of serving as a clean and efficient energy carrier. Certain semiconductors are able to harness the energy of photons and direct it into water electrolysis in a process known as photoelectrochemical water splitting. Triple junction devices integrate three semiconductors of different band gaps resulting in a monolithic material that absorbs over a broader spectrum. Amorphous silicon (a-Si) is one such material that, when stacked in tandem, posesses water-splitting capabilities. Even though a-Si is capable of splitting water, it is an unstable material in solution and therefore requires a coating to protect the surface from corrosion. A stable, transparent material that has the potential for corrosion protection is silicon nitride. In this study, silicon nitride thin films were grown using DC magnetron sputtering with varying amounts of argon and nitrogen added to the system. X-ray diffraction indicated amorphous silicon nitride films. Current as a function of potential was determined from cyclic voltammetry measurements. Mott-Schottky analysis showed variation in flatband potentials with n-type behavior. Absorption and transmission measurements indicate variation in band gap values ranging from 1.90 to 4.0 eV. Corrosion measurements reveal that the silicon nitride samples exhibit both p-type and n-type behavior. Photocurrent over a range of potentials was greater in samples that were submerged in acidic electrolyte. Silicon nitride shows good stability in acidic, neutral, and basic solutions, indicative of a good material for corrosion mitigation.

The Effect of Ether and Hydroxyl Moieties on the Properties of Structurally Diverse Ionic Liquids. *VANESSA HERNANDEZ (Queensborough Community College, Queens, NY 11364) JAMES WISHART (Brookhaven National Laboratory, Upton, NY 11973).* The attractive properties of ionic liquids, including negligible vapor pressure, high conductivity, low flammability, low melting points and recyclable nature, makes them ideal as environmentally friendlier solvent alternatives. They are currently being extensively investigated as alternative reaction media. We have prepared several series of ionic liquids containing cations based on pyrrolidine, imidazole, pyridine, and dabco species bearing ether and hydroxyl substituents. We report here on the synthesis and physical characterization of these types of compounds and the effect of the ether and hydroxyl functionalities. Previous reports have indicated that these substituents have an effect on viscosity. The characterization of these compounds is important because ultimately we want to be able to "custom design" ionic liquids to exhibit desired physical properties such as viscosity, conductivity and melting point. Variation in physical properties can be achieved by interchanging various cations and anions. Cations investigated include quaternary ammonium salts with hydroxyl or ether substituents. Anions investigated include phosphate, bis(trifluoromethanesulfonyl)imide, dicyanamide, bis(oxalato)borate and halides. The cations were first synthesized by reaction of an amine with an alkyl halide to produce a quaternary ammonium halide salt. The halide salt was then converted to a phosphate, bis(trifyl)imide, dicyanamide and bis(oxalato)borate to give potential ionic liquids. The conversion was achieved using metathesis reactions of the halide salt with the metal salt or acid of the desired anion. Structural confirmation was done using C-13, H-1 and P-31 NMR. Samples are analyzed for residual halide and water content and then characterized for their physical properties. Preliminary results indicate conductivity values of bis(trifluoromethanesulfonyl)imide species at 20°C in the range of 0.20 mS/cm and viscosity in the range of 500–550 cP. Continuing studies will focus on synthesizing and characterizing similar compounds with different anions and comparing their physical properties.

Computational Fluid Dynamics and Electrochemical Modeling of a Sulfur Trioxide Electrolysis Cell for use in the Westinghouse Hybrid Sulfur Cycle. *KATHERINE HOHNHOLT (Massachusetts Institute of Technology, Cambridge, MA 02141) DEBORAH J. MYERS (Argonne National Laboratory, Argonne, IL 60439)*. Recently hydrogen has become an exciting new alternative for fueling automotive transportation. Hydrogen, however, has to be produced. One proposed cycle is the Westinghouse Hybrid Sulfur Cycle, which uses the electrolysis of water and sulfur dioxide to produce sulfuric acid and hydrogen. Subsequently, the sulfuric acid is thermally decomposed to sulfur trioxide. Additionally, the sulfur dioxide is regenerated by thermal decomposition of sulfur trioxide. The cycle is promising because it requires less electrical energy then pure water electrolysis. A major disadvantage to this cycle, however, is the extremely high temperatures (>1,000°C) required for sulfur trioxide decomposition. An additional electrolysis cell designed to decompose sulfur trioxide at lower temperatures (500°–600°C) is one proposed solution to this problem. In order to better understand the potential of this alternative, an electrochemical and fluid dynamics model was developed using the commercial code – Star-CD. A previous model developed at Argonne National Laboratory used to model water electrolysis was updated to change the thermodynamic and fluid properties of the new cell. Additional adjustments to the cell model were made in order to improve the calculation of three key variables: the exchange current, limiting current, and diffusivity. In order to determine the feasibility of the temperature range chosen, the thermodynamic stability of the electrolyte was examined. The stability calculations suggested that the electrolyte would be more stable at higher temperatures. The model was run at varying temperatures and product concentrations to examine the effects on cell properties and production. Increasing temperature and decreasing sulfur dioxide inlet mass fraction both increased current density and thus production through the cell. However, they also decreased the voltage efficiency of the cell and increased temperature gradients.

Synthesis of Niobium Selenide Nanoparticles. *KYLEE HYZER (University of Missouri-Rolla, Rolla, MO 65409) JOHN SCHLUETER (Argonne National Laboratory, Argonne, IL 60439).* Several attempts were made to synthesize niobium selenide nanoparticles. Common synthetic processes such as reverse micelle synthesis and the introduction of a capping ligand were studied. Various niobium and selenium reagents were used in the synthesis. This study is still being

conducted and there are many results of experiments that still must be analyzed.

Microwave Synthesis and Characterization of Pyridine-based Ionic Liquids including Vitamin(B3). *ANNU IPE (Queensborough Community College, Bayside, NY 11364) JAMES WISHART (Brookhaven National Laboratory, Upton, NY 11973).* Ionic liquids are salts that are liquid at or below room temperature. Ionic liquids have no measurable vapor pressure and are considered environmentally friendlier than the volatile organic solvents currently being used such as benzene, toluene and methylene chloride. We are exploring the synthesis of ionic liquids from pyridine-based precursors including bio-renewable compounds, such as nicotinic acid (Vitamin B3) using a microwave reactor. Performing the synthesis using microwave energy saves both time and energy. Synthesis performed by conventional methods may take days, whereas in a microwave reactor synthesis is achieved in less than thirty minutes. The potential ionic liquids are synthesized by reacting nicotinic acid with a variety of alkyl and aryl halides to prepare the corresponding quaternized halide salts. The halide salts are then converted into a series of ionic liquids with varying anions including phosphate, bis(trifluoromethylsulfonyl)imide (NTf_2) and dicyanamide. Physical properties including melting point, viscosity, conductivity and water content will be investigated. Preliminary results indicate that we have successfully prepared pyridinium ionic liquids containing hydroxyl and ether substituents with phosphate and NTf_2 anions. Nicotinic acid (an analog of pyridine) was more difficult to alkylate and reaction with most alkyl halides was unsuccessful. However allyl bromide was found to be a successful alkylating agent for quaternizing nicotinic acid. Future research will focus on relating the structure of these new compounds to their properties.

A Systematic Search for New Bismuth and Lead Based Oxide Scintillators and Semiconductors. *CHRISTOPHER JESSAMY (North Carolina Agricultural and Technical State University, Greensboro, NC 27411) STEPHEN DERENZO (Lawrence Berkeley National Laboratory, Berkeley, CA 94720).* In recent times, the steady increase in the uses of radiation detectors has imoposed a great need for higher efficiency and lower costs of detector production. Through such an acheivement, applications ranging from medical imaging to weapons detection may be realized. Prompted by this demand, our research focuses on the discovery of new radiation detectors. In this manuscript we report the results of a systematic search for such detectors that have structures based on lead and bismuth. In this work we synthesized and characterized four compounds: Bi_2TeO_5, $PbTeO_3$, $Ca_2Bi_2O_5$, and Compound A. We were able to identify four semiconductors (Compound A and Compounds 1-3) by DC ionization under gamma irradiation.

Adsorption and Unfolding Kinetics of Ovalbumin on a Diethyl Aminoethyl Surface. *ALISHA JOHNS (University of Washington, Seattle, WA 98195) STEVEN GOHEEN (Pacific Northwest National Laboratory, Richland, WA 99352).* Proteins that are soluble in aqueous media will frequently adsorb and unfold on solid surfaces. This process is responsible for many of the physiological properties of proteins including enzyme activity, their structural behavior in vivo, protein-protein interactions as in blood coagulation, transport processes, etc. In this study, ovalbumin was studied as for its adsorption, retention, and unfolding properties on the anionic surface of diethyl aminoethyl, DEAE. This investigation examined both the changes in retention and recovery of ovalbumin under gradient chromatographic conditions. Several soluble proteins have already been studied in this manner. The trend for three proteins has been to unfold more rapidly with the molecular weight of the protein. A linear relation was found between the logMW and unfolding kinetics. Ovalbumin was adsorbed at 27 degrees C and pH 7.4 while eluting with a linear salt gradient. Additional experiments involved retaining the protein on the surface for various periods of time using a dilute salt butter before they were allowed to elute. Such a process caused the quantity of the material eluted to change, but not elution pattern. To date, the Ovalbumin recovery data needs further evaluation. A calculation was performed to explain how logMW can correlate with unfolding kinetics. The calculation assumes rigid planar surfaces and spherical proteins. The calculation correlates with previous observations in which an increase in the logarithm of the molecular weight of the protein is proportional to the amount of time required for 50% of that protein to unfold.

Caffeinated Ionic Liquids. *KIJIANA KERR (Queensborough Community College, Bayside, NY 11364) JAMES WISHART (Brookhaven National Laboratory, Upton, NY 11973).* Ionic liquids are defined as materials containing only ionic species without any neutral molecules and exhibiting a low melting point (usually below 100°C). Recently there has been an increased interest in preparing ionic liquids from biorenewable precursors. We have been investigating the potential of using caffeine as a precursor for ionic liquids. Preliminary attempts to quaternize caffeine by attaching a hydroxyl, ether and benzyl substituents to the C-3 position of the imidazole ring have been unsuccessful or required long reaction time. We are currently repeating these reactions using microwave assisted synthetic techniques and other alkylating reagents. Microwave assisted synthetic reaction conditions such as temperature, the nature of the reaction solvent and length of reaction have been continuously varied, however the results have also proven inconclusive. Once successful the quaternized salts will be converted to ionic liquids bearing various anions and the physical properties will be investigated. The results of the microwave assisted synthesis and the physical properties of the ionic liquids will be reported.

Optimization of Synthetic Clay Materials for Advanced Energy Applications: Deep Hydrodesulfurization Activity of Ni/Mo/S Synthetic Clays and Controlling Organo-Density of Grafted Synthetic Clays. *GREGORY KUZMANICH (University of Illinois at Urbana-Champaign, Champaign-Urbana, IL 61801) KATHLEEN CARRADO (Argonne National Laboratory, Argonne, IL 60439).* Contributions towards two projects for the Catalyst Design Group were made developing synthetic clays for two different applications. One project provides supports for hydrodesulfurization (HDS) catalysts. The other is optimizing organo-grafted materials for possible use in specialty polymer-clay nanocomposites or in solar energy applications. Synthetic clays derived from silica sol have been loaded with a Co/Mo/S mixture and examined as a less expensive materials, more efficient catalyst to desulfurize crude oil. The clays were tested with collaborators at Pennsylvania State University (PSU) to measure the conversion of dimethyl dibenzothiophene, and the results indicated that desulfurization was obtained at a rate similar to a current commercial catalyst. The project now is to determine whether a synthetic clay loaded with a Ni/Mo/S mixture would produce conversions equal to or better than commercial catalysts. The synthetic clays have been made from various silica sols or ion-exchanged versions of pre-made clays. These clays were then characterized by x-ray diffraction (XRD) and thermal gravimetric analysis (TGA) to determine their structure and composition, as well as by N2 porosimetry to determine adsorption/desorption isotherms, surface areas, and pore volumes. All of the clays produced synthetically were determined to be pure. These clays will be loaded with Ni/Mo/S by Professor Song at PSU and tested for their HDS activity. The second project prepares synthetic clays using alkoxysilanes. The goal of this project is to combine alkoxysilanes and organoalkosysilanes in various mixtures in order to create materials of varying densities of organo groups grafted to the silicate surface. Controlling the spacing between organic groups in this fashion can have effects on affinities for polymer-clay nanocomposite applications. In addition, further derivitization of the organo groups can be utilized for bonding both electron donor and acceptor groups for solar energy applications. The clays synthesized were made by combining various ratios of tetraethoxysilane and phenyltriethoxysilane, and they indicated the formation of silica clay through the use of XRD. The amount of organic material was tested through the use of TGA. The results were promising that organo density can be controlled using various silicon-containing sources.

The Relationship of Soil and Water Chemistry to the Preservation of Salamander Habitats in the Long Island Pine Barrens. *SONYA LAMB (North Carolina Agricultural and Technical State University, Greensboro, NC 27411) TIM GREEN (Brookhaven National Laboratory, Upton, NY 11973).* Although salamanders are the dominant vertebrate population in the ponds of the eastern United States, little is known about their habits. As a result, the extent of their decline worldwide is unknown. Growing urban development is converting woodlands and wetlands, reducing aquatic and terrestrial salamander habitat. Consequentially, most salamanders are threatened by habitat loss and water pollution. Forty percent of North American salamander species are considered to be at risk and the Eastern Tiger Salamander has been listed as endangered since 1983. Long Island Pine Barrens is the northern limit of the tiger salamander in its known range and a stronghold for this species. The purpose of this study is to develop an understanding of the chemical and biological factors that affect salamander population and distribution, identify possible threats to viability, and contribute to the development of a management plan to protect this species. Field studies and analysis activities include soil and water measurements important to the ecological functioning of coastal ponds in the Long Island Pine Barrens—Peconic River Complex. Water and soil samples were collected and analyzed in four

natural ponds and were analyzed using colorimetric and spectroscopic methods. Multiple soil samples prepared in accordance and water samples were further analyzed for metals using inductively coupled plasma–atomic emission spectrometer (ICP). Tiger salamanders appeared to thrive in areas with low concentrations of pollutants and moderate levels of natural factors such as dissolved oxygen. The presence of tannin–lignin and the amount of suspended solids had an affect on the salamander populations showing that salamanders prefer an oxygen-rich environment that contains a low amount of decaying matter. According to our research, steady water depths are desired by the species as well. This work was completed as a small portion of the implemented Wildlife Management Plan being conducted by the Environmental and Waste Management Services Division at Brookhaven National Laboratory. The soil and water chemistry of ponds with and without tiger salamanders was analyzed in order to further investigate the decline of the species as well as aid in the conservation of salamander habitats.

The Effect of Ionic Liquids on Conformationally-Controlled Intramolecular Electron Transfer in a Peptide-Bridged Donor-Acceptor System. *HEATHER LEE (Rutgers University, Piscataway, NJ 08854) JAMES WISHART (Brookhaven National Laboratory, Upton, NY 11973).* In recent years, room-temperature ionic liquids (IL) have become popular media for a variety of chemical processes, including the storage of solar energy by photoinduced electron transfer, due to their intrinsic properties such as negligible volatility, high thermal stability, and high conductivity. Peptide bridged electron donor-acceptor systems have been important tools for studying electron transfer, and previous work has shown that various solvents influence the conformation of the peptide bridge and thereby control electron transfer rates. The cis/trans isomerization of proline peptides is a case in point. We report here on the influence of IL on rates of electron transfer across the diproline bridge in tetramethylrhodamine-pro2-dimethyphenylenediamine (TMRA-Pro2-DMPD). A distribution of intramolecular electron transfer rates is expected due to different proline cis/trans conformational distributions depending on the polarity of the IL. The experiment will be investigated in four different IL: N-methyl-N-hydroxypropylpyrrolidinium dicyanamide, N-methyl-N-hydroxypropylpyrrolidinium bis(trifluoromethanesulfonyl)imide, N-methyl-N-butylpyrrolidinium dicyanamide, and N-methyl-N-butylpyrrolidinium bis(trifluoromethanesulfonyl)imide. Methods of IL preparation were developed using microwave-assisted organic synthesis, and the IL were characterized for their physical properties. Combinations of different cations (containing alkyl or hydroxy alkyl substituents) and anions (hydrophobic or hydrophilic) resulted in IL with varying polarities. Using Reichardt's dye, a standard solvatochromic probe, the normalized solvent polarity indices ETN span a large range: 0.84, 0.70, 0.56 and 0.55 for $P1_{prOH}NTf_2$, $P1_{prOH}DCA$, P14DCA, and $P_{14}NTf_2$ respectively. TMRA-Pro2-DMPD is expected to have distributions of cis/trans configurations that depend on the polarity and hydrogen bond-donating ability of the IL. Time-correlated single-photon counting has been used to measure emission lifetimes (and electron transfer rates) of TMRA-Pro2-DMPD in each of the four IL. Electron transfer rates will be calculated when the corresponding controls are completed. Inferences will be made concerning the influence of the IL on peptide conformation and electron transfer energetic.

Effect of Ozone on Nicotine Desorption from Model Surfaces. *SHARON LEE (University of California Berkeley, Berkeley, CA 94720) HUGO DESTAILLATS (Lawrence Berkeley National Laboratory, Berkeley, CA 94720).* Environmental Tobacco Smoke (ETS) can cause harmful respiratory diseases when present in enclosed spaces. Although ETS is composed of many different compounds, nicotine is used as its tracer. Due to nicotine's ability to sorb onto and desorb from different materials at different rates, its interaction with these materials must be further investigated. Therefore, desorption profiles of nicotine with household surfaces such as Teflon, cotton and wallboard is important to study. Using a 200-L chamber, nicotine desorption profiles were observed on these three surfaces. In order to test conditions similar to those present in ambient air, different humidity and ozone levels were also explored. All samples were collected using Tenax tubes and analyzed with a gas chromatographer. Preliminary results indicate nicotine desorption was significantly reduced in the presence of ozone under most experimental conditions. On cotton surfaces in humid air, the competition between ozone and water for reaction with nicotine on cotton surfaces and water's ability to react reversibly with nicotine led to higher concentrations of nicotine in the chamber. In addition, mechanisms proposed for ozone and nicotine reaction products supported this observation due to water's ability to also react with the pyrrolidinic ring. Unlike cotton, Teflon chamber experiments with humid and dry air showed the expected decrease in nicotine concentrations when ozone was added into the chamber. This observation was attributed to the hydrophobic nature of Teflon surfaces. Wallboard experiments showed a larger concentration of ozone was needed in order for a pseudo first-order reaction to occur. However, future experiments relating to wallboard must be investigated in order to compare its desorption profile with cotton and Teflon surfaces. Also, studies relating to water hydrogen bonding interactions with surfaces would be beneficial to understanding surface reactions of ozone, water, and nicotine.

Effect of Microbial Activity on the In Situ Immobilization of Uranium via Phosphate Amendments. *KATARINA MALATOVA (Rochester Institute of Technology, Rochester, NY 14623) DAWN WELLMAN (Pacific Northwest National Laboratory, Richland, WA 99352).* Immobilization of subsurface uranium plumes via in-situ precipitation with phosphate has been proposed as an alternative remediation technology to standard pump-and-treat methods. Initial investigations regarding the immobilization of uranium via phosphate amendments have centered on inorganic reactions and show promise, but the impact of microbiologic activity on the proposed phosphate amendments and overall remediation strategy is unknown. Natural microorganisms obtained from sediments taken from the Hanford Site (southeastern Washington State) and a pure culture of Arthrobacter globiformis, the most occurring bacteria within the natural extract, were investigated for their effect on the degradation and utility of phosphate amendments for in situ remediation of uranium and on the long-term stability of target uranyl-phosphate minerals. A series of batch experiments were conducted under conditions representative of the Hanford subsurface environment, in the presence and absence of a minimum amount of carbon (0.1% yeast extract), T = 23°C and pH 8. Experiments were conducted in the absence of carbon to asses the effect of adding a source of phosphorus to a carbon limited environment, which is representative of the Hanford subsurface, on microbial growth. Preliminary results indicate that microbial activity is significantly greater in the presence of both uranyl-phosphate minerals and aqueous phosphate amendments; the presence of carbon appears to provide minimal contribution to the degree of microbial activity within the system.

Surface Studies of Cesium Absorbed on Aluminum and Paving Brick. *GAVIN-AJANI NAVARRO & MICHELLE MALONE (University of the Virgin Islands, St. Thomas, VI 00801) GREGG LUMETTA (Pacific Northwest National Laboratory, Richland, WA 99352).* Ever since September 11, 2001, terrorist attacks using Radioactive Dispersive Devices (RDD) has been a major concern. RDDs are weapons that combine conventional explosives with radioactive materials. Cesium-137 is one possible radioisotope that might be encountered in an RDD. Understanding how cesium (and other radionuclides) interacts with urban surfaces is needed to provide the scientific basis for developing strategies for responding to and recovering from RDD attacks. In this work, cesium hydroxide (CsOH) was used as the source of cesium contaminant. The two urban surfaces that were investigated were aluminum and paving brick. CsOH was placed on samples of both materials. The samples were dried in an oven and then were placed inside the high vacuum chamber of a combined X-Ray Photoelectron/Auger Spectrometer. Control samples of aluminum and paving brick without added Cs were also placed inside the vacuum chamber in order to obtain reference spectra. The samples were then analyzed to determine surface composition. After comparison with reference spectra, Cs peaks were detected on the aluminum surface and one of the paving brick samples (# 2). On the aluminum spectra, peaks of Cs were detected at 75 eV and 724 eV. Aluminum and oxygen peaks were also detected. On the paving brick sample # 2, Cs peaks were observed at 75 eV and 724 eV. Other peaks that were observed are calcium, silicon, sodium, and oxygen.

Exploring the Solution Phase Conformations of a Cyclic Porphryin Hexamer by Combining Molecular Simulations with High-Angle X-Ray Scattering Data. *KRISTY MARDIS (Chicago State University, Chicago, IL 60628 and Argonne National Laboratory, Argonne, IL 60439).* The determination of the structure of macromolecular complexes is a crucial step in the design of supramolecular assemblies. The usage of such complexes often depends on their ability to maintain a particular conformation in solution. Unfortunately, the common techniques of solidstate X-ray diffraction and solution phase NMR are often inadequate for supramolecular assembly structural determination. High-angle X-ray scattering provides a complementary technique for solution phase structural determination. When used in conjunction with molecular simulations, high-angle X-ray scattering allows for the testing of structural models and the measurement of

solution state configurational dispersions. The current work focuses on performing molecular simulations on a cyclic diphenylethyne-linked porphyrin hexamer. Such porphyrin based structures are important in photochemistry and energy transfer applications. Constant pressure temperature simulations using the Charmm 22 force field in explicit solvent (toluene) were able to accurately reproduce the experimental scattering data. The conformations present in the simulation indicate that the prophyrin subunits undergo a great deal of twisting motion-some becoming nearly parallel with the plane of the ring. These results provide new insight into the structural flexibility of this complex in solution and will allow a structural basis for the understanding of the photophysical and host-guest possibilities of the hexameric porphyrin assembly in solution. Furthermore, the success of this project as a testcase for the combination of simulation and high-angle x-ray diffraction data for the determination of macromolecular structure supports our plan to engage in additional simulations of cytochrome c porphyrin complexes important as possible energy-transfer devices.

Synthesis of Aryl and Akyl Substituted Ionic Liquids. *HEIDI MARTINEZ (Queensborough Community College, Bayside, NY 11364) JAMES WISHART (Brookhaven National Laboratory, Upton, NY 11973).* Ionic Liquids continue to attract widespread attention because of their potential as environmentally friendlier solvent alternatives. We have previously reported on the synthesis of a series of symmetrical quaternary ammonium ionic liquids. These ionic liquids were of unique structural types bearing phosphate and bis(trifyl)imide anions. However, the symmetrical nature of the cations resulted in ionic liquids with high viscosity, an undesirable property for most applications. We report here on the synthesis of less symmetrical analogs of the compounds previously prepared with the goal of producing less viscous ionic liquids. Particular focus is on the synthesis of quaternary ammonium cations bearing aryl and alkyl substituents. Investigation of the effect on the physical properties of ionic liquids resulting from this structural variation of the cation involved is also being investigated. Benzyl chloride was the main reagent used for the synthesis of aryl salts whereas short chain alkyl halides were used to synthesize the alkyl substituted ammonium salts. The reactions were done under low temperature reflux conditions with stirring. The resultant compounds were purified using various methods including modified charcoal and alumina columns. The halide salts of varying structural types were converted into ionic liquids using four different anions. This was achieved mainly by metathesis reactions using the metal salt or acid of the desired anion. Structure confirmation of the product was performed using C-13 and H-1 NMR. Liquids are screened for residual halide and water content and then characterized. Physical properties including conductivity, viscosity, melting point, density and solvent properties will be studied.

The Modeling of Porphyrin Supramolecular Assemblies Using Langevin Molecular Dynamics. *JOHN MASSEY (Chicago State University, Chicago, IL 60628) KRISTY MARDIS (Argonne National Laboratory, Argonne, IL 60439).* A molecule's conformation determines much of its biological, physical and chemical properties. Therefore, an accurate understanding of these conformations is critical to the understanding of the structure, function and properties of these assemblies. There is a need for methods that resolve the structure and dynamics of supramolecular architectures in solution. One method particularly suited to supramolecular assemblies in solution is high-angle X-ray diffraction. To take full advantage of the data provided through high-angle x-ray diffraction, molecular models of the assemblies must be constructed and their scattering patterns compared to the experimental data. In this work, Langevin dynamics using the Charmm 22 force field were used to construct models of a cyclic Zinc porphyrin hexamer. The goal was to determine if Langevin dynamics could provide accurate models of the solution structure by comparing scattering patterns calculated from the models to the high-angle X-ray diffraction data. Equilibration required relatively high collisional frequencies greater than 20. The models matched the experimental results in the region of 0.01 Å-1 to 0.6 Å-1. In the region of 0.6-1.1 Å-1, the match was to a lesser extent with an additional peak present in the calculated scattering pattern. The high collisional frequencies employed did not allow enough flexibility and kept the structure too close to the starting minimized structure. Longer runs may alleviate this problem. A greater insight into the flexibility of this molecule in solution was gained.

Calorimetry of In Development Dispersion Nuclear Fuels. *THOMAS MCDONALD (Northwestern University, Evanston, IL 60208) J. RORY KENNEDY (Idaho National Laboratory, Idaho Falls, ID 83415).* The Reduced Enrichment for Research and Test Reactors (RERTR) project develops new fuels for the conversion of civilian research and test nuclear reactors from high enriched uranium to low enriched uranium fuels and targets. Fundamental physical properties of new fuels are needed to accurately model how the fuels will behave in and out of a reactor. Using a heat flux differential scanning calorimeter, the enthalpy of reaction and reaction onset temperatures were determined for two uranium-molybdenum-aluminum dispersion type fuel mixtures. The reaction onset temperatures for the two fuels were found to be very similar. However, the enthalpy of reaction was smaller for the fuel containing less uranium. These measurements are one of the many steps necessary to qualify new nuclear fuels for the RERTR program, whose aim is to reduce the threat of nuclear proliferation.

The Use of Carbon Nanotube Modified Electrodes as a Method to Detect Organophosphates. *MARIA MELLEN (Orange Coast College, Costa Mesa, CA 92627) YUEHE LIN (Pacific Northwest National Laboratory, Richland, WA 99352).* Organophosphates (OPs) are neurotoxins found in pesticides and chemical warfare agents that have the potential to be introduced into water supplies. Recent studies have shown that carbon nanotubes (CNTs), in conjunction with amperometric techniques, can be utilized to make a highly sensitive OP biosensor. This would significantly improve upon current methods to detect OPs, which include gas and liquid chromatography; these techniques are more time-consuming, and cannot be performed on-site. Because OPs work by inhibiting the ability of the enzyme acetylcholinesterase (AChE) to break down the neurotransmitter acetylthiocholine (ATCh), both AChE and ATCh have been considered as a means to indirectly detect the presence of OP compounds. Using CNTs, we have been able to immobilize AChE onto a working electrode which can be used in conjunction with a potentiostat. The potentiostat applies voltage to the aqueous sample then measures the produced current. When the enzyme-modified electrode is introduced to ATCh, an increase in current is observed as the substrate is broken down into acetate and thiocholine (TCh). However, when the electrode is incubated in a sample containing OP, then retested with ATCh, the current does not reach the same levels as previous, signifying inhibition of AChE, and therefore, OP presence. Although this method for detecting OPs shows great potential, additional research is necessary. In the future, it should be possible to use this method alongside a fluid injection system, making the process more automated and reproducible. The data could then be extrapolated to make accurate predictions of OP concentrations in unknown samples.

Solubility and Speciation Studies of Manganese in Aqueous Manganite Solutions. *DANIEL NIEPORT (Diablo Valley College, Pleasant Hill, CA 94523) HEINO NITSCHE (Lawrence Berkeley National Laboratory, Berkeley, CA 94720).* Manganite (MnOOH), a manganese oxide mineral, has been shown to reduce highly soluble, aqueous mobile plutonium (VI) to relatively insoluble plutonium (IV). The physical characteristics of manganite which predict this redox reaction disagree with experiment. The conflict lies in that Mn^{2+} reduces Pu(VI) to Pu(IV) while in theory manganite is made of only Mn^{3+} ions that could reduce hexavalent plutonium by oxidation of Mn^{3+} to Mn^{4+}. However, should the manganese oxidation occur, the formation of manganese dioxide, MnO_2 would be observed. Manganese dioxide has a very low solubility and would precipitate as a solid. The formation of any solids other than manganite was not observed in the reported plutonium reduction experiments. The question that the research attempted to answer was if manganite solution that is in contact with air contains any Mn^{2+} in addition to Mn^{3+}. The presence of Mn^{2+} in Pu(VI) solutions would explain the observed plutonium reduction. In this work, we determined the total aqueous concentration of manganese in equilibrium with the solid of manganite by Inductively Coupled Plasma Optical Emission Spectrometry (ICP-OES). We then developed three electrochemical techniques, anodic stripping linear scan voltammetry (ASLSV) and differential pulses anodic stripping voltammetry (DPASV) on a hanging mercury drop electrode (HDME), a sitting mercury drop electrode, and a rotating disk mercury film electrode (RDEMF) to determine whether any Mn^{2+} ions and at what concentration are in the supernatant aqueous solution that is in equilibrium with the solid manganite. The range of total manganese concentration varied with the pH of the manganite solutions, ranging from 5×10^{-4} M to about 5×10^{-9} M, for pH 4.6 and 9.4, respectively. The manganite solubility reached a minimum at about pH 8.7, which was below the detection limit of the ICP-OES. Once manganite's physical properties are properly defined, better predictions can be made about redox reactions with manganite and plutonium compounds. Understanding plutonium manganite interactions in nature will result in better management and cleanup of plutonium contaminated sites.

Conditioned Place Preference to Inhaled Acetone and the Effects on Locomotor Behavior and 18FDG Uptake. *JENNIFER C. PAI (Cornell University, Ithaca, NY 14853) STEPHEN DEWEY (Brookhaven*

National Laboratory, Upton, NY 11973). Acetone is a component in many inhalants that have been widely abused. While other solvents have addictive potential, such as toluene, it is unclear whether acetone alone contains addictive properties. The locomotor, relative glucose metabolism and abusive effects of acetone inhalation were studied in animals using the conditioned place preference (CPP) paradigm and [18F]2-fluorodeoxy-D-glucose (18FDG) imaging. The CPP apparatus contains two distinct conditioning chambers and a middle adaptation chamber, each lined with photocells to monitor locomotor activity. Adolescent Sprague-Dawley rats (n=16; 90-110 g) were paired with acetone in least preferred conditioning chamber, determined on the pretest day. The animals were exposed to a 10,000 ppm dose for an hour, alternating days with air. A CPP test was conducted after the 3rd, 6th and 12th pairing. In these same animals, the relative glucose metabolism effects were determined using positron emission tomography (PET) imaging with 18FDG. Following the 3rd pairing, there was a significant aversion to the acetone paired chamber (190.9 ± 13.7 sec and 241.7 ± 16.9 sec, acetone and air, respectively). After the 6th pairing, there was no significant preference observed with equal time spent in each chamber (222 ± 21 sec and 207 ± 20 sec, acetone and air-paired, respectively). A similar trend was observed after the 12th pairing (213 ± 21 sec and 221 ± 22 sec, acetone and air-paired, respectively). Locomotor analysis indicated a significant decrease ($p < 0.05$) from air pairings to acetone pairings on the first and sixth pairings. The observed locomotor activity was characteristic of central nervous system (CNS) depressants, without showing clear abusive effects in this CPP model. In these studies, acetone vapors were not as reinforcing as other solvents, shown by overall lack of preference for the acetone paired side of the chamber. PET imaging indicated a regionally specific distribution of 18FDG uptake following acetone exposure. Further studies using different concentrations are required to better understand the locomotor and behavioral effects of acetone. This study confirms that the combination of microPET and the CPP paradigm can be used to elucidate the effects of abused solvents vs. non-abused solvents in inhalants.

A Visual Survey of the Effects of Various Parameters on the Plating Rate and Quality of High Purity Electroformed Copper. *TASHI PARSONS-MOSS (Mills College, Oakland, CA 94613) ERIC HOPPE (Pacific Northwest National Laboratory, Richland, WA 99352).* Copper of unprecedented purity is needed to serve as the building material for shields and cryostats of ultra-low background germanium spectrometers. High purity copper is electroformed in a Sulfuric Acid-Copper Sulfate plating bath using a reverse pulse plating (RPP) power supply. Structural integrity of copper is determined by the crystal structures formed and is important to the application described. Various changes in the plating conditions were tested and the products were visually assessed under a microscope. Changes in current density, RPP waveform, plating time, convection mechanism, and plating bath chemistry were tested. A conductivity probe and thermocouple were suspended in the plating bath and connected to a chart recorder to monitor the conductivity and temperature of the bath solution during plating. The average current was held constant during each plating session and average voltage was logged and allowed to fluctuate. Periodic samples of the bath solution were collected and tested for [$CuSO_4$] using a spectrophotometer. Each electroformed copper sample lacked uniformity in crystal structure, thickness and surface texture due to variations in electric field and ion concentration gradients surrounding the cathode surface. No two copper deposits are exactly alike, even when similar conditions are applied. The effects of changing most parameters are dramatic, most obviously with current density. High current densities form rough and pitted copper with little structural integrity and may decrease purity by supporting a wide range of potentials. Poor structural qualities obtained by high current density were accentuated by higher acid concentration. There is some flexibility with forward-to-reverse pulse time ratio, but some off-time in between pulses is necessary for a smooth strong structure. Thiourea is an effective brightening agent but any additive potentially increases contamination in the product. Cupric sulfate concentration seems fairly unimportant as long as a sufficient amount for plating is present. It is very important that the solution be thoroughly mixed during plating, but it is not obvious whether or not it should be done by the common industrial method of air sparge. Various tests of structural strength and purity assays on the products formed remain to be administered. These further tests, as well as many more in-depth formation parameter studies will be needed to fully understand and optimize the process.

Effect of Thiourea Anion Receptors on Cesium Extraction. *CAROL PHAM (University of Hawaii at Manoa, Honolulu, HI 96822) LAETITIA DELMAU (Oak Ridge National Laboratory, Oak Ridge, TN 37831).* Bis(t-octylbenzo-crown-6)calix[4]arene (BOBCalixC6) is a cation receptor with high selectivity for cesium in solvent extraction. When used as co-extractants with BOBCalixC6, anion receptors such as thioureas (RR'N-C(S)-NR'R) may hydrogen bond with counterions of cesium, facilitating the transfer of anions into the organic phase and thus increasing the extraction efficiency. To determine the extent to which a thiourea compound improves cesium extraction as well as the stoichiometry of the process and the importance of the anion's identity, it is necessary to perform a quantitative investigation of the extraction. Previous experiments using chloroform as the organic phase diluent produced complex systems containing apparently both dissociated and ion-paired species. In this project, nitrobenzene was used in place of chloroform to ensure a fully dissociated system, which is expected to follow a simpler model. During the survey portion of the experiment, extractions were performed using three thioureas and the following anions: bicarbonate, bromide, carbonate, chloride, chromate, hydroxide, iodide, nitrate, oxalate, perchlorate, and sulfate. Using radiotracers, the amount of cesium present in the aqueous and organic phases after extraction was determined. Plots relating the distribution ratio to the anion's energy of partition (ΔGp) revealed each thiourea's selectivity towards certain anions. The survey showed that using BOBCalixC6 and an anion receptor together produced a synergistic effect in the extraction of most of the salts tested, especially cesium bicarbonate, but an antagonistic behavior in some cesium perchlorate experiments. From survey data, ΔGp for bicarbonate was determined to be 40.1 kJ/mol. After performing experiments varying the concentrations of salt and thiourea, the SXLSQI program was used to model cesium bromide extraction with one of the anion receptors and obtain thermodynamic data. The model allowed calculation of the equilibrium constants K for complexation of cesium with BOBCalixC6 (logK = 8.55) and of bromide with the thiourea (logK = 3.12). The value for cesium-BOBCalixC6 complexation is in good agreement with the calculation results derived from a different set of experiments carried out in the group. This investigation of anion recognition is part of a larger study of the fundamental principles underlying the properties of new cation and anion receptors.

Development of Corrugated CVD Diamond Stripper Foils. *ROBERT POTTER (Brigham Young University Idaho, Rexburg, ID 83440) ROBERT SHAW (Oak Ridge National Laboratory, Oak Ridge, TN 37831).* Investigations of the growth and production process of micro and nano-crystalline diamond films have been conducted for use as stripper foils in the Spallation Neutron Source (SNS). Due to the expected ion beam power of the SNS currently under construction in the U.S.A., conventional carbon stripper foils are estimated to fail in approximately 10 hours. Chemical vapor deposition (CVD) diamond films have been grown and tested in a simulated SNS environment and were found to have a beam life of over 130 hours. Semiconductor-grade <100> silicon wafers are sonicated in diamond powder slurry to promote uniform nucleation during growth. Microcrystalline diamond film growth is accomplished using a 1,500-watt microwave CVD system with a plasma composition of 1–2% methane 98-99% hydrogen, at 50 Torr pressure and running at 1,300 watts for micro size crystals. Adding argon to the plasma gas produces nano crystalline diamond. Typically 1–2% methane, 8–9% hydrogen and 90% argon at 900 to 1,000 watts and 130 Torr pressure is used. These films were then analyzed using SEM and Raman Spectroscopy to determine continuity, uniformity, and substance. One requirement due to the Linac beam physics is that the diamond stripper foil be free standing, i.e., only supported on one side by silicon. This has led to the development of corrugations in the substrate, using conventional photolithography techniques, that allows a structured diamond film to be grown to increase stiffness and to combat the inherent stress related to the mismatched thermal expansion occurring during the growth process. New photolithography mask patterns are being considered in order to better resist the multidimensional stresses. Another development currently under investigation is a different method to dissolve the silicon substrate without the use of protective Teflon tape, which is difficult to apply and remove without damaging the film. These methods include applying silicon nitride and using KOH etchant instead of HF, or sputtering on a protective metal film. As it has been demonstrated that micro and nano diamond films are robust enough to withstand the purposed SNS beam strength, finalized manufacturing process details are currently being established.

Synthesis and Characterization of $Gd_{5-x}Y_xSi_yGe_{4-y}$. *ERIC POWELEIT (University of Wisconsin, Madison, WI 53715) GORDON MILLER (Ames Laboratory, Ames, IA 50011).* The system of $Gd_5Si_yGe_{4-y}$, while previously studied for its rather unique ability to break and form covalent bonds upon temperature change, is still only partially

understood. This work seeks to further the understanding of this system by exploring similar RE5Tt4 systems of $Gd_{5-x}Y_xSi_yGe_{4-y}$ and $Nd_zEr_{5-z}Ge4$ and observing how their structure and properties differ from those of $Gd_5Si_xGe_{4-x}$. Samples were prepared by repeatedly arc melting stoichiometric mixtures of constituent elements in an argon atmosphere, reaching temperatures of approximately 3,500°C. The structure of each sample was characterized by x-ray powder diffraction. In the $Gd_{5-x}Y_xSi_yGe_{4-y}$ system, two structural transitions were observed, the first occurring between y = 2.5 and y = 3.0 from a Sm_5Ge_4 - type structure to a monoclinic $Gd_5Si_2Ge_2$ - type structure and the second between y = 3.5 and y = 4.0 leading to an orthorhombic Gd_5Si_4 - type structure. Comparatively, the monoclinic phase in $Gd_5Si_xGe_{4-x}$ has been reported in the region between x = 2.012 and x =1.72. This shift in composition suggests that by reducing the volume of the rare earth sites, the formation of covalent bonds between the two-dimensional slabs that define the crystal becomes more favorable. In the $Nd_zEr_{5-z}Ge_4$ system, a structural transition was observed occurring between z = 1.8 and z = 2.0 from a Sm_5Ge_4 - type structure to a monoclinic $Zr_{3.9}Ta_{1.1}Ge_4$ - type structure. These results provide some novel insight into how the RE5Tt4 systems function and suggest that further characterization of these systems may produce a better understanding of their unique structural characteristics.

Carbon Nanotube Modified Glassy Carbon Electrode for the Detection of Enzymatically-generated Thiocholine. *SHAWN RIECHERS (Washington State University, Pullman, WA 99163) YUEHE LIN (Pacific Northwest National Laboratory, Richland, WA 99352).* A carbon nanotube glassy-carbon (CNT/GC) electrode was analyzed for increased sensitivity for the electrochemical detection of enzymatically generated thiocholine. This was accomplished by comparing the cyclic voltammetric and amperometric responses of the CNT/GC, glassy carbon (GC), carbon paste, and gold electrodes. The CNT/GC electrode was shown to give a signal many times greater than that of the GC, carbon paste, or gold electrodes. The added CNT layer lowered the oxidation overpotential (0.15 V) and provided increased sensitivity due to the electrocatalytic activity, rapid rate of electron transfer, and large surface area. Under optimized conditions a detection limit of 5 × 10-6 mol/L was obtained with a residual error of 5.2% (n=10). The CNT/GC electrode was also used in conjunction with constant-potential flow injection analysis to obtain an improved detection limit of 0.3 × 10-6 mol/L as well as an improvement in reproducibility. The increased sensitivity and ability to couple with flow injection analysis makes the CNT/GC electrode a promising platform for an automated biosensor in conjunction with acetylcholinesterase for the detection of organophosphate pesticides and nerve agents.

Molecular Simulations of a Hexameric Porphyrin Supramolecular Assembly using Langevin Dynamics. *TONI SANDERS (Chicago State University, Chicago, IL 60628) DAVID TIEDE (Argonne National Laboratory, Argonne, IL 60439).* There is a need for an accurate method to determine the structure of supramolecular assemblies in solution. X-ray crystallography provides structural information only in the solid phase and NMR cannot distinguish between identical subunits in a common motif in supramolecular assemblies. In contrast, high-angle x-ray diffraction may be an appropriate technique to determine the solution phase conformations of supramolecular structures. To take full advantage of high-angle x-ray diffraction, the experimental scattering patterns need to be combined with scattering data obtained from atomic level molecular models. In this work, we used CHARMM 22 and Langevin dynamics to model a supramolecular complex made up of six porphyrin rings, three containing zinc. When the calculated scattering data from the hexamer model was examined, it was found that simulations with collision frequencies of 20 ps-1, 15 ps-1, 10 ps-1 had similar scattering patterns. However, the calculated scattering pattern displayed a peak around 0.6 Å-1 that is larger than the one present in the experimental data. This larger peak stems from the structure being too organized and rigid. Collision frequencies of less than or equal to 5 ps-1 caused the porphyrin hexamer to unphysically pucker or fold. Because the collision frequency was too small, the frictional drag was not enough to maintain equilibrium ensembles and a shift in the scattering pattern compared to experimental data occurred. If the simulation is run longer than 200 ps there is a possibility that the calculated data will better match the experimental data. In any case, the simulations suggest that the hexamer complex is more flexible than had previously been thought.

Parameterizing Potential-Derived Charge-Dependent Cavity Radii for Continuum Solvation Models: Aqueous Solutes with Oxo, Hydroxo, Amino, and Methyl Functionalities. *CHRISTINE SCHWERDTFEGER (University of Illinois at Urbana-Champaign, Urbana, IL 61801) DONALD CAMAIONI (Pacific Northwest National Laboratory, Richland, WA 99352).* Continuum solvation models are economical to run, and, with advances that allow for molecule-shaped cavities, they have the potential to accurately simulate equilibrium properties of solutes. However, benchmark tests show that existing schemes for defining cavities are unable to consistently and accurately predict the effects of solvation on many neutrals and ions, especially anions. This paper reports on the development of a new protocol for defining the cavities of aqueous solutes. The cavity is defined as interlocking spheres around atoms or groups of atoms in the solute. The sphere radii are determined by simple empirically-based expressions involving the effective atomic charges of the solute atoms (derived from molecular electrostatic potential) that fit the solute molecular electrostatic potential and a base radius. Both of these terms are optimized for the different types of atoms/functional groups in a training set of neutral and charged solutes that include oxo, hydroxo, amino, and methyl functionalities. Parameters in the expressions for the radii were fitted by minimizing residuals between calculated and measured standard free energies of solvation (ΔGs*), weighted by the uncertainty in the measured value. The calculations were performed using Density Functional Theory with the B3LYP functional and 6-311+G** basis set in the Gaussian98 package of programs. The optimized radii definitions reproduce ΔGs* of neutrals and singly-charged ions in training set to within experimental uncertainty and accurately predict ΔGs* of some compounds outside the training set. The mean unsigned error for training set, which is comprised of 11 neutral compounds, 4 cations and 3 anions, is 0.18 kcal/mol. Inherent to this work's approach, the cavity definitions reflect the strength of specific solute-water interactions. We surmise that this feature underlies the success of the approach. The findings offer encouragement for extending to other functional groups to increase the applicability of the scheme and so obtain greater accuracy in using continuum solvation models to predict equilibrium properties of aqueous solutes.

Separation of Plastics from Shredder Residue by Froth Flotation. *SIOBHAN SHAY (Lewis University, Romeoville, IL 60446) BASSAM JODY (Argonne National Laboratory, Argonne, IL 60439).* As landfills in the United States, Europe and Asia become continuously filled, it is necessary for alternatives be found for the material being disposed of in mass quantities. The current objective of the Scrap Recovery and recycling project at Argonne National Lab is to develop an economical method of recovering plastics from "end of life" vehicles in order to reduce the amount of waste from automobiles in land fills. The current processes that are being investigated are known as froth flotation. The objective of the project is to be able to produce pure enough plastic fractions that meet the requirements for recycling through the use of frothers and depressants at various conditions. Final conclusions can not be made during this time because research has not been completed.

Determination of Acid/Base Equilibrium Constants for the Protonation of Triaryl Phosphines in Acetonitrile/Water Mixtures. *ANDREW SHUFF (Texas A&M University, College Station, TX 77844) ANDREJA BAKAC (Ames Laboratory, Ames, IA 50011).* There have been questionable and contradicting values for KH's of different phosphines in literature. Clarification of these values will relieve some of the confusion and aid those seeking to use the values as a vital part of their experiment. The goal of this project was to determine the protonation constants for triphenylphosphine, tri-p-tolylphosphine, tris(p-methoxyphenyl)phosphine, tris(p-trifluoromethylphenyl)phosphine, and tris(p-fluorophenyl)phosphine by UV-Vis and NMR spectroscopies. This was done by measuring the UV absorption or chemical shift of the phosphine in different concentrations of acid with the same ionic strength. The constants were also measured at different solvent mixtures between 50:50 acetonitrile and water (AN)/H_2O (v/v) and 90:10 AN/H_2O (v/v), then tested for a dependence on the fraction of water in the solvent. It was shown that UV-Vis and NMR spectroscopies give results that are identical within the experimental error. Both tris(p-trifluoromethylphenyl)phosphine and tris(p-fluorophenyl)phosphine were determined to not protonate. The protonation constants of the other three phosphines were found to be proportional to the fraction of water in the solvent. For example, the protonation constants for tri-p-tolylphosphine are 32.3 at 90:10 AN/H_2O (v/v), 11.7 at 80:20 AN/H_2O (v/v), and 4.33 at 67:33 AN/H_2O (v/v).

Self-Assembly of Monolayers of Alkylthiol Chains and Oligomers In Silico Using Molecular Dynamics Simulations. *JULIE STERN (State University of New York – Stony Brook, Stony Brook, NY 11794) MARSHALL D.* NEWTON (Brookhaven National Laboratory, Upton, NY 11973). Self-assembled monolayers (SAMs) consist of alkane chains on substrate and are used to form simple models of the

natural phenomena of self-organization and its physical and chemical properties. The alkane chains can be simple hydrocarbons or more complicated saturated chains with additional structure and side groups. In this study, alkythiol chains, hydrocarbon chains on sulfur, and OPE (oligophenyleneethynylene), phenylene-ethynylene oligomers, on sulfur at both ends of the chains, were studied for their self-assembly patterns and properties. These monolayer structures were designed and built in-silico using standard computational software and algorithms including AMBER force fields and Gaussian for the calculation of atomic charges. The "in-silico molecular synthesis protocol" was specifically designed and developed for this study. Molecular dynamics (MD) simulations were used to study structural changes in the SAMs at the atomic level. Starting from the initial molecular packaging of the monolayers and simulating with MD, lower energy stable structures emerged from the alkylthiol and dithiol-OPE monolayers corresponding to the self-assembly pattern. The alkylthiol monolayer produced a pattern of self-assembled tilt. The dithiol-OPE monolayer resulted in a distinctive and ordered herringbone pattern.

Development, Design and Deployment of Passive Samplers for Nicotine. *ELIZABETH STEWART (University of California Los Angeles, Los Angeles, CA 94707) LARA A. GUNDEL (Lawrence Berkeley National Laboratory, Berkeley, CA 94720)*. A passive sampling device for Environmental Tobacco Smoke (ETS) was developed and tested for retention of nicotine and 3-ethenylpyridine vapor. Passive sampling is preferred over active sampling because of the compact size, minimal energy requirement and low cost of the samplers. The devices will be placed into the households of participants in a NIH-funded smoking intervention program. Due to the complex nature of ETS and high basicity of nicotine, measurement of urine cotinine (a metabolic byproduct of nicotine) levels may not be an accurate measure of ETS exposure. The reliability of cotinine as a biological marker for ETS will be determined. Correlation will be made between the level of ETS exposure and the severity of the participants' children's asthma. The passive sampler will provide a more accurate measure of ETS exposure and correct misclassification of exposure status. Tenax-filled thermal tubes were extensively tested in an environmental chamber for 250 minutes while three cigarettes were smoked. Tubes that gave poor results for nicotine retention were repacked with either old or new tenax and retested. The validated, standard method of active sampling with tenax-filled thermal tubes was employed concurrently for comparison. Results from old tubes and tubes repacked with new tenax agree with results from the active samplers. More tests must be done to determine if tubes repacked with old tenax are reliable enough for use in the field. Design and building of a device to deploy and expose the passive samplers in the field has taken place.

Urban Dispersion Program. *DOMINGO TEMPLONUEVO (Suffolk County Community College, Selden, NY 11784) JOHN HEISER (Brookhaven National Laboratory, Upton, NY 11973).* The Urban Dispersion Program was developed to research how a chemical or airborne bacteria and virus that are release in air, will disperse in a city such as New York. The research will greatly help aid evacuation of people within the city and help save lives in case of a terrorist attack. There many mathematical models that already relate the fluid dynamics of chemical dispersion in air given a certain wind direction and speed. However, these models are slightly inaccurate in the city due to many factors that are involve such as car traffic, exhaust vents and building orientation which changes the wind direction in many different areas and elevations. Thus the Urban Dispersion Program or UDP had to simulate a chemical release using a safe known chemical tracer so that existing mathematical models can be compared and calibrated. UDP uses perflorocarbon tracers or PFTs to simulate a hazardous chemical release. PFTs gases is release in the air at a rate of 500 ml/min in different days and time while a device called Brookhaven Atmospheric Tracer Sampler or BATS collects air sample in a given time and time intervals. The BATS contain 23 sampler connected to an air pump that blows ambient air through each of the sampler in consecutive order. These samplers have a chemical compound called Ambesorb that adsorbs PFTs present in the air. Several BATS are scattered around the area of PFTs release point and are ran minutes after the release. There are other samplers that are use a handheld personal air sampler (PAS) that takes only one sample at a time using a Capillary Adsorbent Tracer Sampler or CATS, which also contains Ambesorb. After one run, the BATS and CATS are sent down to Brookhaven National Laboratory for analysis. The samples are then heated up and nitrogen gas is blown through it to desorb the PFTs in the Ambesorb. The PFTs that comes out goes through a gas chromatography and concentrations of each PFT are then calculated. Knowing the concentration and time and place where it was taken for each samples, a general picture of how the tracer spread through out the city is generated using a computer program. The result of the previous UDP research showed the variation of dispersion in different time of day even if the general atmospheric condition was the same. This variance is then accounted for to calibrate existing atmospheric models that can be used in an event of a chemical attack in the city.

Lead Doped Scintillators for Gamma Radiation Detection Synthesized by Room Temperature Sol-Gel Processing. *DUSTIN TRAVAGLINI (University of Florida, Gainesville, FL 32611) BANU KESANLI (Oak Ridge National Laboratory, Oak Ridge, TN 37831).* With a growing focus on homeland security, efforts have been made to improve present radiation detectors. Room-temperature sol-gel synthesis is an effective way to create solid scintillator. The challenge is to create a sol-gel material that is transparent, durable, and crack-free while also containing a radiation absorber and a suitable fluorescence sensitizer. A lead salt, in this case lead acetate, liquid organic scintillators such as a 2,5-diphenyloxazole/1,4-bis-2-(5-phenyloxazolyl)-benzene (PPO/POPOP) mixture and Ultima Gold™, and various siloxane precursors were used in an effort to create a transparent scintillating material for gamma detection. The solid scintillators were then characterized by Energy Dispersive X-ray (EDX) spectroscopy and a photoluminescence study. The EDX shows that the lead is incorporated into the sol-gel matrix of the samples. The photoluminescence study shows that the sol-gels have an emission wavelength in the blue region (425nm) when excited at a wavelength of 385nm. Lead has been doped in the sol-gels up to 6.1 weight percent while still maintaining optical transparency. When a gamma source becomes available, the scintillators will be tested for their detection quality.

Clay Crystallization Mechanisms Probed by Optical Spectroscopy. *JESSICA TYRUS (Benedictine University, Lisle, IL 60532) KATHLEEN A.* CARRADO (*Argonne National Laboratory, Argonne, IL 60439*). Synthetic hectorite clays can be used as heterogeneous catalyst supports and in various other technological applications, thereby placing an importance upon obtaining a knowledge and understanding of the mechanism of clay formation in order to determine an efficient and effective synthetic process. Previous studies focused on the formation of "silica-hectorites," and a silica-clay crystallization mechanism has been proposed. Currently, the mechanism for the complimentary suite of materials referred to as "silane-hectorites" is being studied, and this research focused on using rhodamine 6g perchlorate, a cationic dye, as an optical probe. Successful synthesis of TEOS-hectorite monitored at various time intervals, as well as ion-exchange of silane-hectorite and laponite, with this probe was monitored by X-ray diffraction (XRD), thermogravimetric analysis (TGA), and fluorescence spectroscopy. Data obtained by XRD for ion-exchanges involving each of two concentrations of the dye and both TEOS-hectorite and laponite-RD provided a baseline for the d-spacing of the clays upon full crystallization, as this d-spacing was found to fall between 13 and 15 Å. Data obtained by XRD for the in situ crystallization of TEOS-hectorite at various time intervals allowed for the monitoring of the crystallization of the clay and dye, with clay crystallization beginning after 12 hours. The results obtained via TGA show significant weight losses in the 300–450°C range; these will have to be scrutinized for weight loss from organic dye decomposition versus $Mg(OH)_2$ precursor decomposition due to incomplete clay crystallization. Additional data obtained via fluorescence spectroscopy allowed for the determination of the excitation and emission peaks for the 16-hour crystallization of the clay with 1.0×10^{-5} M dye at 531 nm and 557 nm, respectively. Excitation and emission peaks were not obtained for crystallizations occurring after other periods of time, perhaps due to an insufficient concentration of dye incorporated into the clay.

Ordered Nucleation Sites for the Growth of Zinc Oxide Nanofibers. *JENNIFER WANG (Rice University, Houston, TX 77005) DAVID GINLEY (National Renewable Energy Laboratory, Golden, CO 89401).* Organic photovoltaics (OPVs) offer a promising route to low cost photovoltaic (PV) technology that can be inexpensively manufactured on a large scale for use in power generation and commercial products. Solar power conversion efficiencies of laboratory scale OPV devices have recently reached ~5%; however, projected efficiencies of at least 10% will be required for commercialization. An analogous approach that has arisen recently that can potentially increase efficiencies employs metal oxide semiconductors as the electron acceptor, creating a hybrid organic-inorganic device. This approach offers the advantage that the conduction band of the oxide can be tuned in a systematic way through doping, thus potentially achieving higher photovoltages in the device. Additionally, nanostructures of these materials can be easily grown from precursor solutions, providing a technique to precisely

control the nanoscale geometry. This work focuses on using ZnO, which is known to have high electron mobility (>100 cm^2/Vs), as the electron acceptor. Nanofibers of ZnO can be grown from precursors such as zinc acetate or zinc nitrate to form arrays of nanofibers into which a conjugated polymer can be intercalated to form a composite PV device. The morphology of the nanofiber array is critical to the performance of the device, but current methods of nanofiber growth from a flat, polycrystalline nucleation layer allow for little morphological control. To overcome this limitation, we have created ordered arrays of ZnO nucleation sites with controllable size and spacing. Toluene solutions of diblock copolymer micelles with $ZnCl_2$ incorporated into the micellar cores were spin-coated onto glass substrates and etched with an O_2 plasma to yield hexagonally ordered arrays of ZnO nanoparticles that functioned as nucleation sites. Changing the concentration of $ZnCl_2$ and the molecular weight and ratio of the diblock copolymer resulted in systematic variation in the size and spacing of the nucleation sites. Thermal anneal treatment provided further modification of the nucleation layer, from which ZnO nanofibers were successfully grown from solution, although at present it is not known if the geometry of the as-grown ZnO nanofibers precisely reflects that of the underlying nucleation layer. This work provides a simple and useful method for potentially controlling the nucleation of ZnO nanofibers to be used in hybrid ZnO/organic nanocomposite PV devices.

Olivine Composite Cathode Materials for Improved Lithium Ion Battery Performance. *REBECCA WARD (McDaniel College, Westminster, MD 21157) JOHN VAUGHEY (Argonne National Laboratory, Argonne, IL 60439).* Composite cathode materials in lithium ion batteries have become the subject of great research interest recently as safety issues related to $LiCoO_2$ and other layered structures have been discovered. Both the spinel and olivine families have been studied as possible alternatives to the layered cathodes, but these structures present different problems, as spinels have low capacities and cycle poorly at high temperatures, and olivines exhibit extremely low conductivity. Composites of layered-olivine and spinel-olivine structures could stabilize one another thermodynamically and provide the balance between performance and safety necessary for the use of lithium ion batteries in portable electronic devices, particularly the hybrid-electric vehicle. In this study, layered-olivine and spinel-olivine composites were synthesized from precursor salts using three methods: direct reaction, ballmilling and the core-shell synthesis method. X-ray diffraction images and cycling data show that the core-shell method was the most successful in forming the desired products. The electrochemical performance of the cells containing the composite cathodes varied dramatically, but the low overpotential and reasonable capacities of the spinel-olivine composites make them a promising class for the next generation of lithium ion battery cathodes.

The Hydrolysis Reaction of the Copper-Chloride Low Temperature Thermochemical Cycle. *REBECCA YAPP (Illinois State University, Normal, IL 61761) MICHELE LEWIS (Argonne National Laboratory, Argonne, IL 60439).* Research and development efforts for domestic alternative energy sources are underway. One promising source is hydrogen. Thermochemical cycles are a relatively new technology for producing hydrogen from water. In thermochemical cycles, water and heat are introduced to a series of chemical reactions that operate in a cyclic process. Hydrogen and oxygen are produced and ideally all chemicals are recycled. Thermochemical cycles are of recent interest because of their low greenhouse gas emissions, reasonable efficiency, and compatibility with current nuclear technology. The hybrid copper chloride cycle is one example. This cycle is appealing due in part to its low peak temperature requirement of 550°C. This cycle consists of four reactions; three of which are thermal and the other electrochemical. Two of the thermal reactions are well understood. The hydrolysis of $CuCl_2$ is represented by the following reaction, $2CuCl_2 + H_2O(g) \rightarrow CuCl_2 \bullet CuO + 2HCl(g)$. The challenges associated with this reaction are (1) the apparent need for excess water and (2) the presence of a competing reaction. Instead of 0.5 moles of steam required per mole of $CuCl_2$ up to 40 moles are required. In addition, x-ray diffraction examination shows that some of the $CuCl_2$ decomposes into CuCl. Cl_2 gas is also observed as a by-product of this competing decomposition reaction. The main goals of this project are to experimentally demonstrate the most efficient set of working conditions for the hydrolysis reaction in order to minimize the amount of water and to eliminate the competing reaction. Experiments are being conducted with three different reactor designs to determine the best conditions for the solid-gas interaction. Variables being studied are the dew point (which is related to the total amount of water), flow rate of the humidified nitrogen, and temperature. Preliminary results demonstrate that the overall reaction occurs faster at higher temperatures but the amount of Cl_2 gas produced also increases. Our results indicate that a reactor design that maximizes the contact area between the $CuCl_2$ particles and the steam is important.

Synthesis of Ionic Liquids for Green Chemistry Applications. *MIAO YU (University of Florida, Gainesville, FL 32611) HUIMIN LUO (Oak Ridge National Laboratory, Oak Ridge, TN 37831).* Ionic liquids are essentially organic salts, which are liquid at low temperatures, have negligible vapor pressure, are highly thermally stable, and are non-flammable. These properties and their excellent solvation capabilities for many compounds (organic and inorganic) make ionic liquids particularly attractive for replacing volatile organic solvents and reducing the release of toxic vapors into environments. In this project, methylimidazolium-based ionic liquids with different anions and different alkyl groups were synthesized and their thermal stability measured using thermogravimetric analysis (TGA) to determine the effect of alkyl chain length of the imidazolium ring and the size of the anions on thermal stability. The anions included tetrafluoroborate (BF_4-), hexafluorophosphate (PF_6-), bis(perfluoroethylsylfonyl)imide (BET_1-), and bis(trifluoromethylsulfonyl)imide (NTf_2-), among others. The basic synthesis procedure involves a metathesis reaction. Typically, metal salts containing the corresponding anions (e.g., LiBETI and $LiNTf_2$) and organic salts containing the alkyl and imidazolium groups (e.g., C_4mimBr) were mixed. The resulting ionic liquid was extracted using CH_2Cl_2 and subsequently washed with de-ionized water to remove remaining metal ions (Li or Na) from the reaction mixtures. Using the data from TGA runs, the Tonset temperature, at which the decomposition was initiated, was calculated for each ionic liquid. The value of Tonset for each run was compared to determine the effect of alkyl groups and anion structures on the stabilities of ionic liquids. For the C6 chain, the Tonset temperatures for the BET_1-, NTf_2-, BF_4-, and PF_6- are, respectively, 405, 425, 415, and 365°C. In general, larger anions and longer chains of alkyl groups increase the stability of the ionic liquid.

Determination of Diisopropyl Methylphosphonate and Dimethyl Methylphosphonate and Their Degradation Products in Complex Biological Matrices. *ERIKA ZINK (Washington State University, Richland, WA 99352) ERIC HOPPE, JIM CAMPBELL (Pacific Northwest National Laboratory, Richland, WA 99352).* The organophosphorous compounds, diisopropyl methylphosphonate (DIMP) and dimethyl methylphosphonate (DMMP), are of interest to national security and also play a role as environmental contaminants. Research on the degradation products and their toxicities in diverse matrices is needed. This study describes instrumental and sample preparation techniques used to identify and monitor these compounds and their degradation products in agar, saliva, serum, and aqueous media with the purpose of producing a degradation analysis model for analogous compounds of interest. Residue analysis using gas chromatography/mass spectrometry (GC/MS) and headspace sampling followed by GC/MS were the methods developed for analysis. DIMP and DMMP were successfully analyzed in agar, saliVA serum, and aqueous matrices. The methods were extended to analyze for DIMP and DMMP and their degradation products after fungal decontamination with Poria Cocos. This bioremediation technique could lay the groundwork for clean up of areas contaminated with these and similar compounds. The fungal-based technology will be potentially applicable to decontaminate personnel, equipment, structures, and wide-area sites without damage to items and/or individuals.

Computer Science

Quad-Buffered Stereoscopy for Collegial Education Programs. IAN LUND and JOHNATHAN LUNDGREN *(Jamestown Community College, Jamestown, NY 14701) ROBERT BENNET (Brookhaven National Laboratory, Upton, NY 11973).* Quad-buffered stereoscopic visualization involves generating left and right eye images of an object and delivering each image to its designated eye. This is accomplished through denoting each image with light of opposite polarization. Special glasses are needed to allow light of specific polarization through so each eye receives its respective image. Stereo viewing produces depth (z-axis) in an object, which is not seen in a flat two-dimensional image, or even in a traditional three-dimensional image. As students of math and science often have difficulty visualizing fundamental concepts due to the limits of traditional 3D, stereoscopic rendering has firm academic uses. The goal of this project describes in detail potential uses of stereoscopy in a college curriculum. Some of the most beneficial topics to view in stereoscopy include atomic orbitals, chemical mechanisms, biochemistry, human anatomy, microchemistry, and engineering tools. PyMOL and VMD (Visual Molecular Dynamics) are both molecular

viewers. These programs open up .pdb files (among others), which can easily be downloaded from the protein data bank. The primary molecules viewed are proteins, of which many are stored in the PDB. Atomic electron orbitals can be viewed using Orbital Viewer. Chemistry mechanisms, biology images, and many other things can be found by searching for VRML (Virtual Reality Modeling Language) files. A player can view any VRML file in stereoscopy and be able to rotate the object.

Developing Information Technology Data Management Applications Using PHP and MySQL. *ERIC ANDERS (Iowa State University, Ames, IA 50014) MIKE SKWAREK (Argonne National Laboratory, Argonne, IL 60439).* This project involved developing several systems for managing information technology data required for everyday use. PHP and MySQL provide a framework that allows for rapid development and easy integration with HTML elements. Accessible and efficient systems can be developed in a short amount of time. The PHP and MySQL online manuals provided all of the necessary information to complete the project. I developed several different systems during the course of the project including an application that tracks wireless access point information gathered with Kismet and an application that manages cyber security incident information. While involved in these projects, I investigated new techniques in web design developed to present data as efficiently as possible. One such technique is known as AJAX (Asynchronous JavaScript And XML). AJAX allows data to be displayed to the user's web browser without reloading the page. As new information becomes available, it is instantly displayed to the user.

The Cost of Using MPICH, MPICH2, and the Ganglia GMOND. *BRIAN BAKER (Olivet Nazarene University, Bourbonnais, IL 60914) SUSAN COGHLAN (Argonne National Laboratory, Argonne, IL 60439).* Scientists use clusters and supercomputers to compute complex problems many times more precise and in a fraction of the time needed if the problem were to be run on a single workstation. Scientists want to ensure that each node of the cluster is focusing all of its attention or computing power towards their codes. Other processes on the compute nodes, disk I/O, and network I/O all cause interference with the scientist's code. Pete Beckman, along with help from Kazutomo Yoshii, has designed and implemented a program called Selfish Detour that will calculate the amount of interference, or "noise" (also latency), that these external processes are causing. This program, however, will only calculate the latencies for the system as a whole, and cannot pinpoint the amount of latency caused by a specific application. Comparisons of latencies caused by using MPICH and MPICH2 will be discussed in this paper along with a conclusion of whether MPICH2 is able to lower latency levels as compared with MPICH. Latencies caused by running daemons such as the Ganglia daemon will also be discussed and a conclusion of whether the daemon will be fit to be used in a production environment will be made.

The Response Surface Method: Determining the Minimum Step Size and the Minimum Size of the Region of Interest. *MICHAEL BARNARD (Portland State University, Portland, OR 97207) WESLEY JONES (National Renewable Energy Laboratory, Golden, CO 89401).* The Response Surface Method (RSM) was developed specifically to assist the experimental scientist in minimizing the number of experiments they must run in order to optimize a process or device. Current literature extensively covers the concept behind the method and the statistics involved when measuring the gradient of the response surface. However issues such as, "What size should the Region of Interest (RI) be?", "What should the step size be?", or "When should a quadratic model be used instead of a linear model?" are left to the knowledge of the scientist. By investigating the relationship between the confidence interval associated with the gradient and experimental error, statistically-based analytical answers to these questions can be given. However, new questions arise that must be answered. In this paper, the minimum size of the Region of Interest is expressed as a mathematical function of the desired confidence in the measured gradient. Using the null hypothesis for coefficients, the minimum step size can be expressed as a function of the measured gradient. However, in order for this equation to be useful, more serious consideration needs to be given to the issue of determining when an factor is locally insignificant. A criterion for switching to a quadratic model is a minor result of the Step-Size Equation.

Zoid [Zepto OS IO Daemon]. *IVAN BESCHASTNIKH (University of Chicago, Chicago, IL 60637) PETER BECKMAN (Argonne National Laboratory, Argonne, IL 60439).* The design of IBM's Blue Gene family of super computers scales to thousands of nodes by offloading all system calls made by a compute node to a designated IO node. To facilitate and make the porting of software possible, the system calling interface is transparent to software written for POSIX compliant systems. The native mechanism responsible for servicing forwarded system calls is the Compute IO Daemon (CIOD). This paper introduces and describes the design of ZeptoOS IO Daemon (Zoid), an alternative to CIOD. Zoid is an attempt to construct a scalable system call forwarding mechanism that is designed to emulate CIOD on the BG/L, and integrate with ZeptoOS, a platform independent research operating system meant to scale to systems with millions of CPUs. Zoid has a flexible design which allows user defined behaviour per system call, varying consistency semantics and a choice of cache policies. Another critical feature of Zoid is that it is an open platform for research. Open Source lets scientists explore advanced functionality and new algorithms for BG/L that would otherwise not be possible. Most importantly, Zoid and the ZeptoOS suite is the only available open source choice for the BG/L architecture.

Investigation of Execution Environments for Cluster, Command, and Control (C3). *WESLEY BLAND (Tennessee Technological University, Cookeville, TN 38505) STEPHEN L. SCOTT (Oak Ridge National Laboratory, Oak Ridge, TN 37831).* The Cluster Command and Control Tool Suite (C3) is designed to provide simplified functionality for users and administrators on a cluster of computers by providing a mechanism for operations on distributed machines in parallel. Included in this suite are tools to manage processes, transfer data, and provide support for other tools. Current work includes the implementation of the C3 tools as a client of the SciDAC Scalable Systems Software (SSS) project's Process Manager. The SSS environment uses a component-based systems software architecture for operating large-scale distributed computing systems. The integration of C3 into the SSS environment requires that C3 code be modified to communicate with the SSS Process Manager via the XML schema's specification over TCP/IP sockets. These changes to the C3 transport and execution model will enable the tools to take advantage of the scalability offered by the SSS components.

A Defense-in-Depth Model of Security in Collaborative Systems with the Goal of Robust Prevention, Detection and Response. *AARON BROWN (Gonzaga University, Spokane, WA 99253) DAVE MILLARD (Pacific Northwest National Laboratory, Richland, WA 99352).* Despite increasing concern and interest regarding software security, most software developers continue to treat security as an afterthought. One particular aspect of security that is often over looked is the necessity for a dynamic, adaptive view of secure computing that stresses appropriate security measures for the type of system being designed. This lack of adaptivity is often seen in the development of collaborative systems. Because of their extremely dynamic nature (in terms of user community, data, usage load, and usage method), collaborative systems have several special concerns that are not often addressed by software developers. This paper lays out a generalized defense-in-depth model for collaborative systems covering several methods of attack prevention, detection, and response. Examples used are drawn from work on a system called WebOSB. External references and information are taken from diverse sources such as the Trusted Computer System Evaluation Criteria (DoD-5200.28-STD, often called "The Orange Book"), academic papers and conference presentations, and other published sources such as Secrets and Lies by Bruce Schneier. The paper stresses the importance of not only attack prevention, but also attack detection and response. It also recommends the use of robust systems of auditing, monitoring and logging, and a well-rounded security policy.

Enhancing And Updating The Interactive Envelope Materials Database For Whole-Building Energy Simulation Programs. *BRETT CARMICHAEL (Pellissippi State Technical Community College, Knoxville, TN 37921) JAN KOSNY (Oak Ridge National Laboratory, Oak Ridge, TN 37831).* Thermal resistance of a wall area is used to calculate the flow of heat from one wall surface to another. Decreasing the flow of heat (either containing the heat in cold weather conditions, or keeping it out in warm weather conditions), becomes the main focus of a more energy efficient building. Currently, an average of 45% of a building's energy expense is due to heating and cooling costs. Vast amounts of research have been done within this area, but accurate assessment of data generated has been a hindrance in the past. This is due to the widely varying composition of different buildings, including the details of the buildings, the different wall technologies used, and even the climate the building resides in. Due to the lack of commercial software which can adequately assess whole-building energy efficiency, creation of a user friendly online application has become the focus of the research. The development of the application focuses on three main areas. The first is the complex Whole Wall R-value Calculator. This calculator gives developers and builders the ability to easily

discover the whole wall R-value for any house they are designing, simply by entering basic geometric dimensions and selecting from a list of tested wall systems. The most recent developments in this area include a simple Whole Wall R-value Calculator which runs over the Internet and requires no downloading. Version 2 of the complex is also scheduled to be released. This newest version allows users to select multiple wall technologies within the same building along with implementing significant changes in the user interactivity levels. Single click wall selection and technology assignment allows the user to create complex building structures with little effort. The second area of focus is the Thermal Mass Calculator. It calculates the energy savings of a building based on the configuration of the wall technology and the climate in which the building is located. The final area is the online Hotbox Test R-value Database. This project contains years of hotbox data compiled at the Oak Ridge National Laboratories, and the goal of the database is to present the information in a clear, concise, and user-friendly way. The combination of these three areas helps to incorporate all the aspects needed to make an accurate assessment of whole-building energy efficiency.

Engineering Science and Technology Division Equipment and Calibration Database. *RICHARD CLARK (Pellissippi State Technical Community College, Knoxville, TN 37933) JOHN B. CZACHOWSKI* (*Oak Ridge National Laboratory, Oak Ridge, TN 37831*). To increase the effectiveness in query and report generation and reduce undesirable redundancy and errors introduced in updating data, four separate flat-file databases, through three major revisions, were converted into a unified relational database. Work began with decomposition of the existing flat-file databases into their constituent parts. All the key attributes in the flat-files were identified, the repeating groups were removed and attributes were arranged to be dependent on each primary key. They were then further normalized to remove partial dependencies (attributes that were only dependent on one portion of a primary key) and transitive dependencies (which is a dependency of one nonprime attribute on another nonprime attribute). Microsoft Visio 2003 was the modeling tool used to design the structure of the relational database and the new system was built using Microsoft Access 2003. Lookup tables were identified and created to accommodate the one-to-one and one-to-many relationships present and transaction/bridge tables were created to further delineate the many-to-many relationships into needed one-to-many relationships. Once the basic tables were created the data from the existing flat-file system was extracted and scrubbed to remove inconsistencies and arranged in the proper order and format to be imported to the new relational system. Another aspect of the database was the inclusion of photos of the equipment to help identify items in a remote warehouse. This project will continue with the creation of queries that will be stored to speed up routine and repetitive searches commonly made of the system. From the existing tables and queries, data entry forms will be created that will allow for the management of the equipment, its placement in the laboratories and storage areas' pertinent, recurring calibration and routine inspection schedules of it by and for the equipment custodians.

ZeptoOS and The IBM Blue Gene/L Supercomputer. *CAMERON COOPER (Ohio State, Columbus, OH 43210) PETE BECKMAN (Argonne National Laboratory, Argonne, IL 60439).* The IBM Blue Gene/L supercomputer currently provides more computational power than any other supercomputer architecture in the world. However, without proper software support this system cannot be fully utilized. Many crucial software systems in the IBM Blue Gene/L system are closed-source which prevents modification and fine tuning to maximize system performance. In our research, we have analyzed different systems in the Blue Gene/L and looked for ways that we improve them. In some cases this has required us to replace them with our own, open-source, versions. In particular, we have done this with the I/O Node Kernel and Ramdisk, as well as the CIOD system call forwarder.

Forewarning an Epileptic Seizure through Parallel Computer Analysis. *JASON COX (University of Tennessee, Knoxville, TN 37996) KARA KRUSE (Oak Ridge National Laboratory, Oak Ridge, TN 37831).* Epileptic seizures can be forewarned by quantifying dynamical changes in nonlinear time-serial EEG data. The dynamical changes of an epileptic event are determined using a computer program to determine phase-space dissimilarity (PSD) measures. Computation of the PSD measures involves many different parameters which must be verified to find the set of parameters which gives the best forewarning predictions. Currently, the parameter optimization program can take several days to months to exhaustively test each parameter combination. Waiting this long to receive results makes progress difficult because only a slight change to the analysis or data means starting the program from the beginning. By using methods of optimization and high performance computing, the time to execute the program can be reduced considerably. Currently, an analysis is executed on a single data file multiple times. The file is read and stored into memory each time. Using large amounts of memory to store the file only once will result in the program running much faster than before. Since most of the data files are extremely large and multi-channeled, the use of a supercomputer can make it possible to store all of the data into memory and run multiple analyses on multiple processors. By reducing the time to run the program from months to days, progress towards obtaining the optimal parameters will be more feasible. Once the parameters have been determined, the program can run on a handheld computer and data can be obtained using a portable EEG device, giving the individual with epilepsy a chance to be forewarned of an impending seizure and potentially saving his or her life.

Removing Unused References from the FRAMES-1.x System. *DUARD CRANDALL (Brigham Young University Idaho, Rexburg, ID 83440) FREDERICK RUTZ (Pacific Northwest National Laboratory, Richland, WA 99352).* The Framework for Risk Analysis Multimedia Environmental Systems (FRAMES) is a software platform developed by Pacific Northwest National Laboratory that can be used to create conceptual models of possible contaminant flow through various mediums. These models have access to various parameters whose data needs to be accredited to the proper source. The references for these parameters are stored in a file that is accessed by the FRAMES User Interface (FUI). References contained in these files may, or may not be accessed by parameters in a given scenario. Since a user may wish to remove these unused references from the system, a method was developed that would interrogate both the files containing the references and the parameters, and delete unused references from the reference file. This paper discusses the methods used to remove unused references from the FRAMES 1.x system.

Cryptography as Applied to a Unix Environment. *OLIVER DARIO (Contra Costa College, San Pablo, CA 94806) CHARLIE VERBOOM (Lawrence Berkeley National Laboratory, Berkeley, CA 94720).* Cryptography is the act of enciphering and deciphering messages in secret code. In today's computer systems and networks, the act of enciphering and deciphering messages is applied to the bits of data that we share across networks. The threat imposed on our computer systems by attackers is the primary reason that we have to send messages, or data, in secret code. In its default state, email is typically sent through the Internet as clear text, or unencrypted, which means that a sent message can easily be made viewable. Remote connection protocols such as FTP and Telnet are susceptible to various attacks, such as the man-in-the-middle attack, due to their lack of data encryption during their sessions. The application of cryptography to today's computer systems and networks helps to ensure that electronic information remains in its original form while being delivered, and that it is not falsified in order to gain access to a remote computer. This paper is an analysis of the cryptographic methods supported by the Secure Shell protocol (SSH), a replacement for Telnet, and GNU Privacy Guard (GnuPG), a cryptographic method applied to email messages.

Asynchronous HTTP Request Using AJAX and PHP. *CASEY DAVIS (Big Bend Community College, Moses Lake, WA 98837) DARREN CURTIS (Pacific Northwest National Laboratory, Richland, WA 99352).* By its very nature HyperText Transfer Protocol (HTTP) is stateless. Once a request is made, the server will return the information requested and then cease communication with the client. AJAX (Asynchronous JavaScript and XML) is a method of programming that allows the client to simulate persistent communications with the server. By allowing the developer to use CGI(Common Gateway Interface) programming to define exactly what the client is looking for, the asynchronous requests reduce packet size and reload time, while also making the application less like a web page and more like a desktop application. Using JavaScript on the client-side the developer may initialize an asynchronous HTTP request to the CGI preprocessor, in this case PHP (PHP HyperText PreProcessor). PHP may then make logical decisions about what data is to be presented and returned to the JavaScript. JavaScript will then update only the relevant section of the web browser window, thus making the browser react, seemingly in real-time, without reloading the entire page of data. This new way of using existing technology is adding a whole new facet to the web industry. While all the things that go into making AJAX work are not new, they are being used in many new ways. Google® is putting it to good use with programs such as Google Suggest®, Google Maps®, and most recently Google Earth®. Since AJAX was build to conform to XML(eXtensible Markup Language) standards and is fully DOM(Document Object Model) compliant developers may use AJAX for simple things such as form validation, and list generation, to more complex things like

SVG(Scalable Vector Graphics) which will allow for drawing images on the fly.

Further Development of VBNLTrak. *EDWARD D'AZZO-CAISSER (St. Joseph's College, Patchogue, NY 11772) AHOVIE KPONOU (Brookhaven National Laboratory, Upton, NY 11973).* VBNLTrak, written by Andrew Siemion at Brookhaven National Laboratory, has been used by the Pre-injector group's Electron Beam Ion Source (EBIS) to display the results of tracking simulations for designing the Relativistic Heavy Ion Collider (RHIC) EBIS on a Windows compatible system. Originally designed to replace Field Precision's TriComp 2DTM VTrak, VBNLTrak moved beyond limits in TriComp's visual implementation by handling multiple graph-types at once and by allowing complete graph configuration before a plot, in addition to a variety of customizable options and various output methods. Using Compaq Visual Fortran in conjunction with Interactive Software Services Ltd. (ISS)'s Winteracter Graphics libraries, we continued the progress made on the program by Siemion and resolved some stability issues. Most of the modifications were made in the Winteracter Development Environment (Wide), with the aid of ISS's Graph Designer. VBNL Trak now has the option to save and load data locations from a control list (.TIN), simplifying a graph retrieval process which once required a series of cumbersome dialog boxes. There is also an option to take the files normally specified in the .TIN and save the data inside of a master file (.TRAK), lessening the number of output files cluttering a folder. As a result, program settings were expanded and augmented for these new changes, offering a wider versatility and more pleasant user experience over-all.

Web Content Development and Management Using DREAMWEAVER MX 2004 for the Scientist Team Who Work on the Linear Accelerator Coherent Light Source (LCLS) Project at Argonne National Laboratory (ANL). *ALY DIAKHATE (Borough of Manhattan Community College, New York, NY 10007) CHRISTOPHER KLAUS (Argonne National Laboratory, Argonne, IL 60439).* Scientists at Argonne National Laboratory (ANL) and their colleagues at Stanford Linear Accelerator Center (SLAC) work together on joint projects. While SLAC has its own web site, the Argonne team does not. The purpose of the project is to build a web site similar to the SLAC website, but with a design that is similar to the ANL official web site. To simplify the task, we use a software program known as DREAMWEAVER MX 2004 for its capability to create, maintain and update Hypertext Makeup Language (HTML) pages. We focus on some major points: Set and state our goals (the needs to create this site), Time management (How DREAMWEAVER facilitated us to save time when designing the site), the Presentation, Content management and Navigation of the site.

From Concept to Creation and Implementation: The Web-Based Hour and Dose Tracking and Monitoring System for the Alpha Gamma Hot-Cell Facility. *TYLER DILEO (Pennsylvania State University, University Park, PA 16802) PAUL DOMAGALA (Argonne National Laboratory, Argonne, IL 60439).* Due to the dangerous nature of working with and handling radioactive material there are mandatory regulations set forth by the governing powers that be. There is a strong need for the utmost attention to detail while adhering to such strict policies not only for the facility to remains in operation, but for the ongoing safety of those working both directly and indirectly in and around the hot cells. Though a monitoring system is currently in place, its shortcomings require that an overall more effective system be implemented to ensure that safety regulations and protocol are met on a daily basis. Through knowing merely the purpose and needs of the original spreadsheet and the use of a combination of Hypertext Markup Language (HTML), PHP: Hypertext Preprocessor (PHP) and a Structured Query Language (MySQL) through the aid of Navicat a new web-based system was created from scratch. Those using the original spreadsheet prior to the creation of the web-based database are now able to use the new system in a limited manner. Until this method of data recording has met the satisfaction of all involved it will continue to be used along side the spreadsheet. This database is the first step of many in order to create web-driven records within the Alpha-Gamma Hot Cell Facility (AGHFC). Among those are web-based workslips and real-time radiation dose recordings of the facility.

Two Hybrid Approaches to Increase Activity Analysis Accuracy. *SCOTT EASTERDAY (La Sierra University, Riverside, CA 92515) BARBARA KREASECK (La Sierra University, Riverside, CA 92515) PAUL HOVLAND (Argonne National Laboratory, Argonne, IL 60439).* Automatic Differentiation is the process of translating one program that computes a function f and generating a different program that computes the derivative of that function, f'. Activity analysis is important for AD. Our results show that a dynamic activity analysis enables an average speedup of 28%. We investigated two techniques aimed at reducing the overhead of dynamic activity analysis. One uses a profile-guided activity analysis and the other uses a less-conservative static activity analysis. The results from these techniques are mixed; some benchmarks showed improvement, others performed poorly.

Construction of a Stereoscopic Model of the Solar System. *JASON EMORD (Suffolk County Community College, Selden, NY 11784) GORDON SMITH (Brookhaven National Laboratory, Upton, NY 11973).* The purpose of this venture is to construct a third-dimensional, stereoscopic model of the Solar System by means of Maya 6.5. Accurately scaled three-dimensional representations of the Solar System are virtually non-existent. Vast differences in size, orbital velocity, and semi-major axes present problems for researchers who are trying to realistically portray astronomical bodies. Professors, students, and any interested parties will be offered an up-close-and-personal journey through a small part of the Milky Way Galaxy. Various Internet resources were used to acquire the data necessary for the Solar System's creation. They include, but are not limited to, NASA.com, nationmaster.com, and similar web encyclopedia instruments. Maya 6.5, the program chosen for this project, is an award winning 3-D animation program used by Hollywood production studios in the creation of elaborate special effects scenes. The project was divided into three phases: The first phase involved creating a skeletal model of the Solar System. NURBS spheres represent the planets and their respective moons. Relative sizes were scaled with respect to Jupiter, which made it possible for all the planets to be visible in a single frame. Next, the rotational tilts, orbital inclinations, and orbital eccentricities of the planets were input. Although a method of scaling the relative semi-major axes was found, they were omitted from the final presentation to preserve the single-frame image of the Solar System. The second phase involved planet surface texture maps (skins), acquired from the Internet and wrapped around each sphere. A large sphere was created and shaded black to encompass the Solar System. Phase three involved exporting the model into StereoMovie Maker so that the presentation can be viewed in stereo. Maya's inability to output scenes in Stereo will necessitate its channeling through StereoMovie Maker, a similar program with Stereo capabilities. It will also allow for camera movement throughout the system. Ultimately, this project will function as a platform for those who aspire to build upon the existing model by adding other celestial objects such as galaxies, nebulae, comets, and asteroids.

Lessons Learned Modifying a Web Application That Uses the Java Servlet Technology and MySQL Database. *DANIELLE EVANS (Big Bend Community College, Moses Lake, WA 99357) MITCH PELTON (Pacific Northwest National Laboratory, Richland, WA 99352).* Java™ servlets provide software developers with a simple, consistent mechanism for extending the functionality of a web server. A Java™ servlet uses the Java™ programming language for generating dynamic web content by using the ETL (Extract, Transform and Load) process with the MySQL database engine. MySQL is a RDBMS (Relational Database Management System) that uses SQL (Structured Query Language) for extracting, transforming and loading data in a database. The Apache Tomcat web services' contains an API (Application Programming Interface) library that the Java™ servlets communicate with to post state information. Web application interfaces are generated by a URL (Uniform Resource Locator) request that returns a HTTP (Hypertext Transfer Protocol) document. The FMS (FRAMES Module Server) application is one such application that enables a client to extract data for a pre-defined schema as defined by a program called FRAMES (Framework for Risk Analysis Multimedia Environmental Systems). This schema is contained in a set of text files called dictionaries. Typically a schema provides a framework for naming and storing different elements of information about something. The schema provided by these dictionaries is mapped to the given schema identified by the database being mapped. The FMS application offers users a way to share information that will help make FRAMES a more productive software tool. The FMS application allows for disparate data to be more readily accessed as well as QA/QC (Quality Assurance/Quality Control). Testing, debugging and making this application more user friendly, has revealed problems dealing with the Java™ servlet technology and the JBuilder X development environment. The experiences, problems and their solutions are discussed in this paper. The problems with finding, downloading and using the software needed are prevalent when creating the FMS application that uses the discussed technologies. Testing, debugging and making the application more user friendly have presented unique experiences along with solutions found to make using the software easier are discussed in this document. The solutions to some of the problems were simple and some more difficult.

GWAVA: Java-based Information Retrieval on the Web for the Vitual Autopsy Project. *JUDY EVANS (Roane State Community College, Oak Ridge, TN 37830) LINE POUCHARD (Oak Ridge National Laboratory, Oak Ridge, TN 37831).* Virtual Autopsy is part of the pre-autopsy process performed on combat fatalities. It is performed using a CT-scanner with three-dimensional capabilities. The initial images are sent to the Department of Radiologic Pathology to be further enhanced and interpreted. The final images are stored in a flat file repository. The additional physician findings are reported in the form of medical health records and entered into a database. Presently, retrieval of the database information and the corresponding images is done manually in several steps. The Generic Web Application for the Virtual Autopsy (GWAVA) is a system that follows the best software engineering practices of design, development and deployment. Medical doctors will be able to search certain fields of the database and retrieve relevant information from it as well as the corresponding images. For example a doctor will be able to search a particular description of a wound and the application would retrieve any information and images that pertain to that description. This information will then be used to research weapons and protection systems for soldiers. An architecture using Java Server Pages, Microsoft ACCESS and a Tomcat web server was designed and a prototype is being developed. Particular attention will be paid to secure access and user-based permissions. The medical community uses the Digital Imaging and Communications in Medicine (DICOM) standard. Therefore, the application requires programmatic access to a DICOM viewer. The application is being deployed on a localhost and the ORNL intranet and will be deployed over the web.

Interactive Stereoscopic 3-D Visualization of Time Resolved Plasma Emission Spectra. *OLEKSIY FATYEYEV (Bergen Community College, Paramus, NJ 07652) ROBERT BENNETT (Brookhaven National Laboratory, Upton, NY 11973).* Interactive stereoscopic data visualization is an area of computer graphics providing techniques and algorithms to display large datasets as two- and three-dimensional images, thereby giving scientists the ability to better analyze and discern details in their data. The goal of our effort was to develop and deploy a software package that provides the ability to interpret and visualize arbitrary sized data sets using interactive stereoscopic three-dimensional viewing techniques. Each raw data set consists of a series of frames (two dimensional arrays of emission intensities as a function of wavelength), where each frame is a spectral snapshot of the plasma at a precise unit of time after the initiation (voltage pulse) of the plasma. In order to streamline the processing of the raw data, we have developed a software tool using both open-source and commercial packages: Microsoft Visual Studio .NET 2003 was used as the IDE (Integrated Development Environment) and Visual C++ was the development programming language. We utilized the open-source Visualization Toolkit (vtk) to render the data in three dimensions and another freely available software package, Tool Command Language (Tcl) and its associated graphic user interface (GUI) toolkit (Tk) to create the GUI. This interactive tool will allow the user to study the formation and subsequent decay of active chemical species (excited state atoms, molecules and ions) over the duration of a short-lived plasma event, and should therefore yield greater insight into the underlying plasma processes.

Assessment of Consumer Values – HVAC Units That Improve Indoor Air Quality. *MATTHEW FIELDS (Trevecca Nazarene University, Nashville, TN 37830) MELISSA VOSS LAPSA (Oak Ridge National Laboratory, Oak Ridge, TN 37831).* Heating, ventilating, and air conditioning (HVAC) systems are installed in buildings to regulate temperature and humidity. These systems provide air conditioning, controls for heating, and ducting, which ensures a uniform transfer of cold or hot air throughout a building. HVAC systems are the main energy consumers (more than 40%) in residential homes, according to Department of Energy's 2004 Buildings Energy Databook. According to a new study from The Freedonia Group, the need for HVAC systems is growing with annual growth rates of up to 2.4%. ORNL has an innovative idea for HVAC systems that will not only examine energy costs but will improve homeowners' health and comfort. The California Energy Commission (CEC) is interested in the impact of HVAC systems on homeowners' health. ORNL is working with the CEC to assess what is important to California residents about HVAC systems, including their perceived impact on indoor air quality in homes. Background research on residential HVAC systems and air filtration products is being performed to support this project. A price comparison of HVAC units and air filtration products available at home improvement centers was created to provide a baseline of data on available technology to improve indoor air quality. A database of intermediary and end-user contacts for the market assessment is being developed and discussions are being held with homeowners, utilities, HVAC contractors, home builders, and other organizations including the medical community. Data collected by the ORNL team will be compiled into a report for the CEC. The market assessment will provide the CEC with information needed to determine a path forward for sponsoring R&D on HVAC systems, based on potential consumer demand for advanced systems. This work builds from a successful ORNL project conducted last summer.

Parallel Computation of Blood Flow in Arteries with Moving Walls. *HANNAH FLATH (Columbia University, New York, NY 10027) RICHARD WARD (Oak Ridge National Laboratory, Oak Ridge, TN 37831).* A computational model of realistic blood flow in a section of artery could improve diagnosis and treatment of health problems such as aneurysms and wounds to artery vessel walls. Systems of equations describing fluid and wall behavior are numerically simulated in Parallel Interoperable Computational Mechanics System Simulator (PICMSS), a parallel computational software environment for solving equations using finite element analysis. Currently under investigation are systems of equations published by A. Quarteroni *et al.* in Comput Visual Sci in 2000. These systems include Navier-Stokes and incompressible fluid equations coupled through boundary conditions to wall motion. PICMSS was modified to include these fluid-structure interactions. The algorithm presented by Quarteroni *et al.* was then implemented. The modifications to PICMSS were evaluated through comparison with results from an example of a 2D compliant pipe in the Quarteroni *et al.* publication. Further work is required to complete the modifications.

Keeping System Administrators Informed: Building a Reporting Mechanism for the BCFG2 Configuration Management System. *JOSEPH HAGEDORN (University of Illinois at Urbana-Champaign, Urbana, IL 61801) CRAIG STACEY (Argonne National Laboratory, Argonne, IL 60439).* Bcfg2 is a client-server configuration management tool used to maintain networks of computers. To overcome some of the challenges in maintaining a diverse group of computer configurations, Bcfg2 implements a comprehensive reporting system. This system provides a feedback loop for system administrators to get vital information for effectively managing a network of computers. The uniqueness of a report allows it to hi-light otherwise unobtainable information about possible problems. Reports also can present a variety of other data in an easy to read format to help administrators gain information about the configuration and state of their managed computers, further easing management. Viable information to be included in a report might consist of overall system statistics, discrepancies between specified and actual configuration, invalid configuration, and auditing information. Some requirements in the implementation of the reporting system include; extensibility of reports, flexibility of report delivery mechanisms, the ability to deliver information administrators need. The reporting system implemented in Bcfg2 meets many of these requirements yet can improve with time due to its flexible nature.

Stereoscopic Imaging of Scanning Electron Micrographs. *VALERIE HALL (Nassau Community College, Garden City, NY 11530) JOHN SPILETIC (Brookhaven National Laboratory, Upton, NY 11973).* Scanning electron micrographs exhibit three-dimensional qualities due to the high depth of field inherent in the use of the scanning electron microscope (SEM). Using the program StereoPhoto Maker, we have attempted to render these micrographs viewable in three dimensions. For this to be accomplished, a routine procedure was developed that permitted movement from trial-and-error to a method that yields consistent results. As in conventional photography, creation of a stereoscopic image using the SEM requires a left-eye and right-eye image. SEM stage controls permit sample movement in the X and Y axis, 360 degree rotation, and a tilt of 90 degrees toward and 15 degrees away from the signal detector. Images were captured using successive 2.5 degree increments, horizontal and vertical shifting, and sample rotation. Since rotation could not be measured directly, the SEM-generated scale bar was used to measure increments depending upon magnification. The resultant two-dimensional images were opened in a software application known as Stereo Photo Maker and combined to form a stereoscopic image based on two images of differing perspectives. In addition to the routine method of generating stereo pairs through sample tilting, other methods were also tested. It was determined that lateral shifting does not allow for the production of a visually satisfying stereo image. Rotation, however, produced three dimensional images of equal quality to that of tilted samples. We find that the greater variation of surface structure a sample has, a higher initial degree of tilt is required. However, the study of many more samples will be needed to verify this hypothesis.

Are You Centered? *Automatic Sample Alignment for High-Throughput Protein Crystallography. ANUBHAV JAIN (Cornell University, Ithaca, NY 14853) VIVIAN STOJANOFF (Brookhaven National Laboratory, Upton, NY 11973)*. High-throughput protein crystallography using industrial automation techniques have reduced the time needed to conduct protein structure experiments at many facilities around the world, including the X6A beam line at BNL. A key step in these experiments is protein crystal centering, which can take from ten to thirty minutes to perform manually. Automatic crystal centering would help reduce this time and open up the possibility of a fully computer-controlled crystallography experiment. However, crystal centering algorithms to date rely on human guidance or use heuristics which are not accurate enough to find the crystal in many cases. An improvement over these methods is developed using image processing and machine vision techniques. In addition, shape analysis is used to help distinguish which region corresponds to a crystal. Loop centering, which can center large crystals or perform a rough estimate of crystal position, is improved by analyzing the standard deviation information of the image data rather than pixel intensity. Tests are currently being conducted on a diverse array of image data sets to see how this alternative method compares with previous approaches. If successful, this research would mark an important step in fully automated protein structure experiments.

Conceptual Similarity of Shapes for Feature Extraction/ Comparison Software. *LYONS JORGENSEN (Big Bend Community College, Moses Lake, WA 98837) PATRICK PAULSON (Pacific Northwest National Laboratory, Richland, WA 99352).* To determine the make and model of a car from images the shape of the windows need to be extracted and compared. The comparer needs to analyze similarity in shape independent of scale, rotation, and translation. A new Conceptual Space is a possible solution for comparing qualitative data like shape. We describe a conceptual space for polygons that allows their similarity based on standard distance calculations. The similarity values seem to be consistent and intuitively reasonable. More analysis should be done to compare the results with human perception.

Supporting Information Technology to Take Work Load From System Administrators in Order to Maximize the Volume of Projects Accomplished by the Systems Department of Argonne National Laboratory. *JOE KESTEL (Governors State University, University Park, IL 60466) CRAIG STACEY (Argonne National Laboratory, Argonne, IL 60439).* The goal of my visit at Argonne National Laboratories Math and Computer Science Division was to work in real world IT department the hands on doing of assignments that are taking place in IT departments around the world in the current in exchange for gaining new skills learned during the appointment as with a starter course in programming high level languages like Python and PHP, providing helpdesk support and alleviating administrators of the overhead of some assignments. I also had taken the privilege of building and basic installation of a server and its operating system. I gained knowledge of cluster computer hardware and how a cluster system operates by reassembling getting to re-assemble one in a more effective deployment. Experience with such a machine is obtainable in most IT systems departments.

VisCMAQ: Visualization Tool for EPA's Community Multiscale Air Quality (CMAQ) Modeling System. *MICHAEL KHALIL (New Jersey City University, JERSEY CITY, NJ 07304) DOUGLAS WRIGHT (Brookhaven National Laboratory, Upton, NY 11973).* Simulation models describe worldwide phenomena such as the transport and transformation of trace species in the Earth's atmosphere. Computer visualization plays an important role in the evaluation of model results with observations and in detailed studies of the physical and chemical processes represented in the model. The goal of this project is to enhance the VisCTM model, which was created last summer with additional flexibilities such as reading from NetCDF files. Also, the ability to process multiple time steps for multiple species at the same time. VisCTM would be able to read, and visualize different types of data that is written in C Language. These enhancements will allow the new VisCMAQ to accept an incorporation of data sets for various spatial domains and sets of chemical species. At this process the Visualization of the output from Multi scale Air Quality (VisCMAQ) model will be created. This VisMAQ project will link VisCTM tools with the Environmental Protection Agency's Community Multi-scale Air Quality (CMAQ) Model system; which will utilize VisCTM import files written by the IOAPI library that is built upon the NetCDF file format.

Vulnerability Auditing at the Application Layer of the Open System Interconnect Model. *TRACY KISSIRE (Columbia Basin College, PasCO WA 99301) VAHID S. HACKLER (Pacific Northwest National Laboratory, Richland, WA 99352)*. Research is being performed to assist in the development of efficient processes for identifying and mitigating risk associated with web based applications. Web based applications are highly effective in managing the vast amount of data processed in the business environment. As businesses continue to improve computing and network security, increasingly complex attacks are being directed at web based applications. Vulnerability auditing at the lower levels of the Open System Interconnect (OSI) model is a common procedure; auditing for vulnerabilities at the application level of the OSI model is difficult because of the limitless possibility of exploitation methods. New software tools capable of thoroughly auditing for vulnerabilities at the application layer of the OSI model are needed.

The Diet Problem Case Study Using the Network Enabled Optimization System. *MALCOLM KNOX (Governors State University, University Park, IL 60466) XUEQING TANG (Argonne National Laboratory, Argonne, IL 60439).* The Diet Problem Case Study is a real world application that utilizes the Network Enabled Optimization System (NEOS). The Diet Problem is the most popular case study problem in industry and universities to learn about Linear Programming. When the menu is accessed, and the user makes his/her selections for meals of a day, an error, "Error in write_data program: return code 32256" occurs, and the user does not get to see the results of the least cost menu for his/her selections. If the user wants to change the constraints on the menu, there is an error that displays "Can't open file 'total_cost.out'. We studied C++, Perl, Python, Hyper-Text Markup Language (HTML), A Mathematical Programming Modeling Language (AMPL), and Linear Programming to find out what's missing in the current system. We are writing all the codes in Python to make the case study running again. Python is an object-oriented computer programming language. It's readable, maintainable, portable, and it's powerful. It can be interchanged with other languages, if necessary. Python is easy to use, and easy to learn. Since Python has several advantages over other programming languages, we are converting the code for the Diet Problem over to Python. This way, valuable time and resources are saved. Debugging time is reduced. With all of these advantages, Python provides a better atmosphere, and an easier working environment. I'm working on the write_data module. There are two input files for the module: input.dat, and the food selection from the user. The input.dat file lists the nutrient's name, measuring unit, minimum and maximum requirements, and also the foods nutrient's information. The "write_data" module will generate an AMPL data file called diet.dat, based on the user's selection and input.dat file.

Density Functional Theory-Based Nanostructure Investigation. *ADRIAN KOPACZ (Northwestern University, Evanston, IL 60208) MIHAI ANITESCU (Argonne National Laboratory, Argonne, IL 60439).* The development of software for the investigation of chemical and mechanical properties of nanostructures promises to elucidate phenomena not observed in bulk materials. The method formulates a two-step approach to compute the electronic density distribution in and around a nanostructure and then the displacement of its nuclei. The Electronic Problem employs interpolation and coupled cross-domain optimization techniques through a process called electronic reconstruction. The Ionic Problem, within a quasicontinuum framework, relocates the nuclei of the nanostructure given the electronic density in the domain. The goal of this work is to implement an object-oriented framework that will provide testing mechanisms of the evolving code. Future work will focus on further enhancements to substantially increase the dimension of the nanostructures that can be simulated by using approaches that include accurate density functional theory (DFT) computation.

Biometrics Authentication System Face Recognition Using Eigenfaces. *ELENA LIN (Brooklyn College, Brooklyn, NY 11210) U.S ROHATGI (Brookhaven National Laboratory, Upton, NY 11973).* Identifying an individual from his or her face is one of the most non-intrusive modalities in biometrics, yet it is the most challenging one. The face recognition system is part of the Integrated Biometric Recognition System (IBRS). The goal for the project is to interpret eigenface algorithm and to enhance the clarity of the software documentations. The eigenface algorithm was used for the system, which is the combination of a face feature set. The face recognition system captures images, transforms images, reconstructs new images, compares images and match images with the data template. In order to improve the software documentation, we study and analyze the various algorithms for the clarity and ease of understanding to all users. This analysis reveals that we need to further simply the documentation to help users deploy the software. We conclude the algorithms were

correctly used for a robust application, however the documentation still needs to be improve to complaint with software.

Using Logistical Networking Methodologies to Improve Long Distance Transfer Performance. *DAVID LABISSONIERE (East Tennessee State University, Johnson City, TN 37614) JEFFREY VETTER (Oak Ridge National Laboratory, Oak Ridge, TN 37831).* It is often necessary to move large data sets over great distances across a Wide Area Network (WAN). Due to the design of the congestion control mechanisms in the Internet Protocol suite, the effective bandwidth obtained is often suboptimal. However, by employing Logistical Networking techniques, this performance can be improved. Logistical Networking is a paradigm which uses intermediate time-limited storage to provide buffering areas for data transfers. The foundation of Logistical Networking is the Internet Backplane Protocol (IBP) which allows allocation and access to temporary storage on remote servers. These servers are called depots and are located at strategic points around the Internet. IBP can be used to transfer data indirectly through one or more intermediate depots. To evaluate potential benefits of this technique, the researchers have designed and executed transfer tests of varying data sizes between two systems, both by passing data directly through the network and by passing data in pipelined fashion through an intermediary depot located along the direct network path. When comparing the results of these two transfer techniques, performance improvements can be observed when using the indirect approach when the data size is larger than approximately four megabytes. Even though additional processing is required at each intermediary depot, these costs are outweighed by the performance benefits garnered from shorter transfer distances. Although other potential optimizations have been identified, this work shows the capability of Logistical Networking to improve long-distance data transfer performance.

Developing Interactive Models of Industrial Facilities. *JOSEPH LAKE (University of Tennessee, Knoxville, TN 37996) ROBERT SANDERS (Oak Ridge National Laboratory, Oak Ridge, TN 37831).* After September 11th, 2001, our nation has gained a heightened awareness of the need for greater national security. In order to protect our nation, we must not only protect the public, but also the facilities and infrastructure that permit normal day-to-day life for the population. These facilities include, but are not limited to: power plants, factories, military bases, and government buildings. Determining the best course of action for guarding these facilities and the security analysis of such structures is a daunting task. Due to the uniqueness of each facility, creating a general model is not always possible for real world scenarios. What is required is the ability to create separate models for each critical facility. These models need to be used many times over to generate a variety of different scenarios, and then the data from those scenarios needs to be assessed in a timely manner. Using the Unreal Tournament 2004 (UT2004) Engine, it is possible to make such models that will provide real-time data analysis for agent-based simulations. To create a representative model requires the software packages UnrealEd3.0 and Alias Wavefront's Maya 5.0 PLE, both included with the UT2004 distribution, and Discreet's 3D Studio Max 6.0. Employing these packages and detailed engineering drawings, a model of an industrial facility in the United States has been created. This model contains key systems (i.e. turbines, cooling stations, generators, etc) that will be linked to ORNL's VISAC fault tree analysis code to assess the result of damage to those systems from a variety of terrorist attack scenarios. These simulations will be run using the UT2004 Engine. Areas of interest in the simulations include, but are not limited to: possibility of meltdown, zones of reduced security, and the likelihood of disabling the plant. The ultimate objective of this methodology is to help identify and increase security in vulnerable areas, determine the vulnerability of key system components from internal and external attacks, visualize what subsystems are affected if an attack is successful, and estimate the probabilities of catastrophic events. In the future, manipulation of the Unreal Engine's code to allow for artificial intelligence capabilities that would mimic the behavior of known terrorist groups in an effort to create force-on-force simulations for training purposes may become possible.

Testing the Efficiency of Iterative Methods for Sparse Matrices. *BRIAN LANGSTRAAT (Central College, Pella, IA 50219) MASHA SOSONKINA (Ames Laboratory, Ames, IA 50011).* Matrices are used to store mathematical and scientific information. If a large matrix is made up of mostly zeros, then it is called sparse. Sparse matrices are stored such that each nonzero is recorded by its location within a matrix and zeros are generally omitted. Thus the matrix storage is minimized. Sparse matrices arise in many real-world applications from energy networks and biological systems to weather prediction and engineering. Iterative methods are used to find the value of vector x in the linear system of equations: Ax=b, where A is a matrix (often sparse) and b is a vector. Physicists and chemists utilize iterative methods on parallel computers at the Scalable Computing Laboratory (SCL) to solve large-scale problems involving sparse matrices. MATLAB 7.0 was used to test a variety of iterative methods that solve sparse matrices. Several programs were created to test the iterative methods of generalized minimum residual (GMRES), minimum residual (MINRES), preconditioned conjugate gradient (PCG), and quasi-minimal residual (QMR) on a variety of sparse matrices. A preconditioner is a matrix whose inverse is multiplied to both sides of the linear system of equations which changes how the system is solved to obtain the same solution. Preconditioners were used in several tests which decreased the number of iterations needed. Also, an accurate prediction of final results lessened the quantity of iterations greatly. The residual norms can be found more quickly, if the iterative method, preconditioner, and estimation are selected well. This work will supplement the SCL's ability to use MATLAB for solving sparse matrices.

3D Computer Animation Through Anaglyph Stereo Projection. *JUAN LEON (Bergen Community College, Paramus, NJ 07652) ROBERT BENNETT (Brookhaven National Laboratory, Upton, NY 11973).* Stereoscopic imaging is a process of taking a flat, two dimensional pictures, such as a photograph, and giving it a depth of field. This gives the viewer the illusion that the image is coming out towards them. The easiest way to do this is by taking two identical images and putting them side by side, and then having the viewer look at them through an enclosed viewer, such as the View-master, to get the effect. Though it is easy to get two identical images and a View-master, this process is for individual use only, but with today's advances in computing technology, it is easy to create images in stereo on a desktop PC. In order to create a stereoscopic animation, I had to use software that would allow me to render out stereoscopic images and that would also allow me to use real time stereoscopic renders. Softimage's XSI ended up being the program I used to create my animation, simply because it has an openGL renderer and it has many plug-ins capable of rendering stereoscopic images. I was able to create an electric plasma discharge "overview" in 3D. I created a plasma television, a fluorescent bulb, and a Bunsen burner. The modeling and camera animation were easy to create because I've already had experience working with the software. But because the technology of creating stereo images through a computer isn't set at a universal standard, most of the time in creating the 3D illusion was spent in figuring out the settings that the projector and software had to be in to give the best result.

Monitoring SLAC High Performance UNIX Computing Systems. *ANNETTE LETTSOME (Bethune-Cookman College, Daytona Beach, FL 32114) ADEYEMI ADESANYA (Stanford Linear Accelerator Center, Stanford, CA 94025).* Knowledge of the effectiveness and efficiency of computers is important when working with high performance systems. The monitoring of such systems is advantageous in order to foresee possible misfortunes or system failures. Ganglia is a software system designed for high performance computing systems to retrieve specific monitoring information. An alternative storage facility for Ganglia's collected data is needed since its default storage system, the round-robin database (RRD), struggles with data integrity. The creation of a script-driven MySQL database solves this dilemma. This paper describes the process took in the creation and implementation of the MySQL database for use by Ganglia. Comparisons between data storage by both databases are made using gnuplot and Ganglia's real-time graphical user interface.

Scalable Systems Software. *ZACH LOWRY (Middle Tennessee State University, Murfreesboro, TN 37130) NARAYAN DESAI (Argonne National Laboratory, Argonne, IL 60439).* System software on high performance systems consists of everything below the user applications and above the kernel. When designing and writing system software, a number of different problems are encountered. Scalability is one such problem, and a key concern because system size continues to grow quickly. We discuss the Cobalt system software suite, and the techniques used to over come these scalability concerns.

Stereoscopic Imaging of Scanning Electron Micrographs. *KARISSA MAGGIO (Nassau Community College, Garden City, NY 11530) JOHN SPILETIC (Brookhaven National Laboratory, Upton, NY 11973).* Scanning electron micrographs exhibit three-dimensional qualities due to the high depth of field inherent in the use of the scanning electron microscope (SEM). Using the program StereoPhoto Maker, we have attempted to render these micrographs viewable in three dimensions. For this to be accomplished, a routine procedure was developed that permitted movement from trial-and-error to a

method that yields consistent results. As in conventional photography, creation of a stereoscopic image using the SEM requires a left-eye and right-eye image. SEM stage controls permit sample movement in the X and Y axis, 360 degree rotation, and a tilt of 90 degrees toward and 15 degrees away from the signal detector. Images were captured using successive 2.5 degree increments, horizontal and vertical shifting, and sample rotation. Since rotation could not be measured directly, the SEM-generated scale bar was used to measure increments depending upon magnification. The resultant two-dimensional images were opened in a software application known as Stereo Photo Maker and combined to form a stereoscopic image based on two images of differing perspectives. In addition to the routine method of generating stereo pairs through sample tilting, other methods were also tested. It was determined that lateral shifting does not allow for the production of a visually satisfying stereo image. Rotation, however, produced three dimensional images of equal quality to that of tilted samples. We find that the greater variation of surface structure a sample has, a higher initial degree of tilt is required. However, the study of many more samples will be needed to verify this hypothesis.

Stereoscopic Visualization and its Beneficial Use in the Classroom. *SARAH MAINE (St. Joseph's College, Patchogue, NY 11772) MELVYN MORRIS (Brookhaven National Laboratory, Upton, NY 11973)*. Visualization is an important component in the educational development of students of all ages. Often, a flat two-dimensional image is inadequate for illustrating the complexity of an object, such as protein structure, electron orbitals, or the human body. Stereoscopic visualization theaters provide a solution for educators in need of a powerful three-dimensional visualization tool. Using a polarized projection system, images that resemble three-dimensional holograms can be created to provide a comprehensive model that can be easily manipulated with the use of a computer. Research involved uncovering and exploring various computer programs capable of producing stereoscopic images. The programs were analyzed for ease of use, functionality, their potential for use in a classroom. Several programs were then selected as recommended programs. Using these programs, a general curriculum was developed for use in advanced high school level and college level courses. PyMOL and Visual Molecular Dynamics (VMD) allow the user to visualize molecular structures obtained from a Protein Data Bank (PDB). Other programs that assist in the implementation of these lessons include the Bayer College of Medicine (BCM) Search Launcher, ClustalW (an alignment program), and the Conserved Property Difference Locator (CPDL). These programs were utilized in developing lessons to enhance the general high school and college level biology curriculum. The stereoscopic theater and the developed lesson plans will provide the additional assistance students may require to understand the three-dimensional structures that would otherwise remain as abstract concepts.

Analyzing the Computational Complexity of Hierarchal Clustering Algorithms through the Use of Multiple Performance Metrics. *PHILLIP MARTIN (Clemson University, Clemson, SC 29634) THOMAS E. POTOK (Oak Ridge National Laboratory, Oak Ridge, TN 37831)*. With the advent of several methods for large scale text sorting and classification, it is essential to quantitatively compare each text clustering system. However, this comparison represents a significant challenge when considering the distributed nature and hierarchal structure of some of these methods. To overcome the difficulties in the analysis of each technique, it is necessary to examine the two most important aspects of a system, performance and quality. A system is impractical in the real world if it does not satisfy these two conditions. The IntelliAgents program for text clustering, developed by the Applied Software Engineering Research Group at Oak Ridge National Labs, was selected and then modified to include both a quality and a performance measuring algorithm. The quality measure is based on a modified version of the F-measure algorithm, which utilizes a calculation of precision and recall on document clusters to measure the quality of a clustering result. The performance of the system is observed by evaluating the time each document takes from its introduction into the system until the document is fully clustered. Selecting these methods provides several advantages, including ease of implementation and the applicability to a flat or hierarchal cluster system. Documents in each run consist of various subsets from the Reuters news 21578 text corpus. Testing is performed with 1 to 32 computer nodes in increments of 1 node. The data set is then varied from approximately 3000 to 6000 documents in increments of approximately 1000 documents. The results, as expected, show that as the number of nodes increases from 1 to 32, the time it takes to cluster x documents decreases. As nodes are added for each test, the F-measure of the system is relatively unchanged. The F-measure of the clusters only fluctuates with the change in the document set size. Having a simple and universal measurement, such as the ones in this paper, provides a basis for comparing clustering programs. With this foundation, it may be possible in the future to incorporate self-adjusting clustering algorithms that will balance performance versus quality to create optimally efficient clusters.

Interactive Stereoscopic 3-D Visualization of Time Resolved Plasma Emission Spectra. *DANIEL MASTRANGELO (Bergen Community College, Paramus, NJ 07649) ROBERT BENNETT (Brookhaven National Laboratory, Upton, NY 11973)*. Interactive stereoscopic data visualization is an area of computer graphics providing techniques and algorithms to display large datasets as two- and three-dimensional images, thereby giving scientists the ability to better analyze and discern details in their data. The goal of our effort was to develop and deploy a software package that provides the ability to interpret and visualize arbitrary sized data sets using interactive stereoscopic three-dimensional viewing techniques. Each raw data set consists of a series of frames (two dimensional arrays of emission intensities as a function of wavelength), where each frame is a spectral snapshot of the plasma at a precise unit of time after the initiation (voltage pulse) of the plasma. In order to streamline the processing of the raw data, we have developed a software tool using both open-source and commercial packages: Microsoft Visual Studio .NET 2003 was used as the IDE (Integrated Development Environment) and Visual C++ was the development programming language. We utilized the open-source Visualization Toolkit (vtk) to render the data in three dimensions and another freely available software package, Tool Command Language (Tcl) and its associated graphic user interface (GUI) toolkit (Tk) to create the GUI. This interactive tool will allow the user to study the formation and subsequent decay of active chemical species (excited state atoms, molecules and ions) over the duration of a short-lived plasma event, and should therefore yield greater insight into the underlying plasma processes.

Modeling for 3D Visualization. *KYLE MCCOY (Alfred State College, Alfred, NY 14802) MICHAEL MCGUIGAN (Brookhaven National Laboratory, Upton, NY 11973)*. Of particular interest to the design curricula at Alfred State College (ASC) is the expansion of their current capability to create 3D projections of objects on a 2D computer display using 3D software – specifically Autodesk VIZ 2005 and Maya 6.5. In architecture, using computers to model the interior of a building is much more efficient in giving the viewer a true sense of the space than building cardboard and wood models. The computer generated models are able to give a much better sense of the area than the scaled down physical models because they are created at true scale. Using the 3D visualization theatre on the ASC campus to help showcase student designs, both architectural and graphic, will be very useful in giving the viewer a true sense of the design. The focus of this work is primarily architectural based. Proposed was the transfer of models from the computer software Autodesk VIZ 2005 into the theatre projector. A benefit of this would be allowing students to follow the design process from beginning to end. The level of detail is restricted only by the resolution of the computer program and the practical speed of the theater's workstation. Being able to make this output of the model easily and effectively will be of great value to most of the design curricula offered by ASC. This accomplishment will be made available to any establishment with a 3D visualization theater that would like to teach and show any 3D subject more effectively and efficiently. In order to carry out this task, 3D models of a townhouse complex already planned and designed for ASC were modeled using Autodesk VIZ 2005. These models were then placed in their true environment on the terrain developed in Maya 6.5 and rendered into an animated movie file. This movie will be able to be viewed in stereo in the 3D visualization theatre on the ASC campus. A 'user's manual' was also developed in order to explain in greater detail the process taken to successfully complete this project at Brookhaven National Laboratory.

Development of Biometrics. *VIRAJ MEHTA (State University of New York – Stony Brook, Stony Brook, NY 11794) UPENDRA K. ROHATGI (Brookhaven National Laboratory, Upton, NY 11973)*. Biometric Identification methods are the next level of security in a digital world because they are easy to use but are extremely difficult to compromise. In fact, email passwords and ATM pin numbers can be easily hacked, stolen or misused while biometrics is unique to every human being and uses fingerprints, hand scans, voice samples and iris scans, to identify the person. This technology helps to reduce identity theft and is also used to protect valuable resources of a company or individual. The biometric system can be designed for either individual characteristics such as finger, hand or face, or all of them can be integrated into one identification system. The advantage of integrated system is the increase in the accuracy of identification. An integrated

biometric system was developed that combined fingerprints, face scans and hand scan to identify a person. The results obtained from the integrated hardware with the software were good. The software was able to identify authorized users/personnel 95% of the time. Out of the remaining percentage, 2% went towards giving permissions to unauthorized users, and 3% produced “Invalid Image” errors. This research project is the continuation of work that was done last summer. The biometric software was tested further under different Operating Systems other than Microsoft Windows. The desired Operating Systems selected to be used were Debian Linux and Red Hat Enterprise Linux Version 5. The database of existing users was also modified to create a larger database which is run by Oracle Database 9i. The purpose of having a different OS environment, gave us the ability to further test the software, discover any new bugs and continue to improve the efficiency and the stability of the program. Oracle Database is an industry accepted Database Software Application Suite and having the software use the resources of Oracle Database would allow us to increase the reliability, scalability of the software when deployed in an enterprise. The biometric software uses “generic” off the shelf hardware to make the software cost effective and not making it rely upon proprietary hardware. Digital Persona’s “U.are.U” 4000S sensor is being used for fingerprint recognition, and 2 Logitech QuickCam 4000S webcams were being used for face and hand recognition. The conversion or porting of the biometric software from a Windows to a Linux based environment did cause errors but were resolved with the constant feedback with the help of the developers and other beta testers who had access to the software.

Real-time Harvesting of Distributed Environmental Data for Improved Management of Complex Distributed Water and Power Management Systems. *ELVIRA MEZA (Columbia Basin College, PasCO WA 99301) LANCE VAIL (Pacific Northwest National Laboratory, Richland, WA 99352).* The amount of environmental data that is available and being collected at ever increasing rates exceeds the current ability of most environmental decision makers to acquire and process the data in time to support decision making. Demands for increasing marginal improvements in system performance require decision making to be performed on a real-time basis. This will further increase the demand for faster and more reliable automated systems to harvest data distributed on numerous sources over the Internet. By combining a metadata database with a Java program, remote data sources can be queried and data acquired on either a ‘just in time’ or real-time basis. Java is selected since it has benefits of platform independence and ease of interaction through web browsers. The data harvesting procedure involves the Java program acquiring information about the location and protocol for the web query to acquire the information. Based on this information, the Java program proceeds to acquire the actual data from the Internet source. Java’s exclusive structural design permits the construction of a single application that can run across several platforms. Java is integrated into nearly all major operating systems, and it is built into the most popular web browsers which mean that Java is able to run on practically every Internet connected machine in the world. Also, Java supports multiple threads of execution built into the language .This means that data and code written in Java is easy to understand better than other complex programming language. In addition, Java combines different programming language properties into one language. This makes Java programs faster than other programming languages. This work is a small portion of a much larger initiative within PNNL to develop the next generation of integrated environmental decision support software to enable water and power resources managers the ability to make optimal real-time decisions. Two examples of likely future applications of this approach include: 1) harvesting water related information including stream-flow measurements, snow- pack observations, and remote sensing data on snow cover extent to help calibrate and continuously update the Lab’s Distributed Hydrologic Soil and Vegetation Model to provide reliable stream-flow forecasts and 2) harvest water and fisheries information including real-time reservoir levels and fish passage data to improve the characterization and management of the hydropower system as part of the Lab’s Integrated Energy Operation Center Initiative.

Xing_RK4 and Creation of Interfaces. *AUGUSTUS MIRAGLIA (Appalachian State University, Boone, NC 28607) HAIPENG WANG (Thomas Jefferson National Accelerator Facility, Newport News, VA 23606).* This program will be used at JLab to simulate multipacting (MP) in rectangular waveguides. MP is a resonant electronic process that may happen when a vacuum system is subjected to high radio frequency fields. Xing_RK4 is used to predict power levels at which MP will occur, explore measures to suppress or eliminate MP, and understand the basic characteristics of MP. After fixing some bugs, Xing_RK4 was benchmarked with the data published in using a different math method. Two graphical user interfaces (GUI) were then created. The first GUI is for creating the input files needed to run Xing_RK4. The second GUI is for taking an output file produced by Xing_RK4 and graphing individual electron trajectories of instances where MP will be present. Sweeping frequency parameter was also added to Xing_RK4. The first GUI allows a user to create or edit the input files without using a text editor. It also includes error checking for all variables to limit invalid input. The second GUI will be used to locate and analyze the characteristics of where MP occurs. Together these GUIs will allow other scientists to use Xing_RK4 to analyze different rectangular waveguides. Scientists can quickly view the electron trajectories where MP is present. The GUIs will increase the use of Xing_RK4 for running MP simulations.

Design and Development of a PDA Interface for Cloning and Purification Database Systems. *SOON PARK (Governors State University, University Park, IL 60466) ANDRZEJ JOACHIMIAK (Argonne National Laboratory, Argonne, IL 60439).* One of the researches in the Midwest Center for Structural Genomics (MCSG) is to develop, and optimize new, rapid integrated methods for highly cost-effective determination of protein structures through x-ray crystallography. The cloning database system has been developed for automated gene cloning, gene alteration, and expression using a commercial liquid handling robot system. The purification database system has been developed for the protein purification by implementing a single process stream from cell growth to protein delivery (concentration, characterization). Web applications are available for scientists to access and store their research data to the cloning and purification database systems through a network browser in the MCSG. Mobile computing offers the possibility of dramatically expanding the versatility of computers, by bringing them off the desktop and into PDAs like the Pocket PC, Palm, and Blackberry. This project is to design a PDA application for the cloning and purification database systems. Some of the benefits include improving operational efficiency, reducing human errors, saving time, and increasing accessibility and mobility. The PDA cloning and purification systems make it convenient for scientists to access the databases in the lab while preserving the sophistication of the web application.

A Survey of Web Services Interoperability. *SCOTT PRICE (University of Illinois at Chicago, Chicago, IL 60614) IVAN JUDSON (Argonne National Laboratory, Argonne, IL 60439).* Web Services have become the lingua franca for building service-oriented systems. The development of tools for web service developers takes a significant amount of time, negatively affecting the deployment, and thus the adoption, of web services as a real technology. With the advent of the Web Service Interoperability Organization along with the resulting Basic Profile specifications – which outlines guidelines for interoperable services – toolkits can adhere to a set of standards that can enable interoperability. The selected toolkits are Microsoft’s Visual Studio. NET (VS.NET), Apache Axis for Java (Axis), SOAP::Lite (S::L) for Perl, ZSI for Python and gSoap for C/C++. All of the toolkits require the use of auxiliary software in order for them to work. This includes Microsoft’s Windows XP Professional operating system and Internet Information Services (IIS) web server, Sun Microsystem’s Java 2 Platform, Enterprise Edition (J2EE), the Apache Tomcat web server, and ActiveState’s ActivePerl and ActivePython. A set of simple web services was first designed by constructing a web service definition language file (WSDL). VS.NET was selected to be the provider of these services while the remaining toolkits were used to construct clients that could consume the services. VS.NET, Axis, ZSI and gSoap provided tools within the toolkit to read the WSDL and automatically generate client and server code stubs. This allows the developer to focus solely on writing their specific logic, as opposed to having to meddle with the details of web services. S::L did not provide such a tool; however, the toolkit proved to be easily customizable and achieved interoperability with little fuss. The next step was to create servers using the remaining toolkits and to ensure that all clients and servers were interoperable. The tools provided by VS.NET, Axis, ZSI and gSoap simplified this process. S::L was also easily customizable when acting as a server. While each of these toolkits has documentation, it is often incomplete or lacking in some respect. This survey was aimed at demystifying the process of developing interoperable services by providing ample documentation of our methods.

Configuration File Generation with Python and XML. *KENNETH RAFFENETTI (University of Illinois at Urbana-Champaign, Urbana, IL 61801) CRAIG STACEY (Argonne National Laboratory, Argonne, IL 60439).* There is a need by servers providing network services for a

large number of machines for configuration files that can take a long time to create and update. Systems administrators would be best to devise a system for automatically generating and updating these files from information gathered about the network. When this information is created and/or updated, a single script can easily be run to put the appropriately updated files in place and assure the correct functionality of the network and its hosts. This process can be greatly aided with the use of the Python programming language combined with the data representation abilities of the Extensible Markup Language (XML) to generate files of such nature.

Two Hybrid Approaches to Increase Activity Analysis Accuracy. *LUIS RAMOS (La Sierra University, Riverside, CA 92505) PAUL HOVLAND (Argonne National Laboratory, Argonne, IL 60439).* Automatic Differentiation (AD) is the process of translating one program that computes a function f and generating a different program that computes the derivative of that function, f'. Activity analysis is important for AD. Our results show that a dynamic activity analysis enables an average speedup of 28%. We investigated two techniques aimed at reducing the overhead of dynamic activity analysis. One uses a profile-guided activity analysis and the other uses a less-conservative static activity analysis. The results from these techniques are mixed; some benchmarks showed improvement, others performed poorly.

Identification of CRISPR Elements in Prokaryotes Using Suffix Trees. *TERESA RAMSEY (Jackson State University, Jackson, MS 39217) NIKOS KYRPIDES/PHIL HUGENHOLTZ (Lawrence Berkeley National Laboratory, Berkeley, CA 94720).* Recently, a new class of repeats have been studied. Clustered Regularly Interspaced Short Palindromic Repeats (CRISPRs), are repetitive sequences interspaced by similarly sized non-repetitive spacer sequences ranging in sizes from 21 to 37 base pairs. The identification of these repeats have been analyzed manually by previous researchers. In our study, we create a tool, CRISPR Recognition Tool (CRT), that uses suffix trees to identify CRISPRs. We identified other known repeat finders and compared the running time of those tools to that of CRT. Our results show CRT to be the optimal tool when searching for CRISPR elements.

Wind Turbine Control. *DANIEL RATHE (Iowa Lakes Community College, Estherville, IA 51334) LEE JAY FINGERSH (National Renewable Energy Laboratory, Golden, CO 89401).* Wind turbines are fine machines for generating electricity, but for practical purposes they must start, operate, and shut down automatically. Fortunately, the National Wind Technology Center (NWTC) works with organizations in the U.S. wind industry to design, test, and advance automatic wind turbine control. Currently, the NWTC is implementing a new wind turbine control system in LabVIEW that has the potential to increase the efficiency of wind turbine control research and testing. More efficient research and testing at the NWTC may facilitate quicker advances in wind turbine control systems and increased understanding of such systems; such advances and increased understanding will allow the U.S. wind industry to be more competitive with the global wind industry as well as other sources of energy. The following describes the NWTC's controls research facilities; it describes the basic components of a wind turbine and concurrently shows parameters of these components that are monitored and used to control the wind turbine. Also, the following describes to a limited level of detail how a wind turbine control system gathers and uses the parameters to control a wind turbine. Finally, it illustrates the NWTC's two wind turbine control systems.

Analysis of the Model Facility Geometry of the Visual Interactive Site Analysis Code Using the Java Programming Language. *FREDRICK ROGERS (Norfolk State University, Norfolk, VA 23504) C. DAVID SULFREDGE (Oak Ridge National Laboratory, Oak Ridge, TN 37831).* Visual Interactive Site Analysis Code (VISAC) is a JAVA system that allows the user to simulate and analyze the results of different accidents/incidents ranging from simple individual equipment sabotage to complex sorties that utilize a range of military weapons, simulated truck or car bombs, or satchel charges. VISAC is supplied with a library of facility models that are customizable in both geometry and logic to approximate a number of facilities of interest. Created or customized model facilities can have faults, such as overlaps and voids in the geometry, which may be too small to be visible or even hidden by the complexity of a model. These faults may cause the production of erroneous results in the blast calculation portion of VISAC. The goal is to find such errors and report them so that faults can be easily corrected. To locate the errors, a grid of rays is projected through the model parallel to each of the three coordinate axes. Each ray is then divided into path segments representing the different material regions through which it passes. Interferences and voids are revealed by comparison of the path segment starting and stopping points at the region boundaries. This allows for correction of possible geometry faults.

SensorNet: Combining the Existing to Protect the Future. *ISAIAH RUFFNER (University of the Cumberlands, Williamsburg, KY 40769) DAVID HILL (Oak Ridge National Laboratory, Oak Ridge, TN 37831).* For as long as the United States exists, there will always be a need to manage the ever increasing threat of terrorism. That truth was not fully realized until the attacks on the World Trade Center and the Pentagon in September 2001. Unfortunately, it was only then that Americans realized the real need of early detection. With the rush to appease a demanding public, many agencies, cities, etc. implemented such systems without a true vision for their possibilities, thus resulting in many sensor networks that do little sharing of data (if any) with other networks. This is a problem that the SensorNet project seeks to resolve. The idea of SensorNet is to take existing networks of sensors, create additional networks where needed, and combine everything into one network that is able to access, store, and retrieve that information from any network enabled location. One immediate need for the SensorNet project was the lack of an application which would allow users to view events that had already taken place at transfer truck weigh stations. An application had already been developed by David Feaker that allowed an operator to look at the data in real time, however, it was not designed to allow reach-back capabilities. The SensorNet Weigh Station Viewer needed to be similar in design to the existing application to promote familiarity, and it needed to provide some additional functionality. The application was designed using the Java programming language and JavaWebStart technology, which allows a Java application to be installed and run remotely. It provides users with the ability to study the data taken, including data from various radiation detection devices, as well as provides images and data that provide physical descriptions of the trucks.

Creating a New Plug-In for Gatan's Digital Micrograph and Jeol's Scanning Transmission Electron Microscope. *KEVIN RYAN (SUNY Albany, Albany, NY 12222) HUILIN LI (Brookhaven National Laboratory, Upton, NY 11973).* Digital Micrograph (DM), written by Gatan Inc., allows remote control of the Scanning Transmission Electron Microscope (STEM), powerful data manipulation for analysis, and customization using their included Software Developers Kit (SDK) plus a high level scripting language. The new Plug-In was created to enable researchers who are working with fragile organic specimens to have full control of the microscope so they can preserve their sample. Many of the built in functions of DM were used, however, this was just a base to build on and improve. The Plug-In was created using Microsoft's' Visual Studio .NET 2003 to compile and revise the SDK while the scripting language built the user interface and incorporated the newly created functions into DM. Whenever a problem was encountered referring to Gatan's support pages or various websites, for example http://www.felmi-zfe.tugraz.at/dm_scripts/dm_scripts/index2.html, would always aid in resolving the situation. When the project was first started the script source code was quite small and basically provided the user interface with no functionality behind it. The script went through many changes during its maturity, like all computer programs in development. After much testing and debugging the program was completed, allowing the researchers to change the magnification and control the beam center and scanning speed. This lets them move and scan different areas digitally instead of manually moving the stage the specimen is on. The advantages of these digital movements are much more precise shifts, which are needed because the specimens are only several hundred nanometers long. Another feature of the program permits the researchers to save their settings in three different modes (focus, search and exposure) to easily locate and capture the image without damaging the frail specimen. At the end of development the program was a multiple file script to create a more powerful interface with a compiled Dynamic Link Library (DLL) behind it that can communicate with and manage the microscope with greater accuracy.

The Identification and Characterization of CRISPR patterns in Prokaryotic DNA. *FAREEDAH SABREE (Jackson State University, Jackson, MS 39217) NIKOS KYRPIDES (Lawrence Berkeley National Laboratory, Berkeley, CA 94720).* Clustered Regularly Interspaced Short Palindromic Repeats (CRISPRs) are commonly found in the DNA of prokaryotic cells. CRISPRs are comprised of multiple short direct nucleotide repeats that range in size from 21 to 37 base pairs, and are interspaced by similarly sized non repetitive DNA sequences. They possess a common leader sequence that is usually adjoined along either side of the CRISPR pattern. In this paper, we discuss our extensions to the work of Jansen ***et al.*** They found more than forty prokaryotic species with CRISPR patterns. We extend their research

by re-examining the organisms found by them and searching for new patterns in some species that have been sequenced since their research was completed in 2002. We use the computer software, CRISPR Recognition Tool (CRT), which we developed to find CRISPR patterns along with the Integrated Microbial Genomes (IMG) system (Joint Genome Institute's (JGI) data management system). Upon finding new CRISPR patterns, we characterize and compare them to previous results of other studies. When comparing, we take into consideration the length and the frequency of the patterns. From our search of CRISPR patterns, we found these characteristics: from the 27 organisms, the repeat length ranged in size from 19 in Yersinia pestis KIM to 37 base pairs in Thermus Thermophilis HB27, Porphyromonas gingivalis W83, and Methylococcus Capsulatus BATH. Also, the largest CRISPR loci found was Geobactersulfurreducens PCA with 143 repeats. Overall, the average repeat length of the CRISPR was 32 base pairs. Hopefully, CRT will aid in the discovery of the biological function of CRISPR patterns.

The Administrative Task of Adding a New Computer to an Existing Network. *GABRIEL SANCHEZ (State University of New York – Stony Brook, Stony Brook, NY 11790) CHEO TENG (Brookhaven National Laboratory, Upton, NY 11973).* The National Synchrotron Light Source (NSLS) uses Hewlett-Packard UniX (HP-UX) machines to monitor the daily operations and data collection of particle accelerators. However, these machines must be maintained in order to safely continue the research carried out by the scientists that utilize the NSLS facility. In order to upgrade the NSLS network to a newer HP-UX operating system version, a test machine is securely configured on the existing network, and if there are no compatibility issues, it is safe to upgrade every computer on the network using the test machine's configuration. As part of the system administrative tasks, I developed small resident software designed to report idle users and tracking the location of every computer connected to the private network to maintain the security of the network. Whenever a new machine is configured onto a network, it must successfully initiate the Network Information Service (NIS), the Domain Name System (DNS), and the Network File System (NFS). When invoking NIS and DNS, this test machine acts as a client that connects to a server, then both the server and the client need specific configuration files edited so that the server can recognize the client as part of the network. The purpose of NFS, however, is to mount file systems from one machine onto another, so NIS and DNS must be carried out before this takes place.

Hyperlink Topology: A Plausible Search Engine Technique? *JESSE SCHUSS (Onondaga Community College, Syracuse, NY 13215) SCOTT BUTNER (Pacific Northwest National Laboratory, Richland, WA 99352).* Search engines are a fact of life now. They are used throughout the world to make life easier by returning relevant results to a user's query. As the web grows, however, search engines become more ineffective and new techniques are required. New web analysis techniques are required to keep up with the growth of the web. Link topology is currently used by search engines to aid in ranking their results. However, link topology has not been used by itself to examine the web. Utilizing a crawler, SOLAME, we gathered data from the web and constructed a relatively small database. Specifically, hyperlinks were examined, collected, and categorized. We then constructed a matrix of source-destination hyperlinks and, using Euclidean distances of column vectors from the matrix, plotted the results using IN-SPIRE to reduce a multidimensional space down to a conceptual two or three dimension visualization. The results revealed that within the visualization of IN-SPIRE web sites were clustered together along the bounds of the planar domain. That there was hyperlink clustering reveals sites that have similar subject matter content, thus proving that the link topology of a web site reveals some information about its content. This result was expected, following the logic that sites would link to sites with similar subject matter. Whether that site had arguments for or against the first was not taken into account for this project. This explorative step into new topological analysis of web site is just one part of a growing effort to analyze the web on part of the entire web community. Though the initial results were based off of a small database, they have yielded enough information to warrant further studies. Predictably, more topic specific and argument category result sets (i.e., sites for or against) can be achieved through the use of a contextual engine to analyze the text surrounding the link.

NIS and NFS Security – An introduction to a Secured Network Information Services and Network File Systems. *NOPPOL SETOBOL (Contra Costa College, San Pablo, CA 94806) CHARLES VERBOOM (Lawrence Berkeley National Laboratory, Berkeley, CA 94720).* Laboratories today typically consist of having a couple of workstations that are assigned to specific scientists for that department. These workstations are independent of each other and do not share files unless manually transferred from one workstation to another. Account management configuration and data backup must to be done manually for every machine. An alternative to this setup is using a Linux client-server model implemented with Network Information Services (NIS) and Network File Systems (NFS). These services allow client workstations to have the same configuration files and file systems. User account information and home directories will exist on all configured workstations that are configured with these two services. Managing accounts and backing up data is easily done from the server. Unfortunately, there are a lot of security vulnerabilities that exist when using these two protocols. The following research paper will discuss the stability, vulnerability and comparison of NIS and NFS client-server model to a secured independent workstation. The results will determine whether a client-server model with NIS and NFS can be as secure as an independent workstation in a working environment.

Developing a G2 Software Bridge. *WALLACE SHEEHAN (University of Colorado, Boulder, CO 80301) JOSEPH FARMER (National Renewable Energy Laboratory, Golden, CO 89401).* The Process Development Unit (PDU) — a bioethanol plant — at the National Renewable Energy Laboratory (NREL) is managed by control software called G2. Data from the PDU equipment is made available on the network by Opto22 controllers in the plant. To facilitate communications between the Opto22 controllers and G2 a piece of interpreting software called a G2 bridge is required. The G2 bridge is written in C or C++ and runs independently of either G2 or Opto22. It translates messages from G2 to Opto22 and back. Through the course of developing this bridge it has become apparent that the ideal solution for controlling the PDU is not G2. Rather, it seems more efficient to have a piece of software designed specifically for communicating with Opto22 controllers in the PDU. Because G2 is intended to be generic control software, it requires a great deal of maintenance. Although a custom application would be less robust than G2, it would be easier to use and the loss of generality would not affect the performance of the software as far as the PDU is concerned.

MetaMind: A Meta-data Extraction Tool for Classifying Web Content Using Domain-Specific Context and Content Heuristics. *STEVE SILVA (Washington State University, Pullman, WA 99163) SCOTT BUTNER (Pacific Northwest National Laboratory, Richland, WA 99352).* Developing software agents which can reliably classify web documents is an important prerequisite to widespread adoption of semantic web technologies. Effective agents must be able to process large numbers of web documents in a timely and cost effective manner, while providing for classification accuracy that is comparable to that of a human reader. This research paper discusses the design and implementation of the MetaMind tool, along with preliminary results obtained from the web-based classification of environmental compliance assistance documents. MetaMind is a meta-data extraction tool designed to (1) extract domain-specific meta-data attributes from web documents; and (2) use these meta-data attributes (along with additional context clues) to aid in classifying these documents against predefined, hierarchical subject taxonomy. MetaMind's classification and meta-data extraction rules are based on both document content (analysis of word frequency and word/phrase position) and context cues (including web domain and path structure, analysis of inbound and outbound hyperlinks, etc). In order to facilitate integration with other applications, MetaMind is being implemented as a web service using a combination of Java Servlet technology and JESS, a Java-based Expert System Shell developed by Sandia National Laboratory. An extended form of the Rich Site Summary standard (RSS) is being used to present the resulting meta-data information to the user. MetaMind is being developed to support the US EPA's Compliance Assistance Clearinghouse, an online meta-data repository focusing on documents providing regulatory interpretation and assistance to the business community. While MetaMind is being developed for application to a specific and relatively narrow domain, we believe that many classification tasks are similarly constrained within narrow subject domains. In such applications, classification heuristics encoded as production rules can be used very effectively without suffering the problems of scaling and maintainability that often occur when such approaches are applied to broader subject areas.

Modeling for 3D Visualization. *WENDY SIMPSON (Alfred State College, Alfred, NY 14802) MICHAEL MCGUIGAN (Brookhaven National Laboratory, Upton, NY 11973).* Of particular interest to the design curricula at Alfred State College (ASC) is the expansion of their current capability to create 3D projections of objects on a 2D computer display using 3D software – specifically Autodesk VIZ 2005 and Maya 6.5. In architecture, using computers to model the interior

of a building is much more efficient in giving the viewer a true sense of the space than building cardboard and wood models. The computer generated models are able to give a much better sense of the area than the scaled down physical models because they are created at true scale. Using the 3D visualization theatre on the ASC campus to help showcase student designs, both architectural and graphic, will be very useful in giving the viewer a true sense of the design. The focus of this work is primarily architectural based. Proposed was the transfer of models from the computer software Autodesk VIZ 2005 into the theatre projector. A benefit of this would be allowing students to follow the design process from beginning to end. The level of detail is restricted only by the resolution of the computer program and the practical speed of the theater's workstation. Being able to make this output of the model easily and effectively will be of great value to most of the design curricula offered by ASC. This accomplishment will be made available to any establishment with a 3D visualization theater that would like to teach and show any 3D subject more effectively and efficiently. In order to carry out this task, 3D models of a townhouse complex already planned and designed for ASC were modeled using Autodesk VIZ 2005. These models were then placed in their true environment on the terrain developed in Maya 6.5 and rendered into an animated movie file. This movie will be able to be viewed in stereo in the 3D visualization theatre on the ASC campus. A User's Manual was also developed in order to explain in greater detail the process taken to successfully complete this project at Brookhaven National Laboratory.

Development of Software to Aid in Standardization and Consolidation of Optics Lattice Description Data that Model an Accelerator. *RYAN SLOMINSKI (James Madison University, Harrisonburg, VA 22807) YVES ROBLIN (Thomas Jefferson National Accelerator Facility, Newport News, VA 23606).* Optics lattice description data sharing at Jefferson Lab is currently done by copying data by hand or by using various conversion utilities. Sharing this data is difficult because it is stored in various non-standard formats and is scattered throughout the lab. In this project, three software utilities were developed to aid in the adoption of a new system for standardizing and centralizing optics lattice description data storage at Jefferson Lab. The first, OptiM2AML, converts OptiM, a non-standard optics lattice description data format, into Accelerator Markup Language (AML), a standard format. The second, AML2Database, inserts AML data into a database; and the third, Database2AML, retrieves AML data from a database. The utilities are written in the Java programming language and modeled with Unified Modeling Language (UML) diagrams. The goal of this project was to develop software that could be easily understood, operated, maintained, and extended. To this end, many known solutions and design patterns are incorporated into the work. The credibility of the software is demonstrated by UML diagrams, software design patterns, object-oriented design principles, software testing, and documentation.

Design and Development of a PDA Interface for Cloning and Purification Database Systems. *RAKEYA SMITH (Governors State University, University Park, IL 60466) SOON-OK PARK (Argonne National Laboratory, Argonne, IL 60439).* The objective of the research being conducted in the Midwest Center for Structural Genomics (MCSG) and Bioscience division is to develop, and optimize new, rapid integrated methods for highly cost-effective determination of protein structures through x-ray crystallography. Our near term goal is to improve a user application, which the biologist use, for the advancement of research data storage and mobility. We are faced with the task of modifying the cloning application so that it will be feasibly useable on all PDA's. We want to provide some of the desktop functionality of the application on PDA's. While developing the application there were precautions we took. We developed the application to be user friendly and made sure we had data validation, to reduce errors on data entry that is stored in the database. There are several advantages to this application: It increases the quality and efficiency on the data collection and analysis. It minimizes data entry errors. The data is collected electronically from various sources. Scans the devices and import it into the database by using a scanner on the PDA. It increases accessibility and mobility.

Construction of a Stereoscopic Model of the Solar System. *JONATHAN SMOLANSKY (Suffolk County Community College, Selden, NY 11705) GORDON SMITH (Brookhaven National Laboratory, Upton, NY 11973).* The purpose of this venture is to construct an accurate, stereoscopic model of the Solar System by means of Maya 6.5. Accurately scaled three-dimensional representations of the Solar System are virtually non-existent. Vast differences in size, orbital velocity, and semi-major axes present problems for researchers who are trying to realistically portray astronomical bodies. Professors, students, and any interested parties will be offered an up-close-and-personal journey through a small part of the Milky Way Galaxy. Various internet resources were used to acquire the data necessary for the Solar System's creation. They include, but are not limited to, NASA.com, nationmaster.com, CelestiaMotherlode.com, and similar web encyclopedia instruments. Maya 6.5, the program chosen for this project, is an award winning 3-D animation program used by Hollywood production studios in the creation of elaborate special effects scenes. The project was divided into three phases: The first phase involved creating a skeletal model of the Solar System. NURBS (non-uniform rational b-splines) spheres represent the planets and their respective moons. Relative sizes were scaled with respect to Jupiter, which made it possible for all the planets to be visible in a single frame. Next, the rotational tilts and orbital inclinations of the planets were input. This was followed by the planets' relative distances and orbital eccentricities. The second phase involved planet surface texture maps (skins), acquired from the Internet and wrapped around each sphere. A large sphere was created and shaded black to encompass the Solar System. Phase three involved exporting the model into StereoMovie Maker so that the presentation can be viewed in stereo. Maya's inability to output scenes in Stereo will necessitate its channeling through StereoMovie Maker, a program with Stereo capabilities. Ultimately, this project will function as a platform for those who aspire to build upon the existing model by adding other celestial objects such as galaxies, nebulae, comets, and asteroids.

Floating-Point Intensive Particle System Algorithms Implemented on the Graphics Processing Unit. *JOSHUA STRATTON (University of Tennessee, Knoxville, TN 37922) GEORGE FANN (Oak Ridge National Laboratory, Oak Ridge, TN 37831).* Graphical processing units (GPUs) have increased in programmability, speed, and computational capabilities. GPUs were originally designed for graphical purposes such as basic 2D rendering (GUIs, prompts, etc.) and 3D animations, while the central processing unit (CPU) controlled much more diverse tasks such as managing the operating system, peripherals and user applications. Recently GPUs have been designed specifically for physics-based games and have improved dramatically in floating-point capabilities—required in most 3D algorithms—allowing higher performance than most CPUs can provide. As the FLOPS/cost ratio of the GPU increases faster than the CPU, the GPU becomes a more and more practical tool for some types scientific computing. Using Cg, a particle-system algorithm written for the CPU has been ported to the GPU. This transition has improved the overall performance by taking advantage of the GPUs floating-point performance. Current GPUs can only perform 32-bit arithmetic, which is precise enough for many applications. Our paradigm is applicable to future 64-bit GPUs as well.

Construction of a Stereoscopic Model of the Solar System. *DOUGLAS TAMMANY (Suffolk County Community College, Selden, NY 11784) GORDON SMITH (Brookhaven National Laboratory, Upton, NY 11973).* The purpose of this venture is to construct an accurate, third-dimensional, stereoscopic model of the Solar System by means of Maya 6.5. Accurately scaled three-dimensional representations of the Solar System are virtually non-existent. Vast differences in size, orbital velocity, and semi-major axes present problems for researchers who are trying to realistically portray astronomical bodies. Professors, students, and any interested parties will be offered an up-close-and-personal journey through a small part of the Milky Way Galaxy. Various Internet resources were used to acquire the data necessary for the Solar System's creation. They include, but are not limited to, NASA.com, nationmaster.com, and similar web encyclopedia instruments. Maya 6.5, the program chosen for this project, is an award winning 3-D animation program used by Hollywood production studios in the creation of elaborate special effects scenes. The project was divided into three phases: The first phase involved creating a skeletal model of the Solar System. NURBS spheres represent the planets and their respective moons. Relative sizes were scaled with respect to Jupiter, which made it possible for all the planets to be visible in a single frame. Next, the rotational tilts, orbital inclinations, and orbital eccentricities of the planets were input. Although a method of scaling the relative semi-major axes was found, they were omitted from the final presentation to preserve the single-frame image of the Solar System. The second phase involved planet surface texture maps (skins), acquired from the Internet and wrapped around each sphere. A large sphere was created and shaded black to encompass the Solar System. Phase three involved exporting the model into StereoMovie Maker so that the presentation can be viewed in stereo. Maya's inability to output scenes in Stereo will necessitate its channeling through StereoMovie Maker, a similar program with Stereo capabilities. It will also allow for camera movement throughout the system. Ultimately, this project will function

as a platform for those who aspire to build upon the existing model by adding other celestial objects such as galaxies, nebulae, comets, and asteroids.

The Diet Problem Case Study Using Network Enabled Optimization Systems (NEOS). *XUEQING TANG (Governors State University, University Park, IL 60466) JORGE MORE (Argonne National Laboratory, Argonne, IL 60439).* The Diet Problem Case Study is a real world application that utilizes the Network Enabled Optimization System (NEOS). The Diet Problem is the most popular case study problem in industry and universities to learn about Linear Programming. When the menu is accessed, and the user makes his/her selections for meals of a day, an error, "Error in write_data program: return code 32256" occurs, and the user does not get to see the results of the least cost menu for his/her selections. If the user wants to change the constraints on the menu, there is an error that displays "Can't open file 'total_cost.out'. We studied C++, Perl, Hyper-Text Markup Language (HTML), A thematical Programming Modeling Language (AMPL), and Linear Programming to find out what's missing in the current system. We are writing all the codes in Python to make the case study running again. Python is an object-oriented computer programming language. It's readable, maintainable, portable, and it's powerful. It can be interchanged with other languages, if necessary. Python is easy to use, and easy to learn. Since Python has several advantages over other programming languages, we are converting the code for the Diet Problem over to Python. This way, valuable time and resources are saved. Debugging time is reduced. With all of these advantages, Python provides a better atmosphere, and an easier working environment. I'm working on the write_data module. There are two input files for the module: input.dat, and the food selection from the user. The input.dat file lists the nutrient's name, measuring unit, minimum and maximum requirements, and also the foods nutrient's information. The write_data module will generate an AMPL data file called diet.dat, based on the user's selection and input.dat file.

Stereoscopic Visualization Laboratories and Tools for College Curricula. *NICK TAYLOR (Jamestown Community College, Jamestown, NY 14701) MELVYN MORRIS (Brookhaven National Laboratory, Upton, NY 11973).* Quad-buffered stereoscopic visualization involves generating left and right eye images of an object and delivering each image to its designated eye. This is accomplished through denoting each image with light of opposite polarization. Special glasses are needed to allow light of specific polarization through so each eye receives its respective image. Stereo viewing produces depth (z-axis) in an object, which is not seen in a flat two-dimensional image, or even in a traditional three-dimensional image. As students of math and science often have difficulty visualizing fundamental concepts due to the limits of traditional 3D, stereoscopic rendering has firm academic uses. The goal of this project describes in detail potential uses of stereoscopy in a college curriculum. Some of the most beneficial topics to view in stereoscopy include atomic orbitals, chemical mechanisms, biochemistry, human anatomy, microchemistry, and engineering tools. PyMOL and VMD (Visual Molecular Dynamics) are both molecular viewers. These programs open up .pdb files (among others), which can easily be downloaded from the protein data bank. The primary molecule viewed is proteins, of which many are stored in the PDB. Atomic electron orbitals can be viewed using Orbital Viewer. Chemistry mechanisms, biology images, and many other things can be found by searching for VRML (Virtual Reality Modeling Language) files. A player can view any VRML file in stereoscopy and be able to rotate the object.

Modeling Dynamics in the Kah Framework. *CHARLES TREATMAN (Oberlin College, Oberlin, OH 44074) ED FRANK (Argonne National Laboratory, Argonne, IL 60439).* Kah is a framework for large-scale systems biology applications. However, Kah does not provide facilities for simulating reaction dynamics. An extensible object model is developed for representing reaction dynamics in the Kah framework, and a number of dynamics types are implemented. Converters are developed to connect the new object model to external generators for simulation of reaction systems. The dynamics model is used to reproduce results from a paper on modeling the MAP Kinase pathway in order to verify the validity of the object model. The ModelEditor, an existing Kah application, is modified to allow interaction with the new dynamics simulation capabilities of the Kah framework.

WSND: An Architecture for Wireless Sensor Networks. *ISAAC WASILESKI (University of Chicago, Chicago, IL 60637) PETE BECKMAN (Argonne National Laboratory, Argonne, IL 60439).* The rise in popularity of wireless sensor networks composed of small "motes" capable of gathering data, performing a small amount of processing, and communication over ad-hoc wireless networks, has led to the necessity for an integrated architecture, not only on the mote level, but on the level of data processing and user interaction. There already exist programs for controlling the motes, for visualizing data, and for debugging the network, however, what is needed is a modular architecture that allows built-in and custom components to co-operate in managing the network. The WSND system provides a low-overhead system to do just that, and incorporates a number of components to demonstrate the capabilities of the system. In its current incarnation, the system can gather data from a self-organizing ad-hoc network of motes, feed this data into event listeners or data handlers, detect and respond to events, collect data into a relational database, and visualize raw messages, graphical plots of sensor data, or routing graphs in near real-time. The key is that it is trivial to extend the system in any way - for instance, by writing new event detectors, which can be developed in high-level scripting languages. In this manner, the system can be adapted easily to any desired task.

Reconfigurable Computing with the SRC-6: System Architecture, Performance Data, and Efficient System Utilization. *DAVID WORSHAM (Georgia Institute of Technology, Atlanta, GA 30332) JEFFERY VETTER (Oak Ridge National Laboratory, Oak Ridge, TN 37831).* The SRC-6 is SRC computing's flagship hybrid computing system. Using a combination of DLDs (Dense Logic Devices), such as microprocessors, and DEL (Direct Execution Logic), such as FPGAs, this system can provide large performance gains over traditional computing systems for highly repetitive or computationally intensive problems. Performance data was collected on this system, including bandwidths for the various memory interconnects and timings for various aspects of executing code on the FPGAs, in an attempt to better understand how to utilize the system in an efficient manner. This data was acquired by performing work on the system, such as sending data across memory buses, and using a nanosecond accurate timer to measure how long this work took. This data confirmed SRC's numbers, which was expected. These results will be used as reference data in further papers concerning the SRC-6 system.

Analysis of the Model Facility Geometry of the Visual Interactive Site Analysis Code Using the Java Programming Language. *RODNEY WRIGHT (Norfolk State University, Norfolk, VA 23504) ROBERT SANDERS (Oak Ridge National Laboratory, Oak Ridge, TN 37831).* Visual Interactive Site Analysis Code (VISAC) is a JAVA system that allows the user to simulate and analyze the results of different accidents/incidents ranging from simple individual equipment sabotage to complex sorties that utilize a range of military weapons, simulated truck or car bombs, or satchel charges. VISAC is supplied with a library of facility models that are customizable in both geometry and logic to approximate a number of facilities of interest. Created or customized model facilities can have faults, such as overlaps and voids in the geometry, which may be too small to be visible or even hidden by the complexity of a model. These faults may cause the production of erroneous results in the blast calculation portion of VISAC. The goal is to find such errors and report them so that faults can be easily corrected. To locate the errors, a grid of rays is projected through the model parallel to each of the three coordinate axes. Each ray is then divided into path segments representing the different material regions through which it passes. Interferences and voids are revealed by comparison of the path segment starting and stopping points at the region boundaries. This allows for correction of possible geometry faults.

MetDataCNV, a Windows-Based Software Tool for Converting TD-6201 and Solar and Meteorological Surface Observational Network Meteorological Data for Use in the CALMET Meteorological Model. *NOAH ZEMKE (Big Bend Community College, Moses Lake, WA 98837) FREDERICK RUTZ (Pacific Northwest National Laboratory, Richland, WA 99352).* The CALMET meteorological model requires surface and upper air meteorological data as input for running a simulation. TD-6201 upper air meteorological data and Solar and Meteorological Surface Observational Network (SAMSON) surface meteorological data can be used by CALMET but not in their original formats. While the legacy FORTRAN executables READ62 and SMERGE can convert the SAMSON and TD-6201 files, they require that an input text file be hand edited before their execution. Time consuming alterations of input files that are not edited accurately could cause errors at run-time in the CALMET processor. A software application named MetDataCNV has been developed to solve these problems by having a user friendly interface automatically create the input files, then execute the READ62 and SMERGE executables at the click of a button. The MetDataCNV integrates a graphical user interface, process manager, and two FORTRAN processors. The graphical user interface allows the user to select meteorological station

data and begin the process manager. The process manager controls the flow of input files and execution of the FORTRAN processors. The FORTRAN Processors executed by the process manager use the input files created, to convert the meteorological station data files to a format readable by the CALMET processor. MetDataCNV effectively converts the TD-6201 and SAMSON formats with limited involvement from the user. This tool alleviates the need to make tedious changes to the input files by hand, and the separate execution of the two FORTRAN processors. MetDataCNV has the potential of being integrated with DUSTRAN. This paper will describe the design and development of the MetDataCNV tool.

Engineering

Metrics for the Comparative Analysis of Geospatial Datasets with Applications to High-Resolution Grid-Based Population Models. *KATHLEEN ABERCROMBIE (Auburn University, Auburn, AL 36849) AUROOP GANGULY (Oak Ridge National Laboratory, Oak Ridge, TN 37831).* Geospatial data sciences have emerged as critical requirements for high-priority application solutions in diverse areas like the mitigation of natural or man-made disasters and the assurance of energy, communication and transportation networks. This research develops metrics for comparative analysis of geospatial datasets, specifically for quantifying the relationships within variables, generating measures of difference among datasets, and measuring the value of data in the context of the end-use. This case study focuses on two high-resolution, grid-based population datasets: the LandScan database available from the Geographic Information and Science Technology (GIST) group at Oak Ridge National Laboratory (ORNL) and the Gridded Population of the World (GPW) database available from the Center for International Earth Science Information Network (CIESIN) group at Columbia University. Metrics for quantifying the spatial relationships within multiple geospatial variables include spatial auto- and cross-correlation as a function of lags. This research computes and displays these metrics as three-dimensional surfaces to visualize the relationship between the LandScan databases and one ancillary variable: nighttime lights from satellite imagery. Quantifying metrics for the difference among multiple datasets include spatially aggregated measures like normalized mean squared differences, fractional area coverage, and analysis of grid-based differences through histograms. The spatial cross-correlation metrics described earlier can also be used as spatially-aware measures of difference when the two datasets are supposed to convey identical information. The third set of metrics was designed to measure the usefulness of the databases in the context of end-use. The metrics are based on the number of times the population exceeds certain threshold values in both or one of the datasets, and include the accuracy, bias score, probability of detection, false alarm ratio, probability of false detection, threat scores, equitable threat scores and receiver operating curves. Case studies appear to suggest that GPW is suitable as a residential population model, while LandScan Global is more suitable as an ambient population model, confirming significant difference in the end-use for man-made or natural disasters, security threat scenarios and impact analysis. The metrics utilized in this research can be easily generalized to other geospatial datasets and application domains.

Determining the Optical Properties of Biological Tissue Samples Using an Integrating Sphere Method. *MARCUS ALLEGOOD (Gainesville College, Gainesville, GA 30503) JUSTIN BABA (Oak Ridge National Laboratory, Oak Ridge, TN 37831).* The wavelength dependent interaction of light with biological tissue is an important tool used to determine tissue optical properties. To accurately determine these optical properties for different types of tissue at specific wavelengths would be beneficial for a variety of different biomedical applications. In order to collect the needed data for the multitudes of different wavelengths in a timely and accurate manner, a fully automated computer program and process was developed. The hardware used included an integrating sphere, spectrometer, and a collimated light source. Scattered light intensity inside the sphere was recorded by the spectrometer as either transmitted or reflected light from the tissue sample. LabVIEW was used to write the programs to collect raw intensity data from the spectrometer, to convert the data into a format for C code execution, and to compute the optical properties based on the collected data. To make the process fully automated, the LabVIEW and C code programs were linked together into one single program to allow data to be passed between the two instantly. The automated program was tested using a neutral density filter and the execution of the program was successful. Future work will entail testing of actual known tissue phantoms to check for accuracy before proceeding to utilize the system to characterize actual tissues. Ultimately, the data collection process and algorithms developed through this effort will be applied to build models for light interaction with biological tissue samples.

Pneumatic Shifter for 5-Speed Manual Transmission. *SHAWN ALLRED (University of Wyoming, Laramie, WY 82070) MIKE DUOBA (Argonne National Laboratory, Argonne, IL 60439).* Over the course of this internship at the Advanced Power train Research Facility (APRF), I was challenged with many projects; the main one was to design a Pneumatic Shifter for a 5-Speed Manual Transmission. This task involved a lot of mechanical, electrical, fabrication, and programming work. The purpose of the pneumatic shifter is to be able to shift a standard 5-Speed manual transmission with the push of a button without the transmission actually being in the vehicle. This involved controlling two levers that have to be precisely moved into the right position at the right time with air cylinders and electronic solenoids to shift the devise called MATT. MATT is simply a large metal platform on a rolling chassis that has been equipped with a gasoline engine and a scalable inertia 100Kw AC induction motor. These two are in-line allowing the use of just the gasoline engine, just the electric motor, or both to power the rear tires. The MATT platform emulates a hybrid electric vehicle. The 5-Speed transmission sits at the rear, just before the rear drive shaft. Future work will focus on using the MATT for testing other engines and motors including a hydrogen engine. The goal of this study is to study the impact of various degrees of hybridization on fuel economy, emissions, performance, cost, etc.

The SPEAR 3 Vacuum System, An Analysis of the First Two Years of Operation (2004 and 2005). *REBECCA ARMENTA (University of California Los Angeles, Los Angeles, CA 90024) HAROLD A. MORALES (Stanford Linear Accelerator Center, Stanford, CA 94025).* SPEAR 3, a synchrotron radiation source at the Stanford Linear Accelerator Center, has been in operation for the past two years. SPEAR 3 was designed to achieve high beam lifetimes while operating at a higher current level than previously achieved with SPEAR 2. Maintaining high electron beam lifetimes within the ring allows users to perform their experiments with a consistent supply of high current synchrotron radiation. The purpose of this analysis is to evaluate the SPEAR 3 vacuum system's performance during the 2004 and 2005 runs while considering methods to optimize and improve vacuum system conditioning, especially within the pumping system, so that a recommended plan of action can be created for the FY 2006 run. Pressure data obtained from the gages attached to pumps, temperature data obtained from thermocouples located at various locations around the ring, and beam lifetime projections help to provide some indication of the health of the electron beam, but the true conditions within the beam chamber can only be extrapolated. Data collected from sensors (gauges, thermocouples, etc.) located around the ring can be viewed and extracted from a program created at the Stanford Synchrotron Radiation Laboratory (SSRL) called Historyplot. The data showed that the beam lifetimes in 2005 were much greater than they were in 2004, but it did not provide a clear indication as to why this occurred. One variable of major importance between the 2004 and 2005 runs is the Titanium Sublimation Pump (TSP) flash frequency (flashing is the process in which Titanium from filaments within the pump is sublimated onto the wall surfaces of the pump, where it removes gas molecules from the system by chemisorption). The data indicated that pressures in 2005 could have been lower, based on a comparison between 2004 pressures, if the TSPs were flashed more frequently than they were in 2005. However, the data from 2004 and 2005 does not provide enough information to accurately determine an optimal conditioning frequency, though it does provide enough information to formulate a recommended plan of action for the next run. It appears that flashing at a high rate during the beginning of a run and at a lower rate as the run progresses may be the most effective pumping approach to further improve the vacuum level of the ring. It is recommended that the SPEAR 3 vacuum system should be operated in this way next year.

Use of a Superheterodyne Radiometer for Passive Detection of Chemical Plumes. *UTHAM BALACHANDRAN (University of Illinois at Urbana-Champaign, Champaign, IL 61820) SASAN BAKHTIARI (Argonne National Laboratory, Argonne, IL 60439).* A radiometric sensor is a passive instrument which detects electromagnetic radiation given off by various agents. Since the radiometer is a passive instrument, it does not need to transmit a signal for detection. The instrument sensitivity and ability to detect sources from large distances compared to optical methods makes this technology ideal for various applications including remote sensing and profiling of the atmosphere as well as weather and humidity measurements. In this study, however, the focus is the radiometer's ability to detect hot chemical plumes at distances of several hundred meters and greater. The

Friis Transmission Equation leads us to expect that as the distance increases, the signal will drop at 1/R2 with R being the distance between the transmitter and receiver. Setting up the experimental system was a multi-step procedure, requiring calibration and alignment prior to detection of the plumes. The system output needed to be temperature calibrated so that it is best tuned on the desired source. A 150 GHz millimeter-wave beacon was used at various distances to align the radiometer's antenna. The detected signal from the plume was split into sixteen channels, allowing for a more precise observation at each part of the frequency band. To better characterize the system, several measurements were made in order to fit the data to a 1/R2 curve. In these experiments, the signal did not appear to drop as rapidly as the equation indicates. This was likely caused by variables such as antenna gain and directivity that were not taken into account in our simplified equation. Although there are aspects of this technology such as the design of high-frequency solid-state devices and signal processing techniques that can be further improved, such systems are expected to make major contributions in the area of remote chemical sensing.

Beam Impulse Dynamics: Transient Behavior in Microcantilevers. *SARIT BARHEN (Washington University in St. Louis, Saint Louis, MO 63130) THOMAS THUNDAT (Oak Ridge National Laboratory, Oak Ridge, TN 37831).* The microcantilever of an atomic force microscope is a dynamic system that exhibits useful resonance behavior. Although best known for its service in sensing applications, the microcantilever is gaining popularity in external applications as its unique probing capabilities continue to improve and secure recognition. Theoretically, this system can be modeled in a variety of forms, with one of the most common schemes treating the system as a single mass attached to a spring with a dashpot (the point-mass model). In this case only the temporal aspects of the system are considered and the cantilever's motion is modeled via a second order ordinary differential equation. Such models however, are somewhat unrealistic in that they have a single degree of freedom and ignore the physical extension of the cantilever. Thus, to more accurately portray the microcantilever system, the beam equation is considered. As a fourth-order partial differential equation, the beam equation involves both the temporal and spatial attributes of the system, with the ensuing eigenvalues and eigenfunctions representing the cantilever frequencies and their corresponding modes. Of particular interest is the effect of a short duration impulse applied to the microcantilever of an atomic force microscope. This impulse is observed to create a phenomenon of beats which occur within the system's oscillations. This is verified experimentally for a triangular cantilever, and modeled theoretically as both the analytical and numerical solutions to a fourth-order partial differential equation for the spatial and temporal attributes of the cantilever.

Fabrication of a GC Power Supply for the Thomas Jefferson National Accelerator Facility (JLab) Free Electron Laser (FEL) Electronics Systems. *NATHAN BELCHER (The College of William and Mary, Williamsburg, VA 23186) KEVIN JORDAN (Thomas Jefferson National Accelerator Facility, Newport News, VA 23606).* The magnets designated as GC corrector dipoles provide fine vertical steering correction at two positions in each of the 180-degree bends of Jefferson Lab's FEL electron beam line. Because of the tight quarters in the beam line, a Panofsky Quadrupole was combined with a dipole to create the GC magnet. The innovation of the design comes from using the existing coils that generate quadrupole field to also generate dipole field. But, the circuitry must be designed in such a way that the dipole magnets are biased independent of the voltage across the quadrupole coils. Because of the necessity for independent biasing, the circuit was designed as a push-pull bridge circuit with a floating ground side and a real ground side. Beginning with two circuit boards that contained excessive oscillations from an incorrect offset in the push-pull circuit, tests were run to analyze the extent of the oscillations. From these tests, various resistors and capacitors were added to filter the oscillations. The gains of several parts of the boards were changed to enhance stability, and outside shunts were added to dissipate heat from the main circuitry. After this stabilization, the boards were measured against the actual input voltage to analyze the offset voltage. This offset voltage was trimmed by the potentiometers on the boards to create boards that would produce the correct output current with respect to the input voltage. These working boards will be installed in the chassis and integrated into the electronics system. In the future, another chassis will be fabricated and integrated into the electronics system.

The Heat Loss Analysis and Commissioning of a Commercial Helium Dewar. *MARCUS BELLAMY (University of New Mexico, Albuquerque, NM 87131) JOHN WEISEND (Stanford Linear Accelerator Center, Stanford, CA 94025).* A low temperature cryostat suitable for many different experiments will be commissioned at the cryogenic test facility at SLAC. The scope of the project is to make commission a commercial Helium dewar. The building of the top flange will be followed from its design phase through to its finished assembly. In addition, diagnostic tools such as thermometry, level detector, pressure gauge, transfer lines for He and N_2, vent lines with relief valves for He and N_2 will be incorporated. Instrumentation to read and plot this data will also be included. Once the cryostat is assembled, we will cool down the cryostat to measure its performance. A typical consumption rate of Helium will be measured and from this, the overall heat leak to the dewar will be calculated. A processing instrumentation diagram (PID) of the dewar system was created with SolidEdge and was later approved and published as an official SLAC document. The plots comparing the liquid level changes of the 36 inch probe with the time and the heat loss as a function of time proved to be a valid indication that the data was interpreted and recorded correctly and that the dewar was put together successfully.

Calculation of Release Rates of Gaseous Species from Surfaces at Ultra-High Vacuum. *STEVEN BENARIO (University of Illinois at Urbana-Champaign, Urbana, IL 61801) J.P. ALLAIN (Argonne National Laboratory, Argonne, IL 60439).* When performing surface interaction experiments at Ultra-High Vacuum, it is often important to have a detailed understanding of exactly what gaseous species are being generated and consumed by the chemical reaction taking place at the sample surface. There are not currently any tools available to distinguish between gaseous species of the same atomic mass. Using a linear analysis of partial pressure measurements by atomic mass along with known breakdown percentages of gaseous species by atomic mass, the process of determining partial pressure by species should be refined and automated. The present paper finds that by making use of the Moore-Penrose Matrix Inverse in a readily available programming environment, it is possible to calculate the partial pressures of gaseous species in a UHV environment using data from a residual gas analyzer. This allows for the direct and simple computation of generation and consumption rates of specific species in situ in a UHV research environment.

Modeling Bi-directional Thermosyphon Solar Water Heaters. *KYLE BENNE (University of Missouri-Rolla, Rolla, MO 63304) JAY BURCH (National Renewable Energy Laboratory, Golden, CO 89401).* Solar water heating has the potential to significantly reduce the demand on fossil fuel energy sources. A typical solar water heating system includes a solar collector, a tank, and a pump to circulate flow through the system. A thermosyphon design eliminates the pump by utilizing the buoyancy of the hot fluid to naturally drive the flow. By eliminating the pump, a passive design has the potential to further reduce the demand on fossil energy, increase system reliability, and reduce the cost of a solar water heating system. The challenge is accurately modeling the flow rate generated by the siphon, particularly during the nighttime when reverse siphoning is possible. Reverse flow has traditionally been avoided though it can be utilized by consuming a portion of the tank's stored energy to prevent freezing. A program has previously been written for the TRNSYS software to model the flow rate in a thermosyphon, however it failed to simulate low and reverse flow cases. The present work corrects this limitation with several improvements. Most notably, the fluid head contributed by each internal node of the system's components was calculated in place of computing the fluid head based on the average temperature of each component. Secondly, the Crondt-Freidricks-Louie (CFL) condition was implemented, which states that the distance traveled by the fluid during a time step must not exceed the length of the element. As expected, the results provided by the model indicate a strong correlation between the height of the tank above the collector and the magnitude of the reverse siphoning. It has been observed that while reverse siphoning has the ability to prevent nighttime freezing, significant energy is lost from the storage tank. Using the tool developed in this work, it is possible to quantify energy lost in reverse thermosyphoning and determine the usefulness of reverse siphoning for freeze protection.

Assessing the Accuracy of Simulated Energy Use Predictions for Whole Buildings: Comparison between Measured and Modeled Building Energy Consumption. *ALENA BENNETT (University of Puget Sound, Tacoma, WA 98027) KIMBERLY M. FOWLER (Pacific Northwest National Laboratory, Richland, WA 99352).* In order to demonstrate that building designs are highly energy efficient, simulation tools that accurately predict whole building energy consumption are necessary. The purpose of this paper is to compare simulated (or modeled) total site energy consumption predictions for buildings to their actual measured energy consumption in order to assess the accuracy

of simulation tools. Modeled and measured energy consumption data were extracted from four National Renewable Energy Laboratory (NREL) technical reports. Five design model energy use predictions were compared to actual building energy use data collected from meters over the period of a year at BigHorn Home Improvement, Cambria Office, Lewis Center year 1, Lewis Center year 2, and Merrill Center. The difference between the modeled energy consumption and actual energy consumption was -12%, -39%, 23%, -7%, -41% respectively (a negative percent denotes under predicted energy consumption). A 25% difference resulted between the Lewis Center year 1 model simulated with TMY2 (typical meteorological year v.2) weather data and the same model simulated with actual weather data for March 2001- February 2002. The results demonstrate that, for this data set, energy consumption of buildings is highly dependent on weather and generally design models over estimate the energy performance of buildings.

Modeling of Electronic Components with Reliability Prediction Methods. *SAMIR BHARGAVA (California State University Long Beach, Long Beach, CA 90840) TSONG-LUN CHU (Brookhaven National Laboratory, Upton, NY 11973).* Electronic components are present in any proposed digital system, and can be effectively modeled in conjunction with reliability prediction prior to realization of a system in hardware. One will examine will examine the methods of determining reliability of electronics using two different statistical methods. Specifically, Military Handbook (MIL-HDBK-217F) and Prism can effectively model electronic components failure rates. Military Handbook relies on past experience with similar components and stress conditions to predict future performance. Military Handbook examines the effect of die complexity, case temperature, thermal resistance, operating supply voltage, active thermal design maximum current, maximum power dissipation, junction temperature, package design, environment, quality level, and improvement of design, on the failure rate of a component. Prism applies the effect of system level parameters, such as, environment, operating temperature and year of manufacture, as well as, component level parameters for computing junction temperature using four different methods of calculation. Due to more detailed input specifications at the electronic component level, Military Handbook generates more plausible results in capturing the differences among different electronic components within the same category. Prism grouped electronic components within the same category to have identical risk assessment, and applies junction temperature calculation methods at the component level. Prism can quickly model the effect of varying system level parameters to gauge the effect of the system on failure rates. Military Handbook generally results in a more conservative estimation of component failure rate and may not fully capture improvements in electronics reliability. Prism may oversimplify results for component failure rate by lumping too many electronic components in the same category, for example, all microprocessors and memory.

Validation of an Indoor Calibration System for Pyranometers. *AMY BOWEN (Baylor University, WACO, TX 76798) STEVE WILCOX (National Renewable Energy Laboratory, Golden, CO 89401).* Calibrated radiometers are essential to any climate change research or renewable energy applications that require accurate solar energy measurements. Instrument calibration produces a regulated instrument, by adjustment or assignment of a calibration factor, through comparison with a standardized reference. Because radiometers are used outdoors, their calibration is typically performed outdoors. However, outdoor calibration is often restricted by varying or poor weather conditions. Kipp and Zonen's indoor calibration system will provide flexibility in calibrations if it is compatible with different manufacturer's radiometers. Using a data set of 17 pyranometers, comparison of the outdoor responsivities with responsivities using the indoor calibration system provides insight into the functionality of the system. The pyranometers' responsivities from the two methods were typically within 1% of each other. However, two instruments deviated from their outdoor responsivities by about 6%, indicating that an instrument may occasionally respond differently to the indoor and outdoor light spectrums. Excluding the results from the outlier instruments, the mean bias error between indoor and outdoor responsivities was 0.06%. An infrared-correction method was also examined, and differences were slightly higher, averaging 0.33%. The indoor calibration system results have a 4.41% uncertainty and are recommended for use in applications where this is acceptable. Further investigation and experimentation concerning the unusual outlier case will be necessary to identify other instruments that may behave similarly.

Super-Conducting Undulator Development. *JEAN CHRISTIAN BRUTUS (State University of New York – Stony Brook, Stony Brook, NY 11790) JOHN SKARITKA (Brookhaven National Laboratory, Upton, NY 11973).* Mechanical engineers and scientists from Brookhaven National Laboratory have been collaborating to design high-quality radiation insertion devices such as wigglers and undulators to achieve the required parameters necessary to perform state of the art research at the National Synchrotron Light Source (NSLS). However, as the goals of science advance, engineers have to create new devices to meet the scientific demands. The elliptical super-conducting undulator is one such new art device. To produce this undulator, various design prototypes for winding, cooling and manufacturing methods must be developed. For the design, we used Autodesk Inventor Computer Aided Design (CAD) software. This CAD software helps create and document the design from which the prototype will be manufactured. Computer Aided Manufacturing (CAM) software was used with a Computer Numerical Control (CNC) machine to automatically manufacture components of the undulator. GibbsCAM software is used to convert CAD files into codes that the CNC machine can read to fabricate a part. After learning the program, we have come to the point where an initial design has been prototyped out of wax. This method prevents damage to tools should there be errors in the codes. Improvements in the shape and different winding and cooling techniques are still being considered. When the undulator is completed, its performance will be evaluated in the X-ray ring of the NSLS. This work constitutes the initial phases of development for a new technology that will be incorporated in the construction of the NSLS II at the Brookhaven National Laboratory.

External Switch Fabric Deployment at Brookhaven National Laboratory. *JEAN ROBERT JR. BRUTUS (State University of New York – Stony Brook, Stony Brook, NY 11790) W. SCOTT BRADLEY (Brookhaven National Laboratory, Upton, NY 11973).* The advent of 802.11 wireless networking has brought about the proliferation of user-installed wireless access points (WAPs) on the internal campus network of Brookhaven National Laboratory (BNL). Seen as a potential security risk, these WAPs are being migrated to an external switch fabric. These new external networks for wireless devices join numerous existing external networks that serve various purposes. These networks are logically out in front of the campus network firewall, but traverse the same physical links and devices as the internal campus networks. In a qualitative investigation, considerations were made based on: user needs; security posture requirements and fiscal resources. A physically separate and logically distinct switch fabric was designed to isolate inherently less secure external network traffic from the internal campus network. This external infrastructure of switches and trunks is interconnected with fiber optic cables due to the distances between buildings. The project consisted of the analysis, the design and migration processes. This involved configuring switches so they can efficiently communicate on the same network being the new external switch fabric. Once major components of the external wireless switch fabric were installed, partial migration of the old network system to the newly installed switches was executed and tested. With this upgraded system, the advantages were numerous: easy access to the new external wireless network using existing WAPs; wireless network and support equipment designed to sustain an expanding wireless network user community; external network allowing users access to a network disparate from the main BNL campus; newly deployed network allowing visitors easy internet access when on campus; eradication of potential security risk for the internal network and improved reliability. This project is a small part of major upgrades that are being done on the Brookhaven National Laboratory (BNL) campus network in order to enhance its network performance and security. Future work will continue until the external switch fabric is totally implemented throughout the campus and fully operational by the end of December 2005.

Modeling the Optical Performance of Parabolic Trough Solar Concentrators. *ANITA BUDHRAJA (Northwestern University, Little Rock, AR 72212) TIM WENDELIN (National Renewable Energy Laboratory, Golden, CO 89401).* Parabolic trough solar concentration is currently the lowest cost solar power technology available on a large scale. Encouraged by the Western Governors' Southwest 1000 MW Concentrating Solar Power Initiative as well as by state and federal incentives for solar energy, the National Renewable Energy Lab (NREL) Concentrating Solar Power research team is currently working to improve parabolic trough technology and increase its cost effectiveness in the U.S. and abroad. Specifically, the team devotes much of its parabolic trough development efforts to evaluating and improving concentrator optics. This paper examines how the optical performance of parabolic trough concentrators is affected by concentrator geometry,

manufacturing imperfections and misalignment problems that occur in the field. More specifically, the optical effects of tracking offset, tracking twist, receiver misalignment, aperture width, receiver size, parabolic slope error and some combinations of these factors are investigated. Using the Solargenix trough design as a basis, optical analysis involves determining the exact shape of the trough using the VSHOT test procedure, building detailed but adaptable optical models of the parabolic trough system in Microsoft Excel, evaluating the optical performance of these models with SolTrace raytrace software, and analyzing SolTrace output data using Microsoft Visual Basic. This study has found that the geometry and alignment precision of parabolic trough concentrators can strongly affect their optical performance. For the Solargenix design in particular, tracking offset, tracking twist and receiver misalignment in the transversal direction are the most significant issues. Further, increasing the receiver size accelerates heat loss without significantly boosting optical performance, increasing the aperture width allows the trough to intercept more solar energy without significantly reducing optical performance, and reducing the parabolic slope error is worthwhile, especially if the receiver is made smaller. With the tools built in this project and the information presented in this paper, parabolic trough solar concentrating technology is better armed to shape a sustainable world.

Simulation Model of a Proton Exchange Membrane Electrolyzer Using PSCAD Simulation Software. *BRIAN BUTTERFIELD (California Polytechnic State University, San Luis Obispo, CA 93407) BENJAMIN KROPOSKI (National Renewable Energy Laboratory, Golden, CO 89401).* Currently, staff at the National Renewable Energy Laboratory (NREL) Distributed Energy Test Facility are conducting research on integrating renewable power systems with electrolyzers to produce hydrogen from clean energy sources. One electrolyzer that is being tested uses a proton exchange membrane (PEM) stack that spits water with direct-current (DC) electricity into hydrogen and oxygen. To interconnect a renewable energy system such as a wind turbine, to the electrolyzer, a power electronic converter must be used to convert variable frequency voltage and current to constant voltage direct current electricity. To help in the understanding of how the power system for the electrolyzer works, a model of the electrolyzer based on empirical data is being developed in PSCAD (an electrical simulation tool). Based on this measured data, a model has been developed using curve-fitting and interpolation techniques. These techniques are translated into the PSCAD simulation software via control and circuit components. The PEM Stack model is voltage and temperature dependent, as is the actual component, and can reproduce data similar to that of the PEM Stack's actual measured data. This paper will describe the implementation of the techniques and processes used to model the PEM Stack, as well as verify the model's ability to reproduce data similar to actual measured data.

Limitation of YBCO on Heat Transfer and Stability in High Temperature Superconducting Magnets. *JENNIFER CARNEY (University of Tennessee, Knoxville, TN 37916) ROBERT DUCKWORTH (Oak Ridge National Laboratory, Oak Ridge, TN 37831).* The thermal conductivity of composite YBa_2Cu3O_x (YBCO) tapes was measured to better understand heat transfer in the multilayer structures that are often found in high temperature superconducting (HTS) magnets. Knowledge of the conduction heat transfer through the wire's components – buffer layers, substrate, YBCO and stabilizer – can allow for the efficient selection insulating materials that can provide dielectric strength and improve heat transfer for a second generation (2-G) YBCO tapes. A test setup was designed to measure the effective thermal conductivity of composite YBCO tapes. Various sample stacks that were composed of different materials such as copper, kapton, YBCO and Apiezon© N grease for example were placed between two platinum thermometers and below a heater bobbin. Through variation of the number and type of materials, the background heat loads were quantified so that the properties of the YBCO and candidate insulation materials were accurately measured. After each sample stack was cooled down in an ice bath (273 K), a heater load was applied and the temperature difference across the sample was measured. From the temperature difference, the total thermal resistance was then used to calculate the effective thermal conductivity of the samples. Additional measurements were done at liquid nitrogen temperatures (77 K) although measurements at 273 K allowed for a broad cross section of data to analyzed quickly without sacrificing a meaningful comparison. The measurement of the thermal conductivity was impacted by the contact pressure and the materials that were used to secure the thermometers to the sample stack. A comparison of the role of these factors on the thermal conductivity measurement will be presented. It was found that the composite YBCO tape results were consistent with known thermal properties of substrate, buffer layers, YBCO and stabilizer at 273 K. The overall thermal resistance did improve when kapton was replaced with Apiezon© N grease. These results were applied to a series of preliminary experiments where the stability of composite YBCO tapes was characterized and the removal of heat along the length and across the thickness of the composite YBCO tape was studied. The heat transfer across the thickness of the tape can be improved slightly, but additional measurements are needed. This will assure whether candidate insulation materials for HTS coils can provide tangible improvement in the coil stability.

A Rhodium Bound Polymer Matrix as a Biosensor and an Electrochemical Enzymatic Reactor. *MELISA CARPIO (University of California Berkeley, Berkeley, CA 94720) JOHN B. KERR (Lawrence Berkeley National Laboratory, Berkeley, CA 94720).* Creating a polymer matrix is important because it can be used to coat an electrode for use as a sensor in biosensing devices or in synthetic enzymatic reactors. Such devices can detect, record, and transmit information regarding the presence of, or physiological changes in, different chemical or biological materials in the medicine and the environment. They can also be used to drive bioprocesses at rates that are useful for production of chemicals and fuels. The goal of this research is to synthesize a polymer matrix and to test the capability of such a matrix in an enzymatic reduction reaction. The reaction of interest is the reduction of a ketone (benzylactone) to an alcohol (4-phenyl-2-butanol). This reaction is run using a rhodium catalyst complexed with one of two ligands (bispyridine or bisimidazole), NAD^+, and alcohol dehydrogenase as an enzyme. The rhodium is reduced from Rh(III) to Rh(I), which reacts with water producing a hydride that specifically reduces NAD^+ to 1,4-NADH, which then reacts through the enzyme with the ketone to make alcohol and regenerate NAD^+. Electrochemical experiments have shown that at room temperature and pH 7, the ketone was successfully reduced to alcohol for both the bispyridine and bisimidazole ligands. Future work includes attaching the synthesized ligands, the NAD^+, and the enzyme to an allyloxy-ethoxy comb polymer to create a matrix that will bind the rhodium catalyst. Finally, the entire polymer matrix can be used to coat a carbon electrode that carries the electrons between the electrode and the enzyme. Such a system has a variety of applications including the medical field as a glucose or urea sensor, in the environmental field as a detector of harmful chemicals and as a bioreactor system for conversion of photons to chemicals and fuels.

Review and Application of Thermodynamic Data Related to Pyroprocessing. *ALESSANDRA CARREON (Rice University, Houston, TX 77005) MICHAEL SIMPSON (Idaho National Laboratory, Idaho Falls, ID 83415).* Electrorefining is a pyroprocessing technique that allows for the co-recovery of actinides via electrotransport. This is a useful concept in that it permits the separation of uranium, plutonium, and minor actinides from other fission products in spent nuclear fuel. Various thermodynamic factors affect the yield of such separations, though specific conditions must first be met to expect a viable outcome. These conditions depend upon the type of species desired to obtain as deposits—usually uranium and plutonium. In order to perform the required calculations necessary to predict and model actinide deposition, thermodynamic data must be consistent and standardized for universal application. A set of data has thus been compiled and is herein compared to employ for further use in electrorefining problems. Correlations for thermodynamic data based on species-dependent properties are also of interest to further field progress.

Conceptual Design of Isotope Separator On-Line Target for Rare Isotope Accelerator. *ADAM CARROLL (University of Arizona, Tucson, AZ 85719) CRAIG BRADLEY (Oak Ridge National Laboratory, Oak Ridge, TN 37831).* Isotope Separator On-Line (ISOL) is one of the two types of targets that are being conceptually designed for the Rare Isotope Accelerator (RIA); a 400 kW accelerator for ions from hydrogen to uranium, with the goal of providing a better understanding of exotic nuclei. The ISOL target is composed of a main target, the tungsten core and a secondary target of 133 uranium carbide disks that surrounds the tungsten. Three essential design objectives of the ISOL target were evaluated, (1) cooling the target during beam operation, (2) analyzing the beam window, and (3) ease of replacement with remote handling equipment. The secondary target is thermally cooled by water flowing through two sets of pipes that spiral around the uranium carbide disks. The tungsten is directly cooled by water flowing through small spiraling channels in the tungsten. This is achieved by encasing the tungsten inside a pipe to force the water through the channels at 300 psi. The ion beam goes through the pipe to contact the tungsten making the pipe the target beam window. To ensure that the pipe can manage both the internal pressure of the water and the thermal gradient created by the beam passing through it, Mechanica, a finite element analysis

program, was implemented to calculate the theoretical stresses the pipe will experience. By analyzing a range of wall thickness from 0.5 to 1.5 millimeters with two materials, stainless steel and aluminum, it was discovered that aluminum at 1.5 mm allows the greatest factor of safety. The ISOL target needs to be replaced frequently because of the high level of energy the tungsten receives, making the target radioactive to the point it must be handled completely remotely. To make the process simple the target only has four Hiltap water connections. The electrical power connects automatically when the target is placed in the base of the target module. Handles, hook plates, and alignment pins are also added to guide the target in and out of the target module to make replacement less difficult. The ISOL target is a continually changing design as new ideas are modeled and analyzed. With every small change or addition the ISOL conceptual target becomes a little closer to becoming a reality.

Attachments for Remote Tools and Equipment for Remote Operations. *ADAM CARROLL (University of Arizona, Tucson, AZ 85719) CRAIG BRADLEY (Oak Ridge National Laboratory, Oak Ridge, TN 37831).* The Spallation Neutron Source (SNS) will be a facility with the capability of creating large quantities of neutrons for material science research. The neutrons are generated by high energy protons hitting a mercury target, releasing neutrons and high radiation. The Target Cell, a heavily shielded room for maintenance of the mercury target, contains four pairs of through-the-wall manipulators and one pair of servomanipulator arms attached to a bridge crane to perform maintenance in the Target Cell. The manipulators function best with tools modified for their grippers. Some recent Target Cell projects have been directly related to the development of attachments to everyday tools to be operated by manipulators. For example, there are three pneumatic torque wrenches used remotely in the Target Cell to torque nuts and bolts. In order for the larger torque wrench to be properly positioned for the mercury target bolts, the torque wrench must be capable of being held by a hoist hook in both horizontal and vertical directions. To solve this problem a stainless steel handling bail was attached to both ends of the wrench. Special bends are added to hold the hook in place over the center of gravity in both directions. The hoist hook, with help from the manipulator's arm, will move between both positions. The two smaller pneumatic torque wrenches require a remotely attachable reaction bar to counter the torquing force applied to a nut or bolt. The small wrenches need several reaction bars of various lengths and shapes for torquing different bolts throughout the Target Cell. Another example of a Target Cell project involves the mercury piping supports. The mercury pipe is held in support cradles. Some cradles are adjustable in both horizontal and vertical directions while most only in the vertical direction. All support cradles help align the pipes when being remotely replaced. The adjustments to the cradles are made by turning hex nuts on threaded rods connected to a plate that holds the pipe. Once the adjustments are completed and the pipe connected the nuts must be locked since the vibration of the mercury flowing through the pipe can slowly loosen the nuts and lower the pipe. A removable attachment was designed to be placed over the nuts. The attachment reacts against the side of the cradle keeping the pipe in the correct position. The SNS Hot Cell requires both modified tools and other adaptations for remote operations in its unique environment.

Medium Energy Sn^+ Implantation in Ru Single Layer Mirrors. *CHRISTOPHER CHROBAK (University of Wisconsin, Madison, WI 53706) JEAN-PAUL ALLAIN (Argonne National Laboratory, Argonne, IL 60439).* The process of energetically vaporizing, compressing, and ionizing materials produces various species of debris that is problematic for the lifetime of plasma-facing EUV (Extreme UltraViolet) collector optics. The IMPACT (Interaction of Materials with charged Particles And Components Testing) facility has been testing various collector optic samples under simulated charged particle irradiations to assess the effect of different debris species on the performance and thus the operational lifetimes of these optics. Tests include using ion beams to expose samples to controlled fluxes of mono-energetic Sn^+ ions, an evaporator to direct thermal Sn flux onto samples, and annealing samples at high temperature (80–100°C). The effects of these exposures are monitored in situ using AES (Auger Electron Spectroscopy), LEISS (Low-Energy Ion Scattering Spectroscopy), and collection of sputtered atoms for mass measurement with a QCM-DCU (Quartz Crystal Microbalance – Dual Crystal Unit) system. In addition, the effects of exposures are measured ex-situ with AFM (Atomic Force Microscopy), XRR (X-Ray Reflectivity), and in-band EUV reflectivity. Results show convincingly through complementary metrology techniques that energetically implanted Sn atoms in Ru single layer mirrors diffuses readily, minimizing its impact on the mirror's EUV reflectivity.

A Performance Comparison of Air-cooled and Evaporative Refrigeration Condensers in a Typical U.S. Supermarket. *ERIC CLIFFT (Rose-Hulman Institute of Technology, Terre Haute, IN 47803) MICHAEL DERU (National Renewable Energy Laboratory, Golden, CO 89401).* Supermarket refrigeration systems in the United States use enormous amounts of energy. However, energy efficient devices such as the evaporative condenser exist today that could cost effectively improve their future performance. Using eQUEST Refrigeration version 3.55, a supermarket near Denver, Colorado is modeled to experiment with the energy and cost savings incurred by replacing refrigeration system air-cooled condensers with their evaporative counterpart. As anticipated, the simulations convey both environmental and economic benefit associated with the use of evaporative condensers in a dry climate. In fact, the model predicts annual electricity savings of 208,800 kWh and reductions in utility costs by $12,322 each year. Clearly, evaporative condensers offer a practical way to mitigate U.S. energy use and foreign dependence, making them deserving of a spot in the supermarket refrigeration systems of the future.

Development of an Enhanced Base Component for the Brookhaven Atmospheric Tracer Sampler. *JOHN CORNWELL (Duke University, Durham, NC 27708) RAY EDWARDS (Brookhaven National Laboratory, Upton, NY 11973).* The Brookhaven Atmospheric Tracer Sampler (BATS) is an integral part of the Perfluorocarbon Tracer Technology (PFT) developed at Brookhaven National Laboratory. The BATS is used to actively sample released PFT by pumping air through adsorbent filled tubes. It is comprised of two components: the IID which contains the adsorbent tubes, and the base, which contains the pump and electronic control systems. Although the BATS lids are still state of the art, the electronic logic within the bases has become outdated over the past 20 years. The bases lack programmability and are prone to failure in the field. The main goal of this internship was to design a cost-effective replacement base with complete flexibility in terms of sampling periods as well as programmability through a wireless interface. The Netburner 5272 processor board was selected for its speed, data capacity, and also its easy-to-use TCP/IP interface with an available 802.11b wireless expansion card. This device was programmed to serve a dynamic web page and allow sample periods, the real time clock, and other settings to be programmed simply by navigating the website and filling out forms. The pumping system was also replaced with a miniature diaphragm pump paired with a flow meter to allow the Netburner to implement a feedback controller. This allows for precise volumes to be sampled. A working prototype was constructed with a new pump, flow meter, and processor. Almost every design constraint was met and the prototype includes functioning wireless programming, backup data storage, and a pumping system controlled through a negative feedback loop. Although the prototype demonstrates proof-of-concept of the improved base unit, more work still needs to be done. A custom circuit board needs to be designed to hold all of the electronics and everything needs to be mounted in an enclosure. After these improvements the device will be ready to be tested during an actual PFT release.

The Construction of a Drain Trench to Prevent Floating in Building 911. *JUAN CRUZ (Bronx Community College, Bronx, NY 10452) ALAN RAPHAEL (Brookhaven National Laboratory, Upton, NY 11973).* During a big storm, the sewer system around Building 911 gets so overwhelmed by all the water that the entire facility floods. The terrain around Building 911 is shallow, such that the facility is lower than the surrounding landscape. As a result, in an event of a storm, water from the buildings on high elevations, such as the Graphite Research Reactor and nearby facilities drain down to the area around Building 911. To address this problem, first, we need to survey the land. Surveying was done using a laser level and a measuring rod. There are 'Rim' elevations stored in our archives. We use these as a reference; we then used the measuring rod to find elevations on the surrounding area. We surveyed an area of 7,440 squared feet. Then, we found the elevations of the parking lot in front of Building 923. This gave us an idea of how deep our pond could be and if we could have a slope for the water to run to the pond. We found the pond could be 5 to 6 feet deep and that there is a slope in the parking lot. Using a pay loader, we are going to dig a 19,200 cubic feet hole next to Building 923. We used the excavated soil to fill a hole next to Building 811. We will use this hole to store all the gallons of water that run from the parking lot to Building 911 and 912. The water will go into the pond via trench drain. We designed all the drawings for this project using AutoCAD. The drawings show pretty much how everything will look and work. These drawings will then be given to the contractor and the Environment Protection to be reviewed. Once the hole is dug we would have a place to store the storm run-off in an area of 48,611 square feet. With the help of the

"basin" we are hoping to lessen the effect of storm water running into Building 911 and 912.

Calibrating the U.S. Transportation Sector for the Consolidated Impacts Modeling System (CIMS). *BRANDON CURRIE (University of California Santa Cruz, Santa Cruz, CA 95064) JOE ROOP (Pacific Northwest National Laboratory, Richland, WA 99352).* This paper documents an attempt at calibrating the U.S. transportation sector for the Consolidated Impacts Modeling System (CIMS). When the U.S. transportation sector is calibrated properly, CIMS can forecast how changes in transportation demand affect fuel use and gas emission levels. If CIMS can be calibrated for not only the transportation sector, but also the other 14 economic sectors it covers, it can be a powerful resource for making energy policy decisions. We used a two-step process to do the calibration. We first entered historical standard data and then quantitatively adjusted the model. Our approach to adjusting the model is also a two-step process. First we sought to calculate the share that different transportation demand sub-categories have of the overall demand for transportation. Second, we tried to calculate the share that individual transportation modes had of their respective groups. After adjustment, CIMS should produce fuel use and gas emissions levels equal to the entered historical standard data. We were not able to completely calibrate the U.S. transportation sector for CIMS. Calibration for fuel values ranged from 0.3% to -4915.94%. We believe holes in the data and the use of multiple years for standard historical data may have been the primary reasons for the wide-ranging results that emerged from our calibration attempt. Based on our results, we suggest that future efforts to calibrate the transportation sector include the development of an accurate system of estimation for transportation demand shares and transportation mode competitive shares.

Self-Calibrating Sensor for On-Line Density Measurement. *RYAN DEAN (Massachusetts Institute of Technology, Cambridge, MA 02139) MARGARET GREENWOOD (Pacific Northwest National Laboratory, Richland, WA 99352).* Researchers at Pacific Northwest National Laboratory have developed and on-line computer controlled sensor to calculate the density of fluids based on ultrasonic reflections. A stainless steel hexagonal pipe length fitted with 5MHz transducers bonded on opposing sides of the pipe was able to obtain eleven echoes within the pipeline wall due to multiple reflections of the longitudinal wave. The process of creating a water calibration file, by taking the fast Fourier transform (FFT) of each echo in water, and plotting the natural logarithm of the amplitude of the liquid divided by water allows for exact density calculations. After acquiring the specific reflection coefficient at the solid-liquid interface (SLI) of each sugar water (SW) solution a computer program calculates the density using a sequence of equations. This natural logrithim plotting step is the key to making the sensor self calibrating, unaffected by small changes in pulsar voltage. Results in testing 16 SW solutions with varying weight percentages ranging from 10% to 60% concentration showed densities acquired using the sensor were very similar to those taken by hand utilizing a laboratory pycnometer. Our findings make possible application in quality control pipelines as non intrusive measurement devices or as a safety monitoring units likely. Since this sensor does not directly interact with the fluid it is ideal for situations where a fluid can not be exposed to specific materials present in similar instruments.

Fabrication of Spiral Bio-Reactor Light Sheets. *JEANNE DUCE (Florida State University, Tallahassee, FL 32302) DUNCAN EARL (Oak Ridge National Laboratory, Oak Ridge, TN 37831).* Hydrogen is typically created from electrolysis or thermo-chemical production. Electrolysis requires large amounts of energy while producing hydrogen at a low efficiency rate. An alternative to these processes is to use algae as a biological means of creating hydrogen from sunlight. Exploiting the photosynthesis and respiratory characteristics of algae, a photobioreactor is envisioned that could produce significant volumes of Hydrogen without the use of electricity. Oak Ridge National Laboratory (ORNL) and the National Renewable Energy Laboratory (NREL) are collaborating to develop a prototype spiral geometry photobioreactor that efficiently captures sunlight to fuel the bioproduction of Hydrogen. A significant component of this prototype is the Spiral Bio-Reactor Light Sheet used to distribute sunlight within the bioreactor. The design of the Spiral Bio-Reactor Light sheet consists of plexi-glass sheets that have been rolled into a spiral shape. Micro-etches on the back of the sheet disperse the sunlight in a uniform and controlled manner. The spiral shape of the light sheet allows the sunlight to be dispersed over a large surface area, allowing for maximum algae illumination and production of Hydrogen. In this way the Spiral-Bio Reactor Light Sheet can create hydrogen in an efficient manner without the use of electricity. Chlamydomonas reinhardtii is one type of algae that is capable of converting sunlight into hydrogen photosynthetically, and would be an excellent choice in the Spiral-Bio Reactor Light Sheet. Depriving sulfur to the growth medium of Chlamydomonas reinhardtii causes oxygen production during photosynthesis to decrease. The culture's consumption of oxygen creates an anaerobic condition which instantaneously induces the production of hydrogen. Hybrid Solar Lighting (HSL) is a light source that utilizes direct sunlight taken from a roof top collector and concentrates the sunlight into optical fibers that are supplied to light fixtures. These optical fibers are feed into the spiral shaped plexi-glass. The Spiral Bio-Reactor is in-cased to allow the Hydrogen to be extracted and stored. Work is still in progress and final results expected by September.

Development of a Calibrated Hydrogen Engine Model for the Evaluation of Multi-Cylinder Hydrogen Internal Combustion Engines (H_2ICE). *CIPRIANO DURAN (New Mexico State University, Las Cruces, NM 88001) MATTHEW THORNTON (National Renewable Energy Laboratory, Golden, CO 89401).* This research includes working with hydrogen internal combustion engines and the development of a calibrated engine model for use in stand-alone applications and in conjunction with vehicle systems-level analyses of H_2ICEs. The goal is to implement preexisting test data from a hydrogen-fueled single-cylinder test apparatus (SCTA) in various multi-cylinder hybrid vehicle configurations. They include H_2ICE/battery and H_2ICE/fuel cell configurations, utilizing vehicle systems analysis (VSA) software to evaluate the performance and efficiency of hybrid vehicle powertrains versus conventional vehicle powertrains (e.g., gasoline ICE). Particular attention is given to calibrating the modeled combustion to a near-exact match of the empirical data to ensure that the model will be functional for sensitivity analyses and other engineering applications. This offers engineers the opportunity to create and evaluate various engineering options in a timely, efficient, and cost-effective manner. Anstalt für Verbrennungskraftmaschinen's (AVL) (or Institute for Internal Combustion Engines) one-dimensional engine cycle simulation code BOOST version 4.0.4 is the engine-modeling tool employed. This research demonstrates the feasibility associated with modeling empirical data for rapid result finding and R&D cost reductions while concurrently demonstrating the viability of H_2ICE/battery and H_2ICE/fuel cell configurations.

Water-Gas Shift Catalyst Development. *GINA FAZIO (University of Illinois at Urbana-Champaign, Urbana-Champaign, IL 61820) THEODORE KRAUSE (Argonne National Laboratory, Argonne, IL 60439).* The reforming of infrastructure fuels such as natural gas, liquefied petroleum gas, gasoline, or diesel is one option for producing a hydrogen-rich gas, termed reformate, for fueling fuel cells. In addition to H_2, reformate contains other compounds such as carbon dioxide, carbon monoxide, nitrogen, and water. For use with polymer electrolyte fuel cells, reformate must undergo additional process steps to reduce the CO concentration because CO poisons the Pt anode catalyst. The water-gas shift (WGS) reaction is one of the process steps used in most fuel processing schemes to reduce the bulk of the CO concentration. In the WGS reaction, CO and H_2O react to produce CO_2 and H_2 in the presence of a catalyst. Two important criteria for the catalyst are that it enhances the WGS reaction rate and that it does not promote side reactions, such as the methanation reaction ($CO + H_2$) which produces methane and consumes H_2. Certain metals such as ruthenium are very active for both the WGS and methanation reactions. The objective of this project is to develop new catalysts based on ruthenium that are highly active for the WGS reaction but do not produce methane. Our approach is to alloy ruthenium or cobalt with a second metal with the aim of reducing or eliminating the methanation reaction while not affecting the WGS reaction. Nineteen different catalyst formulations were prepared by incipient wetness, co-impregnation, or deposition-precipitation. The catalysts were tested in a microreactor system to determine their activities for the WGS and methanation reactions and to determine their long-term durability. Most of the formulations tested showed moderate to high CO conversion, and all produced methane. The best performing catalyst was a Ru-Sn catalyst which displayed the highest CO conversion and the lowest methanation formation.

Reactive Power Benefits of CHP Systems. *JASON FOSTER (Tennessee Technological University, Cookeville, TN 38505) ABDOLREZA ZALTASH (Oak Ridge National Laboratory, Oak Ridge, TN 37831).* Combined Cooling, Heating, and Power (CHP) systems enjoy greater efficiency over individually operated electric and thermally activated (TA) systems by using waste heat from power production as input to TA systems. However, a new benefit of CHP is dynamic reactive power (RP) for voltage regulation. There is a growing deficit of RP reserves due to the changing market. The lack of adequate RP and the inability to transport it from central generation to load is one of the main culprits of the past blackouts. Incorporating functionality

into existing or new equipment, RP compensation can be spread over the distribution systems. For mass implementation of CHP-based RP, a standardized control system with minimal communications must be employed and its benefits demonstrated. For the developmental stage, a programmable real-time controller is being used along with mathematical models of the CHP-based RP system and practical test data. The specific technologies being investigated include synchronous motors/generators used as synchronous condensers and prototype inverters for reactive power compensation. In this investigation a 250 hp synchronous motor will interface with the ORNL distribution system. The power inverters will simulate the end-user interface for energy sources such as microturbines and fuel cells. Eventually, several different technologies will be operated in parallel at different injection points. Current methods of RP compensation are mainly based on transporting RP over long distances from central generators or by capacitor banks with expensive switchgear. Also, capacitors cannot provide continuous or dynamic RP and lose their effectiveness at lower voltage when most needed. The project is well suited for ORNL, which owns its distribution system and can make the necessary modifications. Also, ORNL's power supplier, TVA is one of many project partners. ORNL's facilities division will reduce RP compensation at the substation and operate dynamic loads to provide for more meaningful test results. To gain widespread acceptance by the electric power industry, the benefits and impacts of CHP-based RP must be well understood. Ultimately, this project will lead to the development of "rules of thumb" for operation that can easily and reliably be applied.

Rechargeable Batteries. *SARAH FRISINA (Lesley University, Cambridge, MA 02138) STEVE JOHNSON (Lawrence Berkeley National Laboratory, Berkeley, CA 94720).* Today's world having electricity is necessary for living. In countries like Mexico India and China electricity is reserved only from the elite. Because electricity is so hard to come by, many of these countries do not have sufficient light to perform basic tasks like reading. In order to help with this problem the Environmental Energy Technology Division is working on a Light Emitting Diode (LED) solar powered lighting system that will be affordable for people of all economic statuses. In order to maximize the efficiency of the system the proper rechargeable battery must be found. By talking to a number of experts in the field it was found that the two batteries that are best suited for the solar application are Lead Acid batteries. The Cyclon batteries are often used for solar application, and are powerful and light enough to use in a portable flashlight type system. The Genesis batteries are larger and provide more power needed in a stable brighter stationary system.

Enhancement of Air Cooled Condensers for Geothermal Power Production. *BRIAN FRONK (Pennsylvania State University, University Park, PA 16801) CHUCK KUTSCHER (National Renewable Energy Laboratory, Golden, CO 89401).* Electricity generated from geothermal sources offers a more sustainable alternative compared to current methods of generation. Identified resources could provide up to 22,000 MW of clean sustainable power to the U.S. grid. A large capital and operational cost of geothermal electric production are the air-cooled condensers found in the cycle. In order for geothermal to become more economically competitive, improvements in efficiency and reduction in costs of these units is necessary. Using a small-scale air cooled heat exchanger, different fin types and exchanger tube configurations were tested for optimal heat transfer and input fan power required. A plain fin was used as a control case and two experimental perforated fin types were tested. Tubes were configured in a conventionally staggered array, in-line and a 90 degree offset configuration. When heat transfer per bare tube area and hydraulic power required per bare tube area was compared for each fin / configuration combination, the conventional plain fin and standard staggered array performed the best. While the plain fin in a staggered array outperformed the perforated fins, this does not necessarily mean other types of enhanced fins won't provide improved performance. This research is part of ongoing work involving novel fin types and condenser optimization. It is the goal of NREL to reduce the cost of geothermal electricity by $0.01 kWh by the 2010.

Characterizing the Performance of a Proton-Transfer-Reaction Mass Spectrometer by a Rapid Cycling Tenax Preconcentrator. *SHAUN GARLAND (Shasta College, Redding, CA 96049) MICHAEL ALEXANDER (Pacific Northwest National Laboratory, Richland, WA 99352).* Volatile organic compounds (VOCs) are species of interest for atmospheric modeling, worker chemical exposure and medical studies. Sometimes the required detection limits for these compounds is below the capability of existing real-time instrumentation. Preconcentrators have been implemented as an inexpensive way to amplify chemical signals and improve detection limits. Proton-transfer-reaction mass spectrometry (PTR-MS) has been used as a tool for studying low concentrations of VOCs, but it lacks the capability to differentiate chemical signal contributions from isobaric compounds. In this work, behavior of a newly designed Tenax TA preconcentrator when coupled with a PTR-MS is characterized. This novel preconcentrator design allows rapid temperature cycling, maintaining near real-time response. The preconcentrator was exposed to a sample gas of toluene in varying concentrations and loading times between and then thermally desorbed for analysis by PTR-MS. The effects of preconcentrating multiple analytes simultaneously were also investigated as well as the chromatographic effects of the preconcentrator. A linear behavior was observed when the integrated ion count rates (ICPS) from thermal desorption peaks were regressed against both varying loading times at a constant toluene concentration and varying concentrations with constant loading times. From these trends, it is possible to determine the concentration of a VOC by knowing its ICPS from thermal desorption peaks from a known preconcentration time. Peak height ion count rates representing ultimate detectability were amplified by factors up to 257 times the original signal, extending the range of the PTR-MS from 50pptv to nearly 250 parts per quadrillion. This corresponds to an ultimate sensitivity of 200 parts per quadrillion with 20 minute time resolution. Quantitative preconcentrator behavior was demonstrated using ICPS from these ion peaks and were amplified as much as 148 times their original signal. Results from multi-analyte desorption indicate that chromatographic separation is possible with a Tenax preconcentrator and further details are discussed. The dramatic increased in sensitivity with near real-time response, combined with chromatographic resolving capability opens up new areas of research requiring the detection of ultra-trace organic species using PTR-MS.

Friction and Wear of Nearly Frictionless Carbon and Super Hard Coatings in Dry Nitrogen, Isobutane, and Hydrogen. *FRANCISCO GUTIERREZ (Illinois Institute of Technology, Chicago, IL 60629) GEORGE FENSKE (Argonne National Laboratory, Argonne, IL 60439).* The purpose of the project is to assess the tribological parameters of Nearly Frictionless Carbon (NFC-6) and Super Hard Coating (SHC) on steel under dry nitrogen/Isobutane/Hydrogen environments. The speed, load, and environment were kept constant while considering the coated and uncoated surfaces as the independent parameters. A High Frequency Reciprocating Rig (HFRR) recorded the friction coefficient between the sliding surfaces. An optical profilometer was used to estimate the amount of material removed. An optical microscope was used for visual identification and measurement of coating thickness. Raman Spectroscopy was used to assist in determining whether the surfaces became more amorphous or crystalline. Overall results indicate that specimens under isobutane provide lower friction and higher wear resistance than specimens under hydrogen gas. The results indicate that a combination of bare steel/NFC6 ball and bare steel/NFC6 plate provides the lowest coefficient friction. NFC6 ball-SHC plate, NFC6 ball-NFC6 plate and NFC6 ball-Bare plate in hydrogen gas display short life (low wear resistance) but results display a coefficient of friction significantly smaller than any friction measured in isobutane. Future work should include revalidating some of the experiments for reliable results, introducing new independent variables such as speed, load and temperature. In addition, a detailed analysis of the surfaces in contact may provide an understanding at the microstructural level.

Monthly CO_2 Emissions Due to Natural Gas Flaring/Venting and Cement Manufacture. *KIM HAND (Georgia Institute of Technology, Atlanta, GA 30332) TJ BLASING (Oak Ridge National Laboratory, Oak Ridge, TN 37831).* Radiatively active "greenhouse" gases, such as carbon dioxide (CO_2) and methane (CH_4), influence the climate system. Because of its abundance, CO_2 is by far the most influential of these gases. Until recently, only annual data on fossil-fuel CO_2 emissions were available. However, as numerical models of the carbon cycle, which predict future atmospheric CO_2 and CH_4, become increasingly sophisticated, the need for sub-annual (e.g., seasonal) values of carbon emissions increases. Monthly CO_2 emissions from fossil-fuel consumption in the United States have recently been estimated. Therefore, the work reported here focused on release of natural gas at the well sites (not reported as fuel consumption) and on cement manufacture, which is a major industrial source of CO_2 emissions. Values of several parameters had to be obtained to calculate optimally precise emissions estimates. For natural gas, only total amounts released are reported. The fractions combusted to CO_2, released as uncombusted CH_4, and released as soot were not well known before this study. These fractions are important because CO_2, CH_4, and soot have substantially different impacts on the environment. The literature review and engineering calculations completed for this project indicated that about 98% of reported flared/vented natural gas is combusted to

CO_2. In cement manufacture, CO_2 is produced when raw material, including limestone, is heated to produce clinker, an intermediate product used to make cement. Calcium and magnesium carbonates ($CaCO_3$ and $MgCO_3$, respectively) release CO_2 when heated, and leave the resulting calcium and magnesium oxides (CaO and MgO, respectively) in the clinker. The amounts of CaO and MgO in the clinker indicate how much CO_2 was released. On average, 64.6% of the clinker mass is CaO, and about 2% is MgO. However, the error term for M_gO is almost as large as the mean, so carbon from $MgCO_3$ is currently disregarded by the United States Environmental Protection Agency and the Intergovernmental Panel on Climate Change. Some clinker is reduced to dust, most of which is recovered and re-used, but an estimated 2% escapes unreported. The reported clinker values are multiplied by 1.02 to account for this. With the above information obtained in this study, and routinely reported data, the optimally precise monthly values of carbon emissions (as CO_2) from gas flaring and cement manufacture for the United States were estimated.

Engineering and Economic Analysis of Water-saving Fixtures. *ANTONY HAYES (Merced College, Merced, CA 95348) BLAIR HORST (Lawrence Livermore National Laboratory, Livermore, CA 94550).* Reducing water consumption reduces water purchasing and pumping costs, as well as sewer discharge fees. The proposal is to replace urinals that are not water efficient at the Lawrence Livermore National Laboratory (LLNL). Before executing such a project, locations of replacements must be known, justification and the benefits of such a project must be clear, provided in the form of a preliminary analysis of water, energy, and monetary savings. Reducing water consumption and discharge to the sanitary sewer reduces costs as well as contributes towards compliance with various regulations. An initial investment consisting of purchase and installation of low-flow fixtures would result in long-term savings for the LLNL. This project includes surveying the restrooms at LLNL to inventory the toilets, urinals, faucets, showerheads, and lighting controls. Water volume saved by installing the fixtures is the most important factor. The other factors are the price of electricity, water, and sewage per unit of water. Based on the amount of water saved, we can calculate electricity savings, sewer savings, and water savings. These savings, and the costs for purchase and installation of the fixtures are used to calculate simple payback, the metric used to determine where retrofits are economically justified.. A simple estimate shows that the LLNL could save 28 million gallons of water per year, which results in a savings of over $285,000 per year by replacing water closets and urinals with low flow fixtures. The simple payback of replacing the fixtures at LLNL is just over 3 years. This project could reduce the total use of water at LLNL by over 9%. Future work will yield more accurate and in-depth knowledge of the benefits of executing such a project. This work was performed under the auspices of the U.S. Department of Energy by University of California Lawrence Livermore National Laboratory under Contract W-7405-Eng-48.

Heat Radiation Studies for the Neutralized Drift Compression Experiment Injector System. *ELIZABETH HERNANDEZ (Ventura Community College, Ventura, CA 93030) MATTHAEUS LEITNER (Lawrence Berkeley National Laboratory, Berkeley, CA 94720).* The Accelerator and Fusion Research Division at Lawrence Berkeley National Lab is currently designing the Neutralized Drift Compression Experiment (NDCX-II) in order to develop low-cost high line charge density acceleration for High Energy Density Physics (HEDP) experiments. The NDCX consists of an accel-decel injector, a matching section, and a slow wave accelerating structure surrounded by high field transport solenoids to contain the beam. The NDCX injector ion source has to be operated at a temperature of 1,500 K. In order to predict misalignment of the source electrodes due to local heating we used Pro/Engineer CAD and ANSYS FEA software computations as well as analytical analysis, using radiation formulas. The best performing electrode configuration had a minimal misalignment. This turned to be the horizontal design when reducing the energy loads in the ion source it did not make significantly changes to the electromagnetic waves that hold and compress the ion beam. Thermal as well as structural simulations determined the changes of the actual theoretical design in the ion source.

Spark Plug Erosion in Natural Gas Engines. *BRYCE HUDEY (University of South Florida, Tampa, FL 33620) TIM THEISS (Oak Ridge National Laboratory, Oak Ridge, TN 37831).* Spark plugs in industrial natural gas engines demand a longevity and reliability surpassing that of ordinary automotive spark plugs. While current models are designed for 4000 hours of continuous use, demand exists for plugs with an engine lifespan of up to 8000 hours without failure. A critical limiting factor in the lifetimes of these plugs is the erosion of the electrode terminals. In order to characterize possible erosion and failure processes, spectroscopic analyses of breakdown arcs were conducted on ten sets of used plugs. By varying the spark timing and the environment's gas and pressure, spectral signatures from materials such as nickel, calcium, or hydrogen were isolated and examined. Since the sets were each in engines for times ranging between 100 and 5,200 hours, material content was compared with plug age and possible trends were scrutinized, but this trend comparison failed to yield any clear conclusions. A vacuum was applied to view hydrogen spectra for plugs from an Exhaust-Gas-Recirculation (EGR) engine to understand their unique erosion characteristics. The increased levels of found in these plugs might be related to their relatively high erosion rates. Computer analysis of the data determined the frequency of the arc's tendency to alternate between two distinct breakdown points on the plug's arcing surfaces. Though suspected of contributing to the erosion pattern, new data shows that each plug's affinity for sparking consecutively on one side varies widely from plug to plug within a common set. This discovery might mean there are more processes at work that are not yet fully understood. This, coupled with the quantity and variety of elements represented in the emission spectrum, may shed some light on the effects of possible erosion processes.

Restructuring RELAP5-3D. *JOSHUA HYKES (Pennsylvania State University, University Park, PA 16802) GEORGE MESINA (Idaho National Laboratory, Idaho Falls, ID 83415).* The RELAP5-3D source code is unstructured with many interwoven logic flow paths. By restructuring the code, it becomes easier to read and understand, which reduces the time and money required for code development, debugging, and maintenance. A structured program is comprised of blocks of code with one entry and exit point and downward logic flow. IF tests and DO loops inherently create structured code, while GOTO statements are the main cause of unstructured code. FOR_STRUCT is a commercial software package that converts unstructured FORTRAN into structured programming; it was used to restructure individual subroutines. Primarily it transforms GOTO statements, ARITHMETIC IF statements, and COMPUTED GOTO statements into IF-ELSEIF-ELSE tests and DO loops. The complexity of RELAP5-3D complicated the task. First, FOR_STRUCT cannot completely restructure all the complex coding contained in RELAP5-3D. An iterative approach of multiple FOR_STRUCT applications gave some additional improvements. Second, FOR_STRUCT cannot restructure FORTRAN 90 coding, and RELAP5-3D is partially written in FORTRAN 90. Unix scripts for pre-processing subroutines into coding that FOR_STRUCT could handle and post-processing it back into FORTRAN 90 were written. Finally, FOR_STRUCT does not have the ability to restructure the RELAP5-3D code which contains pre-compiler directives. Variations of a file were processed with different pre-compiler options switched on or off, ensuring that every block of code was restructured. Then the variations were recombined to create a completely restructured source file. Unix scripts were written to perform these tasks, as well as to make some minor formatting improvements. In total, 447 files comprising some 180,000 lines of FORTRAN code were restructured. These showed significant reduction in the number of logic jumps contained as measured by reduction in the number of GOTO statements and line labels. The average number of GOTO statements per subroutine dropped from 8.8 before restructuring to 5.3 afterwards, a reduction of 40%. The maximum number of GOTO statements in any subroutine dropped from 213 to 99, a factor of 2.1. Finally, the maximum number of statement labels dropped from 210 to 43, a factor of nearly 5. While many blocks of code remain unstructured, a much greater fraction of the code is now structured. These measurements indicate a serious reduction in degree of interweaving of logic paths.

Electronic Beam Monitor. *CHRISTOPHER JAMES (Prairie View A&M University, Prairie View, TX 77642) MIKE JOHNSON (Lawrence Berkeley National Laboratory, Berkeley, CA 94720).* The Nuclear Science Division of the 88' Cyclotron has designed an electronic beam monitor (EBM) in the cave 4B vacuum chamber. The initial prototype, consisting of a memory chip, mounted on a solenoid driven mechanical arm in the heavy ion vacuum chamber, is described. This prototype is composed of materials that react well under vacuum. The mechanical arm discussed here moves in and out of the beam remotely to alternately apply beam to the chip and the part being tested. Electronic sources that produce little noise under vacuum are necessary to prevent interference with the readouts. Future work will enable the beam to hit the memory chip and read the number of upsets the chips sees without interference, providing users with a functional check to ensure that the appropriate beam is hitting their device.

Modeling of Solid Oxide Fuel Cells and Manipulation of Steam-Methane Reformation Rates. *DANIEL JARBOE (Washington State University, Pullman, WA 99163) KURTIS RECKNAGLE (Pacific*

Northwest National Laboratory, Richland, WA 99352). Direct internal reforming (DIR) offers a number of economic and performance benefits for solid oxide fuel cells (SOFC) that run on natural gas. However, the endothermic impact of the steam-methane reforming reaction increases the thermal stresses within the cell during DIR operation. These stresses can be alleviated by increasing the activation energy of the reaction, thus slowing the rate of the reforming process. Unfortunately, this modification can also reduce the electrochemical performance of the cell. A series of numerical simulations of DIR-SOFC operation were performed to examine this trade-off between thermal integrity and electrochemical performance. A computational modeling tool developed at Pacific Northwest National Laboratory (PNNL) for simulating SOFC operation was used. Simulations were performed on a single planar SOFC cell. Seven activation energy values were considered. Each activation energy value was investigated with four cell voltage values in order to construct performance curves and reveal any voltage dependencies. For each case, the cell power and maximum on-cell temperature difference (MOCTD) were calculated. These values represent measurements of the electrochemical performance and thermal stresses respectively. Simulation results indicate that the cell power and MOCTD both increase as the activation energy is reduced. Reducing the activation energy will yield improvements in performance without significant MOCTD penalties over a limited range of high activation energies. When the activation energy is further reduced to values below this range, the cell power converges towards a maximum value while the MOCTD increases sharply. The results also indicate that no single voltage value produces the minimum MOCTD for all power output values. Based on these relationships, a strategy for maximizing the power output for a given safe MOCTD through the optimal selection of activation energy and cell voltage values is proposed.

Determination of Energy Generated in an Electrical System in Case of an Electrical Accident and Calculating the Possible Hazards and Risks. *GREGORY JIMENEZ (SUNY New Paltz, New Paltz, NY 12561) SWAPNA MUKHERJI (Brookhaven National Laboratory, Upton, NY 11973).* Unusual occurrences such as arcing and short circuit faults in an electrical circuit produce potentially dangerous events such as an Arc-Flash and an Arc-Blast. Both are equivalent to an explosion. Limited, Restricted, and Prohibited Approach Boundaries have been determined from the following electrical standards such as National Fire Protection Association (NFPA) 70 (National Electrical Code), NFPA 70E (Standard for Electrical Safety in the Workplace) and the Institute of Electrical and Electronics Engineers (IEEE) 1584. Electrical software, “Power Tools for Windows” by SKM Corporation is used to calculate the energy generated by an electrical system. We can also use this software to calculate the Personal Protective Equipment (PPE) needed for possible hazards and risks. By going out in the field with a qualified electrician, we were able to verify information needed to design more accurate one line diagrams of some facilities in Brookhaven National Laboratory. This diagram details the circuits, connection and all electrical equipment utilized. The information gathered is then applied to Power Tools for Windows software for calculations on electrical systems. This work is a new study at Brookhaven National Laboratory that will improve Brookhaven’s safety standards.

Electronic Beam Monitor. *QUINCY JOHNSON (Prairie View A&M University, Prairie View, TX 77446) MIKE JOHNSON (Lawrence Berkeley National Laboratory, Berkeley, CA 94720).* The Nuclear Science Division of the 88’ Cyclotron has designed an electronic beam monitor (EBM) in the cave 4B vacuum chamber. The initial prototype, consisting of a memory chip, mounted on a solenoid driven mechanical arm in the heavy ion vacuum chamber, is described. This prototype is composed of materials that react well under vacuum. The mechanical arm discussed here moves in and out of the beam remotely to alternately apply beam to the chip and the part being tested. Electronic sources that produce little noise under vacuum are necessary to prevent interference with the readouts. Future work will enable the beam to hit the memory chip and read the number of upsets the chips sees without interference, providing users with a functional check to ensure that the appropriate beam is hitting their device.

Photon Mask Research and Design for the Advanced Light Source Sector 4 Vacuum Chamber Protection. *SETH KARPINSKI (Columbia University, New York, NY 10025) STEVE MARKS (Lawrence Berkeley National Laboratory, Berkeley, CA 94720).* MERLIN, a low energy, high resolution beamline, will incorporate an Elliptically Polarizing Undulator (EPU 90) that is currently in the design phase at the Advanced Light Source (ALS) located at Lawrence Berkeley National Laboratory (LBNL). The MERLIN EPU 90 will be located in sector 4 at an angle of 1.25 mrad relative to the central axis, downstream of the existing EPU 50. Installing MERLIN will orient the electron beam such that the associated high-energy photons will intercept the vacuum chamber wall, potentially damaging the wall. Before the installation process can proceed this safety issue must be remedied. Currently top and bottom photon masks exist on respective halves of the chamber, intended to block EPU 50 photons from the chamber wall. The goal of the analysis is to redesign masks such that photons from both EPU 90 and EPU 50 are intercepted. The new design must be able to maintain a temperature so as not to compromise the structure of the masks or the required chamber pressure of 10–19 Torr. Ray Tracing is used to define the required mask configuration (that which fully shields the vacuum chamber). We present a thermal analysis of the new design. Temperature rise is examined via ANSYS 9.0 Workbench (finite element analysis program), ultimately yielding a 3-D model of the photon mask displaying temperature variance within the entire volume (based upon load specification). Results show that at an operating energy of 1.9 GeV for EPU 50 and 90 as well as operating energy 1.5 GeV for EPU 50, the temperature increase and gas release are comparable to the present situation. Therefore the new mask performance associated with these cases is acceptable. Further analysis of EPU 90 operating at 1.5 GeV is needed; the temperature increase (52°C) appears to be acceptable, however gas load issues must be addressed. Additional research will also include how new mask geometries may affect beam dynamics. These issues are all critical to the implementation of the MERLIN EPU 90 at the ALS.

Measuring and Analyzing the Transport Properties in Superconducting Films. *BRANDON KILLIAN (North Carolina Agricultural and Technical State University, Greensboro, NC 27408) ALBERT GAPUD (Oak Ridge National Laboratory, Oak Ridge, TN 37831).* This project is part of ORNL ongoing progress in developing high temperature superconductors (HTS) for industrial applications, most especially to eventually replace conventional conductors in transmission lines with HTS wires. This accomplishment would allow transmission of current with significantly fewer energy losses. HTS are materials that have no resistance to the flow of electricity below transition temperature, T_c, and where T_c is above the boiling point of liquid nitrogen (77K). Transport properties were measured, specifically the resistivity and critical current density, J_c, on thin films of the HTS material $YBa_2Cu_3O_7$ (YBCO) made here at ORNL and at North Carolina A & T (NCAT) in order to assess the quality of films and to determine the effects of enhancing magnetic flux pinning. Effective flux pinning prevents current-induced dissipative motion of the quantized magnetic flux lines (vortices) within a superconductor, thereby potentially elevating J_c. Since flux pinning can arise from nanoscale defects in the superconductor, we examined samples in which were added nanoscale impurities. Measurements were made in cryogenic systems with a superconducting magnet capable of supplying a large applied magnetic field (up to 14 Tesla) and varying the field orientation σ over a wide range. The samples are cooled to controlled temperatures from T_c to as low as 4K (boiling point of liquid helium). At each fixed temperature, the samples were measured at different applied magnetic fields (H), and at different angular orientations (σ) of the sample in the field. We have found that introduction of oxide nanostructures with sufficient lattice mismatch dramatically elevates Jc over a broad range of fields and field orientations; therefore this kind of film processing should be very promising for HTS applications. Furthermore, we have found this information to be critical to the optimization of processing conditions for the development of superior-quality YBCO film at NCAT.

Designing an Optical System to Extend the Working Distance of a Surface Scanning Laser Confocal Displacement Meter. *MICHAEL KORNHAUSER (University of Rochester, Rochester, NY 14627) PETER TAKACS (Brookhaven National Laboratory, Upton, NY 11973).* A surface scanning laser confocal displacement meter, by means of a fast oscillating tuning fork and an optical lens system, measures a targeted surface’s height to within .01 microns. In order to measure accurately, the working distance between the surface in question and the device must be 6mm with a range of .3mm in either direction. Extending the working distance to beyond 60 mm, while keeping the accuracy to within 1 micron and the range approximately the same, is necessary in order to examine the surface of a thick telescopic lens. Zemax is a computer program designed to model and optimize optical lens systems. After careful inspection of the scanning laser, it can be modeled accurately in Zemax and its working distance extended using an added lens system. From this, an actual lens system can be built which is very similar to the model created in Zemax. The working distance can be extended to beyond 60 mm, but there is no conclusive evidence as of yet as to whether the accuracy is sufficiently small. As

for the range, it actually increased by a large amount and thus does not limit the ability to examine the telescopic lens.

Fire Modeling Analysis of Laboratory Facilities. *ALAN KOUCHINSKY (University of Maryland, College Park, MD 20740) MICHAEL KRETSCHMANN (Brookhaven National Laboratory, Upton, NY 11973).* The occurrence of a fire in a typical laboratory environment can be detrimental to the research being conducted, the everyday operations of the building, as well as the monetary value associated with the destruction of the facility. In order to develop an accurate fire model for a laboratory room, a quantitative investigation of the combustibles and flammable liquids present, is needed, as well as the dimensions of the room, the materials of construction, and openings for natural ventilation. These parameters will determine the worst case fire scenario for a specified laboratory. The more combustibles and flammable liquids present, the greater the potential of a fire occurring causing work stoppage for months and millions of dollars worth of damage. Using CFAST (Computational Fire and Smoke Transport), a DOE (Department of Energy) sanctioned fire modeling program created by NIST (National Institute of Standards and Technology), a calculation of the time evolving distribution of smoke, fire gases, and the temperature throughout the building during a specified fire is determined. Two research labs were chosen to be modeled based on the rooms being classified as a high hazard, due to the flammable liquids present and nonexistence of suppression systems. Room A had an area of 1040 ft^2 with a ceiling height of 19 ft. Room B had an area of 506 ft^2 with a ceiling height of 8 ft. For each lab, the worst case scenario was modeled, which meant there was natural ventilation allowing a constant air supply to feed the fire, as well as 100% of the flammable liquids stored in the lab were spilt on the floor. Based on the type of flammable liquids and the amount of gallons spilt on the floor, using a Fire Dynamics Tool created by the Nuclear Regulatory Commission (NRC), the heat output of the fire and duration was determined of the insipient fire. Comparing the results of each simulation over a 15 minute interval, Room A showed that the fire only had an immediate impact on the room of origin due to the high ceilings for the hot upper layer of gases and smoke to concentrate. Room B differed in that the hot gases and smoke was confined to the lower ceiling, which caused them to bank down and fill not only the room of origin but the adjacent corridor. This work is a starting point to help analyze the need for suppression systems or other means of protection due to the high risk associated with a specific room or overall building use.

Database Management for the Accelerator Systems Division Design and Drafting Group for the Advanced Photon Source of Argonne National Laboratory. *RYAN KRONE (Valparaiso University, Valparaiso, IN 46383) PAUL CHOI (Argonne National Laboratory, Argonne, IL 60439).* The drawings prepared by the Design and Drafting Group represent every part that used in the construction of the APS. These drawings are all saved for reference in maintenance and improvements. A database called ProIntralink is used to store and organize the drawings. The management of these files is critical to reliability and productivity. My project was to organize these drawings using the Document Control Center Systems/Electronic DCN System, AutoCAD, ProEngineer, ProIntralink, and various websites and network drives. My first task working with the Design and Drafting Group was to organize recently finished drawings. I had to take the paper drawings and store them according to their WBS number. After the information for every part was correct, I had to open every part and make sure that its component interface attributes, mate and insert, were correct. I then worked on checking that all the files in ProIntralink have a WBS number. If they were missing or had an incorrect WBS number, it had to be properly labeled. The last project I worked on was to provide the documentation of various assemblies based on their parts list by printing a paper copy if necessary.

Reduced Enrichment for Research and Test Reactors Foil Production. *JEFFREY LARSON (Brigham Young University, Provo, UT 84602) CURTIS CLARK (Idaho National Laboratory, Idaho Falls, ID 83415).* It was our task to develop a process for making larger (>1 inch width) low enriched UMo foils. It had already been shown that small (<1 inch width) foils could be made. Two processes were investigated for producing these foils. The first process investigated was roll casting. In this method, metal is arc melted in a crucible and bottom poured directly onto spinning copper rollers which cool and flatten the metal into a foil. Stainless steel was substituted for UMo to test this method. Some success was achieved with this process but the yield was low, (one good foil for ten casts), due to thickness variation, holes, and crucible material contaminants. These foils would require additional cold rolling to bring them to the right size. The cold rolling caused the foils to spoon and twist due to the uneven thickness of the foils. The second process investigated was ingot casting. In this process the metal was arc melted in a crucible and bottom poured into a rectangular copper mold, producing a rectangular ingot. The ingot was cold rolled into a foil with the correct thickness. This process also substituted stainless steel for UMo and proved to be very repeatable, though, defects were found to be in some of the foils. These defects were holes, cracks, or contaminants (crucible material). A casting of U10Mo was made using this process and an acceptable ingot was formed. We have yet to cold roll an ingot of UMo. Although from earlier tests the smaller ingots of UMo rolled adequately. Both of these methods required annealing to relieve surface tension in the foils or else cracking would result. Resistance annealing proved to be an efficient way of annealing the foils. An apparatus was used to stretch the foil slightly as current was being passed through it. This apparatus would straighten and anneal the foil simultaneously. An optical pyrometer was used to ensure proper annealing temperature. This method was used with stainless steel foils and proved to be adequate. It is assumed that the UMo will anneal similar to the stainless steel. An annealing apparatus has been designed to anneal the UMo and is in the process of being built. As of now, ingot casting appears to be the most repeatable method for creating foils. Roll casting might be improved with tighter process controls such as improved temperature consistency, metal flow, cleanliness of rollers, and crucible quality.

Optimizing a Prototype for the Production of Medical Ice Slurry. *JEFFREY MA (Stanford University, Stanford, CA 94305) KEN KASZA (Argonne National Laboratory, Argonne, IL 60439).* Injection of micro-particulate ice slurry to induce cell-protective hypothermia offers significant advantages over current techniques for internal organ cooling in surgical and medical emergency settings, including a faster cooling rate and higher cooling capacity. While a preliminary prototype machine has integrated ice slurry production into an automated, medical-grade process, a more exact understanding of specific components of the design is needed in order to improve its efficiency and slurry ice load. Using calorimetric quantification of ice loading as a measurement of the quality of the ice slurry, we tested several parameters influencing the production process, including mixer design, cooling optimization, processing time, and the physical contour of the machine reservoir as it affects mixing efficiency and subcooling. Through our tests, we have been able to achieve a 45% slurry ice load with reproducibility (improved from 25%), accumulate a better understanding of the factors affecting the production process, and establish an improved procedure and prototype for an ice slurry production machine. This reported work is part of a larger project to develop and implement a more effective technique of induced cell-protective hypothermia for cardiac arrest and stroke victims as well as patients of certain minimally invasive surgeries.

Two Types of Gas Cleanup Technologies Used in Integrated Gasification Combined Cycle Power Plants. *AARON MARROQUIN (Santa Rosa Junior College, Santa Rosa, CA 95401) STEVE A. SHANKLE (Pacific Northwest National Laboratory, Richland, WA 99352).* Integrated gasification combined cycle (IGCC) power plants are next generation electricity generating facilities. These new high technology plants operate by gasifying coal rather than burning it, which leads to a more efficient use of coal and less waste production. However, as with pulverized coal (PC) plants, potentially harmful pollutants are produced and need to be captured prior to combustion in a gas turbine (GT). Because higher efficiency is possible by keeping the temperature of the coal-derived gas (syngas) elevated, industry has been looking at hot gas cleanup (HGCU) technologies. HGCU uses components that are able to operate in the elevated temperature gasification environment. Ceramic candle filters and chemical adsorbents are two technologies that appear to have an important role in an IGCC plant. Ceramic candle filters remove particulate material (PM) from the syngas stream. Chemical adsorbents utilize chemical reactions to remove sulfur from the syngas. Both technologies are reusable through back-pulse cleaning and recharging for ceramic candle filters and chemical adsorbents, respectively. Gas cleaning is necessary to prevent damage of downstream components such as the GT. This paper will discuss ceramic candle filters and chemical adsorbents that will most likely be used in an integrated gasification combined cycle plant.

Web-Based Data Acquisitions Systems Utilizing the Rabbit Microprocessor. *BRENDAN MATHEWS (West Virginia University, Morgantown, WV 26505) JOHN MUSSON (Thomas Jefferson National Accelerator Facility, Newport News, VA 23606).* In 2004, Jefferson Lab began what is known as the trim card project to update the cards controlling the current flow to the trim magnets within the accelerator. Also a card was created a card to perform general housekeeping on

the system such as take care of gain selection, and multiplex various inputs. It was decided that these cards could also be used to measure a variety of analog signals from various test equipment. However, in order to use them efficiently for data acquisitions systems, another smarter board would be required to drive the devices. The goal of this project was to find a board that would allow these cards to create a generic, web-based, and user-friendly dada acquisitions system. The card chosen to drive these boards was the Rabbit Core Microprocessor 2200 (RCM2200) because it was able to utilize Ethernet, RS232, and Serial peripheral interface (SPI) connections, which allowed for a wide variety of communication options. The Rabbit's hundreds of factory-defined functions, allow the users or programmers modify the programs interface creating a very generic system whose design could be left entirely to the system's users. Overall, the field tests have shown that the Rabbit performs very well efficiently controlling the digital meters and allowing users complete control of the system from a simple web interface.

Analysis of Thermoxid Sorbents for the Separation and Purification of Molybdenum-99. *HEATHER MAYES (University of Illinois at Chicago, Chicago, IL 60607) CANDIDO PEREIRA (Argonne National Laboratory, Argonne, IL 60439).* To address nuclear proliferation concerns, the Reduced Enrichment for Research and Test Reactor (RERTR) Program is investigating the technology needed to convert the nuclear reactors used for the production of $^{99}M_o$ which currently use high-enriched uranium (HEU, containing =20% ^{235}U) targets, to use low-enriched uranium (LEU, containing =20% ^{235}U) targets. The targets are dissolved in nitric acid. $^{99}M_o$ is subsequently recovered from the dissolved column by elution on an alumina column. To produce $^{99}M_o$ from an LEU target, approximately five times the uranium content is required, which poses challenges for separating the $^{99}M_o$ from the less-refined material since alumina is less effective at high uranium concentration. Using a more efficient sorbent to separate the $^{99}M_o$ from the dissolved target would allow for smaller purification columns and a limited amount of liquid waste. We have identified a sorbent produced by the Thermoxid Scientific and Production Company which selectively adsorbs molybdenum from solutions containing high concentrations of uranium. We tested this sorbent in a packed column with a solution simulating a dissolved LEU target. At flow rate of 3 mL/min through a 1 mL bed volume with 2 cm column height, thirty percent breakthrough was observed in eight bed volumes, and fifty percent in less than twenty-three bed volumes. Lowering the flow rate to 0.5 mL/min resulted in a fifty percent breakthrough in forty-five bed volumes. In both cases the adsorption appeared to be limited, with a high breakthrough corresponding to poor molybdenum retention. More studies will need to be completed to determine if modifying the experimental parameters could result in better molybdenum separation.

Spark Plug Erosion in Natural Gas Engines. *COLIN MCCLELLAND (Wabash College, Crawfordsville, IN 47933) TIM THEISS (Oak Ridge National Laboratory, Oak Ridge, TN 37831).* Spark plugs in industrial natural gas engines demand a longevity and reliability surpassing that of ordinary automotive spark plugs. While current models are designed for 4,000 hours of continuous use, demand exists for plugs with an engine lifespan of up to 8,000 hours without failure. A critical limiting factor in the lifetimes of these plugs is the erosion of the electrode terminals. In order to characterize possible erosion and failure processes, spectroscopic analyses of breakdown arcs were conducted on ten sets of used plugs. By varying the spark timing and the environment's gas and pressure, spectral signatures from materials such as nickel, calcium, or hydrogen were isolated and examined. Since the sets were each in engines for times ranging between 100 and 5,200 hours, material content was compared with plug age and possible trends were scrutinized, but this trend comparison failed to yield any clear conclusions. A vacuum was applied to view hydrogen spectra for plugs from an Exhaust-Gas-Recirculation (EGR) engine to understand their unique erosion characteristics. The increased levels of found in these plugs might be related to their relatively high erosion rates. Computer analysis of the data determined the frequency of the arc's tendency to alternate between two distinct breakdown points on the plug's arcing surfaces. Though suspected of contributing to the erosion pattern, new data shows that each plug's affinity for sparking consecutively on one side varies widely from plug to plug within a common set. This discovery might mean there are more processes at work that are not yet fully understood. This, coupled with the quantity and variety of elements represented in the emission spectrum, may shed some light on the effects of possible erosion processes.

Optical Distance Measurement Device for Eye Surgery. *EILEEN MCFADDEN (Colorado School of Mines, Golden, CO 80401) JUSTIN BABA (Oak Ridge National Laboratory, Oak Ridge, TN 37831).* During a microsurgical procedure called a vitrectomy, surgical equipment is inserted into the eye through 1.4 mm diameter holes in the par plana to repair retinal damage. Currently, surgeons gauge the distance between the surgical tools and the tissue surface using their sense of touch coupled with limited visual feedback from a fiber optic light source. This touch feedback system necessitates the application of adequate contact force to provide a sensation of surface contact, which may lead to unintended surface penetration and tissue damage. Therefore, a fiber optic probe coupled with the surgical tool is needed to aid the surgeon by accurately reporting the distance from the end of the tool to the tissue surface, particularly for delicate surgeries. To accomplish this, an optical approach based on specular reflection from the tissue surface was investigated. Preliminary data was collected on chicken breast tissue and cardboard using three different detector-to-emitter spacing probes, with each probe consisting of a muli-wavelength light emitting diode (LED) source with wavelengths of 660, 810, and 940 nm and a silicon photo-detector. The chicken breast tissue was chosen to represent a birefrignent, i.e. structurally aligned, homogeneous sample and the cardboard to represent a homogeneous non-birefrigent sample with an expectation that the retinal surface will have structural characteristics that fall somewhere in between. Repeatable results using both chicken and cardboard demonstrated trends corresponding to the inverse square law for a Gaussian input beam intensity profile. The reported findings of distance versus intensity show that as the detector-to-emitter spacing decreased, the useful range of the sensor increased, thus supporting the implementation of a fiber optic coupled LED and photo-detector sensor for surgical tool-to-surface distance measurement.

Computer Aided Engineering Analysis in the Development of the Liquid Helium eBubble Cryostat. *GAVIN MCINTYRE (Rensselaer Polytechnic Institute, Troy, NY 12180) MARGERETA REHAK (Brookhaven National Laboratory, Upton, NY 11973).* Prior to the fabrication and experimentation, the eBubble cryostat undergoes structural, thermal, fluid dynamic and electrostatic analysis using ANSYS Classic and ANSYS Workbench. The analysis is important to the success of the experiment, because specific boundary conditions are set. To obtain proper data, no distortions can exist in the electric field. Depending on the analysis type, 2 and 3 dimensional models were constructed using computer-aided drafting software (Pro/Engineer and/or Mechanical Desktop), and imported into ANSYS. The structural and thermal models were developed using minimal symmetric sections of 3 dimensional drawings in ANSYS Workbench, while the electrostatic and fluid dynamic studies were done using an axisymmetric 2 dimensional drawing in ANSYS Classic. The structural analysis focused on the forces applied to the experiment and the material properties of the components. Stress analysis and deformation simulations were created to ensure that the combination of multiple bolt loads and an internal pressure of 1.05 bar did not surpass the ultimate tensile stress of 4.3 Mega Pascals (MPa). The applied forces created a maximum stress of 1.8 MPa, which is well in the acceptable range creating a minimal deformation of .29 centimeters in specific locations. Since the experiment is held at 4.4 Kelvin, thermal and fluid dynamic analysis determined any potential temperature loss that was within the appropriate range between various materials, as well as motion that could occur within the liquid helium due to temperature differentials. A few variations of electrostatic models were tested in order to pursue the best plausible electric field. The desired field would produce completely parallel electric potential lines, which will attract the freed electrons to the measurement components in a non-circuitous manner. The 2 variations consisted of copper rings with applied voltages or a printed circuit board with charged extrusions, both ranging from ground to -100,000 volts (V). The analyses, with the specific boundary conditions, proved that the chosen materials and designs functioned to specifications. The structural analysis proved to withstand all forces, and the liquid helium satisfied the thermal conditions, since the helium remained stationary. Although the circuit board had more of a variation in voltages, the rings produced a field with the most parallel potential lines, and a basic design was moved closer to fabrication.

Database Management of AutoCAD and ProEngineering Drawing Using Intralink. *ANDREW MIKLOS (University of Illinois at Chicago, Chicago, IL 60561) PAUL CHOI (Argonne National Laboratory, Argonne, IL 60439).* The Design and Drafting Group of the Accelerator Systems Division creates all the engineering drawings needed to manufacture parts for the Advanced Photon Source at Argonne National Laboratory. The purpose of this project was to ensure that all the completed drawings were organized into an electronic database. The first task was to reference the paper copies and organize them into filing cabinets as permanent references. Some of the drawings needed to

be edited to ensure that they had the appropriate titles and attributes. Some drawings were created from scratch and provided to the machine shop to be manufactured. The final task was to check assemblies to learn what parts were pending or free. The result of this work will save the designers time when searching for and using drawings. By adding titles, the drawings can accessed easily. By adding attributes, the drawings have automatic features that make them more user friendly. In conclusion, this project work helped me to learn more about engineering as well as making a significant contribution to the efforts in my division.

Cyber Security Issues Within the Engineering Science and Technology Division (ESTD). *SHANE MORRISON (Bevill State Community College, Fayette, AL 35555) TERRY HEATHERLY (Oak Ridge National Laboratory, Oak Ridge, TN 37831).* Information systems have become one of the most used and necessary tools in today's society. During the course of a normal day, the majority of the world's population interacts with some type of computerized system. Whether it is a computer, PDA, cell phone, automobile, shopping (Debit and Credit cards) or a medical system, people are going to interact with some type of computer system. From the infancy of the ARPANET in 1968, the first prototype of today's Internet, there have been cyber security concerns because neither business nor individual wants to lose sensitive data. In more current times, these types of concerns are no different today at the Oak Ridge National Laboratory (ORNL). With the escalating rate of more complex viruses as well as the propagation of spy-ware, identity theft, system failures and the loss of sensitive data have unfortunately become more probable. Therefore, the main goal of this project is to research the evolving methods required to resolve dynamic cyber security issues. In conjunction, various software applications were used to detect, quarantine and remove different types of active cyber security vulnerabilities. Thus, cyber security specialists apply this research by electronically scanning and monitoring information systems within their responsible organizations. Upon finding issues, we use numerous methods to resolve and help to prevent future vulnerabilities from reoccurring. Therefore, continuous cyber security research is a necessity. Routine monitoring and the correction of the problems help to prevent damage to sensitive data and mission critical systems. This proactive cyber security strategy contributes not only to daily dividends that can be measured economically, but also to the world-class research occurring at ORNL.

GREET Vehicle Cycle Model. *UMUT OCAK (Pellissippi State Technical Community College, Knoxville, TN 37933) PAULA MOON (Argonne National Laboratory, Argonne, IL 60439).* The GREET vehicle model is a simulation of studies of energy use and emissions of vehicle cycles. It includes passenger cars, SUVs, minivans and heavy and light duty trucks. The types of vehicles are conventional cars, hybrid cars and fuel cell cars. The GREET vehicle model considers the energy used and emissions throughout the whole life cycle of these type of vehicles. This includes everything from the time the raw materials are acquired to disposal and recycling. This report focuses on the passenger car part of the vehicle cycle. The passenger car excel spreadsheet is a major part of the formula used in calculating the energy use and emissions of vehicles. In order to calculate the energy use and emissions, the material breakdown elements in the passenger car spreadsheet needed to be inputted for conventional, hybrid and fuel cell vehicles. The dismantling reports received from car manufacturers were one resource that was used for this project. These reports had the complete material breakdown of different vehicles. Other related reports were also used and experienced researchers of this study area were contacted for any information needed. After the passenger car spreadsheet dataset was complete, the energy use and emissions data were used after ensuring that the formulas were appropriate. The energy use and emission formulas were linked to passenger car spreadsheet and material spreadsheets.

Synthesis of PLGA-mPEG Nanospheres by Combining Oil-in-Water Emulsion Solvent Evaporation and Nanoprecipitation Techniques. *STAVAN PATEL (Cornell University, Ithaca, NY 14850) MICHAEL KAMINSKI (Argonne National Laboratory, Argonne, IL 60439).* The goal of this research project is to develop magnetic nanospheres for their use in toxin removal systems. Magnetic nanospheres encapsulated with magnetite, and their surface covered with ligands, which corresponds to specific toxins or antigens will be developed. These magnetic nanospheres will be intravenously injected into a human body where these particles will be able to bind to toxins such as cesium, anthrax lethal factor, risen toxin, and others present in the body. These magnetic nanospheres will be removed from the human body by allowing them to pass through a strong magnetic field. This research distribution of 75 nm, 120nm, 150nm, 200nm, and 250nm to ensure proper flow of nanospheres through the circulatory system, and to achieve toxin removal efficiency. The PLGA-mPEG block copolymer nanospheres were synthesized using a combination of oil-in-water emulsion solvent evaporation method, and nanoprecipitation techniques. Nanoprecipitation techniques is a one step nanosphere synthesis technique, which presents numerous advantages, in that it is a straight forward technique, rapid and easy to perform. It requires two miscible solvents and ideally the polymer should dissolve in the organic solvent, but not in the non-solvent. When the polymer/solvent solution is added to the non-solvent, under gentle stirring conditions, nanoprecipitation occurs by rapid desolvation of polymer. Oil-in-water emulsion solvent evaporation technique is a two step synthesis technique, which uses energy (ultrasound, vigorous mixing or both) to emulsify the immiscible organic and aqueous phases. Step one requires two completely immiscible solvents, where ideally the polymer is dissolved in the organic solvent and added to the inorganic non-solvent, while it is sonicated or vortexed for a short period of time. Step two requires that the emulsified solutions be stirred gently for 48 hrs – 96 hrs to completely evaporate the organic solvent from the emulsion. Generally, 100 nm – 300 nm nanospheres with a narrow mono-modal distribution can be synthesized using the nanoprecipitation technique. To synthesize a nanosphere of size less that 100 nm, we combined the nanoprecipitation and the oil-in-water emulsion solvent evaporation technique, where energy of the oil-in-water emulsion solvent evaporation technique is used along with the nanoprecipitation solvents to generate emulsions.

Grid Monitor Development and Deployment Project Summer 2005. *CHRISTOPHER PAVESE (Gonzaga University, Spokane, WA 99258) MIA BOSQUET (Pacific Northwest National Laboratory, Richland, WA 99352).* Grid Monitor Development and Deployment Project was a 2005 Department of Energy's (DOE) Office of Science's Summer Undergraduate Laboratory Internship (SULI) project hosted at the Pacific Northwest National Laboratory (PNNL) in which the team developed a visual tool that monitors the real-time frequency fluctuations of the US Power Grid. For development Visual Basic, Visual C++ and Visual Web Development programming suites were used to produce a windows viewer, a screensaver; as well as, the supporting documents and the website. The team was challenged to complete an extensive design, development, testing and deployment procedure prior to public release of the software within the ten week time constraint of the SULI Program. As a result of the team dynamics, the requirements of the project were achieved. At the end of the program the project was complete and the software was deployed in Beta Version via the http://gridwise.pnl.gov/ website. The team's final report details future work for subsequent versions and deployment requirements to fulfill future demands of GRIDWISE™, Grid Friendly™, Grid Monitor, PNNL, DOE, Universities' Science Education programs, and the general public.

Application of Graphite Foam Heat Exchangers in Neutron Sample Environment Systems. *NATHAN PORTER (Utah State University, Logan, UT 84321) LOUIS J. SANTODONATO (Oak Ridge National Laboratory, Oak Ridge, TN 37831).* Temperature control is crucial for many neutron scattering measurements. The demand for cryogenic systems which operate over a wide temperature range and rapidly lock into a set point is growing furiously. The scope of this research is evaluation and implementation of graphite foam to enhance the thermal performance (i.e., ability to promptly reach the temperature extremes) and set point performance (i.e., the ability to rapidly alter and stabilize on a desired temperature) of a closed cycle helium gas refrigerator system. The work involves an inter-division ORNL collaboration between the Spallation Neutron Source and Metals and Ceramics Division. Measurements of special graphite foam developed at ORNL provided thermal conductivity values throughout the temperature range of interest (3 to 300 K). The conductivity of the foam was measured in a conductance test by placing the foam between two isolated copper blocks. The thermal conductivity measurement came from a calculation of the temperature difference between these blocks. The measurements indicated a high conductivity (greater than 100 $W/m^2 \cdot K$ at 20 K). These results warranted the design, fabrication, and testing of a graphite foam heat exchanger module. A heating module, also fabricated with graphite foam, is incorporated in the design for rapid stabilizing and raising temperatures. A first generation prototype was produced and installed within a "pilot plant" cryogenic system. Testing shows set point stabilization is greatly enhanced, and that the thermal performance weakens being critically dependent on the details of the installation. However, enhancements transpired with the testing of each new configuration refinement within the testing apparatus.

An Improved Pneumatic Frequency Control for Superconducting Cavities. *GREGORY PUCKETT (Southern University and A&M College, Baton Rouge, LA 70813) GARY ZINKANN (Argonne National Laboratory, Argonne, IL 60439).* The ATLAS (Argonne Tandem Linear Accelerator System) super conducting cavities uses a pneumatic frequency control system to compensate for frequency deviations from the master oscillator frequency. The pneumatic frequency control unit was created in 1978 and has slew rates as low as 30 Hz/sec to 500 Hz/sec. The present system is slow in maintaining the master oscillator frequency due to frequency deviations. An improvement has been proposed that could reduce the time for the pneumatic frequency control system to reach the master oscillator frequency. Free hand sketches and computer software designs were implemented in the design stage of the new device. Frequency and physical displacement measurements were also taken and calculated to find that when the RF control module system is working properly the displacement can be kept within $6x10^{-7}$ inches and the pressure can be controlled within $5x10^{-4}$psi.

Real-Time Electrical Grid Frequency Filtering and Graphical Display Using the Visual Basic and C Programming Languages. *CODY RAY (University of Montana, Missoula, MT 59801) DONALD HAMMERSTROM (Pacific Northwest National Laboratory, Richland, WA 99352).* The Grid Friendly(TM) Grid Monitor was developed at Pacific Northwest National Laboratory and is currently a vital component within the Grid Friendly Appliance (GFA) Laboratory and the new Power Systems Communication Laboratory (PSCL). The software developed at PNNL allows anyone interested to view the dynamics of our electric power grid in real-time. Currently there is very little real-time grid monitoring software available to the public. The few programs available are web-based or limited to use by scientists and engineers for off-line grid analysis. Using the Visual Basic programming language, we have created a user friendly application for use by anyone interested in the electric grid of the United States. The software contains a self adjusting filter to compensate for noise and several educational features. These include a histogram plot, and a raw data exporting function so that electrical grid data may be used for educational purposes in other software packages. We also improved the already existing screensaver, written in the C programming language.

The Use of Computer Aided Energy Simulation Program to Assist in Energy Efficient Design and or Retro of Commercial Buildings. *DOROTHY RICHARDSON (Lane Community College, Eugene, OR 97401) BING LIU (Pacific Northwest National Laboratory, Richland, WA 99352).* Given current economic and environmental constraints on energy resources, the energy issue plays an important role in the design and operation of buildings in today's society. Understanding the effects of the decisions made in the design and operation of a building can assist in reducing the energy consumption. Alternative building design strategies, such as the U.S. Department of Energy's DOE-2 Energy Simulation Program allow designers, owners and facility managers to evaluate the design strategies, energy standards compliance and economic optimization of a building before starting construction. Making good design decisions early in the design process ensures energy cost savings throughout the life of a building. By using these programs, it is possible to identify the modifications which would contribute to significant energy and demand reductions, and to gauge the buildings economic viability. This systematic approach to evaluating design strategies is the key to considering the many options without impacting the overall construction costs. The importance of ensuring buildings are energy efficient is increasingly being recognized – driven by rising energy costs and global warming. By using these programs we will see building designers, owners and facility managers taking an active roll in energy savings, conservation and environmental responsibility.

Analysis of Heavy-Ion Beam Images and Comparison to Retarding Potential Analyzer Measurements. *BETH ROSENBERG (University of California Berkeley, Berkeley, CA 94549) PETER SEIDL (Lawrence Berkeley National Laboratory, Berkeley, CA 94720).* It has been predicted that world energy demand will soon outstrip the currently available energy sources. Fusion energy is a potential solution to this problem if it can be controlled and converted into electricity in an economically feasible manner. One type of potential fusion energy plant is heavy-ion beam drivers employed in inertial fusion. As part of the High Current Experiment (HCX), we seek to understand the injection, transport and focusing of high-current ion beams, by investigating the interactions of background-gas and electrons (which can deteriorate the beam quality), with the primary K^+ beam. We present here a method of analyzing the electrostatic potential distribution due to the beam space charge within the grounded conducting vacuum pipe. This method enables tracking of ions arising from the ionization of background gas atoms by the incident K^+ beam. The beam intensity distribution is obtained from images gathered using a scintillator placed in the beam path. These data are used to calculate the expelled ion energy distribution, which is then compared to data collected from a Retarding Potential Analyzer (RPA). The comparison of the image analysis with RPA measurements is in fair agreement, given model and experimental uncertainties. Some remaining issues to be explored include the apparent correlation of maximum beam potential with RMS beam size, the systematic effect of background subtraction in the images, as well as possible 3D effects. The completed method increases capacity to investigate and understand the physics of intense beams, furthering the development of a viable heavy-ion driver for an inertial fusion power plant, which is intended to make fusion energy an affordable and environmentally attractive source of electric power.

The Hydrolysis Reaction of the Low Temperature, HybrID Thermochemical Cupric Chloride Cycle. *MATHEW ROWE (Louisiana State University, Baton Rouge, LA 70803) MICHELE LEWIS (Argonne National Laboratory, Argonne, IL 60439).* Thermochemical cycles are being developed as an alternative and cleaner method in the production of hydrogen. Nuclear or solar energy sources will be utilized for the high energy demands of the thermochemical cycles. Our goal is to develop a cycle that has a maximum temperature of 550°C, does not produce green house gases, does not run under extreme pressures or temperatures, and does not produce highly hazardous chemicals. The hydrolysis reaction is $2CuCl_2(s) + H_2O(g) \rightarrow CuCl_2$ $CuO(s) + 2HCl(g)$. The main objective was to determine both a viable reactor design and a complete system with the ability to control and maintain a constant water vapor content in the nitrogen carrier gas, system temperature, and system pressure. A fixed bed reactor design was utilized inside a Pyrex tube that was placed in a temperature controlled furnace. The overall system used two mass flow controllers, two cold water baths, saturation bubbler, hygrometer, temperature controlled furnace, and water trap to strip hydrogen chloride gas that was monitored by a pH meter. Initial results show a need for as much as sixteen parts water for every part cupric chloride, decomposition of cupric chloride to copper chloride at higher temperatures, and gas-solid particle contact problems. The use of air baffles before and after the reaction vessel has been employed to help with the contact problems. Also, lower temperatures are being used to help reduce the amount of decomposition of cupric chloride. The results suggest that a fluidized bed reactor should be employed to ensure proper contact of solid particles and gas to promote the reaction. The current overall system design has removed most of the instability in the system with only slight variations coming from the change in humidity and temperature in the laboratory. The current project is to institute a fluidized bed reactor and to update old equipment. In time, only two to six parts water to one part cupric chloride will be needed.

Single-Cell Noise Spectrum Analysis for Gene Circuit Characterization. *DAR ROY (The Hebrew University of Jerusalem, Jerusalem, ISRAEL 91904) MICHAEL L. SIMPSON (Oak Ridge National Laboratory, Oak Ridge, TN 37831).* The capability to characterize natural and engineered gene circuits could be beneficial on both academic and industrial fronts by gaining more understanding of intra- and inter-cellular biological processes and structure-function relationships. To explore the frequency distribution of stochastic processes in gene circuits, Green Fluorescent Protein (GFP) expressing gene circuits were constructed on high copy number plasmids in Escherichia Coli bacterial cells. Experiments concentrated on two different types of circuits: (1) Non-regulated gene constructs differing in protein degradation rates, and (2) Autoregulated negative-feedback gene constructs where gene expression is repressed by the binding of a repressor protein at an operator site in the promoter. Laser confocal microscopy (Leica SP2) with a 488 nm Ar source was used to acquire 4-8 hour time-series fluorescence data (500-550 nm) from excited bacterium populations. Cell doubling time was controlled by varying growth temperatures. Single-cell fluorescent output was extracted from microscopy images by tracking individual cells using computer-imaging software to calculate mean pixel intensity. GFP noise was defined as this output's deviation from the population's mean fluorescence. A common reference point from calculated biased Autocorrelation Functions (ACFs) for this time-series noise data (time lag at which the ACF decayed by ½) was used as a measure of noise bandwidth (Fnbw) for gene circuits. An increase in Fnbw with decreasing cell doubling time was observed for all the gene constructs. In addition, an increased bandwidth of about two-fold was seen for the autoregulated gene circuit as opposed to the unregulated circuit. This increase in bandwidth was predicted by a previous theoretical study for these gene circuits and is consistent with negative feedback theory. Additional

spectral measurements and model interpretation may reveal significant information on enzyme kinetics, feedback mechanisms, epigenetic motifs, and kinetic parameter fitting of these gene circuits. Ultimately the physical sciences approach to biological systems may be at the forefront of molecular-scale engineering and help enhance the biologist's tools for discovering underlying structure of gene circuits and networks.

Developing "Cool Roof" Criteria for Direct Nailed and Vented Roof Decks. *BENJAMIN RUDOLPH (Virginia Polytechnic Institute and State University, Blacksburg, VA 24551) WILLIAM A. MILLER (Oak Ridge National Laboratory, Oak Ridge, TN 37831).* Solar reflectance and thermal emmitance affect the surface temperature of a roof, which in turn drives the heat transfer penetrating through the roof. A roof with 0.70 solar reflectance and 0.75 thermal emmittance is defined as a "cool roof" by California's Title 24 prescriptive requirements. However, the Title 24 formula has been found to be too restrictive for "cool roofs" in the low emmittance range. In this project, a more accurate prescriptive requirement formula was developed which considered emmittance, reflectance, and the R-value of various roofs across the 16 California climate zones. Running ORNL's STAR roof calculator, a numerical computational tool, a thermal energy balance was developed to approximate the changes required for two different roofs to produce equal heat flow, and thus cooling load, through the roof. The venting of the underside of a roof surface also provides thermal benefits for comfort cooling. Published literature demonstrates a reduction in the daytime heat flux penetrating a counter-batten tile roof as compared to a direct nailed shingle roof, but the energy savings associated with venting are difficult to quantify. Due to the inclusion of a subsurface air channel in many modern roofs, the thermal energy balance must involve natural convection to be complete, which the Tile Roofing Institute is keenly interested in implementing within Title 24. Using CO_2 as a tracer gas, the mass flow of air inside the channel has been calculated to be in the range of .026 lbs/sec. The next step is to develop formulas which relate mass flow to solar irradiance, wind speed, wind direction and outdoor air temperature. In addition to prescriptive requirements considering reflectance, emmittance and R-value, it is hoped that a more comprehensive set of requirements considering air channels will be developed.

Completing Phase III of Chipmunk Electrical Packaging Upgrade. *YEVHEN RUTOVYTSKYY (Three Rivers Community College, Norwich, CT 06360) VINCENT J. CASTILLO (Brookhaven National Laboratory, Upton, NY 11973).* At the Brookhaven National Laboratory (BNL) Collider-Accelerator (C-A) Complex radiation exceeding levels for safe human occupancy are produced as a standard by-product of normal operations. The "Chipmunk" is the radiation monitor that is used for radiation protection and up to 100 chipmunk monitors are located strategically around the C-A Complex during Beam operations. Since the chipmunk was designed in the early 80's, its electrical packaging is outmoded and needs to be updated. This update will enhance features of the old design that experience has shown necessary. These include independent circuit boards which will facilitate troubleshooting and repair along with a backplane in place of hand-wiring. This update is expected to curtail cost and reduced the manufacture cycle from 14–16 months to 3–5 months. The schematics for the project were drawn using MS Visio. My project is a culmination of a three-years effort by CCI students, who worked on the various electrical changes to the original model of the "Chipmunk". Testing and engineering critique of this and subsequent prototypes will lead to a model that is ready for mass production.

Thermal Stability of Linac Coherent Light Source Fixed Support. *ALEJANDRO SAUCEDO (Illinois Institute of Technology, Chicago, IL 60616) SUSHIL SHARMA (Argonne National Laboratory, Argonne, IL 60439).* Advanced Photon Source scientists at Argonne National Laboratory are designing a fixed support system for a 4th generation light source, the Linac Coherent Light Source (LCLS). It is required that this support system remain thermally stable while air temperature in the LCLS tunnel fluctuates. In this study, special emphasis was placed upon situations where rapid changes in temperature occur. Finite element analysis and transient heat transfer calculations were performed to predict and select the best design options. A cylindrical mild steel stand was chosen as the fixed support. This stand was insulated to dampen the temperature fluctuations. To record the changes in temperature, resistance temperature detectors and temperature transmitters were utilized. The experimental results show that the thermal insulation can eliminate the effect of rapid changes in air temperatures, and can reduce the effect of slow temperature change by a factor of three.

Simulation-Modeling of Environmental Conditions in the New, Naturally-Ventilated San Francisco Federal Office Building. *JOSHUA SPERLING (University of Colorado, Boulder, CO 80303) PHIL HAVES (Lawrence Berkeley National Laboratory, Berkeley, CA 94720).* This study uses computer simulation to examine the effect of different shading strategies on interior comfort conditions during periods of peak high temperature readings in the new, naturally-ventilated San Francisco Federal Building (SFFB) scheduled for occupancy in 2006. The EnergyPlus building energy simulation program was used to quantify the role of different shading elements in reducing solar gain and glare, and smoothing out interior natural daylight distribution in order to ensure long-term energy savings and occupant comfort. More specifically, this paper examines the effects of shading by operable blinds, overhangs and side fins attached to the façade, and surrounding buildings. Results indicate that a combination of shading elements can reduce the peak indoor temperature by ~5 K on hot summer afternoons, providing a significant improvement in thermal comfort conditions.

Theory and Design of a Portable, Quantitative, Airborne, Particulate Matter Sensor. *GEORGE STERN (Gonzaga University, Spokane, WA 99258) MICHAEL APTE (Lawrence Berkeley National Laboratory, Berkeley, CA 94720).* The health affects of airborne particulate matter (PM) has become a growing concern for environmental policy makers and regulators around the globe. Some types of PM have been linked to asthma, cancer, and other respiratory diseases. To establish beneficial and cost effective regulations, much more research must be conducted to determine exposure rates for natural and man-made PM and local baseline levels of naturally occurring PM must be quantified. Research on PM has been limited by the commercially available equipment which is bulky, heavy, and prohibitively expensive. To conduct statistically significant population-based studies and in a statistically significant number of locations, new measuring equipment had to be developed. The equipment had to operate in real time and be accurate, small, lightweight and cheap. Two different prototype models based on the same theoretical concept are being developed and will have the potential to be marketed. Using Van der Waals forces and either thermophoresis or electrostatic forces, the prototypes deposit particles onto a piezoelectric surface which vibrates at a characteristic frequency determined by external electrical circuitry. As the mass on the piezoelectric surface increases, the frequency of vibration decreases and the electronic circuitry converts the change in frequency into the weight of the particles sampled. Concurrently, by measuring the PM's absorption of IR and UV radiation, the type of particles being weighed can be identified and reported. Initial testing of all of the basic parts for each prototype was conducted. Each piece was revised and will be combined with other pieces to create a deployable product. During this SULI session, an improved stable, temperature compensated, quartz crystal oscillator was developed for mass sensing in a quartz crystal microbalance PM detector.

EM Ground-Wave Propagation Prediction Using Finite Difference Time Domain (FDTD) Method and Antenna Modeling (100 kHz) for Theater Position System (TPS) Broadcast Applications. *WEI TAN (University of Colorado, Denver, CO 80120) PAUL EWING (Oak Ridge National Laboratory, Oak Ridge, TN 37831).* The finite difference time domain (FDTD) approach is rapidly becoming a popular computational method in electromagnetic (EM) propagation prediction due to its extreme simplicity, compared to traditional frequency domain approaches, and its capability of modeling antennas of complex geometries that are difficult to analyze by other methods. The challenge of this research is to model various antenna designs with XFDTD software tools and to select the optimum one for transmission of reference signals in a large-area ground-based radiolocation system. The validation process focuses on three main steps. The first is to construct the physical dimensions of these antennas and then simulate their EM field effects. The simulation presents the field propagation in a graphical format, meanwhile calculating the numerical values of the real and imaginary parts of the port impedance. The second step is to compare these results with the ones obtained in a paper published in an IEEE journal paper using the NEC-4.1 (Numerical Electromagnetic Code) method of moments code. The final step is to explain the discrepancies between results yielded from these two methods. The results of the simulation will be used to guide the construction of an antenna to be physically built and tested with appropriate equipment at a later time.

Determination of Top Load Length of a Marconi Antenna to Achieve a Resonant Frequency of 3.2 MHz. *WEI TAN (University of Colorado, Denver, CO 80202) JOHN WILGEN (Oak Ridge National Laboratory, Oak Ridge, TN 37831).* The Theater Positioning System (TPS) requires choosing a certain type of antenna to operate at 3.2

MHz as a ground wave transmitter. A 50-foot Marconi antenna with a top load is chosen for ease of assembly of five temporary transmitters. The top load consists of the upper portions of four guy wires that intersect at the top of the vertical wire, and which are oriented at an angle of 67 degrees from the horizontal direction. The challenge of this research is to determine the length of these four top load wires so as to realize an antenna that resonates at 3.2 MHz. The determination process has three main steps. The first is to come up with an estimation of length by modeling antennas with a range of top load lengths to see which one has a resonant frequency closest to 3.2 MHz. The simulations are done by running finite different time domain (XFDTD) software. Meanwhile, other parameters of interest are obtained, such as reflection coefficient and the real part of antenna impedance for each antenna with a specific length of top load. The second step is to build a prototype which is 1/100 the size of an actually one, then use a network analyzer to measure the resonant frequency, reflection coefficient and the real part of antenna impedance. The third step is to tabulate and compare the results acquired with computational and experimental methods and explain the discrepancy between them. The computer simulation showed that the length of the top loads from the intersection to the lower end needs to be between 20 ft and 22 ft long (a 2-foot range), in order to make this antenna resonate at 3.2MHz. Since the cell size was set as 2 ft per cell when the FDTD simulation was done, the 2 ft range has reached resolution limitation of the model. Meanwhile, a 1/100 scale prototype was built and network analyzer measurements were completed and compared with the modeling simulation.

Investigate the Collection Capacity of Filter Media Using a Ground Based Airborne Particulate Collection System. *COURTNEY TAYLOR (Bevill State Community College, Fayette, AL 35555) JOHN E. SMART (Pacific Northwest National Laboratory, Richland, WA 99352)*. Monitoring atmospheric particulate concentration with selected filter media is a key capability in environmental studies used to measure important airborne signatures. Knowledge of particulate collection capacity for high efficiency filter materials enables researchers to define sampling specifications. This study will report empirical data collected using 3M Brand GS-100 filter media used in the vicinity of Richland, Washington. A 15 horsepower roots blower pump was used to pull in excess of 3500 cubic feet per minute thru a six inch diameter filter section. High volume air sampling combined with the high efficiency collection media resulted in relatively short sampling periods with measurable debris collection. Collected particulate mass was correlated to differential pressure measurements and corresponding face velocity. Meteorological conditions, such as temperature, wind velocity, wind direction, relative humidity, and atmospheric pressure, were recorded. Photographs of the particulate collection and the surrounding air conditions will be presented. Measurements of the face velocity, differential pressure across the filter, and the net weight of the collected particulates were recorded at frequent intervals during filter loading and are included in the tables and appendix. The design of air sampling equipment and collection routines will benefit from this resulting data set. Researchers will use this data to help define sampling duration, sampling media type, and pump specifications. Continued work may include assessment of other high efficiency filter media.

Thermal Stability of Linear Coherent Light Source Fixed Support. *BHARAT THAKKAR (Illinois Institute of Technology, Chicago, IL 60616) SUSHIL SHARMA (Argonne National Laboratory, Argonne, IL 60439)*. The Linear Coherent Light Source (LCLS) will be hosted by the Stanford Linear Accelerator Center (SLAC). Currently, the project is in engineering & design phase. The undulator, support stands, and cam movers are being designed at APS. The thermal stability of the undulator support system was critically analyzed using finite element technique and the important thermo-mechanical parameters were experimentally verified. Change in position of undulator while the temperature fluctuates and any rapid changes in temperature were monitored for 35 hours continuously. With appropriate insulation, support material, and heat sink design; the design goal of variation in 0.7-meter stand height within plus or minus three microns was successfully achieved.

Meteorological Modeling for the 2003 Mexico City Experiment. *CARMEN THOMAS (Texas A&M University-Kingsville, Kingsville, TX 78363) V. RAO KOTAMARTHI (Argonne National Laboratory, Argonne, IL 60439)*. The impact anthropogenic activities have on the earth's atmosphere, biosphere and oceans is of increasing concern. Rapid industrialization and urbanization is contributing to a decrease in air quality across many parts of the earth. There are several scientific studies currently underway to understand and mitigate air quality problems in large urban centers with populations in excess of 10 million people, referred to as megacities. One such effort is the Megacities Impacts on Regional and Global Environments and exploratory field campaigns of the Mexico Valley Metropolitan Area (MVMA), conducted during April-May of the year 2003. During this period air pollutants such as NO_x, ozone, and hydrocarbons variables were measurements. This data set provides the basis for a much larger Max-Mex project planned for March 2006 in the same region. The focus of Max-Mex is on understanding the regional-scale dispersion of aerosols generated in the Mexico City plume into the regional atmosphere, evaluating the sources, sinks and aging of black carbon and evaluating the radiative impacts as constrained by the measured aerosol physical and chemical properties and their distribution. Here we present results from a regional scale meteorological model (MM5) simulation for April 2003 over the Mexico City and surrounding regions. A nested version of the MM5 model with an outer 12km domain covering much of the country of Mexico and inner domain at a horizontal spatial resolution of 4 km, surrounding Mexico City and surroundings, was used for the simulations. The MM5 output was compared with data from several meteorological stations located within the model domain. The analysis showed the temperature to be within 2°C of the measurements at one of the sites. Further analysis of the model results and preparation of dynamic inputs for a regional scale air quality model from these MM5 results will be performed in the near future.

The Consequences of Demolishing the Main Stack. *SABRINA THOMPSON (State University of New York – Stony Brook, Stony Brook, NY 11575) ALAN RAPHAEL (Brookhaven National Laboratory, Upton, NY 11973)*. The environmental cleanup effort at Brookhaven National Laboratory is addressing the decommissioning of the Brookhaven Graphite Research Reactor (BGRR) and the High Flux Beam Reactor (HFBR). One component of the decommissioning is the main stack. The main stack was built in 1947 to support the BGRR's air cooling system and was used in that capacity until 1969 when science mission of the BGRR was terminated. When the HFBR was built, it was situated to take advantage of the existing stack; the HFBR operated from 1965 to 1996. Several other buildings have been connected to the stack over the years. Since neither the BGRR nor the HFBR is in operation, there is no longer a need for a 320-foot stack. The other, smaller buildings connected to the main stack could be accommodated by a smaller stack, if necessary. By researching historic drawings of the area surrounding the stack, we were able to find out which buildings had been connected to the stack. Drawings of the buildings' ductwork and heating, ventilating, and air-conditioning (HVAC) air flow systems were analyzed. Then field verification was performed at the different buildings to assure which buildings were currently using the stack and to verify existing conditions. After analyzing the drawings and existing conditions at the different buildings, we have come to find out which buildings are currently using the stack. Buildings which do not require air discharge will have their disconnections designed. We have found that Building 801 is the only building that really needs a stack to meet air discharge regulations. The plan is to design one or two smaller stacks for building 801.

Pressure Distribution Simulation for ERL Loop Vacuum System. *MICHAEL TIEN (Hobart and William Smith Colleges, GeneVA NY 14456) H.C. HSEUH (Brookhaven National Laboratory, Upton, NY 11973)*. The Energy Recovery Linac (ERL) is a R&D project to test the principles of electron cooling for the Relativistic Heavy-Ion Collider (RHIC). The major components of the ERL loop are currently being designed and fabricated. Ultrahigh vacuum is required for the ERL loop vacuum systems to reduce the electron-residual gas scattering, and to minimize gas migration and particulate contamination to the super-conducting radio frequency (RF) accelerating cavity. The effect of the quantity, speed, and distribution of ion pumps on pressure distribution in the ERL was modeled using a computer simulation program called Vac-Calc. The simulation indicates that the designed pressure of low 10-9 Torr can be optimally achieved with 20 L/s ion pumps positioned approximately every two meters.

Heat Exchanger Studies for Supercritical CO_2 Power Conversion System. *AKIRA TOKUHIRO (University of Missouri-Rolla, Rolla, MO 65409-0170) STEVE LOMPERSKI (Argonne National Laboratory, Argonne, IL 60439)*. Recent investigations conducted under DOE Nuclear Energy Research Initiative program have demonstrated the benefits of the supercritical CO_2 power conversion system, including significant reductions in plants costs, size and complexity coupled with an increase in plant efficiency. The supercritical CO_2 power conversion system is being seriously considered for application to some of the Generation IV nuclear energy systems such as Gas (Cooled) Fast Reactor (GFR), Lead Fast Reactor (LFR) and Sodium Fast Reactor

(SFR). It may also be adopted by the Very High Temperature Reactor (VHTR) for cogeneration of hydrogen and electricity. One of the key components for the supercritical CO_2 power system is the regenerative heat exchanger known as the recuperator where heat exchange between two flowing streams of supercritical CO_2 takes place. While the benefits of the supercritical CO_2 Brayton cycle derive from the unique thermophysical properties of supercritical CO_2 (e.g., density and specific heat), these same properties also present technical challenges to the recuperator design. To maximize the benefits of the supercritical CO_2 power conversion system, a compact heat exchanger would be required. Basic heat transfer data, such as heat exchanger performance data, under reactor-relevant conditions are needed in order to develop an improved design for application to the supercritical CO_2 power conversion system. The ANL-University of Missouri-Rolla (UMR) collaborative project has been awarded funding under the DOE Office of Nuclear Energy, Science and Technology (NE). The summer 2005 marks the start of the collaboration.

Evaluation of the Energy Performance of the Site Entrance Building at the National Wind Technology Center. *ANDREW TUPPER (Colorado School of Mines, Golden, CO 80401) PAUL TORCELLINI (National Renewable Energy Laboratory, Golden, CO 89401).* By incorporating energy efficient design and renewable power generation, the Site Entrance Building (SEB) at the National Wind Technology Center (NWTC) was built to achieve net-zero site energy use. The building neared the net-zero target in 2004, but has never achieved net-zero use for a full year. By analyzing long term SEB data, collecting information on plug loads, and observing building use, the following recommendations will be made to allow the building to achieve net-zero status. During the summer months, foil backed sheathing should cover the Trombe wall. The clerestory window should be open when cooling is required. The other windows shall remain closed unless the heat pump is turned off. Installing power strips, which are to be turned off when not in use, should minimize plug loads. The existing absorbed glass mat (AGM) batteries should be replaced with a larger bank of flooded lead cell batteries. An uninterruptible power supply (UPS) for the computer is redundant and should be removed pending battery replacement. The inverter, wind turbine, and PV voltage settings should be adjusted to increase system efficiency. By following these recommendations, it has been calculated that the building will be able to achieve net-zero status within the next year.

Fire Modeling Analysis of Storage Facilities. *SEAN VAZ (Suffolk County Community College, Selden, NY 11784) MICHAEL KRETSCHMANN (Brookhaven National Laboratory, Upton, NY 11973).* Brookhaven National Laboratory has numerous facilities with various fire hazards within. I was selected to observe a number of storage facilities on site to determine their fire load and to model the building to see what the outcome would be in a fire emergency situation. The buildings were chosen based on identifiable concerns with particular chemicals within the structure. I used a program called Cfast to create a fire model of these facilities to determine the ending result in a fire situation. This program uses information such as, size of the building, fire load, and most important the specific heat release rate of the main fire and combustibles in the room. I use this tool to tell me the temperature of the room and the actual wattage of the fire. By telling us how hot the fire becomes at different layers in the building, and the temperature of the opposing rooms, I can accurately say if there is extreme concern for a hazardous plume release or if the fire doesn't reach the flashpoint of the hazard in question. The Nuclear Regulatory Commission (NRC) has fire dynamics tools that were used to verify the results that were acquired from the Cfast model. After telling us if our fire model was very accurately formed we were able to then able to take the results of the program and make copious graphs to present our data.

Construction of a Block on Ring Test Machine for the Study of Wear Preventative Properties of Surface Textures, Coatings and Lubricants. *MICHAEL WAYNE (Brigham Young University Idaho, Rexburg, ID 83460) GEORGE FENSKE (Argonne National Laboratory, Argonne, IL 60439).* Much of industry is concerned with friction and wear of materials, especially in the use of bearings and gears which are used in engines and other machinery. Oil is commonly used to lubricate sliding surfaces. There are many failure modes in oil lubricated sliding. One especially severe mode is "scuffing". Scuffing is a point of lubrication and material failure that exhibits a sudden and extreme jump in friction force, resulting in large material wear. The construction of a block on ring test machine was done to further the study of scuffing, using various surfaces, coatings, and lubricants. The block on ring test machine, that was built, takes real time measurements of the load, speed, friction force, temperature and number of rotations that are made during the test through the use of data acquisition software. The principle of the block on ring test machine is that a stationary block, using pneumatic pressure is pushed with increasing force against a rotating ring, until scuffing occurs. Scuffing is said to occur when the friction coefficient suddenly increases ant the lubricating ability of the oil is lost. Tests were run of stock and polished steel specimens in (Mobil) PAO10 mineral oIL using a 22.3 N increase in load every minute until scuffing occurred. For a better understanding of scuffing, a test was stopped prior to scuffing in order to view the wear of contact areas. This test resulted in minimal wear as compared to tests where scuffing was allowed to occur. A repeat test was performed with polished specimens, which did not scuff, but resulted in the formation of an iron oxide and removal, and an increase in friction force, where the test was stopped for evaluation. Future experiments will involve the use of a hard carbon coating (Near Frictionless Carbon Coating-NFC6), a nitride coating, and laser surface textured (LST) specimens, where micro-dimples are made into the surface of the specimen to serve as lubricant reservoirs and to catch wear debris.

Performance Analysis of a Second Order ΣΔ ADC With Electornics Noise Using MATLAB and SIMULINK. *JOSH WERRMANN (University of Kentucky, Lexington, KY 40506) M. NANCE ERICSON (Oak Ridge National Laboratory, Oak Ridge, TN 37831).* In the field of signal processing, the sigma delta analog to digital converter (SDADC) is particularly useful for high resolution digitizing of signals. This high resolution is accomplished by oversampling and quantization noise shaping. Mathematical representation of SDADCs is difficult, and continues to be problematic. Closed form representation has not been shown in the known literatures. Accordingly, SDADC developments typically involve simulations in which signals are sampled and calculated at some defined time interval. In this manner, long sequences of output data can then be processed in the frequency domain to assess SDADC effectiveness. Furthermore, SDADCs are constructed by utilizing integrated circuit techniques, thus making the fabrication of prototypes not only time consuming, but costly, with costs ranging from a few thousand to greater than $100,000. This renders it advantageous to have a computer simulation readily available to quickly assess ADC performance characteristics with user specific input variables which simulate real world conditions. The focus of this work is the development of tools for assessing SDADC performance based upon MATLAB and SIMULINK. With these tools, an accurate input noise spectra can be generated which represents the dominant electronic noise sources (white noise, 1/f noise), and includes noise folding, enabling evaluation on the effect these sources have on a 2nd order SDADC. These tools can further be used to analyze the effect that any individual component, such as the various gains in the modulator or the input voltage may have on the various performance metrics, including the signal to noise ratio (SNR), dynamic range (DR), and total harmonic distortion (THD). The success of the simulations will be determined based upon how closely the simulations are in accord with theory.

Comprehensive Process Description of a Wet Scrubber Used for Cleaning Biomass-Derived Syngas in the Thermo Chemical Process Development Unit at the National Renewable Energy Laboratory. *KRISTIN WILLIAMS (University of Colorado, Boulder, CO 80309) STEVEN PHILLIPS (National Renewable Energy Laboratory, Golden, CO 89401).* The main product of biomass gasification is syngas, a gas composed primarily of hydrogen, carbon monoxide, carbon dioxide, and methane. Higher molecular weight hydrocarbons, commonly referred to as tars, also form during this process as undesirable byproducts and are removed in a scrubbing system. Mass balance calculations around the Thermo Chemical Process Development Unit (TCPDU) currently yield a carbon mass closure of approximately 85%. This project aimed to amass a data set that would improve the mass closure through enhanced analysis of the product gas stream and measurements from additional exit streams. The carbon mass balance was improved to 89.6% using the more comprehensive data, and the remaining carbon is attributed to accumulation within the system. A second goal was to develop an ASPEN simulation of the scrubber system. The model output was compared to experimental results with generally good agreement except for minor species. Reducing the output temperature of a heat exchanger was examined using the model, with the prediction that the concentrations of HCN and NH3 in the exit gas will decrease. Preliminary tests investigated adding biodiesel to the TCPDU as a scrubber liquid. Biodiesel was mixed with a sample of scrubber water to examine the partitioning of organics between the diesel and water phases. Using Gas Chromatograph Mass Spectrometry and Liquid Chromatography, it was determined that essentially all of the tars remained in the water phase, except for

approximately 15% of the phenol. Based on these results, biodiesel will not be added to the current scrubber configuration.

Design of Mock-up Target for the Spallation Neutron Source. *RYDER WINCK (Rice University, Houston, TX 77005) ERIC CRAIG BRADLEY (Oak Ridge National Laboratory, Oak Ridge, TN 37831).* The Spallation Neutron Source is a research facility currently under construction at Oak Ridge National Laboratory. The facility will produce neutrons by bombarding a mercury target with a beam of protons. The mercury is contained in a stainless steel vessel that must be replaced several times a year. The Mercury Target must be removed remotely due to high radiation. During Integrated System Testing, operators will practice removal and installation of the Mercury Target. A mock-up of the Mercury Target was needed to avoid potential damage to the Mercury Target that costs about one million dollars and would take months to reproduce. The objective of this project was to design a mock-up target of the real Mercury Target. A basic mock-up target existed at the start of the project. However, it differed significantly from the Mercury Target in many critical dimensions. The Mock-up Target was modified to mimic the Mercury Target in dimensions corresponding to transportation and placement. Before physically modifying the Mock-up Target, a computer aided design program, Pro/Engineer Wildfire 2.0 (Pro/E), was used to digitally model the initial Mock-up Target, compare it to the Mercury Target, and make drawings of the Mock-up Target to give to the fabricators. The Mock-up Target is considered as a "below hook lifting device" and is designed to comply with DOE Standard 1090, Section 14.2.1, which states that lifting devices must have a factor of safety of three based on the yield strength of the material. To check for this, a sub-program of Pro/E, Mechanica, was used to run finite element stress analysis on the part of the Mock-up Target that would be receiving the highest stresses. In addition to Mechanica analysis, stress calculations were done by hand. A formal stress analysis report was written to document that the Mock-up Target would comply with the DOE Standard. Although the Mock-up Target is not yet fabricated, the design is successful in that it fulfills the requirements in a safe and inexpensive way by modifying the current Mock-up Target to the proper specifications. The Mock-up Target will allow for remote handling practice that is as realistic as possible without the risk of using the million dollar Mercury Target.

An Update of Cryogenic Systems Operating Procedures. *ERROL YUKSEK (Old Dominion University, Norfolk, VA 23529) DANA ARENIUS (Thomas Jefferson National Accelerator Facility, Newport News, VA 23606).* The Cryogenic Systems Group at Thomas Jefferson National Accelerator Facility (JLab) has seen many changes to the equipment, systems, and operating procedures since their initial commissioning phases of the early 1990s. JLab's cryogenic systems include the Central Helium Liquefier (CHL), the End Station Refrigerator (ESR), the Cryogenic Test Facility (CTF), and the associated Cryogenic Distribution Systems in the Linear Accelerators (LINACS), the Experimental Halls, and the Test Lab. Because of the changes made to these systems, an update of the cryogenic operating procedures was required in order to maintain correct execution of the various transient and steady state operations. It is of great importance for large and complex operating systems, such as JLab's cryogenic systems, to maintain current operating procedures for safe, efficient, and continuous operation. Based upon a review of flow schematics, mechanical drawings, engineers' notes, inspection of systems, and observation of maintenance operations, an understanding of these systems' fundamental principles has provided enough insight and information to support revisions to the operating procedures. Once an understanding of the relevant issues had been attained, procedures which needed immediate attention and revision were identified and revised. In addition, new operating procedures were created as needed. The revised operating procedures will be available on the Cryogenic Systems Group's network drive to anyone that needs to learn how to operate the cryogenic systems.

Testing and Development of Cryogenic Radiation Detector for Superconducting Radiofrequency Cavity Field Emission Mapping. *PHILLIP ZELLNER (Virginia Polytechnic Institute and State University, Blacksburg, VA 24061) DAN DOTSON (Thomas Jefferson National Accelerator Facility, Newport News, VA 23606).* During operation and testing, Jefferson Lab's Superconducting Radiofrequency (SRF) cavities give off radiation known as field emissions. Field emissions greatly limit the efficiency and maximum output of SRF cavities. For optimum performance, sources of field emissions must be located and removed. Currently, field emission measurements are made outside the stainless steel cryogenic dewar, making them rough estimates. For effective field emission mapping, a radiation detector must be placed inside the helium dewar and be exposed to the 2 K liquid helium. As a result of much research and experimentation, a cesium iodide (CsI) detector has been selected to perform the task. The detector was calibrated and then mounted on a cryogenic test stand, pointing directly down the axis of an SRF cavity pair during routine testing. Data was then gathered from the detector and compared with the power levels and rough field emission data. While there was a correlation, more testing is needed to develop a stronger correlation for greater precision. Once this detector has been fully tested, a precise rotating apparatus must then be developed to carry an array of these detectors into the helium dewar. Data gathered from such a device could then produce a 3-D model of an SRF cavity's field emissions, making defect detection easy.

Environmental Science

An Observational Study of Guided Discovery Science & Math Activities that Promote Environmental Education. *BRANDI MILLER (California State University Fresno, Fresno, CA 93740) KATHY BARRETT (Lawrence Berkeley National Laboratory, Berkeley, CA 94720).* At the Lawrence Hall of science, where education is number one, I was able to be apart of a full summer of various observational studies of guided discovery science and math activities that promote environmental education. On a regional outreach program I assisted the Family First Health Department at Lawrence Hall of Science (LHS) introduce healthy foods to kids and parents at a local elementary school in Hayward, CA. Additionally there were stations set up to teach them about what parts of the plants we eat (fruit, seed, flower, leaf, etc), what cereals are low in sugar, small activities to get your blood pumping, and taste testing! Another approach to guided discovery learning was the summer camps, both the local day camps and overnight regional camps. Both were activity based, with science (and or math) lessons and of course some fun time! They both exhibited environmental education and both showed to be exciting and fun for the participants (and for me as well). A new approach to teaching math was taught by the Growing Learning Community at a two week workshop. This included daily (sometimes multiple) "Math in the Garden" lessons, a approach to teaching K-6 math lessons in a Garden setting, rather than the normal classroom setting and using the garden as a learning tool. We, the workshop, designed a lesson using the Japanese style of Lesson Study and implemented it on a group of kids, courtesy of the UC Berkeley Botanical Garden summer education program. Then we reworked and revised the lesson based on the data we collected and implemented the lesson again on a different group of kids to see how our revisions worked out. In all the settings described above, environmental education adds a tangible aspect to learning and the kids respond well to the new environment as well as the new approach. As one kid told another after hearing her comment of, 'Hey this is fun, I like this!' "I thought you didn't like MATH!"…she didn't realize it was math and not just an activity.

An Inter-comparison Study to Evaluate the Discrepancy in the Measurement of Air Temperature. *EMMANUEL ALABRE (NY City College of Technology, Brooklyn, NY 11201) COLIN FREDERICSON (City University of NY Brooklyn, NY 11201) MICHAEL REYNOLDS (Brookhaven National Laboratory, Upton, NY 11973).* Instruments to estimate meteorological variables have evolved with the science of meteorology. Great advances have been made, especially over the past few decades, in the speed at which meteorological variables have been collected, archived, analyzed, and used to prognosticate. For basic meteorological studies, thermometers, barometers, hygrometers, anemometers, psychrometers, and other meteorological instruments are readily available, common place, and state-of-the-art. The current suite of meteorological instruments uses sensors that are advanced enough to convert an electronic variable (voltage or resistance) into a meteorological variable. However, the accuracy of the measuring instruments has not kept pace with the rapid increase in the acquisition and use of the estimated meteorological variables. Since the climate system is sensitive to even tenths-of-a-degree change in regional temperature, for example, it is important that the meteorological variables, especially temperature, are measured accurately. This study, therefore, particularly focuses on temperature measurements that are made with modern instrumentation. Preliminary results indicate that widespread temperature discrepancies abound between the instruments, and that the differences may be directly related to the state of the atmosphere, the type of shield that is used to house the temperature sensor, and the temperature sensor's time constant.

Use of Artificial Burrows by Burrowing Owls (*Athene cunicularia*) at the HAMMER Facility on the U.S. Department of Energy Hanford Site in the Summer of 2005. *AMANDA ALEXANDER (Genesee Community College, Batavia, NY 14036) MICHAEL SACKSCHEWSKY*

(Pacific Northwest National Laboratory, Richland, WA 99352). In 2003 the U.S. Department of Energy (DOE) constructed an Emergency Vehicle Operations Course (EVOC) at the Hazardous Material Management and Emergency Response Training and Education Center (HAMMER) in the southern portion of the Hanford Site. Preliminary surveys during 2001 identified an active burrowing owl (*Athene cunicularia*) burrow and three burrowing owls within the proposed development area. Burrowing owls were classified as a federal species of concern, a Washington State "candidate" species, a WDFW priority species, and a Hanford Site Biological Resources Management Plan Level III resource. Therefore, a mitigation action plan was established that included the installation of twenty artificial burrowing owl burrows around EVOC in the spring of 2003. The mitigation plan stated that a five percent annual use in the artificial burrows by burrowing owls was to be considered a success. In July 2005 a field survey of the EVOC artificial burrow complex was conducted to determine use and demography at each burrow site. Burrow locations were mapped and signs of activity (feces, owl tracks, castings, feathers) were recorded. Out of the twenty burrows, twelve were found to be active. Of the eight inactive burrows three appeared to have been previously active during the 2005 breeding season. A total of nineteen owls were counted but demography could not be determined. It appears that the EVOC mitigation exceeded burrow use goals during 2005. Continued site monitoring and maintenance, according to mitigation plan guidelines should be conducted as prescribed.

Developing Analytical Techniques Used to Determine Potential Metabolites of the Atrazine in Complex Biological Matrices. *EMIKA ALLEN (Concordia University, Portland, OR 97211) JIM CAMPBELL (Pacific Northwest National Laboratory, Richland, WA 99352)*. Atrazine (ATR), 2-chloro-4-(ethylamino)-6-(isopropylamino) - 1, 3, 5-triazine, is the most commonly used s-triazine herbicide in the United States and Europe. However, concern is rising regarding detecting exposure in humans using noninvasive bio-monitoring techniques (i.e. saliva samples). In order to detect and quantify ATR and its metabolites, knowing how ATR metabolizes is essential. There are several publications on how ATR metabolizes; however, there is a question concerning the identification of the metabolites. For this reason, developing an analytical technique to confirm published information about the major metabolites of ATR is necessary. Before analyzing ATR, S-9 fractions consisting of rat liver microsomes were tested to determine if the enzymes were still active. Chlorpyrifos (CPF) was added to the S-9 fractions, and to simulate metabolism, they were incubated for 1 hour at 37°C. After extracting the analyte with ethyl acetate and derivatizing with N-(t-butyldimethylsilyl)-trifluoroacetamide (MTBSTFA), the samples were analyzed in order to detect the major metabolite of CPF which is 3, 5, 6-trichloro-2-pyridinol (TCP), using gas chromatography/mass spectrometry (GC/MS). Mass spectra from the derivatized CPF samples were compared with those from TCP standard samples, and the results showed that the enzymes were still active. ATR was then added to the S-9 fractions for detection of potential metabolites. The S-9 fractions were incubated for 1 hour at 37°C, extracted with ethyl acetate, and analyzed using GC/MS. Preliminary results, as indicated by a comparison of the mass spectra from the metabolized and non-metabolized ATR samples, show little or no metabolism at incubation for 1 hour for extractable materials. This means the samples either need to be derivatized to make ATR metabolites less polar and more volatile or that they never metabolized and need to be incubated for longer than 1 hour.

Identification of an *Arabidopsis thaliana* Mutant Having a T-DNA Insertion in an NIA Gene. *PETER ANTHOPOLOS (University of Tennessee, Knoxville, TN 37996) LEE E. GUNTER (Oak Ridge National Laboratory, Oak Ridge, TN 37831)*. The overarching hypothesis of this study is that a single-enzyme change affecting an important biological process (e.g., nitrate assimilation) will translate across multiple levels of biological organization to produce predictable responses at the ecosystem level. Long term plans consist of exposing wild-type (WT) and transformed *Arabidopsis thaliana* (nitrate reductase deficient or nia-) to ambient and elevated levels of atmospheric CO_2. Additionally, the competitive interaction between the WT and nia-) will be recorded at the various CO_2 levels, as will the interaction between the carbon and nitrogen cycles. The goal of the project described herein was to identify additional nia- mutants for the study. Two genes in Arabidopsis code for nitrate reductase, and the objective was to identify two classes of Arabidopsis mutants: the first class consisted of mutants having an Agrobacterium T-DNA insertion in NIA1, the first gene for nitrate reductase, and the second class consisted of mutants having an insertion in NIA2, the second gene for nitrate reductase. Each of the seed lines acquired for this project had a putative T-DNA insertion in either NIA1 or NIA2. The seeds were germinated and DNA was extracted from the seedlings. Polymerase chain reactions (PCR) were performed on the DNA using two types of primer pairs: (1) primer pairs designed to detect only the wild-type allele of NIA1 (but not NIA2) or vice versa and (2) primer pairs designed to detect only the presence of a T-DNA insertion in NIA1 (but not NIA2) or vice versa. Initial analysis was completed on three seed lines: Salk 004181 (putative insertion in NIA1), Salk 075996 (putative insertion in NIA2) and Salk 138297 (putative insertion in NIA2). Through PCR, the presence of a T-DNA insertion was confirmed in the Salk 138297 seed line and an individual homozygous for the insertion was isolated from that population. Southern blotting will be performed using DNA from Salk 138297 seedlings to ensure that no other T-DNA insertions are present in the genome, as there is a significant chance that two or more T-DNA insertions resulted from the transformation. PCR indicated that neither of the remaining two seed lines had an insertion at the specified location. The project was successful in that one of the two desired classes of mutants, i.e., the NIA2 mutant, was isolated. Additional seed lines will be tested in an ongoing effort to identify a mutant having an insertion in NIA1.

Textural Analysis of High-Resolution Imagery for Classifying Shrub Canopy Cover on the Hanford Site. *SAMUEL BADER (Southern Nazarene University, Bethany, OK 73008) JERRY TAGESTAD (Pacific Northwest National Laboratory, Richland, WA 99352)*. Sagebrush (*Artemisia spp.*) ecosystems once dominated much of the western part of North America, but millions of hectares have been degraded, fragmented, or lost due to human activity. The loss of sagebrush habitat has large impacts for populations of many sagebrush obligate wildlife species. Land managers need methods to quantify and monitor the shrub canopy cover for the sagebrush ecosystems that remain. Current methods of relating semi-arid shrub canopy cover and/or density to spectral variables derived from remote sensing imagery have varied in success. Textural analysis has advantages over traditional spectral-based classification because it produces a consistent histogram from which a threshold can be chosen relating to shrub objects in imagery. It also aids in equalizing variations in background brightness making shrub objects more distinguishable. Models were developed to map shrub canopy cover on the U.S. Department of Energy's Hanford site, located north of Richland, WA using percent canopy cover measured on 100 m^2 plots located throughout the Site and image analysis of aerial photography. Common shrub species on the site include big sagebrush (*Artemisia tridentata*), gray rabbitbrush (*Ericameria nauseosa*), green rabbitbrush (*Chrysothamnus viscidiflorus*), bitterbrush (*Purshia tridentata*), and spiny hopsage (*Grayia spinosa*). Canopy cover was mapped by applying a texture model to high-resolution aerial photos (.29 m) taken May 1, 2002. Results of the texture model were degraded to 5 m to provide a more realistic scale for percent shrub canopy cover assessment. Accuracy assessment of 48 plots yielded an $R^2 = .70$. Despite difficulties encountered because of poor geo-referencing on sections of the imagery as well as a field data collection methodology designed for a different type of study, textural analysis appears to be successful for accurately classifying shrub canopy cover. Better geo-referenced imagery and field data collection designed for this type of study would likely give a better and more realistic display of the efficacy of textural analysis to classify shrub canopy cover from remotely sensed imagery.

Analysis of HYSPLIT Computed Particle Trajectories Using Data Acquired by. *LESLIE BARAN (Northern Illinois University, DeKalb, IL 60115) CARL BERKOWITZ (Pacific Northwest National Laboratory, Richland, WA 99352)*. In July 2005, scientists from Pacific Northwest National Laboratory, Texas A&M University and the University of Massachusetts, Amherst conducted the Southeast Texas Transport Study of the pollution plume originating at the Houston Ship Channel in Houston, TX. The study had many goals, one of which was assessing how accurately models depicted the plume as it traveled across eastern Texas. Using specially designed controlled altitude balloons to tag the plume and a Twin Otter research aircraft loaded with equipment used to measure the pollutants, the composition and transport of the plume could be monitored. The balloon recorded wind speed, wind direction, GPS location, temperature and other meteorological data. Using the GPS location recorded by the balloon, trajectories were made of the path of the balloon. These "real" trajectories were compared to Hybrid Single-Particle Lagrangian Integrated Trajectory (HYSPLIT) computed trajectories generated before each flight. Models for the HYSPLIT trajectories used in making the trajectories were the Final (FNL) Global Data Assimilation System (GDAS) and the Eta Data Assimilation System (EDAS 40km). It was discovered that despite its lower spatial resolution (191 km as opposed to 40 km), the HYSPLIT

trajectories produced by the FNL forecasted the path of the balloons more accurately than EDAS.

Measuring Algal Biomass and Rate of Growth by Chlorophyll Fluorescence. *ADAM BARLEV (Contra Costa College, San Pablo, CA 94806) WILL STRINGFELLOW (Lawrence Berkeley National Laboratory, Berkeley, CA 94720).* Nitrate contamination of water is a growing problem. Nitrates cause the eutrophication of rivers, wetlands, estuaries, and bays. Nitrate is a serious threat to groundwater, particularly in the west. The primary source of nitrates in the environment is agricultural activity. Currently agricultural runoff isn' t treated before entering the environment. The most cost effective method for treating nitrate is biological denitrification. However, all denitrification bioreactors currently in operation use an added carbon source or fuel that must later be removed at added expense. A methane fueled denitrification bioreactor is advantageous because methane is inexpensive and methane is easily removed from the treated water. We hypothesized that methane could be used to fuel biological denitrification. A Bioreactor was constructed and inoculated with bacterial communities from wetland sediments high in nitrate and low in oxygen. Methane was added and a simulated nitrate-polluted groundwater was prepared and introduced into the bioreactor. The nitrate concentration was measured daily by UV spectrophotometry. Gasses given off by the bioreactor were monitored by gas chromatography. The bioreactor was monitored for the growth of the biomass responsible for denitrification. The turbidity of the effluent, as measured by absorbance at 590 nm, provided a measure of suspended bacterial biomass. The bioreactor was effective for removing nitrate. Initial concentrations of 23.75 ppm nitrate-nitrogen were reduced to less than 0.1 ppm. However, the initial rate of denitrification was insufficient for large scale application. To increase the denitrification rate, several attempts were made at increasing the biomass concentration in the bioreactor. The bioreactor was spiked with methanol, trace metals and yeast extract. All of these overtures failed to induce the accumulation of biomass. While the idea of methane fueled denitrification seems promising, the suspended growth bioreactor had shortcomings. Growth of a bacterial film on the tubing and walls of the apparatus indicates a fixed-film bioreactor might be a more effective design. To transform the bioreactor into a fixed-film design, high surface area pall rings could be added to the main reaction chamber.

Polymer Recovery from Automobile Shredder Residue: Separation Techniques and Analysis. *RYAN BEAMS (Wheaton College, Wheaton, IL 60187) BASSAM JODY (Argonne National Laboratory, Argonne, IL 60439).* Increasing costs of waste disposal combined with rising prices for virgin materials has caused recycling of discarded materials to become an important alternative. Obsolete automobiles are among the major sources of recyclable materials, contributing 14.5 million tons of steal from North America in 2003 alone, due to the high content of valuable metals and plastics. Recovery of the plastics after removal of the metals from the remaining automobile shredder residue (ASR) involves more complicated techniques for recovery and analysis. By using the polymers' characteristics, such as density and hydrophobicity, chemical separation techniques can be developed to create pure fractions of polymers. Acylonitrile butadiene styrene (ABS), polystyrene, polypropylene, polyethylene, and polycarbonate are among the target polymers for recovery. Separation conditions are tested in the laboratory and analyzed using spectroscopy and wet chemistry. Solution conditions are then tested on a large scale separation at the pilot plant on site. Successful separation and analysis has been demonstrated for a variety of ASR materials as well as electronics residue.

An Intercomparison of Particulate Samplers Used on the Hanford Site. *KATHERINE BEEM (Susquehanna University, Selinsgrove, PA 17870) BRAD FRITZ (Pacific Northwest National Laboratory, Richland, WA 99352).* The National Ambient Air Quality Standards set by the U.S. Environmental Protection Agency (EPA) include airborne particulate matter as a criteria pollutant. Correctly measuring the concentration of particulate in ambient air is important for regulatory compliance in addition to health concerns related to particulate matter. Particulate measurements are made with a variety of instruments because of cost, availability, or the type of measurement that is being made. Measurements made with different types of instruments can vary considerably making it important to know how well results from different instruments relate to one another. Measurements at the Hanford Site in Richland, Washington, were used to compare of several different instruments. The instruments used to take measurements include TEOM series 1400a, E-BAM, MiniVols, a 2-inch open-faced medium volume sampler, and a 4-inch open-faced high volume sampler. The TEOM and E-BAM show a very strong linear correlation while the MiniVol demonstrated no correlation with the other instruments that were used. The 2-inch open-faced and 4-inch open-faced TSP samplers had comparable measurements. Measurements of TSP with the 2-inch open-faced sampler correlated very well to TEOM PM10 measurements indicating TSP at Hanford is composed mostly of PM10.

Assessment of Mercury Deposition from a Coal-Fired Power Plant in Texas. *ALVERTIS BOYD (Miles College, Birmingham, AL 35227) LATOYA FEAGIN (Miles College, Fairfield, AL, 35604) TERRY SULLIVAN (Brookhaven National Laboratory, Upton, NY 11973).* Mercury is known to be an environmental toxicant. Elemental mercury dispersed into the atmosphere during burning/mining of coal is reported to accumulate in the soil and vegetation. The mercury, when transformed to organic mercury, poses health risks for the humans and the surrounding wildlife. In March 2005, the EPA created new allowances and standards for mercury emissions in coal-fired power plants. A site in Texas, near to a power plant that burns lignite coal was chosen for assessment studies of mercury in surrounding soils and vegetation. About 100 public property locations near the power plant were sampled. Using Geographical Positioning System (GPS), these specific sampling sites were chosen and soil and vegetation sampling carried out within a ten-mile radius of the power plant. A total of 514 samples were collected that included surface soIL vegetation and soil taken from a depth of about 10 cm from surface. To assess the predicted mercury deposition pattern, an atmospheric dispersion model was used and directional wind and rainfall amounts on an hourly basis were taken into account. A comparison of modeled and measured data will be made after the samples were sent back to Brookhaven National Laboratory. Total mercury analysis of the samples is being accomplished through thermal processing of the samples using the DMA-80 (Direct Mercury Analyzer, Milestone Inc.). A specific amount of the soil sample is weighed and loaded in an auto sampler. The samples are sequentially decomposed at 750°C, converted to elemental mercury in a catalytic converter (600°C) and finally desorbed as elemental mercury in an atomic absorption sample tube. For the surface soils the maximum moisture on a dry basis for mercury concentration was 111.4 ng/g, while the minimum moisture was 7.6 ng/g. The average of the moisture data was calculated as 33.5 ng/g. The data was analyzed to determine if elevated levels of mercury occur near the power plant. The interpretation of the data showed that there was no evidence of a 'hot spot', a large area of mercury concentrations compared to background.

Semi-quantification of Holocene-age Columbia River Sediments From the Hanford Reach Using X-ray Diffraction (XRD) and Comparison to Modern Columbia River Sediment. *BARBARA BURKHOLDER (Texas Christian University, Fort Worth, TX 76129) H. TODD SCHAEF (Pacific Northwest National Laboratory, Richland, WA 99352).* The discovery of an extensive network of Holocene-age Columbia River fluvial terraces and bedforms within the Hanford Reach of south-central Washington has opened the question of whether sediments eroded and deposited by the Columbia River over the past 10,000 years have significantly changed. Fifty-eight Holocene-age Columbia River sediment samples were collected from major fluvial terraces and point bars within the Hanford Reach, the last "free-flowing" segment of the Columbia River. Bulk and clay fractions of these samples were analyzed for mineralogical components and their corresponding relative abundances using X-ray diffraction (XRD). The bulk of the Holocene-age sediments is primarily composed of quartz and sodium-rich plagioclase feldspar, composing approximately 28 wt-% and 22 wt-%, respectively. Smectite and illite dominate the clay fraction, with abundances averaging around 42 wt-% and 38 wt-%, respectively. The presence of sodium-rich plagioclase and illite suggests the sediments may have originated in a plutonic or metamorphic environment, such as the Northern Cascades. Overall, the Holocene-age sediments were comparable to sediments presently being deposited by the Columbia River, suggesting the fluvial processes influencing the Columbia River today are similar to processes that influenced it over the past 10,000 years.

Acclimation Period and Effect on Temperature and Light Response in *Populus grandidentata and Betula alleghaniensis* Grown in Three Temperature Regimes. *CHRISTINA CAMPION (Rhodes College, Memphis, TN 38112) CARLA GUNDERSON (Oak Ridge National Laboratory, Oak Ridge, TN 37831).* Rising concentrations of atmospheric carbon dioxide are projected to increase global air temperatures by 1 to 4.5°C in the next century. If modern ecosystems are to remain unchanged through such rapid climatic warming, it is necessary that plants be able to physiologically acclimate to said increases in growth temperature. To investigate whether species differences in temperature response or adjustment are important to modeling photosynthetic and other responses to warming climates,

four deciduous tree species (*Quercus alba, Betula alleghaniensis, Liquidambar styraciflua, and Populus grandidentata*), have been grown for four years in replicated open-top chambers with three separate temperature treatments: ambient air temperature (A), 2°C above ambient (E^2), and 4°C above ambient (E4). These species were selected in order to study the responses of deciduous trees to atmospheric warming as most acclimation research has focused on coniferous or other evergreen trees. Photosynthetic temperature response curves were collected from *P. grandidentata* and *B. alleghaniensis*. Optimal temperatures (Top+) were then determined and compared statistically with air and soil temperature history for each chamber. Experimental Topt were then compared with meteorological data collected by chamber. In *P. grandidentata*, evidence from 2004 and 2005 indicated an acclimation to daytime average temperature of the preceding 2.5 days. Data from B. *alleghaniensis* in 2003 and 2004 indicated a faster response of 1.5 days, indicating higher fitness as well as complete acclimation. Light response curves in *P. grandidentata* and *B. alleghaniensis*, taken in the A and E4 treatments, showed no significant difference in light compensation point, quantum yield, or rate at saturating light accompanying the temperature acclimation. Knowledge of the acclimation of photosynthesis to temperature allows predictions to be made concerning the future composition of forests and the chances that, specifically, these two species will survive given a moderate rise in temperature.

The Use of Agricultural Modeling to Predict the Potential Supply of Biomass Feedstocks over the Next Ten Years and to Describe Economic Impacts. *BENJAMIN CLEMENS (University of Virginia, Charlottesville, VA 22904) BOB PERLACK (Oak Ridge National Laboratory, Oak Ridge, TN 37831).* As the price of oil continues to increase, the United States government is increasingly looking to alternative fuel sources to replace crude oil demand. Though hydrogen power shows great promise in the future, many analysts believe that more immediate solutions are required. One possibility to bridge this energy gap is the use of biofuels, which are refined from products ranging from corn grain to specially harvested grasses made specifically for energy use. A considerable amount of biomass feedstock is currently available, and more could become available depending on government pricing programs and advances in technology. Modeling of the results shows that the availability of cellulosic biomass feedstocks such as switchgrass, corn stover, and wheat straw is highly dependent on yield and price. Using current technology and tillage practices, 200 million dry tons of cellulosic residue could be harvested at a farmgate price of $50/dry ton by 2014. These two sources alone could replace as much as 12% of gasoline demand, providing a clean, domestic alternative to foreign oil. Regional analysis shows that regions that can produce corn stover closely mirror the largest corn-producing regions, while switchgrass production will be centered on the Mississippi River Valley, the Great Plains, and the Southeast coast. Crop residues can be profitably harvested at prices as low as $30/dry ton, while switchgrass must compete with conventional crops for acreage, and therefore does not displace a significant amount of cropland below prices of $40/dry ton. Increased acreage of switchgrass would lead to a uniform rise in the prices of major crops, resulting in a substantial increase in net returns at the same time that government payments decline. This reduction in payments allows the government to borrow against future savings to subsidize switchgrass startup expenses, a necessary incentive given the high cost of beginning switchgrass crops. Current ethanol plant technology cannot keep up with the forecasted increase in production, so new ethanol plants must be built with the ability to process cellulosic biomass.

Goodness Glacious: Demonstrating Glacial Mass Balance and Flow in the Classroom. *JENA DAVIS (Brigham Young University Idaho, Rexburg, ID 83440) MITCH PLUMMER (Idaho National Laboratory, Idaho Falls, ID 83415).* Glaciers are a dramatic display of nature's forces and are increasingly a world wide indicator of global warming. To illustrate not only how glaciers help to carve and shape mountains, but also how they function and respond to climate, we have developed an inquiry-based learning unit which includes three recently developed hands-on activities and computer animations which describe the mechanics of glaciers. The first of these is simulating a glacier by making plaster flow in an open channel. The principal goal of this exercise is to illustrate how plaster flow acts to produce a variety of common glacial features, like crevasses, moraines, and piedmont lobes. One of the shortcomings of such a presentation however, is that it gives a misleading sense of glacier mechanics. In our second demonstration, we focus on the mass balance of glaciers, how and why they respond to climate change and how they can reach a steady-state condition. This includes a hands-on demonstration of the steady state process in which students are the accumulators and ablators of a mountain basin and "ice" blocks are the flowing ice. By changing the rates at which students add or remove "ice" blocks from their position in the valley, we illustrate how the ice mass can reach steady state and respond to climate change. Finally, we relate the concepts presented in the classroom to research on past and present glaciers using a series of animations of digitally simulated glaciers using a 2-D glacial model that simulates the advance and recession of glaciers to climate change. Simulations include growth of the last maximum glacial surge in the Tetons, the Sierra Nevada and the Wind River Ranges. Simulations also include illustrating advance or recession of modern glaciers in the Tetons and in the Mount Saint Helens crater. With these new hands-on activities and animations, students will better understand the physics and mechanics of glaciers while being able to recognize glacial structures and consequences in the world around them.

Understory Composition of the Long Island Pine Barrens. *MIRANDA DAVIS (Binghamton University, Binghamton, NY 12159) TIM GREEN (Brookhaven National Laboratory, Upton, NY 11973).* The Pine Barrens of Long Island is a unique community that must be properly managed in order to preserve the diverse array of flora and fauna it supports. Without management involving prescribed burnings it is likely that the Pine Barrens will disappear through natural succession leading to an oak-based climax community. In general the Pine Barrens are dominated by *Pinus rigida* and other shrub species that are believed to be facilitated by regular burning; however, very few studies have been conducted in this area. In order to better understand this sequence of succession and the importance of this community, we have studied the vegetational composition of the under-story in both pine and oak-based communities on Long Island. By examining random plots within both forest types we calculated the percent composition of different plant species and a diversity index for the under-story of both oak and pine-based forests. While both communities have a shrub layer dominated by the same species (*Gaylussacia baccata, Vaccinium palidum, and Quercus ilicifolia*) and have similar levels of diversity, we found that the relative proportions of these species differ between the forest types. Results illustrated the vegetational differences between these two distinct communities, which may be critical to the survival of the diverse fauna the Pine Barrens are known for.

Particulate Carbon and Gas/Particle Partitioning of Aromatic Hydrocarbons in Seattle. *JEFF DUARTE (Shasta Community College, Redding, CA 96001) LARA A. GUNDEL (Lawrence Berkeley National Laboratory, Berkeley, CA 94720).* A correlation between airborne particulate pollutants and increasing counts of respiratory and circulatory illness has the U.S. Environmental Protection Agency searching for accurate methods of assessing human exposure to particulate carbon. Depending on location, particulate carbon makes up 30-50% of the total particulate mass in the atmosphere. Using the integrated organic gas and particle sampler (IOGAPS), this study seeks to minimize sampling artifacts and to find a relationship between organic and elemental carbon (OC and EC) and polycyclic aromatic hydrocarbon (PAH) concentrations as an approach to particulate carbon exposure determination.It was found that the hypothesis was supported by the data: without a denuder in the sampling method pathway to separate/collect SVOC (semi-volatile compounds), sampling artifacts formed which complicated the research.

Urban Dispersion Program, Looking Forward to a Better Understanding of Air Flow Contamination and Transportation in Urban Environments. *RAMON FERNANDEZ GARCIA (Bronx Community College, Bronx, NY 10453) JOHN HEISER (Brookhaven National Laboratory, Upton, NY 11973).* The Urban Dispersion Program was developed by the U.S. Department of Homeland Security with additional support from the U.S. Department of Defense – Defense Threat Reduction Agency, the U.S. Department of Energy, and the U.S. Environmental Protection Agency. The primary objective of this four-year (2004-2007) program is to enhance NYC's emergency response capabilities following a chemical release. This program will release tracers in the urban canyon areas of NYC and collect air samples in the area, roughly 4 square kilometers. The portable samplers will be placed in and out of the study area to collect samples of the tracer tagged air. The release systems will be releasing a safe, inert tracer gas into the air to tag the air so that the movement of the air can be followed as it travels through the city. These gases can be perceived at units of femtoliter/liter the same as parts per quadrillion or 10-15. The portable samplers to be used in these projects are the "Brookhaven Atmospheric Tracer Samplers" (BATS) and "Capillary Atmospheric Tracer Samplers" (CATS). Later the gases collected by these samples are desorbed into a gas chromatograph, which analyses the tracers in the air samples and gives us the information of where the tracers "per- fluorocarbons"

traveled. There was an experiment conducted around Madison Square Garden in March of 2005. This data set should provide very accurate knowledge of how the air behaves in and around this area of NYC as well as within building interiors. Two more intensive projects using PFT's are planned for August 2005 and April 2006.

Home Range Size and Spatial Ecology of Eastern Hognose Snakes (*Heterodon platirhinos*). *WENDY FINN (University of Rhode Island, Kingston, RI 02872) JEREMY FEINBERG (Brookhaven National Laboratory, Upton, NY 11973).* Once considered an abundant species on Long Island the eastern hognose snake, *Heterodon platirhinos*, is now found only in small fragmented portions of the species former range. After 1996, *H. platirhinos* was incorrectly believed to be extirpated from Long Island as there were no sightings of the species until 2001 when the species was rediscovered again at Brookhaven National Laboratory (BNL). Since the spring of 2003, radio telemetry studies have been conducted at BNL on *H. platirhinos* to learn more about the factors triggering this species decline. In this study, radio telemetry was utilized to discover more information about the snakes' habitat preferences, mortality rates, and home range sizes. The study consisted of eight snakes that were tracked and monitored daily with the use of GPS/GIS. Aside from tracking, snout vent length, total length measurements and weights were recorded opportunistically to obtain data on growth rates and possible nesting behavior in the snakes. Snakes were active on 67% of days tracked during a portion of the activity season for the species. Preliminary data collected for home ranges displays a maximum home range of 10.7 ha for SN30 with the a minimum size of 0.4 ha for SN41. The data collected from this study will be used to further enhance the conservation of this Special Concern status species.

Health Based Provisional Advisory Levels for the Initial Study of Contaminants In Drinking Water and Air: Acute, Short Term, and Long Term Exposures. *DANIEL FRANCIES (Estrella Mountain Community College, Avondale, AZ 85323) MARGARET MACDONELL (Argonne National Laboratory, Argonne, IL 60439).* The U.S. Environmental Protection Agency (EPA) is developing PALs (provisional advisory levels) which are health based exposure levels for contaminants that terrorists could release into buildings, drinking water supplies, or the air. The PALs are for industrial chemicals, poisons, biological agents/biotoxins, and radionuclides that could be obtained and released by terrorist organizations. The EAD (Environmental Assessment Division) is working with the EPA in developing these PALs so the world can be prepared by knowing how to deal with a future contaminant release. Each contaminant must be assessed accurately, and in developing the PALs scientist research all studies, experiments, and exposures related to a specific contaminant. The PAL must address the toxicodynamics and toxicokinetics of the contaminant and consider acute and short term studies, longer duration studies, and acute lethality studies. The information is then assessed and evaluated in developing a concentration level that the population can consume without significant side effects; if there are side effects they need to be reversible and full recovery needs to take place.

An Inter-comparison Study to Evaluate the Discrepancy in the Measurement of Air Temperature. *COLIN FREDERICSON (City University of New York, Brooklyn, NY 11201) MICHAEL REYNOLDS (Brookhaven National Laboratory, Upton, NY 11973).* Instruments to estimate meteorological variables have evolved with the science of meteorology. Great advances have been made, especially over the past few decades, in the speed at which meteorological variables have been collected, archived, analyzed, and used to prognosticate. For basic meteorological studies, thermometers, barometers, hygrometers, anemometers, psychrometers, and other meteorological instruments are readily available, common place, and state-of-the-art. The current suite of meteorological instruments uses sensors that are advanced enough to convert an electronic variable (voltage or resistance) into a meteorological variable. However, the accuracy of the measuring instruments has not kept pace with the rapid increase in the acquisition and use of the estimated meteorological variables. Since the climate system is sensitive to even tenths-of-a-degree change in regional temperature, for example, it is important that the meteorological variables, especially temperature, are measured accurately. This study, therefore, particularly focuses on temperature measurements that are made with modern instrumentation. Preliminary results indicate that widespread temperature discrepancies abound between the instruments, and that the differences may be directly related to the state of the atmosphere, the type of shield that is used to house the temperature sensor, and the temperature sensor's time constant.

Diversity of Ammonia Monooxygenase (amoA) Genes in Groundwater Treated with Urea to Promote Calcite Precipitation. *STEPHANIE FREEMAN (University of Arizona, Tucson, AZ 85721) YOSHIKO FUJITA (Idaho National Laboratory, Idaho Falls, ID 83415).* The diversity of the ammonia monooxygenase (amoA) gene found in DNA isolated from groundwater was characterized by amplification of amoA DNA using polymerase chain reaction (PCR), Restriction Fragment Length Polymorphism (RFLP), and sequencing. The amoA gene is characteristic to nitrosifying bacterIA such as ammonia oxidizing bacteria (AOB). The DNA extracts were derived from an experiment where dilute molasses and urea were sequentially inserted through a well into the Eastern Snake River Plain Aquifer (ESRPA) to examine whether such amendments could stimulate enhanced ureolytic activity. The hydrolysis of urea into ammonium and carbonate serves as the basis for a potential remediation technique for trace metals and radionuclide contaminants that co-precipitate in calcite. The ammonium ion resulting from ureolysis can promote the growth of AOB. The goal of this work was to investigate the effectiveness of primers designed for quantitative PCR and to evaluate the effect of urea additions upon the population diversity of groundwater AOB. PCR primers designed to target a portion of the amoA gene were used to amplify amoA gene sequences in the groundwater DNA extracts. Following PCR, amplified gene products were cloned into vectors and then transformed into competent *Escherichia coli* cells, after which, colonies containing unique gene sequences were isolated. Sequences were analyzed by RFLP, a DNA restriction technique that can distinguish different DNA sequences, to gauge the initial diversity and unique clones were subjected to DNA sequencing. Initial sequencing results suggest that the primers were successful at specific detection of amoA sequences and the RFLP analyses suggested that the diversity of amoA sequences in the ESRPA decreased with the additions of molasses and urea.

Zinc-Induced Sulfur Speciation in Plants as Determined by XANES Spectroscopy. *DAVID FRUMBERG (Cornell University, Ithaca, NY 14853) JENNY HUANG (Cornell University, Ithaca, NY 14853) MARK FUHRMANN (Brookhaven National Laboratory, Upton, NY 11973).* In order to establish the allocation of metals within plants, speciation of coordinated compounds to metals must be determined. Sulfur, an integral element to plant chemistry, exists as various species in plants and soils and coordinates with different metal species. To determine the extent that metal exposure affects S speciation, samples of *Thlaspi arvense* and *Brassica* rapa and their soils were examined. Plants were grown in natural potting soil for two weeks, and then 2600 µg and 5200 µg aliquots of zinc acetate were added to soils. Plants were allowed seven days for accumulation whereupon samples for roots, leaves, and soil underwent X-ray absorption spectroscopy (XAS) at beamline X-15B at the National Synchrotron Light Source. K-absorption edges for S standards were determined by X-ray absorption near-edge spectroscopy (XANES) between 2472 eV and 2481 eV to assess changes in S speciation in roots and leaves. An intermediate peak was observed at 2475 eV at different concentrations in the roots of both plants, suggesting systematic differences in the biochemical processing of S. In response to Zn exposure, all plants showed a systematic increase in sulfate at 2481 eV. The lack of any change in reduced species of leaves confirms that only sulfate is transported by vascular tissue. Knowing how a plant exposed to metals may respond can provide insight to more effective accumulation of contaminants from soils (phytoremediation). This knowledge can also substantiate the impact of metal accumulation on humans, via our consumption of plants affected by S-containing agricultural fertilizers and compounds.

Evaluating the Effects of Tailwater Irrigation on Soil Salinity and Discharge Water Quality. *HEATHER GRAHAM (Occidental College, Los Angeles, CA 90041) NIGEL WT QUINN (Lawrence Berkeley National Laboratory, Berkeley, CA 94720).* Inorganic salts are a natural component of soil that arise during the process of geologic erosion. Typically, rainwater naturally leaches salts into lower portions of the soil profile. However, in arid regions such as the San Joaquin River Basin of California lack of rainfall and climatic conditions increase surface evaporation and upward capillary flow resulting in reduced leaching. The geologic composition of this area causes both the soil and surface water to be saline. Because of this, agricultural runoff is highly saline and detrimental to receiving water bodies. The excess salt in water can harm aquatic organisms and cause problems for downstream users. State regulations limit the amount of salts that agricultural users are permitted to discharge into receiving waters. In order to comply with these regulations irrigation districts are exploring techniques and technologies that can improve drain water quality without increasing soil salinity. This study examines the use of agricultural runoff or 'tailwater' as an irrigation water source. Four sites were chosen within

the Patterson Irrigation District in the San Joaquin River Basin that have similar irrigation, surface drainage and crop histories but different water sources of varying quality one of which is tailwater. An EM salinity survey of each field revealed that while irrigation water is generally proportional to soil salinity other factors were affecting the salt level. A field receiving irrigation water 27% more saline than another had the same soil salinity but likely had better subsurface drainage. Flow and EC data at the drain site into the river before and after implementation of the tailwater recovery system indicated a 47% decrease in salt discharge into the river. This study suggests that with proper drainage and soil management tailwater can be used as a source of irrigation water. Tailwater recycling also decreases quantity of discharge water as well as improving the overall quality.

A Study of the Age Class Structure of *Quercus alba, Quercus coccinea* and *Quercus velutina:* A Comparative Analysis of Quercus Species Reproduction as an Indicator of Forest Succession within the Long Island Pine Barrens Core Area. *KATHRYN GUTLEBER (Connecticut College, New London, CT 06320) TIMOTHY GREEN (Brookhaven National Laboratory, Upton, NY 11973).* Investigation of the age class structure of Quercus species within the Long Island Pine Barrens Core Area is an important aspect of monitoring the health of the Pine Barrens. The reproduction of *Quercus alba, Quercus coccinea* and *Quercus velutina* is a primary indicator of the possibility of the successional change from a pine to an oak dominated forest. The rates of reproduction for *Quercus alba, Quercus coccinea* and *Quercus velutina* can also be used to foresee the possible dominance of one particular Quercus species in forest succession. By comparing the numbers of seedlings, saplings and mature trees, the success of reproduction for these three different Quercus species was analyzed. The numbers of seedlings and saplings were recorded through the use of four two-meter wide belt transects within sixteen by twenty-five meter plots. These plots were located within the Pine Barrens subtargets of Pitch Pine, Pine-Oak, Oak-Pine and Coastal Oak forests. The number of mature trees was recorded within these same plots. This study found the success of reproduction of *Quercus alba*, *Quercus coccinea* and *Quercus velutina* within Pitch Pine, Pine-Oak, Oak-Pine and Coastal Oak forests to be relatively low. Within the four different forest communities surveyed, *Quercus alba, Quercus coccinea* and *Quercus velutina* all displayed a low number of saplings, indicating that current reproduction of these Quercus species is not very successful. No one Quercus species was repeatedly more successful in reproduction than any other. There are several factors that may influence this trend, including exposure to light, levels of litter and duff, and deer browse. Although the current levels of reproduction for Quercus species are relatively low, they still remain an important indicator of forest succession from pine to oak dominated forests, and need to be continually monitored within the Long Island Pine Barrens Core Area.

Improving the Accuracy of Real-Time Black Carbon Measurements. *OLIVIA HAESLOOP (Yale University, New Haven, CT 06520) THOMAS KIRCHSTETTER (Lawrence Berkeley National Laboratory, Berkeley, CA 94720).* In order to better understand the health and climate impacts of aerosol black carbon (BC), this project began calibration of the aethelometer, the most widely used instrument for real-time BC measurements. The aethelometer measures light attenuation (ATN) through a filter upon which aerosols are collected, then calculates the amount of BC using the equation BC = ATN/σ, where σ is the attenuation coefficient, given by the manufacturer as16.6 m^2/g (at 880 nm). Recent studies, however, raise doubt that σ is constant but rather support a calibration of σ as a decreasing function of particle loading. Initial tasks carried out in this project to improve BC measurements were the assessment of a filter effect on apparent measured absorption and the assessment of the aethelometer given a source of pure BC. To study the filter effect, flame samples were collected from a constant, highly stable inverted flame using four filter lots. No apparent difference was found between filter lots. Subsequently, to assess the aethelometer given a BC source only, one filter lot collected samples from the steady flame and was compared to the readings taken in parallel by the aethelometer. Initial filter data confirms a steady BC output by the flame while the aethelometer shows a cyclical decrease of BC due to the incorrect calibration. Further study is necessary to quantify the relationship between ATN and BC, as well as future experiments evaluating the aethelometer in the presence of mixed aerosol sources and diesel emissions.

Population Survey and Analysis of Banded Sunfish in Zeke's Pond. *KATIE HEISER (Lafayette College, Easton, PA 18042) TIMOTHY GREEN (Brookhaven National Laboratory, Upton, NY 11973).* Banded sunfish (*Enneacanthus obesus*) are listed in New York State as a threatened species. During the Peconic River restoration at Brookhaven National Laboratory, approximately 200 Banded Sunfish were relocated to Zeke's Pond in an effort to conserve the population. Although the pond originally had a native population of Banded Sunfish, it is thought that they were nearly eradicated when it evaporated to a mere puddle in 2002. An accurate survey and assessment of the population is now needed to determine the success of the conservation project. Therefore, seine nets were used to sample sections of the population. From these samples, a population density in the pond was determined and a total population was estimated. Approximately 1,200 Banded sunfish were surveyed and released back into the pond. Different regions of the pond were sampled in an effort to minimize sampling error. This random sampling seemed to show that the population was relatively evenly distributed throughout the pond. The health and reproductive success of the fish was also assessed. The standard length of the fish was determined before they were released. With this information, the average size and age of the population can be continually surveyed and monitored. Since the sunfish have very few predators in Zeke's pond, they have been able to reproduce rapidly. This rapid reproduction has greatly increased the population size. Conservative estimates place the population at well over 100,000 Banded Sunfish. Since the population has grown so much, the average length of the population has shifted to under 40 mm. The youngest size class has clearly become the largest. With such success in the first years after relocating the fish, it is likely that they will continue to do well in Zeke's pond. It is hopeful that some of the population can be reintroduced into the Peconic River following the restoration project.

Analysis of the San Joaquin River: An Example of Techniques and Parameters Used in Assessing Levels of Water Quality. *KATHLEEN HUTCHISON (University of Rochester, Rochester, NY 14627) WILLIAM T. STRINGFELLOW (Lawrence Berkeley National Laboratory, Berkeley, CA 94720).* It is important to be able to quantify water quality in order to talk about and set goals for impaired water bodies. However, water quality remains difficult to define, and the important aspects of the quality of a given water body changes from case to case. One fundamental component unfailingly taken into consideration is the effect on aquatic life. An example of a water body classified as impaired is the San Joaquin River (SJR), which is cited for its critically low dissolved oxygen (DO) levels. The DO sag has harmfully impacted Chinook salmon in the area. Large blooms of algae upstream of the Stockton Deep Water Ship Channel are believed to be related to the significantly low DO levels. In this study, six parameters related to algal growth and water quality are measured at 20 sites along the SJR and its tributaries, and a water quality ranking of the different sites is produced. The result is that a clearer picture of relative areas of water quality can be better deciphered, and some sites in particular are prioritized for further study.

Abstract Evaluation of Canopy Estimation Techniques Used in Monitoring the Central Pine Barrens of Long Island. *MATTHEW KULL (Binghamton University, Binghamton, NY 13902) TIMOTHY GREEN (Brookhaven National Laboratory, Upton, NY 11973).* The Central Pine Barrens of Long Island is an important and unique region of an ecosystem of which little is known. Due to anthropogenic disturbance, however, there is an ever-decreasing amount of this important community type. The Central Pine Barrens of Long Island is instrumental for maintaining a proper functioning aquifer essential for Long Island and thus merits study. A baseline index for the Pine Barrens is currently underway, but the effectiveness and accuracy of the protocol used is unknown. One of the most important parts of scientific endeavors is maintaining repeatability. I evaluated the densitometer measurements to check for accuracy and repeatability, using repeated plots to highlight both. The repeated plots demonstrated possible problems in terms of repeatability and accuracy, having large differences between the first and second data sets. The data also showed large discrepancies between the measured densitometer readings and visual estimation, indicative of inaccuracies most likely from observer bias. The purpose of using the densitometer is to have a more accurate measurement than estimation, but if the densitometer is not accurate this can cause problems with naming the community type and may merit amending the Protocols.

Analysis of Radionuclide Adsorption onto Bauxsol™ "Red Mud" in Simulated Hanford Ground Water. *CAITLIN LABRIE (Gonzaga University, Spokane, WA 99258) JEFF SERNE (Pacific Northwest National Laboratory, Richland, WA 99352).* The efficacy of uranium-238 and other radionuclide removal by two types of Bauxsol™ (red mud) material in simulated Hanford groundwater at differing pH was studied in order to ascertain its effectiveness as a remediation method for radionuclide contaminated groundwater. Batch adsorption experiments using simulated groundwater were performed with A2

SC Bauxsol™ (red mud neutralized with sea water) and Activated SC Bauxsol™ which had been further treated with ferric sulfate ($Fe_2(SO_4)_3$) · $7H_20$). Five different concentrations of uranium-238, technetium-99, iodine-129, and chromium (VI) were spiked into groundwater and then contacted with each Bauxsol type for 24 hrs. The 5 uranium trials were also run at pHs ranging from 6.6 to 9.6. Results showed no uptake for Tc (as pertechnetate [TcO_4-], I as iodide [I-], or Cr as chromate [CrO_4^2-]. Uptake of uranium onto Activated Bauxsol™ decreased as pH increased, and for A2 SC Bauxsol the uptake formed a "U" shaped distribution with the least uptake at approximetly pH 8.3. A leachability test found that uranium attachment to Activated Bauxsol™ involves strong surface complexation and that the solid must be treated with strong acid in order to remove the uranium; while the majority of uranium bound to A2 SC Bauxsol™ can be simply desorbed by a carbonate-rich or groundwater solution. Thus uranium binding to A2 SC Bauxsol is mostly surface adsorption. These results were expected since the contaminants exist as anions and Bauxsol (made of Fe and Al hydrous oxides) sequesters cationic species more strongly at neutral to slightly basic pH values. Without further manipulations such as acidifying the groundwater/adsorbent slurry or using reducing agents such as calcium polysulfide, Bauxsol™ is not a useful option for remediation of the key problematic radionuclides in Hanford groundwaters.

Coal Gasification and Wyoming's Role. *CHRISTIE LARSEN (Brigham Young University Idaho, Rexburg, ID 83440) RICHARD BOARDMAN (Idaho National Laboratory, Idaho Falls, ID 83415).* The world's natural resources are quickly diminishing. As individual countries run out of natural resources they begin to depend on other nations for energy. When one studies the location of fossil fuel resources and calculates the remaining reserves, it is evident that a change in energy production must soon occur. According to the current reserves-to-production ratio (R/P), the world will be completely void of oil in 39 years and natural gas in 65 years. Despite the depletion of petroleum resources, coal is still quite abundant. For example, Wyoming contains a significant amount of coal which could be used to provide large amounts of electricity. This could aide the state's economy which, according to the 2000 Census is struggling. Traditionally, coal burning plants have emitted a considerable amount of pollutants, including Nitrogen Oxides (NO_x) and Sulfur Dioxide (SO_2). Today's modern plant is a gasification plant versus the older coal pulverization plant. Even though this is an improvement, some Wyoming residents do not want to lose their pristine views and unscathed beauty to pollution, even though better paying jobs would assist the economy. The Idaho National Laboratory (INL) is supporting the development of Integrated Gasification Combined Cycle (IGCC) Plants by presenting the benefits of gasification to potential energy production companies, educating the people of Wyoming. Another goal is to improve gasification technology. These plants can also be engineered to produce hydrogen, synfuels, and chemicals in order to reduce our reliance on petroleum. IGCC plants have the potential to create a sizeable amount of energy through the use of the hydrogen they produce. Wyoming coal has a hydrogen to carbon ratio that is close to 1:1, which reduces the amount of CO_2 released when burned. Another advantage is Wyoming's location to California and other large energy consumers. When comparing pollutant emissions from IGCC plants and Pulverized Coal (PC) plants, it is clear that IGCC plants release relatively fewer pollutants. The gasification of Wyoming coal would provide the United States with cleaner energy and an opportunity to reduce its dependence on foreign sources of energy. Consequently, Wyoming's economy would benefit from higher paying jobs.

Comparison of Snag Dynamics in Four Forest Community Types of the Central Pine Barrens. *CHAUNCEY LEAHY (Community College of Rhode Island, Warwick, RI 02886) TIMOTHY M. GREEN (Brookhaven National Laboratory, Upton, NY 11973).* The Long Island Central Pine Barrens (CPB) contains a variety of threatened forest communities that require active management. To determine future management practices the Foundation for Ecological Research in the Northeast (FERN) has initiated a forest health-monitoring project to evaluate potential forest health indicators (*e.g.* amount of available habitat) in the CPB. Snags (standing dead trees) provide suitable habitat for a variety of forest wildlife. The goal of this research was to quantify the abundance of snags in four of the forest community types in the CPB, to determine which contains a greater amount of available habitat. Field data was collected at forty random plots (16 x 25 meters, 400m²), using the Monitoring Protocols for Central Pine Barrens Field Plots prepared by Michael S. Batcher. The field data collected at the forty plots was analyzed to estimate the abundance of snags in the targeted community types and establish the average diameter at breast height (dbh) of snags in each community type. Data analysis shows that the community type with the greatest incidence of snags/acre is coastal oak forest followed by oak-pine, pine-oak, and pitch pine, respectively. However, more data is needed to increase the accuracy of the findings. The greatest average dbh exists in oak-pine forest, but when a standard deviation is applied to the data it shows there is no difference in the range of dbh's in each community type. This research is ongoing and when the data presented here are linked with future data, they can be used to determine the health of the forest.

Mammoth Extinction: A Discussion of the Popular Theories and Scientists' Next Steps. *ALLISON LEDESMA (University of Washington, Seattle, WA 98115) GEORGE V. LAST (Pacific Northwest National Laboratory, Richland, WA 99352).* There are several theories as to why the mammoth became extinct in North America during the late Pleistocene Epoch. This group of theories includes but is not limited to: Climate Change; First Contact; Human Overkill; Keystone Herbivore Extinction; and the Deadly Virus Theory. Popular opinion as to which theory is more correct has changed over the years. Several articles were reviewed from each camp of thought in order to acquire a well-rounded understanding of the issue, including articles by Paul S. Martin, the spokesperson for the Human Overkill Hypothesis movement, and Donald Grayson, who is campaigning towards a better understanding of the Climate Change Theory. This study dovetails with Pacific Northwest National Laboratory's interest in the late Pleistocene's catastrophic Ice-Age flooding of Lake Missoula and how the flooding has shaped the geology of the Northwestern United States and doomed many of its late Pleistocene fauna. This paper brings five of the major extinction theories together for the first time, weighing their positive and negative aspects against each other in order to consider more carefully which theory is most accurate; and as a caveat, reviews possible research paths which scientists may pursue in light of these theories.

New York City Urban Dispersion Program Madison Square Garden Field Study – March 2005. *MIGUEL LOPEZ (Bronx Community College, Bronx, NY 10453) TERRY SULLIVAN (Brookhaven National Laboratory, Upton, NY 11973).* The primary objective of this Urban Dispersion Program (UDP) is to improve understanding of wind and pollution transport pattern in NYC. This program will help to improve the safety and quality of life of New Yorkers. This project is divided in two parts: measurement and analysis. To study the wind, three different kinds of anemometers were used to measure wind speed and direction. The 2D measures horizontal wind speed and direction, the 3D measures vertical winds and turbulence in addition to horizontal winds, and the sodar measures wind speed and direction as a function of height up to a few hundred meters above the instrument. A total of eighteen meteorological systems were located at fifteen different locations and heights around the Madison Square Garden (MSG) area. Perflurocarbon tracers (PFT) were used as a tracer because PFT are safe, non-toxic and can be detected at extremely low concentration, parts per quadrillion (1 in10^{15}). For collecting information of PFT concentration, Brookhaven Atmospheric Tracer Sampler (BATS) and Capillary Adsorbent Tracer Sampler (CATS) were used at different locations around the field of study. According to the analysis of the data collected so far from the first field study in March 10 and March 14, 2005 the concentration of PFT varied depending with the position of the release and the tracer sample and the direction of the wind. Concentration pattern did not always follow the prevailing wind because the course of the wind varies in the canyons formed by the tall buildings and narrow streets. This information is helping to understand airborne transport of contaminants including those from biochemical incident or terrorist attack. Two more intensive projects using PFT's are planned for August 2005 and April 2006.

Monitoring a Mitigation Wetland: Changes in the Diversity of Vegetation in Wetland R at Argonne National Laboratory, Illinois. *NICHOLE LYCZAK (Elmhurst College, Elmhurst, IL 60126) KIRK LAGORY (Argonne National Laboratory, Argonne, IL 60439).* Wetlands are known for their diverse biota. However, they are being depleted at an alarming rate across the United States. During the 1990 construction of the Advanced Photon Source (APS) at Argonne National Laboratory in DuPage County, Illinois, 1.8 acres of wetland were destroyed. To comply with current wetland regulations, a mitigation wetland (Wetland R) was created with the same total area south of the APS construction site. Wetland R was sampled from 1992-1996 to determine the frequency of plant species, relative cover, and water surface area. Annual monitoring of Wetland R began again in 2002 and has continued through 2005. The purpose of this study was to monitor changes in Wetland R through time; particular attention was given to any changes in the relative abundance of dominant species and the number of invasive species present. In 2005, 0.25 m2 quadrats were

randomly placed along 10 transects established in the 2004 study. The plant species present, percent cover and Braun-Blanquet index were recorded for each quadrat. The origin (native, non-native), coefficient of conservatism (C), and wetland status for all species present were also documented. A total of 64 species were collected from the quadrats in Wetland R and identified. Of these species, 13 are non-native to the Chicago region. Fifteen species found in previous years were not seen in 2005. The 10 most abundant species were also identified using the mean percent cover and compared to the dominant species found in previous studies. The only species that was considered to be an abundant species all nine years was *Phalaris arundinacea*, a species not native to the Chicago area. The percent cover of *Alisma triviale*, which is native, and *Cirsium arvense*, a non-native species, has also increased significantly from 2003-2005. It is evident from this study that the diversity of plants found in Wetland R has increased significantly since 1992. Of the 10 dominant species found in Wetland R in 2005, only three were invasive species. Native plants with high C values such as *Leersia oryzoides* and *Sagittaria graminea* appear to be thriving in Wetland R, indicating that the quality of the wetland is improving. It is recommended that annual monitoring of Wetland R should be continued to determine trends in species abundance. Active management of native species (e.g., planting, controlled burns), and control of non-natives will be needed to preserve biodiversity of the wetland.

Analysis of the Habitat of Henslow's Sparrows and Grasshopper Sparrows Compared to Random Grassland Areas. *KRISTEN MAIER (University of Illinois at Chicago, Chicago, IL 60607) ROD WALTON (Fermi National Accelerator Laboratory, Batavia, IL 60510).* Henslow's Sparrows are endangered prairie birds, and Grasshopper Sparrows are considered rare prairie birds. Both of these birds were abundant in Illinois, but their populations have been declining due to loss of the grasslands. This begins an ongoing study of the birds' habitat so Fermilab can develop a land management plan for the Henslow's and Grasshoppers. The Henslow's were found at ten sites and Grasshoppers at eight sites. Once the birds were located, the vegetation at their sites was studied. Measurements of the maximum plant height, average plant height, and duff height were taken and estimates of the percent of grass, forbs, duff, and bare ground were recorded for each square meter studied. The same measurements were taken at ten random grassland sites on Fermilab property. Several t-tests were performed on the data, and it was found that both Henslow's Sparrows and Grasshopper Sparrows preferred areas with a larger percentage of grass than random areas. Henslow's also preferred areas with less bare ground than random areas, while Grasshoppers preferred areas with more bare ground than random areas. In addition, Grasshopper Sparrows preferred a lower percentage of forbs than was found in random areas and a shorter average plant height than the random locations. Two-sample variance tests suggested significantly less variance for both Henslow's Sparrows and Grasshopper Sparrows for maximum plant height in comparison to the random sites. For both birds, the test suggested a significant difference in the variance of the percentage of bare ground compared to random sites, but only the Grasshopper Sparrow showed significance in the variation in the percentage of forbs compared to random locations. Further research should survey additional areas where the birds are found that were not studied for this paper so that the sampling can be as thorough as possible.

VisCMAQ: Visualization Tool for EPA's Community Multiscale Air Quality (CMAQ) Modeling System. *SOLOMON MAINYE (New Jersey City University, Jersey City, NJ 07305) DOUGLAS WRIGHT (Brookhaven National Laboratory, Upton, NY 11973).* Simulation models describe worldwide phenomena such as the transport and transformation of trace species in the Earth's atmosphere. Computer visualization plays an important role in the evaluation of model results with observations and in detailed studies of the physical and chemical processes represented in the model. The goal of this project is to enhance the VisCTM model, which was created last summer with additional flexibilities such as reading from NetCDF files. Also, the ability to process multiple time steps for multiple species at the same time. VisCTM would be able to read, and visualize different types of data that is written in C Language. These enhancements will allow the new VisCMAQ to accept an incorporation of data sets for various spatial domains and sets of chemical species. At this process the Visualization of the output from Multi scale Air Quality (VisCMAQ) model will be created. This VisMAQ project will link VisCTM tools with the Environmental Protection Agency's Community Multi-scale Air Quality (CMAQ) Model system; which will utilize VisCTM import files written by the IOAPI library that is built upon the NetCDF file format.

Predictions of the Growth and Steady-State Form of the Mount St. *Helens Crater Glacier Using a 2-D Glacier Model*. *MELANIE MCCANDLESS (Tufts University, Medford, MA 02155) MITCHELL PLUMMER (Idaho National Laboratory, Idaho Falls, ID 83415)*. Since the 1980 eruption of Mount St. Helens, a glacier has been growing around the lava dome in the volcano's crater. Informally known as the Crater Glacier, the ice mass averages approximately 100 meters in thickness and is reportedly the fastest growing glacier in the continental United States. In 2004, the glacier contained about 120 million cubic meters of snow and ice, a volume roughly equivalent to that of all the glaciers that existed on the mountain prior to the 1980 eruption. The size that this glacier may eventually reach, as it grows toward a steady-state condition, is of considerable interest because the storage of water in the crater increases the risk of mudslides that could result from even minor eruptions – increased activity in the crater during 2004 lifted and cracked the glacier and pierced it in at least two places. To estimate how this glacier may develop in the future and what size it might eventually obtain, we are modeling glacier development in the crater using a general purpose 2-D glacier simulator designed to examine the climatic sensitivity of alpine glaciers. The simulator includes a detailed treatment of effects high-relief topography on net radiation, a physically-based treatment of the other components of the surface energy balance and a transient solution to a set of non-linear equations describing 2-D ice flow. Using this model, whose inputs are primarily a digital elevation model (DEM) and pseudo-vertical lapse rates and precipitation gradients, we calibrate to the observed Crater Glacier development by adjustments to uncertain energy balance parameters, like albedo. With the calibrated model, we predict what the glacier might look like in the future, and describe the primary uncertainties involved in predicting its evolution. Results should be useful as a means of improving risk analysis associated with the geologic hazards that the volcano represents.

Comparing Non-Stratified vs. Temperature-Stratified Classifications for Mapping Groundcover of *Bromus tectorum* (cheatgrass) in Southern Idaho using MODIS Satellite Imagery. *MARY METZCAR (Ball State University, Muncie, IN 47304) JANELLE DOWNS (Pacific Northwest National Laboratory, Richland, WA 99352)*. *Bromus tectorum* (cheatgrass) is an annual grass from Eurasia that has invaded semi-arid and arid shrublands in the Intermountain West. Land managers need information to aid in mitigating the spread of *B. tectorum* and planning for land use, restoration and fuels management. Remote sensing imagery can provide information describing the location and density of cheatgrass stands over large land areas. The first objective of this study was to develop maps indicating low, medium, and high cheatgrass cover on Bureau of Land Management Lands in southern Idaho using training data for areas of varying levels of cheatgrass cover and Moderate Resolution Imaging Spectroradiometer (MODIS) imagery. A second objective was to evaluate whether ancillary cumulative temperature information can be incorporated to improve the identification and classification of cheatgrass. The classification process used a multi-temporal image cube constructed using Normalized Difference Vegetation Index (NDVI) values from MODIS imagery (compiled over 16-day periods) for a portion of southern Idaho for eleven different time periods. Maps predicting cheatgrass groundcover (low, medium and high cover) and cheatgrass presence/absence were generated in ERDAS IMAGINE® using the maximum likelihood classifier, Mahalanobis distance classifier, and minimum distance classifier with two different sets of signatures and training data. Resulting cheatgrass classifications were assessed with 46 known ground points to determine the overall classification accuracy for each method with and without stratification by temperature. Comparisons indicate using temperature stratification improves overall map accuracy for predicting cheatgrass cover or presence. For the maximum likelihood classifier, stratification increased accuracy from 34.8% to 52.2% for the cover class map and from 54.3% to 65.2% for the presence/absence map. Results indicate temperature-stratified classification methods and MODIS imagery can provide better presence/absence maps of *B. tectorum* than non-stratified classification methods.

An Analysis of the Processes By Which Be-7 is Spread Throughout the Experimental End Stations of a Continuous Electron Beam Accelerator Facility. *JAMES MURLA (St.* Vincent College, Latrobe, *PA 15650) ROBERT MAY (Thomas Jefferson National Accelerator Facility, Newport News, VA 23606)*. In the Continuous Electron Beam Accelerator Facility of Jefferson Lab, there is a certain amount of radiation caused by the unintended interaction of the electron beam with surrounding surfaces, especially the walls of the downstream beam line after the beam passes through the physics target in the

experimental end station. Be-7 is one of the radioisotopes formed by the interaction of this radiation with molecules of oxygen and nitrogen in the air is Be-7. Apparently, Be-7 atoms either become attached to dust, are transported as an aerosol, or are spread throughout the end station by some combination of both where they tend to collect on air filters, fan surfaces, and electrostatically charged surfaces. Although its radiotoxicity is very low, when Be-7 collects, it can exceed surface contamination limits in localized areas, called hot spots, requiring decontamination. A detailed mathematical model has been developed to describe ion production, attachment, and interaction with Be-7, based on the conceptual model presented by Bob May (2003), which has been simplified by incorporating some well-researched assumptions. This model considers the influence of electrostatics, kinetics, and aerosol particle growth. Although Be-7 has a valence of +2, it remains electrically neutral and, being a relatively light ion with a high root mean square (RMS) velocity, electrostatics seems to play a small role in comparison to that of kinetics. Because of this, it appears that the most prevalent means by which Be-7 attaches to aerosols is by impaction on surfaces. A possible solution to the problem of Be-7 contamination is considered; a method of hydrating the air local to the Be-7 source to catalyze the production and growth of condensation nuclei, which serve as a mechanism for the collection of Be-7 atoms. These condensation nuclei may be collected and easily discarded.

Generation of *Populus* Aux/IAA RNA$_i$ Constructs, Soil Acclimation of Transgenics and Standardization of RT-PCR Technique for Confirmation of RNA$_i$ Effect. *MEGAN O'SHAUGHNESSEY (Purdue University, West Lafayette, IN 47906) UDAYA C. KALLURI (Oak Ridge National Laboratory, Oak Ridge, TN 37831)*. Over the past centuries CO_2 levels have been increasing causing increased global warming and climate changes. Plants play an important role in terrestrial carbon sequestration owing to their natural ability to fix atmospheric CO_2 through photosynthesis. This study concentrates on identifying and characterizing genes that control the fate of belowground carbon in plants. *Populus* is an excellent model for this study because it is a fast growing tree, has its genome entirely sequenced, and has well established molecular biology and transformation tools. Auxin is a hormone that plays a major role in plant bioprocesses such as cell division, cell elongation, vascular development and root formation. Cell walls are a long-term sink for carbon from photosynthates, thus auxin helps to indirectly control carbon storage levels. The AUX/IAAs gene family is involved in auxin signaling and response. Therefore, in this project, Populus AUX/IAA RNA$_i$ constructs were created out of transgenic plants. The functional role of the specifically down-regulated AUX/IAA gene can be elucidated through observation of phenotypic changes in the transgenic plants. Hence, RNA$_i$ constructs for specific genes will ultimately help in understanding the possible functional roles these genes play in carbon sequestration. To this end, gene-specific fragments were amplified from Populus genomic DNA though PCR techniques and then directionally cloned using a D-TOPO pENTR reaction, resulting in an entry clone that is subsequently used to create an expression clone using pCAPT vector in a gateway technology based recombination reaction. Upon sequence confirmation, the expression clone was introduced into *Agrobacterium* C58 cells for use in *Populus* transgenesis. Transgenic plants were generated from this work. Acclimation of tissue culture plants to the greenhouse conditions was carried out gently and carefully. Transgenic tissue samples were studied microscopically to screen for phenotypic differences. RT-PCR was used to measure the extent of down-regulation achieved in the transgenic plants. These studies will allow us to directly observe whether the targeted gene has been down regulated as expected and will also provide further insight into the role of AUX/IAA genes in carbon allocation.

Identification of Metal Resistance Genes in Microbial Communities from Atlantic Fleet Weapons Training Area (AFWTA) Facility in Vieques, Puerto Rico using Microarray Techniques. *ERNIE PEREZ (University of Puerto Rico at Mayaguez, Mayaguez, PR 00681) CHRISTOPHER W. SCHADT, TERRY GENTRY (Oak Ridge National Laboratory, Oak Ridge, TN 37831)*. The Atlantic Fleet Weapons Training Area (AFWTA) facility, which is located in the eastern part of Vieques, PR, includes land areas, waters and cays impacted by 63 years of military training operations, largely by the U.S. Navy. Samples from the island of Vieques, Guánica, PR and Adjuntas, PR (same geoclimatic zone) were collected in May, 2005. The Functional Gene Array (FGA) technique was used to study the microbial community. Metal resistance genes for Cd, Pb, Hg, Al, and others were included in the analysis. Using different methods, DNA was extracted and purified from the microbial communities in the samples. The community DNA was amplified using the Whole Community Genome Amplification (WCGA) with different quantities (50ng/uL, 100ng/uL and 200ng/uL) of template. The amplified template was labeled with Cy5 fluorochrome dye. Hybridization was performed between the samples and a FGA probes encompassing functional genes for a variety of microbial processes including approximately 4,546 probes for metal resistance gene targets. The objective is to identify metal resistance genes from the AFWTA facility in Vieques, Puerto Rico and compare the results with the ones obtained from the forests in Guánica and Adjuntas. It is believed that a low biomass due to contamination at the AFWTA facility caused difficulties in its DNA extraction. The MoBio-Soil Extraction-Protocol seemed to be the method with the best extraction results. After many attempts, it was concluded that the WCGA made better amplifications using a 50ng/uL concentration of template. The labeling was performed with the expected outcomes. The results obtained from this analysis will provide the tools to identify the profile of genes involved in metal resistance and also develop some strategies for the island's restoration.

Strontium and Calcite: A Remediation Approach for Cleanup at the Hanford Site. *AYESHA PERGADIA (Purdue University, West Lafayette, IN 47906) DAVID BLANCHARD (Pacific Northwest National Laboratory, Richland, WA 99352).* Surface analysis techniques have been used in the past as a way to investigate methods to expedite the remediation of Sr-90 contamination at the Hanford site. In order to develop these techniques for remediation, investigations need to be done to analyze the binding properties of different compounds that could potentially be used for this cleanup. In this investigation specifically, the binding properties of strontium to calcite were examined using the surface analysis techniques of XPS, AES, and SIMS. XPS or X-ray photoelectron spectroscopy is a surface analysis technique that identifies certain elements by irradiating a sample using monoenergetic soft x-rays and sorting them by their distinctive energies. SIMS or Secondary Ion Mass Spectrometry is a process that can utilize a mass filtered beam of argon, oxygen, or cesium to strike a surface and remove the outermost surface atoms. In our investigation we used argon to conduct this process. The emitted atoms were then detected by a mass spectrometer and then classified. Our third surface analysis technique was AES, or Auger Electron Spectroscopy. This technique engaged the chemistry of our sample's surface by measuring the kinetic energy of the ejected Auger electrons. The energies detected were then used to identify the composition of our surface. The specific strontium compound that we used was SrF_2. This was carefully measured out and placed on the surface of calcite prior to investigation. The percent concentration of the elements found on our sample's surface was determined using a data analysis software called CasaXPS. Our results showed us that there is a very slight affinity of SrF_2 to calcite. This affinity exits in a very small percent concentration, and only at the surface. The last few trials using the SIMS provided us with no evidence of Strontium, showing us that the element was sputtered off as we tried to examine the deeper layers of our sample. This experiment is a subset of a larger study that is being done to eventually study the effects of different Strontium compounds such as, $Sr(OH)_2$, $SrSO_4$, and $Sr(NO_3)_2$ to different surfaces such as M_gO, CaO, and TiO_2.

Odonate Species Survey in Correlation with Air Temperature and Precipitation at Brookhaven National Laboratory. *SANEDDY QUEZADA (Hostos Community College, Bronx, NY 10451) TIM GREEN (Brookhaven National Laboratory, Upton, NY 11973).* Odonate emergence data and summer weather conditions were the subject of research at Brookhaven National Laboratory for the summer of 2005. The project attempted to compare meteorological data from the summers of 2003, 2004, and 2005 and its correlation with the distribution and richness of Odonates at Brookhaven National Laboratory. The purpose of the project is to obtain accurate data that will assist in the understanding of Odonate emergence and behavior in correspondence with humidity, precipitation, and air temperature. The project utilizes weather records of the last two summers, courtesy of the National Weather Service located at Brookhaven National Laboratory. Data from the past two summers from the Environmental and Waste Management Services Division at BNL are also being applied to fulfill the goal of this project, as well as current sampling and assessment of the many wetlands on the BNL site. While sampling the ponds, a new species was added to the New York State list of Odonates Celithemis verna or Double-Ring Pennant. Also, one of the three threatened damselflies (*Enallagma recurvatum*) was recorded for the first time at BNL this summer. Further research is required for complete and accurate conclusions. Future work for this project will focus on the investigation and search for the two other threatened damselflies *Enallagma minusculum and Enallagma pictum*.

Comparison of Adaptive Sampling Designs in Determining the Contamination Footprint at a Contaminated Site. *ABBEY RECHNER (University of Illinois at Urbana-Champaign, Champaign, IL 61820) ROBERT JOHNSON (Argonne National Laboratory, Argonne, IL 60439).* Contamination must be cleaned up for the health of society and the environment. Adaptive sampling, a sampling design based on results of previous samples and spatial correlation, is needed at contaminated sites to find the exact boundary or the footprint of the contamination within some margin of error. But the number of samples needs to be minimized to eliminate unnecessary cost. At one contaminated site, this research compared three types of adaptive sampling designs: the Bayesian Approaches to Adaptive Spatial Sampling (BAASS) computer program, an experiment with two sets of employees and three heuristic methods. BAASS uses Bayesian statistics and Geostatistics on a rectangular grid. The experiment with two sets of employees tested how the average person sampled given either no information or a probability of contamination distribution. The heuristic methods- diamond, hexagonal, and modified hexagonal- had no information, were constructed on a triangular grid and were algorithmic. False clean error (the amount of dirty area left dirty), false dirty error (the amount of clean area cleaned), and the number of samples taken were recorded for the adaptive sampling designs relative to the number of possible samples. The percent of samples, false clean error and false dirty error for BAASS were 5.6%, zero and 0.010, respectively. The percent of area sampled, false clean error and false dirty error for the set of employees supplied with no information, on average, were 8.8%, 0.007 and 0.070, respectively. The percent of area sampled, false clean error and false dirty error for the set of employees supplied with a probability of contamination distribution, on average, were 6.7%, 0.023 and 0.024, respectively. The percent of area sampled, false clean error and false dirty error for the diamond method were 6.9%, 0.007 and 0.016, respectively. The percent of area sampled, false clean error and false dirty error for the hexagonal method were 6.0%, 0.016 and 0.050, respectively. The percent of area sampled, false clean error and false dirty error for the modified hexagonal method were 7.8%, 0.007 and 0.009, respectively. Therefore, BAASS is the best adaptive sampling design for this contaminated site because it had the least false clean and false dirty errors and did so in the smallest percent of area sampled. To study whether BAASS is truly a better adaptive sampling design, this research should be replicated at other contaminated sites.

Cataloging and Indexing the Data Holdings of the Carbon Dioxide Information Analysis Center using the ORNL Metadata Editor and Mercury. *KRISTEN REEVES (Southeastern Louisiana University, Hammond, LA 70402) THOMAS A. BODEN (Oak Ridge National Laboratory, Oak Ridge, TN 37831).* The Carbon Dioxide Information Analysis Center (CDIAC) serves as the primary data repository for The United States Department of Energy's (DOE) Global Change Research Program (GCRP). This program facilitates data acquisition and data management activities necessary for basic research on global change, promotes the enhancement of modeling designed to improve representation of Earth system interactions, and develops advanced analytic methods to facilitate fundamental research. CDIAC maintains hundreds of data sets related to climate change. These data have been submitted to CDIAC by researchers around the world. One of CDIAC's primary goals is to make well-documented data sets visible and available to users worldwide via the Web. To reach this goal computing resources have been invested to improve Web-based access, visualization, and retrieval of CDIAC data holdings. Specifically, CDIAC has developed and implemented the CDIAC OME (ORNL Metadata Editor) and the CDIAC version of Mercury. OME is a Web-based tool used to fully document databases by collecting the appropriate metadata (i.e. definitional data that provides information about, or documentation of, other data managed within an application or environment). For this project, the OME was used to generate new metadata for many of CDIAC's data holdings. This metadata consisted of author information, thematic area, beginning and end dates of measurements, variables, data location, etc. Existing OME entries were revised, embellished, and consolidated, where appropriate, to lend better organization and ease navigation. Once the metadata had been collected from the various sources an XML (eXtensible Markup Language) file was created on the development server. These XML files were then harvested by Mercury each night. Mercury is a Web-based search engine used to search for metadata and retrieve associated data. CDIAC staff helped review the metadata collected, and made the appropriate edits needed to assure the most accurate description of data. The OME was then used to modify the existing XML files. Finally, those files were moved to the CDIAC development server, where they were used nightly by the CDIAC version of Mercury to build a locator file; this is also where the catalog is built. Mercury indexes the catalog and makes it searchable on the CDIAC web-site. Mercury then allows users to query the catalog by keyword, subject, title, and author to find the specific data sets they will need for research.

Interspecies Metabolism of Halogenated Acetic Acids. *QASIM REHMAN (Michigan State University, East Lansing, MI 48825) IRVIN SCHULTZ (Pacific Northwest National Laboratory, Richland, WA 99352).* Disinfected drinking water typically contains a mixture of di- and tri-halogenated acetic acids (HAA's), which are known hepatocarcinogens. It has been well documented that tri-HAA's undergo substantial microsomal metabolism, forming di-HAA's as the primary metabolite. In vitro metabolism of these acetic acids were studied-particularly tri-bromo acetic acid (TBA), chloro-dibromo acetic acid (CDBA), and tri-chloro acetic acid (TCA)-in rat, mouse, and human liver microsomes. Rat control microsomes and di-chloro acetic acid (DCA)-pretreated rat microsomes were compared in respect to their tri-HAA metabolism. DCA-pretreatment in rats both induces and increases the amount of the cytochrome P450-2E1 isoenzyme (CYP-2E1), which we had speculated was the main site of metabolism of these tri-HAA's. This comparison pointed to a notable increase in the amount of consumption of TBA and CDBA and an increase in production of their respective metabolites-di-bromo acetic acid (DBA) and bromo-chloro acetic acid (BCA)-in DCA-pretreated rat liver microsomes when compared with the controls. A comparative study of the metabolism of TBA and CDBA was also done in the microsomes of control mice and in CYP-2E1 gene knockout mice, which lacked this isoenzyme. These studies indicated a small decrease in consumption of TBA and CDBA and a slight decrease in the production of their respective metabolites in those mice without CYP-2E1 when compared with the controls. In human liver microsomes, CYP-2E1 monoclonal antibodies were used in an immunoinhibition study. Compared with the controls, the CYP-2E1-immunoinhibited microsomes showed a notable decrease in metabolism of CDBA and a corresponding decrease in the production of BCA. These collective results indicate that CYP-2E1 does play an important role in the metabolism of these tri-HAA's and the consequent production of di-HAA's. However, results also suggest that CYP-2E1-at least in the realm of these three species-is not the sole enzyme involved in this metabolic pathway, and that significant differences appear to exist between mice and humans. Also, in agreement with past in vivo and in vitro studies, TCA was shown to be a poor substrate for rat microsomal enzymes.

Analyzing Mexico City's Air Quality Data to Better Understand the Sources, Sinks, and Chemical Modification of Black Carbon Aerosols. *JUANITA RIOJAS (Texas A&M University-Kingsville, Kingsville, TX 78363) V. RAO KOTAMARTHI (Argonne National Laboratory, Argonne, IL 60439).* To contribute to the understanding of the sources, sinks, and radiative properties of black carbon (BC), a field experiment is planned by the Department of Energy Atmospheric Science Program (DOE ASP) in the year 2006 in and around Mexico City. As a precursor to this experiment, measurements were made in Mexico City of BC and other aerosols during 2003. In this study, these measurements were analyzed to understand the sources of the BC aerosols and evaluate the significance of a primary sink. These issues were addressed using: measurements of BC from El Centro Nacional de Investigacion y Capacitacion Ambiental (CENICA) site, the aid of data analysis software such as KaleidaGraph, backward air-parcel trajectory calculations using HYSPLIT 4 model, and Fire Map derived from satellite datasets. Black carbon wavelength measurements varied between the IR band and the UV band. The two hypotheses for this behavior were (a) the BC during these periods were chemically different from the rest of the time series i.e. had a different source or (b) high values of relative humidity modified the locally emitted BC giving its absorption a dependence on wavelength. When comparing the backwards trajectories to the satellite pictures of the Yucatan Peninsula forest fires, we were able to see that BC in the air was due to the forest fires during some of these times. The results of the correlation analysis between relative humidity and concentration of BC indicated only a few time periods with strong correlations. The correlations were not consistent enough to conclude that relative humidity was the only factor affecting the BC behavior. We were also able to prove that the rain events did not wash out all the BC in the air. Aerosol emission inventories currently do not include information resulting from burning of biomass or forest fires. Therefore, it is important to continue with the DOE ASP in 2006 in order to update aerosol emission inventories. Studying the air quality in Mexico City will help us understand more about the air pollution problems that exist throughout the world.

Aerosol Activation: Theoretical Predictions versus Observations. *ROOSEVELT RIOJAS (University of Texas Pan-American, Edinburg, TX 78501) V. RAO KOTAMARTHI (Argonne National Laboratory, Argonne, IL 60439)*. It has been hypothesized that microscopic anthropogenic aerosol particles are having direct and indirect affects on earth's radiation budget. The aerosols impact the radiation incident on the earth's surface directly by absorbing the incoming radiation or by scattering. The indirect affect of aerosols results from their role in activation of cloud droplets and as a result the possibility of increased aerosol concentrations leading to enhanced cloud formation or an increase in the number of cloud droplets in a given cloud. This indirect effect of aerosols on the radiation budget is by far the least known and understood process in the current climate models. Here we use measurements made in the atmosphere to evaluate a recently developed parameterization for predicting aerosol activation leading to the formation of cloud droplets. We are primarily focusing on data collected during an ARM IOP, conducted during May 2003 from Twin-Otter measurement platform; these fights were flown over the Southern Great Plains site, a facility near north central Oklahoma. The aircraft was equipped with standard meteorological sensors to retrieve temperature, pressure, humidity and more sophisticated ones were used to measure cloud droplet number concentration. The aquired data was then used to constrain a numericla model simulating aerosol activation (developed by my professor, Dr. H. Abdul-Razzak) to predict the number of droplets formed under the measured conditions. The data and model results were plotted using Excel and IDL program. The analysis suggests that the observed data and the numerical model are qualitatively similar, except when zero or negative updrafts velocities were present. Since cloud formation and aerosol activation occurs only under updraft conditions, the activated aerosols measured during the flight pass suggests an anomalous measurement of aerosol activation, possibly a result of the coarse integration time used by the instrument. This indicated that field researchers in future studies may need to employ even higher frequencies of data collection for aerosols to obtain better constraints for model evaluation and developing new and improving current parameterizations.

The Inter-relationship of Energy Efficiency and Water Supply Technology in the Northeastern United States: Existing Systems and Future Research Possibilities. *CARISSA SALVATO (Binghamton University, Vestal, NY 13906) ANN REISMAN (Brookhaven National Laboratory, Upton, NY 11973).* Brookhaven National Laboratory (BNL) is currently researching requirements for energy-efficient water supply and water treatment technology in the Northeastern United States under a national energy-water nexus initiative. For this research, it is necessary to compile information on existing energy-water devices and programs to provide Brookhaven National Laboratory with possible future research areas. Initial online searches, both across the web and within scientific journals, were conducted. The Elsevier Search engine was operated to obtain scientific journal articles relevant to topics on co-location of power plants and wastewater treatment facilities, membranes in wastewater treatment and constructed wetlands. Information was sorted by both topic and relevance to Brookhaven's energy-water initiative. This information was then complied and presented to the energy-water group at BNL. Information acquired during data searches will help to structure the path of future energy-water research by identifying the most promising areas for further inquiry.

Stabilization of Arsenic-Bearing Residuals in Polymeric Matrices. *JACQUELINE SHAW (University of Arizona, Tucson, AZ 85721) WENDELL ELA (Pacific Northwest National Laboratory, Richland, WA 99352).* The USEPA's new standard for arsenic in drinking water (10 µg/L) has motivated research to safely and effectively dispose of arsenic-bearing solid residuals (ABSR) produced in water purification. This research investigates the use of polymeric matrices to encapsulate three different sorbents commonly used in the water industry to remove arsenic. Arsenic containing granular ferric oxy/hydroxide and ferric hydroxide amended alumina residuals were encapsulated in rubber-epoxy composite matrices using an aqueous-based, environmentally benign, manufacturing flowsheet. Arsenic leaching of encapsulated and unencapsulated residuals was evaluated using the standard Toxicity Characteristic Leaching Procedure (TCLP) and the more aggressive California Waste Extraction Test (CA-WET). The structure and composition of the resulting polymeric waste forms were analyzed using Scanning Electron Microscopy (SEM). Arsenic, iron and aluminum concentrations were evaluated using Inductively Coupled Plasma Optical Emission Spectroscopy (ICP-OES). The results showed that waste forms of the polymer encapsulated ABSR crushed for testing retain good leaching resistance, with arsenic levels typically 10 times lower than the unencapsulated ABSR and below the federal Toxicity Characteristics (TC) standard of 5 mg/L. When compared with conventional cement matrices containing the same ABSR, the polymeric matrices encapsulated 4 times more waste (loading levels in excess of 60 wt%) and leached arsenic at levels 1-2 orders of magnitude lower than cement.

Effects of Changes in Canopy Composition on Understory Vegetation in the Long Island Pine Barrens. *ANDREW SIEFERT (Pennsylvania State University, University Park, PA 16802) TIMOTHY GREEN (Brookhaven National Laboratory, Upton, NY 11973).* Pine barrens are rare and important ecosystems found on coarse, droughty, nutrient-poor soils in the northeastern United States. The Central Pine Barrens, located on Long Island in Suffolk County, New York, are a mosaic of communities representing different stages of forest succession, from open canopy pitch pine (*Pinus rigida*) and scrub oak (*Quercus ilicifolia*) barrens to closed canopy pitch pine and finally coastal oak forests. Although the succession of overstory vegetation has been modeled, the effects of changes in overstory composition and increased canopy cover on understory vegetation are not understood. To explore this, overstory and understory cover data were sampled in study plots in the Central Pine Barrens. Understory cover and species richness were analyzed as a function of overall canopy cover and relative pitch pine and hardwood cover. Shrub cover decreased as total canopy cover and relative hardwood cover increased. Conversely, herbaceous plants were more abundant in areas with dense, oak-dominated canopies. Dominant understory species were similar in most areas, though *Quercus ilicifolia* abundance declined with increased canopy cover. Species richness varied greatly between plots, but the differences were not well explained by canopy characteristics. This research contributes to our understanding of understory vegetation—its composition, dynamics, and relationship with the overstory—in the Central Pine Barrens, and provides information that will assist in the management of this important natural resource.

Analysis of the Ecosystem Carbon and Nitrogen Stocks from a Prescribed Burn Seeking to Increase Soil Carbon Sequestration. *LINESHA SIMS (Bevill State Community College, Fayette, AL 35555) ROSER MATAMALA (Argonne National Laboratory, Argonne, IL 60439).* The soil organic matter (SOM) contained in a prairie is rich and deep and has vanished over the past several years. Agricultural practices, such as tillage, depleted the SOM reservoir, reduced soil fertility, and released CO2 into the atmosphere. The purpose of the proposed project is to study the mechanisms of carbon loss and accrual under different management practices seeking to increase soil carbon sequestration. One major strategy to prevent SOM loss and increase carbon sequestration in the soil is to restore degraded soils and long-term cultivated lands to native vegetation. Designated prairies within Fermi National Accelerator Laboratory (Fermilab) were prescribed bi-annual burnings to reduce weeds and encourage the establishment of native grasses. Samples were taken before and after the fire to compare the difference in the ecosystem carbon and nitrogen stocks. The samples were properly prepared and placed in the elemental analyzer instrument. The carbon content was measured by infrared absorption and the nitrogen was determined by thermal conductivity in a horizontal combustion system at approximately 1300°C. When comparing the total system's carbon and nitrogen stocks before and after the prescribed burn, we found there to be no significant differences. We believe a drought may have delayed the plant productivity, while reducing the water availability. We did notice that the carbon and nitrogen content of our research was similar to other simulated effects of an annually burned prairie. This work is a small portion of a much larger project being researched. We will next research the compounds such as nitrates and soil respiration that are in the soil as well as analyze the elements in the charcoal and ashes produced by the fire. This data will contribute to the annual carbon budget for the prairie to explain the differential net ecosystem exchange before and after the burn.

Home Range Estimates and Habitat Preferences of Spotted Turtles (*Clemmys Guttata*) Assessed Through the Utilization of Radio Telemetry, GPS, and GIS Technology. *FRANK SMITH (University of Rhode Island, Kingston, RI 02914) TIM GREEN (Brookhaven National Laboratory, Upton, NY 11973).* Beginning in the fall of 2003, a behavioral ecology study of the spotted turtle, *Clemmys guttata*, implementing radio telemetry was initiated at Brookhaven National Laboratory (BNL). Both hatchery-raised (headstarted) and native spotted turtles were radio tracked in order to discern anomalous behavior in hatchery-raised turtles and the applicability of the raise-and-release method in reestablishing viable spotted turtle populations in native habitats. Individuals from the study group were monitored

regularly, habitat data gathered and positional data logged utilizing GPS technology. The GPS points gathered were used to map hypothetical home ranges for each turtle using GIS technology. No significant difference was found between the summer 2004 headstarted turtle home range sizes and the summer 2005 headstarted turtle home range sizes (Student t-test, a = 0.05, p = 0.3073). Also, no significant difference was found between the combined 2004 and 2005 headstarted turtle home range sizes and the combined 2004 and 2005 native turtle home range sizes (Student t-test, a = 0.05, p = 0.6088). Because the spotted turtle is considered a species of special concern in New York State, the results of this study are relevant to conservation policy.

The Distribution of Plant Species in Relation to Hydrologic Conditions at a Mitigation Wetland at Argonne National Laboratory, Illinois. *ELIZABETH SNYDER (University of Illinois at Chicago, Chicago, IL 60612) KIRK LAGORY (Argonne National Laboratory, Argonne, IL 60439).* Wetlands are valuable ecosystems, not only for plants and animals, but also for people throughout the world. For years, wetlands were destroyed because people did not see their value. Then, in 1990, the "no net loss" policy, which called for wetland conservation, was established in the U.S. This policy stated that for every wetland destroyed, a new one of equal size would have to be created to replace it. Three wetlands were destroyed at Argonne National Laboratory because of the construction of the Advanced Photon Source. In order to keep with the policy, Wetland R was created using topsoil from these destroyed wetlands. Since 1992, this wetland has been observed by scientists interested in the area's vegetation abundance and distribution. These same studies were carried out in the summer of 2005, along with a study of the most abundant species and their distribution in relation to the hydrology of the wetland. In order to determine plant cover, ten transect lines were established and 50 quadrat points were laid out, five per line. Plant cover was estimated visually and using the Braun-Blanquet index. A 0.25m^2 frame was used to encapsulate each quadrat. Once vegetation was determined, a scientific symbol was given to each species, along with its wetland status, origin (native vs. non-native), and coefficient of conservatism. A Global Positioning System device was used to map the surface area of the water. Sixty four plant species were identified during this study: 51 native to the area and 13 non-native. Based on mean percent coverage, ten species were identified as the most abundant. The distribution of species was strongly influenced by the hydrologic condition, and location correlated well with the species' wetland indicator values. At the end of the study, Wetland R was completely dry due to drought conditions. Overall, Wetland R is a fully functioning wetland. Not many mitigation wetlands survive but this one has been succeeding due to proper monitoring and management. While it does contain non-native species, it is covered mostly with species native to the area. Continuing controlled burnings and herbicide applications will help ensure that non-native species do not take control of the site. The lack of water this year had little effect on the plant life, but how it may affect this study next year is unknown. Plant distribution based on hydrology should continue to be studied for this reason.

Preparation for Possible Terrorism Threats to Water and or Air: Emphasis on Acute and Short-Term Exposures. *JERUSHA SPARKS (Southern University at New Orleans, New Orleans, LA 70126) MARGARET MACDONELL (Argonne National Laboratory, Argonne, IL 60439).* There are current standards regulating the public water and air supply. These standards consider lifetime exposures to specific chemicals or contaminants rather than acute or short-term exposures. Shorter exposure duration standards are needed in possible cases of terrorism in which higher concentrations of these contaminants can be tolerated in order to continue or restore usage of these supplies. The Environmental Protection Agency (EPA) supplied a list of possible contaminants to be studied. Background information was initially collected for each contaminant studied this summer in order to determine threat, fate, the potential for interactions, detectability, and current standards and guidelines available through other organizations. For each contaminant studied, research about previous experiments performed was reviewed in order to determine relevant studies upon which to base the Provisional Advisory Levels (PALs). Sensitive populations and possible tolerant populations were discovered, noted, and taken into consideration as well. These studies were organized into a matrix for clarity and organizational purposes. Subsequently, an accurate PAL was derived for many of the contaminants undertaken. This portion is only a small part of the entire scope of the project.

Synthesis of pALS Plasmids Containing Fluorescent Protein Genes for Insertion into *Shewanella oneidensis* for Analysis with Confocal Microscopy. *ALLISON SPENCER (Whitman College, Walla Walla, WA 99362) DAVID E. CULLEY (Pacific Northwest National Laboratory, Richland, WA 99352).* Bioremediation is an essential component of stabilizing and decontaminating radioactive materials present on DOE sites. *Shewanella oneidensis'* ability to reduce different metals for respiration make it a prime candidate for environmental cleanup. Analysis of *S. oneidensis* using confocal microscopy is essential for a complete investigation of how the bacterium exercises control over its ability to use different metals as electron acceptors. As confocal microscopy requires fluorescence for visualization, genes coding for fluorescent proteins will need to be inserted into the chromosomal DNA of *S. oneidensis*. Cloning of four different fluorescent gene sequences located in AKN plasmids was done using PCR with a Phusion polymerase. Cloned sequences were ligated into pKD4 vectors to create the pALS plasmids. Plasmids were electroporated into competent *E. coli* cells to be screened for gene incorporation. Using Epi-Fluorescent microscopy and ultraviolet light, all four newly created pALS plasmids were screened for fluorescence. Analysis showed each fluorescent protein gene sequence had been successfully inserted into the pKD4 vector. All pALS plasmids contain Gentamicin resistance as well as either a green, yellow, cyan or red fluorescent protein gene flanked by two Tn7 transposon sites. From here, the next step is to incorporate the Tn7 region from the pALS plasmids into the attTn7 site on *Shewanella's chromosome*. This is done with a helper plasmid that encodes for the transposition pathway.

A Comparison of Litter Densities in Four Community Types of the Long Island Central Pine Barrens. *DANA TIEVSKY (University of Rochester, Rochester, NY 14627) TIMOTHY GREEN (Brookhaven National Laboratory, Upton, NY 11973).* The condition of the Long Island Central Pine Barrens has been an area of ecological concern for the past three decades. In 2003, the Foundation for Ecological Research in the Northeast (FERN) was founded to support scientific research in the Pine Barrens. FERN's groundbreaking project is the Central Pine Barrens Monitoring Program, for which field research began during the summer of 2005 at Brookhaven National Laboratory. The purpose of this research is to determine the current status of forest health in order to promote longevity and conservation in the Pine Barrens, as well as to learn what research should be done in the future. Specifically, litter densities from Pitch Pine, Pine-Oak, Oak-Pine, and Coastal Oak habitats were compared in order to justify the succession of the Pine Barrens and prepare for future prescribed forest fires. Using Geographic Information System (GIS) and Global Positioning System (GPS) technology, random plots of land were selected throughout eastern Long Island. These twenty-five by sixteen meter plots of land were then thoroughly surveyed. As part of the protocol, litter and duff depth data were collected at twenty points along each of the ten line transects in the plot. Pitch Pine forests were found to have the most litter, with an average depth of 8.58 centimeters (cm). Pine-Oak forests have an average litter depth of 7.48 cm. Oak-Pine and Coastal Oak forests have comparable litter depths. Oak-Pine forests have an average litter depth of 4.81 cm while Coastal Oak forests have an average litter depth of 4.41 cm. A comparison of the vastly different litter densities of the four community types yields results that are consistent with the previously determined succession of the Pine Barrens and shows that litter density plays a key role in aiding forest succession. In the future, data collected under the Central Pine Barrens Monitoring Program can be used to determine a threshold for litter density in order to prescribe forest fires at appropriate times and preserve the Pine Barrens in the most effective manner.

Synthesis of Zirconium Oxo Phosphate for Application in Uranium(VI) Removal. *LYNDSAY TROYER (Whitman College, Walla Walla, WA 99362) WOOYONG UM (Pacific Northwest National Laboratory, Richland, WA 99352).* This study attempts the synthesis of uniformly porous zirconium oxo phosphate and investigates its use as a sorbent for Uranium (VI) removal from solution phase in varying background conditions including pH, ionic strength, and carbonate concentration. The zirconium oxo phosphate was synthesized successfully and was characterized by TEM, IR spectroscopy, XRD, and nitrogen adsorption. By these methods, the material was found to be a highly ordered nanoporous material with hexagonal pore structure. Several sets of batch adsorption experiments, both open and closed to the atmosphere, at a pH range from 3–10, and at ionic strengths of 0.1 M and 0.5 M $NaNO_3$, were allowed to react to equilibrium for 48 hours to determine the percent Uranium(VI) adsorption. The compared results showed a lower Uranium (VI) uptake at low pH (3–4) and high pH (8–10), and also at high ionic strength (0.5 M $NaNO_3$), and in open systems. This result was expected because of the known affect of these background conditions on the interaction between dissolved uranyl ions and the charged sorbent surface. From a linear isotherm,

the K_d for a closed system with 0.1 M $NaNO_3$ and a pH of 8.05 ± 0.23 was calculated to be 38,147 mL/g. This value, in comparison to that of other synthesized materials, indicates the high efficiency of the zirconium oxo phosphate as a sorbent for Uranium (VI) removal.

Physiological Adjustments of Leaf Respiration in *Betula alleghaniensis* and *Quercus rubra* Grown at Varying Temperatures. *ASHLEY VOLLMAR (Pellissippi State Technical Community College, Knoxville, TN 37933) CARLA A. GUNDERSON (Oak Ridge National Laboratory, Oak Ridge, TN 37831)*. Global air temperatures are predicted to rise 1° to 4.5°C by the year 2100. This climatic change can have a great effect on the succession and migration of temperate deciduous forest species. Most physiologically based models of forest response to climatic change focus on the ecosystems as a whole instead of on individual tree species, assuming that the effects of warming on respiration are generally the same for each species, and that processes can not adjust to a changing climate. Experimental data suggest that physiological adjustments are possible, but there is a lack of data in deciduous species. In order to correctly model the effects of climate change on temperate species, species-specific respiration acclimation (adjustment) to rising temperatures is being determined in this experiment. Two temperate deciduous tree species *Betula alleghaniensis* (BA) and *Quercus rubra* (QR) were grown over a span of four years in open-top chambers and subjected to two different temperature treatments; ambient and ambient plus 4°C (E4). Between 0530 hours and 1,100 hours, respiration was measured over a range of leaf temperatures on several comparable, fully expanded leaves in each treatment. Circular punches were taken from the leaves and dried at 60°C to determine leaf mass per area (LMA). Respiration rates at a common temperature in both species decreased by at least 4°C with increasing growth temperature, indicating a large degree of physiological acclimation. Foliar mass per area decreased with increasing growth temperature for both species. It can be concluded that there is a relationship between leaf respiration and foliar mass as it relates to respiratory acclimation, and that these two species had similar patterns of adjustment to warming.

Characterization of Sulfate-Reducing Bacterial Populations in a Uranium-Contaminated Aquifer in Oak Ridge, Tennessee. *AMY VOSS (Auburn University, Auburn, AL 36849) TERRY GENTRY (Oak Ridge National Laboratory, Oak Ridge, TN 37831).* The Field Research Center (FRC), located near Oak Ridge National Laboratory in Oak Ridge, Tennessee, contained four unlined ponds that were used for waste disposal during the years 1951 to 1983. As a result, the soil and groundwater of the FRC are contaminated with uranium-containing waste that has potential to infiltrate local water supply. Bioremediation procedures currently under development involve the use of microorganisms to reduce uranium from U(VI) to U(IV), thus lowering its solubility and reducing the potential for offsite migration. Many sulfate-reducers have been verified to also reduce uranium. The dissimilatory sulfite reduction (dsrA/B) genes were used to detect the presence of sulfate-reducing bacteria potentially capable of U(VI) reduction. The Polymerase Chain Reaction (PCR) was used to amplify the prospective dsrA/B genes in samples collected from the groundwater well FW-106. Gel electrophoresis was performed to confirm that PCR amplification produced the correct-sized fragment. A clone library was constructed from 16S rDNA and dsrA/B PCR products, creating approximately 300 clones containing the genes. These clones were screened to determine the size of the insert. Gel electrophoresis indicated that the inserted fragments were the correct size, and these inserts were then sequenced. A phylogenetic tree constructed for the dsrA/B clones showed that FW-106 was dominated by a single population. Comparison of the putative dsrA/B sequences with those from known organisms indicated that the clones were likely not from dsrA/B genes. However, genes that were found are highly unique and will be used along with a metagenomic sequencing project to determine if indigenous microbial populations have potential to reduce uranium. Knowledge of specific sulfate-reducing populations at the site will allow conditions to be managed for optimal U(VI) reduction.

Stress Response Phenomics in *Desulfovibrio vulgaris* Ferric Uptake Regulator (FUR) Mutants. *KAREN WEBSTER (University of California Berkeley, Berkeley, CA 94720) TERRY C. HAZEN (Lawrence Berkeley National Laboratory, Berkeley, CA 94720)*. Bioremediation is potentially a very powerful technique for containment of hazardous waste, particularly metals and radionuclides. Controlling and manipulating naturally-occuring microorganisms to handle hazardous waste would be effective, cost-efficient and environmentally sound, especially compared with other remediation techniques. Before the organisms can be properly applied to contaminated sites, they must be fully studied and characterized. One microorganism, *Desulfovibrio vulgaris Hildenborough* (DvH), is particularly promising for use in remediation efforts. To understand this organism's capabilities and application potential, it is first necessary to study and elucidate its phenotypical characteristics and optimal growth environment. Special DvH mutants (JW707) have been designed lacking a specific, metabolically significant, ferric uptake regulator gene. By comparing these altered DvH phenotypes to those of the wild-type we can elucidate the significance of the "knocked-out" gene and it's relation to DvH stress response. Stress factors such as metal and radionuclide concentrations, salt, nitrate and nitrite concentrations, and other factors such as temperature and pH have a large effect on the proliferation of DvH biomass. By applying these stress factors in a controlled fashion, we can quantify their effects and the role they play in the growth response of DvH as compared to JW707 in various environments. Biolog in Hayward has developed the Omnilog Phenotype Microarray system for highly efficient phenotypic analysis of microorganism cultures. Biolog's Phenotypic Microarray (PM) plates are designed to screen ~2,000 phenotypical characteristics at once, ranging from osmotic pressure response, to folate synthesis. The Biolog "MT" plates were also used for further analysis of particularly important stressors, such as NaCl and $NaNO_3$ for determination of minimum inhibitory concentrations (MICs), and comparison with the PM plates. The PM data was successfully acquired and a portion was used for comparison to MIC data. The remaining bulk of PM data was passed along to VIMSS colaborators for further analysis. The determined MICs for the stressors applied to JW707 are as follows: NaCl, 175 mM; $NaNO_3$, 60 mM; KCl, 275 mM; $NaNO_2$, 1.6 mM. MIC data will also be used by VIMSS colleagues in the future.

Long Term Impacts of Fire on Grassland Carbon Balance. *LAURA WELLS (University of Colorado, Boulder, CO 80305) MARGARET TORN (Lawrence Berkeley National Laboratory, Berkeley, CA 94720).* I analyzed soil and vegetation samples from the Southern Great Plains (SGP) test bed in Oklahoma for C, N, and ^{13}C to establish total ecosystem carbon estimates for a burn experiment. The experiment aims to uncover the long term effects of fire on the grassland ecosystem carbon balance. This is important on two levels. First, because fire could change the rate of photosynthesis and respiration of vegetation due to loss of biomass or change in community composition, fire management could impact global climate change. Second, if in fact fire is a significant factor, grassland is the most widely found ecosystem in the SGP and holds proportionally more carbon than other ecosystems, so it is of strategic importance. This experiment is designed with two fields, one was burned to assess the post fire ecosystem carbon changes and the other was kept unburned as a control to quantify future changes. However, in order to establish that fire was the cause of any changes, we must establish that the sites were statistically the same before the fire. This was achieved by analyzing soil and vegetation samples from both fields for %C, %N, and ^{13}C using an elemental analyzer and a mass spectrometer. Ten replicate quadrants per field were sampled by on-site staff for seven classes of vegetation and litter. Preliminary data from the vegetation analysis shows that the fields are in fact statistically similar, with C and ^{13}C values for each field falling with in the other's standard error. This indicates that any differences in the fields after the fire will in fact be a result of the burn. The sites were managed by the USDA Grazing land Research Laboratory and the project was sponsored by the DOE Atmospheric Radiation Measurement Program.

Assessment of Mercury Deposition from a Coal-Fired Power Plant in Texas. *JOSEPH WILLIAMS (Miles College, Birmingham, AL 35208) TERRY SULLIVAN (Brookhaven National Laboratory, Upton, NY 11973).* Mercury is known to be an environmental toxicant. Elemental mercury dispersed into the atmosphere during burning/mining of coal is reported to accumulate in the soil and vegetation. The mercury, when transformed to organic mercury, poses health risks for the humans and the surrounding wildlife. In March 2005, the EPA created new allowances and standards for mercury emissions in coal-fired power plants. A site in Texas, near to a power plant that burns lignite coal was chosen for assessment studies of mercury in surrounding soils and vegetation. About 100 public property locations near the power plant were sampled. Using Geographical Positioning System (GPS), these specific sampling sites were chosen and soil and vegetation sampling carried out within a ten-mile radius of the power plant. A total of 514 samples were collected that included surface soil vegetation and soil taken from a depth of about 10 cm from surface. To assess the predicted mercury deposition pattern, an atmospheric dispersion model was used and directional wind and rainfall amounts on an hourly basis were taken into account. A comparison of modeled and measured data will be made after the samples were sent back to Brookhaven

National Laboratory. Total mercury analysis of the samples is being accomplished through therft5mal processing of the samples using the DMA-80 (Direct Mercury Analyzer, Milestone Inc.). A specific amount of the soil sample is weighed and loaded in an auto sampler. The samples are sequentially decomposed at 750°C, converted to elemental mercury in a catalytic converter (600 °C) and finally desorbed as elemental mercury in an atomic absorption sample tube. For the surface soils the maximum moisture on a dry basis for mercury concentration was 111.4 ng/g, while the minimum moisture was 7.6 ng/g. The average of the moisture data was calculated as 33.5 ng/g. The data was analyzed to determine if elevated levels of mercury occur near the power plant. The interpretation of the data showed that there was no evidence of a 'hot spot,' a large area of mercury concentrations compared to background.

Development of Toxicological Matrices, Standard and Guideline Tables, and Provisional Advisory Levels for Contaminants Released in Water and Air. *MEGAN WILLIAMS (University of New Orleans, New Orleans, LA 70148) MARGARET MACDONELL (Argonne National Laboratory, Argonne, IL 60439).* With the potential for terror attacks on the rise throughout the world, measures are being taken to reassure the safety of Americans. One mode toward protecting the country is to set provisional advisory levels (PALs) for potential threat contaminants that may be released by terrorists into the public drinking water supply and/or air. These contaminants that we research include biotoxins, toxic industrial chemicals (TICs), biological and chemical warfare (CW) agents, as well as radionuclides. An initial step is to evaluate current standards and guidelines to channel near-term decisions of contaminant exposure controls for the general public. Once we have evaluated preexisting guidelines, we the gather information to create toxicological matrices from which PALs are set for each contaminant. Our primary focus is to set initial PALs for ingestion. We also consider the inhalation aspect of contaminants in the secondary phase of the PALs.

Exploring Optimal Growing Conditions For Hydrogen Production by *Rhodopseudomonas palustris*. *SARAH WOODS (Lipscomb University, Nashville, TN 37204) QIANG HE (Oak Ridge National Laboratory, Oak Ridge, TN 37831).* *Rhodopseudomonas palustris* is widely distributed in natural environments and is one of the most metabolically versatile bacteria ever described. It is capable of phototrophic hydrogen production and CO_2 assimilation, which are of great significance for H_2 production as an alternative fuel and carbon sequestration to reduce greenhouse gas emission. However, many questions remain unanswered before technologically feasible processes can be developed for hydrogen production. In this study various growth conditions were explored with the aim to determine the effect of carbon source, nitrogen source and oxygen on the phototrophic growth and hydrogen production potential of *R. palustris*. During this study, *R. palustris* was grown in 30ml anaerobic culture tubes with 10ml of degassed medium and closed with rubber stoppers and aluminum seals. Cultures were incubated under light at 30°C under anaerobic conditions (100% N2 headspace) to simulate photosynthesis. Various amounts of different organic substrates, nitrogen sources or oxygen were added to the cultures to test their impact on growth. Growth was monitored spectrophotometrically at 660 nm to avoid optical interference from the cell pigments. Growth curves of R. palustris revealed that acetate allowed optimal growth with the most rapid growth rate (doubling time of approximatly 3.5h) and the highest yield (OD660>2). More moderate growth on fumarate and succinate were also observed. Therefore, acetate being a more reduced substrate is a better carbon source for cell mass than fumarate and succinate. In contrast, growth on pyruvate was minimal with final OD660 of 0.091. Because pyruvate contains more reducing equivalents than acetate yet provided much less growth, this indicates the significant energetic obstacles that prevent the efficient assimilation of pyruvate. Nitrogen source is another growth impacting factor for hydrogen production of *R. palustris*. Compared with nitrogen-fixing growth, the presence of fixed nitrogen (NH4+-N) increased the growth yield by 35%, explaining the ammonia inhibition of hydrogen production is due to the inhibition of nitrogen fixation process, which is responsible for hydrogen evolution. Results show that the phototrophic growth of *R. palustris* and its potential for hydrogen production is affected by the type of organic carbon source, the presence of oxygen, and the form of nitrogen. For hydrogen production processes to make way in the future, these factors should be taken into consideration.

Analysis of the Vegetation in the Meadow Fritillary Habitat. *DOROTHY WYRZYKOWSKI (University of Illinois at Chicago, Chicago, IL 60607) RODNEY WALTON (Fermi National Accelerator Laboratory, Batavia, IL 60510).* The detrimental effects of habitat fragmentation and loss in the Midwest have created an increasing challenge to preserve rare and endangered species. Meadow Fritillary butterflies, uncommon in the Chicago region, yet found in Fermi National Accelerator Laboratory in Batavia, Illinois, are considered to be highly remnant-dependent with specific habitat preferences and needs. The natural area index rating, an assessment of vegetation in Kane County, was measured at three locations. Using a butterfly transect monitoring method, in conjunction with a quadrat study, the percent of several plant species in each quadrat, maximum plant height, and percent of bare ground was measured. A multiple linear regression analysis revealed that relative abundance of butterflies was found to be statistically significant to the percent cover of violets and dandelions. All three sites had a low natural area index rating, contradicting the widely accepted belief that Meadow Fritillaries are highly remnant-dependent. Further research is suggested for evaluating the specific needs of Meadow Fritillaries and their preferred habitats.

Properties of Colloidal Silica Nanoparticles in Aqueous Solution With Organic and Inorganic Cations. *JENNIFER XU (University of Southern California, Los Angeles, CA 90007) WEI WANG (Oak Ridge National Laboratory, Oak Ridge, TN 37831).* The adsorption of various ionic species onto silica nanoparticles causes variations in their apparent surface charge, stability, and other properties. These changes of characteristics are of especial interest because of their potential to be used in the analysis of river sediments (composed mostly of sand or silica) when different toxins are introduced and become adsorbed onto these nanoparticles. While many past studies have focused on alkali metal salts, this study has also examined the effect of varying pH, as well as different concentrations of large organic molecules and phospholipids on the zeta potential of the silica nanoparticles. Using a dynamic light scattering technique (DLS), both the effective diameter and the zeta potential of spherical silica nanoparticles (~40 nm in diameter, highly purified and monodisperse, neutral pH) in aqueous solution with concentrations of different cations ranging from 0 to $1x10^{-2}$ mol/L were investigated. These cations include four alkali chloride salts, four quaternary ammonium cations, and a phospholipids (DPPC). The effect of pH on the plain silica nanoparticles was also studied, both with and without an electrolyte (0.01 M KCl) in aqueous solution. From the pH variation experiment, it was observed that the aqueous KCl greatly stabilized the zeta potential fluctuation concomitant with the variation of pH. The trials with both the organic and inorganic cations indicate that the effective diameter of silica colloidal nanoparticles increases with increasing size of the cation, as does the zeta potential. With larger cations the zeta potential increased more dramatically than when the colloid is in solution with smaller cations. Therefore, larger cationic molecules cause greater flocculation and aid in the precipitation of silica nanoparticles. Additionally, a total organic carbon (TOC) analysis was done to determine the amount of adsorption of DPPC on colloidal silica. The result shows that there is a linear relationship between amount of DPPC adsorbed and the concentration of the DPPC in solution with the silica particles. If these behaviors can be predicted in river water where the alkalinity, pH, or concentrations of various disposed organic wastes can be predicted, sedimentation in rivers can be selectively formed and more accurately determined. This study is part of a larger project dealing with various properties of many other types of nanoparticles.

Effects of Temperature and Relative Humidity of Indoor Air on Workers' Health in U.S. Office Buildings. *PENGQIAN YUAN (University of California Berkeley, Berkeley, CA 94720) MARK J. MENDELL (Lawrence Berkeley National Laboratory, Berkeley, CA 94720).* It is unknown how the thermal properties of indoor air within buildings affects the health of the buildings' workers. In order to find this relationship, temperature and relative humidity (RH) data within 100 buildings across the United States were compiled and merged with lower respiratory symptom outcomes surveyed amongst office workers within each building using a statistical analysis software, SAS. After obtaining a new variable, humidity ratio, from temperature and relative humidity in order to decrease dependence of both these variables, bivariate analyses were conducted on each lower respiratory symptom (cough, shortness of breath, tightness of chest, and wheeze) and on the overall lower respiratory group response. Following the analyses, odds ratio estimates were plotted against the temperatures and humidity ratios categorized into five ranges for each symptom. It was seen that the trendlines of the symptoms versus temperature outcomes all appeared to be concave parabolas. It is held that there is possibly an ideal temperature in which workers have the fewest lower respiratory symptoms. The odds ratios estimates versus humidity ratios were not as consistent as the trends for symptoms against temperature and also had greater noise. Therefore, it did not give enough evidence for a concrete conclusion. Further studies will be needed to test for confounding variables and will contain multivariate analyses with

variables such as age and gender. This work is only a small portion of indoor air study as analyses on other symptom groups such as upper respiratory, mucous membranes, and neurological outcomes are needed as well.

General Sciences

Experimental Investigation of the Light Transmission Method for Measuring Black Carbon Aerosol Mass. *JEFFERY AGUIAR (University of the Pacific, Stockton, CA 95211) THOMAS KIRCHSTETTER (Lawrence Berkeley National Laboratory, Berkeley, CA 94720).* Black carbon (BC) is a product of incomplete combustion and is strongly light absorbing. Carbonaceous aerosols perturb the earth's energy balance with space thereby introducing global and regional climate changes. There is significant uncertainty associated with atmospheric aerosol research due to the differing experimental methods and instruments that exist to measure aerosol mass and optical properties. Using thermal and optical techniques, the group studied the evolution of organic and black carbon from sampled quartz filters was studied. In this study, a dual sampling routine was used to monitor the reported BC concentrations both from a stable BC-emitting source and in a Caldecott Tunnel vehicular emissions survey. The dual sampling setup consisted of using both an aethalometer and filter based technique. After the data sets were collected and compared, the uncertainty associated with measuring carbonaceous aerosols was observed. A data correction based on a varying sigma value as function of transmission was implemented to the aethalometer data to illustrate the same observed trend seen in the filter samples. In order to calculate an accurate BC concentration, a varying sigma value must be assumed to account for the non-linearities associated with filter-based sampling artifact.

Growing and Learning Community Combing Lesson Study with Math in the Garden. *STEPHANIE BIRCH (California State Domiguez Hills, Carson, CA 90747) ALAN GOULD (Lawrence Berkeley National Laboratory, Berkeley, CA 94720).* The Growing and Learning Community (GLC) is an institute designed to encourage teachers to implement lesson study at their host schools while developing school garden which can be used to teach Math lessons. Lesson study is the main process of teacher development in Japan. Instead of spending a majority of their time focusing on curriculum development teachers involved involved with lesson study use their time to focus on the success of a lesson by gathering students observations and data. GLC is combing lesson study with Math in the garden by educating teachers on the lesson study cycle by using Math in the garden lessons as an example lesson study. Lesson study consist of a school goal, selecting a lesson to study, observation of the students during the lesson, debriefing and modification session, teaching the lesson a second time with the suggested modification, collecting more observations of students and final debriefing session. Through this lesson study process teaching gain a better understanding of how the students learning process. Teachers also gain a support network among other teachers and learn about alternative teaching techniques. Lesson study is a new method of teacher development in the United States which can bring a new focus to teaching by putting the attention on students instead of standards.

Location and Trends of Ice Age Floods Erratics in the ALE Unit, Hanford Reach National Monument. *RICK EDWARDS (Montana State University, Bozeman, MT 59715) BRUCE BJORNSTAD (Pacific Northwest National Laboratory, Richland, WA 99352).* The Ice Age Floods in Montana, Idaho, Washington and Oregon dramatically changed the landscape along their paths. Along with massive erosion, large quantities of ice rafted debris, or erratics, were deposited in slackwater areas along the paths of the floods. The study area is located on the northeast slope of Rattlesnake Mountain in south central Washington, an area relatively undisturbed by humans. The goal of the study is to map the erratics and determine from the data collected as much as possible with regard to water height and possible extrapolation of iceberg sizes. The ice rafted debris was mapped using a Global Positioning System unit. At the same time lithology, size, roundness, shape and degree of weathering were also determined and recorded. This data was entered into a mapping program and an Excel spreadsheet. With the data in a manageable format, trends were noted and hypotheses were generated as to water depth and why certain features were found in particular places. There were three types of erratic groupings found: singular erratics, erratic clusters with many rocks and negligible topographic relief and bergmounds with many rocks and up to several feet or more of topographic relief. A majority of the erratics were found on the up current side of arroyos on Rattlesnake Mountain. Erratics were found from 528 feet to 1,177 feet above sea level (asl) with an average of 846 feet asl with a standard deviation of 135 feet. Erratic clusters found from 549 feet to 1063 feet asl with an average elevation of 937 feet and a standard deviation of 119 feet. The bergmounds were found between the elevations of 554 and 970 feet with an average elevation of 793 feet and a standard deviation of 116 feet asl. The lack of any ice rafted debris above 1,177 feet asl indicates this elevation as the likely maximum elevation of the floodwaters. The size and extent of the feature found, erratic, erratic cluster or bergmound were controlled by the size, thus draft of the iceberg that deposited the debris. Single erratics were carried by all sizes of icebergs and thus were deposited more widely whereas erratic clusters and bergmounds were deposited from much larger icebergs, thus needed much deeper water, therefore are distributed over a lower range of elevations.

Intensive Research Institute-Cosmic Ray Detector. *MARLENA GUTIERREZ (Reedley College, Reedley, CA 93654) TOM KNIGHT (Lawrence Berkeley National Laboratory, Berkeley, CA 94720).* This summer I, along with the Intensive Research Institute, worked in four different workshops. The workshop I will be discussing is that of the Cosmic Ray Detector. Our main focus was where do cosmic rays come from, the earth or the atmosphere. To answer this question we built a cosmic ray detector. This detector would enable us to conduct experiments in an attempt to answer this question. To increase the efficiency of the detector we constructed an entirely new frame for the detector. Our frame was an octagon shape. This allowed for two more detection angles, 30° and 60°. To test our detector we took it to Mount Diablo and Caldecott Tunnel. We concluded from our tests at Mount Diablo, as elevation increases so do the number of counts detected. At the Caldecott Tunnel we found that earth and man made substances act as a barrier for the cosmic rays, decreasing the number of counts detected. Therefore, our experiment concluded that cosmic rays come from the atmosphere, not the earth.

Purification and Crystallization of a Putative PhoH-like Protein from *C. diphtheriae*. *TIFFANY HOAGE (University of Wisconsin-Stout, Menomonie, WI 54751) ANDRZEJ JOACHIMIAK (Argonne National Laboratory, Argonne, IL 60439).* One of the goals of the Midwest Center for Structural Genomics (MCSG) is to determine the structure of novel and important eukaryotic and bacterial proteins having specific amino-acid sequences and unknown functions. By characterizing the structures, functions of the proteins may be better understood, new protein folds may be identified, and in some cases new pharmaceuticals can be developed. One of the proteins currently under study at the MCSG in collaboration with the Structural Biology Center (SBC) at Argonne National Laboratory is a putative PhoH-like protein naturally found in *Corynebacterium diphtheriae*, MSCG code APC 82804. It represents a unique class of phosphate starvation-inducible proteins with putative ATPase activity. To determine the protein's structure using x-ray crystallography, crystals that diffract x-rays to at least 3 angstroms (Å) resolution are required. A crystallization condition that produces macroscopic crystals has now been found for APC 82804. The protein used for crystallization was expressed from the recombinant plasmid pMCSG7 that contained the gene coding for APC 82804 in Escherichia coli host strains BL21-Gold (DE3). The protein was purified on a Ni-NTA column. Mosquito protein crystallization robot was used to screen for crystallization conditions. Crystals formed in wells containing 2.0 M sodium formate and buffer at pH 7.0 and 8.5. These conditions were further optimized, one of which produced macroscopic crystals that diffracted x-rays to 5.25 Å resolution. Further optimization will be necessary to improve crystallization for structure determination. Once the structure is obtained, it can then be analyzed to determine the function of APC 82804 within *C. diphtheriae* and possibly be used to prevent the bacteria's toxic effects in humans.

Optimizing System of Information Routing Devices to Accompany Sensor Infrastructure and Deliver Information Promptly at Minimal Cost. *JOHN PENUEL (University of Florida, Gainesville, FL 32611) HUMBERTO GARCIA (Idaho National Laboratory, Idaho Falls, ID 83415).* This paper explains some ideas proposed for implementation and optimization of an information routing system about a city. The paper explains the need for information routing devices and the types available. The types considered are stationary routers and random-route mobile routers. Heuristics are presented for placement of stationary routers. A modification (for the discrete case) of the quadratic line search algorithm is provided for use in optimization of the number of random-route mobile routers to implement in the system. The optimization of the router infrastructure is performed using discrete event simulation, and simulation parameters are addressed in appendix A. Appendix B contains the results of an ad hoc testing

session of the Discrete Quadratic Line Search Algorithm as compared to a discrete bisection style line search algorithm.

Testing of X-ray Active Pixel Sensors for Recording Data from STEM. *JARED SCHWEDE (Yale University, New Haven, CT 06520) PAVEL REHAK (Brookhaven National Laboratory, Upton, NY 11973).* An X-ray Active Pixel Sensor (XAMPS) made for recording data from the Scanning Transmission Electron Microscope (STEM) is being tested. Previous tests using an electron beam of this 32 x 32 matrix of 180 micron silicon square pixels showed less than ideal behavior. It appeared that some of the columns were nonfunctional, indicating that some of the parallel electronics should be tested and perhaps replaced. A simple light source obstructed by a cover with a hole of diameter 1 mm created a beam that was demagnified to about the order of the pixels, much finer than the broad electron beam used previously, to make more refined tests of the sensors. An x-y table equipt with two stepper motors that could precisely determine the position of the light source was used to move the light beam on the sensor. Observations discovered a broken chip and faulty contacts. Replacement increased resolution and general performance, which had been poorer than in previous tests. Other components frequently broke before the installation of a cooling fan. Changes to the LabVIEW visualization program yielded satisfactory images. These tests of the XAMPS are one of many continuing tests of this sensor. This sensor is part of an ongoing project to increase STEM's available information.

Analyzing the Relationship Between Earthquakes and Geology: A Key to Understanding the Seismic Gap in Central Idaho. *SADIE SPRAGUE (University of Idaho, Moscow, ID 83843) STEVE REIDEL (Pacific Northwest National Laboratory, Richland, WA 99352).* Since 1873 there have been 2,507 earthquakes in Idaho. Central Idaho is the site of most earthquakes. There is a seismic gap located between Borah Peak and the Idaho/Montana border. To understand the gap, one solution is to relate earthquakes to geology. Strong earthquakes may occur in igneous and metamorphic rocks. Earthquakes in these rocks may take place at great depth. Small magnitude earthquakes may occur in continental and marine rocks. Earthquakes in the continental rocks should occur near the surface. If there is a relationship between earthquakes and geology the seismic gap may be better understood. It may also explain why few earthquakes occur on the Snake River Plain and the Idaho Batholith. Earthquake data were found at the Digital Atlas of Idaho website before beginning the project. Knowing crust layer thickness, rock types in Idaho, and earthquake data, rock layer thicknesses were then found. The rock layer thicknesses were found online and then the layers were associated with rock units using the Idaho Geologic Map. The rock units were then assigned to the rock types on the geologic map. Knowing the rock type thickness allowed geology data to be analyzed with earthquake depth and magnitude. The result of the project is that there is a relationship between earthquakes and geology. This relationship allowed the seismic gap to be better understood. The rocks found in this area are marine rocks and they are located near the surface. With marine rocks near the surface there is not enough pressure to cause them to fracture creating earthquakes.

Material Sciences

Tuff Cell Solid Oxide Fuel Cell Design and Fabrication. *ERIC ANDERS (Iowa State University, Ames, IA 50011) JOHN DAVID CARTER (Argonne National Laboratory, Argonne, IL 60439).* The Solid Oxide Fuel Cell (SOFC) has the capacity to change the face of energy consumption in our society. There are, however, a few obstacles still in the way. For example, typical SOFCs are expensive and brittle. The Tuff Cell SOFC, developed at Argonne National Laboratory, was designed to counter these problems. Metal cell supports act as a fuel flow field and provides the cell with superior support and strength. The electrolyte and anode are comprised of multi-layered tape castings of both zirconia and nickel oxide ceramics. We report on advances in the fabrication process that have increased the yield rate of functioning cells, and the development of techniques for repairing defective cells.

Grain Size Measurements using Image Analysis Software. *EDUARDO ARAMAYO (Illinois Institute of Technology, Chicago, IL 60616) MICHAEL PERSHING (Oak Ridge National Laboratory, Oak Ridge, TN 37831).* Grain size measurements of metallographic specimens produced from software, such as Clemex Vision, can be generated much more rapidly than measurements taken by hand, greatly simplifying the analysis process. The standard for grain size measurement is set in ASTM E112, which defines a scale for grain size. The standard also explains how to take these measurements, offering a few different methods involving grain intercepts per test line. Clemex Vision software analyzes images based on routines that must be written and adjusted by the user for each field or image. A well written routine simply and easily gives accurate grain size measurements that include much more information than what is available from hand measurements, such as exact grain counts, grain area, length distribution, and anisotropy. Furthermore, the grain size can be verified through multiple methods at once rather than taking multiple counts for the same field. This work presents the results of routines that determine grain size by three different analysis methods in addition to a manual count method. The methods show good agreement giving confidence in the accuracy of the analysis. Comparing the results of image analysis on Nb-1Zr after a one-hour, 1530 °C anneal process with an image of the same material after a two-hour, 1530 °C anneal process illustrates important differences in average grain size and grain size distribution. These image analysis routines greatly simplify the grain analysis process while providing more detailed information.

Cross-Correlation of Thermal and Optically Induced Structural Changes in Arsenic Trisulfide Thin Films. *VERONICA AUGUSTYN (University of Arizona, Tucson, AZ 85719) S.K. SUNDARAM (Pacific Northwest National Laboratory, Richland, WA 99352).* Chalcogenide glasses (based on S, Se, Te) exhibit dramatic photoinduced changes in their physical and optical properties. These phenomena can used to create a variety of integrated photonic structures through controlled, localized, changes in the refractive index of the glass. However, successful application of such photo-modified structures requires that these glasses are stable under service conditions. Understanding the structural modification processes in these materials is central to successfully exploiting their photosensitivity as well as maximizing their environmental stability. The present study examines the effect of both thermal and optical exposures on the optical and structural characteristics of As_2S_3 evaporated thin films. Thin film samples were exposed to different environments and analyzed using optical absorption and X-ray diffraction (XRD). A red-shift of over 5 nm was observed in the optical absorption edge for samples stored for up to 15 days in a controlled environment chamber (50°C, 72% relative humidity) and illuminated by a light emitting diode (LED) at 507 nm. A similar shift in the absorption edge was also observed after annealing the as-deposited films at increasing temperatures (110°C, 130°C, 150°C, and 170°C). An additional shift in the absorption edge of the thermally annealed specimens was observed in the films after subsequent optical exposure (100 J/cm2 total fluence) at 514 nm. All absorption edge shifts were correlated with structural modifications observed using XRD that indicated the as-deposited short-range, realgar-based, structural units (As_4S_4) were converted to orpiment (As_2S_3) moities. The corresponding changes in refractive index in the thermally annealed films were obtained from an analysis of the interference fringes in the absorption spectra. The refractive index of the film was found to increase with increasing annealing temperature, reaching a maximum of + 0.14 at a wavelength of 1000 nm after treatment at 170°C. The results indicate that both optical and thermal exposures activate similar structural modification processes in the films. These changes in structural configuration are consistent with the relaxation of the high-energy structural states in the thermally evaporated material.

An Analysis of the Affected Behavior of PVDF Due to Various Backing Materials. *JASON BARTLETT (City College of San Francisco, San Francisco, CA 94117) MICHAEL KINTNER-MEYER (Pacific Northwest National Laboratory, Richland, WA 99352).* PVDF film is a piezoelectric material capable of sending or receiving a broad range of frequencies when used as an ultrasonic signal interpreter. This article addresses the questions of how different backing materials affect this characteristic of PVDF and whether or not that effect is dependent upon the film's thickness. Using a general material testing matrix, a series of transmitters were constructed for empirical experiments to qualitatively probe for the answers. Fourier transforms were derived from each transmitter by two different methods and compared to determine the exact effects the different backing materials have upon the PVDF's transmittance properties. Using the air backed data as a standard, each tested backing material is compared and discussed in relative terms. Also, all relevant graphs are provided.

Ionogel-Templated Synthesis of Cadmium Sulfide Nanoparticles. *GISSELLE BENITEZ (University of Puerto Rico at Mayaguez, Mayaguez, PR 00681) MILICENT FIRESTONE (Argonne National Laboratory, Argonne, IL 60439).* Nanoparticles have been studied for many years mostly because of their physicochemical properties such as optoelectronic and photovoltaic devices. Previous work in the Firestone lab has focused on ionogel templated synthesis of gold nanoparticles. 1-Decyl-3-methylimidazolium chloride was combined with an aqueous gold solution yielding a 2-D hexagonally ordered mesostructural gel.

Upon irradiation of this composite, anisotropic gold (Au) nanoparticles were obtained. In this report we describe two extensions of this prior work: 1) Development of a covalent (polymerized) ionogel as a template of scaffold for the in-situ formation; aggregation of gold nanoparticles. 2) The synthesis of semi-conducting nanoparticles within an Ionogel was also explored. Gold nanoparticles were grown combining 1-decyl-3-vinylimidazolium chloride with an aqueous gold solution. Using photochemical irradiation, the polymerized ionic liquid and the aqueous gold solution was reduced to create gold nanoparticles. Cadmium sulfide nanoparticles were created by adding 1-decyl-3-methylimidazolium chloride to an aqueous cadmium chloride solution and exposing it to hydrogen sulfide gas. These nanoparticles were formed and studied using UV-Vis, SAXS, and POM.

Optimization of the Growth of High Temperature YBCO Superconductor Films Using Metal Organic Deposition Technique and RABiTs Substrates. *NAMITA BISARIA (Princeton University, Princeton, NJ 08544) MARIAPPAN PARANS PARANTHAMAN (Oak Ridge National Laboratory, Oak Ridge, TN 37831).* $YBa_2Cu_3O_{7-x}$ (YBCO) coated conductor research using the solution deposition method has made progress in recent years towards the development of low cost superconductor wires. The potential uses of superconducting wires for electric power applications include underground transmission cables, oil-free transformers, superconducting magnetic-energy storage units, fault-current limiters, high-efficiency motors, and compact generators. A modified and low cost solution process has been developed to grow the high performance YBCO superconductor films. This solution process uses a variety of different organic precursors that decompose to form YBCO and consequently there is flexibility in what compounds can be used as a precursor. This experiment uses the more stable copper propionate instead of copper trifluoroacetate as was found in previous and documented research. In the process of growing YBCO superconducting films, there are four general steps that have been followed and tailored to the new precursor and require optimization in this research. They are: the solution preparation from metal organic salts, the decomposition phase, the conversion process, and the final characterization through x-ray diffraction analysis and four probe current transport measurement of the superconductor films. The growth of these films was mediated by a stack of buffer layers (CeO_2, YSZ and Y_2O_3) on a textured Ni-W substrate. Preliminary results show that the YBCO films prepared by this process yielded a competitive critical current of 140 A at 77 K. The details of the synthesis and characterization of superconductor films are reported in detail.

Weight Predictions for Infiltrated Kernel Nuclear Fuel. *LINDA BLAKE (Seattle Pacific University, Seattle, WA 98119) LYNNE ECKER (Brookhaven National Laboratory, Upton, NY 11973).* Nuclear fuel capable of operating at higher temperatures will be vital for the next generation of nuclear reactors. Infiltrated Kernel Nuclear Fuel (IKNF) consists of graphite kernels infiltrated with uranium and coated with alternating carbon-containing layers to protect the kernel and contain fission products. For IKNF to be a viable process for a manufacturing facility, one needs to be able to control the amount of fuel in the kernels. Currently, Brookhaven has laboratory notebooks from previous IKNF experiments and is interested in completing development of the fuel fabrication technique. The purpose of this research was to review, develop, and verify a model that can be used to predict the weight gain (uranium loading) during the IKNF process. Data was extracted from the lab notebooks from the previous experiment and compared to the values obtained by a model. Also, experimental parameters were varied in order to determine which variables impact the uranium loading. The model correctly predicts trends in the data. Predictions for weight gain from the model were compared to the experimental data and found to match, or follow closely, the raw data curves. However, there are still unknown parameters that may significantly impact the quantitative predictions. Once new experimental data is available, the unknown parameters can be accounted for and integrated into the models. The ability to predict the weight gain contains numerous advantages. By controlling the number of infiltrations, one can control the amount of fuel in the kernels. It was demonstrated that enough uranium was infiltrated into the graphite that a viable commercial fuel was obtained. Also, the density control allows for ample space to remain available in the kernel to retain fission products. IKNF properties make it an excellent option for the VHTR. The developed models will assist in the next stages of this research.

Fabrication of Anodic Aluminum Oxide Membranes for Catalytic Coating Using Atomic Layer Deposition. *KURTIS BLOHM (Hope College, Holland, MI 49423) GREGORY KRUMDICK (Argonne National Laboratory, Argonne, IL 60439).* Anodic aluminum oxide (AAO) has recently gained importance in many frontiers of nanoscience due to the nearly perfect hexagonal array of closely packed alumina nanopores that are generated in an aluminum sample. The purpose of this project is to use AAO membranes as a substrate for the formation of nano separation membranes and catalytic membranes when coated with a catalyst using atomic layer deposition (ALD). By varying parameters of the AAO synthesis procedure such as electrolyte, voltage, temperature, anodization time, etching time and number of anodizations, a membrane with ideal pore dimensions for ALD coating can be obtained. The barrier layer inevitably formed by this process can be removed by chemical etching after successive anodizations, resulting in a permeable “wafer.” To minimize grain boundaries, the Al is degreased and annealed to produce an ordered microstructure as well as electropolished to remove any impurities and dislocations on the surface that may produce an uneven charge distribution. The laboratory has been designed to provide flexibility in the fabrication of AAO membranes. Analysis of the dimensions and ordering of the AAO membranes will be conducted with SEM (Scanning Electron Microscopy) and AFM (Atomic Force Microscopy). After analysis, the membranes will be coated using ALD to adjust pore size down to the atomic level and to apply catalytic materials for the production of catalytic membranes.

High Temperature Steam Electrolyzer Materials Development. *TODD BOGE (Iowa State University, Ames, IA 50013) JENNIFER MAWDSLEY (Argonne National Laboratory, Argonne, IL 60439).* Due to the increasing interest in hydrogen as a fuel, research is needed to make the production, storage, and transportation of hydrogen more efficient and economical. One of these hydrogen production processes is water electrolysis at high temperatures using heat from a nuclear reactor, known as high temperature steam electrolysis (HTSE). HTSE utilizes solid oxide electrolysis cells, which are based on the current solid oxide fuel cell (SOFC) technology, to split steam into hydrogen and oxygen. Previous studies at ANL have shown that $La_{0.7}Sr_{0.2}FeO_3$ (LSF-ns), $Pr_{0.5}Sr_{0.5}CoO_3$ (PSC), and $La_{0.8}Sr0.2CoO_3$ (LSC) are better air electrodes at temperatures below 900°C than the current SOFC benchmark material, $La_{0.8}Sr_{0.2}MnO_3$. The current study focused on improving the performance of LSF-ns, PSC, and/or LSC using two different strategies. The first strategy was to increase the triple-phase boundary area between oxygen-bearing gas, the oxygen electrode, and the electrolyte by mixing the LSF-ns and LSC powders with an electrolyte material, either gadolinium-doped ceria or yttria-stabilized zirconia (YSZ) powder. The second strategy was to grade the grain size and density of the LSF-ns and PSC, using a gel precursor to create a denser, smaller-grained thin layer on the electrolyte followed by a thicker layer made from larger grained powders. Half-cells of the materials were evaluated using electrochemical impedance spectroscopy (EIS) at temperatures between 800° and 900°C. After analyzing the EIS data, it was found that the PSC with graded density made using the gel precursor had area specific resistances lower than any material previously tested. Work was also done to improve the hydrogen/steam electrode because the current SOFC hydrogen/steam electrode (a nickel-YSZ cermet) oxidizes under the high steam conditions of HTSE. Ten single-phase, non-metallic materials were identified as having the properties needed for an improved hydrogen electrode. These materials were synthesized and are currently in the process of testing alternative materials for the hydrogen/steam electrode via EIS.

An Artificial Nacre. *DEANNA BRITTON (University of Tennessee, Knoxville, TN 37996) APRIL MCMILLAN (Oak Ridge National Laboratory, Oak Ridge, TN 37831).* Many structured organic-inorganic composites exist in nature. An example is mother-of-pearl, or nacre, which was investigated in this study. Nacre possesses an ordered brick-and-mortar arrangement composed of alternating layers of inorganic aragonite ($CaCO_3$) approximately 500 nm in thickness and an organic protein matrix 50 nm thick. Nacre is well known for its excellent mechanical properties in particular its high toughness and strength, and these superior qualities can be attributed to the arrangement of the organic/inorganic elements which combines the elasticity and toughness of the protein layers and the strength and hardness of the aragonite. In order to develop an understanding of how organic and inorganic structures assemble, a synthetic approach was utilized to reproduce the structure of nacre. This study carried on the work of Dr. Nicholas Kotov, Oklahoma State University. Kotov fabricated the layered structure through demonstration of a technique called layer-by-layer assembly. Layer-by-layer assembly involves alternate immersions of glass slides in solutions of negatively-charged clay called montmorillonite, the bricks, and positively-charged polyelectrolyte called poly(diallydimethylammonium) chloride (PDDA) which serves as the mortar. Currently, a calibration curve for Layer Thickness versus

Immersion time is being generated in order to understand the growth kinetics of the layers. The ability to manufacture artificial nacre may provide lightweight, rigid composites for biological tissues that possess a similar structure such as bone and teeth.

Stabilization of Arsenic-Bearing Residuals in Polymeric Matrices. *SAVANNAH BURNSIDE (University of Arizona, Tucson, AZ 85721) WENDELL ELA (Pacific Northwest National Laboratory, Richland, WA 99352).* The USEPA's new standard for arsenic in drinking water (10 µg/L) has motivated research to safely and effectively dispose of arsenic-bearing solid residuals (ABSR) produced in water purification. This research investigates the use of polymeric matrices to encapsulate three different sorbents commonly used in the water industry to remove arsenic. Arsenic containing granular ferric oxy/hydroxide and ferric hydroxide amended alumina residuals were encapsulated in rubber-epoxy composite matrices using an aqueous-based, environmentally benign, manufacturing flowsheet. Arsenic leaching of encapsulated and unencapsulated residuals was evaluated using the standard Toxicity Characteristic Leaching Procedure (TCLP) and the more aggressive California Waste Extraction Test (CA-WET). The structure and composition of the resulting polymeric waste forms were analyzed using Scanning Electron Microscopy (SEM). Arsenic, iron and aluminum concentrations were evaluated using Inductively Coupled Plasma Optical Emission Spectroscopy (ICP-OES). The results showed that waste forms of the polymer encapsulated ABSR crushed for testing retain good leaching resistance, with arsenic levels typically 10 times lower than the unencapsulated ABSR and below the federal Toxicity Characteristics (TC) standard of 5 mg/L. When compared with conventional cement matrices containing the same ABSR, the polymeric matrices encapsulated 4 times more waste (loading levels in excess of 60 wt%) and leached arsenic at levels 1-2 orders of magnitude lower than cement.

Friction Stir Welding of Nickel-based Superalloy Inconel 738 and Friction Stir Weld Defects in Aluminum Alloy 5454. *DEBORAH CARLSON (South Dakota School of Mines and Technology, Rapid City, SD 57701) S. A. DAVID (Oak Ridge National Laboratory, Oak Ridge, TN 37831).* Friction stir welding (FSW) is a relatively new solid-state joining technique in which a pin tool is inserted into a seam between two pieces of material and rotates at sufficient speed to plasticize the material. The pin tool travels along the length of the seam and welds the materials together. This research project involves two tasks involving FSW. The first task is to apply FSW techniques to the nickel-based superalloy Inconel 738 and to characterize the welds made. Traditionally, FSW has only been applied to low-temperature metals such as aluminum alloys and more recently to steels, but FSW of nickel-based superalloys has never been attempted before. A successful three inch weld was performed with a tungsten alloy pin tool at 12.7 mm/min and 800 rpm. The cross-section of the weld was characterized with optical and scanning electron microscopy. Results showed fine grains and also dissolution and re-precipitation of gamma prime particles inside the grains in the stir zone. Further research will be conducted on refining the welding conditions and analysis of the microstructure with transmission electron microscopy. The second task is to examine defects that occur during FSW of aluminum alloy Al 5454-H32 under certain welding conditions. Trials were performed at different translational and rotational speeds and the welds were characterized with optical microscopy. Torque, the forces in the X and Z directions, power, and energy were examined with the set welding parameters to find a correlation with the formation of weld defects. Temperature profiles across the length of the welds were calculated using heat flow analysis. In addition, hardness tests were conducted over the weld profile for several samples. Upon analysis of the data, it was determined that a correlation exists between defect formation and an increase in power, caused by an increase in torque and rotational velocity. This increase in power also leads to higher temperatures in the weld region. Monitoring the power consumed during FSW may provide an effective means of controlling defect formation.

Interdiffusion Behavior in RERTR Fuels Using Composition Profile Data. *MATTHEW CARLSON (Brigham Young University Idaho, Rexburg, ID 83440) DENNIS KEISER (Idaho National Laboratory, Idaho Falls, ID 83415).* Working this summer as an Intern at the I.N.L.'s M.F.C., I had the privilege of working with Dr. Dennis Keiser. We investigated interdiffusion behavior in RERTR fuels using composition profile data that was generated from actual fuel plates using a scanning electron microscope. Multicomponent, multiphase interdiffusion theory was then employed to calculate interdiffusion data from these profiles. To increase the efficiency of this process, a computer program was created using the computer code Maple. This computer program consisted of nine steps: First, data points were entered directly into Maple in matrix form. Second, concentration (atom fraction) data was plotted as a function of position (micrometers). Third, the plotted data was fit using a cubic-spline approach. Fourth, the Matano plane, or plane of mass balance, was calculated for each component. Fifth, the interdiffusion flux was calculated for each component as a function of position. Sixth, the interdiffusion flux was plotted for each component and checked, for consistency, to make sure that the sum of the fluxes at each position added to zero. Seventh, average effective interdiffusion coefficients were calculated by applying integration by parts, which is very straightforward using Maple. Eighth, effective penetration depths were calculated to get an idea of how far each component penetrated into the diffusion zone. Completion of this project has increased my understanding of the field of materials science, as well as the field of computer programming. I know that creating the above-mentioned computer program has enhanced my ability to program using Maple 9.5. The work experience gained at the INL has strengthened my scientific background, and this will serve me well as I explore other fields of science.

Magnetic Field Effects on the Tempering Behavior of SAE 1045 Steel. *CARLOS CORREA-LOCKHART (Florida A&M University, Tallahassee, FL 32304) GERARD M. LUDTKA (Oak Ridge National Laboratory, Oak Ridge, TN 37831).* The heat treatment or tempering of steel is a required process to develop the appropriate combination of properties of strength, ductility, and toughness for the intended use. Tempering is a thermal process whereby the quenched-in metastable martensite phase decomposes into a combination of ferrite with an extremely fine dispersion of iron carbide (Fe_3C). This process of heat treatment requires a large amount of energy to take the steel to the high austenitization temperature and subsequently quench and temper the metal. Prior research has shown that magnetic processing significantly accelerates the transformation kinetics for the decomposition of the parent paramagnetic austenite phase to any of the ferromagnetic transformation products when temperatures are below the ferrite phase T_c (Curie temperature). This research endeavor is investigating the hypothesis that since iron carbide also has a T_c of 210°C in the tempering temperature regime that accelerated tempering kinetics can be achieved in a SAE 1045 steel by conducting this process below the Fe_3C T_c under the influence of magnetic field. In this study tempering experiments were preformed as a function of tempering temperature above and below the T_c and various magnetic field strengths. If this hypothesis is substantiated, the steel will temper at a lower temperature faster, which in turn, conserves the amount of energy used to process the steel. The application of the magnetic force to the heat treatment of steels will not only conserve energy, but will make heat treatment of steel more cost effective. To determine the direct effects of the magnetic fields on the steel specimens, Scanning Electron Microscopy (SEM), and Orientation Imaging Microscopy (OIM) analyses were used for quantitative microstructural evaluation along with microhardness measurements to compare tempered sample mechanical properties. The results and conclusions of this investigation will be presented in addition to providing recommendations for future research to optimize and implement this concept for specific industrial applications.

Synthetic Approaches to Develop Electrochemically Active Metal Based Mesoporous Structures. *ANTHONY CRISCI (University of Illinois at Urbana-Champaign, Champaign, IL 61820) MILICENT FIRESTONE (Argonne National Laboratory, Argonne, IL 60439).* Mesoporous silicas are structured materials that possess an ordered 2D hexagonal array of parallel cylindrical channels with tunable pore diameters (e.g., 30-70Å). Mesoporous silicas such as MCM-41 and SBA-15 have been used primarily as passive frameworks in which active guests (e.g., catalysts) are housed. Less work has been performed on preparing active mesoporous materials that could be used to control the functionality of the intercalated guest. In this report, we describe several synthetic approaches used to develop an electrochemically active ordered mesoporous structure composed of gold. An aqueous gold salt is mixed with a surfactant-based template which is ordered by thermal treatment. Photochemical or chemical reduction is applied to reduce the gold ions (Au^{3+}) to Au0 which initiates the formation of interconnecting gold bonds encompassing the template. The surfactant-based template is removed through washing with water. Analysis of a surfactant-free sample by small angle x-ray scattering (SAXS) indicates a highly ordered, autonomous structure remained after washing. A Nitrogen adsorption study is scheduled to determine the surface area and aperture diameters of the gold mesopore product. The current focus is on the development of an efficient standard synthesis protocol for metallic mesoporous materials (e.g. gold); to enable the production of functionalized mesopores.

Gas Flow Characteristics of Various Discrete Jet, Close-Coupled Gas Atomization Nozzle Designs. *JAMES CRONIN (Clemson University, Clemson, SC 29632) IVER E. ANDERSON (Ames Laboratory, Ames, IA 50011)*. To gain a further understanding behind the gas flow characteristics in discrete jet, close-coupled gas atomization, high speed photography, aspiration testing, and velocity probe testing have been conducted on gas-only flows from various nozzle geometries currently used for experimental atomization processes. Experiments indicate that a certain degree of control over the atomization process can be obtained by utilizing the gas-only flow trends that arise from the design variables of these nozzles. The variables considered were: atomizing gas composition, nozzle jet configuration (angle, number, and size), and melt tube insert parameters (length and chamfer angle). These were arranged into a test matrix to isolate gas flow and pressure trends associated with each of the individual variables. Initial results from a combination of Schlieren images and aspiration pressure data were obtained for the formation of the Mach disk in relation to operating pressure and nozzle geometry. The findings show that a shorter insert tube length (2.286 mm) is a major factor for forming a Mach disk at a lower pressure with a minor factor being a wide jet apex angle (45°). These and other resulting fluid flow trends can now be used in conjunction with future research to enable gas atomization process designs that minimize mean size of the powders produced, reduce the standard deviation of the powder batch, and improve the overall efficiency.

Internal Nitridation of Fe-Al Alloys in Air. *MATTHEW DWYER (Lehigh University, Bethlehem, PA 18015) BRUCE PINT (Oak Ridge National Laboratory, Oak Ridge, TN 37831).* Ferritic Fe-Al (10–20 at % Al) compositions are being evaluated for coatings in high temperature oxidizing environments including the next generation of ultra-supercritical steam plants. Ferritic compositions have been found to have a lower thermal expansion coefficient than intermetallic FeAl or Fe_3Al and, therefore, have fewer coating-substrate thermal expansion mismatch problems than intermetallic coatings. However, the lower Al content in ferritic alloys reduces the oxidation resistance of these materials because less Al is available to maintain a protective Al_2O_3 layer. Consequently, additions of 1–5% Cr (all compositions in at.%) to Fe-Al alloys have been investigated as a way to increase their oxidation resistance. Recently, it was discovered that cast materials with 14% and 19% Al containing 0–5% Cr additions underwent extensive internal oxidation and nitridation in air at 900°C. The purpose of this study was to quantify the extent of internal attack as a function of Al and Cr content after 5,000 h at 900°C and as a function of temperature at 700–1,000°C. Cast ingots are used to study oxidation behavior to assist in coating development. Both light-optical microscopy and scanning electron microscopy were used in conjunction with imaging software to quantify the extent of attack. The internal attack for this set of materials was unusual because the depth of penetration generally increased for the Fe-19Al alloys compared to the Fe-14Al materials. Also, the volume of internal precipitates increased with Cr content for the Fe-19Al alloys. Specimens of Fe-19Al-2Cr showed no internal attack at 700 or 800°C, but extensive internal attack at 900° and 1,000°C. Alloys containing 1.1Ti showed no internal attack after the same exposures. This beneficial effect may be due to the effect of Ti on the oxide morphology. In plan view and in cross-section, the oxide on the Ti-containing alloys was relatively flat compared to the buckled oxide on the alloys without Ti. The buckling of the surface oxide may cause cracks that allow nitrogen and oxygen to penetrate deep into the material. Because Fe-Al coatings are limited to the 500–700°C range, the severe internal attack that was observed at 900° and 1,000°C is not likely to affect coating performance.

Cross-Correlation of Thermal and Optically Induced Structural Changes in Arsenic Trisulfide Thin Films. *HELEN FAN (University of Arizona, Tucson, AZ 85719) S.K. SUNDARAM (Pacific Northwest National Laboratory, Richland, WA 99352)*. Chalcogenide glasses (based on S, Se, Te) exhibit dramatic photoinduced changes in their physical and optical properties. These phenomena can provide the basis for the optical patterning of refractive index to fabricate useful optical device structures in the glass for a variety of integrated photonic applications. In addition, these glasses need to be stable in service conditions. Understanding structural modification processes in these materials is central to successfully exploiting their photosensitivity as well as maximizing their environmental stability. The present study examines the effect of both thermal and optical exposures on the optical and structural characteristics of As_2S_3 evaporated thin films. Thin film samples were exposed to one of two different environments and their resulting optical absorption and X-ray diffraction (XRD) results were compared. A red-shift of over 5 nm was observed in the optical absorption edge for samples stored for up to 15 days in a controlled environment chamber (50°C, 72% relative humidity) and illuminated by a light emitting diode (LED) at 507 nm. A similar shift in the absorption edge was also observed after annealing the as-deposited films at increasing temperatures (110°C, 130°C, 150°C, and 170°C). An additional shift in the absorption edge of the thermally annealed specimens was observed in the films after subsequent optical exposure (100 J/cm^2 total fluence) at 514 nm. All absorption edge shifts were correlated with structural modifications observed using XRD that indicated the conversion of short-range, realgar-based structural units (As_4S_4) to orpiment (As_2S_3). The corresponding changes in refractive index in the thermally annealed films were obtained from an analysis of the interference fringes in the absorption spectra. The film index was found to increase with increasing annealing temperature, reaching a maximum of +0.14 at a wavelength of 1000 nm after treatment at 170°C. The results indicate that both the optical and thermal exposures activate similar structural modification processes in the films. These changes in structural configuration are consistent with the relaxation of the high-energy structural states in the thermally evaporated material.

Analysis of Holes in Coated Fuel Particles, Calculation of the Ratio of Resin to Sand in a Manufacturing Mold, and Observation of Glass Fiber Properties in a Polypropylene Sample Using X-ray Tomography. *PAUL FIKSE (Allegheny College, Meadville, PA 16335) G.E. ICE (Oak Ridge National Laboratory, Oak Ridge, TN 37831)*. X-ray tomography serves as a nondestructive means of creating 3-D images of samples with volumes from 5μm^3 to 5mm^3. It is often used to detect imperfections in manufacturing processes. Laser drilled holes in inert coated fuel particles were measured for depth and diameter of entry incision, the percentage of sand in a manufacturing mold was roughly estimated, and properties of glass fibers dispersed in a sample of polypropylene were observed. An individual sample is placed between a 5 micron diameter x-ray source and a detector (which consists of a microscope, a crystal, and a CCD). The sample is rotated about its axis and a number of images are taken. Each image depicts the amount of x-ray absorption for the particular orientation. Using a parallel-beam back projection algorithm, a 3-D reconstruction of the sample is obtained. Slices of tomograms were taken depicting the entry diameter of incision and a cross section of the incision depth for 6 C-SiC-C-Zr inert fuel particles. Two tomograms were also taken (inner and outer regions) of the sand mold used for lost foam cast molding - a process popular in automobile manufacturing. Slices of varying depth were taken from each and then analyzed with Photoshop® and ImageJ® for the percentage of sand present. The sample was found to be nearly consistent throughout with approximately 80.5% sand. Slices from a fiber-reinforced polypropylene tomogram were used to find the coordinates of the individual glass fibers' endpoints, with which an estimate of average fiber length was calculated. The isolated fibers were found to average 1,073 μm in length, far shorter than the length of bundled fibers, which were the majority of fibers present. The tomography machine proved only somewhat useful for examining the sand sample, yet highly effective in detecting contrast in the carbon layers of the fuel particles as well as the glass fibers in the polypropylene sample.

Elevated Temperature Compression Properties of Unirradiated V-4Cr-4Ti. *MICHAEL FRYD (Lawrence University, Appleton, WI 54911) MYCHAILO TOLOCZKO (Pacific Northwest National Laboratory, Richland, WA 99352)*. V-4Cr-4Ti is a potential structural material currently being investigated for post-ITER fusion reactor concepts. Vanadium alloys are attractive because of their relative resilience to becoming radioactive and their resistance to high temperature creep. To obtain information on the deformation properties of this material, compression tests of cylindrical unirradiated 3 mm diameter by 3.5 mm tall specimens from heats 832665 and NIFS-1 were performed at 250°C and ~415°C at a strain rate of 5x10-4 s-1. The yield stress for the NIFS-1 heat was 222 MPa at 250°C and 213 MPa at ~415°C. Yield stress for heat 832665 was 244 MPa at 250°C and the average yield stress was 236 MPa at ~415°C. The power law strain hardening (PLSH) exponent for the NIFS-1 heat was 0.28 at 250°C and 0.34 at ~415°C. The PLSH exponent for heat 832665 was 0.3 at 250°C and 0.27 at ~415°C.

The Effect of Nickel Oxide on the Thermal Properties of an Alkaline Earth Silicate Sealing Glass for Planar Solid Oxide Fuel Cells. *ROBERT GOW (Montana Tech, Butte, MT 59701) YEONG-SHYUNG CHOU (Pacific Northwest National Laboratory, Richland, WA 99352)*. Current research on planar solid-oxide fuel cells (SOFCs) has shown them to be an efficient, environmentally friendly source of energy. One of the many remaining barriers to seeing a commercially viable SOFC has been the sealant. The sealant must prevent the direct mixing of

fuel and air, be stable it oxidizing and reducing conditions, and most importantly it has to survive hundreds to thousands of thermal cycles during routine operations. For the glass or glass-ceramics approach, the sealant is required to have a closely-matched coefficient of thermal expansion (CTE) to that of the SOFC components; otherwise the seal would fracture and cause the total failure of the stack. Current glass seal developments have focused on alkaline-earth based aluminosilicate glasses. One problem was the decrease of CTE during aging. A possible solution was proposed by adding a stable phase element with a high CTE. In this study, we selected nickel oxide as the high CTE phase in a SrO–CaO silicate glass. Two approaches were used to incorporate NiO (up to 15%) into the glass. One was the melting glass approach, and the other was a composite approach. Both thermal and mechanical properties were characterized. The results of dilatometry showed a decreasing CTE with increasing NiO content for the melting glass approach, whereas opposite results were observed for the composite approach. The difference was discussed with x-ray diffraction analysis. The 10 volume percent NiO in the composite approach was used for sealing tests. A hermetic seal was found and the microstructure was characterized with electron microscopy.

Salt Flux Experiments for Secondary Aluminum Processing. *JONATHAN HAVENGA (Iowa State University, Ames, IA 50011) GREGORY KRUMDICK (Argonne National Laboratory, Argonne, IL 60439).* The aluminum industry consists of two basic components: primary and secondary aluminum production. Primary aluminum production involves the reduction of alumina (Al_2O_3) into aluminum using the Hall-Héroult process. Secondary processing is the remelting of aluminum scrap to produce 'new' aluminum or alloys, rather than using alumina as the source of the raw material. This process is much more energy efficient than primary aluminum production. Current secondary aluminum processing requires various methods used to improve recovery of aluminum by minimizing oxidation and metal melt loss. One method utilizes a salt flux; the most commonly used mixtures are approximately equal portions of NaCl and KCl with small amounts of a fluoride compound. Other fluxes offer potential advantages over this mixture, yet have not been proven for possible industrial use. This experiment seeks to determine if the advantages of using a new flux are great enough to motivate research on a larger scale. To do this, different mixtures of the salt flux will be melted with aluminum chips, stirred, and then analyzed after cooling. The analysis will evaluate how well the different fluxes improve aluminum recovery by determining how much oxidation takes place, if the flux contaminates the metal, and the flux composition and oxide content after melting. The experiments are currently being performed.

Fischer-Tropsch Synthesis Catalyzed by Nano-Sized Iron. *NATHAN HOULD (State University of New York – Stony Brook, Stony Brook, NY 11793) DEVINDER MAHAJAN (Brookhaven National Laboratory, Upton, NY 11973).* The Fischer-Tropsch (F-T) reaction is used commercially to synthesize clean liquid hydrocarbon fuels from synthesis gas (syngas). Syngas is a mixture consisting primarily of CO and H_2 produced by coal gasification or steam reforming of natural gas (>90% CH_4). The F-T syngas conversion is achieved with catalysts based on Fe, CO and Ru. The aim of this project was to evaluate a nano-sized catalyst to ameliorate the prevalent problems with the F-T synthesis, those being low space time yield and product selectivity. This research utilized nano-particles of iron oxide (a-Fe_2O_3) to drive the F-T reaction and collected data to yield fundamental insight into the process mechanism. Catalyst phase and morphology and the subsequent reaction product slate and fractional conversion were comparatively analyzed to develop a superior F-T process. The catalyst was evaluated in the slurry phase at 0.73 MPa and 493 K with a custom built continuous flow process unit. This unit consisted of a 1 liter constant stirred tank reactor (CSTR) and had provisions for gas, liquid and slurry sampling. The product slate was analyzed with chromatographic methods developed to quantitatively identify aliphatic C5-C10 liquid hydrocarbons, C1-C5 gaseous hydrocarbons products, C1-C6 alcohols, and CO H_2, O_2, N_2, and CO_2 gases. Analysis employing these methods was used to determine the extent of reaction and showed the nano-particles (3nm MPD) have a propensity to yield paraffins; the liquid phase products consisted of >30% C10+ hydrocarbons. Gas phase analysis shows that methane was 0.24% of reactor effluent and C2-C5 gaseous hydrocarbons were each <0.1% of reactor effluent. Mössbauer data were used to identify the phase of the catalyst. The initial phase of the catalyst was a-Fe2O3 and the quenched catalyst phase was a mixture of oxides and carbides that was predominantly magnetite (Fe_3O_4). It follows that the active catalyst phase is magnetite or the remaining carbide phase is highly active. A more detailed catalyst material analysis was conducted with transmission and scanning electron microscopy. Ultimately, this research shows F-T synthesis is subject to conversion constraints via pressure; therefore, the F-T process should be run at pressures >0.825 Mpa to scale up to an advanced F-T process.

Quality Control of Material Thickness Using Ultrasonic Scanning. *BENJAMIN JOHNSON (University of Washington, Seattle, WA 98195) MORRIS S. GOOD (Pacific Northwest National Laboratory, Richland, WA 99352*). High precision characterization techniques are needed to assure quality control. In industrial settings, quality control often needs to happen at production rates. The current quality control procedure exchanges chemicals to change the index of refraction for an optical test. We proposed acoustic microscopy as a feasible high speed inspection measurement method as well as to eliminate a chemical waste stream from processes such as chemical baths. Using time of flight measurements both to the surface and through materials, it is possible to quantify thickness as well as shape parameters. To demonstrate that acoustic microscopy was a viable method, we simulated data produced by the current inspection method. With the time of flight and temperature of the water medium measured, shape and thickness could be calculated. Data was acquired at predetermined increments in order to reproduce current visual results and processed using Microsoft Excel to construct a visualization of the sample. A proof of concept test was conducted where the sample was normally scanned. This procedure proved very easy to compare thickness at all points and was consistent between repeat runs of the same specimen. Corroboration by another measurement technique is needed to evaluate performance; however, data quality was high and confidence exists that the technique will be proved successful in future work. Assuming this is performed successfully, an automated system is invisioned that could acquire all measurements almost instantaneously from multiple transducers as samples pass by a sensor. This would provide fast and reliable quality assurance, eliminate the element of human error or inconsistency, and provide an objective quantitative evaluation. Furthermore, this would save time, the cost of chemicals used by the current method, and thereby prevent a waste stream.

The TuffCell. *JONATHAN KIDD (Iowa State University, Ames, IA 50014) JOHN DAVID CARTER (Argonne National Laboratory, Argonne, IL 60439).* Solid Oxide Fuel Cells (SOFC) have been in the developmental stages for quite a few years. SOFC's are high temperature fuel cells that operate between 650° and 1000°C with an efficiency of 50 to 60%. SOFC provide an electrochemical reaction that produces electricity, with the total cell reaction being the oxidation of hydrogen or hydrocarbon fuels. Argonne National Laboratory is developing a new design concept for the SOFC called the TuffCell-a metallic bi-polar plate supported design. The goal with the TuffCell is to create a fuel cell that is rugged, compact, and simple to produce. The TuffCell is currently produced through tape casting methods paired with a stainless steel support system. This paper focuses on the sintering process that involves a high temperature hydrogen furnace and electrode gel, and their application for SOFC's and testing purposes. It examines the problems that were encountered in both the sintering profiles and the testing of the electrode gels. SOFC have the potential to provide a cleaner energy source, a reduced dependence on outside nations, and a wide variety of professional and personal applications.

Chemical Analysis of Sump Water in Pressurized Water Reactors. *JUSTIN KIESER (University of Texas at El Paso, El Paso, TX 79968) JONG HEE PARK (Argonne National Laboratory, Argonne, IL 60439).* During a Loss of Coolant Accident (LOCA) within the containment vessel of a pressurized water reactor (PWR), it possible for the discharged high temperature, high pressure radioactive water stream to displace thermal piping insulation comprised of Calcium Silicate (CalSil). This material then enters the sump water storage tank which contains Tri-Sodium Phosphate (TSP) to maintain a neutral pH. Aside from this actual material accumulating on the sump filtration screens, leached CalSil solution reacting with TSP, $3CaSiO_3 + 2Na_3PO_4 \rightarrow Ca_3(PO_4)_2 + 3Na_2SiO_3$, can form precipitates that may collect on the filtration screens and also accumulate on the inner piping walls, preventing the required amount of sump water from cooling the impaired reactor core. In order to study the reaction and determine an unsafe concentration of TSP, simulations and experiments were performed to study the formations of ions from both reactants, measuring conductivity as a function of time and temperature. A titration was also executed to examine the formation of obstructing precipitates. Based on titration and visual observation, a TSP concentration ranging from 250 ppm to 1,000 ppm forms the largest amount and greatest size of Calcium Phosphate, $Ca_3(PO_4)_2$ precipitates reaching 4 mm in diameter which pose the maximum threat for these particles to coalesce and cover a large majority of filter screen surface area. After 1000 ppm concentration is

surpassed, $Ca_3(PO_4)_2$ begins to dissolve while the solutions pH rises to basic level between 8.0 and 8.75. A rise in pH allows for the high iso-electric $Ca_3(PO_4)_2$ to bond with the inner steel piping walls, causing further precipitate accumulation which reduces sump water flow and increases head loss.

Theoretical Plotting of Thermodynamic Data Using the Thermocalc Software and Comparison with Established Data with an Emphasis in Radiological Fuels. *TRAVIS KOENIG (Colorado School of Mines, Golden, CO 80401) IRINA GLAGOLENKO (Idaho National Laboratory, Idaho Falls, ID 83415).* Thermodynamic data for various nuclear fuels is available and needs to be implemented for the generation of phase diagrams and other thermodynamic plots to be used in predicting various fuel alloy behaviors. Thermocalc is a thermodynamic modeling software capable of generating a variety of plots, however, it has not yet been fully evaluated and its use is limited by knowledge of the software. By implementing a database on nuclear fuel elements it is possible to generate accurate plots exhibiting the behavior of various fuel alloys to be used in power plants. These plots will then be compared with established or theoretical data from previous work to check validity and make predictions. The procedure involved in generating these graphs also needs to be documented. Working closely with the Thermocalc software developers and laboratory workers in the lab it is possible to generate plots for use in the prediction of nuclear fuel behavior of various alloys of Americium, Plutonium, Neptunium, Uranium, and Zirconium. These plots will be compared with previous and current work to create accurate predictions as well as the generation techniques documented. When comparing data established in situ with plots generated with Thermocalc, it was found that accurate plots were possible to generate, with only minimal discrepancies, plots of thermodynamic behavior of various alloys. However, with the software's limitations in modeling intermetallic phases, the Np-Zr phase diagram was difficult to interpret and further research will be required. This is part of an ongoing project to fully implement the Thermocalc software along with data established in this lab and previous work to accurately predict various fuel alloy behavior for use in nuclear power plants.

Fabrication of Titania Nanotubes on Glass and Transparent Conducting Oxide Substrates by Anodization of Titanium Films. *ANDREW LEENHEER (Colorado School of Mines, Golden, CO 80401) DAVID GINLEY (National Renewable Energy Laboratory, Golden, CO 89401).* Arrays of titania (TiO_2) nanotubes could potentially provide a good electron-conducting contact for organic thin-film solar cells. In this work, we fabricated titania nanotubes by anodizing thin films of titanium on both glass and transparent conducting oxide (TCO) substrates. Titanium thin films (500-700 nm) were deposited by radio-frequency (RF) sputtering. Films were anodized in acidic electrolytes containing small amounts of hydrofluoric acid at constant voltage ranging from 7 to 15 volts. After anodization, scanning-electron microscope (SEM) analysis revealed a nanotube structure. Titania nanotube structures were successfully grown on glass in an electrolyte containing sulfuric acID trisodium citrate, and potassium fluoride, with nanotube diameters around 50 nm. By monitoring the anodization current over time, the stages of nanotube formation were elucidated. Additionally, nanotubes were formed on a TCO substrate by anodizing in an electrolyte containing acetic acid and hydrofluoric acid. The dimensions and shape of the nanotubes appear to be controlled by the voltage, electrolyte pH, and anodization time. While not completely transparent, the arrays fabricated are promising for use in organic solar cells.

SPIDER Interferometer for Characterization of Femtosecond Pulses. *EDWARD LIKOVICH (Harvard University, Cambridge, MA 02138) ROBERT W. SCHOENLEIN (Lawrence Berkeley National Laboratory, Berkeley, CA 94720).* A SPIDER (Spectral Phase Interferometry for Direct Electric-field Reconstruction) interferometer is used to measure the time-dependent intensity and phase of an ultrashort optical pulse. Arbitrary optical fields, including ultrafast laser pulses, are characterized by the complex fields $E(\omega)=|E(\omega)|\exp[i\varphi\omega]$ or $E(t)=|E(t)|\exp[i\varphi t]$ which are related by the Fourier transform. In order to fully characterize ultrafast optical pulses, $\{E(\omega),\varphi(\omega)\}$ or $\{E(t),\varphi(t)\}$ must be determined. SPIDER achieves this by generating a pair of frequency-sheared copies of the input pulse through the use of nonlinear frequency mixing. The interferogram between these sheared replicas is analyzed to extract the intensity and phase properties of the pulse. By combining $|E(\omega)|$ and $\varphi(\omega)$, pulse shape can be completely determined. Ultrashort pulse compression can be optimized using SPIDER through direct observation of the phase of the amplified pulse, as opposed to iterative procedures of trial and error that must be used without SPIDER. In doing so, SPIDER provides real-time feedback that is useful in the optimization of pulse compression for time-resolved spectroscopy. Data analysis algorithms were designed and programmed using LabVIEW, and real-time phase retrieval (~2 Hz) was simulated using realistic input pulses under optimal conditions for the experimental parameters. A SPIDER interferometer was designed, assembled, and aligned using a low-power Helium-Neon laser. Femtosecond pulses with 800 nm wavelength were sent into the SPIDER, and the resulting interferograms were captured by the spectrometer. These interferograms were analyzed by the LabVIEW program, which extracted information about the relative time separation of the two short pulses and the phase offset of the SPIDER setup, which will be used as the calibration data for the SPIDER. Further study includes the introduction of the SPIDER into a hollow-fiber pulse compression system where it will provide real-time feedback necessary to optimize the compression of extremely short pulses (<10 fs). The SPIDER will eventually be deployed on the Femtosecond Beamline at the Advanced Light Source.

An Analysis of the Affected Behavior of PVDF due to Various Backing Materials. *WINSTON LYONS III (South Mountain Community College, Phoenix, AZ 85042) MORRIS S. GOOD (Pacific Northwest National Laboratory, Richland, WA 99352).* PVDF film is a piezoelectric material capable of sending or receiving a broad range of frequencies when used as an ultrasonic signal interpreter. This article addresses the questions of how different backing materials affect this characteristic of PVDF and whether or not that effect is dependent upon the film's thickness. Using a general material testing matrix, a series of transmitters were constructed for empirical experiments to qualitatively probe for the answers. Fourier transforms were derived from each transmitter by two different methods and compared to determine the exact effects the different backing materials have upon the PVDF's transmittance properties. Using the air backed data as a standard, each tested backing material is compared and discussed in relative terms. Also, all relevant graphs are provided.

Preliminary Surface Study of the Low-Temperature Baking Effect on Niobium. *LAURA MACINTYRE (Norfolk State University, Norfolk, VA 23504) ANDY T. WU (Thomas Jefferson National Accelerator Facility, Newport News, VA 23606).* Study has shown that the performance of niobium (Nb) Superconductive Radiofrequency (SRF) cavities can be improved by baking the cavities in air or in ultra-high vacuum (UHV) at temperatures ranging from 100° to 150°C. This low-temperature baking improves the quality factor (Q_o) and the Q-slope which appears at high fields in Q_o vs. Eacc curves for Nb SRF cavities. So far, primarily x-ray photoelectron spectroscopy has been used to study this low-temperature baking effect in terms of the possible changes of the surface chemical information of niobium. However, the detailed mechanism responsible for the improved performance is not clear. It has been proposed that oxygen diffusion into the bulk of Nb or disassociation of Nb_2O_5 may be responsible for the improved performance. Direct confirmation from surface analyses has yet to be done. In this study, Nb samples treated by buffered chemical polishing were baked at 120° and 160°C in air and at 120°C in UHV and compared to an unbaked sample. Relevant analytical surface tools were used to observe the Nb samples. Metallographic optical microscope images and 3-D profilometer surface scans showed no significant changes in grain structure or surface morphology after baking. On the other hand, the number of field emissions was found to be reduced significantly after baking in UHV as observed using scanning field emission microscopy. Data obtained from secondary ion mass spectrometry showed that indeed the low-temperature baking induces oxygen diffusion into the bulk. This study may affect Nb SRF cavity treatment procedures in the future and eventually improve the performance of Nb cavities used in particle accelerators.

Analysis of Old Copper Synchrotron Light Absorbers from the Stanford Positron Electron Accelerating Ring. *SARA MARSHALL (Franklin W. Olin College of Engineering, Needham, MA 02492) BENJAMIN SCOTT (Stanford Linear Accelerator Center, Stanford, CA 94025).* Synchrotron light absorbers intercept synchrotron radiation to protect chamber walls from excessive heat. When subjected to the high temperature of the beam, these absorbers undergo thermal stress. If the stress is too great or fatigues the material, the absorbers may fail. These absorbers are designed to last the lifetime of the machine. Any premature cracking could result in a leak and, consequently, loss of the ultra high vacuum environment. Using secondary and backscattered electron techniques, several sections of a used copper absorber were analyzed for material damage. Chemical analyses were performed on these samples as well. Comparing the unexposed sections to the sections exposed to the electron beam, few cracks were seen in the copper. However, the exposed samples showed heavy surface damage, in addition to crevices that could eventually result in material failure. Significant corrosion was also evident along the water

cooling passage of the samples. These findings suggest that further investigation and periodic inspection of absorbers in SPEAR3 are necessary to control corrosion of the copper.

Hydrogen Storage Properties of Nanomaterials. *JACOB MCMAHON (University of California Davis, Davis, CA 95616) SAMUEL MAO (Lawrence Berkeley National Laboratory, Berkeley, CA 94720).* Alternatives to fossil fuels have become necessary to prevent the adverse effects of carbon dioxide emissions on the environment. Fossil fuels used to create gasoline produce such emissions, but hydrogen is a clean burning source of energy. However, conventional hydrogen storage methods are impractical and dangerous. Current hydrogen storage methods employ cryogenic containers to maintain hydrogen as a liquID or pressurized tanks containing hydrogen gas. Since hydrogen has a very low density, there is not much hydrogen per pressurized container and it is therefore volumetrically inefficient. In order to have a practical amount of hydrogen to fuel a car with a pressurized tank of hydrogen gas, one would need a tank that takes up a large quantity of the cars space. In addition, a large pressurized tank of hydrogen is extremely flammable and explosive. Storing hydrogen in the liquid form for fuel is much more volumetrically efficient, but is very costly as hydrogen needs to be kept below -252.8°C in order to stay in the liquid form, and must be kept in a heavily insulated cryogenic container. Storage of hydrogen by means of a volumetrically efficient and safe method in nanoporous materials is the goal of this research. Several nanomaterials were tested at isothermal conditions from 0 to 20 bar using a gravimetric analyzer including aerogel, a mix of single and multi-walled carbon nanotubes, multi-walled nanotubes (MWNT), and carbon black particles. Preliminary results show that aerogel may be a candidate for hydrogen storage with a 2.10% mass uptake of hydrogen at room temperature. The aerogel also shows about 1.45% mass uptake of hydrogen at 463°C. Both carbon nanotube samples, and the carbon particles show small uptake of hydrogen at room temperature. The multi-walled nanotubes and carbon particles show a steady decrease in mass uptake as the pressure of hydrogen increases. Further experiments must be conducted to ensure that the aerogel uptake of hydrogen is real, and to discover why the uptake of the MWNT and the carbon particles went down over time.

Electrochromic Tunable Windows: Development of a Gas Phase Counter Electrode to Simplify the Device Stack. *BRENDEN MILLSTEIN (Harvard University, Cambridge, MA 02138) JONATHAN SLACK (Lawrence Berkeley National Laboratory, Berkeley, CA 94720).* Global energy consumption for conditioning large office buildings demands annual energy expenditures in the hundreds of billions of dollars, much of which could be saved by the use of electrochromic windows. Electrochromic windows can be tuned across their range of optical states in mere minutes, allowing optimization of interior lighting levels while providing dynamic control of solar heat gain and radiative energy losses from conditioned space. Current electrochromic devices utilize solid-state counter electrodes for ion storage which are technically difficult to engineer and costly to manufacture. This paper focuses on the development of a catalytic ITO/Pd layer coupled with a dilute H_2 gas reservoir to replace the solid-state counter electrode. Layers of the prototype device stack ranged from 3 to 500 nm, and were deposited onto ITO-coated glass at process pressures varying from 2-10 mTorr by DC magnetron and RF sputtering. The use of a cartridge-mask system allowed the creation of multiple device stacks on a single substrate, facilitating side-by-side analysis of the unique geometries. A device consisting of ITO, WO_3, ZrO_2, Pd, ITO, and a final Pd cap layer was found to exhibit successful electrochromic optical switching in the presence of a 4% H_2, balance Ar, gas reservoir. The device stack colored with the application of 1.5v, and returned to its transparent state (bleached) at 0v applied. The applied potential was necessary only during switching; once tuned the device remained in its optical state. Research was also begun on an electrochromic reflective window that could offer even greater energy savings due to its ability to modulate between reflecting and transmitting states across the full solar spectrum. Both technologies require further research for optimization, but hold promise as energy efficient features of the modern building envelope, capable of delivering billions of dollars in energy savings to the US economy.

Data Acquisition Issues for Phosphor Thermometry. *ROBERT MOORE (University of Louisiana at Lafayette, Lafayette, LA 70504) STEVEN W. ALLISON (Oak Ridge National Laboratory, Oak Ridge, TN 37831).* Phosphor thermometry is used for non-contact remote access temperature measurements. Certain characteristics of phosphor emission, like decay time, are temperature dependent and can be correlated with a reference to provide a method of temperature measurement. In order to achieve the correlation needed, every aspect of the calibration procedure must be fully understood. In early testing, several divergences from previous calibrations of La2O2S:Eu were discovered. The calibration curve produced in these experiments diverged from the previous values for temperatures that exceeded 70°C. Certain aspects of the equipment setup and software appeared to cause these small differences. In addition, to investigate calibration effects from excitation source changes, a series of light emitting diodes (LEDs) were tested with a fluorescent ruby target. The ruby exhibited a similar response to two different LED wavelengths (405 nm and 435 nm). The procedures studied here are just examples of the characteristics of commonly used equipment for calibrations and excitation sources. The testing suggests that even the smallest changes can affect results in unexpected ways and must be understood in order to improve this thermometry approach.

Template-Assisted Chemical Vapor Deposition (CVD) Growth of Carbon Nanotubes. *STEVEN MUI (Columbia University, New York, NY 10027) STANISLAUS WONG (Brookhaven National Laboratory, Upton, NY 11973).* Carbon Nanotubes (CNTs), which are composed of cylindrical layers of graphene, can exhibit novel mechanical and electronic properties depending on their diameter, chirality, and assembly. In order to understand the potential functions and applications of carbon nanotubes that extend to both physical and biological sciences, fabricating a variety of carbon nanotube structures becomes necessary. Using the chemical vapor deposition (CVD) method with an alumina template, various gases, and catalysts, we can produce a number of CNT types, which can then be analyzed with a number of microscopic and spectroscopic techniques. In particular, we are interested in fabricating multi-walled carbon nanotubes (MWNTs). Using an alumina membrane that was placed in tube furnace, a gas mixture of 30% ethylene and 70% helium, heated at 670°C, was flowed over a 6h period to form MWNTs in the nanoscale pores of an alumina template. The alumina template was dissolved by immersing the membrane in 10M NaOH solution followed by centrifugation to remove the NaOH. The nanotubes were characterized by different microscopic and spectroscopic techiques, including SEM, TEM, AFM, UV-Vis and FTIR. The analyses show the presence of MWNTs as well as single walled nanotubes (SWNTs). Further purification protocols are necessary before additional forms of analysis can be used to verify the presence of MWNTs as well as single-walled carbon nanotubes (SWNTs). This work, involving the fabrication of a variety of CNT structural motifs, will contribute to further research involving electronic and biological applications of composite nanomaterials.

Parameter Variations for Low Temperature Synthesis of Carbon Nanofibers. *MATTHEW MUSGRAVE (James Madison University, Harrisonburg, VA 22807) MICHAEL L. SIMPSON (Oak Ridge National Laboratory, Oak Ridge, TN 37831).* Carbon nanofibers are cylindrical structures of stacked modified graphene sheets with a wide range of diameters and lengths. The synthesis of vertically aligned carbon nanofibers (VACNFs) by plasma enhanced chemical vapor deposition is conventionally done by heating a silicon substrate with nickel catalysts patterned on it and then creating an ammonia and acetylene plasma above it. By adding oxygen to the gas mixture the intent is to provide catalytic oxidation of the acetylene that should heat the catalyst particles allowing the substrate heater to operate at lower temperatures. By growing carbon nanofibers at a lower temperature a larger range of substrates can be used. Currently the VACNFs are grown at temperatures around 700°C. The synthesis of the vertically aligned carbon nanofibers is optimized at decreasing substrate temperatures by changing the ratio of ammonIA acetylene, and oxygen in the plasma and the power of the plasma. If there is too much ammonIA carbon nanofibers are damaged and lose the catalyst particles, and nanofibers will be covered in silicon oxide or completely etched away. If there is too much acetylene, the catalyst particles will be covered by a carbon film and VACNF synthesis will be impossible. A strategy was developed in that small changes to one parameter are made and the other parameters are adjusted after the quality of the material is assessed by scanning electron microscopy (SEM) and x-ray energy dispersive spectroscopy (EDS). SEM images of the carbon nanofibers are captured for determination of morphology, shape, height, and density measurements, and EDS is used to determine the concentration of carbon, silicon, and oxygen in the fibers. The images of nanofibers grown with oxygen are compared with images of a control group of nanofibers synthesized without oxygen. The results collected so far are preliminary, but it can be concluded that oxygen is not detrimental to the synthesis of VACNFs and can play a similar role as ammonia in etching amorphous carbon. Additionally small changes in the gas flow value of oxygen yield large differences in the appearance of the nanofibers compared to changes in the gas flow value of ammonia.

Resolving Electromigratory Issues Via Nanomaterial Implementations. *CHRISTOPHER NACHMIAS (Georgia Institute of Technology, Atlanta, GA 30332) ARLENE WU ZHANG (Brookhaven National Laboratory, Upton, NY 11973).* Electromigration affects almost all integrated circuit and microelectronic device design, production, and functionality. This phenomenon occurs due to an overwhelming amount of current density passing through increasingly smaller conducting vias which comprise electronic devices. Causing cracks and voids in the connections and severely hindering operation, electromigration will continue to limit the various performance aspects of electronic devices unless a solution is realized. One such solution may be the use of nanotechnology, whether it is the popular nanotubes or emerging nanowires, in devices to curb the effects of electromigration. Nanotubes and nanowires have exhibited extraordinary conductive and electrical properties which make them a promising alternative to common copper and silicon devices today, despite some difficulties with utilizing these materials. Several materials were utilized to study and interpret the situation of electromigration issues at present and the possible implementation of nanomaterials. Extensive use of the proceedings within varying scientific and technological conferences discussing nanomaterials and microelectronic device fabrication were observed and analyzed. In accordance to these references, several online periodicals relating to the research field were observed as this is a developing technology and breakthroughs occur daily. Finally, discussion with others directly related to the research fields was conducted. Through the research, it was observed that, as stated previously, nanotubes and nanowires present themselves as viable alternatives to present microelectronic vias. Various methods exist to develop these materials, however harnessing their full capability is yet to have been achieved. Such considerations as the chemical orientation of these materials, their functional lifetime, and fabrication concerns are issues that are still open for further exploration and must be examined. It is clear that ultimately, to some extent some of the current means toward microelectronic circuit fabrication and development will have to progress in another direction due to limitations presented by electromigratory issues. The failure of the devices due to these issues is at the root of nanomaterial research and exploration to other alternatives as well. The benefits of using nanomaterials are overwhelming, however overcoming inherent difficulties associated with them may limit their time toward fruition as a common place implementation in the field.

Refurbishment of High Temperature Creep Frames for Generation IV Nuclear Reactor Material Testing. *NATHAN OTTINGER (University of Tennessee, Knoxville, TN 37996) TIMOTHY MCGREEVY (Oak Ridge National Laboratory, Oak Ridge, TN 37831).* Generation IV nuclear fission reactors promise to be more efficient and produce less nuclear waste than reactors already in operation. Six reactor designs have been chosen as part of Gen IV, each with sustained operation temperatures ranging from 510°C to 950°C. One such reactor, the Very High Temperature Reactor (VHTR), will produce electricity as well as hydrogen for use in fuel cells. High temperature creep tests are necessary to obtain creep properties of materials appropriate for these reactors. The Applied Test Systems (ATS) creep frames are structurally in excellent condition. However, the Instron self-aligning hydraulic grips used to hold and equally distribute force throughout the specimen's cross section were either overheating to the point of meltdown or had lost hydraulic pressure. These grips were systematically taken apart and thoroughly inspected. In most cases, the overheating problem was found to be blocked coolant passages. Those without hydraulic pressure were completely rebuilt. Seals were replaced and the grips were refilled with hydraulic fluid. The creep frames also require some new load cells since the Gen IV tests will require significantly less load than the current load cells. CAD drawings were made for a hydraulic grip to load cell adapter plate that will accommodate the new load cells. Capacitance extensometers are currently needed for seven of the machines. Portions of previously used extensometers exist, and CAD drawings will be made of the parts needed to turn the portions into usable extensometers. Financial limitations will make the completion of this refurbishment highly unlikely. However, by the projects conclusion, the hydraulic grips will be ready for long term high temperature tests, the load cells will be ready to mount, and several more machines may have operable extensometers.

An Investigation of the Dependence of Fracture Toughness on Crystallographic Orientation in Single-Crystalline Cubic (ß) Silicon Carbide. *GEORGE PHARR (Rice University, Houston, TX 77005) YUTAI KATOH (Oak Ridge National Laboratory, Oak Ridge, TN 37831).* Along with other desirable properties, the ability of silicon carbide (SiC) to retain high strength after elevated temperature exposures to neutron irradiation renders it potentially applicable in fusion and advanced fission reactors. However, properties of the material such as room temperature fracture toughness must be thoroughly characterized prior to such practical applications. The objective of this work is to investigate the dependence of fracture toughness on crystallographic orientation for single-crystalline ß-SiC. X-ray diffraction was first performed on the samples to determine the orientation of the crystal. Nanoindentation was used to determine a hardness of 39.1 and 35.2 GPa and elastic modulus of 474 and 446 GPa for the single-crystalline and polycrystalline samples, respectively. Additionally, crack lengths and indentation diagonals were measured via a Vickers micro-hardness indenter under a load of 100 gf for different crystallographic orientations with indentation diagonals aligned along fundamental cleavage planes. Upon examination of propagation direction of cracks, the cracks usually did not initiate and propagate from the corners of the indentation where the stresses are concentrated but instead from the indentation sides. Such cracks clearly moved along the {1 1 0} family of planes (previously determined to be preferred cleavage plane), demonstrating that the fracture toughness of SiC is comparatively so much lower along this set of planes that the lower energy required to cleave along this plane overpowers the stress-concentration at indentation corners. Additionally, fracture toughness in the <1 1 0> direction was 1.84 $MPa \bullet m^{1/2}$, lower than the 3.46 $MPa \bullet m^{1/2}$ measured for polycrystalline SiC (which can serve as an average of a spectrum of orientations), further demonstrating that single-crystalline ß-SiC has a strong fracture toughness anisotropy.

Method for Creating Gradient Porosity in Sintered Nickel Components. *MORGAN POLIKOFF (University of Illinois at Urbana-Champaign, Urbana, IL 61801) K. SCOTT WEIL (Pacific Northwest National Laboratory, Richland, WA 99352).* Titanium is widely used for orthopedic implants, due to its biocompatibility and high strength-to-weight ratio. In recent years, interest has been shown in creating titanium components with a graded porous microstructure. With greater porosity in the center of the part and higher density in the edges, the components would more closely replicate the properties of natural bone. The goal of the present study was to establish processing techniques for producing sintered metal bodies with graded porosity. As a surrogate for titanium, nickel was chosen for its inertness to carbon, nitrogen, and oxygen impurities and ease of sintering. A binder system of naphthalene, stearic acID and ethylene vinyl acetate was mixed with nickel powder to allow the pre-sintered body to be shaped by pressing. The use of a naphthalene-based binder system is advantageous because the naphthalene can be sublimed at low temperatures (~60-80°C). In combination with controlled drying and cold isostatic pressing (CIP) protocol, the use of naphthalene allows the porosity of the body to be tailored. Spherical, 400 mesh nickel powder was mixed with the binder system in 45%, 55%, 60%, and 65% ratios by volume and pressed into discs. The discs were subjected to drying and CIP under varying conditions. The working hypothesis was that by subliming different amounts of naphthalene from the discs in a vacuum oven before CIP, the sintered nickel components would exhibit varying degrees of gradient porosity. Inadequate green strength of the partially de-bindered nickel discs was a problem initially, but this was overcome by carrying out an initial CIP step before de-bindering. After a series of drying curves was established for the discs at different temperatures, the discs were CIPed and sintered in a high-temperature furnace. The data revealed a positive correlation between final density and naphthalene removal - as more naphthalene was removed from the samples prior to CIP, the final density increased. Also, with decreased nickel loading in the initial mixture, final density decreased. Metallurgical analysis will be conducted on the sintered samples to determine their porosity and examine their cross-sectional microstructure. Future study will focus on the use of a modified naphthalene-based binder system, as well as an effort to enlarge the pores by employing nickel carbonate in place of pure nickel. These techniques will also be generalized to titanium and other metals.

Evaluation of Titanium Aluminide and Silicon Nitride Valves Using Elastic Optical Backscattering Techniques. *DAVID POTEMPA (Bradley University, PeorIA IL 61606) JIANGANG SUN (Argonne National Laboratory, Argonne, IL 60439).* Silicon nitride and titanium aluminide are advanced materials that exhibit excellent thermal properties, wear resistance, and corrosion resistance. It is because of these characteristics that they are ideal for use as engine valves. In order to assist in bringing these advanced materials into commercial realization, it is our task here at Argonne National Laboratory to provide information on the design, manufacturing, and structural performance of these valves. Using elastic optical backscattering techniques, surface and subsurface defects are detected and analyzed to predict

valve fractures or confirm the origins of a fractured valve. Images obtained from newly refinished silicon nitride valves show less surface and subsurface machining damage than previously recorded. Since a primary cause of failure in ceramics is the propagation of a surface crack developed during machining, less surface and subsurface machining damage implies a stronger valve. Titanium aluminide valves, scanned for the first time, provide for excellent images of surface machining damage. Their poor optical translucency prevents deep scans of subsurface defects. Additional tests and subsequent scans will be necessary to determine the structural performance of these valves. These scans are the first in a planned program of alternating scan and rig/engine tests. As the program continues, additional rig/engine tests and subsequent scans will provide more information regarding the structural performance, future manufacturing, and future design of these valves.

Sputter Rate Variations in Porous low-k dielectric Thin Films Exposed to Isopropanol Using the Auger Electron Spectrometer and the X-ray Photoelectron Spectroscopy. *BRIAN PULTZ (San Joaquin Delta College, Stocktion, CA 95207) SCOTT LEA (Pacific Northwest National Laboratory, Richland, WA 99352).* Porous nanomaterials exhibit different sputtering properties than their dense counterparts upon ion beam exposure. Previous experiments have show that there are some increases in the sputter rate after the low-k dielectric (LKD) films have been exposed to isopropyl alcohol (IPA). This work is intended to sort out some of the reasons for the observed sputter rate differences after these films have been exposed to IPA. These experiments were carried out using both x-ray photoelectron spectroscopy (XPS) and Auger electron spectroscopy (AES) using samples from the same wafer. For each spectrometer, four samples were used: a control that had not been exposed to IPA, a sample that was analyzed within 15 minutes of exposure to IPA, a sample that was analyzed 72 hours after exposure to IPA, and a sample that was analyzed after exposure to IPA and placed in vacuum for 72 hours. The results showed that the samples that had been exposed to the IPA have a lower sputter rate (greater sputter time) than the untreated samples. This was true for both the XPS and the AES analysis. Analysis of the samples 72 hours after IPA exposure showed a partial recovery of the initial sputter rate. This recovery was more pronounced for the sample that had been placed in vacuum for 72 hours prior to analysis. These results suggest that the added mass in the films due to the presence of IPA accounts for the decrease in sputter rate observed in previous experiments.

Photonic Bandgap Material Fabrication via Two-Polymer Micro-Transfer Molding. *XUEYING QIN (Carleton College, Northfield, MN 55057) KRISTEN CONSTANT (Ames Laboratory, Ames, IA 50011).* Photonic bandgap materials, also known as photonic crystals, are materials that exhibit a photonic bandgap, which is a phenomenon that prevents a specific set of wavelengths of electromagnetic radiation from propagating through the crystal. Two-polymer micro-transfer molding is a novel technique for the fabrication of these crystals, and can be performed much more cost-effectively with a minimal loss in efficiency than traditional photonic crystal fabrication techniques. By using pre-made silicon wafer molds, a mixture of polydimethylsiloxane (PDMS) is poured onto the pattern and the pattern is then cured in an oven for several hours, allowing the PDMS to solidify. When removed, the PDMS mold now has the pattern imprinted in it, in the form of many small channels in its surface, whose size and spacing depend on the desired wavelength bandgap. These channels are then filled with polyurethane (PU) and are then cured under ultraviolet light to allow the PU to solidify. The sample area is now coated with optical cement (PA), a glass cover slip is attached, and then the sample is once again cured in a UV oven. Afterwards, the PDMS is peeled off and the remaining PU structure is transferred onto the glass slide. The work done by this group aims to improve the PU-stage of sample fabrication. This method is desirable in that it does not need to be performed in clean-room facilities, and therefore is far more cost-effective than traditional methods. The single-layer samples can then be used in 3-dimensional crystals via a method of stacking also being developed by this research group. This is all a part of a larger effort to develop cost-effective, efficient techniques for the fabrication of 3D photonic bandgap materials.

Alternative Methodologies for Neural Networks that Predict Charpy Toughness Properties. *STACEY RADEN (University of Tennessee, Knoxville, TN 37966) JOHN M. VITEK (Oak Ridge National Laboratory, Oak Ridge, TN 37831).* Modeled after the human brain and its neural connections, artificial neural networks are nonlinear analytic tools that identify patterns between input and output data and can then be applied to predict behavior. A neural network is formed from multiple layers consisting of an input layer constructed from input nodes, a specified number of "hidden" layers constructed from "hidden" nodes, and an output layer constructed from output nodes. This advanced investigative tool was applied to the problem of predicting Charpy toughness in welds as a function of alloy composition, weld conditions, and heat treatment. The intent of this project was to compare these two methodologies to determine which approach is better suited for predicting the toughness of a weld. The first approach produced a neural network which predicts the Charpy value for given metal composition, welding conditions and heat treatment. This approach considered seventeen material inputs and one output (toughness). The second approach made use of the accepted fact that toughness versus temperature behaves in a sigmoidal fashion. The data were pre-processed to produce the parameters of a sigmoid function for each condition and a neural network was created to predict these curve parameters. This approach used sixteen material inputs and four outputs (four curve parameters). The first step in the analysis was to identify the optimum network architecture for each model (the optimum number of hidden nodes). Neural networks with a range of hidden nodes were trained and tested (up to twenty nodes for the first approach and up to six nodes for the second approach). Several pairs of training and testing data were considered to allow for the inherent noise in such an analysis. For the first approach (direct prediction of toughness), an architecture containing five hidden nodes was the optimal architecture. For the second approach (prediction of parameters for toughness versus temperature curve), the optimal architecture contained two hidden nodes. After calculating the root mean square error for both approaches, the first approach (direct calculation of Charpy toughness) seemed to be the most accurate. However, this method also seems to reproduce noise in the data and therefore may not be the best method to predict Charpy toughness.

Comparison of "Ridge" Like Structures Induced by Light and Heavy Ions on Single Crystal $SrTiO_3$ Surfaces Using MeV Implantation. *LEE REAM (Yakima Valley Community College, Yakima, WA 98908) V. SHUTTHANANDAN (Pacific Northwest National Laboratory, Richland, WA 99352).* The understanding of nano-structures has become increasing interest due to their applications in several areas. In particular, there is a high demand for high surface area nano-structures oxide materials due to their applications in heterogeneous catalysis. It has been recently showed that periodic "ridge" like structure with high surface area can be synthesized on $SrTiO_3$ single crystal surface by grazing angle ion implantation. In the present work, influence of the mass of incident ions on these ridge like structures were systematically studied using Rutherford backscattering spectrometry (RBS), Proton Induced X-ray Emission (PIXE), scanning electron microscopy (SEM), and energy dispersive x-ray emission (EDX). Heavy (Gold) and light (nickel) ions with different ion doses and energies were implanted at grazing angle direction to the surface at 300 K in $SrTiO_3$ (100) single crystal surfaces. Measurements of the samples were conducted directly after implantation. RBS measurements from the sample implanted with gold show that the gold is uniformly distributed to a depth of 400 nm from the surface. Total dose of implanted gold and nickel were obtained by PIXE. SEM micrographs obtained from these samples show that the surface of the implanted region underwent substantial rearrangement and formed "ridge" like structures. These "ridge" like structures are periodic in nature with wavelengths ranging from 0.5 to 4 microns and formed throughout the implanted region with the average heights of 0.2 to 4 microns. SEM micrographs further reveled that there is a strong correlation exists between the directions of the ridges and the mass of the incident ion beam. It was noticed that with the heavy ions the ridges that formed were parallel to the beam. While, with the light ions, the ridges formed perpendicular to the direction of the incident ion beam.

Radiation Damage in Structural Stainless Steels. *DAVID RIVERA (University of Texas at El Paso, El Paso, TX 79968) OMESH K. CHOPRA (Argonne National Laboratory, Argonne, IL 60439).* Austenitic stainless steels (SS's) are widely used in nuclear reactor cores around the world. Their superior fracture toughness, durability, and relatively high strength make these materials a prime candidate for use in reactor core internal components. However it has been shown that extended periods of neutron irradiation can have a severe detrimental effect on such materials, namely a marked reduction in ductility and fracture toughness coupled with a drastic increase in material yield strength. Slow strain rate tests (SSRT's) were conducted on several irradiated SS tensile specimens in simulated boiling water reactor (BWR) conditions. All tests were conducted with a strain rate of 1.65×10^{-7} s^{-1} and a pressure of 1,300–1,450 psi at 289°C. After failure, the specimen fracture surfaces were examined using a scanning electron microscope

in order to asses the extent of intergranular and transgranular fracture. The results of the SSRT's reveal the characteristic increase in yield stress and reduction in ductility experienced by samples subjected to irradiation. Nearly all the 304 and 316 SS alloys followed a similar trend in work hardening behavior in that each individual alloy experienced a tendency to work harden at the same rate regardless of irradiation dosage. This leads to the possibility of a unique critical true stress existing for every austenitic SS alloy. Changes in yield strength as a function of displacements per atom (dpa) were plotted and showed to correlate reasonably with the previous model proposed by Oddeta & Lucas. These changes in yield strength and ductility are brought about by the creation of many small defects within the material consisting of a vacancy and a self interstitial atom (SIA). Such defects have a tendency to group together and form dislocation loops, which in turn inhibit other dislocations from moving thus increasing yield strength and decreasing ductility and fracture toughness. Reduction of fracture toughness leaves the material susceptible to irradiation assisted stress corrosion cracking (IASCC). The depletion of Cr at the grain boundaries (GB's) is believed to be the primary cause of IASCC, such a reduction in Cr at the GB's leads to the preferential attack of corrosion at these sites. This investigation is part of a much larger research effort focused on studying the effects of radiation on austenitic SS's in order to increase the life expectancy and efficiency of current and future nuclear reactors.

Initialization, Optimization and Integration of Ultra-High Speed Photography for Rapid Solidification Processes. *DAVID SAUER (University of Missouri-Rolla, Rolla, MO 65401) R. WILLIAM MCCALLUM (Ames Laboratory, Ames, IA 50011).* An Ultra-High Speed camera has been acquired by the Materials and Engineering Physics Program at Ames Laboratory to study rapid solidification processes. The camera, a Phantom v7.1 manufactured by Vision Research Inc., is state of the art in digital rapid photography. The camera is capable of 160,000 digital images per second at a resolution of 32 x 32 pixels. Using melt spinning as the model process, the image acquisition system has been optimized for optics, image size and rate (320 x 320 pixels at 8,000 images per second), and attached data collection. A matrix of rapid solidification runs were performed and analyzed for characteristic flow parameters as derived from acquired images. Representative images from the experimental matrix of solidification runs, spanning multiple parameters, were analyzed for dynamic fluid flow dimensions. Two main variables were verified as influences on the melt pool characteristics, wheel speed and ejection pressure. When wheel speed increased, the melt pool length showed a hyperbolic slope with the melt pool length approaching a minimum value of 2 mm. When ejection pressure was changed, the melt pool height changed in a characteristic inverse linear fashion. With these results, the rapid solidification process will be better understood and the characteristics of the product will be more easily identifiable with the parameters applied during the melt-spin process.

The Solubility of Magnesia in Molten Lanthanum Chloride-Magnesium Chloride Mixtures. *TIMOTHY SCARPINATO (Syracuse University, Syracuse, NY 13244) GREGORY KRUMDICK (Argonne National Laboratory, Argonne, IL 60439).* In response to the ongoing pursuit for a better fuel economy, more viable methods for producing primary magnesium are being examined. With its superior strength-to-weight ratio and low density, magnesium has the potential to significantly reduce vehicle mass and be utilized in a variety of other applications. Previous research has suggested that the LaC_{l3}-MgC_{l2} (lanthanum chloride-magnesium chloride) electrolyte system is a strong candidate for magnesium production through MgO (magnesia) electrolysis. While an earlier study has suggested that magnesia is highly soluble in this system, no details of the measurements were given. The results of our study do not support this, indicating a much lower solubility. However, the solubility did increase with increased molar percentage of LaC_{l3} in the system, as reported in literature. To study the solubility, the LaC_{l3}-MgC_{l2} mixture was placed and sealed in a graphite crucible and heated in a crucible furnace to the desired temperature. Samples were taken before adding the magnesia crystals and at successive time increments after the magnesia addition. The experiments were run between 4 and 7 hours and agitated throughout to ensure complete saturation. According to the results, the system is saturated rather quickly, supporting its use in magnesia electrolysis. An investigation on the discrepancies between this study and previous work should be conducted. Future efforts will focus on exploring the level of solubility needed for this system to be an acceptable electrolyte and optimizing the electrolyte based on the solubility curve.

Production of Corrugated Micro- and Nanocrystalline Diamond Stripper Foils for the Spallation Neutron Source Using Chemical Vapor Deposition. *DANIEL SHOEMAKER (University of Illinois at Urbana-Champaign, Urbana-Champaign, IL 61801) R.W. SHAW (Oak Ridge National Laboratory, Oak Ridge, TN 37831).* Microwave plasma chemical vapor deposition (MPCVD) has been used to produce single-edge supported, micro- and nanocrystalline diamond films for use as stripper foils in the Spallation Neutron Source (SNS). Beam simulations have predicted that diamond foils will provide a longer lifetime in the SNS H- beam (38 mA at 1 GeV) than conventional carbon foils, while the geometry of the SNS accumulator ring requires foils that are supported by only one edge. The freestanding diamond must have dimensions of at least 12 mm x 20 mm and an areal density of ~350 μg/cm^2, which corresponds to a thickness of ~1.0 μm. Films were deposited on silicon substrates, which were pretreated to enhance diamond nucleation in the MPCVD reactor by scratching in an ultrasonic bath using a slurry of diamond particles in methanol. The highest nucleation density was obtained by using a mixed slurry containing 0.3 g of 30–40 μm and 0.3 g of <0.25 μm diameter diamond particles in 20 mL of methanol. Microcrystalline diamond films were grown using MPCVD operating at 1,300 W power in a 2% CH_4 98% H_2 atmosphere at 50 torr. Films for use in the SNS typically were deposited in 110 min, while use of the mixed scratching slurry enabled growth of fully continuous films in less than 25 min. Nanocrystalline films were deposited at 900–1,000 W in a 90% Ar atmosphere with 1–2% CH_4 and 8–9% H_2 at 130 torr. Due to cooling after deposition, the thermal expansion mismatch between diamond and silicon causes considerable stress in the film, which leads to scrolling once the substrate has been etched away. To prevent curling, photolithography was used to pattern 7 μm-deep U-shaped channels in the substrate, which ran along the unsupported edges of the foil and covered 20–40% of its area. The corrugated foils remained flat after their backing was removed. While microcrystalline films with high nucleation density were sufficiently robust for transport and beam testing, nanocrystalline films have shown superior mechanical strength, fewer pinholes, and decreased surface roughness. These smoother films are expected to exhibit more reliable stripping efficiencies. Future work on this project will focus on making improvements to the processing techniques based on the results of nanocrystalline film beam testing in the Los Alamos Proton Storage Ring and the SNS.

In-Situ Electrical Biasing in a TEM. *AMANDA SIMENS (Lehigh University, Bethlehem, PA 18015) ANDY MINOR (Lawrence Berkeley National Laboratory, Berkeley, CA 94720).* Observing a microstructural change of nanoscale materials has historically relied on ex situ electrical measurements combined with ex post facto Transmission Electron Microscope (TEM) analysis. Recently, a new custom built electrical biasing holder designed for the JEOL 3010 TEM at NCEM has made it possible to measure the electrical properties of a sample while simultaneously observing the microstructural evolution at high spatial resolution. In order to characterize the electrical performance of thin films and nanostructures, we first need to gain a better understanding of the microstructural changes that occur under an applied bias. This study investigated three different materials with the biasing holder including gold nanowires, carbon nanotubes, and polymeric liquid crystals. The gold nanowires served as a control and as a means of calibrating the biasing holder. Experiments suggest that even though liquid crystals such as poly(2,5-2'ethylhexyloxy-p-phenylene vinylene) have the potential to align under an applied bias, adhesion forces between the film and the substrate prevented it from doing so. The carbon nanotube samples were investigated for the possibility of forming nanoscale electrode gaps for molecular electronic applications. The intention was to characterize the resistive heating of the nanotubes to a degree that they could be predictably controlled.

Erosion Resistance of MoCuN Coated Steel. *SULAV SINGH (University of Illinois at Urbana-Champaign, Champaign, IL 60439) JULES ROUBORT (Argonne National Laboratory, Argonne, IL 60439).* The objective of this research is to characterize and understand erosion behavior of various films deposited under different conditions on stainless steel substrates. Experiments were performed at Argonne National Laboratory to evaluate the erosion resistance of coated substrates using SiC particles having 143 μm diameter, at incidence angles of 20°, 45°, and 90°, and velocities of 30 m/s and 100 m/s. Introduction Engineered coatings are very beneficial for machine components to protect them from severe environmental conditions. However, these environmental conditions, often erode, in service, and break down the coatings over time. Thus, there is a need to understand the erosion behavior of these protective coatings in order to prolong and improve their life. The present study was conducted on MoCuN

(molybdenum copper nitrite) coating on 304 stainless steel substrates, in order to better understand and characterize the erosion resistance of this coating. Experimental Details To characterize the erosion rate, the ANL particle slinger was used to erode coated substrates. The particle slinger can erode ten samples simultaneously, though for this experiment only three samples were eroded at a time. The particle slinger mechanically accelerates solid particle abrasives onto a sample's surface at a predetermined velocity and angle in a vacuum. Several MoCuN coated steel substrates were eroded at velocities of 30 m/s and 100 m/s and at impact angles of 20°, 45°, and 90° using SiC erodent. The thickness of the coating is between 4 and 5 microns. Following each trial, the eroded substrate was cleaned by applying an air jet onto the sample to remove any unwanted particles. The weight loss of the sample was then measured on a balance with a sensitivity of 0.1 mg. This data was then used in a computer program that calculated erosion rate. My Contribution In this experiment I ran all the trail runs. Then, I collected data and measured the weight loss of the material. After the weight loss was recorded I inputed the recorded data into the computer program that calculated the erosion rate. When this was completed, I analyzed the results with my supervisor, in order to understand the behavior of the coated substrates erosion characteristics.

Formation of Epitaxial MgO Thin Films on Textured Ni-3 at% W Substrates by *dc* and *rf* Reactive Magnetron Sputtering. *BETHANY SPENCER (North Carolina Agricultural and Technical State University, Greensboro, NC 27411) DHANANJAY KUMAR (Oak Ridge National Laboratory, Oak Ridge, TN 37831).* Robust high temperature superconducting (HTS) wire is a layered composite comprised of a HTS compound, usually $YBa_2Cu_3O_7$ (YBCO), deposited on intermediate oxide layers grown on a metal/metal-alloy substrate. Buffer layers are generally required between the HTS film and the metal substrate in order to prevent oxidation of the substrate material and chemical poisoning of the superconducting thin film. Consequently, there is a great need to develop buffer architectures that could prevent inward oxygen diffusion to the metal substrate. In this context magnesium oxide (MgO) is very appealing because it has a much lower oxygen diffusion coefficient than other oxide buffer materials studied. If MgO can be grown epitaxially on the metal substrate, both the efficiency and the robustness of 2nd generation superconducting wires (coated conductors) could be significantly improved. Deposition parameters of a reactive magnetron sputtering process were varied in order to study whether an epitaxial film of MgO could grow on a biaxially textured Ni-3 atomic% W (Ni-3 at% W) substrate. Film growth took place in a mixture of argon or argon 4% hydrogen and water vapor (H_2O) which was used as a controlled, low-level oxygen source. Two inch Mg and MgO targets were used for the metal source. The temperature, power, partial pressure of (H_2O), and deposition time were varied for each experimental run. X-ray diffraction techniques were used to determine the crystal structure and the quality of the deposited films. *dc*-sputtering with the Mg target failed to yield crystalline MgO films. This is mainly due to the high vapor pressure of Mg at the sputtering temperatures. However, *rf*-sputtering with the MgO target was successful. X-ray diffraction analysis indicated that the MgO and Ni-3 % W la+yers had good in- and out-of-plane alignment and were cube-on-cube oriented. Atomic force microscopy measurements indicated an increase in surface roughness with the sputtering temperature. At temperatures below 400°C and H_2O pressures above $1x10^{-6}$ Torr, (00l) oriented MgO films were successfully grown. More experiments should be performed to narrow down the parameters for the growth of MgO films with optimal orientation and intensity. Ultimately, the performance of MgO buffer layers should be tested with the electrical properties of HTS coatings.

Comparisons of Austenitic Cast Stainless Steel Alloys Used for Steam Turbine Casings. *CORY STINTON (University of Tennessee, Knoxville, TN 37996) PHILIP J. MAZIASZ (Oak Ridge National Laboratory, Oak Ridge, TN 37831).* Current materials used for turbine casings under high temperatures and pressures are reaching their maximum temperatures and thus, their maximum reliable performance limits will soon also be attained. CF8C-Plus and CF8C-Plus+Cu/W, two variations of standard CF8C, are austenitic cast stainless steel alloys that have been developed by Oak Ridge National Laboratory (ORNL) and Caterpillar to replace these current materials, in order to increase the efficiencies and maximum operating temperatures of steam turbines. Specimens of each variation of the two new steels were aged at 700°C, 750°C, 800°C, and 850°C, for 3,000 hours. Tensile and Charpy specimens were tested at room temperature (25°C) to obtain statistical data for comparison. The specimens tested at room temperature, which were aged at 750°C, were then selected to be further examined in the Scanning Electron Microscope (SEM) for fracture mode and microstructure analysis. When comparing the tensile data, CF8C-Plus and CF8C-Plus+Cu/W have Ultimate Tensile Strengths similar to CF8C, but their Yield Strengths are considerably higher than that of CF8C. The Charpy data showed that CF8C was the least ductile, that CF8C-Plus+Cu/W was the most ductile, and that the CF8C-Plus was in-between these two. Tensile ductility was much lower in the as-cast specimens of the CF8C-Plus+Cu/W than the aged specimens, but the opposite was true for CF8C-Plus. The SEM showed the presence of delta ferrite in the CF8C samples, but its presence was not detected in the other two new materials. The higher Yield Strength of CF8C-Plus and CF8C-Plus+Cu/W indicate that these materials are stronger after aging and more desirable than CF8C, which has similar Yield Strength and much lower ductility after aging due to the presence of weakening delta ferrite.

Micro Fabrication of Patterned Sm2O3-doped CeO_2 Electrodes on an Yttria-Stabilized Zirconia Electrolyte. *CASEY STRATTON (Washington State University, Pullman, WA 99163) OLGA MARINA (Pacific Northwest National Laboratory, Richland, WA 99352).* Yttria-Stabilized Zirconia (YSZ) electrolyte disks with patterned Samaria-Doped Ceria (SDC) electrodes were fabricated using microphotolithography. The pattern of the electrodes had variable triple phase boundary (place where the electrode, electrolyte and gas meet). A photosensitive polymer layer was deposited on the electrolyte in a pattern negative to a desired electrode pattern, heat treated, and exposed with high intensity ultra-violet (UV) light. After that the layer was developed. SDC was deposited using direct current sputtering technique. Annealling time and temperature, polymer thickness, UV exposure time, and developing time were varied to produce a highly defined pattern. Polymer and excess of SDC that was not in direct contact with electrolyte was washed away by acetone. The obtained patterned electrode was analyzed by optical profilometry and optical microscopy.

Nanoparticle Sensors For Biological Medicine. *AMEER TILLMAN (Washington State University, Pullman, WA 99163) NOVELLA BRIDGES (Pacific Northwest National Laboratory, Richland, WA 99352).* Our work is to focus on making nanoparticles that will be used as a non-invasive method to monitor intracellular trafficking and the transfection of genes. The nanoparticles characterize gradients in oxygen tension and gene expression that occur in the biofilms. The nanoparticles are made by a few different procedures such as the Ormosil and Sol-gel pebble formation. The Ormosil formation makes silica particles which are used for gene delivery. This gene delivery can deliver antibiotics or any of the other medicines that could help to kill these biofilms, once something is found that can kill them these will be really useful. These nanoparticles also determine where and how much oxygen there is in the biolfilms. This can show you how bacteria are respiring and functioning and allows you to optimize conditions so you can, for example, prevent corrosion, enhance bioremediation, or enhance chemical production.

Rhenium Penetration in a Castable Refractory Block. *BRONNIE TINSLEY (Central Washington University, Ellensburg, WA 98926) MICHAEL SCHWEIGER (Pacific Northwest National Laboratory, Richland, WA 99352).* Technetium is a radioactive element that results as a by-product from the production of nuclear weapons. Unfortunately, technetium has proven to be difficult to contain and efforts are underway to get it cleaned up. A method called bulk vitrification is currently under development that will allow technetium to be stored in large blocks of glass. The base component that makes up the glass is the desert soil found on the Hanford Reservation in Eastern Washington. Powerful electrical currents are used to heat the soil until it melts into glass in a process called vitrification. The glass melt process is contained in a block of heat resistant material called a refractory. During the melt process, the refractory block can be exposed to technetium and if it is porous enough, some of the technetium can become trapped in the refractory rather than the glass. Rhenium is an element that behaves similarly to technetium chemically but is not radioactive, and therefore is used as a surrogate for technetium in laboratory testing. In order to understand the penetration of rhenium in the refractory pores, a refractory sample was ground to dust in thin layers and the resulting dust analyzed by Inductively-Coupled Plasma Mass Spectroscopy (ICPMS) to determine the amount of rhenium each dust sample contained. The results from ICPMS showed that the distribution of rhenium in the refractory was somewhat uniform over the length of the refractory that was tested.

Magnetic States of a 50% $La_{2-2x}Sr_{1+2x}Mn_2O_7$ Bilayered Manganite Sample. *ALEXANDER TUMMINELLI (Cornell University, Ithaca, NY 14850) KEN GRAY (Argonne National Laboratory, Argonne, IL 60439).*

Layered Manganites are proving to be useful in the study of electron spin and the magnetic field that it induces. Recently, we've been able to isolate a sample with x close enough to 50% so that the chemical formula is essentially $La1Sr_2Mn_2O_7$. While this sample's conductivity states are not dominated by magnetic ordering, the data was sufficient enough to allow us to study further states that are dominated by charge ordering and orbital ordering. The data needed to be collected between temperatures of 5 and 300 Kelvin, so liquid helium and liquid nitrogen were both used in a cryogenic system to cool the sample to appropriate temperatures. It was also required that data be collected with different amounts of current running through the sample at different places on the sample, so a wide array of electrical connections needed to be attached to the sample. Data collection was completed using a combination of LabView programs, temperature controllers, voltmeters and a current source. The data we collected very clearly shows that a high current running through the sample will alter the states that the sample experiences. While these states appear to be dominated solely by charge and orbital ordering, they could prove useful in studying the magnetic ordering of other samples by allowing us to understand more fully the basics behind charge and orbital ordering. Studying this sample is only a part of a larger project directed at determining the magnetic properties of layered manganites as a whole, including other percentages of Lanthanum and Strontium.

Development of an ASTM Graphite Oxidation Test Method. *ZACHARY VANE (Virginia Polytechnic Institute and State University, Blacksburg, VA 24061) TIMOTHY BURCHELL (Oak Ridge National Laboratory, Oak Ridge, TN 37831).* Graphite, one of the three allotropes of carbon, is a very useful material because of its unique chemical structure and properties such as mechanical strength, chemical inertness, and electrical conductivity. In order to advance our knowledge of various graphite brands, further research must be conducted to gain a greater insight into the process and effects of oxidation on graphite properties. Although the key processes and controlling elements of graphite oxidation have been identified, the behavior of this material during and after oxidation is not well established. Knowledge of this behavior is crucial in understanding what happens to the various graphite components in nuclear reactors. Thermogravimetric analysis (TGA) of small samples of AG 13-01, 20-20, and PGWX graphite at the Oak Ridge National Laboratory (ORNL) has been used to increase scientific understanding of the relationship between the rate of oxidation and the flow rates of gases, temperature, and the intrinsic reactivity of graphite. This helps to identify the more oxidation resistant forms of graphite. These TGA results then serve as a reference point for validating a potential procedure for characterization of larger samples using a vertical tube furnace (VTF). The information gathered from these experiments is geared towards the development of an American Society for Testing and Materials (ASTM) test method for the oxidation of graphite. Though only a few runs have been conducted, preliminary results have proved promising as data from both the TGA and VTF methods yielded almost identical activation energies. More research on all of the types of graphite is needed, but such results suggest that the current ORNL procedure using the vertical tube furnace may become a reliable ASTM test method.

Polymer Ionogel-Templated Synthesis of Gold Nanoparticles. *LEGNA VARELA (University of Puerto Rico at Mayaguez, Mayaguez, PR 00680) MILICENT FIRESTONE (Argonne National Laboratory, Argonne, IL 60439).* Nanoparticles have been studied for many years mostly because of their physicochemical properties such as optoelectronic and photovoltaic devices. Previous work in the Firestone lab has focused on ionogel templated synthesis of gold nanoparticles. 1-Decyl-3-methylimidazolium chloride was combined with an aqueous gold solution yielding a 2-D hexagonally ordered mesostructural gel. Upon irradiation of this composite, anisotropic gold (Au) nanoparticles were obtained. In this report we describe two extensions of this prior work: 1) Development of a covalent (polymerized) ionogel as a template of scaffold for the in-situ formation; aggregation of gold nanoparticles. 2) The synthesis of semi-conducting nanoparticles within an Ionogel was also explored. Gold nanoparticles were grown combining 1-decyl-3-vinylimidazolium chloride with an aqueous gold solution. Using photochemical irradiation, the polymerized ionic liquid and the aqueous gold solution was reduced to create gold nanoparticles. Cadmium sulfide nanoparticles were created by adding 1-decyl-3-methylimidazolium chloride to an aqueous cadmium chloride solution and exposing it to hydrogen sulfide gas. These nanoparticles were formed and studies using UV-Vis, SAXS, and POM.

Magneto-Optic Imaging Studies of Diluted Magnetic Semiconductor and Exchange Bias Systems. *ZACHARY WEBER (Kenyon College, Gambier, OH 43022) ULRICH WELP (Argonne National Laboratory, Argonne, IL 60439).* The Magneto-Optical Imaging (MOI) technique relies on the Faraday rotation of polarized light to make magnetic domains visible. The MOI is adaptable to a wide variety of systems; in this study, MOI was used to examine films of a diluted magnetic semiconductor, $Ga_{1-x}Mn_xAs$, and an exchange coupled magnetic metal multilayer system, Co/FeF_2. Both of these systems are of interest in the development of spintronics devices, such as nonvolatile memory. In this study, MOI and magnetization measurements of $Ga_{1-x}Mn_xAs$ indicated that both as-grown and annealed samples had biaxial easy magnetization along the [100] and [010] directions. As temperature increased, the easy magnetization axis turned to the [110] direction and became uniaxial. The rotation of the easy magnetization axis orientation is due to the competing, temperature dependent anisotropy energies from the tetragonal structure of $Ga_{1-x}Mn_xAs$ (biaxial easy magnetization) and layer-by-layer surface reconstruction (uniaxial easy magnetization). The annealed sample demonstrated greater magnetic inhomogeneity, possibly indicating the presence of increased Mn clusters or interstitials. The Co/FeF_2 sample demonstrated a unidirectional field bias after cooling at high fields perpendicular to the c-axis. The same sample also seems to demonstrate separate regions with exchange bias in opposite directions after cooling at high fields parallel to the c-axis. These results support the notion that magnetic domains in the antiferromagnet give rise to the exchange bias.

Transient Liquid Phase Bonding Development. *JARED WIGHT (Brigham Young University Idaho, Rexburg, ID 83460) CURTIS CLARK (Idaho National Laboratory, Idaho Falls, ID 83415).* Transient liquid phase bonding (TLPB) is a process that employs a liquid eutectic which diffuses into a parent material. For the Reduced Enrichment for Research and Test Reactors (RERTR) program, aluminum 6061 is used as a parent material while silicon is used to form the eutectic. Silicon is deposited on a piece of aluminum and put in a hot press to create the bond. The RERTR program is currently developing this process for cladding a newly developed uranium-molybdenum monolithic fuel foil. Work on cladding the monolithic fuel foil began with selecting silicon as the material to create the eutectic with aluminum. A previous patent was used to determine how to apply the silicon to the aluminum plate. This was done by creating a silicon "paint" and painting it on the surface. Bonding times, temperatures, and pressures were studied to determine the optimal procedure. Ultra-sonic scanning was used to determine bond integrity. Initial results were promising but not satisfactory for testing in the reactor due to incomplete bonding. Recent literature research and novel ideas have led to many new variables that needed to be tested to make TLPB a valid bonding process for the RERTR project. Three key areas were targeted for development work: initial cleaning, silicon application, and actual bonding procedures. The current process includes mechanical and chemical cleaning and silicon application by flame spraying. The assembly is then put in a hot press near the eutectic temperature and held at 1000 psi for 30 minutes. This is now creating very desirable bonds. Future work will include development of the bonding parameters, inclusion of TLPB fuel plates in the next RERTR test in the Advanced Test Reactor, and plans for scaling up the process for larger foils. More work will also need to be done to create a good bond with a desirable grain structure.

Retained Austenite Decomposition in SAE 52100 Steel Using Magnetic Fields. *BRIE WITHERSPOON (Florida A&M University, Tallahassee, FL 32304) GERARD M. LUDTKA (Oak Ridge National Laboratory, Oak Ridge, TN 37831*). When hypereutectoid steel is raised to a high temperature such as 800°–900°C and then rapidly cooled, the material undergoes phase transformations such as austenite to martensite, carbide, bainite, or pearlite. In some instances for high quench rates the austenite may not completely transform to martensite and undesirable, residual austenite is retained in the final microstructure. Thermodynamic arguments predict that ambient temperature magnetic field treatment will reduce the amount of retained austenite in hypereutectoid as-quenched steel samples. The goal of this research is to determine the influence of various magnetic field processing parameters on the final amount of retained austenite in a SAE 52100 steel. Demonstration and implementation of this novel concept would ultimately reduce the amount of energy used in the processing of hypereutectoid steels for industrial use. Since in commercial practice retained austenite becomes stabilized against conversion to martensite after ~2 hours following a quench, one series of tests were done varying the amount of time the samples were held after being quenched from 850°C to see if magnetic fields can overcome this detrimental issue. Other variables investigated were the amount of time a magnetic field was applied to the samples, and its field strength. X-Ray diffraction, optical microscopy, Scanning

Electron Microscopy (SEM), and Orientation Imaging Microscopy (OIM) analyses were run on eleven samples for microstructural evaluation, and to determine the remnant amount of retained austenite (for conversion efficiency). X-ray data provide quantitative information regarding the amount of phase constituents in the microstructure, specifically martensite and austenite. The optical microscopy and SEM show qualitative information about the microstructure such as grain size and morphology. The OIM analysis shows textured or preferred grain orientation, phase identification and quantitative metallography, such as grain size. This presentation will summarize the results of this investigation and discuss their ramifications for potential industrial applications. Student Name: Brie Bedford Witherspoon School Student Attends: FAMU-FSU College of Engineering Names of Mentors: Dr. Gerard Ludtka, Dr. Roger Jaramillo Division: Metals and Ceramics Division Program: DOE Faculty and Student Teams

Synthesis and Characterization of Glucose-Sensitive Diblock Copolymers. *CHRISTOPHER WONG (Northwestern University, Evanston, IL 60201) SURYA MALLAPRAGADA (Ames Laboratory, Ames, IA 50011).* A diblock copolymer consisting of poly(ethylene glycol) (PEG) and 4-(1,6 dioxo-2,5-daza-7-oxamyl)phenylboronic acid (DDOPBA), has been synthesized via reversible addition fragmentation transfer (RAFT) polymerization. The DDOPBA polymer is an anionic polyelectrolyte with a pKa ~ 7.8. In aqueous solutions, glucose forms a charged complex with the phenylboronic acid moiety of the DDOPBA resulting in a dual hydrophilic-hydrophilic block copolymer. In the absence of the glucose the DDOPBA block is uncharged and becomes insoluble, resulting in the formation of micelles with DDOPBA cores and PEG corona structure. The molecular characteristics of this novel block copolymer were characterized with 1H NMR and size exclusion chromatography. Reversible, glucose dependent micellization in aqueous solution, around physiological pH, was shown with multi-angle laser light scattering (MALLS) and quasi-elastic light scattering (QELS). This material has potential applications in food processing and sensing technologies.

Unforeseen Heating During the Ultrasonic Welding of Aluminum Alloys. *LING XU (Georgia Institute of Technology, Atlanta, GA 30332) ZILI FENG (Oak Ridge National Laboratory, Oak Ridge, TN 37831).* Ultrasonic welding is a relatively new process to join two metal plates in a lap weld. For the ultrasonic welding process, the plates rest on an anvil while the sonotrode pushes down on them, applying heavy pressure. The sonotrode conveys the ultrasonic frequencies which cause heat, friction, and structural breakdown in the welded material. It has been discovered that stress patterns occur in areas far away from the weld area that are induced by unforeseen heating of such area. This creates obvious concerns for the feasibility of ultrasonic welding in the manufacturing environment. It is the purpose of this experiment to test that when a second weld is made on two plates that have already been joined, if the extraneous heating created by the second weld will have an effect on the initial joint. To test the effect of extraneous stress, two welds were made on each set of plates to test the impact of welds on each other. The time set of the weld was the initial variable in order to find the time which allows for maximum heating in the expected areas. Single welds were made under different time sets to see at what time the two plates would be fully bonded. The distance between the two welds was the primary variable to find if there is an optimal distance where the heating occurs. Spacing between the two welds ranged from 1 inch to 3 inches, in quarter inch increments. Further testing determined the effect a second weld had on two plates that are already joined by the first weld. The amount of heating was determined by the intensity values of the increased stress areas as recorded by an infrared video camera. The experiment determined that the second weld indeed caused heating on the first weld and sometimes even broke the original bond. The ultrasonic vibrations created by the second weld, affected the first weld in a high degree, creating enough stress within the weld to create heating and possibly failure.

Medical and Health Sciences

Effects of HZE Radiation on Motor Functions of the Brain. *ODIANOSEN AYEWOH (University of Maryland Eastern Shore, Princess Anne, MD 21853) ONARAE RICE (Brookhaven National Laboratory, Upton, NY 11973).* The effects of cosmic radiation on the brain were studied. This was done in order to aid the National Aeronautics and Space Association (NASA) in evaluating possible brain damages to astronauts that may result from exposure to heavy ions on a three year voyage to Mars. In this study animals (rats) were irradiated at the NASA Space Radiation Lab (NSRL) with ^{56}Fe ions in order to simulate one aspect of the effects of cosmic radiation. There were three groups of radiation doses: 0 cGY, 120 cGY and 240 cGY. We utilized two behavioral methods: The Rotational Rod Machine (Rotorod) and Locomotive Motor Skill Monitoring Boxes (LocoMotor Boxes). Rotorod is a device with four bi-level compartments with a rotating bar in the middle, which rotates at either a fixed speed or increasing speeds, that measures motor agility and motor learning. The Locomotor boxes work on a system linked to a monitoring computer. The interior of the boxes have infra-red beams that form a grid and traverse the entire area within the box. Each time the animal moves and breaks a beam it is registered as activity. Our results showed that heavy ions, such ^{56}Fe, contributed to the damage of the nigro-striatal dopamine pathway, which is primarily responsible for movement. Deprenyl (selegiline), used to treat Parkinson's Disease, is an irreversible inhibitor of monoamine oxidase B, and has shown to be a neuro-protector. Our study also revealed that the ^{56}Fe particles caused decreased locomotor activity, as well as, deficits in motor agility and motor learning. In addition, Deprenyl was shown to have a significant impact on the group of animals with the highest irradiation level on the brain.

Differentiating Between Different Forms of B-Cell Chronic Lymphocytic Leukemia Using FT-IR Spectroscopy and its Clinical Relevance as a Diagnostic Tool. *JEFFREY BORACK (Binghamton University, Binghamton, NY 13902) LISA MILLER (Brookhaven National Laboratory, Upton, NY 11973).* B-cell chronic lymphocytic leukemia (B-CLL) is a disease that follows two completely different clinical courses. Two forms of the disease, in which either the IgVH gene is mutated and there is low expression of ZAP-70 and CD38, or the IgVH gene is not mutated and there is higher ZAP-70 and CD38 expression, follow a benign or more aggressive clinical path respectively. Furthermore differences in transmembrane signaling through the B-cell antigen receptor exist in these subgroups and these differences have been suggested as a central explanation for the differences in biology and outcome in the disease. By using infrared spectroscopy and an automated cluster analysis tool it is hoped to determine if there may be any clinically applicable diagnostic tests that can be conducted to differentiate between different forms of B-CLL. To accomplish this, B-cells from patients have been isolated and placed on IR reflective slides. IR spectra were taken from ~300 cells/sample using a Spectrum™ Spotlight™ FT-IR microscope with an aperture size of 25 mm2 in reflection mode. The IR spectra were analyzed using OPUS 5.0 cluster analysis. Averages of each sample were taken and then clustered using vector normalization and Ward's algorithm. Results show that distinct clusters form with the highest degree of clustering around the lipid absorption region (2,900–3,100 cm^{-1}). Clusters did not develop as well for protein and nucleic acid regions. It is believed that the results found in the lipid region can be attributed to differences in membrane composition and/or lipid concentration and clusters may represent patients with different transmembrane signaling properties and possibly disease progression rate, although these remain undetermined as of yet. In the future, more tests will be conducted on additional samples to try and establish a higher degree of statistical relevance between these observations and the V-gene mutation information available on the B-CLL cases.

The Use of MicroPET and Autoradiography to Study Radiation Damage to the Brain. *SASHEEN FERGUSON (State University of New York – Stony Brook, Stony Brook, NY 11790) ONARAE RICE (Brookhaven National Laboratory, Upton, NY 11973).* The objective of our research is to employ MicroPET imaging to evaluate the effects of irradiation with ^{56}Fe particles on the brain, and ultimately to estimate human neurological risks from HZE radiation of prolonged missions beyond the geomagnetosphere as astronauts embark on an estimated three year mission to and from Mars. In this study animals (rats) were irradiated at the NASA Space Radiation Lab (NSRL), during NSRL 4, with ^{56}Fe ions at either doses of 0 cGy, 120 cGy or 240 cGy in order to simulate one aspect of cosmic radiation. We tested animals six and nine months post-irradiation with microPET to assess possible deterioration to the brain. The glucose analog [18F] FDG was used to measure glucose uptake, and eventually metabolic glucose rates, in various brain regions, such as the hippocampus and substantia nigra. It is hypothesized that HZE particles may cause damage to the brain, specifically the hippocampus and striatum, which may lead to numerous complications including early onset of Parkinson's disease or memory loss. Our Results showed that there was no significant damage or differences between doses at the regions of interest. We need to conduct further studies at a longer time frame post irradiation in order to assess the effects of irradiation with ^{56}Fe particles on the brain.

Operation Stabilization and Implementation of Dual Headed Scintimammography Detector in the Detection of Breast Cancer. *CLARISSA FREEMAN (Hampton University, Hampton, VA 23668) STAM MAJEWSKI (Thomas Jefferson National Accelerator Facility, Newport News, VA 23606).* Although the idea of a dual-headed breast-specific scintimammography detector imaging system is not new, it has never been fully developed and implemented in a clinical setting. In Scintimammography, a nuclear medicine technique, radiopharmaceuticals emitting a radiotracer that marks biological processes specific to breast cancer are used in conjunction with a gamma-imaging detector system. The dual headed system is an improvement over both standard mammography and single-headed systems in that its two cameras combined view of the breast allows it to detect lesions in dense breast tissues, near breast implants, post-surgical scars. The goal of this study was to improve and achieve sufficient and crucial operational stability of the system prior to its implementation in the hospital and to get the detector in a clinical setting as soon as possible. The first steps in the process of stabilization were (1) careful calibration of both detector heads and (2) making sure that all internal hardware, cabling, and external components could withstand movements of the gantry. To calibrate the system, we used a sixty-four channel readout to test detector function of four ADC boards along with data acquisition software developed based on Sparrows Corporation's Kmax development package. The system has been successfully calibrated, and the machine will be implemented at the George Washington University under the care of Dr. Rachel F. Brem, Director of the Breast Imaging and Intervention Center.

Progress Towards Development of a System for Intracellular Extraction From Living Cells Utilizing Carbon Nanofibers. *STEPHEN JONES (Earlham College, Richmond, IN 47374) TIM MCNIGHT (Oak Ridge National Laboratory, Oak Ridge, TN 37831).* Due to their size and mechanical strength, vertically aligned carbon nanofibers (VACNF) provide an excellent platform for intracellular manipulation and probing. By attaching antibodies specific for an intracellular molecule of interest to a VACNF array and then impaling cells with the VACNFs, it may be possible to extract or probe for a molecule of interest in a living cell. The goal of the project is to confirm that this system will work by extracting and identifying an abundantly available species, tubulin, from tissue cultures of the Chinese Hamster Ovary (CHO) cell line. Initial attempts employed an EDC-mediated condensation of avidin protein onto the VACNF array and subsequent binding of biotinylated antibodies specific for tubulin. Cells could then be impaled on the VACNF's upon which the antibodies would putatively bind unpolymerized tubulin dimers. The tubulin would then be identified on VACNF's using a fluorescently tagged taxol compound, which has affinity for the tubulin dimer. This procedure was attempted in-vitro with bovine tubulin, but it was difficult to qualify success via taxol fluorescence because of native fluorescence of the fibers. To overcome this problem, the original procedure has been modified so that quantum dot conjugated anti tubulin antibodies will now be used for identifying fibers with bound tubulin. This procedure was attempted and succeeded in showing a clear difference between samples and negative controls. However the protocol was not reproducible to an acceptable extent, so further tests must be performed. However the preliminary results suggest that the basic protocol is feasible as proposed, and give some indication as to problems that must be overcome in the future. The biggest flaws in this procedure are the native fluorescence of the fibers (single to noise ration), and the sensitivity of fluorescent techniques. Future experiments may use radioactively labeled antibodies to resolve these problems.

Severity of Executive Impairment in Depressed Cocaine Addicts. *ROLINDA MCINTOSH (Medgar Evers College, Brooklyn, NY 11203) RITA GOLDSTEIN (Brookhaven National Laboratory, Upton, NY 11973).* Cocaine abuse continues to be a major societal problem. From recent studies conducted at Brookhaven, there has been substantial evidence that cocaine use is associated with neuropsychological impairments. The aim of this study was to examine the effect of self-reported state depression on executive functioning, including planning, shifting, cognitive interference, decision-making, and problem solving abilities in substance dependent individuals (SDI). Participants were 64 cocaine abusers (14 females and 50 males) between the ages of 20–55. They self-reported depression using the Beck Depression Inventory (BDI), a 21-item self-report instrument intended to assess the severity of symptoms of depression within the two weeks prior to and including day of testing in adolescents and adults. Subjects with BDI scores in the range of 0-15 were considered not to be depressed (N=43), and those who scored above 15 were considered depressed (N=21). As part of a larger neuropsychological battery, all subjects were administered several measures of executive functioning. These included the Stroop Task, the Wisconsin Card Sort Task (WCST), Trails Making Test (part B), the Letter-Number Sequencing Task, mazes from the Wechsler Intelligence Scale for Children (WISC), Symbol Digit Modalities Test, and the Attention Network Test conflict subscale. Reading subscale of the Wide Range Achievement Test (WRAT) and design matrix of the Wechsler Adult Intelligence Scale (WAIS) were administered for assessment of overall level of intelligence. No significant differences were found between the depressed SDI and the non-depressed SDI in any of the inspected neuropsychological tasks, as assessed by univariate t-tests. Future studies with larger sample sizes and additional specific executive functioning task, such as the Bechara's gambling task are needed to determine the importance of the relationships between state depression and executive functioning in drug addiction.

Conditioned Place Preference Responses to SB-277011-A in Dextroamphetamine Sulfate Addicted Rats. *LESLEY RUSSELL (College of the Holy Cross, Worcester, MA 01610) ANDREW GIFFORD (Brookhaven National Laboratory, Upton, NY 11973).* Dextroamphetamine sulfate, a member of the amphetamine family, is a central nervous system stimulant often used to treat attention deficit disorder (ADD) and attention deficit hyperactivity disorder (ADHD) in children. Dextroamphetamine sulfate is also commonly used to treat narcolepsy. Amphetamine use causes storage vesicles in the central nervous system to release the excitatory neurotransmitters dopamine and norepinephrine. While amphetamine usage at first causes feelings of euphorIA these feelings ultimately give way to deep depression and fatigue due to the depletion of dopamine and norepinephrine stores in the mesolimbic areas of the brain. The cycle of euphoria followed by depression often leads to amphetamine addiction. While a number of neurochemical pathways are involved in creating drug addiction, the dopaminergic pathway, specifically, is associated with the reinforcement of addictive substances and behaviors. Five types of receptors exist within the dopaminergic pathway (D1-D5). Past research has shown that the D2 class of receptors, in particular the D2R receptor, is essential in creating and sustaining drug addiction. Recently, however, a substantial body of literature has accumulated pointing also to the D3R receptor as playing a vital role in drug addiction. Current research has revealed that SB-277011-A, a highly selective D3 receptor antagonist, decreases cocaine-seeking behavior, ethanol-seeking behavior, ethanol consumption, nicotine conditioning, and nicotine-triggered relapse. Using a place preference paradigm, this study examines the effects of SB-277011-A when administered to dextroamphetamine-addicted rats (i.p.) at a dose of 3 mg/kg, 10 minutes before being posited into the place preference apparatus. The data shows that rats given a 3 mg/kg injection (i.p.) of dextroamphetamine sulfate exhibited significant drug seeking behavior. Also, despite the administered dose of SB-277011-A, dextroamphetamine addicted rats continued to exhibit a considerable amphetamine place preference, suggesting that the D3 receptor does not play a large role in amphetamine seeking behavior. This project is intended to help advance the present knowledge of the role the D3R receptor plays in drug and substance addiction and abuse.

Nuclear Sciences

Substance Based Fingerprint Analysis Using Infrared Spectromicroscopy. *RODGER BAILEY (California State University Fresno, Fresno, CA 93702) TOM KNIGHT (Lawrence Berkeley National Laboratory, Berkeley, CA, 94720).* Traditional fingerprint analysis has involved the comparison of the physical characteristics of a fingerprint, using the patterns of various ridges as a means of identification for an individual. Infrared Fingerprint Spectroscopy focuses on the tiny traces of material that remain in the fingerprints after handling a substance. Molecular bonds in substances move in three distinct patterns, symmetrical, asymmetrical and bending. When these bonds are moving in a symmetrical or bending pattern, they interact with IR light and absorb energy at various frequencies, depending upon the substance. Each type of bond moves, or resonates, at a specific frequency. By measuring the frequency of absorbed infrared light, chemical bond information can be obtained and the substance can be identified. This adds another dimension to fingerprint analysis by matching trace particles in a fingerprint to a specific substance. An infrared spectrum was obtained from an unidentified substance by mixing the sample with KBr, compressing it into a crystal and analyzing it in the FTIR Spectrometer. The spectrum indicated the presence of Silicone in the sample. Two fingerprints were obtained, one as a control and the other contaminated with the unknown substance.

Each fingerprint was analyzed, using the FTIR Spectrometer, and their respective infrared spectra were compared with that of the unidentified substance. The spectrum obtained from the control fingerprint did not indicate the presence of Silicone. The spectrum obtained from the contaminated fingerprint matched that of the unidentified substance, conclusively linking the fingerprint with the substance. Beyond identifying unknown compounds, IR Spectroscopy can be used to determine what chemical groups are present in a compound and its optical conductivity.

Optimum Fuel Design for the One-pass Deep Burn Concept. *JEROME CASE (University of Wisconsin, Madison, WI 53706) TAEK K. KIM (Argonne National Laboratory, Argonne, IL, 60439).* The objective of the Deep Burn Modular Helium Reactor (DB-MHR) project is to maximize the transmutation of heavy elements, especially plutonium, in spent fuel from Commercial Light Water Reactors (LWR's) while providing a safe, clean, reliable and competitive source of electricity. This study provides a TRISO fuel configuration, which balances burnup of transuranic actinides, including overall burnup and plutonium transmutation, and the cycle length for a four-batch fuel cycle. This optimized configuration is intended for future design and core performance calculations for the once-through, single-phase fuel DB-MHR design. The most favorable fuel design found in this study has a 224μm diameter fuel kernel and a packing fraction of 15%. This combination results in a fuel-to-moderator ratio, cycle length and transmutation similar to previously recorded configurations. Specifically, a fuel-to-moderator ratio of 0.0003255 supplies a cycle length of 272 days and a transuranic transmutation rate of 57.9%. Plutonium transmutation is 61.3% and the total burnup of the fuel is 544 GWd/t.

Hydrogen Cost Analysis Simulation in Flow. *QUAN COHEN (Robeson Community College, Lumberton, NC 28358) JUAN FERRADA (Oak Ridge National Laboratory, Oak Ridge, TN, 37831).* The Department of Energy (DOE) has designed a model, known as H2 Analysis (H2A), which addresses the economic aspects that must be considered while attempting to transition hydrogen as a fuel source into society. H2A has estimated all costs of production, storage, and modes of delivery from the storage facility to the distribution site in its "scenarios." The scenarios contain data that represent the implementation of a hydrogen economy such as projected feedstock and utility prices and labor costs. Delivery methods such as pipeline, truck tube-trailer equipment operation, and maintenance are included in the simulation. This module, however, will focus on the associated delivery costs of gaseous and liquid hydrogen from its storage facility to its distribution site in a truck tube-trailer. The project objective is to create a user-friendly interface that will display the main variables associated with hydrogen transportation. The user has the option of using H2A Projections in the code's database or entering other values if there is a variance. Flow is the simulation process and modeling tool used for analysis, developed by Oak Ridge National Laboratory (ORNL) that will be used to produce the module. Python is the scripting programming language used to execute Flow spreadsheets. The data used for Flow's code was extracted from two of DOE's twenty spreadsheets. The sequence of calculation steps were coded in Flow by using the reverse engineering method, which determined how the equations in the DOE spreadsheet were calculated. DOE spreadsheets had to be examined to determine the various forms of data compiled and differentiate the user-inputs from the calculated variables. This module produced results consistent with those produced by DOE's H2A spreadsheets. It allows for flexible and friendlier interaction with the user. In conclusion, this is a significantly small portion of the DOE hydrogen economy project.

Neutron and Gamma Ray Multiplet Analysis for the Determination of Plutonium Mass. *MELISSA CRAWFORD (University of Florida, Gainesville, FL 32608) SARA POZZI (Oak Ridge National Laboratory, Oak Ridge, TN, 37831).* Nuclear safeguards methods are being developed at ORNL and elsewhere to nondestructively determine the mass of fissile material. Recent efforts have studied the multiplicity of neutrons and gamma rays emitted by spontaneous and induced fissions in fissile samples. The present work aims at developing a reliable method for determining the mass of the samples. The proposed analysis relies on a series of experiments that were conducted on plutonium oxide samples at the JRC in Ispra, Italy, using a GHz processor developed at ORNL. The detectors used were liquid scintillators, which are sensitive to fast neutrons and gamma rays. The setup consisted of two 2x2 detector arrays, placed opposite each other, with a plutonium oxide sample set equidistant from them, inside of an AT400 container. The measurement setup was simulated using the MCNP-PoliMi code, and multiplet analysis was performed on both the simulated and the measured data. The distribution of multiplets describes the number of times n detections occur following a single fission, where n includes neutron and gamma ray counts. This work shows that it is possible to determine a relationship between the multiplet distribution and the mass of Pu-240 in the sample. Our results show that the Pu-240 mass can be predicted to within 7.8% in the mass range of 50 to 2500g. This information, together with information on the sample's composition, allows us to determine the mass of Pu-239. This work has a bearing on nuclear nonproliferation programs and will lead to more sophisticated analyses that can be applied to homeland security issues.

Benchmarking of Monte Carlo Codes and Sensitivity Analysis of Physics models in Monte Carlo N-Particle eXtended for High Energy Projectile-Target Interaction. *JERRAD DEASON (Prairie View A&M University, Prairie View, TX 77446) JEFFREY O. JOHNSON (Oak Ridge National Laboratory, Oak Ridge, TN, 37831).* Neutral and charged particle transport phenomena is described with the Boltzmann transport equation. The numerical solution of the Boltzmann transport equation is applicable to various fields of nuclear engineering and physics. One such numerical technique, the Monte Carlo method, provides stochastic solutions to the particle transport calculations utilizing detailed three-dimensional geometry. Recent implementation of heavy ion transport capabilities has advanced the applicability of these codes to space and high energy physics problems. MCNPX (Monte Carlo N-Particle eXtended) and PHITS (Particle and Heavy-Ion Transport System) are two such multi-purpose particle and heavy ion transport codes that implement the Monte Carlo method and are ideally suited for characterization of high energy charged particle interactions and heavy ion transport design studies. However, the application of these codes currently has limitations as they are relatively new and unverified, particularly in the energy regimes where charged particle interaction data is sparse or absent. In these regions codes rely on physic model calculations to compute interaction probabilities. The work performed here was to validate and benchmark these two transport codes against the quantitative data collected from a peer-reviewed journal article. The article reports secondary neutron spectra measurements at discrete angles from a target to the scintillator detectors. The report presents the comparison of measured values with the computational results for two targets (water and lead) at nine different angles (0°, 6°, 15°, 30°, 45°, 60°, 90°, 120° and 150°) with a specific energy distribution at each angle. Additionally, for the lead target, calculations were performed at two different incident alpha energies (710-MeV and 640-MeV) and compared to the measured data. The resulting data extracted from the codes, are graphed on a log-log plot to illustrate the difference between the measured and computational neutron spectra at the various angles. The simulated geometries for the water target were then subjected to several alterations in the computational structures and physic mode implementations, such as, removing the columbic barrier parameter, and changing the physics models from the program defaults (Bertini and ISABEL) to the CEM2K model. These additional calculations were performed to compare the sensitivity of the physics models on the neutron production spectra.

Evaluation of a 3D Design Information Verification System for Uses at Oak Ridge National Lab. *CAROL DUDNEY (University of Tennessee, Knoxville, TN 37916) MICHEAL WHITAKER (Oak Ridge National Laboratory, Oak Ridge, TN, 37831).* Through a joint research cooperative with the European Commission's Joint Research Center, Oak Ridge National Laboratory (ORNL) has been given access to the 3D Design Information Verification (3D-DIV) system. This is a laser scanning system that can determine if an object has been moved as little as five millimeters. ORNL will test the 3D-DIV system to evaluate the systems limitations, applicability to ORNL, and function within nuclear installations. Five different experiments will be conducted. Scans will be taken from several well marked spots and subsequent verification scans will be taken at various distances from the original positions to test the importance of the placement of the laser. The use of barcodes in conjunction with the 3D-DIV system will be examined to determine other possible field applications. The response of the system to highly reflective materials at different angles will be evaluated. The next experiment will deal with layers of piping similar to that in nuclear facilities. And finally, the ability of the system to scan through different mediums (e.g., thin glass, colored water) will be assessed. The results obtained from these tests will be presented.

A Method to Determine the Minimum Energy Threshold and Coarse Low Energy Calibration for PVT Based Detectors Using the Lower Level Discriminator. *ALISON EARNHART (Juniata College, Huntingdon, PA 16652) JIM BORGARDT (Pacific Northwest National Laboratory, Richland, WA, 99352).* Radiation portal monitors (RPMs) play a critical role in ongoing attempts to intercede illicit radiological

sources. RPMs widely utilize polyvinyl toluene (PVT) based detectors which have relatively high durability and low cost, but intrinsically poor energy resolution. However, a pulse height analyzer does provide some spectroscopic information allowing broad energy windowing (EW) algorithms to be employed as a complement to less specific gross count measures when detecting radiation. Quantifying the low energy sensitivity and low energy calibration of these detectors presents unique obstacles since the photon interaction in PVT is dominated by Compton scattering events, masking full energy peaks in the energy range of interest, and driving an increase in the count rate in the low energy region. A method to gauge the sensitivity of PVT detectors and generate a coarse low energy (~5keV to ~80keV) calibration by varying the lower level discriminator (LLD) setting and tracking the net count rate from a source has been investigated for several commercial PVT-based RPM systems using 55Fe, 109Cd and 241Am. Parameters in a Fermi function were adjusted to fit the resulting integral pulse height data and the derivative of the generated fit function, representing the differential pulse height spectrum, was determined. The presence of a peak in the derivative of the count rate for a source signified the presence of a photopeak, and provided a means of assessing the low energy sensitivity of the detector. Additionally, observed peaks in such differential pulse height curves for multiple sources with peaks in the 5keV to 80keV range allowed a coarse low energy calibration to be established.

Validation of SCALE (TRITON) Isotopic Predictions for Light Water Reactor Spent Fuel. *DANIEL GILL (Pennsylvania State University, University Park, PA 16802) STEVE BOWMAN (Oak Ridge National Laboratory, Oak Ridge, TN, 37831).* The ability to accurately predict the nuclide composition of spent fuel samples over the course of time is important in a wide variety of applications. These applications include, but are not limited to, the design, licensing and operation of radioactive waste transport systems, interim waste storage, and a permanent waste repository. The isotopic depletion capabilities of the new SCALE (Standardized Computer Analyses for Licensing Evaluation) control module TRITON, coupled with ORIGEN-S, were evaluated using spent fuel assays from several commercial light water reactors. The type of reactor analyzed was the pressurized-water-reactor (PWR) with both standard and mixed-oxide fuel (MOX) assemblies. Calculations were performed using the functional modules NEWT and KENO-VI. NEWT is a two-dimensional, arbitrary geometry, discrete ordinates transport code and KENO-VI is a multigroup, Monte Carlo transport code capable of handling complex three-dimensional geometries. To validate the codes and data used in depletion calculations, numerical predictions were compared with experimental measurements for a total of 21 samples taken from the Calvert Cliffs, Obrigheim, and San Onofre PWRs. Similar comparisons have previously been performed at the Oak Ridge National Laboratory (ORNL) for the one-dimensional SAS2H control module. The SAS2H, TRITON/KENO-VI, and TRITON/NEWT results were compared for corresponding samples. All analyses showed that TRITON/KENO-VI and TRITON/NEWT produced typically similar results, leading to the conclusion that the transport/depletion models are performing correctly. For the San Onofre MOX assemblies, TRITON obtained depletion results nearly the same as or better than SAS2H for all nuclides considered. The average difference between calculated and measured values was below 1 % for ^{235}Uand around 5 %for ^{239}Pu. The results for the Calvert Cliffs and Obrigheim PWRs were in most cases also comparable to previous SAS2H results. The calculations performed in this validation study demonstrate that the depletion capabilities of TRITON accurately model spent fuel depletion and decay and are similar to those of SAS2H, which previous ORNL studies have concluded qualifies as a basic tool for predicting isotopic compositions of spent fuel.

Obtaining Region Dependent Reaction Rates using MCNP4C for the International Criticality Safety Benchmark Evaluation Project Zero-Power Reactor 6/7 Benchmark. *THOMAS GOTER (University of Missouri-Rolla, Rolla, MO 65401) STEVE LOMPERSKI (Argonne National Laboratory, Argonne, IL, 60439).* Benchmark calculations for the International Criticality Safety Benchmark Evaluation Project (ICSBEP) prove to be useful in the validation of new codes and cross section data. Improved codes and updated cross section data in turn leads to better neutron path modeling and simulation. We use Monte Carlo N-Particle transport code, commonly known as MCNP, to calculate the regional reaction rates for the ICSBEP benchmark for Assembly 7 of Zero Power Reactor 6 (ZPR 6/7). A ZPR is a rudimentary experimental reactor operated at such a low power that a coolant is not required. In order to accurately simulate the reactor assembly, exact dimensions and nuclide compositions must be known. For simplification of the problem the as built geometry was transposed to an R-Z geometry. The transposition was automatically accomplished through the use of VIM, but an error in criticality still resulted from it. VIM is a separate nuclear criticality safety code which also is used in benchmark evaluations. The reaction rates desired are fission production, fission, radiative capture, (n, 2n) production and leakage. After the results are calculated they are then compared with results from VIM. The difference between VIM and MCNP is how they treat the resonance range of the cross section. Error calculations showed a very small amount of relative error between the two codes. There was a much larger error between the as-built criticality and the R-Z criticality. This means that the transposition through the use of VIM was the cause of that error since the as-built model obtained a criticality level much closer to the actual ZPR 6/7 experimental value. Future work will be to continue adding to the database of benchmarks for the ICSBEP and to encourage a greater level of international cooperation in the ICSBEP.

Evaluation of Electromagnetic Pump Data and Examination of Theoretical Mechanisms for Performance. *VERNON GUTHRIE (Clemson University, Clemson, SC 29631) GRAYDON L. YODER, JR. (Oak Ridge National Laboratory, Oak Ridge, TN, 37831).* The removal of heat developed in a nuclear reactor requires a pumping system to circulate a fluid through the reactor and then to a heat exchanger. Liquid metals are advantageous for use as the working fluid for cooling nuclear reactors because they have very high thermal conductivities and pumps can be used without moving parts. Electromagnetic (EM) pumps are often used for pumping liquid metals because of the problems conventional pumps have with liquid metals. Since EM pumps have no moving parts, they require no seals or bearing systems. The Annular Linear Induction Pump (ALIP) is a type of EM pump which produces flow in an electrically conductive fluid by the interaction of the currents induced in the liquid metal with the magnetic field created by the stator windings. Analysis of pump data obtained from a test loop containing an ALIP pumping liquid mercury provides insight into evaluating and maximizing pump performance. The product of differential pressure across the pump and volumetric flow rate through the pump is the work put into the fluid. Comparing this work to the product of the pump's input voltage and current allows the determination of pump efficiency. While pump data revealed efficiency values under 1%, these results were consistent with those expected for mercury ALIP pumps. The maximum efficiency calculated from test data was .78%. This value occurred at a differential pressure of 114.4 kPa, a volumetric flow rate 0.616 L/s, and a pump input power of 8.98 kW. In comparison, the efficiency value was .99% when using the pump manufacturer's data at the nominal operating point of 253.3 kPa, 0.4 L/s, and 10.2 kW. This effort supports a larger project designed to develop a space reactor power system capable of providing spacecraft power and propulsion for as long as fifteen years.

Determining Specific Activity of [^{13}N] Ammonia. *JONATHAN HOFFMAN (Elcamino Community College, Torrance, CA 90503) JIM O'NEIL (Lawrence Berkeley National Laboratory, Berkeley, CA, 94720).* The specific activity of a radioactive species is a quantization of the amount of radioactive isotope in comparison with non radioactive isomers within the same species. This quantitative assessment is generally expressed as a ratio of activity (e.g. mCi) to mass (grams or moles). In the context of diagnostic radiopharmaceuticals, specific activity provides a method of measuring the concentration of a radioactive drug to a non radioactive drug. Maximizing the specific activity within a given substance helps to minimize the potential of unwanted side effects. Therefore the higher the specific activity of a drug, the smaller the amount of injected non radioactive drug. Using High Performance Liquid Chromatography-Ion Chromatography (HPLC-IC), ammonium ions were separated from injected samples and their concentrations where determined by electrochemical conductivity detection. A series of injections were made onto a Hamilton PRP-x200 Cation Exchange column at a flow rate of 2 ml/min at a constant pressure of 900psi. Measuring the detector response per injected mass of ammonium nitrate standards (0.15mmol/L to 0.000015mmol/L) provided data for a standard absorbance curve. Subsequently, the standard curve can then be used in determining concentrations of unknown ammonium samples by comparison to the detector response. Radioactive samples of [^{13}N] ammonia can then be analyzed for radioactivity using a dose calibrator, and the concentrations can be determined by the HPLC-IC and standard curve. Thus the specific activity is provided by calculating the ratio of radioactivity to mass of the sample. Furthermore, a calibration curve for the conductivity detector was successfully constructed. Future studies using radioactive [^{13}N] ammonia can now refer to the ammonium curve in order to calculate the specific activity of an unknown sample.

Simulation of Cosmogenic Backgrounds in Underground Detectors. *KAI HUDEK (Colorado School of Mines, Golden, CO 80401) KEVIN LESKO (Lawrence Berkeley National Laboratory, Berkeley, CA, 94720).* This project is intended to further the understanding of neutron backgrounds in Majorana. Neutrons produced by cosmic muons in rock surrounding an underground facility can generate irreducible backgrounds in detectors and in some experiments determine the sensitivity. Understanding the muon-induced production and the response of underground detectors to neutrons is crucial for the design of next generation low background experiments. Surface muons are generated using the rejection method and used as inputs for neutron generating distribution functions. These distribution functions are, in turn, sampled using the rejection method and the resulting neutrons are input into MaGe, the Majorana Monte Carlo package.

Millimeter Wavelength RADAR Detection of Air Ions and Aerosols Produced From Ionizing Radiation. *MIKE HULL (University of Illinois at Urbana-Champaign, Urbana Champaign, IL 61820) NACHAPPA GOPALSAMI (Argonne National Laboratory, Argonne, IL, 60439).* Current methods of detecting ionizing radiation sources depend on the detector physically lying within the range of the radiation. For many sources, this is a matter of an inch or two in air. As a more versatile means of detecting radiation, a millimeter wave-length RADAR system is being developed and calibrated. To test the RADAR, it is first necessary to design an experiment where a known activity of radioactive substance is released into a controlled volume with variable temperatures and humidities, including the supersaturation humidities found in the atmosphere (above power plants, e.g.). For this purpose, the processes of droplet formation, vapor condensation, air chilling and adiabatic expansions were studied, and in the end, a 12” cube transparent polycarbonate chamber was carefully designed and then constructed. With consideration of the temperature and pressure ranges required for the experiment, appropriate and relatively inexpensive humidity detector, thermometer, and pressure gauge were procured. Testing is currently being done on this chamber to see whether the method of uniform cooling is sufficient to reach supersaturation, or whether condensation will occur before the center has cooled, and thus a volume expansion technique is required. The answer to this research is a necessary one for the further development of the millimeter RADAR radiation detector.

Hydrogen Economy Costs Model Simulations. (HyTrans). *MARCUS JACKSON (South Carolina State University, Orangeburg, SC 29117) JUAN FERRADA (Oak Ridge National Laboratory, Oak Ridge, TN, 37831).* There is a need to develop interfaces between the already existing models and the global model of the hydrogen economy. Many transportation models have been developed using current oil fuels and future hydrogen fuel. However, these existing models and analytical tools are difficult to integrate and execute separately for analyzing efficiently and effectively the transition towards a hydrogen economy. Using the graphically oriented simulation software package FLOW and the process modeling scripting language Python various interfaces were developed to simulate different aspects of using hydrogen based on existing computerized transportation models (HyTrans developed at ORNL). FLOW simulated hydrogen economy scenarios by developing process flow sheets and analyzing capital, operating and unit production costs of these scenarios. Each scenario consisted of a selected production process, one delivery mechanism, and one type of retail. Several simulations were developed and run to compare the various alternatives and determine solutions beneficial to the U.S. Department of Energy Hydrogen Program. Results show that these simulations are accurate and consistent with the HyTrans model. This project is a small portion of a much larger project being pursued by the U.S. Department of Energy’s Hydrogen Program to develop an efficient transition plan for a future use of hydrogen. In conclusion, the results suggest that this goal is achievable but current studies must be evaluated in order to accurately model an effective hydrogen economy.

Intensive Research Institute. *MEAGAN JAMIESON (Fresno State, Fresno, CA 93726) TOM KNIGHT (Lawrence Berkeley National Laboratory, Berkeley, CA, 94720).* The Intensive Research Institute participated in four, two week workshops: (1) Building a Cosmic Ray Detector with Howard Matis, (2) Natural Terrestrial radioactivity with Allan Smith, (3) Neutron Activation with Howard Shugart, and (4) Finger Print Analysis and spectromicroscopy with Michael Martin. Our main goal is to relate newly acquired knowledge and skills from the workshops to high school and middle school mathematics and science standards. We built a cosmic ray detector and proved through experiment that cosmic rays come from the atmosphere not the earth. In the workshop Natural Terrestrial radioactivity we conducted two experiments. We tested an air filter and soil near our building to see what elements they contain. The air filter contained Uranium and Thorium. The soil contained Uranium, Thorium and Potassium. We bombarded three types of medals with neutrons in the workshop, Neutron Activation. In doing this experiment three isotopes were created; Cobalt (Co-58), Magnesium (Mg-27), and Sodium (Na-24). A forensics type experiment was conducted using infrared spectroscopy. We tested a powdery substance and found which spectra’s it contained. We then analyzed the spectra of two sets of fingerprints, one with the powdery substance and one without. The powdery substance and the fingerprint with the substance had some of the same spectra’s. The main goal was achieved because we came up with standards for every workshop and we now have more ideas of lesson plans that can be used to relate science and mathematics.

Comparison of Electron Beam Diffraction and Soft X-ray Attenuation Methods to Achieve Approximate Thickness of Lithium Charge State Stripper for RIA. *ANTONIO JOHNSON (University of Missouri-Rolla, Rolla, MO 65409) STEVE LOMPERSKI (Argonne National Laboratory, Argonne, IL, 60439).* The Rare Isotope Accelerator is a high priority new facility that will provide researchers with the opportunity to learn more about short-lived isotopes that are too unstable to study with conventional facilities. This type of accelerator is capable of delivering high-energy radioactive beams of isotopes from Hydrogen to Uranium for experiments relating to astrophysics and nuclear science. The high-energy radioactive beams are more effective at reaching their final speeds (~0.81 c) if they are stripped of their electrons by a charge-state stripper. Experiments have shown that lithium can withstand a 12 MeV/u ion beam in high vacuum. Research has also shown that the thickness of the liquid lithium charge state stripper is a key parameter to determine the behavior of the lithium as it interacts with the ion beam. Therefore the thickness of the lithium film must be measured and monitored. Many techniques have been investigated to monitor and/or measure the thickness of the liquid lithium film. The search for the most promising technique is primarily based on commercial availability and difficulty of implementation. The electron beam diffraction and soft X-ray attenuation techniques are the most promising methods among many possibilities for example, micrometer types, interferometry, laser triangulation, Terra Hertz wave, and Eddy currents) because they meet the standards needed to drive the RIA project further toward completion. Many criteria are used to judge the suitability of a particular film thickness measurement technique. These include hardware and software, compatibility, development cost, accuracy, reliability, and safety. Inside the lithium loop, the equipment is exposed to high temperature (250oC), high vacuum (2x10-4 Torr), and the possibility of lithium splashing. Equipment that can perform in this environment without disrupting the very nature of RIA system is required. The electron beam diffraction method is the better choice for the reason that it is commercially available, less expensive, easier to administer, and more productive in a vacuum bakeable environment than soft x-ray attenuation.

Improving Cadmium Zinc Telluride Detectors Through In-Depth Analysis and Collaboration. *KYLE KOHMAN (Kansas State University, Manhattan, KS 66502) ALEKSEY BOLOTNIKOV (Brookhaven National Laboratory, Upton, NY, 11973).* Cadmium Zinc Telluride (CdZnTe) crystal is a material that shows great potential for detection of gamma and X-rays because it provides a high gamma ray stopping power, high energy resolution, and can be operated at room temperature while remaining much more compact than other detector assemblies. These properties make it useful for applications in fields such as nuclear medical imaging, Homeland Security, and astronomy. The ability to consistently produce good quality crystals has not yet been achieved, thus holding back the potential impact of these devices on current technology. This study gives a better understanding to the properties of CdZnTe crystals for detection in hopes to achieve consistent production of superior quality crystals for detectors. Vendors send Brookhaven National Laboratory (BNL) samples of their CdZnTe material to test quality and to seek advice for improvements. These crystals go through an array of tests to give the vendor a detailed understanding of what their crystals’ characteristics are. By using the X-ray beam from the National Synchrotron Light Source (NSLS) at BNL, the energy transmission of the crystal is analyzed. X-ray diffraction is also performed at the NSLS to attain a topographical map of the crystal. Infrared images are taken to observe precipitates in the material. The crystal is then polished and made into a detector. Its detection capabilities are analyzed by counting radiation at different voltages. The data is then analyzed to try and observe correlations between the crystal properties and the detector performance. A better understanding of what material properties affect detectors is achieved. Feedback

is then provided to the vendors of the material to help them improve their crystal growth techniques. Eventually this will lead to production of improved quality CdZnTe crystal, making CdZnTe detectors more useful. This allows for the implementation of better detectors in industry and the advancement of other fields like nuclear medical imaging, Homeland Security and astronomy.

Microbeam Radiation Therapy in the Treatment of Tumors. *NATAN LENJO (Bronx Community College, Bronx, NY 10453) AVRAHAM DILMANIAN (Brookhaven National Laboratory, Upton, NY, 11973).* Radiation therapy is one of the principal methods used in the treatment of tumors, especially brain tumors. The problem faced by the current methods of treatment is the limitation brought about by the radiosensitivity of normal tissues surrounding the tumor, therefore placing considerable constraints in the adequate delivery of the radiation dose(s) to the tumor. Microbeam Radiation Therapy (MRT) appears to address this problem. MRT uses an array of parallel, thin planar slices of synchrotron-generated X-rays (microbeams) and is commonly administered in a single dose in the treatment of animal tumors. The irradiation of tumors with microbeams appears to spare normal tissue, including the central nervous system, while damaging the tumor. To demonstrate the application of MRT in the treatment of brain tumors, male rats, 200-225 g, were injected with $1x10^4$ cultured 9L gliosarcoma (9LGS) cells into their striatum 4 mm left of the midline, at the bregma level. These cells were implanted 5 mm beneath the surface of the skull using a 27-gauge needle. It took 14 days for the cultured cells to grow into tumors measuring 4 mm in diameter. The rats with 9L gliosarcoma brain tumors were exposed to a microbeams with a median energy of 120 keV. A total of 32 tumor-inoculated rats were used in this experiment; 24 were irradiated and 8 were left unirradiated as controls. The rats were monitored closely after the irradiation, euthanizing any that showed signs of neurological disability. In the previous MRT studies histological examinations 4 months after the irradiations or later showed that no tumor or tumor residue were visible, and that the brain tissues showed no significant level of damage. Those earlier results suggested that MRT can destroy tumors at a relatively high efficacy rate with little or no normal tissue damage. However, the present study is still ongoing and no conclusive results can be reached at this time.

Digital Signal Processing for Active Pixel Sensors. *JEFFREY LEVESQUE (Rensselaer Polytechnic Institute, Troy, NY 12180) HOWARD MATIS (Lawrence Berkeley National Laboratory, Berkeley, CA, 94720).* Active pixel sensors (APS) have been a promising development in complimentary metal-oxide semiconductor (CMOS) technology. The Relativistic Nuclear Collisions group at Lawrence Berkeley National Laboratory has proposed using active pixel sensors in a new vertex detector to measure short-lived particles resulting from high energy collisions at the Relativistic Heavy Ion Collider (RHIC). The expected performance must be evaluated before implementing an APS detector. In this study, a standard threshold-based algorithm was used to compare efficiencies before and after applying a Gaussian smoothing digital signal processing (DSP) technique to APS data. Different levels of noise were attained by recording data at several operating temperatures using the MIMOSA-5 chip, provided by the Institut de Recherches Subatomiques (IReS) of Strasbourg, France. Simulated particle hits were embedded at known locations in the data, and then a hit-finding algorithm was used to search for these hits. Overall efficiencies were calculated by integrating percentages of found hits over a 1.0 GeV/c pion energy spectrum for the MIMOSA-5. Results were compared based on efficiency versus the number of incorrect hits found. For all studied noise levels, smoothed data achieved higher efficiencies at reasonable false hit totals. Gaussian smoothing was therefore deemed to be effective method for improving APS efficiency.

The Density of Actinide Solutions at Varying Concentrations and Temperatures. *RACHEAL MARTINDALE (Purdue University, West Lafayette, IN 47907) CHARLES WEBER (Oak Ridge National Laboratory, Oak Ridge, TN, 37831).* In order to build more effective models, nuclear criticality safety research has recently found the need to obtain additional density data for aqueous solutions of various actinide compounds as well as hydrofluoric acid. Information was collected from internal Oak Ridge National Laboratory (ORNL) sources in addition to open literature. Internal sources include logbooks belonging to ORNL researchers beginning in the 1950's in the areas of criticality research and chemical science and technology research, the annual progress reports of the Neutron Physics Division of ORNL from the same time period, and other ORNL internal research reports. Open literature searched includes journals and compilations published in the chemical and nuclear sciences. Data regarding aqueous solutions of uranyl fluoride (UO_2F_2), uranyl sulfate (UO_2SO_4), uranyl chloride (UO_2Cl_2), thorium chloride ($ThCl_4$), thorium nitrate ($Th(NO_3)_4$), and hydrofluoric acid (HF) was found and compiled. This data was then evaluated statistically and analyzed for error in preparation for input into a small experimental program.

An Analysis of Variations in the Half-Lives of Long-Lived Isotopes. *CAROLYN MELDGIN (Harvey Mudd College, Claremont, CA 91711) RICHARD B. FIRESTONE (Lawrence Berkeley National Laboratory, Berkeley, CA, 94720).* It is commonly held that the half-life of an isotope is a constant. However, there is less agreement between different measurements than one would expect. Analyzing a database of 860 measurements for isotopes with a half-life greater than one day, it was determined that the average X^2, comparing measurements of the same isotope, was 7.04, rather than 1.00, the expected value. The purpose of this analysis was to select a subset of values from the original database that could be considered significant and determine what factor(s) influenced the agreement between values. Statistical analysis revealed that the measurements of half-lives of isotopes with large masses showed larger X^2 values. Nuclei can exist in different energy states, and heavier nuclei have more isomeric states available, often with half-lives comparable to that of the ground state. It is hypothesized that these nuclei show less agreement because when experimenters created the parent isotope for their experiment they created an isomer as well. Different experiments may populate the two states differently leading to varying results. Another factor influencing the measurement in half-life is decay energy. For isotopes with small decay energies, the associated half-lives tend to show poorer agreement. It is possible that the half-lives are affected by the chemical environment of the isotope when the decay energy is small. Spin, parity, fractional uncertainty, and mode of decay do not appear to influence the comparison of measurements.

Transient CO_2 Line Pipe Break Analysis for the Liquid Metal Secure Transportable Autonomous Reactor (STAR-LM). *ALEKSANDAR MILICEVIC (University of Wisconsin, Madison, WI 53715) JAMES J. SIENICKI (Argonne National Laboratory, Argonne, IL, 60439).* A simple transient model for a $400MW_t$ Liquid Metal Secure Transportable Autonomous Reactor (STAR-LM) system has been developed and incorporated into a computer code for a pipe break analysis on the gas turbine Brayton cycle utilizing supercritical carbon dioxide as the working fluid. The transient model was used to determine if a break in the pipe at the turbine inlet would affect reactor power, and to determine what size break would affect reactor power most significantly. A break in the pipe (50 cm in diameter) at the turbine inlet does affect reactor power, and a maximum increase in power (4%) is calculated for a 12.5-cm in diameter sized break.

Out-of-beam Studies of Beta Decay Products Near ^{48}Ca. *JARED NANCE (Beloit College, Beloit, WI 53511) ROBERT JANSSENS (Argonne National Laboratory, Argonne, IL, 60439).* Traditional gamma-ray spectroscopy focuses on 'in-beam', or prompt gamma rays as a probe of nuclear structure. In this paper, I describe a data mining experiment that was performed on data collected at the Gammasphere facility at Argonne National Laboratories that focused on 'out-of-beam' events. These events are typically missed by in-beam studies, as they take longer to produce and are of much lower relative intensity than in-beam reaction products. Using this technique, the existing level schemes for ^{46,47,49}Ca were verified. Furthermore, I propose a new energy level in ^{47}Ca (E=3143keV).

Compact Nuclear Power Source Benchmark Study. *MARK PAULSON (University of Wisconsin, Madison, WI 53715) TAEK K. KIM (Argonne National Laboratory, Argonne, IL, 60439).* The compact nuclear power source (CNPS) design was a small medium-enriched uranium-graphite-moderated reactor developed at Lose Alamos National Lab (LANL). Although the program was canceled before a complete demonstration CNPS was built, a series of critical experiments were performed at LANL given the unique CNPS core design. Today the most likely candidate for a Generation IV reactor is a Very High Temperature Reactor (VHTR) with similar design parameters as the CNPS. However, the published literature pertaining to the CNPS critical experiments does not consistently report the reactor's design parameters. This paper presents the results of a series of Monte-Carlo method benchmarking and sensitivity modeling of the CNPS design. The various CNPS configurations reported in the literature were evaluated and results of core eigenvalues and core physics data was compared. The modeling results were comparable but did not exactly reproduce the values found in the CNPS literature. The sensitivity results provide a more accurate understanding of the CNPS design and bias of benchmarking data. However, further modeling is needed to

develop the CNPS benchmark problem for application to a VHTR Gen IV reactor design.

Background Mitigation of Highly-Segmented HPGe Detectors in a Low-Background Environment. *MICHELLE PERRY (Florida State University, Tallahassee, FL 32301) KEVIN LESKO (Lawrence Berkeley National Laboratory, Berkeley, CA, 94720).* We present the first study of a highly-segmented HPGe detector with pulse shape discrimination in a low background environment. The detector consists of an 8x5 higly segmented coaxial HPGe crystal shielded with 5 cm of normal lead. Data was collected at the Oroville low-background counting facility to study detector behavior and backgrounds applicable to the proposed Majorana neutrinoless double-beta decay experiment. Waveform analysis and development of data analysis methods for the detector is presented.

Unveiling a New State of Matter: Studying Quark-Gluon Plasma with Charm Hadron Probes. *LARA PIERPOINT (University of California-Los Angeles, Los Angeles, CA 90095) KAI SCHWEDA (Lawrence Berkeley National Laboratory, Berkeley, CA, 94720).* Fifty-one institutions worldwide are working in collaboration to create and study a new state of matter called quark-gluon plasma (QGP) with the Solenoidal Tracker at RHIC (STAR) device at Brookhaven National Laboratory. Characterization of QGP, if it exists, can be accomplished by studying charm-quark hadrons in STAR. However, in order to observe charm hadron behavior, more precise measurements are needed than those currently possible with the detectors in place. The relativistic nuclear collisions group (RNC) at Lawrence Berkeley Lab is developing a new detector subsystem that will utilize active pixel sensing (APS) technology to measure charm hadrons in STAR. One of its main science goals will be to reveal the transverse momentum spectrum of the charm hadrons in gold-gold collisions. Monte Carlo simulations of the new sub-system detector (Heavy Flavor Tracker, or "HFT") show that it will be successful in distinguishing the spectrum of charm hadrons in the non-flow (no QGP) case from the spectrum in the flow (QGP) case.

Detection of Illicit Uranium Masked by the Presence of More Active Radioisotopes. *STEVEN SAAVEDRA (University of New Mexico, Albuquerque, NM 87131) IAN GROSS (Oak Ridge National Laboratory, Oak Ridge, TN, 37831).* Identification of unknown radioactive sources is a necessary process. With the heightened level of interest in the prevention of illicit trafficking of radioactive materials, new methods for the detection and characterization are being developed and evaluated. These methods are focused on detection of Uranium in the presence of more active radioisotopes to reduce the probability that an adversary could import fissile Uranium, an improvised nuclear device (IND) or a stolen nuclear weapon masked by a legitimate radioactive material shipment. An experiment was performed to detect the presence of Uranium by gamma spectroscopy utilizing a high purity Germanium (HPGe) radiation detector. A radioactive sample containing Uranium and an unknown radionuclide was placed in close proximity to a HPGe radiation detector with a Beryllium window end cap. An energy spectrum was collected for analysis. Analysis of the gamma peaks in the spectrum indicated that the sample was Ho-166m. None of the traditional photo peaks from Uranium were identified in the spectrum as the Ho-166m peaks overwhelmed the spectral results. By a non-traditional method of characteristic X-ray identification, the presence of Uranium was verified by identifying its characteristic X-ray peaks in the acquired spectrum. The energies of these characteristic X-rays, as listed in the nuclear decay tables, are 94.3 keV, 98.4 keV, 110.4 keV and 114.4 keV. The Uranium gamma peaks could not be seen in the acquired spectrum due to the large difference in specific activity on the order of 6 orders of magnitude between Uranium and Ho-166m, 1.922 10-6 Ci/g and 1.8 Ci/g respectively. The presence of Uranium, and other low specific activity radionuclides in the presence of high specific activity isotopes, can be verified through the non-traditional means of characteristic X-ray identification. This method is limited in the fact that the isotope can neither be qualified nor quantified through this method. To determine other artifacts such as enrichment or isotopic makeup more active means, such as sampling or active interrogation, would need to be employed.

Advanced Liquid-Liquid Separations. *DENISE SCHUH (University of Wisconsin, Madison, WI 53706) JOANNA MCFARLANE (Oak Ridge National Laboratory, Oak Ridge, TN, 37831).* Centrifugal contactors have many distinct advantages compared with conventional technologies for liquid-liquid extraction operations. The small size and high processing throughput of centrifugal contactors facilitate process intensification, i.e., the minimization of process size and material inventories. These reductions significantly improve process economics. Three systems were analyzed; diethylene glycol dibutyl ether (dibutyl carbitol) with nitric acid, 1-butyl-3-methyl imidazolium bis(perfluoroethyl sulfonyl)imide (bmim BETI) with water, and bmim BETI with cyclohexane. The data obtained can be used to create an accurate model to predict optimum performance. The systems were examined using a laboratory-scale, commercially available 5-cm-diameter contactor. Multiple data points were collected by varying the speed of the rotor, the weir size, the pump frequency, the pump stroke, the ratio between the two pumps, and the concentration of the liquids, which provided valuable information as to when the system would fail. Many physical and chemical properties of the three systems have also been determined, such as: calculating the surface tension using a contact angle meter; using a ring tensiometer, another method to measure the surface tension; determining the dispersion number by agitation; determining the density using Archimedes Principle; and determining the viscosity using a Brookfield Rheometer. For the dibutyl carbitol and nitric acid system, using weaker acid than 0.1M is not feasible due to the extremely poor separation time. Poor separation time was also measured with 1M nitric acid because the dibutyl carbitol was found to be contaminated with an unidentified substance. This particular system was examined because it is used in the purification of noble and heavy metals (e.g., gold and uranium) by selective extraction from aqueous solutions. The ionic liquid systems are currently being tested to gain more knowledge about them with hope they may be used for commercial processes in the future.

Creating an Interactive Timeline of Events Pertaining to the Creation and Completion of a Nuclear Waste Repository at Yucca Mountain, Nevada. *SCOTT SPYCHALA (University of Missouri-Rolla, Rolla, MO 65401) STEVE LOMPERSKI (Argonne National Laboratory, Argonne, IL, 60439).* Realization of nuclear waste storage in the United States including delays to date in the Yucca Mountain Project is well known as a tremendous challenge from the perspective of Federal project management. As with any major governmental project (The Hoover Dam, ORNL's Spallation Neutron Source) the Yucca Mountain Project (YMP) requires several governmental entities to make individual but coordinated decisions. The Nuclear Waste Policy act requires that all responsible bodies submit reports containing performance metrics and objectives. While these reports are issued separately and progress stepwise to a common goal, there is very little examination of the dynamics of the project in its entirety. The Yucca Mountain Interactive Timeline (YaMIT) project is an attempt to statically and dynamically model the YMP as a whole. In order to create the static model, the dynamic modeling program Vensim was used. We created a static model that identifies stakeholders and their tasks along one axis, with time along the other. Task to task relationships are connected by functional arrows. While Vensim was able to provide initial logic for the dynamic model, limitations prevented full development, so the programming language Java was used to complete of the simulation. Constant, linear and non–linear utility functions in time were incorporated into tasks that downstream predicted an end-of –project timeline. The dynamic model may be, in scope and with respect to utility functions, a breakthrough in large-scale project modeling. This dynamic portion of the YaMIT project is especially useful in determining the influence of multitask coupling and sensitivity analysis. We are developing a first-of-a-kind user friendly interface to assess the impact of decisions and completion of tasks in multi-stakeholder Federal projects.

Cosmic Rays: A Trip into the Atmosphere. *CHRISTOPHER TAYLOR (West Hills College, Lemoore, CA 93245) TOM KNIGHT (Lawrence Berkeley National Laboratory, Berkeley, CA, 94720).* The constant bombarding of cosmic rays (charged particles originating from either the sun or super nova) upon the earth's atmosphere has been a concern for scientist for over 100 years, and in years past and present, a major obstacle for NASA and airline workers. Since Victor Hess' balloon ride with an electroscope, scientist have known that the higher the altitude the more cosmic rays that will be detected. Scientists have often wondered if these particles have negative effects on the human body if too closely exposed to them. Using a cosmic ray detector which was built with the following components: 1) Scintallator paddles; captures falling rays and turns them into light, 2) Photo Multiplier Tubes (PMT); captures these light rays, 3) Circuit board; turns signal from PMT into a quantitative number, and 4) The detector's outer shell; gave 3 different angles of collection (30,60,90 degrees), and picking two places to take the readings, one high in elevation (Mt. Diablo) and one barricaded by man made structures (Caldecott Tunnel), scientists will be able to show if and how the atmosphere and structures affect these particles. This test will show that while altitude increases the amount of rays detected, concrete and earth block many of them. NASA and the FAA need to

be aware and concerned about these rays in hopes of protecting our nations astronauts, airline pilots and attendants from these rays and their possible harm.

Optics Analysis of the Hall A High Resolution Spectrometers. *ANDREW WHITBECK (University of Rochester, Rochester, NY 14445) DOUG HIGINBOTHAM (Thomas Jefferson National Accelerator Facility, Newport News, VA, 23606).* Experiment E94-107 at Thomas Jefferson National Accelerator Facility (JLab) will measure hypernuclear spectra. Because certain hypernuclear states are extremely close in energy, the Hall A High Resolution Spectrometers (HRS) will need to be calibrated to a higher precision than previously reached. Analysis of elastic optics data taken on a tantalum target at various momenta around a central momentum of 1.85 GeV/c was done in an effort to achieve a momentum, dp/p, full width half max (FWHM) resolution of 1×10^{-4}, the projected design limit of the HRS. Cuts were first applied to the optics data files in order to isolate useful events. The data files were then run through an optimization program to recalculate the optics matrix elements. Other systematic checks were done on various parts of the spectrometers. A FWHM resolution of 1×10^{-4} has been attained as a result of this optimization. With this improved HRS resolution, the current hypernulear experiment should be successful in its measurements.

Nuclear Data Extracted for Use in Burnup Credit Calculations. *SUSAN WILLIAMS (Texas A&M University, College Station, TX 77843) DON MUELLER (Oak Ridge National Laboratory, Oak Ridge, TN, 37831).* Burnup credit is a negative reactivity credit caused by a decrease in the amount of uranium-235 and the accumulation of other nuclides in nuclear reactor fuel while it has been used to generate power. Realistic bounding operating conditions can be used in fuel burnup modeling to support realistic conservative burnup credit calculations. Reactor operating data extracted, organized, and processed from documents from several commercial nuclear power plants offer valuable information for nuclear fuel burnup calculations. Axial burnup distributions, fuel temperatures, and moderator densities were among some of the information extracted for reactors such as Crystal River, Sequoyah, Three Mile Island, and Quad Cities. In addition, soluble boron concentrations were obtained for pressurized water reactors. This and additional data will be used to more accurately model nuclear fuel burnup. This work is part of a larger project that's main goal is to safely and economically transport commercial spent nuclear fuel in casks.

Numerical Analysis of Benchmark Data Using MCNPX. *ERIC WRIGHT (Prairie View A&M University, Prairie View, TX 77446) JEFFREY O. JOHNSON (Oak Ridge National Laboratory, Oak Ridge, TN, 37831).* Developments in the radiation transport codes for high energy radiation transport have triggered the applicability of these codes to new areas of research within the high energy physics and the NASA communities. These codes are now being utilized to analyze secondary particle production from Galactic Cosmic Ray (GCR) and Solar Particle Event (SPE) interactions in space environments. Similarly, they are also applicable to the analyses associated with target selection and design for advanced high energy particle accelerators and associated shielding. MCNPX (Monte Carlo N-Particle eXtended), an extended version of the industry standard Monte Carlo N-Particle transport code (MCNP), is being evaluated for such applications. MCNPX provides a complete 3D simulation of the problem geometry. It also provides the ability to utilize nuclear cross section libraries, when available, and physics models for particle types and energies where tabular nuclear data are not available. The results from MCNPX calculations, performed to benchmark neutron production from high energy source (alpha) - target interactions, were compared to measured values reported in a peer-reviewed journal article. This work was performed to better understand the limitations of the MCNPX physics models and to validate the code's applicability to heavy ion accelerator target design. The analysis was performed for a focused 710 MeV alpha ion beam on four different target materials: Water, Carbon, Lead and Stainless Steel (SS). The computational results are compared with the measured data at nine different angles; seven forward angles (0, 6, 15, 30, 45, 60, and 90) and two back angles (120 and 150) with a specific energy distribution at each angle. The source-target-detector geometry was modeled explicitly with all the details that were documented in the journal article. The calculations were performed to attain 10% uncertainty or better. In most cases sixty million source particles were simulated in a parallel mode (Parallel Virtual Machine, PVM) on a 24 node Linux Cluster, "cpile," within the Nuclear Science and Technology Division (NSTD) of Oak Ridge National Laboratory (ORNL). This work supports the benchmark efforts of the Radiation Shielding Group of NSTD for applying MCNPX to target station design for particle accelerators such as the Rare Isotope Accelerator (RIA) and Spallation Neutron Source (SNS).

Cost Analysis of the Hydrogen Economy Using FLOW. *SHANNON WROBLEWSKI (Tennessee Technological University, Cookeville, TN 38505) JUAN J. FERRADA (Oak Ridge National Laboratory, Oak Ridge, TN, 37831).* As the need for alternative fuel and energy sources increases, efforts to analyze the cost and viability of these sources also increase. One of the cost analysis models the Department of Energy (DOE) is currently using is known as H2 analysis, or H2A. H2A estimates the cost of production, delivery, and storage of hydrogen, giving a cost in $/kg of hydrogen. The H2A model looks at several different scenarios, such as transporting hydrogen as a compressed gas through a pipeline, as a compressed gas by truck, or as a liquid by truck. Currently, these models are all calculated in Excel on different spreadsheets. Using, reverse engineering, a step by step process was developed by which each step of the H2A model could be programmed into a simulation software package known as FLOW, named for its ability to create flow sheets and created at Oak Ridge National Laboratory. Python, a process modeling scripting language, was the computer language used due to the fact that it is already embedded in FLOW. After a module was made, it was then checked to make sure it corresponded to the values found in the H2A calculations. Then the module could be used in a flow sheet to compare similar types of operations, such as the transportation methods mentioned above. This allows the user to more easily compare different methods used in the H2A analysis in several ways. First, FLOW is a graphical program and does not show intermediate calculations as in the spreadsheets used in H2A. Second, several methods of transportation, storage, or other components of the hydrogen economy can be compared on the same flow sheet. Finally, user inputs are easily manipulated as in Excel. This project is a small but important part in the DOE's analysis of the hydrogen economy. It allows quick, yet accurate use of H2A analysis spreadsheets in an easy to use graphical format, allowing this small section of the hydrogen economy to be modeled more effectively.

Radiation Damage Studies at the Advanced Photon Source. *JAMES YOUNG (Diablo Valley College, Pleasant Hill, CA 94523) MARIA PETRA (Argonne National Laboratory, Argonne, IL, 60439).* The rare-earth permanent magnets in the insertion devices (IDs) of a storage ring are subjected to a harsh radiation environment that can lead to radiation-induced demagnetization significant enough to require the removal of the magnets for remagnetization. Integrated radiation dose measurements on the IDs give an indication of their radiation sensitivity and lifetime in the radiation environment of the accelerator facility and identification of regions where the probability for damage is highest. To date, at the Advanced Photon Source (APS) 7 GeV electron storage ring, the most severe radiation damage has been observed in those sectors that are equipped with small 5-mm vacuum chambers (i.e., sectors 3 and 4). The dose profile along the length of the ID in sector 4 was measured with alanine dosimeters, and magnetic measurements on that ID were also performed following a 3-month-long operation period (i.e., the 2005-1 run.) Helmholtz coil measurements of the magnetic field degradation of a sampling of magnets from the sector 4 ID were performed. The recorded doses along the length of the ID revealed significant dose nonuniformities with the highest doses being observed towards the downstream end of the ID where the greater magnetic degradation also occurs. In addition, transverse Hall probe x-scans of sample magnets from that ID showed that the sample magnets are primarily demagnetized directly under the beam. This study, as part of the continuing ID dosimetric and magnet damage studies on the APS IDs produced results consistent with previous studies. These results will contribute to the body of knowledge concerning the determination of the threshold for damage and identification of areas where the likelihood of damage is highest.

Evaluation of Russian Seals and Development of Wireless Tracking Systems for Nuclear Safeguards. *DAVID YOUNKIN (University of Tennessee, Knoxville, TN 37996) CHRIS PICKETT (Oak Ridge National Laboratory, Oak Ridge, TN, 37831).* Increased concern for national security is effectuating the development of technologies to, among other things, safeguard nuclear materials. To achieve this goal, wireless tracking systems can be used to monitor the location of a container and tamper-indicating devices (TIDs) can be used to detect unauthorized access into the container. However, these tools must be tested to determine their performance capabilities and characteristics before they can be effectively implemented. Russian supplied wire loop seals (OPP-1M) are TIDs that are noted for their simplicity of design. They are assembled by creating a unique wire pattern between two pieces of glass and then registered in a reader that can then verify the wire pattern image associated with the seal. These seals were tested to

quantify the rate of failure of the reader in the laboratory environment as well as applied to drums to simulate an actual operating environment. The rate of failure in the laboratory is 2 percent in contrast to 4 percent when read on the drums. The data was also analyzed to identify factors that may influence this rate of failure. Another set of Russian TIDs was tested. These fiber-optic based seals transmit radio frequencies to a base station connected to a computer that records the status of the seal. Also, a wireless tracking system using 802.11 wireless routers and active radio frequency tags was set up and preliminary tests done to determine signal strength at given intervals. This system would allow containers to be tracked as they enter and move around a facility. Testing these safeguards reveals their strengths and weaknesses which will lead to a better determination of the levels of nuclear safeguards required to thwart different threats and to provide safer transport and storage of nuclear materials in the future.

Case Study of Radioactive Modeling with Irregular Source Formations. *ANDREW ZURAWSKI (Purdue University, West Lafayette, IN 47906) JAMES TERRY (Oak Ridge National Laboratory, Oak Ridge, TN, 37831).* Dose rates were modeled and measured for 20-foot cargo containers loaded with drums containing hydrated thorium nitrate in two configurations. One configuration consisted of 38 85-gallon drums each containing 825 pounds of hydrated thorium nitrate; the other configuration consisted of 127 30-gallon drums each containing 200 lbs of hydrated thorium nitrate. The decrease of the dose rates with distance were calculated using both line source and point source models. The modeled decrease of the dose rate with distance was compared to the measured dose rate. To relate the modeled unshielded source with the measurements, an effective linear attenuation coefficient was computed. Despite a geometry that appears to be more line-like than spherically symmetric, the point source predictions for dose rates were found to be in much better agreement with the measurements than were the predictions using the line source model.

Physics

Ray Detector. *GUADALUPE AMEZQUITA (Reedley College, Reedley, CA 93654) TOM KNIGHT (Lawrence Berkeley National Laboratory, Berkeley, CA 94720).* Cosmic rays are energetic particles that enter the earth's atmosphere from space. They are produced by the interactions of high-energy particles from space the sun and supernovae. Scientists can not determine the specific source and direction of the charged particle because the magnetic fields in space distort their direction of origin. The cosmic ray detector is made to measure the muon flux as a function of elevation, in these flux muons and anti-muons are produced equally. This is the process in which muons are made: A charged particle in space collides with atoms in the earth's atmosphere, from these interactions pions are given off. Pions decay rapidly but they may interact first and make even more pions, when the pions decay they create high-energy muons and two (unseen) neutrinos. Muons decay slower than the pions. Muons decay into electrons and neutrinos, but the electrons and neutrinos do not have enough energy to be detected by the scintillators in the detector. Muons are the only particles with enough energy to be detected above the noise of the environment. Muons are able to penetrate large amounts of materials without interacting. An example of these materials would be mountains and concrete which were part of our experiment. We took the detector to the Caldecott Tunnel to see if concrete and the mountains on top of the tunnel decreased the amount of muons that would be detected. The result was that the counts did decrease which meant that the concrete and the mountain slowed down the muons. Also, we took the detector to Mt. Diablo to test if the altitude increase the counts of the muons being detected. In result the higher we got on Mt. Diablo the higher the counts were.

Optimizing The $B_s \rightarrow \mu^+\mu^-$ Decay Search At CDF Using an Artificial Neural Network. *BARRY AMOS (Saint Mary's College of California, Moraga, CA 94565) CHENG-JU LIN (Fermi National Accelerator Laboratory, Batavia, IL 60510).* In the standard model (SM), the Flavor Changing Neutral Current $B_s \rightarrow \mu^+\mu^-$ decay is highly suppressed. The SM expectation for this branching fraction is $B(B_s \rightarrow \mu^+\mu^-) = 3.42 +/- 0.54x10^{-9}$, which is about an order of magnitude smaller than the current experimental sensitivity at the Tevatron. However, new physics contributions can significantly enhance this branching fraction. An observation of this decay at the Tevatron would be unambiguous evidence for physics beyond the SM. However, identifying B_s candidates is an experimental challenge due to the small branching fraction and large background contamination in the data. In a previous search, a multivariate likelihood technique (LH) was used to discriminate between signal ($B_s \rightarrow \mu^+\mu^-$ events) and background (non $B_s \rightarrow \mu^+\mu^-$ events). In this analysis, we study the feasibility of using a Neural Network to improve signal and background separation using of data collected by the CDF II detector. To quantify the improvements, we train the Neural Network using the same three input discriminating variables and data sample as the ones used in the LH analysis. The first input variable is the proper decay time of the B_s candidate. The second input variable is the opening angle between the B_s candidate momentum and decay axis, where the decay axis is defined as the vector pointing from the B_s production to the decay vertex. The last input variable is the B_s candidate isolation, which is defined as the ratio of the B_s momentum to the scalar sum of the momentum of other adjacent tracks around the B_s candidate. Using independent samples for testing and training the Neural Network, we were able to optimize the number of training cycles and structure of the network. To train the network we use a standard-backpropagation algorithm. The structure of the network consists of eight nodes in the first hidden layer, six nodes in the second, and a single output node. Our results for the Neural Network show about a 10% increase in signal acceptance with the same background rejection compared to the LH. With future plans of using more input variables to further optimize the Neural Network, we expect to improve significantly the signal acceptance and background rejection.

Balloon-Borne Gamma-Ray Polarimeter (PoGO) to Study Black Holes, Pulsars, and AGN Jets: Design and Calibration. *ZACHARY APTE (Hampshire College, Amherst, MA 01002) TSUNEYOSHI KAMAE (Stanford Linear Accelerator Center, Stanford, CA 94025).* Polarization measurements at X-ray and gamma-ray energies can provide crucial information on the emission region around massive compact objects such as black holes and neutron stars. The Polarized Gamma-ray Observer (PoGO) is a new balloon-borne instrument designed to measure polarization from such astrophysical objects in the 30–100 keV range, under development by an international collaboration with members from United States, Japan, Sweden and France. The PoGO instrument has been designed by the collaboration and several versions of prototype models have been built at SLAC. The purpose of this experiment is to test the latest prototype model with a radioactive gamma-ray source. For this, we have to polarize gamma-rays in a laboratory environment. Unpolarized gamma-rays from Am241 (59.5 keV) were Compton scattered at around 90 degrees for this purpose. Computer simulation of the scattering process in the setup predicts a 86% polarization. The polarized beam was then used to irradiate the prototype PoGO detector. The data taken in this experiment showed a clear polarization signal, with a measured azimuthal modulation factor of 0.35 ± 0.02. The measured modulation is in very close agreement with the value expected from a previous beam test study of a polarized gamma-ray beam at the Argonne National Laboratories Advanced Photon Source. This experiment has demonstrated that the PoGO instrument (or any other polarimeter in the energy range) can be tested in a libratory with a simple setup to a similar accuracy.

Analysis of Sensor Viability for Transmission Lines in Close Proximity to Zero-Potential Grounding Objects. *ALEXANDER BATALLER (University of California Santa Cruz, Santa Cruz, CA 95010) DONALD HAMMERSTROM (Pacific Northwest National Laboratory, Richland, WA 99352).* Zero-Potential Grounding Object (ZPGO) is any object that has the ability to come into contact with Transmission Lines thereby creating grounding for current. Trees are the ZPGO of focus in this study as they are the most common. In order to determine if sensors can be placed on trees that can successfully detect voltage running from Transmission Lines to ground, a quantitative analysis is needed to determine if said voltage will be detectable as a function of distance. By creating Simple Circuit, Voltage as a function of distance, Change in Swing Ratio, and Cross-Sectional Voltage Fields through a Finite Difference Method models (CSVFFDM), voltage data can be acquired using Excel and MatLab. When analyzing voltage data through these various models, the extremely low current values coupled with the high variability in tree conductivity eliminates the chances for conventional voltage readings. Further analysis in mapping CSVFFDM will provide a more accurate representation of Transmission Line models and a possibility for sensor viability on Transmission Line Poles.

Gyrokinetic Stability Studies of the Microtearing Mode in the National Spherical Torus Experiment H-mode. *JESSICA BAUMGAERTEL (University of Washington, Seattle, WA 98105) MARTHA REDI (Princeton Plasma Physics Laboratory, Princeton, NJ 08543).* Insight into plasma microturbulence and transport is being sought using linear simulations of drift waves on the National Spherical Torus Experiment (NSTX), following a study of drift wave modes on the Alcator C-Mod Tokamak. Microturbulence is likely generated by

instabilities of drift waves, which cause transport of heat and particles. Understanding this transport is important because the containment of heat and particles is required for the achievement of practical nuclear fusion. Microtearing modes may cause high heat transport through high electron thermal conductivity. It is hoped that microtearing will be stable along with good electron transport in the proposed low collisionality International Thermonuclear Experimental Reactor (ITER). Stability of the microtearing mode is investigated for conditions at mid-radius in a high density NSTX high performance (H-mode) plasma, which is compared to the proposed ITER plasmas. The microtearing mode is driven by the electron temperature gradient, and is believed to be mediated by ion collisions and magnetic shear. Calculations are based on input files produced by TRXPL following TRANSP (a time-dependent transport analysis code) analysis. The variability of unstable mode growth rates is examined as a function of ion and electron collisionalities using the parallel gyrokinetic computational code GS2. Results show the microtearing mode stability dependence for a range of plasma collisionalities. Computation verifies analytic predictions that higher collisionalities than in the NSTX experiment increase microtearing instability growth rates, but that the modes are stabilized at the highest values. There is a transition of the dominant mode in the collisionality scan to ion temperature gradient character at both high and low collisionalities. The calculations suggest that plasma electron thermal confinement may be greatly improved in the low-collisionality ITER.

Effects of Superhard Nanocomposite Coatings on Friction Between Piston Rings and Cylinders in Automobile Engines. *JEFF BAYERS (Washington University in St. Louis, St. Louis, MO 63105) GEORGE FENSKE (Argonne National Laboratory, Argonne, IL 60439)*. With rising gas prices and ongoing disputes over foreign oil sources, improving fuel economy is a task of great importance. A primary weakness in fuel efficiency in automobiles occurs in engine pistons: as piston rings rub repeatedly against the inside of the cylinders, the resulting friction hinders their movement and consequently excess fuel is impractically expended. Furthermore, this repetitive rubbing can gradually cause wear in both the cylinder liner and the ring, thereby weakening both and decreasing the engine's operating efficiency. Here in the tribology department, which focuses on the physical concepts of friction, wear, and lubrication, we have been testing a recently developed Super Hard NanoComposite coating (SHNC), a wear-resistant lubricant designed to reduce friction between surfaces in contact. Using a High Frequency Reciprocating Rig (HFRR), we can simulate the rubbing of a ring against a liner while measuring the resulting friction, allowing for in-situ testing of the new coating. Because conducting tests using a model engine would be too costly and difficult to monitor, all tests are being performed with the HFRR. The coated liner is tested with a variety of commercial motor oils as a means of determining chemical interaction between the coating and the oils that might also occur in practical environments. On liners for which the coating has been applied and allowed to wear in through initial runs of the HFRR, marked reductions in friction and coefficient of friction have been measured. Friction shows the greatest reduction when the HFRR is operated at higher speeds, although the tests have not exceeded 360 rpm. Comparing different amounts of a single oil type shows relatively insignificant differences between the different quantities of oil. All tests are also conducted with different speed transitions. Data is taken at individual speeds and again as the rig accelerates and decelerates to further simulate actual Ring-On-Liner (ROL) interaction. Further testing will be conducted using different liner and ring combinations such as: both uncoated, coated ring and uncoated liner, and both coated. These tests work in conjunction with other simulations of surfaces in contact to determine the most efficient contact area between two surfaces.

A Method to Determine the Minimum Energy Threshold and Coarse Low Energy Calibration for PVT Based Detectors Using the Lower Level Discriminator. *SARAH BENDER (Juniata College, Huntingdon, PA 16652) RICHARD KOUZES (Pacific Northwest National Laboratory, Richland, WA 99352).* Radiation portal monitors (RPMs) play a critical role in ongoing attempts to intercede illicit radiological sources. RPMs widely utilize polyvinyl toluene (PVT) based detectors which have relatively high durability and low cost, but intrinsically poor energy resolution. However, a pulse height analyzer does provide some spectroscopic information allowing broad energy windowing (EW) algorithms to be employed as a complement to less specific gross count measures when detecting radiation. Quantifying the low energy sensitivity and low energy calibration of these detectors presents unique obstacles since the photon interaction in PVT is dominated by Compton scattering events, masking full energy peaks in the energy range of interest, and driving an increase in the count rate in the low energy region. A method to gauge the sensitivity of PVT detectors and generate a coarse low energy (~5keV to ~80keV) calibration by varying the lower level discriminator (LLD) setting and tracking the net count rate from a source has been investigated for several commercial PVT-based RPM systems using ^{55}Fe, ^{109}Cd and ^{241}Am. Parameters in a Fermi function were adjusted to fit the resulting integral pulse height data and the derivative of the generated fit function, representing the differential pulse height spectrum, was determined. The presence of a peak in the derivative of the count rate for a source signified the presence of a photopeak, and provided a means of assessing the low energy sensitivity of the detector. Additionally, observed peaks in such differential pulse height curves for multiple sources with peaks in the 5keV to 80keV range allowed a coarse low energy calibration to be established.

RIA Rotating Foil Stripper Design. *MICHAEL BERTOLLI (Colorado School of Mines, Golden, CO 80401) JERRY NOLEN (Argonne National Laboratory, Argonne, IL 60439).* Development of the next generation of accelerator facilities, the Rare Isotope Accelerator (RIA), is underway. Its construction will lead to fundamental breakthroughs in the study of unstable nuclei and nuclear physics. In order achieve the goals of RIA a method of proper cooling of integral beam strippers in necessary. Using a pendulum swinging, rotating foil wheel it may be possible to reach the required cooling rates. Several possible cam designs that can be used to cause the pendulum motion are analyzed in this paper. Mathematical models of of the cam designs have been developed and can be used to determine the most desirable configuration. The optimal design depends on several factors, including increasing smoothness of rotation and reducing friction. The disadvantages of each design are detailed, with the cylindrical cam appearing as a strong design option. Design of the foil beam strippers, while integral, is only a small part of the massive collaboration working on RIA in the drive to reach the next level of experimental nuclear physics.

Mapping Strain in Nanocrystalline Nitinol: An X-ray Diffraction Method. *MATTHEW BIBEE (University of California San Diego, La Jolla, CA 92093) APURVA MEHTA (Stanford Linear Accelerator Center, Stanford, CA 94025).* Understanding the mechanical properties of biomedical devices is critical in predicting and preventing their failure in the body. Such knowledge is essential, for example, in the design of biomedical stents, which must undergo repeated strain over their ten year lifetimes without breaking. Computational models are used to predict mechanical response of a device, but these models are not complete; there are significant deviations from the predictions, especially when devices are subjected to repeated multi-axial loads. Improving these models requires comparisons with actual measurements of strained nitinol. Local measurements of the full strain tensor can be made using X-ray diffraction techniques, but they are currently limited to materials whose grain size is larger than the X-ray beam size or require several diffraction patterns produced by rotation of the sample. Nitinol stents are nanocrystalline, with grains smaller than any available X-ray beam. We present a method for measuring the local strain in a nanocrystalline material from a single X-ray diffraction pattern by extending current powder diffraction techniques. The components of the strain tensor are mapped onto a displacement ellipsoID which is then reconstructed from diffraction data through Bragg's law and least-squares fitting. Using simulated diffraction data, we performed sensitivity tests to examine how the accuracy of the method depends on how much of the diffraction pattern is measured. We found that strain can be accurately calculated from measurements of at least three diffraction arcs of at least 20 in length. Thus we believe that our method is a viable approach to calculating strain provided a sufficient amount of diffraction pattern is recorded.

The Universe Adventure Project. *KYRA BOSTROEM (Vassar College, Poughkeepsie, NY 21604) GEORGE SMOOT (Lawrence Berkeley National Laboratory, Berkeley, CA 94720).* Cosmology is a difficult area to study. It is not only constantly changing, but the ideas are abstract, often mistakes are made even by scientists in the field. However, it is also an important field to study. It tells us our history on the largest scale possible, that of the universe. It also gives us hints about our future. How then are teachers to educate themselves enough to teach students cosmology. Very few books are written below the college level and Internet resources are often unreliable. The Universe Adventure is an educational website that seeks to solve these problems. Written by scientists and teachers, it is accurate, current, and at the high school and middle school level. It offers a comprehensive view of cosmology as well as quizzes throughout to test understanding and math problems to challenge students. Along with providing students with information, it also has a page of reference materials for teachers with activities and links. The website has the

advantage of being as up to date with the most current models. This is due in part to the base of the website being at Berkeley lab, where there is ongoing research in cosmology. The currency is also a result of the format of the website, as a website it can easily and quickly be updated. This summer the project underwent some updates. It was edited and consolidated as well as augmented with math problems, in depth side paths, and more information. With the work done so far and future work, we hope the Universe Adventure will allow teachers to bring cosmology to their classroom in a way that is interesting and inspiring to students.

Characterizing the Interactions Between a Photon and a Magnetic Field Gradient. *CHERYL ANN BROWN (Borough of Manhattan Community College, New York, NY 10007) CAROL Y. SCARLETT (Brookhaven National Laboratory, Upton, NY 11973)*. The objective of this experiment is to explore an interaction between photons and a magnetic field gradient. The specific goal of our research is to detect the Fourth Order Feynman Interaction, Polarization of Virtual pairs, and/or Space Time Curvature. The method and main goal of our experiment was to apply Fourier Analysis with the software program FORTRAN. As a result of this, we then applied FORTRAN codes with a Fourier Analysis code to break down vibrations that can effect the photo-receiver sensitivity. By breaking down these vibrations, we can then find the amplitudes which are the frequency contributions to the wave as well as that particular frequency. Depending on the interference pattern, other sounds and vibrations (vibrations on the floor will jump around to about 120 Hertz, the additional vibration may be 60 Hertz that may influence the laser). We will then compare data from the accelerant-meter to the photo receiver of its vibration data with the data of the vibrations that we collect from the Fourier Analysis. With the aspect of Lens Calculations we prepared a data analysis table where, with the measurement of different optical lenses, a telescope to maintain space time curvature effect and a photo receiver at the end of the magnetic beam, we had the ability to calculate the focal point and minimize waist of the beam. To get the calculations of the radius of the beam at the photo-receiver, we applied an optical lens matrices and Jones vectors into a Mathematica program. We then applied several measurements of optical length to the distances of the laser beam and lenses to get precise data, measurements and price estimations for the Lens Experiment. The measured data that we have from the lens matrices and Jones vectors were set up as an “x” and “y” variables to see the proximity and sensitivity of the dimensions. Our results indicated that these dimensions provided the least amount of sensitivity in the waist of the beam, meaning that any lens shift within the error of our instruments would not dramatically affect the waist of our beam. Error bounds equal +/- 1cm. To conclude, the ultimate goal of our experiment was to eliminate outside interference, that contributes to the background noise and to eliminate it when trying to apply the authentic data.

Event Display Tools for the Cryogenic Dark Matter Search (CDMS). *REGINA CAPUTO (Colorado School of Mines, Golden, CO 80401) DAN BAUER (Fermi National Accelerator Laboratory, Batavia, IL 60510).* Dark matter is an attractive solution to the problem of missing matter in the universe as observed in galactic rotation curves and other large body observations. Cold non-baryonic Dark Matter (CDM) emerges as the leading candidate among the other types of dark matter because it has properties required for the formation of the current universe. The Cryogenic Dark Matter Search (CDMS) is using cutting edge technology to aid in the direct detection of Weakly Interacting Massive Particles (WIMPs), a type of CDM. This paper discusses the process by which WIMPs, as well as other incoming particles, are detected by the CDMS experiment and how the data is collected and characterized. Once data is collected, however, accessing the raw data by members of the collaboration is important. This paper also focuses on event display software that allows easy access to raw data. A problem occurs when raw data is stored where there are restrictions to accessing the files. This problem can be solved by incorporating two versions of event display software into general use. The first, written in ROOT, can graph raw data and apply a curve fitting so that, after integrating the curve, the energy of the particle can be determined. The second version, written in CGI for the Internet, can allow access to graphed raw data saved in a site accessible to the collaboration.

Fourier Analysis of Background Vibrations Concerned with High Level Precision in the Detection of Virtual Pair Interaction and Anomalous Space-time Curvature. *DANIEL CARRERO (State University of New York – Stony Brook, Stony Brook, NY 11794) CAROL SCARLETT (Brookhaven National Laboratory, Upton, NY 11973).* Anomalous space-time curvature, analogous to that of general relativity, presents itself outside what is described by the standard model of physics concerning itself not with the induced curved flight path of a photon insofar as general relativity curves space around a massive object. Such photon interactions are not conceived adequately through the standard model which seeks to explain photon interactions as far as a 4th order Feynman interaction. Concerning this, our experiment wishes to facilitate the requirements of general relativity using an electromagnetic basis to further study such photon interactions. Thusly, in accordance to this objective, we will be utilizing a Relativistic Heavy Ion Collider (RHIC) quadra-pole magnet which upon being ramped at a frequency less than 20 Hz will yield a field gradient of 71 T/m where in which an argon laser of 512nm will pass and interact. The virtual pair interaction will resolve for us on a quadri-cell photo receiver, a frequent deviation of the beam equal to that of the magnetic ramping. Of consequence to us, the contribution of background vibrations can also provide deviations in the beam which can eliminate justified results. Therefore, we have worked to develop and analyze the Fourier transformations of background vibrations using comparative analysis of a photo receiver and accelerometer data taken over a span 1minute. Each device was positioned in critical areas near the magnet and the laser for 1 minute each and then alternated. Then utilizing FORTRAN running computers we transformed the vibrations into their components yielding various frequencies and contributions (amplitudes). Comparing the two devices we discovered similar vibration pickup and frequency contributions. From both, a clear and dominant 120 Hz signal was recovered which is expected from operation frequencies of cooling refrigerators surrounding the magnet. Of consequence to the magnet, signals near 20 Hz and below were negligible which gives good indication that background contributions to magnetic ramping will not contribute to false deviations. From these transformations, we are given a quantitative understanding of our background which will enable us to avoid in phase magnetic ramping which can leave ambiguity in our results.

Bettering Communication Among Nuclear Astrophysicists: An Overview of the Computational Infrastructure for Nuclear Astrophysics. *RICK CARROLL (Pellissippi State Technical Community College, Knoxville, TN 37933) MICHAEL SMITH (Oak Ridge National Laboratory, Oak Ridge, TN 37831).* In the past half century there have been numerous advances in the understanding of astrophysical phenomena such as element synthesis during stellar events, and the evolution of the next generation of stars and planets. This progress is a result of the compilation of large datasets consisting of laboratory measurements of thermonuclear reaction rates. Surprisingly, the standard reaction rate library among the astrophysics community, REACLIB, subsists with a decade long lapse in incorporating laboratory findings. In a 2003 article, Michal Smith addresses the importance of centralizing the efforts of world-wide research, and introducing “user-friendly” dissemination and evaluation tools to astrophysicists. The Computational Infrastructure for Nuclear Astrophysics (CINA) project was launched in 2003 to fulfill this need. With this interactive suite, reaction rate information can easily be accessed, updated, and utilized. In order to improve the efficiency and functionality of the suite for nuclear astrophysics studies, CINA is currently undergoing a redevelopment stage. Specifically, efforts are being made to approach real-time retrieval of element synthesis data. Currently, datasets and other essential information used by the interface are stored in text files in a linear fashion. This means that a search for a particular piece of data must start from the beginning of a file and “look” for its target. The goal of the current project is to migrate the text file storage method to a relational database storage method, such as MYSQL, to increase the communication speed of data to the interface, and then to the research community. Once implemented, these improvements to the Computational Infrastructure for Nuclear Astrophysics will aid in the immediate evaluation, distribution and application of today’s laboratory results.

Spectroscopic Studies of Merging Spheromak Plasmas in the Magnetic Reconnection Experiment. *ALEXANDER CARVER (University of Wisconsin, Madison, WI 53706) STEFAN GERHARDT (Princeton Plasma Physics Laboratory, Princeton, NJ 08543).* Magnetic reconnection, the topological breaking and reconnection of magnetic field lines, occurs in many magnetized plasmas e.g. in the solar corona, Earth’s magnetosphere, and tokamaks. The ubiquity of plasmas in the universe and the potential use of current-carrying plasmas in fusion power plants warrant an improved understanding of magnetic reconnection. The Magnetic Reconnection eXperiment (MRX) is dedicated to improving our understanding of magnetic reconnection. We used nine fiber optic guides leading to a spectrometer and CCD camera to measure spectral line widths and shifts along many lines of sight within MRX, hence mapping the MRX ion temperature and

toroidal plasma velocity. This diagnostic allows us to study flow patterns and ion heating during the merging of two spheromaks. 439 MRX shots and spectrometer images were taken over six days. Averaged ion temperatures ranging from 0 to 30 eV were observed. The average bulk plasma flow was away from the observer at the vacuum vessel edge and towards to observer at the vacuum vessel center with velocities up to 15 km/s. Further study of these results will allow comparison with Tokyo University's TS-3 experiment. These measurements and comparisons are another step toward the realization of fusion power plants and the improved understanding of magnetic reconnection. A.J. Carver was supported by the Department of Energy's Summer Undergraduate Laboratory Internship program. Contract number DE-AC02-76CH03073

2-D Modeling of Energy-z Beam Dynamics Using the LiTrack Matlab Program. *SEAN CAULEY (Paine College, Augusta, GA 30901) MIKE WOODS (Stanford Linear Accelerator Center, Stanford, CA 94025).* Short bunches and the bunch length distribution have important consequences for both the Linac Coherent Light Source (LCLS) project at SLAC and the proposed International Linear Collider (ILC) project. For both these projects, it is important to simulate what bunch length distributions are expected and then to perform actual measurements. The goal of the research is to determine the sensitivity of the bunch length distribution to accelerator phase and voltage. This then indicates the level of control and stability that is needed. In this project I simulated beamlines to find the rms bunch length in three different beam lines at SLAC, which are the test beam to End Station A (ILC-ESA) for the ILC studies, LCLS and LCLS-ESA. To simulate the beamlines, I used the LiTrack program, which does a 2-dimensional tracking of an electron bunch's longitudinal (z) and the energy spread beam (δE) parameters. In order to reduce the time of processing the information, I developed a small program to loop over adjustable machine parameters. LiTrack is a Matlab script and Matlab is also used for plotting and saving and loading files. The results show that the LCLS in Linac-A is the most sensitive when looking at the ratio of change in phase degree to rate of change. The results also show a noticeable difference between the LCLS and LCLS-ESA, which suggest that further testing of the effects caused by the Beam Switch Yard and End Station A to determine why the result of the LCLS and LCLS-ESA vary

Simulations of the Electron Cloud Effect for the Large Hadron Collider. *VERNON CHAPLIN (Swarthmore College, Swarthmore, PA 19081) MIGUEL FURMAN (Lawrence Berkeley National Laboratory, Berkeley, CA 94720).* The Large Hadron Collider (LHC), scheduled to begin operation at CERN (the European Laboratory for Particle Physics) in Switzerland in 2007, will collide counter-rotating beams of protons at unprecedented energies of up to 7 TeV per proton and intensities up to 1011 protons per bunch. In this regime, a phenomenon known as the Electron Cloud Effect (ECE) is expected to play a significant role in beam dynamics. Unwanted electrons can be produced in the beam pipe through the photoelectric effect, ionization of residual gas by beam particles, or the production of secondary electrons due to electrons striking the walls. A high electron concentration partially neutralizes the beam, making it more difficult to control. The primary concern for the LHC is that electrons striking the walls of the pipe will deposit heat at a high enough rate to overwhelm the cryogenic cooling system, which is necessary for the accelerator's superconducting magnets to function properly. This paper details the results of computer simulations of the ECE in one of the LHC dipole magnets using the Fortran code POSINST, developed by Miguel Furman and Mauro Pivi at LBNL over a number of years. POSINST simulates a thin slice of the beam pipe over a time interval encompassing many bunch passages. It includes a detailed model of primary electron production, secondary emission, and electron cloud dynamics; however, it does not calculate the effects of electrons on the beam. POSINST simulations were run with bunch spacings of 25 ns and 75 ns, bunch intensities between 4×10^{10} and 1.6×10^{11} protons, and maximum secondary electron yields (δmax) between 1.0 and 2.0. Preliminary results indicate that the cooling system may be overwhelmed at the nominal values of 1.15×10^{11} particles per bunch and 25 ns bunch spacing unless δmax is less than or equal to 1.3. Independent simulations using the ECLOUD code at CERN have produced lower estimates of the average power deposition; we investigated this discrepancy by re-running our simulations with the production of re-diffused electrons turned off (ECLOUD does not consider the contribution of this effect to the population of secondaries). Results of these simulations were in close agreement with CERN results, indicating that because of their unique energy spectrum, re-diffused electrons play an important and unique role in the overall ECE.

Structural Study of 2-Quasiparticle States in ^{254}No. *JEREMY CHAPMAN (Syracuse University, Syracuse, NY 13210) TENG LEK KHOO (Argonne National Laboratory, Argonne, IL 60439).* Heavy nuclei are prone to spontaneous fission. A large shell-correction energy provides a sizeable barrier against fission in some superheavy nuclei, e.g. ^{254}No. Isomers in ^{254}No were studied in a ^{208}Pb(^{48}Ca,2n) reaction to provide data on single-particle energies and pairing. Germanium Clovers detected gamma rays, and a Double-sided Silicon Strip Detector (DSSD) detected electrons and alpha particles. Gamma ray intensities and branching ratios were detected. Gamma rays were found at 53keV from the (7^- or 8^-) isomer to the 7^+ state in a 2-quasiparticle band with $K_p = 3^+$. Gamma rays were also found at 842keV and 944keV from the 3^+ band head to the 4^+ and 2^+ states respectively, in the ground state band. The decay percentage is 15% and 85% respectively.

Analysis of B→ωlu Decays With BaBar. *YIWEN CHU (Massachusetts Institute of Technology, Cambridge, MA 02139) JOCHEN DINGFELDER (Stanford Linear Accelerator Center, Stanford, CA 94025).* As part of the BaBar project at SLAC to study the properties of B mesons, we have carried out a study of the exclusive charmless semileptonic decay mode B→ωlu, which can be used to determine the Cabbibo-Kobayashi- Maskawa matrix element Vub. Using simulated event samples, this study focuses on determining criteria on variables for selection of B→ωlu signal and suppression of background from other types of $B\overline{B}$ events and continuum processes. In addition, we determine optimal cuts on variables to ensure a good neutrino reconstruction. With these selection cuts, we were able to achieve a signal-to-background ratio of 0.68 and a signal efficiency of the order of 1%. Applying these cuts to a sample of 83 million $B\overline{B}$ events recorded by BaBar in e^+e^- collisions at the (4S) resonance, we obtain a yield of 115 ± 19 B→ωlu decays.

Testing and Reparing Detectors for the Møller Polarimeter. *APRIL COOK (Monmouth College, Monmouth, IL 61462) DAVE GASKELL (Thomas Jefferson National Accelerator Facility, Newport News, VA 23606).* The Møller Polarimeter is used to measure the polarization of the electron beam passing through the beam line on its way to the main target in Hall C at JLab. A key component of the detector system is 32 small detectors, made up of a piece of scintillator attached to a photomultiplier tube (PMT). The electron beam hits this wall of detectors and excites the atoms and molecules in the scintillator, which then decay and emit photons. The photons then travel through the PMT and produce a pulse that is sent to a data acquisition (DAQ) program. After several years of use, these PMT's are not working properly and need to be replaced. Before they are repaired, the detectors are tested to see what data they produce at their broken state. Cobalt-60 (Co-60) is then placed directly on the scintillator, to produce signals. After their initial tests, new PMT's are glued onto the same scintillators, using special ultraviolet (UV) curing glue. The new detectors are wrapped tightly with aluminized Mylar and black electrical tape to keep ambient light out. After they are fixed, the detectors are tested again using the same Co-60 source. The signals produced after repairs are compared to the previous data to ensure that they are working better. The detectors have improved since their repairs. They have larger signals at much lower voltages. This will significantly improve the effectiveness of the Møller Polarimeter.

Neutron Attenuation and Monte Carlo Calculations Using the FLUKA Simulation Program. *BRENT COVELE (Rose-Hulman Institute of Technology, Terre Haute, IN 47803) ALBERTO FASSO (Stanford Linear Accelerator Center, Stanford, CA 94025).* Rather than construct thick shielding around radioactive sources to attenuate hazardous radiation, physicists often design winding networks of tunnels to effectively limit the range of radiation while providing access to the source if necessary. However, it is important to know how quickly the radiation attenuates, and instead of planning physical experiments, physicists use complex simulations to model various situations via Monte Carlo calculations. The simulation program used in this experiment was FLUKA. A concrete labyrinth with two legs of lengths 10 d/vA and 20 d/vA (d is the centerline distance, A is the inner cross-section) was designed with an isotropic neutron point source at the mouth of the first leg. Sixty different scenarios were run with twelve energies and five cross-sections to determine the rate of attenuation. A model equation with two empirically determined constants was chosen to be fit to the resultant data. Most of the model curves matched the data in the high energies and in the first leg very well, but it was found that a "second-order" version of the model equation with an extra term in the denominator was better for matching the data from the low energies, especially in the second leg. One constant in the equation was shown to have a beam energy dependency, possibly exponential,

while the other was independent. Both were fairly independent of the geometry, but both also showed remote signs of a linear, geometric dependency, especially in the lower half of the energy groups. Most of the energy curves remained within the upper and lower bounds of the universal transmission curve, although there was some slight intersecting at the upper bound at long distances. Further research is needed to fit a curve to the energy dependency of the first constant as well as corroborate the possible geometric dependencies. It is recommended that data fitting be continued with the second-order equation, including matching it to some high-energy data.

Particle Identification in BigBite Spectrometer for G_{En} Experiment. *KYLE DAMBORSKY (Tulane University, New Orleans, LA 70118) BOGDAN WOJTSEKHOWSKI (Thomas Jefferson National Accelerator Facility, Newport News, VA 23606).* Electron/Pion identification is one of the critical tasks of the detector system in the upcoming GEn experiment at Thomas Jefferson National Accelerator Facility (JLab). Due to the high-energy nature of the electron beam and its collision with a target, multiple pions are produced. These pions produce an excessive counting rate and disrupt the detection of similarly charged electrons whose momenta are to be measured. To reject the pion counts, a lead glass calorimeter is used in the BigBite spectrometer to explore the longitudinal profile of the electromagnetic shower created by the particles. The calorimeter consists of a preshower detector array and a total absorption array, both comprised of lead glass counters. From their distinct shower profiles, pion and electron events can be discerned and an online rejection factor of up to 50 could be achieved, thereby creating a clean trigger apparatus for the G_{En} experiment. Each of these counters passed an extensive examination using cosmic rays, as well as hermicity tests before being added to the BigBite spectrometer, yielding 53 usable detectors. These detectors will be installed in the preshower array of BigBite. Also, a Monte Carlo simulation of the probability of a particle interacting with the lead glass detector was conducted. The average dark current of the usable detectors was -2 nA, while the average voltage required for a 5 mV output signal was found to be -1.5 kV. These results will be used as a starting point for a precise calibration of the BigBite spectrometer in Hall A. The results from the initial stage of a Monte Carlo simulation, eventually meant to model the electromagentic shower inside of a lead glass block, showed that 95.5% of all incident events interact with the preshower detector, 100% of all incident events interact with the total absorption detector, and 100% interact with the entire shower detector. The 100% is only within the tolerance of the written program, which is accurate to two decimal places. This data gives a good estimate as to the expected efficiency of the shower detector.

Ion Beamstop Design for a High Precision Mass Measurement System. *DAVID DANAHER (Monmouth College, Monmouth, IL 61462) GUY SAVARD (Argonne National Laboratory, Argonne, IL 60439).* The precise mass measurement of ions is the main objective of the Canadian Penning Trap (CPT) collaboration at Argonne National Laboratory. The mass measurements require a beam from the Argonne Tandem Linear Accelerator System (ATLAS) to fuse with a target to create the desired reaction products, which diverge due to alpha decay and are refocused for later measurement. Depending on the components of the reaction, some reactions have particles with much greater divergence angles than others. Some measurements are limited by ions displaced at angles greater than what are able to be collected by the current system. A new beamline is being added to collect products with greater divergence angles (±9°). Much of the beam, however, passes through the target without interaction, and will overwhelm the data of the reaction products if left to continue through the system. The method for stopping the beam in the current system is not applicable to the new beam line, so a new solution is required. We developed a system that allows ±2.5° to ±4.5° of beam to be blocked while still allowing most of the desired reaction products to continue through the system. The new beam stop will be built and placed in the new line which is still under construction. With the new beamline in place at the ATLAS facility, the CPT collaboration will no longer be limited to reactions which produce the desired nuclides emerging with low divergence angles. The effect of the new beam line, in conjunction with the beam stop, will be to permit more precise measurements in some cases and make other measurements possible in cases that were not possible before.

Single Gas Electron Multiplier (GEM) Based Gas X-Ray Detector and Ionization Chamber. *JEOFFRI DAVIS (Southern University and A&M College, Baton Rouge, LA 70811) PETER SIDDONS (Brookhaven National Laboratory, Upton, NY 11973).* The signal from an ionization chamber can be improved through the use of an electron multiplication device such as a gas electron multiplier (GEM). This paper will show the results from a one-inch diameter, single GEM based ionization chamber that was designed, built, and tested at the National Synchrotron Light Source (NSLS) at Brookhaven National Laboratory. The chamber was run with an Argon Carbon Dioxide ($ArCO_2$ 90/10) gas mixture at atmospheric pressure and achieved a gain of 130 at a 100 kV/cm electric field across the GEM. In the future, the detector will be further used to characterize samples using Extended X-ray Absorption Fine Structure (EXAFS) and X-ray absorption near edge structure (XANES).

Designing a Current Source for Toroid Integrated Intensity System Calibration. *MELANIE DAY (Rochester Institute of Technology, Rochester, NY 14623) M.A IBRAHIM (Fermi National Accelerator Laboratory, Batavia, IL 60510).* At Fermilab, the toroid integrated intensity system is used to measure beam intensity. This measurement is especially important when lowest possible error is critical, as in the MINIBooNE neutrino oscillation experiment. In order to reduce the error in toroid measurement, a calibration module was commissioned by the MINIBooNE collaborators through Columbia University. However, because of certain dependencies, it was necessary to design a current source to replace the existing pulse generating circuitry of the module. Several current source designs were examined, with special consideration given to the specific needs of the toroid integrated intensity system. Models done in WinSpice simulated the current output for each design. The simulation was then used to analyze the difference between an ideal source and the actual output of each model due to its dependence on change in the terminating resistance of the circuit. In simulation, the final design gave an optimal error margin of approximately +/-1mA for every .1ohm change in terminating resistance, or a +/-.5mV change in the voltage pulse input to the toroid integrator. Simulation suggests this value could be modified by changing the terminating resistor from the current 50ohm load to a higher value resistance. Extensive testing of the model has not yet been done. Future alterations may be necessary to deal with effects that cannot be seen in the simulation. Also, other circuitry in the pulse generator will need to be altered in the future to deal with the new requirements of the current source.

Optimizing the Handling of Large Datasets. *CHRISTOPHER DORAN (DePauw University, Greencastle, IN 46135) FRANK CHLEBANA (Fermi National Accelerator Laboratory, Batavia IL 60510).* Collision Detector at Fermilab (CDF) Run II has recently surpassed 1 fb-1 of integrated luminosity and it is hoped that it will reach at least 6 fb-1 before the Tevatron is decommissioned. The number of events is proportional to the integrated luminosity, and if the goal of 6 fb-1 is reached, the result will be close to 500 TB of raw data. The large amount of data presents a challenge for offline data analysis. The current inclusive-jet dataset, sampled from 500 pb-1 of raw data, requires more than 5 hours to analyze. Steps must be taken to increase the speed and convenience of analyses as the data sample continues to grow. By condensing the data such that it contains only the information necessary for the particular analysis, and/or by running the analysis in parallel on multiple machines, one can increase the speed of analysis significantly. Condensing also makes it easier to store and access the data locally, increasing data access speed and convenience. Results show that the user is able to increase speed by several factors. These strategies will make the growing data sample more manageable, and they may be applied to any analysis of large datasets.

Prototype Data Acquisition System for the Mixed Apparatus Radio-wave Investigation of Atmospheric Cosmic-rays of High Ionization (MARIACHI) Experiment. *EBONY EGGLESTON (Florida A&M University, Tallahassee, FL 32307) HELIO TAKAI (Brookhaven National Laboratory, Upton, NY 11973).* Cosmic rays are high energy charged particles, originating in outer space, that travel at nearly the speed of light and strike the Earth from all directions. These primary cosmic rays contain mainly high energy protons, photons (gamma rays), and atomic nuclei. The MARIACHI experiment seeks to detect cosmic rays of energy 10E18eV or greater via detection of FM and TV band radio wave reflection from cosmic ray initiated ionization events in the stratosphere. The muse for MARIACHI came from a conventional method that radio astronomers detected meteorites and micrometeorites that entered into the Earth's atmosphere. Through the use of the data acquisition and instrument control software LabView, radio reflection waveforms will be acquired and analyzed. LabView is a computer software program which allows graphical development of an instrumental control, signal acquisition, measurement analysis, and data presentation which will enable the design and implementation of a Virtual Instrument (VI) for the analysis of the radio waveforms. The FM radio wave is conveyed from an antenna and incorporated into the LabView program, obtaining

the audio waveform. Frequency discrimination analysis is then performed on the acquired waveform in order to determine whether the detected signal originates from stratospheric cosmic ray induced ionization. This will allow for the detection of signals only due to cosmic ray events. Due to the fact that the project is not yet complete, there are no results indicated. However, in conclusion, the objective of the LabView software is to be able to obtain those signals which are reflected from cosmic ray ionization events through the use of a PC controlled radio receiver and soundcard.

Development of Web Software for Nuclear Decay Data in the MIRD Format. *MANUEL EMERIC (University of Puerto Rico, Rio Piedras, PR 00923) ALEJANDRO SONZOGNI (Brookhaven National Laboratory, Upton, NY 11973).* The Medical Internal Radiation Dose (MIRD) is the dose given to patient's organs during radiation therapy to destroy cancer cells. The organ doses used for a patient are not measured in vivo. The commonly used methods for deriving the organ doses are measurements done in a phantom, an artificial object representing a patient, or computer calculations. We have developed an easy to use web-based MIRD software product for the radiation dose data, which makes the nuclear decay data accessible for a larger group of users. Tables of nuclear and atomic radiations from nuclear decay and decay scheme drawings were produced in the MIRD format from the Evaluated Nuclear Structure Data File (ENSDF). A user interface was written in Hypertext Markup Language (HTML) code scripted with Java as a JSP file (Java Server Pages). The front page requests the user for the desired nuclide. The HTML form code and the JSP script send the nuclide name to the Java code classes that look for the information into the ENSDF database using Structured Query Language (SQL) commands. An image is created on the fly by Java classes showing the decay scheme for each decay mode of the desired nuclide as a ".png" (Portable Network Graphic) image shown with the results. The data results given by the MIRD interface consist of decay modes and their probabilities as well as radiation properties (type, energy, intensity and dose). The image includes energy for each level of the parent and daughter nucleus, level parity, decay mode label and ground state to ground state energy (Q-value). This work is part of the National Nuclear Data Center web page at Brookhaven National Laboratory available for the general public at www.nndc.bnl.gov .

Quality Control of Modules for the ATLAS Pixel Detector. *ERIC FENG (University of California Berkeley, Berkeley, CA 94720) MAURICE GARCIA-SCIVERES (Lawrence Berkeley National Laboratory, Berkeley, CA 94720).* ATLAS is an international collaboration to build the next-generation high energy particle detector for the Large Hadron Collider at CERN. The building block of the ATLAS pixel detector is the "module", which consists of a finely pixilated silicon sensor that is indium bump-bonded to 16 front-end (FE-I3) readout chips. Each of the sensor pixels in a module is read out in parallel by an independent FE-I3 electronics channel via an indium bump bond from each sensor pixel to an FE-I3 input. Quality control of these high-precision FE-I3 chips is vital to ensure the high detector efficiency required to distinguish individual tracks among the hundreds produced every 25ns by the LHC collisions. The purpose of this study is to investigate how "dark" pixels on a module (pixels unresponsive to external charge) may be caused by defective indium bumps on the module's constituent front-end readout chips. First, a sample of bump defects discovered during visual inspection was electrically tested to see if their associated FE-I3 pixels exhibited faulty digital operation, atypically low or high threshold and noise, and too few/too many hits from the source scan. Second, an independent sample of pixels that exhibited electrical abnormalities was traced back to the visual inspection to see if their associated indium bumps had been observed to be defective. By performing cross checks of bump defects with electrical failures of modules, a rubric was constructed by which quantitative measurements of a bump defect such as bump size, shape, and spacing can be used to predict a pixel's efficiency. This rubric will increase both the efficiency and accuracy of quality control in the future.

A Study of Photomultiplier Tubes Response to Scintillators Using Cosmic Rays, Ruthenium 106, and a Neutron Source. *CHRISTINA FENNIMORE (Binghamton University, Binghamton, NY 13902) MICHAEL SIVERTZ (Brookhaven National Laboratory, Upton, NY 11973).* The KOPIO experiment is looking for a rare reaction to explain why matter and anti-matter are not equally distributed throughout the universe. KOPIO uses the AGS proton accelerator to create an intense beam of kaons to study rare decays. One of the rare decays is when a kaon decays into a neutral pion, a neutrino, and an antineutrino. This decay will help us understand CP (charge parity) symmetry violation. CP violation was discovered in 1960, when two different CP eigenstates decayed into the same products. CP violation can help scientists to understand how the universe began, and they are working towards studying CP violation in the KOPIO experiment. Prototype designs for KOPIO Charge Particle Veto detector were tested. The response to neutrons is a concern because the neutron flux is a thousand times greater than the kaon flux, so the response to neutrons was measured with a prototype CPV and a neutron source. Scintillator responses to a thermal neutron source were tested to understand the response of the KOPIO detectors. Scintillator responses were measured using photomultiplier tubes. The photomultiplier tube was calibrated by studying the response from a single photoelectron to see how many photoelectrons were produced. The photomultiplier tube has high amplification and low noise. The responses from cosmic rays and the radioactive source, ruthenium-106, were tested. By moving a 4x5 inch trigger scintillator across a 24.5x8 inch test scintillator the uniformity of response could be determined. The center and the edge of the test scintillator were tested to check the uniformity of the test scintillator. The photomultiplier tubes were attached to pieces of scintillator and the response to cosmic rays, ruthenium 106, and a neutron source were tested. It was found that the photomultiplier tubes were exceptionally responsive towards the neutron response. When further tests are done, the trigger threshold will need to be set at a much higher level. Future studies will establish the most receptive level for the threshold so that the kaons can be observed and the neutrons cannot.

Prototyping a "Pure" Cosine-θ Superconducting Dipole Magnet. *NATHAN FINNEY (Santa Rosa Junior College, Santa Rosa, CA 95401) MICHAEL FUERY (Laney College, Oakland, CA 94607) STEVE A. GOURLAY (Lawrence Berkeley National Laboratory, Berkeley, CA 94720).* Using superposition of tilted elliptical helices, a "pure" cosine-theta dipole magnet has been designed, fabricated and tested using superconducting niobium-titanium (NbTi) wire. The geometry of the NbTi wire was held in place by careful placement of stainless steel pins in a hollow aluminum bore. The entire fabrication and testing process took 3 ½ weeks, due to the simplicity of the design. The theoretical magnetic field at a current of 267 A was calculated to be 1.07 T compared to an experimental value of 1.02 T. The tilted helical geometry yields a pure dipole, with a distribution of magnetic field strength showing uniformity along the section of highest current density. This design allows for one continuous wire to be used during the winding, making it a practical design for the rapid production of dipole magnets used in accelerators. "Pure" COS-θ dipole magnets can be improved by using superconducting materials with higher critical temperatures and external magnetic field tolerances allowing them to be used as insert coils.

Dislocation Generation Under Controlled Thermal Stress. *DOUGLAS GAGNON (Cornell University, Ithaca, NY 14850) BHUSHAN SOPORI (National Renewable Energy Laboratory, Golden, CO 89401).* The objective of this project was to produce dislocations of desired density and with a nearly-uniform distribution in silicon wafers. The dislocations were generated by applying thermal stress to silicon wafers via an optical processing furnace. Controlled stresses were produced by different spatial distributions of temperature. The temperature of the wafers was measured using Chromel/Alumel thermocouples attached to the underside. The temperature of each thermocouple, as well as its spatial location on the wafer, was recorded by a computed program, which graphed the temperature recorded over time. The samples were then defect etched and their dislocations maps were generated by PVSCAN, an instrument that rapidly produces maps of surface defects.

Transport and Imaging of Fluorescent Dust in a DC Glow Discharge Plasma. *WILL GANNETT (Harvey Mudd College, Claremont, CA 91711) ANDREW POST-ZWICKER (Princeton Plasma Physics Laboratory, Princeton, NJ 08543).* The study of dusty plasmas has wide applications, from astrophysics to chip fabrication. A fluorescent dust cloud illuminated by a longwave mercury ultraviolet (UV) lamp rather than the traditional laser has been produced in a DC glow discharge plasma. The luminescence of the dust particles in the wide UV beam allows imaging anywhere in the chamber, making it possible to observe the initial formation of a cloud as well as dust phenomena not in anticipated locations. The luminescence of the dust particles allows them to be recorded by a charge coupled device (CCD) camera at 30 frames per second, which can be analyzed to obtain a two-dimensional velocity profile for the cloud. This velocimetry is far simpler than contemporary laser methods yet provides temporal and spatial resolution sufficient to analyze a variety of dust phenomena, including dust acoustic waves. Using this ability of examining a large spatial range, we can analyze different modes of transport within and between the dust clouds that form in our chamber. A comparison of dust types and illumination sources will be presented, as well as observations of dust cloud formation and transport.

An Automated Method for Characterizing the Relaxedness of Galaxy Clusters. *MATTHEW GEORGE (Harvard University, Cambridge, MA 02139) STEVE ALLEN / GREG MADEJSKI (Stanford Linear Accelerator Center, Stanford, CA 94025).* Relaxed galaxy clusters are useful tools for probing cosmological parameters like the gas mass fraction of the universe. Selecting relaxed clusters for this purpose can be a time-consuming and subjective task, so we present methods to automate parts of the process. We fit elliptical isophotes to a diverse sample of Chandra cluster data and summarize other methods for quantifying relaxedness which will be included in future work. Analysis of the results of tests from isophote fitting, combined with numerical simulations of cluster structures and comparison to previous classifications will allow us to formulate criteria for selection of relaxed clusters. We find that they tend to have core radii less than approximately 60 kpc from King model fits, shifts in isophote centroids of less than 25 kpc over a range in semi-major axes of several hundred kpc, and significantly greater surface brightness profile gradients within 30 kpc of their cores than unrelaxed clusters. These criteria will help with future cosmological work as larger amounts of cluster data are taken and need objective classification.

Deposition and Characterization of Colossal Magnetoresistive La0.8Sr0.2MnO3 Films on a Single Crystal-like CeO_2 Substrate Architecture. *DAVID GETTMAN (California State University Fresno, Fresno, CA 93740) AMIT GOYAL (Oak Ridge National Laboratory, Oak Ridge, TN 37831).* $La_xSr_{1-x}MnO_3$ (LSMO) is one member of a class of metallic magnetic perovskites that show a large change in resistivity in an applied magnetic field, which is referred to as the colossal magnetoresistance (CMR) effect. This property makes the materials attractive from a technological viewpoint for use in hard disk drive read/write heads, magnetic sensors, and magnetic random access memories (MRAM). Some of the major obstacles to the commercial use of these materials are high deposition temperatures and the need to use relatively costly single crystal substrates for epitaxial growth. One inexpensive substrate used for the deposition of epitaxial $YBa_2Cu_3O_7$ superconducting perovskite films are single crystal-like CeO_2 substrate architectures. Films of LSMO with 20% Sr doping were deposited by radio frequency magnetron sputtering under various deposition conditions on a substrate architecture based on these CeO_2 substrates. The films were characterized structurally and morphologically by X-ray diffraction, optical microscopy, and step profilometry. It was discovered that all the deposited films were under-oxygenated using a wide variety of deposition conditions and therefore were not suitable for magnetoresistance measurements. Some discussion of possible reasons for this under-oxygenation is included. Future work will look at overcoming the oxygenation problem, measuring the magnetotransport properties of the LSMO CMR thin films, and depositing other types of half-filled ferromagnetic metals such as Fe_3O_4 which also show CMR effects.

Automated Analysis of SNS Linac Beam Position Monitor Data. *AMELIE GILLMAN (Tennessee State University, Nashville, TN 37209) THEODORE WILLIAMS (Oak Ridge National Laboratory, Oak Ridge, TN 37831).* The Spallation Neutron Source's (SNS) Linear Accelerator (Linac) accelerates pulsed beams of H^- ions for use in neutron production via the spallation process. The accelerator consists of an ion source for H- production, a room temperature normal-conductivity Linac for acceleration of H^- particles to approximately 200 MeV, and a superconducting niobium Linac with a nominal operating temperature of 2 K for acceleration of the beam to 1 GeV (90% the speed of light). In order to reduce beam loss and to improve beam stability, the trajectory of the intense H^- beam must be strictly monitored throughout the Linac. In an effort to characterize and maintain alignment of the beam pulses, beam position monitors (BPMs) located throughout the Linac provide measurements of horizontal and vertical beam centroid displacement, beam phase, and beam intensity. An adaptable, interactive computer program was designed and implemented in MatLab for the purpose of automating the analysis of the data acquired by the BPMs. Program functionality includes generation of frequency distribution histograms and calculation of statistical information including the mean, standard deviation, and root mean square values for individual and multiple BPMs. Data filtering is applied per user-specified options including standard deviation and data variability constraints, as well as cross-parametric correlation of BPM measurement values. The application supports Model Independent Analysis via singular value decomposition (SVD) techniques, which allows for discrimination between temporally and spatially correlated oscillatory modes in the data. These SVD methods provide powerful technique for estimating the BPM resolutions, as well as for identifying coherent motion inherent in the beam. The results of the analysis will be used to characterize and improve the BPM system performance, as well as to aid in identifying the sources of coherent beam motion.

Improving the Raster Scanning Methods Used With X-ray Fluorescence to See the Ancient Greek Copy of Archimedes Work. *ISABELLA GRIFFIN (Norfolk State University, Norfolk, VA 23504) UWE BERGMANN (Stanford Linear Accelerator Center, Stanford, CA 94025).* X-ray fluorescence is being used to detect the ancient Greek copy of Archimedes work. The copy of Archimedes text was erased with a weak acid and written over to make a prayer book in the Middle Ages. The ancient parchment, made of goat skin, has on it some of Archimedes most valuable writings. The ink in the text contains iron which will fluoresce under x-ray radiation. My research project deals with the scanning and imaging process. The palimpsest is put in a stage that moves in a raster format. As the beam hits the parchment, a germanium detector detects the iron atoms and discriminates against other elements. Since the computer scans in both forwards and backwards directions, it is imperative that each row of data lines up exactly on top of the next row. There are several parameters to consider when scanning the parchment. These parameters include: speed, count time, shutter time, x-number of points, and acceleration. Formulas were made to relate these parameters together. During the actual beam time of this project, the scanning was very slow going; it took 30 hours to scan ½ of a page. Using the formulas, the scientists doubled distance and speed to scan the parchment faster; however, the grey scaled data was not lined up properly causing the images to look blurred. My project was is to find out why doubling the parameters caused blurred images, and to fix the problem if it is fixable.

Progress Toward a Liquid Lithium Target and Electron Stripper for the Rare Isotope Accelerator. *IAN GUERASSIO (Colorado School of Mines, Golden, CO 80401) JERRY NOLEN (Argonne National Laboratory, Argonne, IL 60439).* The proposed Rare Isotope Accelerator (RIA) facility will utilize new fragmentation targets and electron strippers that can survive the expected 200 kW of beam power. Liquid lithium offers a unique solution to the problem of dissipating the beam energy by acting as both target and coolant. A flowing, liquid lithium target with Beryllium windows could be used to create radioactive beams in the mass range of oxygen to calcium. A windowless target at the Alkali Metal Experiment (ALEX) facility at Argonne National Laboratory (ANL) already demonstrates that a liquid lithium target can maintain usability in a 200 kW beam. Current experiments are attempting to create a flowing liquid lithium thin film for use as a stripper material.

Investigating the Infrared Properties of Candidate Blazars. *JESSICA HALL (University of Southern California, Los Angeles, CA 90007) SETH DIGEL, GREG MADEJSKI (Stanford Linear Accelerator Center, Stanford, CA 94025).* Blazars are active galaxies with super-massive black holes, containing jets that accelerate plasma material and produce radiation. They are unique among other active galaxies for properties such as rapid variability and the lack of emission lines. The double-peaked spectral energy distribution (SED) found for most blazar objects suggests that synchrotron radiation and Compton scattering occurs in the jets. This study is an investigation of the infrared (IR) spectra of a selected population of blazar candidates, focusing on the IR properties of objects within the three types of blazars currently recognized by their spectral characteristics at other wavelengths. Using blazar candidates found in a recent study of the northern sky (Sowards-Emmerd et al., The Astrophysical Journal, 2005), IRAS data for 12, 25, 60, and 100 μm, as well as any available data from 2MASS and EGRET, were located. The synchrotron peak of the SED of each object was expected to occur anywhere in the infrared (IR) to soft X-ray range. However, peaks were generally found to lie in the IR range, suggesting potential selection biases. An analysis of selection techniques reveals that the figure of merit used in the original survey is engineered to select objects with a Compton scattering peak luminosity occurring in the GeV range, the energy band most easily detected by the upcoming GLAST mission. Therefore, this figure of merit selection process should be used to compile a list of blazar candidates for further study in anticipation of the launch of the satellite.

EXAFS Measurements of Doped Cadmium Sulfide Methods of Analysis. *VIRGINIA HAYES (Chicago State University, Chicago, IL 60636) JUSTIN AKUJIEZE (Argonne National Laboratory, Argonne, IL 60439).* Cadmium sulfide is a photoconductor, radiation detector, and serves as a photovoltaic cell. It exits in two structures wurtzite and zinc blend type cubic. The wurtzite structure is an ABC structure, which makes it hexagonal. The zinc blend cubic structure is the ABA structure and is also the one being studied. Manganese sulfide also shares the same structure as cadmium sulfide. The focus of

this project is to measure the resulting chemical environment of the compound cadmium sulfide when manganese is doped for cadmium in the CdS matrix. In order to do this we carried out fluorescent EXAFS Spectroscopy because of a very high absorption and low transmission of radiation. EXAFS Spectroscopy is a way to determine the local chemical environment of an element (except the lightest) in a structure. The nano materials were of different sizes (18, 23, and 30 Å) and have varying amount of manganese content There were two variables in this study, (thickness of sample, and Mn content) and samples were run ten times each. Further analysis using the Artemis software is required in order to obtain more information from these data.

A New Outlook for Cosmology. *PAUL HIGGINS (Contra Costa College, San Pablo, CA 94806) MICHAEL BARNETT (Lawrence Berkeley National Laboratory, Berkeley, CA 94720).* The Universe Adventure is a website designed to teach high school students and the general public about the fundamentals of cosmology, the study of the dynamics and evolution of the universe. The participant is taken through the history of cosmological models, such as the Geocentric (Greek) and Heliocentric (European Renaissance) models. The Big Bang (present day) model is then discussed, including supporting evidence. The rest of the website is devoted to explaining how the universe has changed from its initial hot, dense state into the current state we now observe and map with our telescopes. What distinguishes The Universe Adventure, is the way in which its physics concepts are presented. There is a liberal use of analogies, metaphors, animation, diagrams, illustrations, photographs, and humor in order to ensure interest and comprehension for high school students, teachers and the general public. The fundamental idea is to break away from academic methods of teaching physics. This website could act as a supplement to course work, or merely as a resource for curious minds. This summer was spent revising existing content, and expanding on that content by creating more in depth explanations, graphics and animation.

Sputter Yield Measurements and Analysis of EUV Lithography Collector Mirrors Under Low Energy Particle Bombardment. *EDWARD HINSON (Middlebury College, Middlebury, VT 05753) J.P. ALLAIN (Argonne National Laboratory, Argonne, IL 60439).* In extreme ultraviolet lithography (EUVL) environments, both laser produced plasma (LPP) and gas discharge produced plasma (GDPP) configurations face serious problems regarding component lifetime and performance under particle bombardment, in particular collector mirrors. For both configurations, debris, fast ions, fast neutrals, and condensable EUV radiator fuels (Li, Sn) can affect collector mirrors. In addition, collector mirrors are exposed to impurities (H, C, O, N), off-band radiation (depositing heat) and highly charged ions leading to their degradation and consequently limiting 13.5 nm light reflection intensity. In an effort to address these issues, the IMPACT (Interaction of Materials with charged Particles and Components Testing) experiment at Argonne National Lab involves in part the calculation of sputter yields on precision optical mirror surfaces. For this project, this entails: a numeric calculation of the QCM collected fraction (O) for various conditions in which yield measurements were taken, an analysis of temperature-dependent effects in QCM response to particle deposition, and collection of sputtering data for various impinging singly-charged inert gases (e.g., Xe, Ar) and radiator fuels (Sn, Li), and calculation from this data resultant sputter yields on glancing incidence mirrors (Ru, Pd, Si/Mo) at bombardment energies in the 100–1,000 eV range at room temperature.

Development of an Auto-convergent Free-Boundary Axisymmetric Equilibrium Solver. *JONATHAN HUANG (Dartmouth College, Hanover, NH 03755) JON MENARD (Princeton Plasma Physics Laboratory, Princeton, NJ 08543).* Large scale internal magnetohydrodynamic (MHD) instabilities have been observed to degrade thermal and fast ion confinement in the core of high-beta NSTX plasmas. Saturated internal kink modes have been observed to flatten the toroidal rotation profile and cause significant and persistent fast ion loss. Both effects likely result from a significant alteration of the magnetic field topology; specifically, the formation of large magnetic islands. Simple models of the perturbed helical flux of these islands have been used successfully to simulate the perturbed soft X-ray emission; however, detailed models of the island magnetic field and comparisons to measurement have not yet been obtained. To simulate the magnetic field from assumed helical and poloidal flux perturbations, a highly modular general toroidal coordinate transformation package has been developed using the IDL programming language. The package includes routines to easily transform between different coordinate systems and to perform all necessary vector operations. Overall, a contravariant/covariant representation of the vector fields is found to be most convenient for performing vector operations in general geometry. Using this computational framework, all components of the perturbed magnetic field can be computed. The code has been benchmarked in 2D against existing equilibrium data and in 3D using simple models of the perturbed helical flux. Future work will compare model predictions of the mode magnetic field to high-time-resolutions Motional Stark Effect data. Further, multiple helicity calculations can now be performed to study non-linear mode coupling. Specifically, it may be possible to test whether instabilities of different poloidal mode number prefer a toroidal phase relationship that minimizes the total magnetic energy of the coupled state.

Optimization of Electronics for "Clover" Germanium Detectors. *CHAD HUIBREGTSE (Beloit College, Beloit, WI 53511) C.J. LISTER (Argonne National Laboratory, Argonne, IL 60439).* Gamma ray detectors are a necessary tool for nuclear physics, and by examining gamma radiation we may more clearly identify the inner workings of the nucleus and further the boundaries of science. Currently the best gamma ray detectors operate by using germanium semiconducting crystals. Argonne National Laboratory has recently acquired three semiconducting Ge "Clover" detectors that each contain four germanium crystals. In order to get the best use from these detectors it is necessary to run several diagnostic tests on them to find their ideal operating settings. The Clover detectors were calibrated for both energy resolution and timing coincidence to prepare them for use in future experiments.

The Theoretical Basis of an EXAFS Measurement of Mn Doped CdS. *CHINEDUM IBEABUCHI (Chicago State University, Chicago, IL 60628) JUSTIN AKUJIEZE (Argonne National Laboratory, Argonne, IL 60439).* Cadmium Sulfide is valuable in its use in sensors, optoelectronic devices, and solar cells. Cadmium sulfide was doped with manganese to observe if theses properties would remain. Due to the smaller size of manganese, it was expected that the structure of cadmium sulfide would be distorted when doped with manganese. This could possibly change the structure from cubic to wurtzite. It was also expected that the structure of cadmium sulfide would change the energy level excitation occurrence. To probe the structure of cadmium sulfide extended x-ray absorption of fine structure (EXAFS), spectroscopy was performed. This paper presents the theoretical concepts behind various EXAFS fitting software. The absorption edges of our samples were typically around 6.5 KeV indicating the presence of Mn. Further analysis using enhanced software will be carried out in due course. When such analysis is concluded, the oxidation state of Mn and bond lengths of immediate neighbors will be obtained.

Prototype Data Acquisition System for the Mixed Apparatus Radio-wave Investigation of Atmospheric Cosmic-rays of High Ionization (MARIACHI) Experiment. *SHANDA JOHNSON (Florida A&M University, Tallahassee, FL 32307) HELIO TAKAI (Brookhaven National Laboratory, Upton, NY 11973).* Cosmic rays are high energy charged particles, originating in outer space, that travel at nearly the speed of light and strike the Earth from all directions. These primary cosmic rays contain mainly high energy protons, photons (gamma rays), and atomic nuclei. The MARIACHI experiment seeks to detect cosmic rays of energy 10E18 eV or greater via detection of FM and TV band radio wave reflection from cosmic ray initiated ionization events in the stratosphere. The muse for MARIACHI came from a conventional method that radio astronomers detected meteorites and micrometeorites that entered into the Earth's atmosphere. Through the use of the data acquisition and instrument control software LabView, radio reflection waveforms will be acquired and analyzed. LabView is a computer software program which allows graphical development of an instrumental control, signal acquisition, measurement analysis, and data presentation which will enable the design and implementation of a Virtual Instrument (VI) for the analysis of the radio waveforms. The FM radio wave is conveyed from an antenna and incorporated into the LabView program, obtaining the audio waveform. Frequency discrimination analysis is then performed on the acquired waveform in order to determine whether the detected signal originates from stratospheric cosmic ray induced ionization. This will allow for the detection of signals only due to cosmic ray events. Due to the fact that the project is not yet complete, there are no results indicated. However, in conclusion, the objective of the LabView software is to be able to obtain those signals which are reflected from cosmic ray ionization events through the use of a PC controlled radio receiver and soundcard.

Understanding Helium Burning in Stellar Evolution Through Nuclear Physics. *DAVID KAHL (Beloit College, Beloit, WI 53511) ERNST REHM (Argonne National Laboratory, Argonne, IL 60439).* The project undertaken by the experimenter is located at ATLAS (Argonne Tandem-Linear-Accelerator-System) and is focused on preparation and

calibration of an ion chamber for a future experiment. As a summer intern, I ran the day-to-day documentation, data collection and on-line data analysis of an ion chamber designed to study the astrophysical important reaction $^{12}C(\alpha, \gamma)^{16}O$. We study this reaction by looking at the β-delayed α decay of 16N. This essay will begin by describing the importance of the $^{12}C(\alpha, \gamma)^{16}O$ reaction to stellar evolution, as well as how we plan to study the reaction in the coming months. From there, our experimental technique will lead the reader to an understanding of our particular setup, as well as the reasoning behind our chosen configuration. It will then follow logically what components of our detection apparatus require thorough testing, the results of that testing, and specifically how the author has contributed to this ongoing research.

Scintillator Response to Neutron Radiation. *RYAN KAUFMAN (SUNY Farmingdale, Farmingdale, NY 11735-1021) L. LITTENBERG (Brookhaven National Laboratory, Upton, NY 11973)*. The KOPIO experiment (simply a pronunciation of the equation upon which it is based) is part of a scientific effort to study CP violation in the decay of K°_L particles into a π° and two neutrinos ($K^\circ_L \rightarrow \pi^\circ \nu\pi\nu$). This particular decay mode of K°_L is believed to exhibit direct CP violation which will be measured and studied. It must be distinguished from other, much more copious decays by the absence of extra charged particles in its final and intermediate states. When these charged particles pass through a scintillating plastic the subsequent light is measured and analyzed. Additionally, neutrons are going to be produced on the order of about two thousand neutrons to one K°_L. Scintillators only give a signal when penetrated by charged particles, and the neutron, as we know, has no charge. It can, however, give a signal via a recoil proton or by neutron capture in the hydrocarbon scintillator. We used an Am/Be neutron source emitting neutrons in the thermal and energetic range. We tested a new scintillator, BC-408, wrapped in Tyvec and light sealed with photographic tape, as well as a complete shashlyk array with nine modules. The shashlyk array had eight modules surrounding one center module, the test module each with its own Thorn EMI 9903b PMT on one end. The PMT's were read out with ADC's (analog to digital converters) in a CAMAC (computer automated monitoring and controlling) crate. This should allow us to see a signal from the neutrons passing through the module directly, and veto signals coming in at angles to the test module, most likely cosmic ray muons. The thermal neutrons give a very low count rate. There is, though, a very high count rate due to the energetic neutrons. If most of the signal is due to energetic neutrons, as this should indicate, there should be more of a signal in the thermal neutron spectrum due to energetic neutrons penetrating the shielding. Simulations are going to be run to determine the source of this discrepancy. This experiment will be very useful to any experiment in a neutron rich environment in which scintillators will be used to make measurements.

Turn-by-Turn and Bunch-by-Bunch Transverse Profiles of a Single Bunch in a Full Ring. *RICHARD KRAUS (University of Nevada, Reno, Reno, NV 89557) ALAN S. FISHER (Stanford Linear Accelerator Center, Stanford, CA 94025)*. The apparatus described in this paper can image the evolution of the transverse profile of a single bunch, isolated from a full PEP-II ring of 1500 bunches. Using this apparatus there are two methods of single bunch imaging; bunch-by-bunch beam profiling can image every bunch in the ring a single bunch at a time with the images of sequential bunches being in order, allowing one to see variations in beam size along a train. Turn-by-turn beam profiling images a single bunch on each successive turn it makes around the ring. This method will be useful in determining the effect that an injected bunch has on a stable bunch as the oscillations of the injected bunch damp out. Turn-by-turn imaging of the synchrotron light uses a system of lenses and mirrors to image many turns of both the major and minor axis of a single bunch across the photocathode of a gateable camera. The bunch-by-bunch method is simpler: because of a focusing mirror used in porting the light from the ring, the synchrotron light from the orbiting electrons becomes an image at a certain distance from the mirror; and since the camera does not use a lens, the photocathode is set exactly at this image distance. Bunch-by-bunch profiling has shown that in the Low Energy Ring (LER) horizontal bunch size decreases along a train. Turn-by-turn profiling has been able to image 100 turns of a single bunch on one exposure of the camera. The turn-by-turn setup has also been able to image 50 turns of the minor axis showing part of the damping process of an oscillating injected charge during a LER fill. The goal is to image the damping of oscillations of injected charge for 100 turns of both the major and minor axis throughout the damping process during trickle injection. With some changes to the apparatus this goal is within reach and will make turn-by-turn imaging a very useful tool in beam diagnostics.

Detecting Extreme Energy Cosmic Rays with RADAR. *ELLYNNE KUTSCHERA (University of Wisconsin, Stevens Point, Stevens Point, WI 54481) HELIO TAKAI (Brookhaven National Laboratory, Upton, NY 11973)*. Currently, cosmic ray showers are detected mainly through the use of scintillator arrays or related ground-based methods. An alternative means of detection may be possible, in particular for Extreme Energy Cosmic Rays. As cosmic ray showers move through the atmosphere, ionization is created. Depending on the energy of the primary cosmic ray particle, the angle of incidence of the shower, and the atmospheric depth of the shower, the ionization may even be dense enough to reflect incident radio waves. The density of the ionization at a given time and location, the position and shape of the ionization, electron lifetime as a function of attachment and recombination rates, and the geometry of radio reflection off the ionization must be understood in order to accurately predict what type of radio receivers are most appropriate for detection as well as where receivers should be located. Several sources of data are combined to describe a physical model of the EECR and radio reflection: simulated showers of EECR, data gathered on ionization lifetime, and geometric analysis of the shower ionization and ground reflection, or footprint. Calculations suggest that reflected radio signals of several microseconds should be receivable, available over areas of tens to hundreds of square kilometers. This information suggests particular types of receiving radio equipment and many possibilities for the placement of receiving antennas.

Background Characterization for Thermal Ion Release Experiments with Radium-224. *HELEN KWONG (Stanford University, Stanford, CA 94305) PETER ROWSON (Stanford Linear Accelerator Center, Stanford, CA 94025)*. The Enriched Xenon Observatory for neutrinoless double beta decay uses ^{136}Ba identification as a means for verifying the decay's occurrence in ^{136}Xe. A current challenge is the release of Ba ions from the Ba extraction probe, and one possible solution is to heat the probe to high temperatures to release the ions. The investigation of this method requires a characterization of the alpha decay background in our test apparatus, which uses a ^{228}Th source that produces ^{224}Ra daughters, the ionization energies of which are similar to those of Ba. For this purpose, we ran a background count with our apparatus maintained at a vacuum, and then three counts with the apparatus filled with Xe gas. We were able to match up our alpha spectrum in vacuum with the known decay scheme of ^{228}Th, while the spectrum in xenon gas had too many unresolved ambiguities for an accurate characterization. We also found that the alpha decays occurred at a near-zero rate both in vacuum and in xenon gas, which indicates that the rate was determined by ^{228}Th decays. With these background measurements, we can in the future make a more accurate measurement of the temperature dependency of the ratio of ions to neutral atoms released from the hot surface of the probe, which may lead to a successful method of Ba ion release.

Localized PEPII Storage Ring Optics Measurements. *JONATHAN LANDY (Caltech, Pasadena, CA 91126) YITON YAN (Stanford Linear Accelerator Center, Stanford, CA 94025)*. The current technique employed to determine the parameters which specify the betatron oscillation in the PEPII ring at SLAC is a global procedure in that the data from each BPM (Beam Position Monitor) is weighted equally. However for more accurate interaction point (IP) measurements, it would be beneficial to weight the data from the BPMs closest to the IP much more heavily. Researchers are thus considering the possibility of developing a technique to determine the oscillation parameters near the IP using as few BPMs as possible. In this paper, allowing BPM gains and cross coupling, we show analytically that given data from N BPMs there remain 6N + 2 degrees of freedom in the matrices $M_{A,A}$, $M_{B,A}$, ...,$M_{N,N-1}$ unspecified by the observable data alone. From this we demonstrate that data from at least 3 BPMs is required to completely specify the system when the transfer maps between BPMs are assumed known, and that 4 BPMs may be more suitable.

Relative Humidity in Limited Streamer Tubes for Stanford Linear Accelerator Center's BABAR Detector. *MARY LANG (Massachusetts Institute of Technology, Cambridge, MA 02139) MARK CONVERY & WOLFGANG MENGES (Stanford Linear Accelerator Center, Stanford, CA 94025)*. The BABAR Detector at the Stanford Linear Accelerator Center studies the decay of B mesons created in e+e- collisions. The outermost layer of the detector, used to detect muons and neutral hadrons created during this process, is being upgraded from Resistive Plate Chambers (RPCs) to Limited Streamer Tubes (LSTs). The standard-size LST tube consists of eight cells, where a silver-plated wire runs down the center of each. A large potential difference is placed between the wires and ground. Gas flows through a series of modules connected with tubing, typically four. LSTs must be carefully tested

before installation, as it will be extremely difficult to repair any damage once installed in the detector. In the testing process, the count rate in most modules showed was stable and consistent with cosmic ray rate over an approximately 500 V operating range between 5400 to 5900 V. The count in some modules; however, was shown to unexpectedly spike near the operation point. In general, the modules through which the gas first flows did not show this problem, but those further along the gas chain were much more likely to do so. The suggestion was that this spike was due to higher humidity in the modules furthest from the fresh, dry inflowing gas, and that the water molecules in more humid modules were adversely affecting the modules' performance. This project studied the effect of humidity in the modules, using a small capacitive humidity sensor (Honeywell). The sensor provided a humidity-dependent output voltage, as well as a temperature measurement from a thermistor. A full-size hygrometer (Panametrics) was used for testing and calibrating the Honeywell sensors. First the relative humidity of the air was measured. For the full calibration, a special gas-mixing setup was used, where relative humidity of the LST gas mixture could be varied from almost dry to almost fully saturated. With the sensor calibrated, a set of sensors was used to measure humidity vs. time in the LSTs. The sensors were placed in two sets of LST modules, one gas line flowing through each set. These modules were tested for count rate v. voltage while simultaneously measuring relative humidity in each module. One set produced expected readings, while the other showed the spike in count rate. The relative humidity in the two sets of modules looked very similar, but it rose significantly for modules further along the gas chain.

Particle Diffusion by Waves in Mirror Geometry. *TIANHUI LI (Princeton University, Princeton, NJ 08540) NATHANIEL FISCH (Princeton Plasma Physics Laboratory, Princeton, NJ 08543).* Due to their relative simplicity, magnetic mirror geometries have been considered as candidate devices for achieving thermonuclear fusion. One byproduct of nuclear fusion is hot "ash," which can breed instabilities that disrupt plasma confinement. Here, we discuss a novel technique that takes advantage of the mirror physics to stochastically cool these particles with radiation. By employing a spatially-localized single-frequency wave, a resonance with particles of a fixed parallel energy is created which selectively perturbs their perpendicular energy in a chaotic manner. Adiabatic invariants guarantee that the particles will return with the same resonant energy profile as they bounce between mirror points. The net effect of the wave is to create a diffusion path along the mid-plane phase space and the larger position space. When the particles diffuse to a low enough energy, they are removed from the system. We demonstrate the physics behind these wave-particle interactions and solve the diffusion equation for this problem using various software tools. The results show how different spatially-varying diffusion coefficients affect the evolution of the particle distribution. The analysis provides a framework for discussing and optimizing specific wave-diffusion problems.

Visible Light Tomography on FRX-L. *ADAM LIGHT (Case Western Reserve University, Cleveland, OH 44106) THOMAS INTRATOR (Los Alamos National Laboratory, Los Alamos, NM 87545).* An optical tomographic system has been developed to analyze plasma structure in the Field Reversed eXperiment – Liner (FRX-L) device at Los Alamos National Laboratory. FRX-L is designed to produce a high-density field-reversed configuration plasma (FRC) for fusion energy research. Visible light emitted by the plasma provides much information about its internal structure and is measured by several diagnostics, including the tomographic system described in this work. The diagnostic system consists of two optical array holders each equipped with eight 200-μm optical fibers arranged in a fan-like geometry. Line-integrated optical brightness data from the fan arrays are converted to a two-dimensional brightness map by tomographic inversion. The system has been calibrated and tested using the known brightness profile of a fluorescent lamp. Inversion routines based on the expansion-in-base-functions method have been developed and preliminary results match the expected hollow density profile of the FRC.

Hardware Testing of the BaBar Drift Chamber. *BRYCE LITTLEJOHN (Principia College, Elsah, IL 62028) JOCHEN DINGFELDER (Stanford Linear Accelerator Center, Stanford, CA 94025).* The BaBar drift chamber provides position, timing, and dE/dx measurements for charged decay products of the Υ(4S) resonance at 10.58 GeV. Increasing data collection rates stemming from higher PEP II luminosities and background have highlighted dead time problems in the drift chamber's data aquisition system. A proposed upgrade, called Phase II, aims to solve the problem with the introduction of rewritable, higher-memory firmware in the DAQ front-end electronics that lowers dataflow through the system. After fabrication, the new electronics components were tested to ensure proper function and reliability before installation in the detector. Some tests checked for successful operation of individual components, while others operated entire sections of the upgraded system in a mockup drift chamber environment. This paper explains the testing process and presents results regarding performance of the upgrade electronics.

Water Quality and Pollution in Our Enviornment. *LAURA LIZARZABURU (California State University Long Beach, Long Beach, CA 90840) CARL SZATHMARY (Princeton Plasma Physics Laboratory, Princeton, NJ 08543).* This unit will consist of a series of experiments about the properties of water and the effects of water pollution. Water is perhaps the most important life sustaining resource on Earth. The importance of unpolluted water in sustaining human, animal and plant life can't be overstated. Yet, each day, millions of gallons of water are lost to various contaminants. Water pollution is a serious global problem. Much of the damage is due to human activity. An important factor that plays a role in the degradation of our water sources is simple ignorance of the affect that our daily activities have on the global ecosystem. Awareness and prevention are important ways to control water pollution. It is essential that we inform our children of these issues regarding water pollution and quality. The knowledge that the students will gain will empower them to make positive changes in the future. This unit will familiarize students with the properties of water and pollutants. It will also allow students to familiarize themselves with common laboratory practices. Students will learn to collect samples in the field and perform water quality tests for nitrates, dissolved oxygen, and pH.

Comparison of Particle Species and Spectra Produced in 25.5GeV/c Proton-Platinum Collisions for the KOPIO Experiment in Different Simulation Packages. *KA HO LO (State University of New York – Stony Brook, Stony Brook, NY 11794) DAVID JAFFE (Brookhaven National Laboratory, Upton, NY 11973).* The KOPIO experiment(E926) aims at searching for the rare decay $K^{\circ}_{L} \rightarrow \pi^{\circ} \nu\pi\nu$ with a predicted branching fraction of 3×10^{-11}. To study this decay, KOPIO requires a large flux of K_L beam. In the experiment, K_L are produced by having a 25.5GeV/c proton beam impinge on a stationary platinum target. Many particles species are produced in the collision. We need to purify the K_L beam as much as possible. Knowledge of the yields and the kinematic properties of the particles produced would be necessary for designing efficient ways of purification. Using Monte Carlo simulations(MC), we study the composition of the neutral beam. We used GEANT3 and GEANT4 for the study, which are MC packages used extensively in high energy physics. We compared the momentum spectra, time spectra and particle composition in different simulations. By comparing the simulation results, some discrepancies among the simulation packages are identified.

Test and Comparison of GEM Foils from Different Manufacturers Under Various Operating Conditions. *PATRICK LYNCH (Bucknell University, Lewisburg, PA 17837) CRAIG WOODY (Brookhaven National Laboratory, Upton, NY 11973).* Gas Electron Multiplier (GEM) foils can serve as detectors for high-energy nuclear particles in a variety of physics applications. Because GEM foils are set to play a major role in upgrades to both the Pioneering High Energy Nuclear Interaction eXperiment (PHENIX) and Solenoidal Tracker At RHIC (STAR) experiments at the Relativistic Heavy Ion Collider (RHIC) located at Brookhaven National Laboratory, it is necessary to test the operation of these foils in regards to their gain and stability as a function of their operating conditions (e.g. pressure, water content in the gas), and as the foils' manufacturing processes are varied. Using a three GEM stack with an Iron-55 source in a 70/30 Argon/CO_2 environment, the electrons produced can be collected and read off as an electronic pulse on an oscilloscope. Knowing the expected primary charge, a GEM foil's gain can be determined through a ratio of final charge to primary charge. When comparing the effect of pressure on the GEM foils' performance, a higher pressure was shown to lead to smaller gain. In addition, increased water concentrations in the detector environment not only resulted in a significant gain increase, but also improved the foils' overall stability. In the comparison of Tech Etch manufactured GEM foils and those manufactured at the CERN laboratory, the Tech Etch foils showed a significantly higher maximum gain, as well as much greater instability. The CERN foils had little to no charge up time (within minutes) at low water levels while the Tech Etch foils required several hours to reach their maximum gain potential. This work is imperative for finding the optimal operating environment for GEM foils so that they can be used effectively and accurately in their applications not only at Brookhaven Laboratory, but also in other research laboratories throughout the world.

Microwave Characterization of Composites with Tungsten Coated Filler Particles. *THOMAS MALONEY (University of Cincinnati, Cincinnati, OH 45221) NICOLA BOWLER (Ames Laboratory, Ames, IA 50011).* Using filler particles in composites allows for the control of the electromagnetic properties of the material. This is useful in the absorption of electromagnetic waves in the microwave spectrum, which has applications in telecommunications, radar systems and microwave heating. In this study, the relative permittivity of composites made with four related types of filler particles was measured at microwave frequencies. The particles used were 3M™ Glass Bubbles A20/1000 sputter coated with tungsten. Two of the particle samples had an aluminum oxide (AlO_x) outer coating. For each of these two different types of particle samples, one batch was dried at 150°C and the other at 350°C prior to sputter coating with tungsten. The particles were infused into a matrix material of paraffin wax. The electromagnetic properties were measured in the frequency range of ~2 to 18 GHz by a 7 mm coaxial reflection/transmission line method. The data was analyzed and showed a dielectric loss in the observed frequency range for all four particle samples. This research shows that the composites filled with the AlO_x coated particles have a higher real and imaginary relative permittivity than those with the non-AlO_x coated particles. The drying temperature of 350°C was shown to shift the dielectric relaxation to a higher frequency while reducing its extent. This indicates that the frequency and amount of absorption can be controlled by the type of particle used, and the filler volume fraction of the sample, allowing composite materials to be tailored for a large number of applications.

Measuring the Friction Drag Reduction of Superhydrophobic Glass in Water. *EVAN MARKEL (Cornell University, Ithaca, NY 14850) JOHN T. SIMPSON (Oak Ridge National Laboratory, Oak Ridge, TN 37831)*. Through several mechanical and chemical processes, the surface structure of glass can be designed to have superhydrophobic properties. A material is defined as superhydrophobic if a drop of water sitting on top of the material beads up to have a contact angle with the surface greater than 150 degrees. (A perfectly superhydrophobic material has a contact angle of 180 degrees.) Among many applications, this glass could be used as an inexpensive coating for the bottom of ships or other watercraft. When the glass is submerged underwater there is a microscopic layer of air separating the surface of the glass from the water. Because this glass is so water repellant, there should be a significant reduction of friction drag in water, compared to normal glass. This project first involves designing and fabricating a magnetic bearing to separate form drag from friction drag in conducting drag reduction experiments. The magnetic bearing is composed of an electromagnet, infrared emitter, detector, and op-amp circuit, which work to levitate an object underneath the electromagnet. The bearing suspends a magnetic apparatus underneath it, which holds a cylinder of the superhydrophobic glass. A circular cylinder of the glass is used because there is no water displacement as it spins, so there is no form drag. The apparatus is then spun using air jets, and a high-speed camera counts the number and frequency of rotations as the glass spins in the water. From this information, a decay coefficient of the water's friction drag can be calculated. The results for the superhydrophobic glass will be compared to those for a control sample of regular glass, and the amount of friction drag reduction will be found and presented. This work is part of a project to design, test, and develop superhydrophobic nano-structured materials.

Velocity Measurements of Turbulent Structures on the National Spherical Torus Experiment (NSTX) with High Speed Cameras. *BRETT MCGEEHAN (Dickinson College, Carlisle, PA 17013) ROBERT KAITA (Princeton Plasma Physics Laboratory, Princeton, NJ 08543).* Measuring the characteristics of edge turbulence in fusion plasma devices allows physicists to better understand the confinement properties of fusion plasmas. Edge turbulence is studied with diagnostics such as gas puff imaging (GPI) and the Shifted Wavelength/Interference Filter Technology (SWIFT) diagnostic. In the GPI diagnostic, a neutral gas puff is introduced at the plasma edge to enhance the visible hydrogen emission so that turbulent structures can be seen with a camera viewing along magnetic field lines. The GPI allows for 2D spatial imaging and temporal resolution of the turbulence. The SWIFT diagnostic can yield additional information on the velocity of the turbulent structures normal to the viewing plane. This technique has been demonstrated with single-point measurements, and its extension to 2D imaging is being investigated. Through the use of an Ultima SE CMOS digital camera, manufactured by Photron, Ltd., turbulent structures are captured at framing rates between 4,500 and 40,500 frames per second with exposure times of 222 and 25 microseconds, respectively. Images from the edge of the plasma were obtained using a helium filter in a helium plasma, and from the region around the center stack in a deuterium plasma using a deuterium filter. Data analysis has shown that for viewing the edge of the plasma, the maximum frame rate that can be used is 13,500 frames per second to yield a useable signal; for center stack viewing, 40,500 fps is possible. *In collaboration with S. Paul and L. Roquemore (Princeton Plasma Physics Laboratory) and N. Nishino (Hiroshima University).

Silicon Wafer Transmission Window for Electron-Pumped Laser Systems. *CHRISTOPHER MCGUFFEY (University of Oklahoma, Norman, OK 73072) CHARLES GENTILE (Princeton Plasma Physics Laboratory, Princeton, NJ 08543).* An electron beam transmission window is being developed as a crucial component for the Electra Krypton Fluoride (KrF) laser at the Naval Research Laboratory (NRL). Such KrF lasers will be employed to provide direct drivers for Inertial Fusion Energy (IFE). The transmission window is composed of a 1/4" thick aluminum frame arrayed with 24 holes, each covered by a 2" round 150 μm thick silicon wafer. The goal is to efficiently allow transmission of a 750 KeV electron beam into the KrF lasing medium. The window must withstand 2.3 atm pressure, high temperature (400°C) from electron bombardment, endure =108 shots and allow high electron transmission efficiency (=80%). Usually, this is achieved with a thin metal foil. However, we believe this method will provide the same transmission efficiency with a greater safety factor in strength because of silicon's mechanical strength, elastic deformation, thermal properties, and electron transmission. The wafers are coated with a 1.2 μm diamond layer to protect the silicon from the corrosive fluorine gas. Silicon wafers are bonded to the aluminum frame using Room Temperature Vulcanizing (RTV) sealant. The RTV becomes a seal that can withstand high temperature and pressure. We tested various RTV sealants for desired performance. We successfully tested individual wafers for strength by applying up to 3.5 atm pressure and baking in a 600°C oven. A prototype window was produced and tested at the laser site at NRL. The overall result was an improvement in durability by a factor of four compared to the previous frame which used square wafers. However, durability is still below operable levels – the wafers shattered after 180 shots. Convection correlations combined with finite element analysis simulations indicate that the silicon wafers were heated well beyond softening temperature. These thermal stresses could have caused the wafers to fail. Conductive RTV and metal contacts should be used in the next round of experiments to provide sufficient heat transfer away from the wafers. Because silicon is a crystal, a repeatable solution can be found that will last practically infinitely. If the proper parameters can be found to handle steady-state operation, silicon windows will provide the desired combination of strength and electron transmission.

Augmentation of Graphical User Interfaces for the Main Injector Neutrino Oscillation Search. *ANDREW MCUMBER (Binghamton University, Binghamton, NY 13902) MARY BISHAI (Brookhaven National Laboratory, Upton, NY 11973).* Graphical user interfaces (GUI) in Java allow physicists straightforward access in managing classifications of streaming data from the networks of complex experiments. For the Main Injector Neutrino Oscillation Search (MINOS), a long-term study of muon neutrino flavors and their anomalous interactions, large volumes of sensor output are likewise conveniently displayed. The Java Analysis Studio 3 (JAS3) package is also implemented, chiefly for its numerous plotting capabilities and real-time data acquisition. The Fermi National Accelerator Laboratory project induces collisions of 120 GeV protons on a target, and observes a subsequent yield of hadrons, requiring that multiple charge monitors are present. Specifically, live proton beam target alignment in the Neutrino Main Injector (NuMI) is portrayed and updated in the GUI. Other critical characteristics of the software include a time plot of proton beam target intensity, a monitor for resultant pion and kaon particles, and muon detectors placed after the hadron decay reactions. An augmentation of existing code is undertaken, as a precautionary measure for budgeting and system alerts. A new GUI catalogues errors that are found by the local beam system. Detailed error categories are plotted and compared. Two trials for error rate monitoring are conducted and yield correlations between proton beam position devices, as well rate inequalities for different time periods in the NuMI research schedule. Memory management is characterized via a Java memory profiler.

Cost-Efficient Fabrication of 3-D Photonic Crystals via Microtransfer Molding. *TRAVIS MONK (Truman State University, Kirrksville, MS 63501) KRISTEN CONSTANT (Ames Laboratory, Ames, IA 50011).* Three-dimensional photonic crystals impede a certain frequency of light independent of the light's incident angle. Methods based on semiconductor processing cost around $250,000 to create a four-layer crystal. Using microtransfer molding, a method of soft

lithography, it is possible to construct photonic crystals cost-efficiently. By pouring poly-dimethyl siloxane elastomer (PDMS) over parallel bars etched in a silicon wafer and curing the PDMS, one can repeatedly create parallel channels in the PDMS. The channels' spacing and size depend on the frequency of light to be impeded. Prying the PDMS from the silicon wafer exposes these imbedded channels. They are then filled with polyurethane (PU) and exposed to high-intensity ultraviolet light, hardening the PU. The PU-filled channels are then coated with polyacrylate (PA). After pressing a glass substrate atop the PU-filled, PA-coated channels, the PU and PA are again exposed to ultraviolet light for solidification. The PDMS is peeled from the glass substrate, leaving bars of solid PU glued to the substrate by the PA. Stacking these layers of PU bars in the 'Iowa State Woodpile Structure', where layers are rotated 90 degrees relative to each other, a mold is created from which one can make a photonic crystal. This crystal has a yield around 70%, meaning microtransfer molding is not yet an acceptable method for fabricating photonic crystals. Methods based on semiconductor processing produce very high quality samples. However, the process is so expensive that samples can only be used for proof of theory. Microtransfer molding, on the other hand, is quite cost efficient, allowing our group to focus on applications of photonic crystals.

Optimization of the Aorsa 1-Dimensional Code. *RYAN MOORE (Georgia Institute of Technology, Atlanta, GA 30332) MARK CARTER (Oak Ridge National Laboratory, Oak Ridge, TN 37831).* The Aorsa 1-dimensional program was written by E. F. Jaeger of the Fusion Energy Division at Oak Ridge National Labs. ORNL and the Princeton Plasma Physics Laboratory use the Fortran code to analyze plasma heating caused by an antenna that couples its radio frequency power to the plasma. The resolution of the analysis is dependent on the physics involved and is computationally intensive. Optimizing Aorsa will allow researchers at ORNL and PPPL to more accurately and efficiently analyze plasma heating by RF Antennas. To increase the resolution and decrease the runtime, three parts of the code were identified for optimization by timing studies. The most expensive subroutine, BESIEXP, calculated the i and j Bessel functions with argument, G, proportional to the ratio of the charged particle gyroradius to the wavelength. BESIEXP was called many times with a wide G distribution with the G's clustered around discrete steps. The subroutine is now replaced by one that interpolates linearly on a table of Bessel functions. The steps of the table are centered around the clusters of G to decrease the error. Interpolation cuts the time spent in BESIEXP by two-thirds. Spacing the table to align with the G distribution gives the same error as an evenly spaced table with 21 times the resolution. A second part of the code that is optimized is the impedance scan used for 3D antenna analysis. A Message Passing Interface now splits the scan among different processors that calculate their values independently and send them to the Master process for ordered output. MPI decreases the time spent in the impedance scan by a factor approximately equal to the number of processors used. The third part of the code identified for optimization was the dense matrix amat, solved for each wave. Preliminary testing shows that making the matrix sparse and using a sparse solver such as MUMPS will save time and memory with minimal error. Continued refinement on Aorsa is needed, but the benefit of the optimization can already be seen.

Optimization of the Muon Stopping Target of the Muon to Electron Conversion (MECO) Experiment. *DAVID MORSE (University of Rochester, Rochester, NY 14627) YANNIS SEMERTZIDIS (Brookhaven National Laboratory, Upton, NY 11973).* Muon to electron conversion is a rare symmetry violating process which MECO proposes to investigate. Natural muon decay in flight is characterized by the expression $\mu^- \rightarrow e^- + \nu \bar{e} + \nu\mu$. It is only in the presence of matter that the process $\mu^- + N \rightarrow e^- + N$ is seen. This is a rare neutrinoless lepton flavor violating process with a maximum bound branching ratio of $10x^{-11}$. This process is characterized by the production of a 105 MeV electron. This energy is the rest mass of the muon and shows a direct conversion. To produce these electrons muons are collided onto a muon stopping target. As such it is important to optimize this target for maximal muon stoppage and to retain high energy resolution (minimize energy loss) for resulting electrons. The target geometry initially proposed was a series of thin disks suspended in the transverse plane. After further study, other geometries were proposed, including a series of 17 cones pointing upstream or downstream of the muons, or a single larger cone pointing downstream. The cones were hypothesized to have a natural advantage over the disks, as the pitch of the electrons, the azimuthal angle from the particle's helical path, ensures that the electrons see less matter when traveling through an angled surface. Electrons lose 2 MeV per centimeter, so this is a major concern. Modifying existing GEANT (a GEometry ANd Tracking package) code, the target geometries were tested for both muons and electrons using ROOT, an object oriented data analysis framework, to compare muon stopping power, electron energy distributions and electron efficiency (what percentage of produced electrons reach the calorimeter). With a 24% increase in energy resolution and a slight increase in muon stopping power this analysis concludes that the series of cones pointing in the upstream direction is the most effective geometry for both muon stopping power and for minimizing electron energy loss.

Exploring Gold Nanoparticle Monolayers with a Langmuir Trough and X-rays. *JESSICA MURRAY (Eastern Illinois University, Charleston, IL 61920) DAVID SCHULTZ (Argonne National Laboratory, Argonne, IL 60439).* Gold nanoparticles show the possibility of being applicable in many different areas of technology due to the particles' collective and individual behavior and characteristics. By examining the nanoparticles' behavior and characteristics, more distinctive and unique qualities of nanoparticles may be known and used to benefit society. However, the difficulty in researching nanoparticles is finding the right conditions to create a solution of nanoparticles that would yield useful experimental data on the behavior of the solution. The purpose of this experiment is to find the conditions to create a uniform gold nanoparticle monolayer. The features of gold nanoparticle films on the surface of pure water were studied with use of a Langmuir trough, optical microscope and an x-ray liquid surface spectrometer. By varying the conditions used for sample preparation, it was found that for every 1 ml of gold nanoparticle solution, 12 µl of dodecanethiol needs to be added to create a uniform film. Also observed was that the temperature of the solution needs to be increased to 37°C while compressing the film to prevent thiol bubbles from sitting on the surface of the film.

Testing For Linearity Using A Two Lamp Method. *DEREK NALLEY (Purdue University, West Lafayette, IN 47907) KEITH A. EMERY (National Renewable Energy Laboratory, Golden, CO 89401).* Photovoltaic devices are rated in terms of their power output or efficiency with respect to a specific spectrum, total irradiance, and temperature. In order to rate photovoltaic devices a reference detector whose response is linear with total irradiance is needed. This procedure documents a procedure to determine if a detector is linear over the irradiance range of interest. Testing the short circuit current versus the total irradiance is done by illuminating a reference cell candidate with two lamps that are fitted with programmable filter wheels. The purpose is to reject nonlinear samples as determined by national and international standards from being used as primary reference cells. A calibrated linear reference cell tested by the two lamp method yields a linear result.

Reconstructing Parton Distribution Functions From Their Moments. *SCARLET NORBERG (Kent State University, Kent, OH 44243) DAVID RICHARDS (Thomas Jefferson National Accelerator Facility, Newport News, VA 23606).* Parton Distribution Functions (PDFs) are used to describe what the inside of the nucleon looks like and to determine the effective degrees of freedom of Quantum Chromodynamics (QCD). One way to determine the PDFs is to compute or to measure their moments. However, if only the first few moments are known it is important to explore the extent to which the shape of the PDF can be recovered. Using the computer-algebra package Maple, we took a known PDF and computed its moments; we then examined the extent at which we could recover the shape of the PDF with a given number of moments. The goal of this project is to show if moments can be taken and PDFs can be found with reasonably amount of accuracy. What one realizes immediately is that one more moment is needed then parameters. Some parameters were discovered using this method and discovering the shape of the PDF. We did discover though despite our best efforts the parameters we got did not give us back the moments we had initial had. They were close but there were still discrepancies. Also, the accuracy of getting the PDF parameters is not very good. There is no way to get the shape of the PDF, if all that is known is a limited number of moments.

Assessment of Hall A VDC Analysis Software Performance through Monte Carlo Simulation. *AMY ORSBORN (Case Western Reserve University, Cleveland, OH 44106) JENS-OLE HANSEN (Thomas Jefferson National Accelerator Facility, Newport News, VA 23606).* The High Resolution Spectrometers (HRS) employed by Hall A at the Thomas Jefferson National Accelerator Facility (JLab) rely on vertical drift chambers (VDCs) for particle tracking. In order to reconstruct particle paths, data from these VDCs are analyzed using custom analysis software ('the analyzer') that builds upon the ROOT data analysis framework. To test the software's abilities and find methods for improvement, it is useful to examine simulated data. In this paper, a

Monte Carlo simulation of the VDC wire chambers was carried out. The simulation was based on an existing framework, which was expanded and improved as part of this project. Realistic effects were incorporated into the simulation to test the analyzer's resolution and tracking limits. Data from this simulation were analyzed, and results were compared with the simulated data to assess analyzer performance. The effects of angle estimation in the track reconstruction algorithm, VDC drift time resolution, random wire firing, and coincident tracks on analyzer performance were examined. It was found that track angle estimation reduces error in track position and slope linear fits by approximately 10% with a drift time resolution of 4.5 ns. In simulations with a drift time resolution of 4.5 ns, a 0.5% probability of random wire firing 99.999% wire efficiency, and angle estimation incorporated, the overall tracking efficiency remained above 90% for all triggering rates ranging from 2 kHz to 700 kHz. Tracking efficiency in reconstructed multi-track events was shown to be below 90% for all rates, falling below 80% for trigger rates above 500 kHz. The simulation may still be improved via the addition of more natural effects such as delta and cosmic rays. Preliminary simulation results show a high level of confidence in trigger track reconstruction but significant failures in the analyzer's processing and identification of multiple tracks. Further analysis of analyzer performance with reconstructed and generated multi-track events is necessary to identify problems in the algorithm's treatment of multiple track events.

Development of a Genetic Algorithm to Parametrize Thermonuclear Reaction Rates from the NACRE Library. *CARLOS ORTIZ (Davidson College, Davidson, NC 28035) MICHAEL SMITH (Oak Ridge National Laboratory, Oak Ridge, TN 37831).* Astrophysicists simulating the processes inside stars that drive stellar explosions depend on large collections of thermonuclear reaction rates. The NACRE collaboration recently evaluated numerous key reaction rates, yet these rates have not been incorporated into REACLIB, a standard collection of over 60,000 rates. Incorporating the NACRE library requires the parametrization of all its rates into the functional form used by the REACLIB community. Implementing object oriented programming techniques in Fortran 90, a genetic algorithm (GA) was designed to fit these reaction rates with seven parameters. The range of these reaction rates may at times stretch over thirty orders of magnitude. The algorithm's implementation was inspired by numerous web sources, in particular the GA FAQ and the GA Archives. Moreover, the use of object oriented concepts was heavily guided by the writings of V. K. Decyk, C. D. Norton, and B. K. Szymanski in the journal of Scientific Programming. Currently, the algorithm generates good solutions in a timely fashion. However, its performance does not match either that of the Levenberg-Marquardt method or that of the Generalized Least Squares method, the latter currently under development for the Computational Infrastructure for Nuclear Astrophysics (CINA). Both of these methods readily fit a sizable portion of the NACRE library within a two percent maximum error, whereas the GA algorithm fits only most areas of the data sets satisfactorily. Still, the performance of both these and other methods depends on the quality of the input set of initial parameters. The task of generating this input could be performed well by the genetic algorithm, thus creating a robust hybrid algorithm. Also, the algorithm's structure readily allows further improvements, such as adding new search strategies and fitting data sets to other functional forms, thus serving as a flexible, much needed tool for researchers. It also allows changing the fitness function from chi squared to any other objective function, thus potentially eventually serving not only as a fitting algorithm, but also as a general-purpose nonlinear optimization algorithm.

Linux-Based Application for the New Generation Digital Pulse Processing-Based Data Acquisition System for Nuclear Physics Experiments. *ZACHARY OWENS (Walter State Community College, Morristown, TN 37813-6899) ROBERT GRZYWACZ (Oak Ridge National Laboratory, Oak Ridge, TN 37831).* Nuclear fusion and fission are, theoretically, ways to produce efficient and clean energy but they need to be economical. Fundamental nuclear physics research is necessary to address some of the energy generation issues. Reliable modeling of nuclei and their nuclear reactions is needed. So there are experiments that test theoretical nuclear models, where novel methods of doing experiments have been developed. Nuclear reactions e.g. fusion-evaporation and reaction products are studied. Rare reaction products are separated with the use of magnetic spectrometers. Single nuclei have to be identified and their decay radiation detected. A combination of detectors and electronic readout system is used to achieve that. Nuclear decay radiation is detected in semiconductor detectors. There is a charge that the detector converts into a voltage pulse and digitizes in the fast sampling electronic board. Signals go through an analog-to-digital converter, which produces a digital image of a pulse at 100 million times per second (100 MHz). Real Time Processing circuitry is analyzing this image and extracting useful information characterizing pulse amplitude, its arrival time and radiation type. This information is extracted from the electronics and stored for further analysis. Readout and control software compatible with other Holifield Radioactive Ion Beam Facility (HRIBF) used systems is being developed. In this project existing Windows XP software has to be converted into Linux, which has better real time performance and reliability, and is easily modified. The software is converted by taking the code from the windows version of the software that runs. Then commenting out all the code that is not working right in Linux then slowly put it back together. The new generation of hardware that will supple this software with data is called Pixie-16 manufactured by XIA LLC. Ca. It comes with a 16 input channel PCI board with 100 MHz sampling Analog-To-Digital-Converter, which has new abilities in storing more information, which also may result in improving detection sensitivity. It is connected to a computer running operating system Enterprise Linux 3 (kernel 2.4). User-friendly interface has to be developed for easier control of the complex tasks of the Pixie-16 board. The Pixie-16 development will enable measurements on rare isotopes and study their properties more accurately.

A Study of Z-plane Capacitance. *HARSHIL PARIKH (University of Illinois at Urbana-Champaign, Urbana-Champaign, IL 61801) SANJAY SWAIN (Stanford Linear Accelerator Center, Stanford, CA 94025).* The BaBaR detector at the Stanford Linear Accelerator Center is currently undergoing an upgrade to improve its muon and neutral hadron detection system. The Resistive Plate Chambers (RPCs) that had been used till now have deteriorated in performance over the past few years and are being replaced by Limited Streamer Tube (LSTs). Each layer of the system consists of a set of up to 10 streamer tube modules which provide one coordinate (Φ coordinate) and a single "Z-plane" which provides the Z coordinate of the hit. The large area Z-planes (up to $12m^2$) are 1 mm thick and contain 96 copper strips that detect the induced charge from avalanches created in the streamer tube wires. All the Z-planes needed for the upgrade have already been constructed, but only a third of the planes were installed last summer. After installing the 24 Z-planes last year, it was learned that 0.7% of the strips were dead when put inside the detector. This was mainly due to the delicate solder joint between the read-out cable and the strip, and since it is difficult to access or replace the Z-planes inside the detector, it is very important to perform various tests to make sure that the Z-planes will be efficient and effective in the long term. We measure the capacitance between the copper strips and the ground plane, and compare it to the theoretical value that we expect. Instead of measuring the capacitance channel by channel, which would be a very tedious job, we developed a more effective method of measuring the capacitance. Since all the Z-planes were built at SLAC, we also built a smaller 46 cm by 30 cm Z-plane with 12 strips just to see how they were constructed and to gain a better understanding about the solder joints.

Study on the Characteristics of Avalanche Photodiodes. *ZACHARY PARSONS (University of South Dakota, Vermillion, SD 57069) MILIND DIWAN (Brookhaven National Laboratory, Upton, NY 11973).* In the past, many particle physics experiments have used Photomultiplier Tubes (PMTs) for light detection. These PMTs, while effective, have some limitations. One alternative is the Avalanche Photodiode (APD). APDs excel in many of these areas that PMTs are found lacking. While APDs are becoming more widely used, they are limited in size, due to increasing noise with increasing size. New techniques are in development to create larger area, high gain APDs with more favorable properties. This study was done to test the basic properties of new large area APDs developed by Radiation Monitoring Devices Inc. (RMD). The properties tested including dark current, gain, capacitance, and series resistance. The RMD APDs were compared to an older APD developed by Hamamatsu. For capacitance and series resistance measurements a LCR meter was hooked to the APDs. For dark current and gain measurements, a picoammeter was connected to the APDs. The capacitance per area for the RMD APDs is less than 1 pF/mm^2 at high bias. The series resistance is rather large, but is greatly reduced when it is specially packaged for use in water. The devices have a high gain, but the surface and bulk current is large. Overall, the results were promising, but further improvements are needed before the APDs are ready for use in experiments.

Photometric Supernova Typing for the SDSS SN Survey. *ELIZABETH RIVERS (Wellesley College, Wellesley, MA 02481) MASAO SAKO (Stanford Linear Accelerator Center, Stanford, CA 94025).* In the fall of 2004 the Sloan Digital Sky Survey (SDSS) 2.5m telescope scanned the southern equatorial stripe for approximately 20

nights over the space of two months. Light curves for over four dozen supernovae (SNe) were collected over time using five colored filters ugriz that together had a range of approximately 3000A to 10500A. 22 SNe were spectroscopically confirmed with follow-up observation. Using the data obtained in the Fall 2004 campaign, preparations are now being made for the Supernova Survey of the SDSS II, a three-year extension of the original project. One main goal of the Supernova Survey will be to identify and study type Ia SNe of up to redshift ~0.4, the intermediate 'redshift desert,' as well as enabling further study of other types of SNe including type 1b/c and peculiar SNe. Most of the SNe found will not have spectra taken, due to time and cost constraints. Thus it would be advantageous to be able to robustly type SNe solely from the light curves obtained by the SDSS telescope prior to, or even without ever obtaining a spectrum. Using light curves of well-observed SNe templates were constructed for comparison with unknown SNe in order to photometrically type them.

Monte Carlo Simulations of Type I X-ray Bursts. *LUKE ROBERTS (Colorado College, Colorado Springs, CO 80936) MICHAEL S. SMITH (Oak Ridge National Laboratory, Oak Ridge, TN 37831)*. Type I x-ray bursts (XRB) occur on the surface of an accreting neutron star in a binary star system. Accreted matter from the normal star is deposited on the surface of the NS and becomes extremely hot and dense. In the steady state burn phase, hydrogen is converted to helium through the B^+ limited CNO cycle, which contributes to the temperature increase on the surface of the NS. Once a high enough temperature is reached in the envelope, a runaway thermonuclear explosion ensues. These thermonuclear explosions are driven by the rp- and αp-processes, which occur on proton-rich unstable nuclei. Almost all reaction rates involving these nuclei have never been experimentally measured. Theoretically determined rates generally have an uncertainty greater than a factor of two. To understand how these uncertainties effect final nuclear abundances and energy generation throughout the burst, a Monte Carlo (MC) simulation using a post-processing element burning code is employed. In the MC simulation, all of the reaction rates are varied simultaneously for each of the 5,000 trials. This is done randomly for each reaction according to a log-normal probability distribution taken from the value and uncertainty of the rate as stated in the literature. We find variations in the nuclear reaction α(2α,γ)12C strongly effect all final nuclear abundances and energy generation throughout the burst. Positron decays of the nuclei ^{21}Mg, ^{24}Si, ^{25}Si, ^{30}S and ^{34}Ar also effect energy generation in the XRB. The final abundances of high mass nuclei are strongly affected by proton captures on nearby nuclei. Upper limits on the uncertainties of final abundances of nuclei were also found. Future work will include verification of results by separate methods and larger numbers of MC trials for more accurate statistics.

Quality Assurance Testing of HDI Circuitry for CMS FPix Detector. *DANIEL ROKUSEK (University of Illinois at Urbana-Champaign, Urbana, IL 61801) GREG SELLBERG (Fermi National Accelerator Laboratory, Batavia, IL 60510).* The Large Hadron Collider (LHC) at CERN will be used to a variety of aspects of high energy physics. One such aspect is the breaking of symmetry in the electroweak force. It has been theorized that the discovery of the Higgs particle could uncover the nature of this symmetry breaking. The Compact Muon Solenoid (CMS) will be used to search for the Higgs, beginning with the Forward Pixel (FPix) detector located at the center of CMS. FPix is a robust particle tracker, featuring silicon strip and pixel detectors. Before the components of FPix can be assembled, it is of the utmost importance that each individual piece of circuitry be tested to verify proper performance. The work presented here consists of quality assurance (QA) testing of the high density interconnect (HDI) circuitry for FPix. Prior to testing the HDIs, software was written to automate the probing process. National Instruments' LabVIEW 7.0 was used to write a custom probing software package. This package uses the NI GPIB (IEEE 488) interface to control a Rucker & Kolles 680A Semi-Automatic probe station and an Agilent 4284A precision LCR meter. Features of the software package include a user interface to enter input data of HDI surface feature locations generated from the HDI Gerber file, perform probing tasks and analysis, and generate output data. Special care was taken to design a HDI alignment sub-routine to allow a user without previous knowledge the HDI circuitry, software, or probe station to perform the QA tests. Results from the testing of the initial batch of HDIs show shorting errors. Errors were manually inspected and verified, and the information was passed onto the HDI design team and to the manufacturer for analysis. Once the errors are remedied, full production of HDIs can be approved and the HDIs will be tested with this software package. Upgrades to the software package could begin with the replacement of the semi-automatic RK680A probe station with an Electroglas 2001X probe station. The incorporation of additional probes and motion stages to the 2001X probe station will result in a fully-automatic flying-head probe station, and will significantly decrease the HDI probing time.

Modeling and Visualizing the Particle Beam in the Rare Isotope Accelerator. *CHRISTOPHER ROSENTHAL (Illinois Institute of Technology, Chicago, IL 60616) BELA ERDELYI (Argonne National Laboratory, Argonne, IL 60439).* Argonne National Laboratory is actively pursuing research and design for a Rare Isotope Accelerator (RIA) facility that will aid basic research in nuclear physics by creating beams of unstable isotopes. Such a facility has been labeled as a high priority by the joint Department of Energy and National Science Foundation Nuclear Science Advisory Committee because it will allow more study on the nature of nucleonic matter, the origin of the elements, the Standard Model, and nuclear medicine. An important part of this research is computer simulations that model the behavior of the particle beam, specifically in the Fragment Separator. The Fragment Separator selects isotopes based on their trajectory in electromagnetic fields and then uses absorbers to separate particles with a certain mass and charge from the rest of the beam. This project focused on the development of a multivariate, correlated Gaussian distribution to model the distribution of particles in the beam as well as visualizations and analysis to view how this distribution changed when passing through an absorber. The distribution was developed in the COSY INFINITY programming language. The user inputs a covariance matrix and a vector of means for the six phase space variables, and the program outputs a vector of correlated, Gaussian random variables. A variety of random test cases were conducted in two, three and six variables. In each case, the expectation values, variances and covariances were calculated and they converged to the input values. The output of the absorber code is a large data set that stores all of the variables for each particle in the distribution. It is impossible to analyze such a large data set by hand, so visualizations and summary statistics had to be developed. The first visualization is a three-dimensional graph that shows the number of each isotope present after each slice of the absorber. A second graph plots any of the six phase space variables against any of the others to see the change in the beam's distribution. Also, the expectation values, variances and covariances of the phase space variables were calculated after the absorber. The distribution that models the particle beam gives the variability that physicists need to simulate many different situations in the Fragment Separator. The statistics and visualizations will allow quick analysis of the particle beam. Both of these developments will contribute to the overall viability of the RIA proposal.

Reconstruction of a 4D Particle Distribution Using Underdetermined Phase-Space Data. *AFSHIN ROSTAMIZADEH (University of California Berkeley, Berkeley, CA 94720) ALEX FRIEDMAN (Lawrence Berkeley National Laboratory, Berkeley, CA 94720).* A well defined 4D distribution that describes the transverse spatial coordinates (x, y) and momenta (x', y') of the particles that make up an intense ion beam is of great value to theorists in the field of particle beam physics. If such a distribution truthfully captures the characteristic of the actual beam, it can be used to initialize an extensive simulation, and can yield insight into the processes that affect beam quality. Creating a proper representative distribution of particles is a challenge because the problem is, in general, quite underdetermined. Data is collected through a pair of "optical slit" diagnostics which provide two 3D distributions, f(x, y, x') and f(x, y, y'); the challenge is to coalesce these into a full 4D distribution f(x, y, x', y'). Further difficulties are introduced because the data is collected at different longitudinal planes and must be "remapped" to a common plane, taking into account the convergence or divergence of the beam as well as any off-centering. This challenge was met by developing a suitable algorithm and implementing it as a "plug-in" for the popular scientific image analysis program ImageJ, written entirely in the Java programming language. The algorithm accomplishes the desired remapping and synthesizes a 4D particle distribution, using Monte-Carlo techniques. Preliminary results show that this reconstructed distribution is consistent with actual data that was gathered from the same experiment using a different diagnostic. Also, "forward" particle-in-cell (PIC) simulations, that use the reconstructed distribution, match actual data gathered downstream in the experiment. Both these results give us some indication that the reconstruction is being done correctly. In addition to the multi-particle synthesis, the plug-in allows for the easy loading of digital data and the output of various plots that are useful to both experimenters and theorists. It also provides a framework by which its applicability can be extended to other types of experiments for which data analysis and simulation-particle synthesis are required.

Testing of Radiation Detectors for the Department of Homeland Security. *PAUL ROVINSKY (Suffolk County Community College, Selden, NY 11784) BIAYS BOWERMAN (Brookhaven National Laboratory, Upton, NY 11973).* The Department of Homeland Security (DHS) is investigating the purchase of millions of dollars worth of radiation detectors. In order to assure that they perform the way the manufacturers claim, the DHS has assigned various government labs to test the manufacturer's claims. This study was primarily concerned with the hand-held radiation detectors, which work through gamma spectroscopy and may have neutron identification. Various sources at various distances are used to test their detection and identification capabilities. The testing method involves placing a source on a table and moving the detector farther and farther away at 0.3m intervals, to the 3m mark. The results vary, depending on the detector. Several detectors did not pick up any radiation above the background level beyond the 1.5m mark, but were still able to identify the source. Others were incapable of identifying the source but noticed the increased radiation. No detectors were able to identify all the sources. More testing will need to be done to draw any valuable conclusions; however, several of the detectors work magnificently under controlled conditions and are ready straight out of the box. The results of these tests will be sent to the DHS for use in determining which detectors will fulfill their needs best.

Beam Loss and Residual Activation Trending Data Analysis for the Spallation Neutron Source. *ARIEL RUFFIN (Tennessee State University Alumna, Nashville, TN 37209) TED WILLIAMS (Oak Ridge National Laboratory, Oak Ridge, TN 37831).* The Spallation Neutron Source (SNS) linear accelerator has several diagnostic tools that are used to measure the amount of beam lost. These tools have been utilized during beam commissioning. Although the commissioning process includes a gradual increase in the beam intensity, the beam pulse width and the frequency of operation, the process also involves characterizing the beam. Some of the processes used to characterize the beam result in increased activation of accelerator components. The Front End, the Drift Tube Linac (DTL), and most of the Coupled Cavity Linac (CCL) of the SNS have been operated. Beam loss data were collected using Beam Loss Monitors and differential Beam Current Monitors. Residual activation data were also taken at various times during and after the commissioning run. Beam loss and residual activation data analysis is conducted according to guidelines specified in the Operations Procedure Manual titled "Procedure for Trending Beam Loss and Radiological Monitoring Data." As part of the analysis, a radiological survey is required. A precision-detailed radiological survey was designed and conducted and compared with the archived pulse-to-pulse beam loss monitor data and the calculated beam losses. The residual activation in the accelerator enclosure was found to be greater than predicted because that activation included losses resulting from exploring the beam characteristics.

Thermal Rate-of-Rise and Cooling Curve as Diagnostic Tools for Closed Cycle Refrigerators (CCR). *ARIEL RUFFIN (Vanderbilt University, Nashville, TN 37209) LOUIS SANTODONATO (Oak Ridge National Laboratory, Oak Ridge, TN 37831).* Temperature control is a crucial aspect of many types of scientific experiments, including most neutron scattering experiments. The Spallation Neutron Source (SNS), which will produce the most intense pulsed neutron beams in the world for scientific research and industrial development, will also develop advanced "sample environment" devices for controlling temperature and/or other sample parameters. The present research is part of the SNS sample environment development program, and involves the development of a new diagnostic technique ("thermal rate-of-rise") which will help debug and optimize commonly-used laboratory devices. This new technique, analogous to the well-known pressure rate-of-rise test, has been applied to a Closed Cycle Refrigerator (CCR) which produces temperatures in the 4 to 300 Kelvin (K) range. The thermal rate-of-rise test is prepared by first conducting the commonly used "cooling curve" diagnostic, where the CCR is actively cooled to its base temperature. The rate-of-rise test then proceeds by turning the machine off and allowing the temperature to drift back to room temperature while recording the data. Shown here is how the thermal rate-of-rise and cooling curves compliment each other and allow one to distinguish between various types of problems, such as inadequate heat shielding and virtual vacuum leaks.

Control of Activated Soil in Building 912, the Alternating Gradient Synchtron (AGS) Complex. *NOREEN SAPANSKI (St. Joseph's College, Patchogue, NY 11772) KIN YIP (Brookhaven National Laboratory, Upton, NY 11973).* When high energy proton particles interact with the targets made of steel, concrete, and copper, a variety of radioactive atoms are produced. Below the targets and primary beam dump, some of these radioactive particles penetrate the concrete and iron layers of floor shielding. To assess whether Building 912 at Brookhaven National Lab sufficiently protects the activated soils below the floor, a scaled drawing of the floor shieldings of the Alternating Gradient Synchrotron (AGS) complex was converted using three dimensional geometry into Monte Carlo N Particle Extended (MCNPX) program. Using the beam line drawings and Monte Carlo calculations, a simulation of the radioactivity in the soil has been conducted. The results of these calculations were then used to draw contour lines in Building 912 that show activity concentrations in the groundwater beneath the soil. The results indicate that the high concentration of radioactive material in the soil lies primarily below the target at $2E^{-05}$ particles per cm^2. These calculations are important because they reveal what happens to the activated soil below the target and beam lines if water penetrates into the activated soil. The output from the MCNPX simulation also indicates the location and size of the radioactive concentration in the soil. These results will also help determine if any changes need to be made in the boundary of the activated soil area so the drinking water is not affected.

Pulsed Electrical Discharge in a Gas Bubble in Water. *ERICA SCHAEFER (Hartwick College, Oneonta, NY 13820) SOPHIA GERSHMAN (Princeton Plasma Physics Laboratory, Princeton, NJ 08543).* This experiment is an investigation of the electrical and optical characteristics of a pulsed electrical discharge ignited in a gas bubble in water in a needle-to-plane electrode geometry. Argon or oxygen gas is fed through a platinum hypodermic needle that serves as the high voltage electrode. The gas filled bubble forms at the high voltage electrode with the tip of the needle inside the bubble. The discharge in the gas bubble in water is produced by applying 5 - 15 kV, microsecond long rectangular pulses between the electrodes submerged in water. The voltage across the electrodes and the current are measured as functions of time. Electrical measurements suggest a discharge ignited in the bubble (composed of the bubbled gas and water vapor) without breakdown of the entire water filled electrode gap. Time-resolved optical emission measurements are taken in the areas of the spectrum corresponding to the main reactive species produced in the discharge, e.g. OH 309 nm, Ar 750 nm, and O 777 nm emissions using optical filters. The discharge properties are investigated as a function of the applied voltage, the distance between the electrodes, the gas in the bubble (Ar or O_2).

Modeling NASA's Deep Impact Mission with Smoothed Particle Hydrodynamics. *SAM SKILLMAN (Harvey Mudd College, Claremont, CA 91711) FRANCIS X. TIMMES (Los Alamos National Laboratory, Los Alamos, NM 87545).* NASA's Deep Impact Mission sent a 364 kg impactor into the path of the comet Tempel 1 with a relative velocity of 10.2 km/s on July 4th, 2005. The mission objective was to determine the physical properties of the comet's nucleus in order to further our theories of the formation of the solar system. This research was focused on modeling the impact using a Smoothed Particle Hydrodynamics(SPH) code written by M.S. Warren. An ideal gas equation of state is used with an adiabatic index of 1.3. The density of the comet is assumed to be constant to the depths that the impactor will reach and ranges between 100-900 kg/m^3 for each individual run. The impact angle was varied until NASA released the known angle of 25 degrees relative to the surface. With the density of the comet set at 500 kg/m^3, our model suggests that the crater will have a diameter of 80 meters and a depth of 43 meters. Further improvement to this simulation would require a more robust equation of state which is outside the realm of this research.

Gain Optimization for the NSTX Power Supply Control System. *JOHN SMITH (Colorado School of Mines, Golden, CO 80401) RONALD HATCHER (Princeton Plasma Physics Laboratory, Princeton, NJ 08543).* A time-saving gain optimization procedure is described for the National Spherical Torus Experiment (NSTX) power supply control system. An algorithm has been designed for determination of the optimal gains for prescribed levels of convergence to the reference current over specified time intervals. Simulink is used to emulate feedback control behavior and plant response while imposing realistic constraints on the power supply and control system models. A MATLAB routine containing the algorithm rates convergence based on weighted considerations of rise-time, steady-state error and overshoot in user-specified regions, adjusting both proportional and integral gains accordingly. Coil reference currents from multiple NSTX shot data files provide set points for benchmarking the algorithm. Use of the MATLAB Optimization Toolbox function lsqnonlin (non-linear least squares) in conjunction with dynamic interval setting has been found to be an excellent candidate for gain adjustment. Eventual application may

include adaptive, efficient gain optimization and setting for the NSTX power supply control system.

Inclusion Analysis and Absorption Measurement in Nonlinear Crystals. *LAURA SMITH (Merced Community College, Atwater, CA 95301) ZHI LIAO (Lawrence Livermore National Laboratory, Livermore, CA 94550).* Yttrium calcium oxyborate (YCOB) is a newly developed nonlinear optical crystal used for second harmonic generation in the Mercury laser. As with any new crystal, optical characterization of the material properties needs to be fully investigated. We are developing two new techniques to detect inclusions and measure optical absorption. With the side illuminating detection examination (SIDE) method, we hope to identify and map the size, density, and the morphology of inclusions. The multi-pass absorption technique (MPAT) will be used to help determine the absorption coefficient of various finished crystalline pieces at near-infrared wavelengths.

Single Gas Electron Multiplier (GEM) Based Gas X-Ray Detector and Ionization Chamber. *RODNEY SNOW (Southern University and A&M College, Baton Rouge, LA 70813) DAVID PETER SIDDONS (Brookhaven National Laboratory, Upton, NY 11973).* The signal from an ionization chamber can be improved through the use of an electron multiplication device such as a gas electron multiplier (GEM). This paper will show the results from a one-inch diameter, single GEM based ionization chamber that was designed, built, and tested at the National Synchrotron Light Source (NSLS) at Brookhaven National Laboratory. The chamber was run with an Argon Carbon Dioxide ($Ar:CO^2$ 90/10) gas mixture at atmospheric pressure and achieved a gain of 130 at a 100 kV/cm field across the GEM. The detector was also characterized using Extended X-ray Absorption Fine Structure (EXAFS) and x-ray absorption near edge structure (XANES).

And There Was Light — Analyzing the Cosmic Microwave Background Using Interactive Data Language. *DANIELLE SPELLER (North Carolina State University, Raleigh, NC 27695) GEORGE F. SMOOT (Lawrence Berkeley National Laboratory, Berkeley, CA 94720).* The discovery of the Cosmic Microwave Background (CMB) is a major development in the field of cosmology that has been instrumental in raising cosmology from a qualitative to a quantitative science, allowing more accurate, precise measurements for fundamental constants and providing a way to discriminate between various theories of cosmic origin and evolution. An important feature of the CMB is the presence of tiny temperature anisotropies in what is otherwise an isotropic and homogeneous sea of radiation. Current theories and models predict a Gaussian distribution for these anisotropies, and much research has been devoted to the statistical analysis of the CMB. We tested the Gaussianity of a small portion of the first year WMAP map (10 degree radius, at [0,90] galactic coordinates) by comparing its statistical moments with those of 1000 Monte Carlo simulated CMB samples. We also formed a rough comparison of the WMAP signal data to a Gaussian of the same mean and standard deviation. It was found that the mean, skewness, and kurtosis of the 94 GHz frequency map fell within one standard deviation of the mean values for the simulations and is compatible within 78% probablility. Qualitatively, the skewness and kurtosis of the WMAP data in comparison with the simulated analysis suggests Gaussianity. This conclusion of Gaussianity is in agreement with several previous studies of the statistical distribution of the background anisotropies.

Gas-Filled Recoil Separation of Heavy Ions at Intermediate Energies. *MATTHEW STERNBERG (University of Oregon, Eugene, OR 97403) GUY SAVARD (Argonne National Laboratory, Argonne, IL 60439).* Current capabilities for the capture of fusion recoils produced at the Argonne Tandem Linear Accelerator System (ATLAS) and used for mass measurements at the Canadian Penning Trap are limited. A method has been developed in which a large range of recoil products at various energies could be efficiently separated from the primary beam. Simulations suggest that recoil products could be captured with initial angles of divergence as large as 12 degrees, improving the current efficiency by as much as 1,000%. Design and construction of the proposed apparatus are currently underway at Argonne National Laboratory. The current laboratory setup is capable of capturing reaction products emitted at angles up to 4 degrees off axis. In the majority of reactions recoil products are emitted at angles within 4 degrees of the primary axis. However, there are many desirable reactions, such as those in which alpha particles are emitted, where the majority of products diverge from the primary axis at angles in excess of 4 degrees. The use of a large bore solenoid magnet has been investigated as a means of capturing a larger range of recoil products. A Monte Carlo simulation has been developed to model the transport of ions through a gas-filled solenoid magnet and different means of disposing of the primary beam have been investigated.

Measuring the Magnetic Field of the ECR-2 Magnet at ATLAS and its Effect on Charged Particle Beams. *CACEY STEVENS (Southern University and A&M College, Baton Rouge, LA 70813) ELIANE LESSNER (Argonne National Laboratory, Argonne, IL 60439).* The purpose of the Argonne Tandem Linear Accelerator System (ATLAS), a particle accelerator at Argonne, is to generate beams of heavy ions for interaction with matter. The charged particles are generated by the Electron Cyclotron Resonance (ECR) source, accelerated by electric fields from radio frequency cavities, and focused or bent by magnets. The current induced magnetic field within a magnet exerts a force on the beam particles which changes their direction of motion. A dipole magnet at ATLAS, known as the ECR-2 analyzer magnet, focuses in both planes due to edge angles of 29.4 degrees and bends an ideal beam 90 degrees to be sent to various experimental areas. In this context, we measured the ECR-2 field to determine its effects on the beam trajectory at different points in the magnet. Using a Hall probe, the magnetic field was recorded by the gauss meter and plotted according to the Cartesian coordinate system. The trajectories of oxygen, krypton, and lead ion beams through ECR-2 are compared to trajectories through an ideal sector dipole using simulations performed on the software program, Particle Beam Optics Laboratory. The simulation of an ideal sector magnet had a uniform magnetic field of 1021 gauss to agree with the maximum value of the magnetic field measured in the ATLAS dipole, 1021 gauss. The plots of the ECR-2 analyzer magnet show gradual decrease in the magnetic field away from the center of the magnet. The comparison of the ideal sector to the ECR-2 magnet shows that the ECR-2 focuses more significantly in the x- and y-planes. In addition,changes in the ECR-2 analyzer magnet due to edge focusing effects.

Unusually Large Magnetostriction Effect at Room Temperature in A-site Ordered Perovskite Manganites. *ANNE STYKA (University of Illinois at Chicago, Chicago, IL 60607) YANG REN (Argonne National Laboratory, Argonne, IL 60439).* The temperature and magnetic field-dependent structural properties of the half-doped A-site ordered manganites $RBaMn_2O_6$ (R = Pr, Nd, $Pr_{½}Nd_{½}$) have been studied using high-resolution high-energy X-ray powder diffraction. The compounds are ferromagnetic at room temperature and antiferromagnetic at lower temperatures. It is found that the lattice parameters of the crystal structure are very sensitive to applied magnetic fields in the ferromagnetic states, while the antiferromagnetic state is unchanging. An unusually large magnetostriction effect is obtained at room temperature, with the magnetostriction of the order of 1,200 microstrain. The observed phenomena is explained in terms of a change in orbital occupancy of the eg electrons from the $d\{x^2- y^2\}$ state to the $d\{3z^2 - r^2\}$induced by external magnetic fields.

The Interactions of Virtual Pairs in the Electro-Magnetic Field. *LISA SUTER (St. Joseph's College, Patchogue, NY 11772) CAROL SCARLETT (Brookhaven National Laboratory, Upton, NY 11973).* The purpose of this experiment is to study the behavior of virtual pairs while traveling through an electro-magnetic field. The effects that we will be looking for include photon-photon scattering, polarization of the virtual particles, and curvature with the presence of a gradient. Our setup will consist of a vacuum-sealed Relativistic Heavy Ion Collider (RHIC) quadra-pole magnet, which will produce a magnetic field gradient of 71 tesla/meter. We will be sending an argon laser through its cavity, producing 1019 photons/second. We want our equipment to be sensitive enough to detect photon-photon scattering. In order to detect a slight deviation in the lasers path, the waist of the beam has to be minimized. At the start of our setup, we will have a telescope designed to focus and minimize waist of the beam. At the opposite end of our magnet, a photon-receiver will be positioned to measure a deviation as small as 10 x 10-9 radians. In order to calculate the waist of the beam at the photo-receiver, we combined lens matrices and Jones vectors into a Mathematica program. A variety of optical lengths and distances between the laser and lenses were used in order to find the optimal measurements. We then set some of the measurements as variables, which allowed us to plot and measure the sensitivity of the dimensions. Our results indicated that the distances between the lenses had a greater influence on the radius of the beam then the optical lengths. Because of this, we focused more on the sensitivity of the setup by finding the rate of change between the distances and the waist. The focal lengths we used were -100 and 200. The distances that provided us with the best results were 67.1cm between the laser and the defocusing lens (D1) and 15.2 cm between the two lenses (D2). With these measurements, we were able to produce a beam with a radius of 2 x 10-6 m at the photo-receiver. The rate at which the radius increased

with any adjustment in D1 was also minimal with these dimensions. With this setup, we will be more accurate in finding any deviation in the path of the argon laser while traveling through the magnet. The trends that we were able to find though these calculations will also help us when preparing further studies with virtual pairs in the magnetic field.

Determining the Rate of Boron 12 Decay in the MiniBooNE Neutrino Detector. *RUTH TONER (Yale University, New Haven, CT 06520) MORGAN WASCKO (Fermi National Accelerator Laboratory, Batavia, IL 60510).* In addition to its main goal of investigating neutrino oscillation, the MiniBooNE collaboration conducts several physics projects involving the search for exotic particles with energies as low as 10 MeV. It is therefore essential to understand all sources of background at this low energy, including that of the beta decay of boron 12. This background appears when cosmic ray muons stop in the detector and are captured by mineral oil carbon 12 nuclei. The most important step in calculating the cross section of this decay reaction in the detector was accurately determining its rate in the detector. The MiniBooNE exotics pre-report predicts that the rate in the MiniBooNE detector should be approximately 11 Hz. Sample data was taken from the detector strobe stream, which had been recorded by the data acquisition system (DAQ) with an external trigger independent of the neutrino beam. A series of filters and pre-cuts were applied to the data, turning the DAQ raw data into a usable set of events with detailed information about energy, event location and time, etc. The total boron 12 decay rate was taken to be the total number of boron 12 events observed divided by the integrated time of observation. The total time for the rate calculation was taken to be the time during which the DAQ recorded good data – i.e., the number of events passing the filters multiplied by their constant time duration. The total number of boron 12 events was taken to be those events passing the precuts and a second series of cuts applied in ROOT, including a rough energy cut only passing those events below 15 MeV. By knowing the rate and the approximate number of detector carbon atoms, the frequency per carbon atom was calculated to be 1.76×10^{-30} Hz. This number can later be used to get a cross section, once the flux of muons stopping in the detector is better understood. Although the order of magnitude seems reasonable, the decay rate number used in this calculation (33.43 Hz) seemed somewhat high. The study therefore recommend a more complicated series of fitting functions to apply weighted cuts and determine a more accurate count for the boron 12 events.

Meson Form Factor and the Convolution Product. *LESLIE UPTON (Hampton University, Hampton, VA 23668) PAUL GUEYE (Thomas Jefferson National Accelerator Facility, Newport News, VA 23606).* At Thomas Jefferson National Accelerator Facility, experiments are performed to extract unobserved key information on the constituents of nuclei through measurements of meson form factor data. The current method requires the knowledge of cross sections. However, this method is currently not accurate enough. The focus of this study is to develop and validate a technique to accurately extract meson form factors based on the combination of the convolution product and Lyapunov stability. Three independent functions f(Q2), g(W) and h(t) mix to form the cross section. The intent is to extract the analytical functions that combined to exactly reproduce the behavior of the cross section by using a deconvolution technique. Finally, the Lyapunov stability algorithm will be applied to insure a unique solution. Using a previosly published algorithim, non-linear and polynomial regressions for the data were calculated. The data was used to determine the functions for f(Q2), g(W) and h(t). These analytical expressions will be used to confirm the exact meson form factor extraction technique. If this technique proves successful, there will be major implications within nuclear physics, medical imaging, and even statistics.

Adapting Devices for a Beamline and EXAFS Measurement. *TIM VANDERLEEST (Chicago State University, Chicago, IL 60628) JUSTIN AKUJIEZE (Argonne National Laboratory, Argonne, IL 60439).* The prototype circuitry for a remote shutter control system was succsessfully designed, created and tested. In addition, a schematic of the circiutry has been created and sent for professional fabrication. This system is needed for control of the intense synchrotron beam that is used in a beamline. Secondly, a specialized sample mount for thin-film EXAFS (Extended X-ray Absorption Fine Structure) measurement was designed and built. The uniqueness of the sample mount is in that the sample can be rotated to perform angle-resolved EXAFS measurements while the sample remains in the beam path.

Extended Source Gamma-Ray Emission from WIMP Annihilation in the Sagittarius Dwarf Elliptical Galaxy. *VIDYA VASU-DEVAN (Columbia University, New York, NY 10027) LARRY WAI (Stanford Linear Accelerator Center, Stanford, CA 94025).* The proximity of the dark matter dominated Sagittarius Dwarf Elliptical Galaxy (position (*l*,*b*) = 5.6°, -14°) allows it to act as an ideal laboratory for the exploration of extended gamma-ray emission from Weakly Interacting Massive Particle (WIMP) annihilation processes in a dark matter-dominated system. Since the matter in our universe is predominantly dark, exploring such processes as WIMP annihilation will lead to a better understanding of cosmology. In order to study this gamma-ray emission, a model for the diffuse background gamma-radiation in the dwarf galaxy's region is extracted from the Energetic Gamma Ray Experiment Telescope (EGRET) data. After validating this model and comparing it to the EGRET diffuse model, the background model is added to effective bleeding-contamination from external point sources and multiple models for the signal-above-background emission. Various models of this emission are tested: a) no source located in region, b) unidentified point source 3EG J1847-3219 from *the Third EGRET Catalog* responsible for the emission and c) extended emission resulting from WIMP annihilation responsible for the signal above background. These models are created through the employment of Monte Carlo simulation methods, utilizing the response functions of the EGRET instrument to simulate the point spread function, energy dispersion and effects of variable effective area depending on angle of incidence. Energy spectra for point sources are generated from the best predictions of spectral indices listed in *the Third EGRET Catalog* and the spectrum for the extended dark matter source is generated from Pythia high energy annihilation simulations. Hypothesis testing is conducted to assess the goodness-of-fit of these models to the data taken by EGRET. Additionally, we hope to expand our analysis by employing the response functions of the imminent Gamma Ray Large Area Space Telescope (GLAST) to our models. This extension should highlight the sensitivity disparities between GLAST and EGRET and show GLAST's potential enhancement of this analysis. This process will allow for forecasting of extended WIMP annihilation emission signatures for the GLAST detector.

Characterizing of Zinc Oxide (ZnO) as a Transparent Conducting Oxide (TCO). *ANDREA VERMEER (Seattle Pacific University, Seattle, WA 98119) XIAONAN LI (National Renewable Energy Laboratory, Golden, CO 89401).* The purpose of this investigation was to characterize undoped insulating zinc oxide (*i*-ZnO) as a transparent conducting oxide (TCO). We studied the optical, electrical, and structural properties of the metal oxide as it was deposited by two different methods: MOCVD (metal-organic chemical vapor deposition) and PECVD (plasma enhanced chemical vapor deposition). The films were etched using plater's tape or black wax and hydrochloric acid. The thickness of each film was measured using a Dektak3 stylus profilometer. Transmission, reflection, and absorption spectrums were analyzed between 300 nm to 2000 nm using a Cary spectrophotometer. Through use of the Bio-Rad HL5500 Hall system, the carrier concentration, resistivity, and mobility of each film were measured. A Scintag X-ray Diffraction machine (XRD) was used to determine the lattice constants and presence of crystalline structures within the thin films. Three sample sets were studied: a set of undoped ZnO films was deposited by MOCVD at temperatures ranging from 200°C to 550°C as well as two sets of undoped ZnO films deposited by PECVD, one set ranging from room temperature to 400°C at a fixed power of 50 watts and one set ranging from 25 watts to 150 watts at a fixed temperature of 200°C. With increased deposition temperatures in MOCVD, the films demonstrated strong preferred (0 0 2) orientation. As the temperature increased, the samples deposited by MOCVD had increased resistivity and decreased carrier concentration. The films deposited by PECVD tended to have a stronger preferred orientation (0 0 2) as the power decreased and the temperature increased. The resistivity of the films deposited by the PECVD decreased with temperature and the carrier concentration increased. The resistivity of the films deposited by the PECVD increased with power at first, then decreased and the carrier concentration increased with increased power. Most of the samples demonstrated transmission that was greater than eighty percent and lattice constants tended to be above the standard. From this data we were able to determine the optimal MOCVD and PECVD deposition conditions for *i*-ZnO.

Electron Tomography: A New Diagnostics Technology for the Spallation Neutron Source Accumulator Ring. *AARON VINCENT (Laval University, Quebec City, QC G1W 1M3) SARAH COUSINEAU (Oak Ridge National Laboratory, Oak Ridge, TN 37831).* The Spallation Neutron Source accelerator ring will accumulate 1014 protons per pulse for the production of neutrons via the spallation process. Operating at such high beam intensities requires a reliable, robust set of beam diagnostics. The high beam intensity in the ring precludes the use of traditional interceptive beam diagnostics used to measure beam density

distributions. Electron tomography is a new non-destructive, non-interceptive beam analysis tool that exploits the trajectory deflection of an electron bunch due to the proton beam electromagnetic field. A two-dimensional scan of the electron beam through the proton beam allows for a complete reconstruction of the two-dimensional cross-sectional proton beam density distribution. Here, the electron tomography system was simulated in an advanced modular programming package that modeled the interaction between a 50 to 200KeV electron beam and the electromagnetic field generated by the proton beam. Realistic electron gun, scanning and detection parameters were used to ensure accuracy and both lateral sweeping and fixed-pivoting hardware setups were studied for the electron gun. The collected data was filtered and the proton beam was reconstructed in MatLab using a modified version of a medical tomography reconstruction algorithm. The resulting reconstructed density profiles were compared with the original proton beam. The effects of sampling resolution, hardware parameters, mechanical error and data filtering were studied, and each parameter was optimized for accuracy of reconstruction and maximization of signal-to-noise ratio. It was found that even when realistic errors were introduced the reconstruction was still accurate enough to warrant the implementation of electron tomography technology in SNS. The reconstruction software developed here will eventually be used to process actual beam data in the SNS ring.

Simulation of Neutron Therapy at the Neutron Therapy Facility Using Geant4. *AMANDA WEINMANN (Saint Mary's University of Minnesota, Winona, MN 55987) ERIK RAMBERG (Fermi National Accelerator Laboratory, Batavia, IL 60510).* Neutron therapy is a type of radiation therapy used to treat malignant tumors. Unlike conventional radiation therapy that uses photons, neutron therapy destroys the cells by interacting with atomic nuclei via several, varying mechanisms. It is important to be able to predict how the neutrons will interact and lose energy in tissue in order to develop unique and effective treatment plans for patients. For this reason, this project sought to create a simulation that could model the energy deposition of neutrons in a patient at the Neutron Therapy Facility (NTF). A simulation toolkit named Generation and Tracking 4 (Geant4) was used. Geant4 is designed to model particles passing through matter, and it is capable of simulating many user-defined details, such as particle generation, physics processes, and geometries. The geometries used by NTF are imported from Computed Tomography (CT) images that meet a medical standard known as Digital Imaging and Communications in Medicine (DICOM). The Hounsfield numbers of the DICOM images are converted into linearly-correlated tissue densities and constructed into Geant4 geometries. Once the geometry is developed, aspects of the neutron beam must be characterized. Other reference materials discuss specifics of the NTF beam. Currently, the simulation models the initial beam spot, energy spectrum, and downstream flux of the neutrons. The beam spot is simulated as the size of the neutron beam that is emitted from 66 MeV protons striking a beryllium target; the neutrons' energies are reproduced from a plot of the NTF neutron energy spectrum; and the downstream flux is simulated as a uniform and flat spatial distribution at the exit of a variable collimator. This simulation is distinctive because, just as neutron therapy is relatively rare compared to photon therapy, most radiation therapy simulations are intended to model photon radiation. It is also different from other techniques because it does not require that ionization profiles be defined for each type of tissue or material. The Geant4 simulation is a useful technique for NTF, but future work must be conducted to describe other aspects of the beam and obtain acceptable accuracy levels.

Investigating the Frictional Effects of SuperHard Nano-Composite Films and Laser Texturing. *MARK WHEELER (Amherst College, Amherst, MA 01002) GEORGE FENSKE (Argonne National Laboratory, Argonne, IL 60439).* Tribology is often applied to the study of the inner workings of automotive combustion engines because small reductions in engine friction could mean savings of several million barrels of gas nationwide and improvements to engine life. Our experiments are conducted with commercial Mobil-1 10W30 formulated motor oil on a "High Frequency Reciprocating Rig" that uses segments taken from stock engine liners and stock engine rings. Using actual pieces of engine increases the realism of the experiments but also introduces alignment issues that can make exactly repeating experiments difficult. A reciprocating rig also imitates the motion of a piston engine, though at much lower rpm. The rig runs from 15 to 300 rpm and delivers loads of 0 to 250N. Our first experiment was the testing of a liner coated with a recently developed "Super-Hard Nano-Composite" with a stock ring. The SHNC sample was tested against a stock sample at room temperature, after a three hour bake in 150°C oil and after a three hour run in 150°C oil. The heated and the heated while running experiments were conducted to test the effects of tribofilms that may be formed by the Mobil-1 oil's additives either thermally or tribologically. Initially the SHNC liner performs about 30% worse than the stock and when baked or baked while running about performs about 20% worse. This contradicts previous experiment on a pin on flat apparatus which showed a roughly 60% improvement over stock after several hours of running. As predicted, wear on the SHNC surface is negligible compared to stock. Our second experiment tested three samples with half of their surface laser textured. The laser texturing in these samples is a pattern of small dimples 2, 5, and 8 microns deep respectively, 100 microns in diameter, and spaced center-to-center by 200 microns. The half textured surface allows for a comparison of the performance versus a stock baseline in every stroke of data. The first and most obvious result from these liners is clear indication that the dimpled surfaces need wearing in (or possibly polishing). Microscope examination reveals that the dimpling process creates a slightly raised ring around the dimple. This raised area wears down with a few hours use and friction is reduced but it has not yet been explored how much wear is optimal. Despite all the dimpled liners performing worse than the stock, the 5 micron dimple depth outperformed the 2 and 8 micron deep liners slightly before and after wear.

Analysis of Beam Position Monitor. *APRIL WHITE (Tennessee State University, Nashville, TN 37209) THEODORE L. WILLIAMS (Oak Ridge National Laboratory, Oak Ridge, TN 37831).* The Linear Accelerator (Linac) for the Spallation Neutron Source (SNS) accelerates negative hydrogen ions to an energy of one billion electron volts. In order to maintain the trajectory of the particles throughout the accelerator, beam position monitors (BPM) are utilized. The BPMs provide valuable information pertaining to the vertical, the horizontal, the phase, and the amplitude of the Linac beam. An interactive computer program was designed and implemented in MatLab for the purpose of analyzing the data acquired by the beam position monitors. Data analysis techniques included generation of statistical data and model independent analysis via singular value decomposition methods. In order to analyze the data created by singular value decomposition, a beam simulation module was generated. To analyze the spatial eigenvectors, the data output of the module was incorporated into the Matlab program. The results of the analysis will be used to improve the BPM's system performance and to obtain system resolution beyond that achieved by individual BPMs.

Period of Validity of Adiabatic Invariance for a Resonant Mathieu Equation. *NATHANIEL WILLIAMS (Whitworth College, Spokane, WA 99251) HONG QIN (Princeton Plasma Physics Laboratory, Princeton, NJ 08543).* The Mathieu equation describes a periodically perturbed harmonic oscillator that is resonant when the ratio of the natural frequency of the oscillator to the frequency of the perturbation is near integer and half integer values. The principle of adiabatic invariance tells us that the action variable of a system will be nearly constant over a time interval of order $1/\varepsilon$ where ε is the order of the rate of change the perturbed system's frequency. Adiabatic invariance is a useful theoretical tool that can greatly simplify calculation. The time scale over which such a simplification is valid must be know before implementation. In plasma physics, adiabatic invariance is the reason why magnetic mirror machines are capable of confining charged particles in a plasma. It is desired to know whether the period of validity of the adiabatic invariant can be extended to higher orders of $1/\varepsilon$. The WKB method, developed by Wentzel, Kramers, and Brillouin, is used to obtain an approximate solution to the Mathieu equation so that its adiabatic invariance can be analyzed. The calculation indicates that the change in the action variable over any interval is of order ε. The approximation turns out to be asymptotic only for periods with length of order $1/\varepsilon^2$. This result verifies the adiabatic invariance for t less than $1/\varepsilon$ and extends the result to order $1/\varepsilon^2$. The adiabatic invariance of the Mathieu equation can be consider constant over time periods up to order $1/\varepsilon^2$. There is reason to believe this can be extended to higher order but this can not be done by the method employed here.

Conservation of Magnetic Moment for Charged Particle Motion in a Time-Dependent Uniform Magnetic Field. *SUNGHWAN YI (Cornell University, Ithaca, NY 14853) R.C. DAVIDSON (Princeton Plasma Physics Laboratory, Princeton, NJ 08543).* The adiabatic magnetic moment invariant for the motion of a charged particle in a spatially uniform, time-dependent magnetic field B(t) is studied numerically. The robustness of the magnetic moment invariant $\mu = mv^2/2B$ is explored for slowly varying and rapidly varying magnetic field B(t), for a charged particle moving in a long solenoid with time-varying current. The numerical method used in this study is a fourth-order Runge-Kutta method, which is used to integrate the nonlinear differential equations for the particle dynamics. Where high accuracy over a long evolution period is desired, a fourth-order symplectic integration method may

be used instead. In the case of a slowly varying magnetic field, where the time-scale of the change in the magnetic field is much larger than the particle gyroperiod, it is shown numerically that the adiabatic magnetic moment m is asymptotic to a recently discovered exact magnetic moment invariant M, which is conserved even for rapidly varying magnetic fields. By examining numerically the effects of various functional forms of B(t) on the conservation of the adiabatic magnetic moment invariant, the precise conditions under which m is conserved are identified. Thus, this work characterizes the validity of the adiabatic approximation of the magnetic moment invariant, a fundamental assumption in plasma physics that has never been rigorously quantified.

Magnetization, Charge Transport, and Stripe Phases in $Nd_{5/3}Sr_{1/3}NiO_{4+\delta}$ Single Crystal. *JUN ZHANG (Cornell University, Ithaca, NY 14853) MARKUS HÜCKER (Brookhaven National Laboratory, Upton, NY 11973).* Stripe phases, in which doped charges are localized along domain walls between antiferromagnetic insulating regions, provide a framework for the electronic structure of doped antiferromagnets such as the superconducting layered copper-oxides. Layered nickel-oxides, such as $Nd_{2-x}Sr_xNiO_{4+\delta}$, though non-superconducting, exhibit stripe phases in which charges are more localized, resulting in higher charge density modulation amplitudes than their cuprate analogs, thus are more amenable for experimental investigations. We study the magnetic and electric-transport properties of a $Nd_{5/3}Sr_{1/3}NiO_{4+\delta}$ single crystal by means of magnetic susceptibility, isothermal magnetization, and electric resistivity measurements. We observe a transition of the magnetic susceptibility with applied field parallel to the c-axis at T ≈ 15 K, which is due to the long-range ordering of Nd^{3+} magnetic moments. A transition of the in-plane resistivity (P_{ab}) is observed at T ≈ 230 K, which indicates the charge stripe ordering that has also been observed in $La_{2-x}Sr_xNiO_4$ at about the same temperature. The out-of-plane resistivity (P_c) exhibits a milder transition at T ≈ 200 K. After the stripe phase transition takes place, the electronic transport exhibits variable range hopping behavior. The resistivity anisotropy (P_c/P_{ab}) shows a sharp drop at the P_{ab} transition temperature with decreasing temperature, which indicates the strong localization of charge carriers in the ab-plane as charge stripes become statically ordered and the system becomes less two-dimensional electronically. Our results are in support of the stripe phase picture of the electronic structure in layered metal-oxides.

Science Policy

Effects of Electric Utilities on a Zero Energy Building (ZEB). *NICOLAS BABCOCK (Colorado State University, Fort Collins, CO 80523) PAUL TORCELLINI (National Renewable Energy Laboratory, Golden, CO 89401).* Buildings consume approximately forty percent of U.S. source energy. However, design technologies, materials, and control systems allow for construction of commercial buildings that consume significantly less energy than minimum code-compliant buildings of identical size. The Office of Energy Efficiency and Renewable Energy (EERE) has set goals for ZEB's to enter the market place no later than 2025. Once built; however, source energy use and site energy costs are regulated largely by the electric utility. This study explores how a high-performance building (HPB) can reach ZEB status with respect to source energy, site energy, energy cost and emissions by varying the generating capacity of the building's photovoltaic (PV) array. Utility rate calculations for energy costs were processed using three tariff structures: a Small Power General Service Tariff (GS), a Time of Use Tariff (TOU), and a Real-Time Pricing Tariff (RTP). A net metering rider was applied to each tariff to explore the cost benefit of exporting energy to the grid. Further, an attempt was made to calculate a variable source-to-site conversion factor (SSCF) that considers time of day, time of year, base load, peak load, generating capacity, and source energy. A variable SSCF is needed to better calculate source energy use and source environmental impacts. Proprietary concerns from surveyed utilities made this exploration largely unsuccessful, however. Evidence suggests a general service tariff with a net-metering rider that pays an equivalent rate for on-site generation is most favorable from a ZEB cost viewpoint. Current rate structures, however, do not provide financial incentives for incorporating energy efficient design into buildings.

Innovation Diffusion Modeling; Tests and Application to the Renewable Energy Sector. *ZACHARY BRATUN-GLENNON (University of Virginia, Charlottesville, VA 22904) DOUGLAS ARENT (National Renewable Energy Laboratory, Golden, CO 89401).* The field of innovation diffusion modeling has proved the ability to accurately predict the adoption of a new consumer good. This science has been applied, in large part, only to consumer durable goods that do not encompass the unique characteristics of renewable energy technologies. For this reason, this study applied diffusion models to the renewable energy market. The Bass Model, Generalized Bass Model, and Nonuniform Influence Model were selected and applied, along with a new combination of the last two, to historical market data for testing. Photovoltaic technology was used, as representative of current renewable energy technologies, for generating a model that sufficiently predicted adoption of this product sector. Because of PV's several uses, three market sectors were determined and comparisons were drawn between each sector and another technology with more historical data. While conventional models were found to adequately predicted consumer good applications, they over-predicted the diffusion of PV. The Nonuniform Influence Model was used to adapt the models for accurate renewable energy diffusion forecasting.

Proposed Patent Law Reform of 2005: Implications for Research Institutions. *JUSTIN KNEITEL (University at Buffalo, Buffalo, NY 14261) CHRISTINE BRAKEL (Brookhaven National Laboratory, Upton, NY 11973).* Recently, reforming the U.S. patent system has become the subject of much discussion. The current system has changed little since 1952. Coupled with a recent increase in the types, volume and complexity of modern patents and patent applications, what were formerly minor or non-existent problems with U.S. patent law have since caused a great amount of difficulty for the USPTO, U.S. court system, and patent seekers alike. In response to this need for U.S. patent law to evolve, the Patent Reform Act of 2005 has been introduced. The effect the Patent Reform Act of 2005 will have on research institutions is greatly different from the effect it will have on corporations. This paper will discuss, in depth, the potential changes to procedure and practice that research institutions will have to make should the changes embodied in the Patent Reform Act of 2005 become part of U.S. patent law. While these reforms are generally held to be an overall benefit to corporations, the changes have potential to be detrimental to research institutions and their technology transfer missions.

Index of Authors

C

D

E

F

G

H

I

J

K

L

M

N

O

P

Q

R

S

T

U

V

W

X

Y

Z

Index of Schools

T

U

V

W

X

Y

PROGRAMS OFFERED BY THE U.S. DEPARTMENT OF ENERGY'S OFFICE OF SCIENCE

http://www.scied.science.doe.gov

UNDERGRADUATE RESEARCH PROGRAMS

CCI: *The Community College Institute of Science and Technology.* This internship program is open to students attending community colleges.

PST: *Pre-Service Teacher Program.* This internship program is designed for students aspiring to become K-12 science, math, and technology educators.

SULI: *Science Undergraduate Laboratory Internship.* This internship program is open to all undergraduate students attending 2 or 4 year colleges or universities.

GRADUATE AND FACULTY PROGRAMS

Albert Einstein Distinguished Educator Fellowship: This program brings K-12 Science, Math, and Technology teachers to Washington, D.C. for a ten-month fellowship with a federal agency or legislative office.

Faculty and Student Teams (FaST): This internship program is open to teams of college faculty members and 2 or 3 undergraduate students.

DOE Academies Creating Teacher Scientists (ACTS) Program: This summer fellowship program is open to K-14 teachers.

OTHER PROGRAMS

Energy Research Laboratory Equipment Program: This program grants available used equipment to institutions of higher education for energy-related research.

Science Bowl: This program is a national math and science competition for teams of public and private high school and middle school students.